The University of Adelaide
Department of Geology and Geophysics

AEROMAGNETIC INTERPRETATION OF THE KANMANTOO GROUP, SOUTH AUSTRALIA

Shanti Rajagopalan
B. Sc. [Madras], M. Sc. (Tech.) [Osmania]

awarded 3.4.90

June 1989

A thesis submitted to the University of Adelaide
in fulfilment of the requirements for the degree of
Doctor of Philosophy

Contents

Appendices B to J in microfiche. Appendices K and L and Errata in the back pocket of this thesis.

List of Figures

The given page numbers refer to facing pages.

Plates are to be found in the back pocket of this thesis.

Plate 1: 1:100 000 detailed interpretation map.
Plate 2: 1:100 000 total magnetic field contour map.
Plate 3: 1:250 000 grey-scale image of the total magnetic field.
Plate 4: 1:250 000 grey-scale image of the total radiometric count.
Plate 5: 1:250 000 regional interpretation map.

List of Tables

The given page numbers refer to facing pages.

Abstract

The Kanmantoo Group has been the subject of many geological studies. Investigators have been hampered by the paucity of outcrop and the absence of markers in the monotonous lithologic sequence. However, magnetic properties show considerable variation. Aeromagnetic information has been integrated with geological and other geophysical data. The interpretation has been achieved by the use of techniques specially developed for this area and constrained by the results of rock magnetism studies.

Magnetic modelling, opaque mineralogy studies and magnetic susceptibility measurements indicate that most magnetic anomalies are caused by near-surface metasediments, granites and granitic gneisses. Opaque oxide assemblages of magnetite ± haematite ± ilmenite in meta-arenites and pelitic schists and of pyrrhotite ± magnetite in meta-siltstones give rise to the dominant magnetic pattern of multiple, linear to curvilinear anomalies which are essentially stratiform. This pattern is occasionally truncated by elongate discordant anomalies caused by magnetite-series granites.

Magnetic character as indicated by the style and pattern of anomalies varies within the study area. Three distinct subzones have been identified: the Kanmantoo Synclinal Subzone (KNSZ), the Karinya Synclinal Subzone (KRSZ) and the Intermediate Subzone (ISZ). The style of magnetic anomalies in the three Subzones is closely linked to changes in metamorphic grade and structural complexity. In the south, continuous, linear, well-defined anomalies delineate the open, upright folds of the KNSZ against a quiet magnetic background. Anomalies in the KRSZ in the north are of similar style though less continuous and describe the regional NS trending syncline-anticline structure. The ISZ trends NNW and separates the KRSZ from the KNSZ. Increase in metamorphic grade together with several generations of macroscopic folding events have created a complex magnetic pattern of multiple, closely-spaced, intense linear anomalies.

The deformational history of the region can be divided into three phases of macroscopic folding, F_{early}, F_{main} and F_{later}. Early macroscopic folds, some possibly isoclinal, are indicated in the ISZ and they constitute the F_{early} event. The second and dominant phase of folding was the F_{main} event during which the open, upright folds of the Kanmantoo and Karinya Synclinorium formed. Fold axes trending NNW seen in the ISZ may have been part of a later F_{later} phase. Faults trending NS, NNW and NE form the major fault systems.

Effective interpretation of geophysical data is critically dependent on presentation formats. The choice of display should be based on survey specifications, aims of the interpretation and characteristics of the magnetic terrain. Where near-surface, linear anomalies predominate, as in the Kanmantoo Group, vertical magnetic gradient maps reflect surface geology. These maps were created by stacking profiles of the gradient and using a non-linear vertical scale such as automatic gain control so as to enhance fine detail while preserving high-amplitude anomalies. The detection of lineaments and other large scale structures was made possible by the use of grey-scale and colour images of individual and integrated geophysical data sets. A vertical magnetic gradient algorithm was developed to interpret two-dimensional dyke anomalies.

Statement

To the best of my knowledge and belief, and except where reference is made herein, this thesis contains no material previously published or written by another person, nor any material that has been accepted for the award of any other degree or diploma in any University.

If this thesis is accepted for the award of the degree, I consent to the thesis being made available for photocopying and loan.

Shanti Rajagopalan
June 1989

Acknowledgements

I would like to thank the following people:

Prof. Boyd for his guidance and for the benefit of his geophysical insight and experience.

CRA Exploration for giving me access to high-resolution aeromagnetic data.

Peter Brooker, John Paine, Andy Mitchell, John Willoughby and Gabor Korvin for advice on geophysics and computing and for their interest in my work.

Colin Gatehouse and Wolfgang Preiss of SADME for critical comments on geology and for reviewing parts of the thesis.

David Love and Robin Gerdes of SADME for providing geophysical information.

Robin Oliver, Ding Pu Quan, Richard Jenkins, Mike Sandiford, Vic Gostin and Ross Both for helpful discussions on structure, metamorphism, sedimentology and opaque mineralogy.

David Clark of CSIRO for information on rock magnetism and Francois Chamalaun of the Flinders University of South Australia for assistance with measurement of remanent magnetization.

Richard Barrett for photographic reproduction of figures, Sherry Proferes for advice on drafting, Wayne Mussared for preparing thin sections, Phil McDuie and John Stanley for assistance with chemical analyses.

Terry Fanning and the Computing Centre of the University and also the National Centre for Petroleum Geology and Geophysics for providing computing facilities.

Martin Holt for advice on the finer points of English expression and Sally Phillips for help with map presentation.

Tom Whiting, Geoff Johnson, Robert Lawrence, Andrew Lewis, Robert O'Dowd, Bernhard Pracejus and Shi Zhi Qun for their companionship and willingness to help.

Andrew Trevorrow for consultations on TEX and PostScript, and for his patience, understanding and encouragement.

The University of Adelaide for granting me a research scholarship and the Department of Geology and Geophysics for the use of facilities.

My parents and family who made it possible for me to pursue my choice of career.

I dedicate this thesis to my parents, R. Rajam and K. S. Rajagopalan. I shall always be deeply appreciative of their support and generosity.

Conventions and abbreviations

The Australian Map Grid (AMG) has been used to provide a base for magnetic, radiometric and interpretation maps. The study area lies within Zone SI-54. All locations are given in terms of the full AMG coordinate system, i.e. 6 digit numbers for eastings and 7 digit numbers for northings. Note that the AMG system is metric. All units used in this thesis belong to the SI system unless specifically stated otherwise.

Abbreviations commonly used are listed below:

SADME South Australian Department of Mines and Energy

CRA Con-Zinc Rio Tinto Australia Exploration Pty. Ltd.

BMR Bureau of Mineral Resources

PACIFIC EXPL. Pacific Exploration Consultants Pty. Ltd.

All polished thin sections and polished blocks referred to in this thesis are catalogued in the rock collection of the Department of Geology and Geophysics, University of Adelaide. They are prefixed by the accession number 873.

The average intensity of the present magnetic field of the earth in the study area is taken to be 60000 nT and the inclination to be $-65°$. The declination varies between 7.5° E and 8° E.

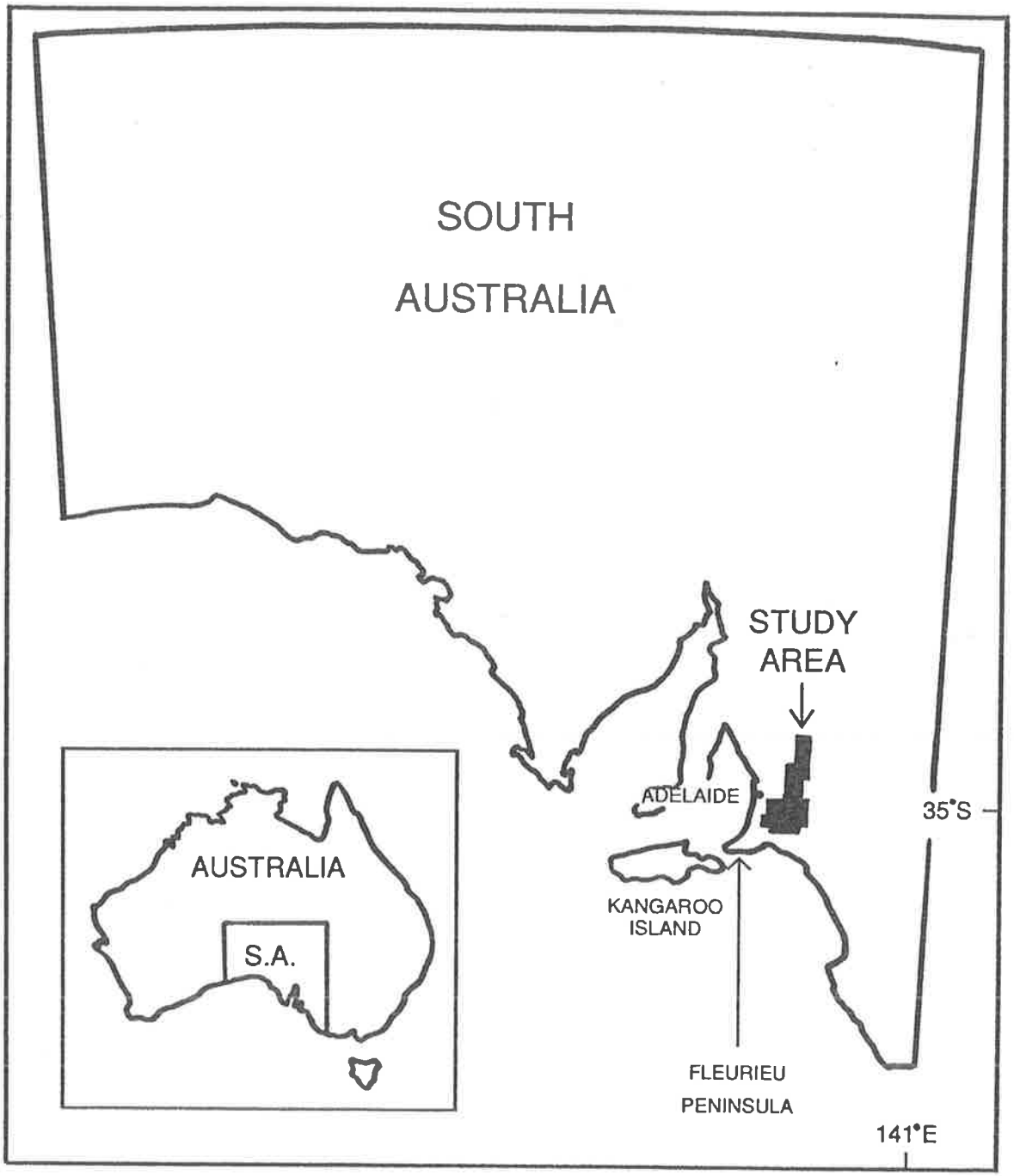

Figure I.1: Location maps showing the position of the state of South Australia within Australia (inset) and the location of the study area (and some localities mentioned in the text) within South Australia. For further detail, see Figure I.2.

Introduction

Metasediments of the Kanmantoo Group are exposed in a synclinorium which is part of the southern Adelaide Geosyncline (Chapter 1). Metamorphosed greywackes, arkoses and siltstones, and occasional limestones and calc-silicates comprise the sedimentary sequence. The amount of information in available geological maps varies, because outcrop is often poor and because there are few markers in what is a rather monotonous lithologic sequence. As a result, after early progress, research into the Kanmantoo Group has stagnated for want of new facts and new ideas. Aeromagnetic surveys provide new facts which may be integrated into current ideas about basin development and tectonics.

The rocks of the Kanmantoo Group outcrop in an arc which extends from Kangaroo Island to Fleurieu Peninsula and the Mt. Lofty Ranges. The boundaries of the main study area (shown in Figures I.1 and I.2) were constrained by the availability of detailed aeromagnetic data.

The aeromagnetic coverage of the study area and surrounding regions is shown in Figure I.2. The southern Adelaide Geosyncline and the western margin of the Murray Basin are covered by regional aeromagnetic surveys. High-resolution aeromagnetic and aeroradiometric data have been collected by CRA over much of the exposed Kanmantoo Group in the Mt. Lofty Ranges. Survey specifications of the different data sets available are summarized in Appendix A.

In this thesis, I present a new perspective on an old problem. This interpretation is based on the integration of aeromagnetic data with aeroradiometric and geological information. In the course of the interpretation, I developed new methods and adapted existing techniques to facilitate the rapid and thorough interpretation of large data sets.

I.1 Aeromagnetic and aeroradiometric interpretation

Aeromagnetic surveys essentially reflect the presence of magnetic minerals in the earth's crust. Of all the airborne geophysical techniques, the aeromagnetic method has by far the greatest depth penetration being able to detect features down to the Curie point geotherm some 20 km or so beneath the earth's surface (Hood *et al.*, 1979). The aeromagnetic method makes an excellent mapping tool (Boyd, 1967) because the signal is unaffected by poor outcrop, the continuity of information provided cannot be matched by ground geophysical or geological surveys, and the regional aeromagnetic coverage now available over Australia makes the delineation of large, previously unrecognized, geological features possible. Recent advances in processing, presentation and interpretation techniques make it possible to integrate the results of magnetic surveys with geological information to produce a consistent overall interpretation (Paterson and Reeves, 1985).

The successful application of the magnetic method is limited by the magnetization contrast, the resolution, accuracy and sensitivity of the magnetometer, and the survey altitude. Anomalies

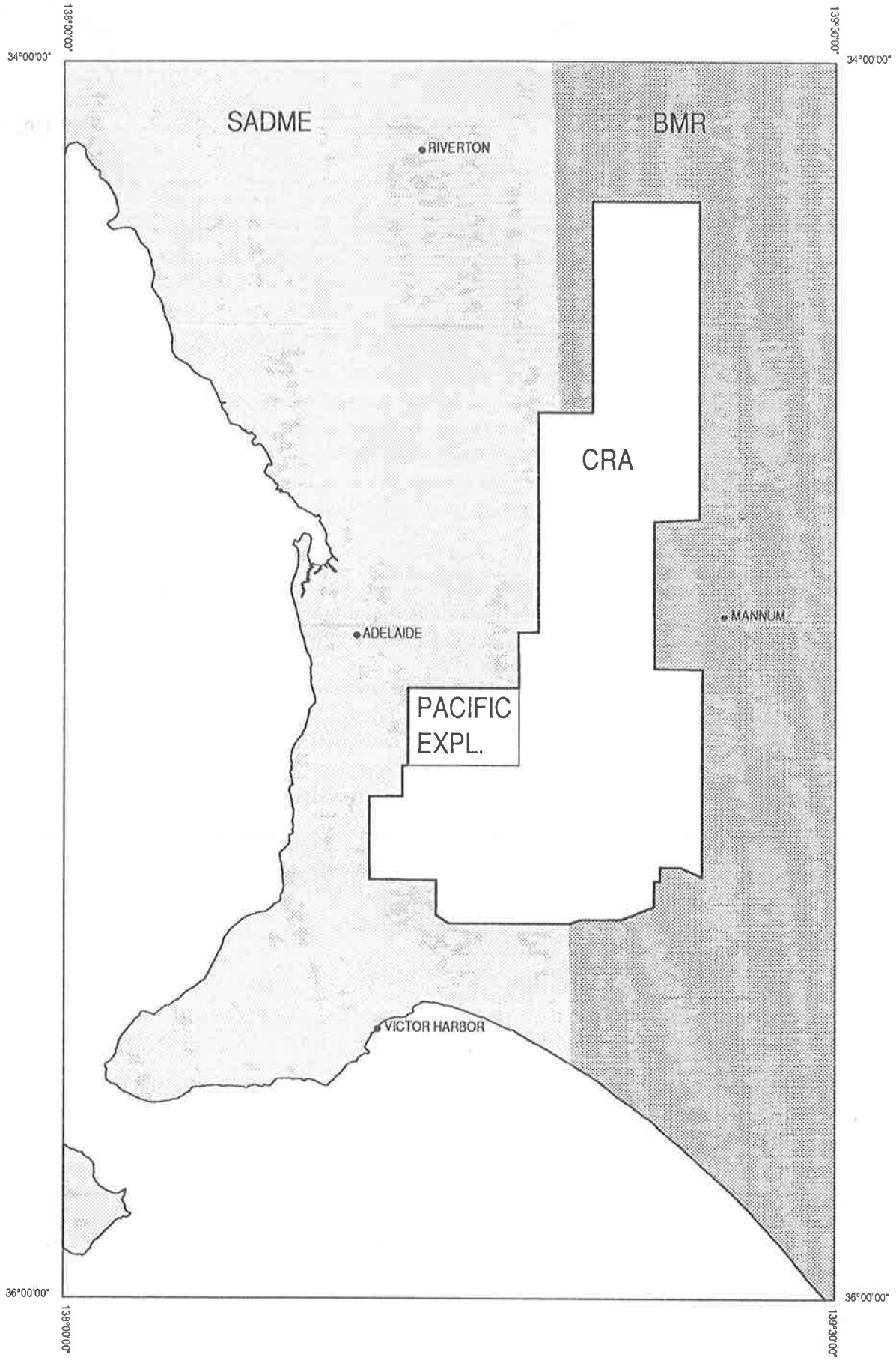

Figure I.2: Aeromagnetic coverage of Mt. Lofty Ranges and adjacent areas with study area outlined. Data — CRA: CRA Exploration, Pacific Expl.: Pacific Exploration, SADME: SADME contour maps (1980, 1983) and BMR: BMR-SADME joint acquisition. Refer to Appendix A for survey specifications.

with amplitudes as small as a few nanoTeslas may be significant and these can be identified in the newer CRA data though not on the older BMR and SADME data.

Initially the study area is divided into magnetic zones, the magnetic texture of each zone described and quantitative estimates of anomaly source parameters determined. Ultimately the information carried in the magnetic data regarding the geology of the area, on both a detailed and regional scale, must be extracted. Interpreting a magnetic survey in terms of geology is often difficult, because the main magnetic mineral, magnetite, is only an accessory mineral in most rocks and therefore rock type classifications which depend on silicate content give no indication of magnetite content. The inherent ambiguity in magnetic interpretation is further compounded by an incomplete understanding of magnetic mineral petrogenesis and rock magnetism.

In contrast to the depth penetration capability of aeromagnetic surveys, aeroradiometric surveys indicate the presence of radioactive elements (K, U and Th) in the top tens of centimetres of the crust. The quality of the data set is severely restricted by the nature of outcrop. These two data sets, one representing a depth profile of the crust and the other a surface map, complement each other and provide information from which the geological processes controlling the presence of the indicator minerals may be deduced.

Radiometric data can be used to map lithology and compute the equivalent radioactive element concentration in the soil or outcrop. The first is possible because variation in the amount of K-minerals (feldspars, clays, micas) is closely associated with variation in lithology. The second is possible only if the survey and instruments were accurately calibrated and has not been attempted in this thesis as the necessary calibration coefficients were not available.

Interpreting large data sets, such as those acquired for mineral exploration surveys, requires appropriate techniques to process and assess them. Different displays enhance different features of the signal. The optimum situation is to vary the format and scale of the presentation to try and reveal unknown and unexpected structures in the area. Though this added processing is time consuming and expensive, it can transform the quality of interpretation.

I.2 Aims of this thesis

The basic aim of this thesis was to provide new facts and ideas and to thus improve and extend the geological model of the area. In order to achieve this, the project was subdivided into a number of smaller parts which are listed below.

1. The study area has been covered by geological maps of varying quality. The first step involved the relating of magnetic and radiometric signatures to the known geology for well-mapped areas and then extending the interpretation beyond these small areas to improve the mapping of adjacent regions.

2. Regional and detailed magnetic maps, and available gravity and seismic data, were used to reexamine the geological setting of the Kanmantoo Group and to test the new models advanced by current researchers.

3. Rock magnetic susceptibility measurements and opaque oxide assemblages were studied to determine the possible sources of magnetic anomalies. The magnetic properties were related to the sedimentary and metamorphic history of the metasediments.

Figure I.3: Detailed locality map of study area showing localities mentioned in text (after SADME base map at 1:1 000 000 scale). The Mt. Lofty Ranges extend from near Yankalilla on the southwest coast to north of Clare.

4. Information regarding the known mineralization was compiled and their geophysical responses compared. This aim was only partly fulfilled and the results are not included in this thesis.

5. To improve the ease and accuracy with which aeromagnetic surveys can be interpreted, new and standard presentation and interpretation techniques were applied and assessed.

I.3 Guide to maps

Many maps are included in this thesis. Some of the important topographic, geologic, aeromagnetic and interpretation maps are listed below. All Plates are in the back pocket of the thesis and Figures are in the text.

1. Location maps:
   Regional location map of the study area: Figure I.1.
   Aeromagnetic survey coverage of the study area and surrounding regions: Figure I.2.
   Places mentioned in the text: Figure I.3.
   1:50 000 topographic map sheets in relation to the study area: Figure A.1.
   Note that 1:50 000 topographic map sheet names are italicized when referred to in the text, i.e. "*Echunga* sheet" refers to the 1:50 000 topographic sheet of the same name.

2. Geological maps:
   Regional setting of the Kanmantoo Group: Figure 1.1.
   Geology of the Mt. Lofty Ranges and surrounding areas: Figure 1.2.
   Metamorphic zones and location of basement inliers: Figure 1.3.
   Granites, granite gneisses and norites: Figures 6.1 and 6.2.

3. Geophysical maps:
   Regional aeromagnetic data: Figure 5.3.
   Total magnetic field contours over the study area: Plate 2.
   Digital grey-scale image of total magnetic field data: Plate 3.
   Digital grey-scale image of total radiometric count data: Plate 4.

4. Interpretation maps:
   Detailed interpretation map: Plate 1.
   Regional interpretation map: Plate 5.

Part I

Geology and rock property studies

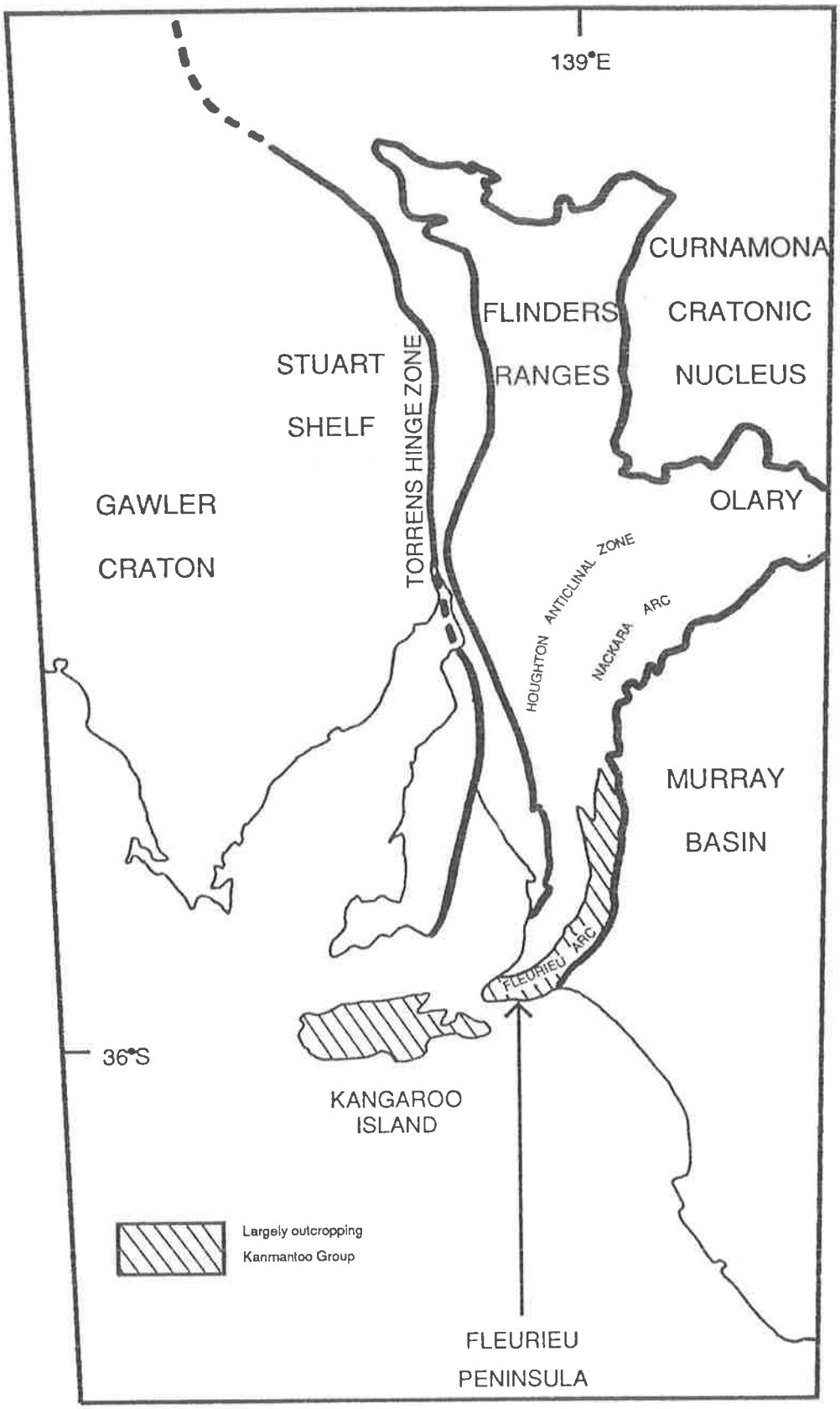

Figure 1.1: The regional geological setting of Kanmantoo Group rocks. The Adelaide Geosyncline consists of the South, Central and North Flinders Zone (Flinders Ranges), the Houghton Anticlinal Zone, and the Nackara and Fleurieu Arcs (Preiss, 1987). Exposed Kanmantoo Group rocks are contained within the outer Fleurieu Arc.

Chapter 1

The geology of the Kanmantoo Group

This thesis is aimed at two groups of earth scientists: those interested in the Kanmantoo Group and in the additional insights which geophysics can provide about local geology; and those who are more interested in the analysis of geophysical data and in the application of the aeromagnetic method to geological interpretation.

Many geologists have worked on the Kanmantoo Group and the earliest references date back to the previous century (e.g. Selwyn, 1859; Brown, 1883). In this chapter I present a brief summary of the geology and establish a geological framework for the thesis. In addition some of the more problematical aspects relating to the deposition and development of the Kanmantoo Group are discussed. References to local geology will be made, where appropriate, in the following chapters on rock properties and interpretation. Readers are referred to Daily and Milnes (1971a, 1972a and 1973), Fleming (1971), Offler and Fleming (1968), Thomson (1969a, 1970, and 1975), Thomson *et al.* (1976), Toteff (1977) and Mancktelow (1979) for extensive discussions on the Kanmantoo Group; to Preiss (1987) for a thorough investigation of the Adelaide Geosyncline; and to von der Borch (1980), Clarke and Powell (1989), Gatehouse *et al.* (in press), Jenkins (1986; in press), Sandiford *et al.* (in press), and Steinhardt (in prep.) among others for current ideas on the tectonic and metamorphic history of the region.

1.1 Regional geology

The Adelaide Geosyncline is an elongate sigmoidal arc which stretches from the Olary region in the northeast and the Flinders Ranges in the north to western Kangaroo Island in the southwest. On Fleurieu Peninsula, the southern Adelaide Geosyncline may be subdivided into the Fleurieu Arc, Nackara Arc and the Houghton Anticlinal Zone (Figure 1.1). The outer Fleurieu Arc corresponds spatially with the exposed Kanmantoo Group (Preiss, 1987). The Torrens Hinge Zone separates "the thin, essentially undeformed sequence on the Stuart Shelf from the thick, folded basinal sedimentary pile" which constitutes the Adelaide Geosyncline (Preiss, 1979).

Sedimentation in the Adelaide Geosyncline started in the late Proterozoic and continued into the early Palaeozoic. The Wilpena Group is the youngest of the lithostratigraphic groups (Thomson, 1969b) which comprise the Proterozoic Adelaide Supergroup (Daily, 1963). Southwest of Adelaide, the Wilpena Group is disconformably overlain by limestone and shale containing Cambrian fauna (Horwitz *et al.*, 1959). These Cambrian rocks belong to the Normanville Group and

are the equivalents of the Hawker Group defined in the northern Flinders Ranges (Dalgarno, 1964). The Barossa Complex, considered to be basement to the Adelaide Supergroup, crops out in five inliers in the southern Adelaide Geosyncline (Mancktelow, 1979).

In the southern Adelaide Geosyncline, the sedimentary basin apparently collapsed soon after the initiation of Cambrian deposition, resulting in the very rapid accumulation of dominantly flysch facies sediments: the Kanmantoo Group (Daily, 1956; Thomson, 1969a; Mancktelow, 1979). The Kanmantoo Group is a thick, essentially non-fossiliferous sequence of metamorphosed greywackes and arkoses, and pelites with occasional calcareous and pyritic units. It overlies the geographically restricted Normanville Group but the nature of the contact has still not been ascertained. Where the Normanville Group is absent, the Kanmantoo Group is in contact with either the Adelaide Supergroup or the Barossa Complex. On the basis of exposed stratigraphy and interpreted cover during Delamerian metamorphism, Mancktelow (1979) estimated that the original thickness of the Kanmantoo Group may have been as much as 20 km. The age of younger granites restrict the period of sedimentation to less than 50 Ma, (Mancktelow, 1979), and perhaps even less than 5 Ma (Jenkins, in press). The uppermost known unit of the Kanmantoo Group is the Middleton Sandstone. Milnes *et al.* (1977) inferred from the intrusion of granites into the Middleton Sandstone that there must have been several kilometres of cover during granite emplacement.

Cambrian sedimentation in the southern Adelaide Geosyncline ended with or before the first deformation of the Delamerian Orogeny, about 505 Ma. The Delamerian Orogeny transformed the sedimentary basin into an orogenic upland and folded the Kanmantoo Group rocks into the Kanmantoo Synclinorium. The orogeny was accompanied by several periods of granitoid intrusion. Increasing temperatures, caused by crustal thickening and granite intrusion, resulted in extensive metamorphism of the sediments. Migmatites are found in the highest grade zone which trends NW from west of Murray Bridge to north of Springton. Madigan (1988) has described the style as being similar to Buchan style metamorphism. The orogeny ended with the decline in temperature and plasticity of the Delamerian fold belt around 450–430 Ma, as indicated by the closure of the *K-Ar* system within biotite and muscovite (Webb, 1976).

Since that time, there has been continual isostatic adjustment leading to uplift and erosion within the fold belt. Glaciation during the Permian produced a series of valleys and monadnocks. Some of the valleys are still filled with Permian sediments (e.g. Inman Valley). Between the Permian and the early Tertiary, the area continued as a stable cratonic block undergoing very gradual weathering and erosion. The weathered landscape was rejuvenated during the Tertiary by block faulting parallel to the regional schistosity, with episodic marine and terrestrial sedimentation continuing to the present day (Mancktelow, 1979).

The present limits of outcrop of the Kanmantoo Group have been set by the Delamerian Orogeny: the original limits are unknown. To the north and west, the Kanmantoo Group is flanked by exposed Normanville Group, Adelaide Supergroup and Barossa Complex. South of Milang and east of the Palmer and Milendella Fault, Caenozoic sediments of the Murray Basin obscure possible Kanmantoo Group rocks except for some isolated and limited exposure. The presence of undeformed Cambrian sediments on Yorke Peninsula constrains the maximum westward boundary of the original basin in which the Kanmantoo Group was deposited. Kanmantoo Group correlatives have been suggested as far afield as the Glenelg River sediments (Wells, 1956).

	Formation name	Dominant lithologies
KANMANTOO GROUP	Middleton Sandstone	arkosic sandstones
	Petrel Cove	siltstones and phyllites
	Balquhidder	greywackes
	Tunkalilla	siltstones and greywackes
	Tapanappa	greywackes and sandstones
	Talisker Calc-siltstone	calc-siltstones
	Backstairs Passage	arkoses and greywackes
	Carrickalinga Head	greywackes and siltstones (*Hyolithidae* and *Lingulella*)
NATURE OF CONTACT UNCERTAIN		
NORMANVILLE GROUP	Heatherdale Shale	slates with phosphatic nodules
	Fork Tree Limestone	limestones *Archaeocyatha* limestone
	Sellick Hill Limestone	mottled limestones and calcareous slates
	Wangkonda Mt. Terrible	limestone member *Hyolithidae* sandstones
MAJOR HIATUS		
ADELAIDE SUPERGROUP		
WILPENA GROUP	Bunyeroo	shales and siltstones
	ABC Range Quartzite	quartzite
	Ulupa Siltstone	green-grey siltstones
	Hallett Arkose	arkose and quartzites
	Seacliff Sandstone	grey-white quartzite
	Nuccaleena	dolomites and siltstones
UMBERATANA GROUP	Upper Umberatana Group	siltstones and sandstones
	Brighton Limestone	limestone
	Tapley Hill	calcareous siltstones and shales
	Sturt Tillite	diamictites, quartzites and slates
BURRA GROUP	Belair Subgroup	siltstones and quartzites
	Saddleworth	dolomitic siltstones
	Stonyfell Quartzite	feldspathic quartzites
	Woolshed Flat Shale	siltstones and phyllites
	Montacute Dolomite	dolomites
	Castambul Formation	dolomitic phyllites
	Aldgate Sandstone	sandstone
MAJOR HIATUS		
BASEMENT: BAROSSA COMPLEX		

Table 1.1: Stratigraphy of the metasedimentary sequence in the southern Adelaide Geosyncline (sources: Abele and McGowran, 1959; Daily and Milnes, 1972a; Mancktelow, 1979; Preiss, 1987).

1.2 Detailed geology

The stratigraphy, structure, metamorphism, igneous intrusion and mineralization within the Kanmantoo Group and relevant adjacent areas are summarized in this section. Most of the information presented in this section is taken from Mancktelow (1979).

1.2.1 Stratigraphy and lithology

All the lithologies described in this section have been metamorphosed to varying degrees. Pre-metamorphic lithologic terms such as sandstones, siltstones, ..., are used here to describe the facies variants and environments of deposition. The stratigraphy and lithology of the Adelaide Supergroup, Normanville Group and Kanmantoo Group are tabulated in Table 1.1.

Metamorphic basement, overlain unconformably by the Burra Group, occurs as five inliers in anticlinal cores in the Mt. Lofty Ranges (Figure 1.3). Western margins of these inliers are commonly faulted (Anderson, 1975), whereas the unconformity is usually preserved on the eastern flanks. The basement rocks, known as the Barossa Complex, are entirely high grade metamorphic rocks, but all have been affected by Delamerian, and possibly pre-Adelaidean, retrograde metamorphism and shearing (Preiss, 1987). The present lithologies include sericite and mica schists, sillimanite and biotite-rich gneisses and various others.

Thomson (1969b) divided the Adelaide Supergroup into four main lithostratigraphic units: the Callana Group, the Burra Group, the Umberatana Group and the Wilpena Group. The Callana Group is not seen in the sequence in the southern Adelaide Geosyncline. The Burra Group unconformably overlies the basement inliers. The Aldgate Sandstone, a sandstone-conglomerate unit which contains heavy minerals concentrated from the basement, is the basal unit. The Burra Group increases in argillite-carbonate units going upwards in sequence. The base of the Umberatana Group is characterized by massive tillite, arkose and quartzite. These are overlain by a thick pile of laminated siltstone and shale with some stromatolitic carbonate which are in turn overlain by a marine glacial sequence and non-marine red sandstone and siltstone.

The Wilpena Group contains a sequence of shale, siltstone, limestone and quartzite. The basal part of the Wilpena Group which consists of the Nuccaleena Formation, Brachina Formation and the ABC Range Quartzite was named the Brachina Subgroup by Plummer (1978). The sequence shown in Table 1.1 is adapted from Preiss (1987) and the term Brachina Subgroup is avoided except when making a reference to previous work. The Ulupa Siltstone occurs near the base of the Wilpena Group and is overlain by the ABC Range Quartzite and the Bunyeroo Formation. Since the Ulupa Siltstone is the most magnetic unit below the Kanmantoo Group, its lithology and chemistry merit attention.

The chemistry of the well laminated green-grey siltstones which make up the Ulupa Siltstone is distinctive, with a characteristic enrichment in TiO_2. The silts are generally aluminous, producing considerable modal chlorite at low grades, and strikingly porphyroblastic andalusite-garnet-staurolite schists at moderate grades. In places, these meta-silts are overlain by massive grey silts and fine grey sandstones, with lesser poorly laminated silts, calc-silicates and rare marble. Occasional grey sandstones which occur above the Ulupa Siltstone are very similar to Kanmantoo Group sandstones (Horwitz *et al.*, 1959).

The base of the Cambrian in South Australia is believed to be the erosional disconformity which separates the quartzites of the Wilpena Group from the base of the Cambrian Normanville

Figure 1.2: Geological map of the Mt. Lofty Ranges showing major structures (after Mancktelow, 1979).

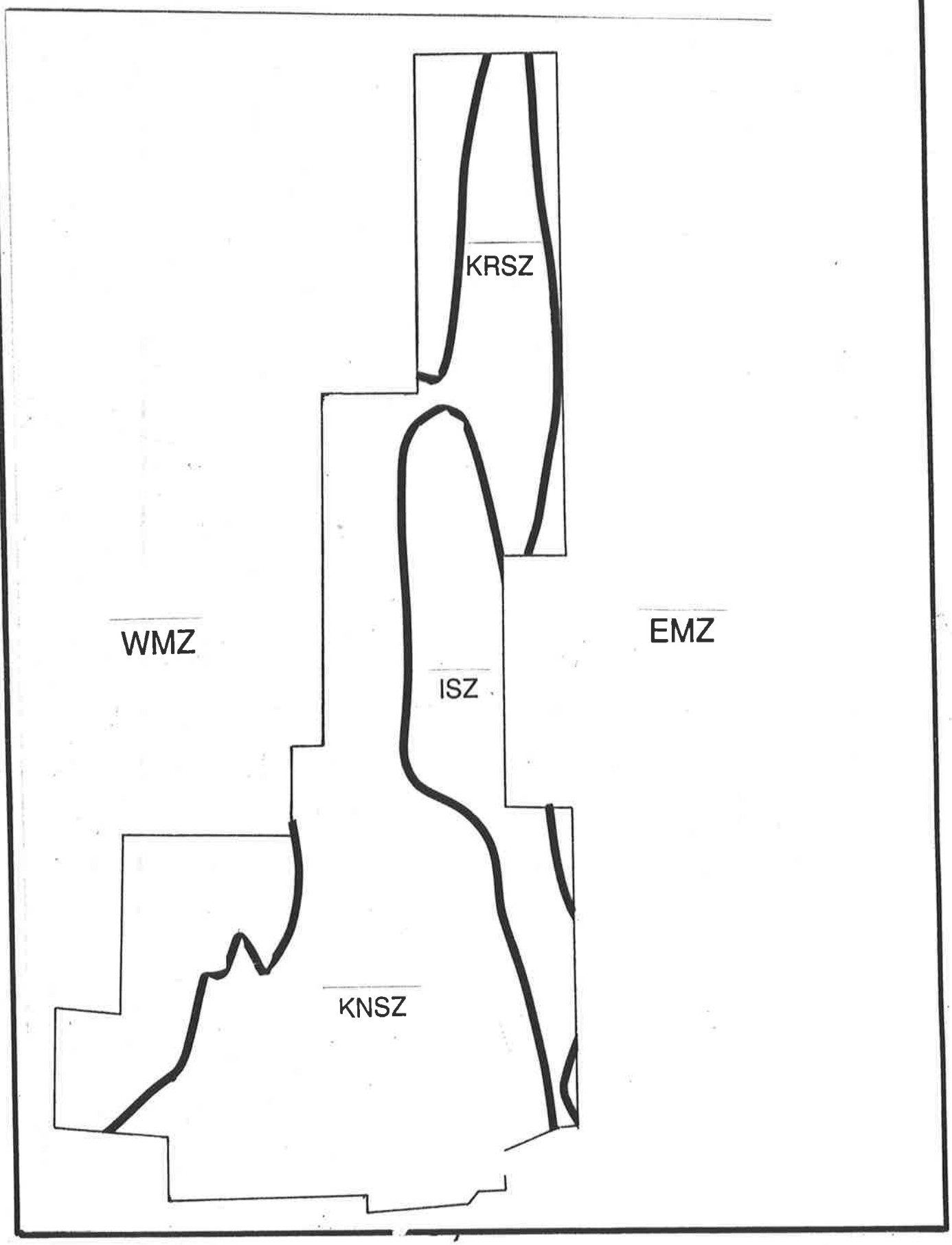
KRSZ
WMZ
EMZ
ISZ
KNSZ

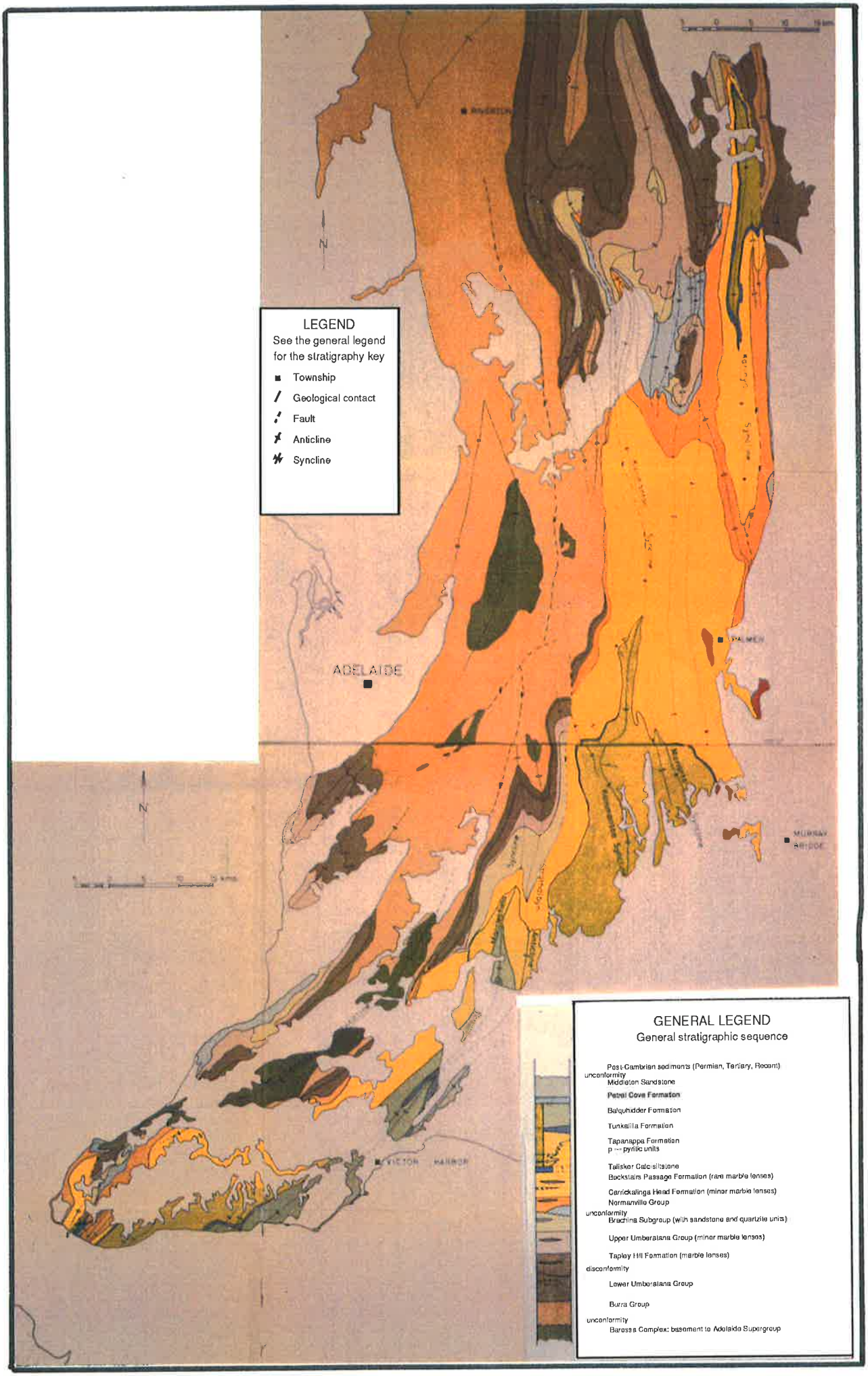
LEGEND
See the general legend for the stratigraphy key
Township
Geological contact
Fault
Anticline
Syncline
ADELAIDE
N
GENERAL LEGEND
General stratigraphic sequence
Post-Cambrian sediments (Permian, Tertiary, Recent)
unconformity
Middleton Sandstone
Petrel Cove Formation
Balquhidder Formation
Tunkalilla Formation
Tapanappa Formation
p — pyritic units
Talisker Calc-siltstone
Backstairs Passage Formation (rare marble lenses)
Carrickalinga Head Formation (minor marble lenses)
Normanville Group
unconformity
Brachina Subgroup (with sandstone and quartzite units)
Upper Umberatana Group (minor marble lenses)
Tapley Hill Formation (marble lenses)
disconformity
Lower Umberatana Group
Burra Group
unconformity
Barossa Complex: basement to Adelaide Supergroup

Group in the Sellick Hill area (Thomson and Horwitz, 1961). Carbonate and phosphate-rich rocks characterize the Normanville Group. The only volcanics found in the southern Adelaide Geosyncline are the Truro Volcanics (Forbes *et al.*, 1972). These are amygdaloidal basalts and trachytes interbedded with the Heatherdale Shale. The Normanville Group is restricted in outcrop. Where Kanmantoo Group sediments are in direct contact with Adelaide Supergroup sediments, the contact often appears concordant. Mancktelow (1979) suggested that Normanville Group deposition was geographically restricted.

Belperio (1985) has equated the quartzite units formerly known as the Macclesfield Quartzite and Mt. Barker Quartzite with the ABC Range Quartzite. This places these units in the Wilpena Group. However, their stratigraphic position are uncertain (Preiss, pers. comm.) and the terms "quartzite at Macclesfield" and "quartzite at Mt. Barker" are used here instead. Similarly, instead of using the terms Macclesfield Marble and Paris Creek Marble, the term "marble at Paris Creek" is used.

The Kanmantoo Group

While the first definition of the Kanmantoo Group was given by Sprigg and Campana (1953), the nomenclature used to describe the sequence in this thesis (Table 1.2) is taken from Daily and Milnes (1972a). The type section of the Kanmantoo Group is along the south coast between Tunkalilla Beach and Rosetta Head (Sprigg and Campana, 1953). In the new classification, the Carrickalinga Head Formation represents the basal unit of the Kanmantoo Group and the Middleton Sandstone the uppermost known unit. All contacts between Kanmantoo Group units are conformable. The younger units are seen mainly on the south coast and on Kangaroo Island and the oldest unit, the Carrickalinga Head Formation, crops out on the south coast and in the Karinya Syncline (Figure 1.2). The lithologies and interpreted environment of deposition are listed in Table 1.2. Much of the Kanmantoo Group outcrop in the main study area is dominated by rocks of the Backstairs Passage Formation, Talisker Calc-siltstone and Tapanappa Formation.

The Carrickalinga Head Formation has been subdivided by Daily and Milnes (1972a) into three members: the Madigan Inlet Member, the Blowhole Creek Siltstone and the Campana Creek Member. In the type section, Madigan Inlet Member forms the bulk of Carrickalinga Head Formation. Blowhole Creek Siltstone and Campana Creek Member represent a transition into the overlying Backstairs Passage Formation. The siltstones of these two members are similar, and are generally weakly to well laminated: the laminae are due to thin graded beds. The proportion of light coloured, feldspathic sandy beds increases towards the top of the Campana Creek Member. Argillaceous and pure limestone occurs within the Blowhole Creek Siltstone (the Milendella Limestone Member: Cooper, 1988), indicating a period of limited clastic sediment supply during Blowhole Creek Siltstone deposition (Gatehouse *et al.*, in press). Along the fold belt, the Carrickalinga Head Formation is of greatly varying thickness. Relative to the south coast, the formation is quite thin north of Truro, though in the Sedan Hill section (road cutting on the road between Sedan and Keyneton), it is much thicker than in the type section (Gatehouse *et al.*, in press).

While the base of the Backstairs Passage Formation is relatively sharp on the south coast, elsewhere it is gradational reflecting the similarities between the lithologies of the upper Carrickalinga Head Formation and the Backstairs Passage Formation. The sandstone facies of the Tapanappa Formation is also similar to that of the Backstairs Passage Formation. Toteff (1977) differentiated the Backstairs Passage Formation into the basal, middle and upper members. However this differentiation has only been applied in restricted areas (e.g. Lawrence, 1980). The basal member is more pelitic; well laminated meta-arkoses and feldspathic meta-sandstones typical of the Backstairs Passage Formation constitute the middle member; and more micaceous

Formation name	Lithologies	Environment of deposition
Middleton Sandstone	fine-grained, light grey arkosic sandstones	shallow marine
Petrel Cove	well laminated meta-siltstones, meta-siltstones, lesser grey phyllites and fine to medium-grained greywackes	deep marine, well below wave base, more distal, lower middle fan to outer fan environment
Balquhidder	coarser grained greywackes, thin interbeds of grey siltstone, grey phyllites and pyritic, carbonaceous phyllites	
Tunkalilla	meta-siltstones, medium-grained greywackes and pyritic, carbonaceous phyllites	submarine fan environment
Tapanappa	Facies variants: 1) medium-grained greywackes, siltstones and siltstones rich in iron sulphides 2) light coloured arkoses and quartz-rich sandstones	
Talisker Calc-siltstone	Facies variants: 1)calcareous siltstones and occasional arkoses 2)aluminous siltstone facies: 3)siltstones with pyrite, pyrrhotite 4)black, carbonaceous, laminated shale	deep water
Backstairs Passage	light coloured, well laminated arkoses and occasional medium-grained greywackes	at or near change in slope in a shallow environment
Carrickalinga Head CAMPANA CREEK MEMBER BLOWHOLE CREEK SILTSTONE MADIGAN INLET MEMBER	 light coloured feldspathic sandstones siltstones and limestones massive, medium-grained, grey feldspathic greywacke with lesser, massive grey siltstone and phyllite	 closer to break in slope below wave base but more distal below wave base, submarine fan

Table 1.2: Kanmantoo Group lithologies and environment of deposition (sources: Skinner, 1958; Mancktelow, 1979; Boord, 1985; Gatehouse *et al.*, in press).

sandstones form the upper member. Greywacke units become more common towards the top of the formation. Channeling is observed at the base of some arkose units. Medium-grained, greywacke units occur occasionally, and rare white quartzites, calc-silicates, and marbles have been found (e.g. Tungkillo Marble Member). In contrast to the overlying formations, no iron-rich siltstone or phyllite units have been found in the Backstairs Passage Formation or in the Carrickalinga Head Formation.

The Talisker Calc-siltstone conformably overlies the Backstairs Passage Formation and in some localities also intertongues with it. The formation changes lithology along strike and has at least four facies variants: calc-siltstone, aluminous siltstone, Nairne pyrite, and black shale facies. It is the best marker horizon in the Kanmantoo Group as its main facies variants, excluding the aluminous siltstone facies, are distinctive and quite different from the underlying and overlying greywackes and sandstones of the Tapanappa and Backstairs Passage Formation.

The pyrite bands originally known as the Nairne Pyrite Member (Thomson, 1969b) were re-defined by Mancktelow (1979) as the Nairne pyrite facies of the Talisker Calc-siltstone. Similarly the black shale known as the Karinya Shale (Thomson, *op. cit.*) is considered by Mancktelow (*op. cit.*) to be the black shale facies of the Talisker Calc-siltstone.

Iron sulphide bands first begin to appear in the Talisker Calc-siltstone. At Brukunga, the Nairne pyrite facies has been mined for its pyrite content. The Talisker Calc-siltstone is also host to *Ag-Pb* mineralization at Talisker, where the calc-siltstone facies crops out.

Greywackes and sandstones comprise the two facies variants of the Tapanappa Formation. Medium-grained greywacke is the dominant lithology of the greywacke facies: conglomerates and phyllites, and siltstones rich in iron sulphides occasionally occur. Going inland along strike, the greywacke facies is replaced by lithologies more typical of the Backstairs Passage Formation. This sandstone facies is dominated by well laminated, light coloured, arkosic and quartz-rich sandstones, the light colour being caused by the lower proportion of biotite. In regions of poor outcrop, where the sandstone facies of the Tapanappa Formation occurs, it is not always possible to determine with certainty the position or continuity of the Talisker Calc-siltstone.

The distinction between the Tapanappa, Tunkalilla and Balquhidder Formation becomes very difficult to apply in the poorly outcropping, higher grade regions north of the type section. The top and bottom of the Tunkalilla Formation are marked by thin, blue-black, pyritic, carbonaceous phyllites. The Balquhidder Formation was distinguished from the Tapanappa Formation by Daily and Milnes (1973), due to the presence of blue-black carbonaceous, pyritic phyllites within the sequence. The Petrel Cove Formation conformably overlies the Balquhidder Formation and is dominated by well laminated meta-siltstone, lesser grey phyllites, and fine to medium-grained greywacke.

The Middleton Sandstone represents the youngest outcropping member of the Kanmantoo Group. The base of the Middleton Sandstone marks a distinct change in sedimentary environment from that of the underlying formations. The exposed Middleton Sandstone is dominated by fine-grained, light grey arkosic sandstones. The sandstones are typically well laminated. It is intruded by the coarse-grained Encounter Bay Granites at Port Elliot and during igneous intrusion must have been overlain by a considerable thickness (between 5–10 km) of younger sediments (Milnes *et al.*, 1977).

The sequence of lithologies from the Carrickalinga Head Formation to the Petrel Cove Formation represents a general deepening of the basin superimposed by several upward-shallowing cycles, and a consequent increase in the distance from the ancient shoreline with time. The relative constancy of facies within the exposed Kanmantoo Group may reflect the constancy of sedimentary environment which existed parallel to the ancient coastline. The Tapanappa,

Tunkalilla, Balquhidder and Petrel Cove Formation were deposited in a submarine fan environment from turbidites flowing episodically from the distributary mouths. Pyritic and carbonaceous siltstone units represent periods of quiescence without sediment supply from turbidite flows.

These sediments are generally non-fossiliferous except for worm tracks and casts in the lower five formations, *Lingulella* in the lower Madigan Inlet Member (Daily, 1963) and *Hyolithidae* in the upper Campana Creek Member (Gatehouse *et al.*, in press).

1.2.2 Tectonics

The Adelaidean sedimentary record is quite thin in the southern Adelaide Geosyncline. In this region, compared to the northern part of the Geosyncline, subsidence may have been less pronounced during Adelaidean time but may have increased rapidly during the Cambrian. Mancktelow (1979) suggests that sudden collapse instigated deposition of the flysch facies Kanmantoo Group, while subsidence in the northern regions may have continued at a steady rate to develop shallower water, shelf facies, carbonates. According to Jenkins (in press), the final extensional phase took place in the Early Cambrian and led to the development of the Kanmantoo Trough by lithospheric stretching.

The source of the Kanmantoo Group sediments is generally believed to have been the Gawler Craton and shelf regions to the west (Daily and Milnes, 1971a, 1973; Thomson *et al.*, 1976; Gatehouse *et al.*, in press). The Glenelg River sediments in Victoria are believed to be Kanmantoo Group correlatives (Wells, 1956). Mancktelow (1979) hypothesizes that during Cambrian times, travelling eastwards into Victoria may have involved movement in a marine basin away from the terrigenous source and towards a calc-alkaline volcanic arc.

As a result of the Delamerian Orogeny, the sediments of the Kanmantoo Group have been folded into a synclinorium. The orogeny transformed the basin into an orogenic upland leading to the sudden influx of immature flysch facies sediments into Victoria. Several periods of granite intrusion accompanied the deformation events. The sigmoidal shape of the fold belt is considered by Mancktelow (1979) to be the result of flattening during the Delamerian D_1 deformation against a curved cratonic or transitional basement margin.

Structure

The structural history of the Kanmantoo Group is complex and polyphase and difficult to unravel. Earlier folds are possibly overprinted and obscured by later folding in the high metamorphic grade areas. Later folds have had little effect on a macroscopic scale on the less highly metamorphosed rocks. Going from the low grade to the higher metamorphic grade rocks, the effect and importance of the different folding events is apparently different. Previous workers have disagreed on the relative importance and the number of folding events which have affected the southern Adelaide Geosyncline. Offler and Fleming (1968) proposed the first regional synthesis of the structural history of the area. Fleming and White (1984) made slight revisions to this model after Mancktelow (1979) gave an alternative and quite different interpretation.

Common to the different structural models proposed is that at least one major deformation event occurred causing the development of macroscopic folds. Subsequent to the development of the macroscopic folds was the development of folds on smaller scales. The net result of the

Delamerian Orogeny was the creation of the Kanmantoo Synclinorium which includes the Macclesfield Syncline-Strathalbyn Anticline pair, the Kanmantoo Syncline, the Monarto Syncline and the Karinya Syncline (see Figure 1.2).

The major differences between interpretations given by Mancktelow (1979), Offler and Fleming (1968), and Fleming and White (1984), is that Mancktelow (*op. cit.*) considered D_1 to be the dominant fold event throughout the region and the cause of the macroscopic folds mentioned above. Offler and Fleming (1968) considered that many of the more obvious macroscopic structures in the eastern Mt. Lofty Ranges were post-D_1 structures. Fleming and White (*op. cit.*) and Offler and Fleming (*op. cit.*) consider F_2 and F_3 to have caused the macroscopic folds, with F_2 being the major fold event. They recognized early, mesoscopic folds which had been refolded. Allen (1977) and Hoesni (1985) have also reported mesoscopic folds which they consider to have formed prior to the event described by Mancktelow (1979) as F_1 and which may therefore correspond to the D_1 deformation described by Offler and Fleming (1968).

Mancktelow (1979) believed most macroscopic folds were F_1 and that the first deformation, D_1 was the major deformation event. The F_1 macroscopic folds generally have large wavelengths on the scale of tens of kilometres. Their axial planes form an arc, swinging in strike from NS east of Adelaide to EW on Kangaroo Island in the south. Along the length of this arc, the orientation and style of F_1 folds consistently changes in transverse sections across the belt. Towards the western or northern side, the folds are more asymmetric, with axial planes dipping more shallowly east (Offler and Fleming, 1968; Daily and Milnes, 1973). Individual fold hinges are less continuous than further east, and adjoining anticlines and synclines commonly coalesce and annihilate each other. Moving south from Adelaide along the fold belt, each successive culminating anticline dies out as another forms thus producing an *en échelon* pattern of elongate domal anticlines migrating southeast. The oldest rocks, the basement inliers, outcrop in these domal culminations.

The corresponding synclinal structure may also migrate towards the SE forming an *en échelon* pattern. North of a line from Adelaide to Palmer, the direction of migration of the major syncline is reversed. Going northwards, the synclinal structure moves eastward with the Karinya Syncline eventually supplanting the Kanmantoo Syncline as the major structure controlling the outcrop of the Kanmantoo Group. Overprinting by D_2 is most common in the higher grade metamorphic zones. Mancktelow (1979) found that the D_2 deformation does not refold F_1 folds on a macroscopic scale as D_1 and D_2 are nearly coaxial.

There have been several periods of faulting. Faulting associated with D_1 is not uncommon, particularly on the steep to overturned limbs of F_1 folds (e.g. Talisker Fault and Alex Lookout Fault). While Mancktelow (1979) maintains that the Nairne Fault is a major structure which cross-cuts and offsets a D_2 fold and must be younger than this event, Toteff (1977; in press) considers it to be the contact between the Kanmantoo Group and the Adelaide Supergroup which has been reactivated during subsequent deformations. The Nairne Fault is likely to be a composite feature: possibly an early thrust in the Macclesfield area and a later fault in the Mt. Torrens-Birdwood-Pewsey Vale area where it cuts D_2 folds (Preiss, pers. comm.).

The present Mt. Lofty Ranges are a rejuvenated Caenozoic topographic feature which was uplifted relative to adjacent basinal areas along steeply dipping, northeast trending, reverse faults (Thomson, 1969a; Stuart and von Sanden, 1972). These faults are important in limiting the outcrop of Kanmantoo Group rocks to both the east and west, but in cross section the vertical offsets are generally small.

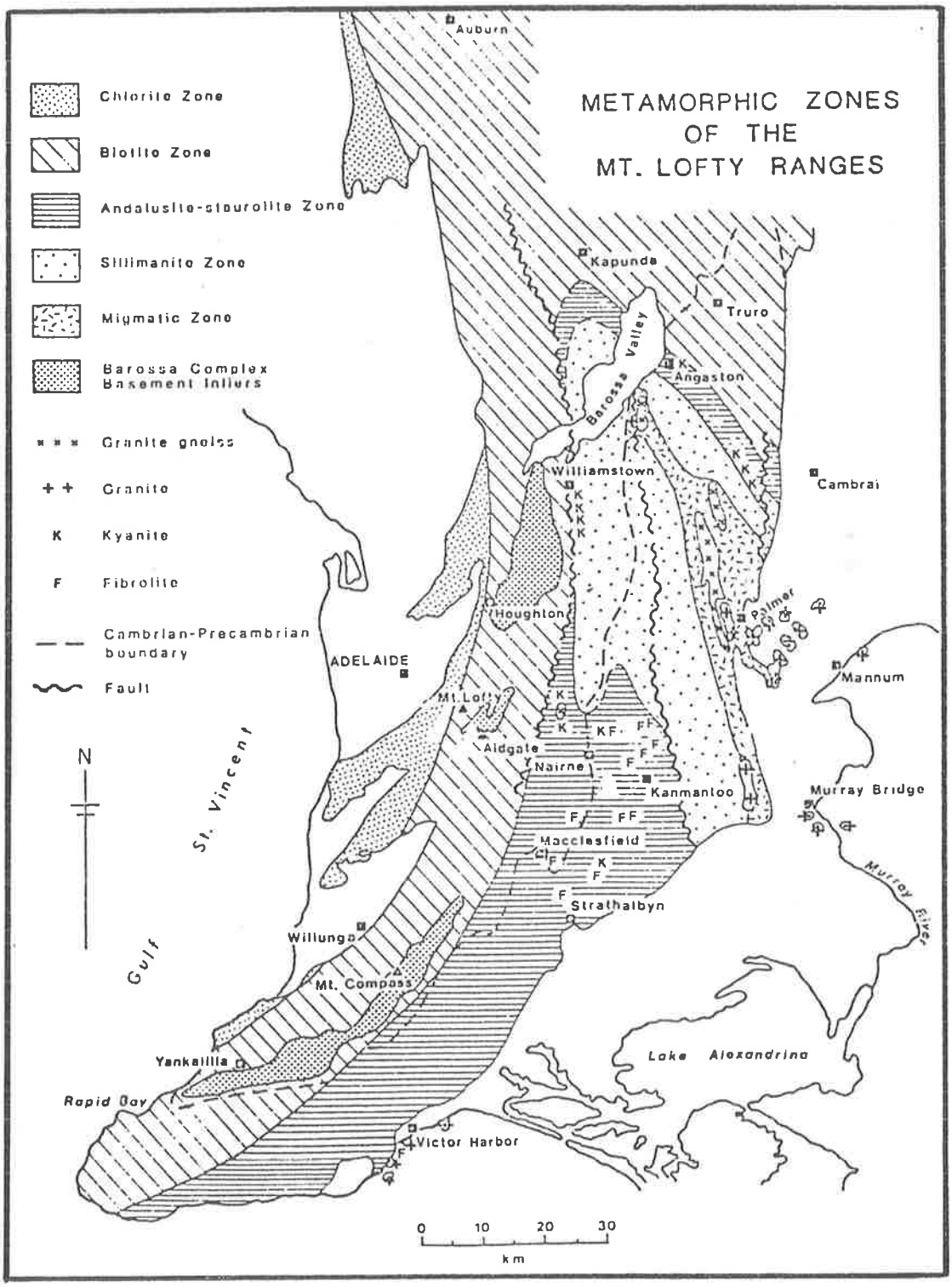

Figure 1.3: Boundaries of metamorphic zones within the southern Adelaide Geosyncline (after Offler and Fleming, 1968). Also shown are the basement inliers.

1.2.3 Metamorphism

Kanmantoo Group sediments have been extensively metamorphosed. The highest grade zone is believed to be the migmatite zone which extends from Murray Bridge to beyond Springton, and trends NNW. North and south of this zone the grade drops away. Mancktelow (1979) identified five metamorphic zones: biotite-muscovite-chlorite, andalusite (kyanite)-staurolite, fibrolite, sillimanite and migmatite. The mapped limits of the migmatite zone are contained completely within the Kanmantoo Group. The boundaries of the different zones are shown in Figure 1.3.

There is a gradual and consistent increase in grain size of the metasediments from the biotite-chlorite-muscovite zone, through the intermediate zones, and into the quite coarse-grained metasediments of the migmatite zone. This suggests that the migmatite zone may be the zone of highest metamorphic grade in the region.

Mancktelow (1979) inferred that the pressure during metamorphism was close to the aluminosilicate triple point because all three Al_2SiO_5 polymorphs occur as intergrown coarse crystals throughout most of the sillimanite zone. The maximum temperature reached by the metasediments in the study area was around 640°–650° C, just below the temperature of first melt formation.

Sandiford *et al.* (in press) use a cordierite-staurolite-muscovite bearing quartz schist from the Kanmantoo Group east of Springton to demonstrate that prograde reactions occurred late in the deformation history, that temperatures reached were between 530°C and 680°C, and pressures between 3–5 kbars. This equates to a depth of burial of the order of 15 km. They conclude that the P-T conditions reflect a severely perturbed thermal regime well in excess of that expected for the conductive heating of tectonically thickened crust and that the additional heat of metamorphism may have been introduced by syn-tectonic magmas.

The timing of the metamorphic events is debatable. Fleming and White (1984) conclude that partial melting began and migmatites were formed in some rocks of the Kanmantoo Group near Palmer before penetrative deformation affected them. They took this to indicate that there existed a significant degree of thermal activity before the effects of the first deformation were imprinted. Fleming and Offler (1968) and Fleming (1971) also found that metamorphism reached at least andalusite-staurolite grade in the Angaston-Kapunda area and in the Dawesley-Kanmantoo area before the effects of F_1 folding were imprinted. Mancktelow (1979) differs from the above researchers and suggests that peak temperatures probably coincided with F_2, and that there was no metamorphism of Kanmantoo Group rocks before the onset of the Delamerian Orogeny.

1.2.4 Igneous intrusives

In the southern Mt. Lofty Ranges, most intrusive igneous rocks are restricted to the Kanmantoo Group. Granitoid intrusions are common in parts of the sillimanite and migmatite zones. Many of these form small stocks less than a few hundreds of metres across (e.g. Mills, 1964; Abbas, 1975), but there are several larger bodies. The Palmer and Monarto Granite are within the main study area, while the granitoids at Murray Bridge, Long Ridge/Sedan, Mannum and Reedy Creek lie to the east of the area. The Encounter Bay Granites are south of the study area. Basic dykes and sills, amphibolites and dolerites outcrop near Cooke Hill, Springton and Woodside. Numerous pegmatite and amphibolite dykes can be found in the migmatite and sillimanite zones. The Black Hill Norite crops out at Black Hill near Mannum. Black Hill

Norite equivalents have been interpreted under cover in the Murray Basin, and other gabbros and basalts have been intersected in drill holes into the western margin of the Murray Basin (Sections 5.2.1 and 6.2.2). The location of the granitoids and norites are shown in Figures 6.1 and 6.2.

Foden *et al.* (in press) have grouped the various intrusives which intrude the Cambrian metasediments into pre-tectonic, syn-tectonic and post-tectonic groups. Partly syn-sedimentary, pre-tectonic intrusion was dominantly mafic and included the deformed amphibolites which outcrop near Cooke Hill, Monarto and Tungkillo. Liu and Fleming (1989) in their study of the amphibolites in the Mt. Lofty Ranges have recorded three generations of amphibolites. Most are small bodies with maximum dimensions reaching one or two kilometres.

Syn-deformation intrusion was characterized by I-type granite intrusives: Reedy Creek Granodiorite, Palmer Granite, Rathjen Gneiss, Encounter Bay Granite and Monarto Granite among others. Post-tectonic intrusion may be associated with an extensional phase during which the Black Hill Norite and mainly A-type granites intruded sediments in what is now covered by Murray Basin sediments.

Geochronological ages determined for the granites are listed below.

1. Palmer Granite: White *et al.* (1967) — 496 ± 31 Ma
2. Encounter Bay Granite: Milnes *et al.* (1977) — 495 ± 6 Ma
3. Granites on Kangaroo Island: Webb (1976) — 470 ± 11 Ma
4. Rathjen Gneiss: Milnes *et al.* (1977) — 526 ± 25 Ma

1.2.5 Mineralization

Base metal mineralization is widely distributed along the length of the Kanmantoo Group, but is generally confined to the Carrickalinga Head Formation, Talisker Calc-siltstone and Tapanappa Formation. The mineralization is of five types: copper deposits, gold deposits, lead-zinc deposits, pyrite-pyrrhotite deposits and silver-lead deposits. The references on which this section are based are as follows: Brown (1908), Seccombe *et al.* (1985), Morris (1988), Spry *et al.* (1988) and Both (in press).

1. Copper deposits are discordant and pipelike and contain chalcopyrite, pyrrhotite, magnetite and pyrite as the major opaque minerals. They occur typically as veins or vein networks within the Carrickalinga Head and Tapanappa Formation. These include the Kanmantoo, Bremer and Royal Keyneton mines.
2. Gold deposits are restricted geographically though not stratigraphically or lithologically. Gold is almost invariably the only economic metal present and is almost always associated with specularite. The gold mineralization probably postdates the Delamerian Orogeny and metamorphism.
3. Lead-zinc deposits in the Tapanappa Formation are apparently concordant and contain pyrrhotite. Magnetite is found associated with the ore at Strathalbyn, but not at Aclare and Wheal Ellen.

The Mt. Torrens lead-zinc prospect is the only example of lead-zinc mineralization associated with the Talisker Calc-Siltstone. The mineralization is stratabound and both pyrite and pyrrhotite are found with it.

Within the Karinya Syncline, the Milendella Limestone Member of the Carrickalinga Head Formation is host to lead-zinc mineralization at Royal Keyneton and Mt. Rhine among others. No magnetite or pyrrhotite has been reported.

4. The Nairne pyrite facies of the Talisker Calc-siltstone has been mined at Brukunga for its pyrite content. A sedimentary origin for the deposit is undisputed. Pyrite and pyrrhotite are the major sulphides.

5. At the Talisker mine, *Ag-Pb-As-Au-Zn* mineralization is found in sandstones of the Talisker Calc-siltstone. No pyrrhotite or magnetite has been reported.

Many of the mineral deposits in the region are associated with pyrrhotite ± magnetite and can therefore be detected on aeromagnetic surveys, though it is not possible to distinguish mineralized magnetic horizons from non-mineralized horizons. Around the Kanmantoo mine, Mancktelow (1979) reported a zone of potassium depletion. Analysis of the potassium aeroradiometric channel could reveal other zones of potassium depletion.

1.3 Discussion

Renewed interest in the Kanmantoo Group is indicated by recent publications (Clarke and Powell, 1989; Foden *et al.*, in press; Gatehouse *et al.*, in press; Jenkins, 1986 and in press; Sandiford *et al.*, in press; ...) and participation in the Kanmantoo Field Symposium organized by SADME (Gatehouse, 1988b). While researchers have new ideas about basin formation, tectonics and metamorphic processes, little additional geological information has been acquired. The issues listed below are central to any model proposed for the Kanmantoo Group.

1. Mode of formation: The term "Kanmantoo Trough" was proposed by Thomson (1969a) and the usage of that name has continued even though "there is no definitive evidence to suggest that either a trough or graben developed" (Gatehouse, 1988b). Steinhardt (in prep.) suggests that the Kanmantoo Group may be partly coeval with the Adelaide Supergroup and may have been deposited on the continental slope of a passive continental margin while the sediments of the Adelaide Supergroup were being deposited on the shelf.

   The depositional environments of the different units in the Kanmantoo sequence has not been resolved. Steinhardt (in prep.) assumes that the Kanmantoo Group generally represents a deep water sequence and suggests that the sequence was deposited on a continental slope. However, not all researchers agree that the environment was dominantly deep water. The Backstairs Passage Formation, Middleton Sandstone, (Mancktelow, 1979; Boord, 1985), and the Madigan Inlet Member of the Carrickalinga Head Formation in the Sedan Hill section (Gatehouse *et al.*, in press) have been interpreted to be shallow marine.

2. Extent and location of original basin: The present limits have been set by the Delamerian Orogeny. To the west, Cambrian sediments on Yorke Peninsula and relatively undeformed Precambrian and Cambrian sediments in Gulf St. Vincent (Stuart and von Sanden, 1972) constrain the maximum western limit. The Glenelg River beds in Victoria are considered by Wells (1956) to be Kanmantoo Group correlatives.

Reference	Area	Formation	Palaeocurrent source
Mills (1964)	southern Karinya Syncline	basal Kanmantoo Group	west
Flint (1978)	West Bay, Kangaroo Island	possible Kanmantoo Group equivalents	west
Boord (1985)	Parson's beach, southern Fleurieu Peninsula	Balquhidder Petrel Cove Middleton Sandstone	northwest northwest west

Table 1.3: Palaeocurrent directions determined on Kanmantoo Group rocks.

3. Nature of contact with underlying rocks: In the type section, the Kanmantoo Group conformably overlies the Normanville Group (Daily and Milnes, 1971a). Where Kanmantoo Group rocks overlie Adelaide Supergroup rocks, the nature of the contact is apparently variable, and in any case, controversial. While Horwitz *et al.* (1959), Thomson (1969a, 1975) and Mancktelow (1979) considered the Kanmantoo Group to be transgressive over Adelaidean rocks, Daily and Milnes (1971a) and Toteff (1977) have argued that over much of the length of the fold belt, the contact is a fault and that the Nairne Fault probably represents the reactivated contact.

   Toteff (1977; in press) maintains that in the Birdwood-Brukunga region, the contact is a fault as basal Kanmantoo Group units strike into the underlying Adelaide Supergroup. His evidence for a fault rests on detailed mapping of the Cambrian Kanmantoo Group and its relationship to the contact. Horwitz *et al.* (1959) originally proposed a conformable succession from the Adelaide Supergroup, through "basal Cambrian" to Kanmantoo Group strata in the area between Ashbourne and Murdock Hill. Much of Toteff's (1977; in press) argument for a faulted contact depends on the redefinition of this "basal Cambrian" succession. Toteff (1977) considers that part of the Wilpena Group, the Carrickalinga Head Formation and the basal units of the Backstairs Passage Formation have been wrongly mapped by Horwitz *et al.* (1959) as "basal Cambrian".

4. Basement to the Kanmantoo Group: Though Cambrian Normanville Group, Precambrian Adelaide Supergroup and Barossa Complex rocks are found on the western and northern boundaries of the exposed Kanmantoo Group, whether these rocks continue under the Kanmantoo Synclinorium is debatable. No volcanics have been found in the Kanmantoo Group sequence. Gatehouse and Jago (pers. comm.) have commenced the study of Truro Volcanics equivalents in the Red Creek section (Karinya Syncline). The contact between the Heatherdale Shale and the Carrickalinga Head Formation appears transitional. Examination of the section is in its early stages but it is possible that these volcanics extend into the basal few metres of the Carrickalinga Head Formation (Gatehouse, pers. comm.).

   The interpretation of limited gravity and seismic data available is not consistent with the presence of oceanic crust (Greenhalgh *et al.*, 1989; Greenhalgh *et al.*, in press)

5. Thickness of sedimentary pile: The original thickness may have been as much as 50 km (Thomson, 1969a) or even as much as 20 km (Mancktelow, 1979). Even if repeated thrusting has increased the thickness (Jenkins, in press), the Kanmantoo Group still represents a great thickness of sediments though it may not be as much as 15 km. Thickness estimates have been mainly based on sections along the south coast where folds and thrusts might not have been recognized.

6. Source of sediments: The generally accepted theory (Daily *et al.*, 1976; Thomson *et al.*, 1976; Mancktelow, 1979; Moore, 1983; Gatehouse *et al.*, in press) has been that the source of sediments in the Kanmantoo Group sequence was the Gawler Craton which was being uplifted while the Adelaide Geosyncline was subsiding. Palaeocurrent directions determined by previous researchers are presented in Table 1.3.

Chapter 2

Rock magnetism and radioactivity

Assessing the geological significance of geophysical anomalies is, or should be, the main aim in the interpretation of geophysical data. This can be achieved by understanding the geological processes and conditions which influence rock magnetism and radioactivity; and by measuring magnetic properties and determining magnetic mineral assemblages in rocks so as to reduce the ambiguity inherent in magnetic interpretation.

The physical properties which determine the magnetism of a rock unit are its susceptibility κ, remanent intensity J and Koenigsberger ratio Q. These properties are controlled by the abundance, composition and form of magnetic mineral grains. The net magnetic response of a rock unit varies with the geological processes which affect the petrogenesis of magnetic minerals.

The radiometric response of rocks is controlled by the amount of potassium, uranium and thorium they contain. The abundance of radioactive elements is directly related to the lithology and geological history.

The following sections summarize the various factors controlling the variation of magnetic and radioactive minerals in different rock types, the rock property measurements made, and the conclusions derived.

2.1 Magnetic minerals and their properties

Magnetic anomalies are caused by the bulk magnetization of rocks which may be separated into two components: magnetization induced by the earth's field (this is κH, the product of magnetic susceptibility and the magnetizing force of the Earth's field, H) and the natural remanent magnetization (NRM) of intensity J. The resultant magnetization is the vector sum of these components. The Koenigsberger ratio, Q, defined to be the ratio of the remanent component to the induced component ($J/\kappa H$), indicates the contribution made by each component to the magnetic anomaly.

The magnetic minerals are generally minor constituents of rocks. For the purposes of magnetic interpretation, the most important magnetic minerals are the titanomagnetites, given by $Fe_{3-x}Ti_xO_4$ where $(0 \leq x \leq 1)$. Other magnetic minerals include the titanohaematites, αFe_2O_3, and the pyrrhotites, $Fe_{1-x}S$, $(0 \leq x \leq .13)$. The magnetic properties of these minerals depends mainly on their chemical composition and domain structure. Many of the magnetic

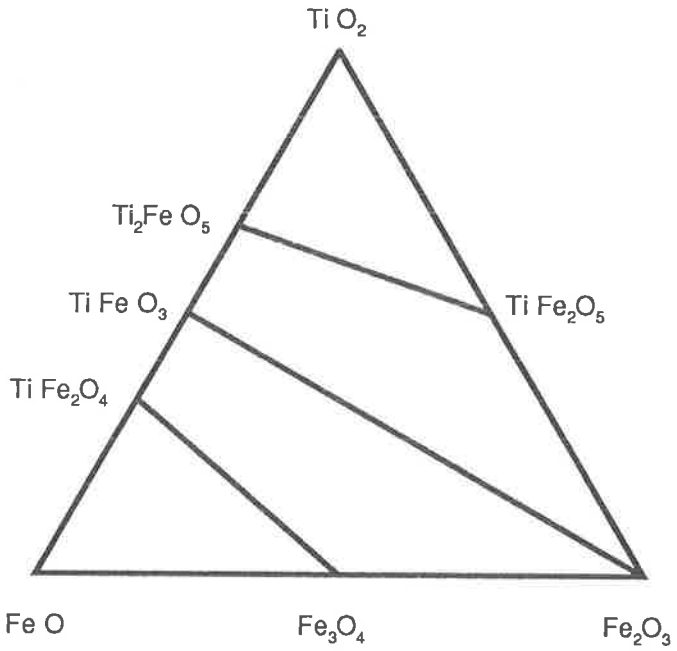

Figure 2.1: The FeO-TiO_2-Fe_2O_3 ternary diagram of rock magnetism (after O'Reilly, 1984).

Mineral	SPM threshold size (μm)	Critical SD size (μm)
Iron	< 0.008	0.023
Magnetite	0.03	0.06
Maghaematite	0.02	0.06
Titanomagnetite ($x = 0.6$)	0.08	0.40
Titanomaghaematite ($x = 0.6, z = 0.4$)*	0.05	0.75
Titanomaghaematite ($x = 0.6, z = 0.7$)*	0.09	2.40
Haematite	0.03	15.0
Pyrrhotite	**0.018	1.60

Table 2.1: Domain structure transition sizes (after Clark, 1983). Equidimensional particles assumed. Critical sizes cited are at 20° C.
* Titanomaghaematite $Fe_{(3-x)R}Ti_{xR}V_{3-R}O_4$, $R = 8/[8 + z(1 + x)]$; V = cation lattice site vacancy, $z = (Fe^{2+}\text{oxidised})/\text{original}\,Fe^{2+})$.
** Calculated from relaxation time equation assuming magnetocrystalline anisotropy constant $K_1 = 3 \times 10^5 \text{erg/cm}^3$ for pyrrhotite.

oxides may be represented, at least approximately, on the FeO-TiO_2-Fe_2O_3 ternary diagram (O'Reilly, 1984) shown in Figure 2.1.

Magnetic properties are critically dependent on domain structure (see Table 2.1). With increasing size, grains of magnetic minerals may be considered to be superparamagnetic (SPM), single domain (SD), pseudo-single domain (PSD) and multidomain (MD). SPM grains possess very high susceptibility and zero remanence and a small fraction can disproportionately affect the magnetic properties of the rock. SD grains have much lower susceptibility but can have relatively intense remanence. The intrinsic susceptibility of MD grains is generally greater than that of SD grains, and for highly magnetic minerals is limited by self-demagnetization to ≈ 0.25 cgs units. PSD grains are small MD grains (≈ 0.1–15μ m) and can retain relatively intense, hard and stable remanence (Clark, 1983).

The susceptibility of the titanomagnetites varies considerably depending on titanium content. Compositions which contain more than 75% ulvospinel are paramagnetic at room temperature and therefore exhibit very low susceptibility. Below this composition the susceptibility is relatively insensitive to titanium content and the observed emu susceptibility of MD magnetite grains is about 0.25 and that of SD grains between 0.1 and 1.1.

Fine grained haematite has a low susceptibility but is capable of carrying a substantial remanence. With increasing grain size ($> 100\mu$ m), the susceptibility and intensity of remanence increase. While pure ilmenite is paramagnetic at room temperature, intermediate composition titanohaematites ($Fe_{2-x}Ti_xO_3$) with x in the range ≈ 0.5 to ≈ 0.8 are ferrimagnetic at room temperature and have high susceptibility and remanence. Of the sulphide minerals, monoclinic pyrrhotite is ferrimagnetic at room temperature.

The NRM of rocks is often complex with several components present. The most important carriers of NRM are the magnetites (particularly fine-grained magnetite and magnetite contaminated by ulvospinel or ilmenite), the titanohaematites of intermediate composition and monoclinic pyrrhotite. Dominantly ilmenitic titanohaematites and monoclinic pyrrhotite often exhibit "self reversal". The magnetic properties of the common magnetic minerals are summarized in Table 2.2 (Clark, 1983).

2.2 Magnetic mineral petrogenesis

The main rock types in the study area are metasediments and granitic rocks. Magnetic minerals in the metasediments may be primary (pre-metamorphic) or secondary (the product of metamorphism). The form and amount of iron in sediments controls the production of magnetic minerals during metamorphism. This section deals with iron minerals in sediments, and the petrogenesis of magnetic minerals in metasediments and granitic rocks.

The oxide minerals are of great value in deducing the conditions of metamorphism for they simultaneously record information about the ambient temperature and the chemical potential of oxygen (μ_{O_2}) during metamorphism (Rumble, 1976). Their importance is out of proportion to their relatively low abundance in most rocks. Magnetic interpretation benefits out of a study of oxide assemblages, and at the same time can benefit metamorphic petrology. This is because rocks with similar lithology but varying oxide assemblage can be differentiated on the basis of their varying magnetic response using a combination of magnetic maps and susceptibility measurements.

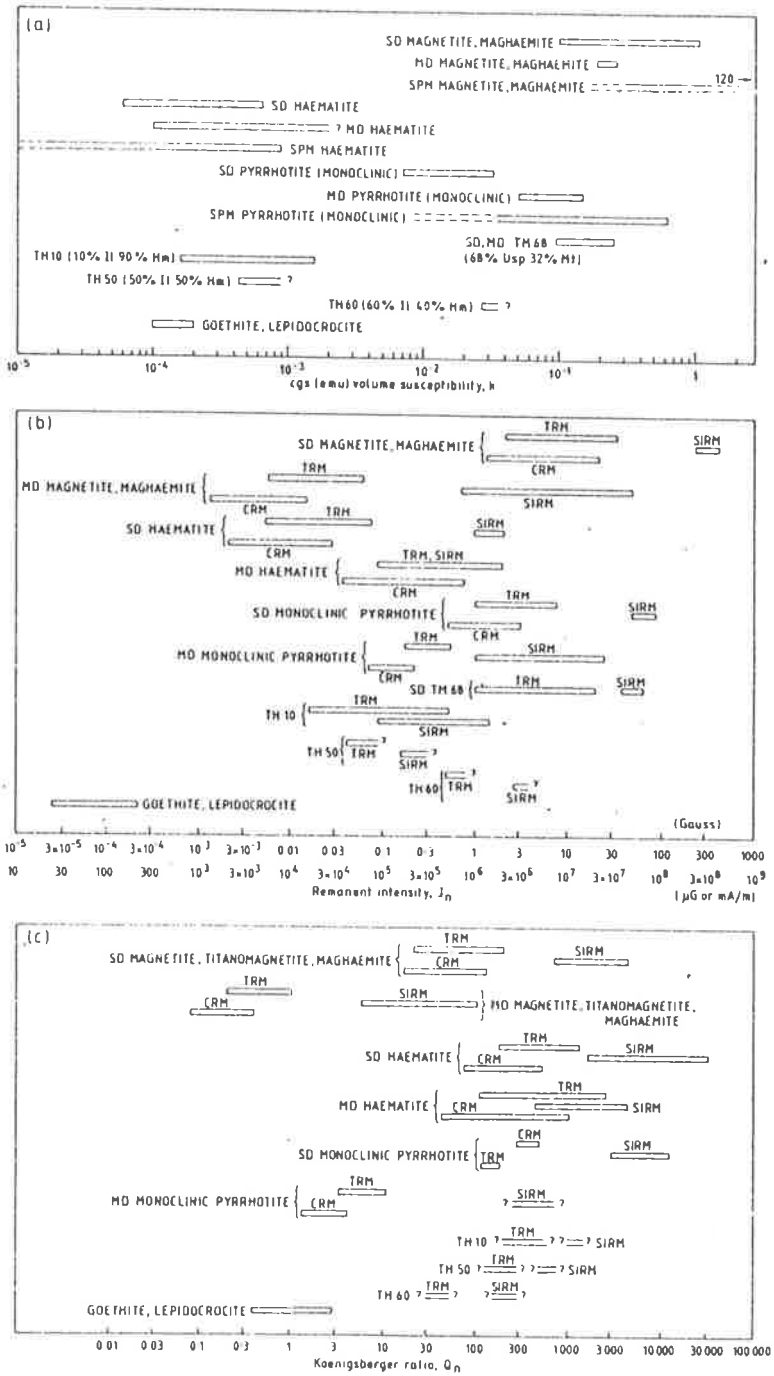

Table 2.2: Magnetic properties of common magnetic minerals (after Clark, 1983).

2.2.1 Sediments

Sediments may contain a great deal of iron, but it is commonly in the form of hydrous ferric oxides, haematite and siderite. It is unusual to find magnetite in sediments except in very minor amounts so that in general, unmetamorphosed sediments may be considered non-magnetic (Grant, 1985a and 1985b). Curtis and Spears (1968) suggest that two distinct sedimentary environments may be recognized: that of the depositional water and that of interstitial (sediment) water. In the former only ferric compounds can be truly stable. Ferrous compounds (pyrite, pyrrhotite, magnetite, siderite and chamosite) are stable beneath the sediment/water interface. The form in which iron minerals occur in sediments is listed below (sources: Carroll, 1958; Curtis and Spears, 1968; Vokes, 1969; Large, 1977; McIntyre, 1980; Willan and Hall, 1980; Grant, 1985a and 1985b).

1. Magnetite:
   (a) Heavy mineral deposits in greywackes, beach sands and placers commonly contain magnetite together with ilmenite and rutile.
   (b) During diagenesis and below the sediment-seawater interface, magnetite may be produced by the reduction of haematite or the oxidation of pyrite.
   (c) Pyrite and/or pyrrhotite and/or magnetite may be precipitated from hot, acidic, sulphide-rich solutions expelled onto the sea floor to form volcanogenic sediments.
   (d) Magnetite in Proterozoic banded iron formations may have formed by chemical precipitation from extensive seas rich in dissolved Fe^{2+} when the atmosphere and hydrosphere were poorer in free oxygen.
2. Ilmenite:
   (a) Greywackes, beach sands and river placers may contain heavy minerals including ilmenite.
3. Haematite and other oxides:
   (a) Haematite and other ferric compounds are the only iron minerals which can exist in true equilibrium with depositional waters and they can be precipitated from normal, depositional waters.
   (b) Haematite persists where there is a lack of organic material so that aerobic conditions are preserved during diagenesis. Haematite forms from diagenetic dehydration of the hydrated ferric oxides. Detrital or secondary haematite and hydrated ferric oxides are often adsorbed onto clay minerals.
4. Pyrrhotite:
   (a) Pyrrhotite, like magnetite, can occur in volcanogenic sediments — see 1 (c) above.
   (b) Pyrrhotite can form by the reactions between detrital iron minerals and bacteriogenic sulphide in anoxic sediments. Pyrite is the stable phase in most sedimentary environments, particularly in marine environments, but survival of authigenic monosulphide phases (precursors to pyrrhotite) is favoured by stagnant aerobic conditions and the absence of sulphur or sulphate.
   (c) Precipitation of pyrrhotite from hydrothermal vents at present day spreading centres has been observed. Older and deeper-water submarine exhalative deposit tend to be pyrrhotite bearing whereas pyrite is favoured in more recent and shallower water deposits.

5. Pyrite and other sulphides:

   (a) In distal marine environments, pyrite and other sulphides can be precipitated in aerobic water masses in which sulphide activities are maintained at non-equilibrium levels by bacteria.

   (b) Diagenetic environments characterized by slow detrital addition, abundant organic matter and readily available sulphate maintaining high sulphide activity, result in all iron compounds tending towards pyrite.

   (c) Detrital pyrite may be found in greywackes.

6. Carbonates — chiefly siderite:

   (a) Siderite is formed in certain freshwater swamps (often associated with coal), and in reducing environments with low sulphide activity and high CO_2, neutral pH. Siderite is unstable in normal marine environments.

7. Silicates — glauconite and other clay minerals:

   (a) Fe^{3+} and Fe^{2+} are incorporated into structures of clay minerals. Glauconite forms where there are very slow rates of deposition and where organic matter is present. Silica must be present, but carbonate and sulphate activities must be very low.

2.2.2 Metasediments

Mancktelow (1979) identified five metamorphic zones within Kanmantoo Group rocks: biotite-muscovite-chlorite, andalusite (kyanite)-staurolite, fibrolite, sillimanite and migmatite. During the regional metamorphism, magnetic minerals could have formed by many reactions, some of which are given below. Magnetite is usually the source of most aeromagnetic anomalies. However, pyrite-pyrrhotite schists occur frequently in the upper Kanmantoo Group sequence and pyrrhotite contribution to magnetic anomalies cannot be ignored.

Production of oxide minerals during regional metamorphism

Magnetite is formed by the breakdown of (Fe, Mg) silicates at all levels of regional metamorphism. Magnetite as opposed to haematite is characteristic of the higher metamorphic grades and is the dominant iron oxide in rocks above the garnet isograd (Thompson, 1972). Pure magnetite is found in banded iron formations (Annersten, 1968), pelitic schists, and quartzites (Rumble, 1973). Magnetite forms euhedral or subhedral porphyroblasts, notably free of inclusions (Banno and Kanehira, 1961; Rumble, 1973). Magnetites from weathered outcrops usually show traces of supergene alteration to haematite parallel to their octahedral faces and may be completely converted to martite pseudomorphs (Ramdohr, 1969).

Some of the different reactions by which secondary magnetite is produced during different stages of metamorphism are shown below (after McIntyre, 1980; Grant, 1985a).

Lower greenschist facies (chlorite-biotite zone: T$\sim$ 250°–350°C)

$$\text{chlorite} + \text{haematite} \rightleftharpoons \text{chloritoid} + \text{magnetite} + SiO_2 + H_2O \qquad (2.1)$$

Upper greenschist facies (biotite-muscovite zone: T $\sim$ 350°–450°C)

$$\text{chlorite} \pm \text{biotite} + \text{haematite} \rightleftharpoons \text{muscovite} \pm K\text{-feldspar} + \text{magnetite} + SiO_2 + H_2O \quad (2.2)$$

Epidote-amphibolite facies (almandine-staurolite-kyanite: T$\sim$ 450°–550°C)

$$\text{chloritoid} \pm SiO_2 \pm O_2 \rightleftharpoons \text{staurolite} \pm \text{almandine} \pm \text{kyanite} \pm \text{magnetite} + H_2O \quad (2.3)$$

Amphibolite facies (sillimanite zone: T$\sim$ 550°–650°C)

$$\text{biotite} \pm SiO_2 \pm O_2 \rightleftharpoons K\text{-feldspar} + (Fe, Mg)\text{silicates} \pm \text{magnetite} + H_2O \quad (2.4)$$

Granulite facies (cordierite zone: T $\sim$ 650°–750°C)

$$\text{hydrous } (Fe, Mg)\ Al\text{-silicates} \pm SiO_2 + O_2 \rightleftharpoons K\text{-feldspar} + (Fe, Mg)\text{silicates} \pm \text{magnetite} + H_2O \quad (2.5)$$

The lamellar intergrowths of ferrianilmenite in magnetite characteristic of igneous rocks is only rarely present in metamorphic rocks (Rumble, 1976). Instead, haematite-ilmenite solid solutions are found in all metamorphic zones in a wide variety of rocks types. There is limited miscibility at metamorphic temperatures along the join Fe_2O_3-$FeTiO_3$ and this results in the exsolution of ilmenite lamellae in a haematite host or vice versa (Ramdohr, 1969). Supergene alteration produces fine-grained intergrowths of rutile and haematite or rutile alone.

The terminology used in describing the oxide minerals has been taken from Buddington *et al.* (1963):

Ferrianilmenite A one-phase grain of ilmenite containing varying amounts of Fe_2O_3 in solid solution.

Titanhaematite A one-phase grain of haematite containing varying amounts of $FeTiO_3$ in solid solution.

Hemo-ilmenite A two-phase grain consisting of titanhaematite lamellae enclosed in a ferrianilmenite host.

Ilmeno-haematite A two-phase grain consisting of ferrianilmenite lamellae enclosed in a titanhaematite host.

The principle mechanisms by which magnetite replaces haematite are given in reactions 2.1 and 2.2. Both reactions involve dehydration, compaction and the production of magnetite-quartzite assemblages. The FeO needed to form magnetite is taken from the silicates (Grant, 1985a). The transformation of the iron oxides from a predominantly haematitic to a predominantly magnetitic composition is more or less completed when rocks have been regionally metamorphosed to upper greenschist facies.

Increasing temperatures favour the breakdown of hydrous (Fe, Mg) silicates into progressively less hydrous and chemically simpler compounds, beginning with complex substances like

chloritoid and ending with simple silicates like hypersthene (see above). Secondary magnetite is produced from these reactions and silica is consumed at all stages of progressive metamorphism; but significant production of magnetite takes place under relatively low-grade conditions — usually in rocks which are haematitic — or under sufficiently high grade conditions that there is a significant breakdown of biotite and amphibole and a loss of silica. Thus there is a general tendency of iron bearing rocks to become more magnetitic with increasing metamorphic grade. Extreme metamorphism seems to be accompanied by a marked reduction in magnetic strength, probably because with migmatization and granitization, iron and titanium oxides will begin to recombine to form magnetite-ilmenite solid solutions (Grant, 1985a).

The two most important controls on the production of secondary iron oxides are total iron content and oxidation state. The amount of iron fixes the maximum amount of iron oxides which can form. The oxidation state controls the partitioning of iron between the oxides and the silicates. Several researchers (Chinner, 1960; Thompson, 1972) argue that metamorphic rocks retain the oxidation state inherited from their sedimentary parent rock rather than experience progressive reduction during metamorphism; i.e. during metamorphism, rocks behave as narrow units "closed" to oxygen. Chinner (1960) determined the FeO and Fe_2O_3 content of a sequence of pelitic gneisses and computed their oxidation ratio defined as molecular $(2Fe_2O_3 \times 100)/(2Fe_2O_3 + FeO)$. On this scale the oxidation ratio of a rock varied from 0 (all ferrous) to 100 (all ferric). Rocks with low oxidation ratios contained iron in silicates and ilmenite. With increasing oxidation ratio, magnetite appeared and finally haematite. Thompson (1972) suggests that the activity of oxygen is clearly buffered owing to its low mobility and that the reaction by which magnetite forms at the expense of haematite is more consistent with dehydration rather than reduction. However, even if the true mobility of oxygen is very low, its apparent mobility may be amplified by the widespread presence of graphite (Miyashiro, 1964).

Production of secondary pyrrhotite during regional metamorphism

Pyrite is the characteristic iron sulphide mineral of shales, slates and low-grade phyllites and schists, whereas pyrrhotite may be the dominant iron sulphide in many higher grade schists and gneisses (Thompson, 1972). French (1968) considered an isograd based on the prograde appearance of pyrrhotite and Rochette (1987) used magnetic susceptibility measurements to map the pyrrhotite-in isograd in the Dauphinois zone in the French Alps. In the same way in which magnetite appears to form at the expense of haematite, pyrrhotite forms at the expense of pyrite but since oxygen and sulphur are clearly buffered in certain mineral assemblages and indirectly buffered in many others, it would appear that the net reaction is one of dehydration rather than reduction (Thompson, 1972). There may also be degraphitization through loss of CO_2 if graphite or carbonaceous material is present. Some reactions by which pyrrhotite may form from pyrite (after Thompson, 1972) are given below.

pyrite + biotite + silica + graphite $\rightleftharpoons$ pyrrhotite + muscovite + SiO_2 + CO_2

pyrite + chlorite + graphite $\rightleftharpoons$ pyrrhotite + chloritoid + SiO_2 + water + CO_2

pyrite + chlorite $\rightleftharpoons$ pyrrhotite + chloritoid + SiO_2 + magnetite + H_2O

Factors which determine bulk magnetic properties in metasediments

The factors controlling the change in magnetic properties during metamorphism are given below (McIntyre, 1980; Grant, 1985a).

Characteristics	Magnetite-series	Ilmenite-series
magnetite	> .1%, up to 2%	
magnetite+ilmenite		less than .1%
magnetic susceptibility (cgs)	$> 100 \times 10^{-6}$	$< 100 \times 10^{-6}$
oxidation ratio	> 31.03%	< 31.03%
$\delta^{34}S$	positive	negative
$\delta^{18}O$	low	high
lithophile elements	depleted	enriched
accessory minerals	magnetite ilmenite haematite pyrite chalcopyrite	 ilmenite graphite pyrrhotite muscovite (monazite) (garnet)
BIOTITE Fe_2O_3/FeO refractive index	 high low	 low high
mineralization	sulphide	cassiterite & wolframite
genetic type	I	I or S

Table 2.3: Magnetite-series vs. ilmenite-series granitoids (after Takahashi *et al.*, 1980; Ishihara, 1981; Grant, 1985a).

Total iron content Iron-rich rocks have a greater magnetite producing potential.

Oxidation state Low ratios favour silicates, higher ratios favour haematite, and intermediate ratios favour magnetite formation.

Degree of metamorphism Deformation and metamorphism cause opaque oxide minerals to recrystallize into coarser structures. Coarsely crystalline magnetite has a higher κ and lower Q than finely crystalline magnetite. Also magnetite is exsolved from solid solutions, and secondary magnetite is formed.

Degree of silica saturation In rocks which have the same amount of iron, but differing amounts of silica, more magnetite will tend to form in those rocks which have less silica.

Original sediments Argillaceous rocks generally have more iron and therefore more magnetite producing potential than arenaceous rocks. Note that placers and greywackes may contain detrital magnetite.

Major element chemistry

1. Increasing aluminium content favours magnetite and muscovite over biotite.
2. Deficiency in titanium results in higher magnetic susceptibilities and less remanence.
3. Absence of carbon favours magnetite production. However, magnetite is stable in graphite bearing rocks under most of the range of metamorphic temperature and carbon dioxide pressure (Miyashiro, 1964).

Pressure Low pressures with opportunity for hydrous diffusion away from the metamorphic zone favours magnetite production.

Temperature With increasing temperatures, biotite starts to break down to produce magnetite. In titaniferous rocks, low temperatures favour magnetite production because at higher temperatures, solid solutions of the iron oxides form instead of pure magnetite.

Water flow Large scale water flow through rocks carries the oxidation state of the original host with it and may therefore be oxidizing or reducing (Henkel and Guzmán, 1977).

2.2.3 Granitoids

Rocks are not classified on the basis of their opaque mineralogy but their silicate assemblages. However, Ishihara (1977) devised the magnetite-series and ilmenite-series scheme for classifying granitoids. This classification is descriptive and is dependent on the presence and amount of magnetite and ilmenite in granitoids. The differences between the two series is presented in Table 2.3. The overall chemical compositions are similar. The magnetite-series granitoids probably evolved at higher temperatures and under higher oxidizing conditions than the ilmenite-series granitoids. The two series of granitoids are considered to have resulted from the prevalence of different oxygen fugacities during evolution of the granitic magmas, in which dissociation of hydrous magmas is a main oxidizing agent for magnetite-series magmas and incorporation of crustal carbon is the most essential reducing media for ilmenite-series magmas. The difference in oxygen fugacity probably accounts for the occurrence of ilmenite in granitoids of lower oxygen fugacities and of magnetite in granitoids of higher oxygen fugacities.

Takahashi *et al.* (1980) have compared Ishihara's (*op. cit.*) classification of granitoids with the I-type/S-type series proposed by Chappell and White (1974). Their conclusion was that all magnetite-series granitoids are indeed I-type but that ilmenite-series may include both S-types

Formation	Magnetic susceptibility $\times 10^{-5}$ SI						
	0–50	50–100	100–500	500–1000	1000–2000	2000–5000	> 5000
US		1	1	2	2		
NG	2						
TV	3	2					
CH	6	1	2				
BP	14	25	69	37	8		
TC	3	3	2	2	1		
TP	3	3	1		1		
MS					7		
PG				2	16		
RG	2	1	3	7	11		
MMG						41	9
MNG	10	5					
EBG	5						
RCG				5	10	2	
BHN						31	
MYL					5		

Table 2.4: Outcrop susceptibility measurements. Abbreviations are as follows — US: Ulupa Siltstone, NG: Normanville Group, TV: Truro Volcanics, CH: Carrickalinga Head Fm., BP: Backstairs Passage Fm., TC: Talisker Calc-siltstone, TP: Tapanappa Fm., MS: Middleton Sandstone, PG: Palmer Granite, RG: Rathjen Gneiss, MMG: Mannum Granite, MNG: Monarto Granite, EBG: Encounter Bay Granite, RCG: Reedy Creek Granodiorite, BHN: Black Hill Norite and MYL: Mylonite. Fm. stands for Formation. See Appendix B for the full list of measurements.

and I-types. Ishihara's scheme is of great use in aeromagnetic interpretation as granitoids can now be classified on the basis of their aeromagnetic signatures. Magnetite-series are associated with major sulphide mineralization whereas ilmenite-series granitoids are related to cassiterite and wolframite mineralization (Ishihara, 1981).

2.3 Rock magnetism and opaque mineralogy of rocks in the study area

The preceding sections have established that rock properties are necessary to constrain and improve magnetic interpretation. Though many researchers have worked on Kanmantoo Group rocks, very few whole rock analyses have been carried out. The opaque mineralogy of the rocks has only rarely been studied (Offler, 1966; Brotherton, 1967; Fleming, 1971; Spry, 1976) as it is more usual to make thin sections of rocks rather than the polished thin section which are required for the study of opaque minerals. Most descriptions of rock types in the literature refer to "opaque minerals" or "iron ores" without any further differentiation. Oxidation ratio measurements have not generally been carried out (for exceptions see Brotherton, *op. cit.*; Fleming, *op. cit.*; Toteff, 1977).

Rock samples and thin sections referred to by previous researchers were not always still available in the rock collection of the Department of Geology and Geophysics, and those which were could not always be located on a map and placed in the appropriate stratigraphic interval. For these reasons, the amount of available rock property data to draw on is severely restricted.

The time available for field work was limited and the area to be covered ($\sim 8000\,\mathrm{km}^2$) was large. It was decided to carry out the following steps so as to acquire a reasonable amount of rock property data.

1. Summarize available data in the form of whole rock analyses and oxidation ratios determined by previous researchers at the University of Adelaide and at the South Australian Institute of Technology. Measure the susceptibility of all properly identified hand samples available from these institutes.

2. From the magnetic interpretation, identify areas where magnetic units may be expected to outcrop, search for the outcrop and measure the magnetic susceptibility over the outcrop. Collect samples for opaque mineral studies, whole rock and ferrous iron analyses.

3. Identify magnetic units suspected of carrying a strong NRM, and collect oriented samples from the outcrop.

To obtain representative susceptibility values, several measurements were made on each hand sample, and between 50 to 100 measurements on every outcrop. Usually most outcrops could quite easily be classed into a small range but for the few outcrops for which several different ranges were observed, the outcrop was divided into the appropriate number of smaller outcrops.

173 localities were visited. Magnetic susceptibility was measured *in situ* and on samples using a Geoinstruments JH-8 susceptibility meter. Polished thin sections and polished blocks from 39 rocks were analyzed for opaque mineralogy. Facilities for whole rock analysis were restricted so only 10 measurements were made, all on rocks from the Backstairs Passage Formation. Ferrous iron determinations were carried out on 21 samples (Backstairs Passage Formation: 14; Ulupa

Formation	Magnetic susceptibility $\times 10^{-5}$ SI						
	0–50	50–100	100–500	500–1000	1000–2000	2000–5000	> 5000
PRE	124	3	12				
BSG	62		39	35	12	4	
NG	42						
CH	125			2			
BP	333	20	66	19	18	4	1
TC	62	6	108	27	1	8	
TP	358		6		2		1
GR	40	1	21	31	6	9	
AMP	45	17	1	1	1		
DIO	9		6		1		
MYL					7		

Table 2.5: Susceptibility measurements on samples. Abbreviations are as follows — PRE: Precambrian rocks below Brachina Subgroup, BSG: Brachina Subgroup, NG: Normanville Group, CH: Carrickalinga Head Fm., BP: Backstairs Passage Fm., TC: Talisker Calc-siltstone, TP: Tapanappa Fm., GR: Granite, AMP: Amphibolite and meta-dolerite, DIO: Diorite and MYL: Mylonite. Fm. stands for Formation. Full details are given in Appendix C.

Siltstone: 1, Middleton Sandstone: 1, Tapanappa Formation: 2, Carrickalinga Head Formation: 1).

To study the significance of NRM, 15 oriented samples were selected. The dip and strike of the top surface of each sample was marked. It was often difficult to orient samples either because of the weathered nature or the schistosity of the sample. As a result, measured directions of the inclination and declination of the remanent field are not reliable though the measurements of intensity are reliable. Several cores were drilled into each sample in order to obtain consistent results. NRM intensity and direction were determined using a Schonstedt spinner magnetometer at the Department of Earth Sciences, Flinders University[1].

For major element and iron analyses, the samples were ground to fine powder using a Siebtechnic tungsten carbide mill. Weathered surfaces had previously been removed. Powder for whole rock analysis was ignited at 960°C to determine the percentage loss of volatiles. 280 mg of ignited sample, 20 mg of sodium nitrate and 1.5 g of flux were mixed and fused in a platinum crucible to form buttons. The whole rock analyses were then determined on a programmable Siemens XRF machine by John Stanley.

Total iron analyses were carried out on 15 samples (4 overlapped with whole rock analyses measurements — see above). All samples were dried at 110°C, then weighed into teflon beakers. Samples (100 mg) were digested with HCl, HF and $HClO_4$ acids, and then made up to volume (100 ml) in the presence of Lanthanum Zirconate (0.2% w/v La, 0.1% w/v Zr) and K (0.12% w/v) and 10% v/v HCl. The solutions were then measured by Atomic Absorption Spectrometry for total Fe% at 372.0 nm Fe line using a Varian AA-6D Atomic Absorption Spectrometer.

To determine ferrous iron content, 400 mg of powdered sample was mixed with 5 ml of water in a platinum crucible. To this mixture, 5 ml of 50% v/v sulphuric acid and 5 ml 50% w/w hydrofluoric acid was added and the crucible heated at 350° C for approximately 20 minutes. This was added to 300 ml of distilled water, 10 ml of 50% v/v sulphuric acid and 30 ml saturated boric acid before titration with a standardized solution of 0.02 normal $CeSO_4$ and the indicator, N-Phenyl anthranilic acid to determine ferrous iron content.

2.3.1 Magnetic susceptibility and NRM

Measurements of magnetic susceptibility were made on outcrops (Appendix B) and tabulated in Table 2.4. Based on quantitative interpretation, a number of shallow magnetic anomalies were chosen. During field work, the surface expressions of the anomalous sources were searched for, and susceptibility measurements made on outcrops in their vicinity.

Measurements were also made on hand samples collected by previous researchers (Appendix C). These results are tabulated in Table 2.5. They were not integrated with outcrop measurements because both distributions are biased for different reasons. Outcrops were chosen based on the possibility of finding rocks capable of giving rise to a detectable magnetic anomaly. Previous researchers probably chose their samples according to the state of weathering and silicate lithology.

Susceptibility values tend to vary from low ($< 100 \times 10^{-5}$ SI), to moderate (100–1000 $\times$ 10^{-5} SI). Some high measurements ($\sim 1000 \times 10^{-5}$ SI) were made and a few very high values ($\gg 1000 \times 10^{-5}$ SI)were recorded.

[1]Dr. F.Chamalaun provided access to the equipment and advised on its usage.

Unit	Sample	Core	Declination degrees	Inclination degrees	Intensity ($\times 10^{-6}$ emu/cc)	Susceptibility ($\times 10^{-5}$ SI)	Q
TC	E14	A1	223	-8	4741	450	12
	E14	A2	200	6	3262		
	E14	A3	190	-4	2975		
	E14	B1	224	-28	6332		
	E14	B2	226	-23	3818		
	E14	B3	216	-19	3259		
	E14	C1	228	-15	3687		
	E16	A1	328	30	16265	800	27
BP	S1	A1	292	-66	898	1000	1.6
	S1	A2	291	-46	1243		
	S1	A3	296	-46	1740		
	S1	B1	321	-61	1504		
	S1	B2	282	-49	1102		
	S1	C1	277	-44	847		
BP	TR5	A1	162	-30	4	210	.03
	TR5	A2	162	-28	4		
	TR5	B1	170	-17	7		
	TR5	C1	174	-24	5		
	TR5	C2	166	-26	5		
	TR5	D1	179	-22	8		
	TR5	D1	180	-22	7		
	TR5	D2	144	-29	5		
	TR5	E1	185	-18	7		
	TR5	E2	180	-18	5		
US	X2	A1	220	-4	2922	1700	2.3
RG	S2	A1	301	-8	107	1500	.04
	S2	A1	298	-2.5	104		
	S2	B1	303	-36	80		
	S2	B2	307	-54	68		

Table 2.6: NRM measurements. Abbreviations: TC: Talisker Calc-siltstone, BP: Backstairs Passage Formation, US: Ulupa Siltstone, RG: Rathjen Gneiss. The average remanent intensity was used to compute the Q ratio.

Susceptibility measurements made on hand samples of metasediments were generally low. Outcrop values were moderate to high especially where the outcrop coincided with a magnetic anomaly. This was expected as a single sample is too small to be considered representative of the larger outcrop from which it had been collected. Analogously, outcrop measurements were expected to be in the moderate to high range as the choice of outcrops were based on magnetic interpretation and it was expected to find magnetic mineral bearing rocks.

Of the metasediments, it is significant that even sample susceptibility measurements of the Ulupa Siltstone (and other members of the Brachina Subgroup) were generally moderate to high. These samples were collected from Kangaroo Island, Cape Jervis, Australia Plains, Mt. Barker Creek and Macclesfield (Appendix C).

The quartzites and marbles of the Normanville Group had low susceptibilities. Outcrop measurements on the Truro Volcanics and its equivalents in the Sedan Hill section and Red Creek section, were all consistently low.

Susceptibility measurements of the Backstairs Passage Formation were often low, and sometimes high. The higher values were obtained in the sillimanite and migmatite zones and were associated with meta-arenites and migmatites. Measurements made on the Middleton Sandstone on Kangaroo Island and at Middleton Beach returned consistently high values. The high susceptibility measurements on Talisker Calc-siltstone rocks were made at the Brukunga quarry where the Nairne pyrite facies of the Talisker Calc-siltstone used to be mined for its pyrite content. Andalusite schists of the Tapanappa Formation at Dawesley and at the Kanmantoo Mine had high susceptibilities. The highest susceptibility measured in the study area (> 1 SI) was recorded over a sample of magnetite ore from the Kanmantoo Mine (Tapanappa Formation).

Based on susceptibility measurements the metasedimentary sequence can be considered to consist of a sequence of basically non-magnetic rocks intercalated with magnetic units. Pelitic schists, pyrite schists, psammites and migmatites are the lithologies associated with magnetic units. The more calcareous lithologies (limestones, marbles, non-pyritic calc-silicates) are generally non-magnetic.

Susceptibility measurements recorded over granites, granite gneisses and the Black Hill Norite were in the moderate to high range with a few exceptions. Susceptibility measurements over the Palmer Granite, Rathjen Gneiss, Reedy Creek Granodiorite and associated granitic bodies, and the Murray Bridge Granite were in the moderate to high range. Measurements over the Mannum Granite and the Black Hill Norite were in the very high range, while the Monarto Granite returned consistently low values. The few samples of amphibolite tested returned low to moderate values. Extensive outcrop of mylonite in the Marne River gave consistently high measurements.

Statistically, at least several hundred oriented samples need to be analyzed before the remanence associated with the various rock units can be understood. It was considered outside the scope of this thesis to conduct a full scale remanent magnetism study. Instead, an exploratory study was conducted to indicate the possible nature of remanence and the specific geological units to be investigated further.

The units suspected of carrying a strong remanence were the magnetic units within the Ulupa Siltstone, the Nairne pyrite facies of the Talisker Calc-siltstone, and the more magnetic of the magnetic units within the Backstairs Passage Formation. Samples from these units and from the Rathjen Gneiss were cored and examined at Flinders University. Nine of the 15 samples shattered during drilling leaving 6 samples. The results of the study are presented in Table 2.6. Samples of the Nairne pyrite facies had the highest Q values (average: 12 and 27). The sole Ulupa Siltstone sample had a Q value of 2.3. The conclusions which can be drawn are that the

Figure 2.2: Opaque minerals in metasediments:

A: Tabular-shaped iron oxides in andalusite schists of the Ulupa Siltstone. Note the microfault in the centre of the photograph. The opaque minerals follow the schistosity of the mica fabric. [Transmitted light, 940μm $\times$ 630μm, sample X3.]

B: Samples of the Ulupa Siltstone often contain all three iron oxide phases: magnetite (left), hemo-ilmenite (top right) and ilmeno-haematite (top centre). [Reflected light, 435μm $\times$ 270μm, sample E8.]

C: Euhedral, almost pure magnetite from a biotite gneiss in the Backstairs Passage Formation. [Reflected light, 950μm $\times$ 630μm, sample T12.]

D: Euhedral magnetite grains showing traces of supergene alteration to haematite parallel to the octahedral faces. [Reflected light, 180μm $\times$ 110μm, sample AN4a.]

E: The degree of martitization varies and the magnetite may be converted to martite pseudomorphs. [Reflected light, 200μm $\times$ 130μm, sample E19.]

F and G: While magnetite is the dominant opaque, particularly in meta-arenites, ilmeno-haematite (F) and hemo-ilmenite (G) is occasionally found. [Reflected light, F: 140μm $\times$ 85μm, sample T9a; G: 180μm $\times$ 110, sample T3(2).]

H: Pyrite (bottom left) and magnetite (centre right) in pyrrhotite (top background) and chalcopyrite (bottom background). Sample from ore bearing schists, Kanmantoo Mine (courtesy of J. Schiller) [Reflected light].


A

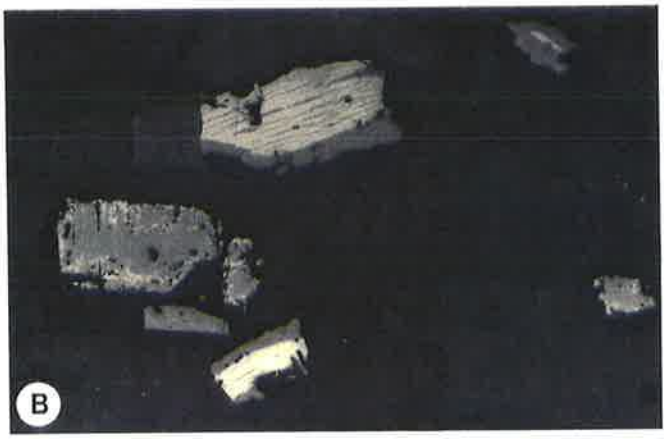
B

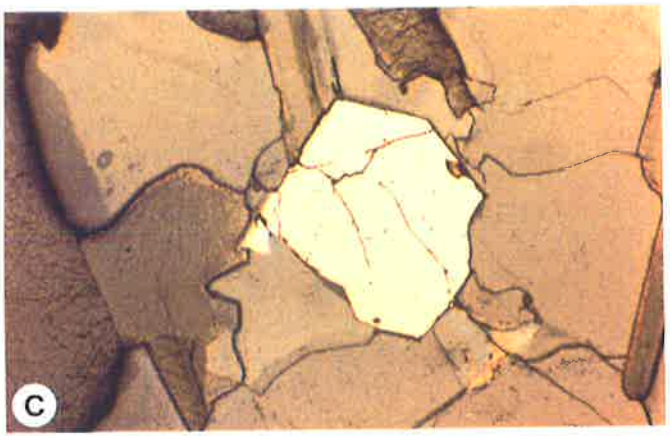
C

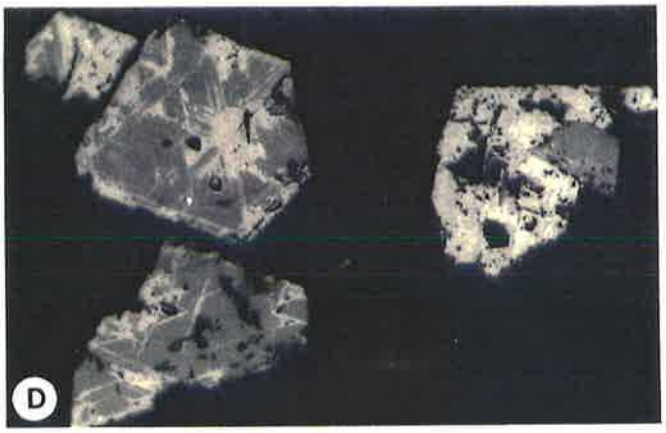
D

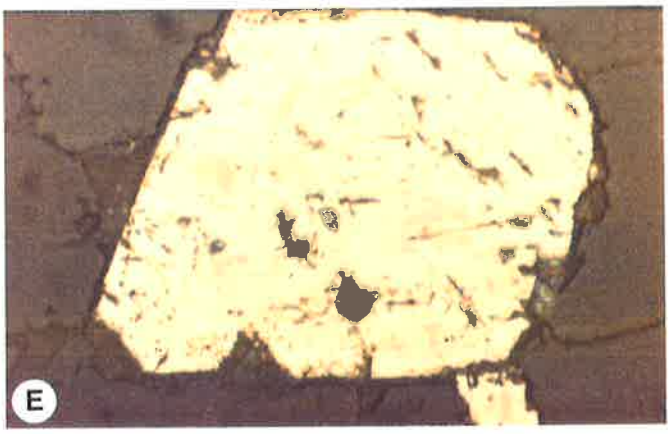
E

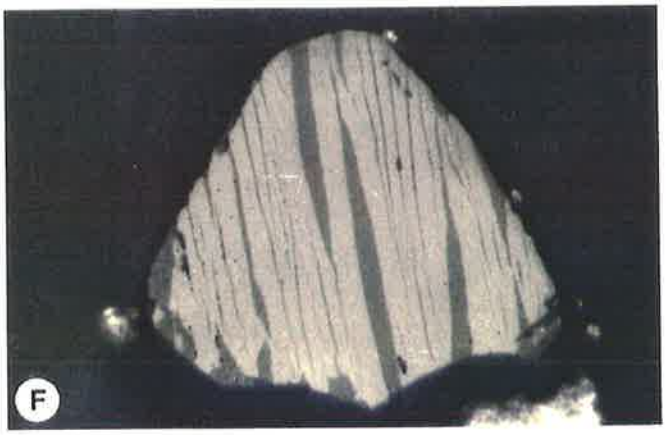
F


G

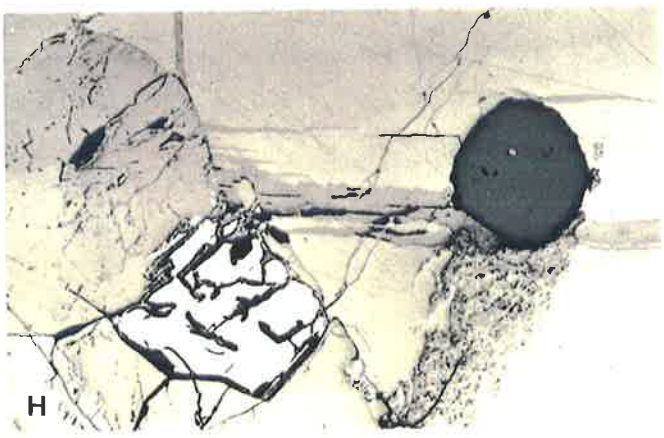
H

Nairne pyrite facies, Ulupa Siltstone and magnetic Backstairs Passage Formation can possess significant remanent magnetism which could affect the modelling of magnetic anomalies. The paucity of data precludes any further interpretation.

2.3.2 Opaque mineralogy and petrogenesis

Polished thin sections were studied under transmitted and reflected light to study the amount and form of opaques present, confirm the identity using the electron microprobe, and study the non-opaques. Eight polished blocks were also studied.

Metasediments

The mineralogy of the thin sections studied shows that the major metasedimentary rock types are meta-arenites, schists (containing andalusite and/or garnet and/or staurolite and/or sillimanite), limestones, calc-silicates and pyritic schists. Minerals common to most lithologies are quartz, feldspars and mica.

The dominant opaque in the metasediments is either magnetite or pyrrhotite or hemo-ilmenite + ilmeno-haematite. The opaque mineral content of the rocks (determined by point count) is presented against the measured susceptibility in Figure 2.4. The opaque mineralogy of the metasediments can be divided into the following groups:

1. No opaques: From the Figure 2.4, it is seen that rocks with few or no opaque minerals have zero to low susceptibilities. This is because the major magnetic minerals are all opaque.

2. Magnetite ± titaniferous iron oxides: The dominant opaque mineral in the meta-arenites of the Backstairs Passage Formation is magnetite. Magnetite forms equant, euhedral porphyroblasts (Figure 2.2C) and is apparently pure and free of inclusions (this is based on limited electron probe data). The average grain size is in the MD size range. Magnetite from weathered outcrops showed traces of alteration to specular haematite (Figure 2.2D). In extreme cases, the magnetite has been completely converted to martite pseudomorphs (Figure 2.2E). Occasional laths of ilmeno-haematite and hemo-ilmenite are found, but only in very minor quantities. Where the magnetites are MD grains and only partially martitized, there is a linear relationship between magnetic susceptibility and opaque content. In rocks with high opaque content but low susceptibilities, the magnetites had been almost completely martitized to haematite.

3. Ilmeno-haematite + hemo-ilmenite: In Figure 2.4, it is seen that rocks with a high percentage of opaques may have low susceptibilities. In some cases, the magnetites have been martitized to haematites. The other main reason is that the dominant opaques are ilmeno-haematite and hemo-ilmenite, which tend to have low susceptibility. In the andalusite schists of the Ulupa Siltstone, this combination of opaques is common. In fact, all three iron oxide phases have been found in the same sample of the Ulupa Siltstone.

   Ilmeno-haematite in the metasediments is always accompanied by hemo-ilmenite (Figure 2.2A, B). The subhedral haematite and ilmenite grains have the form of flat plates; their rectangular cross sections measure up to $75 \times 125 \mu$m. The haematite and ilmenite plates show a strong preferred orientation parallel to the schistosity defined by the mica grains of the pelitic schists. No traces of relict detrital mineral grains were observed. Magnetite is often found in close proximity to the haematite and ilmenite but also occurs in separate parallel bands. The exsolution blebs of ilmenite in the haematite grains and vice versa, indicates a possible cause for strong NRM in the Ulupa Siltstone (Section 6.1.3).

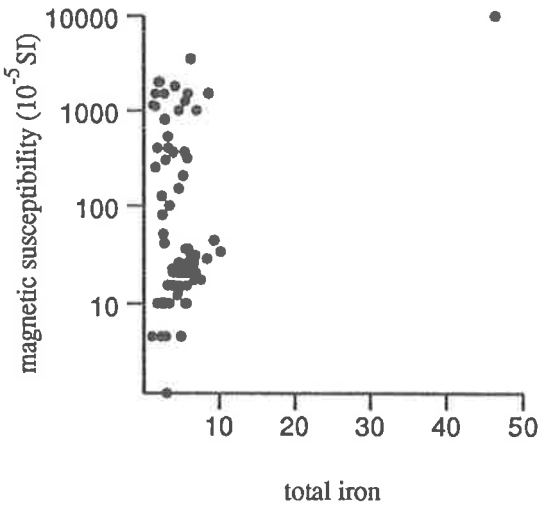

Figure 2.3: Susceptibility vs. total iron content.

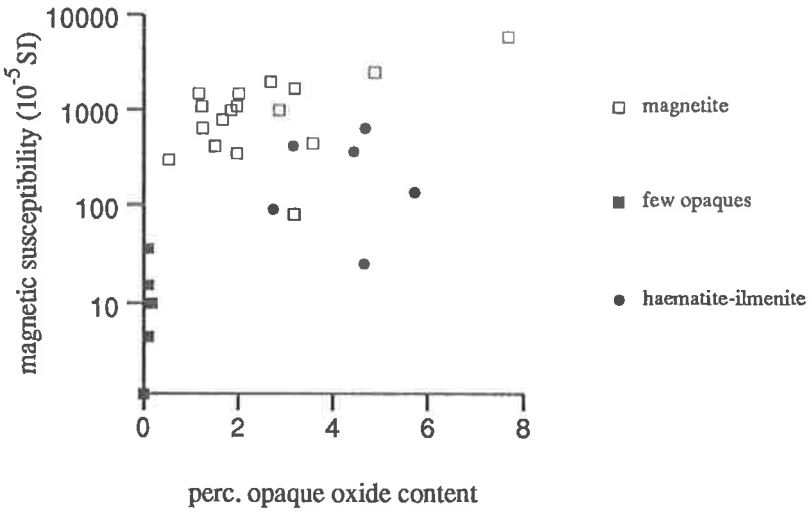

Figure 2.4: Susceptibility vs. opaque oxide abundance.

4. Pyrhhotite ± pyrite ± sulphide ore minerals ± magnetite: Pyrrhotite is found in the Nairne pyrite facies of the Talisker Calc-siltstone, in pyritic phyllites of the Tapanappa Formation and younger Kanmantoo Group formations, and associated with sulphide ore minerals in the mineralized schists of the Tapanappa Formation. It is frequently found together with magnetite.

   In his study of the Nairne pyrite facies of the Talisker Calc-siltstone, La Ganza (1959a) states: "pyrrhotite is present throughout the ore and is somewhat more abundant than pyrite. Unlike the pyrite, pyrrhotite does not form crystals, but instead forms irregular masses which reflect the outlines of the enclosing gangue minerals. Commonly, the pyrrhotite forms plates between laths of muscovite, and these like the muscovite, are aligned parallel with the foliation." La Ganza (*op. cit.*) noted that there were very few inclusions in the pyrrhotite. Graphite is always present but magnetite has not been recorded.

   Meta-pelites and meta-greywackes of the Tapanappa Formation are host to sulphide mineralization (e.g. at Kanmantoo, Wheal Ellen, South Hill and Strathalbyn). Pyrrhotite is found as anhedral grains. Magnetite, together with chalcopyrite and pyrrhotite forms the major primary minerals in the Kanmantoo ore deposit (Figure 2.2H). Magnetite and ilmenite are common in the other sulphide ore deposits but not at Wheal Ellen and Strathalbyn (Both, in press).

Magnetic susceptibility has been used as the parameter common to the graphs shown in Figures 2.3 and 2.4. Graphs of susceptibility vs. oxidation ratio and titanium content are presented for the Ulupa Siltstone, Backstairs Passage Formation and Tapanappa Formation in Figures 2.5, 2.6 and 2.7. Note that the Middleton Sandstone has been grouped together with the Backstairs Passage Formation and the other younger Kanmantoo Group formations with the Tapanappa Formation. Available whole rock analyses have been averaged and tabulated in Table 2.7.

The graph of susceptibility against total iron content showed that while the presence of iron controls whether magnetic minerals can form, and the amount of iron controls how iron is partitioned between the oxides and silicates, susceptibility could not be simply related to total iron content. To produce 1% magnetite in a rock requires only .722% iron. There is a general increase in magnetic susceptibility with oxidation ratio corresponding to the absence or paucity of magnetite at low oxidation ratios and the increasing amount of magnetite formed in rocks with higher oxidation ratios.

The Ulupa Siltstone contains abundant opaques (hemo-ilmenite + ilmeno-haematite ± magnetite). Sediments of the Ulupa Siltstone have been selectively enriched in titanium (Manck-telow, 1979). From Table 2.7 it can be seen that the Ulupa Siltstone is relatively richer in iron and aluminium, and poorer in silica. This combination favours the production of aluminium silicates and titaniferous iron oxides. The conspicuous presence of the titanohaematites in the Ulupa Siltstone is probably a result of this excess titanium. Chinner (1960) found that in his study area only one of 11 samples of pelitic gneisses contained all three oxide phases and that its oxidation ratio was 37. Samples of the Ulupa Siltstone contain all three oxide phases and the oxidation ratio varies between 30 and 55 suggesting that all three iron oxides can exist over a wide range of oxidation ratios.

From Table 2.7, the Backstairs Passage Formation and the Middleton Sandstone tend to have relatively less titanium, low iron and are high in silica. Both these formations contain heavy mineral concentrates. They are more oxidized than the pelitic Tapanappa Formation. During metamorphism, the chemical composition would tend to favour the production of quartz, feldspars and iron oxides. The moderate oxidation ratios favour the production of magnetite

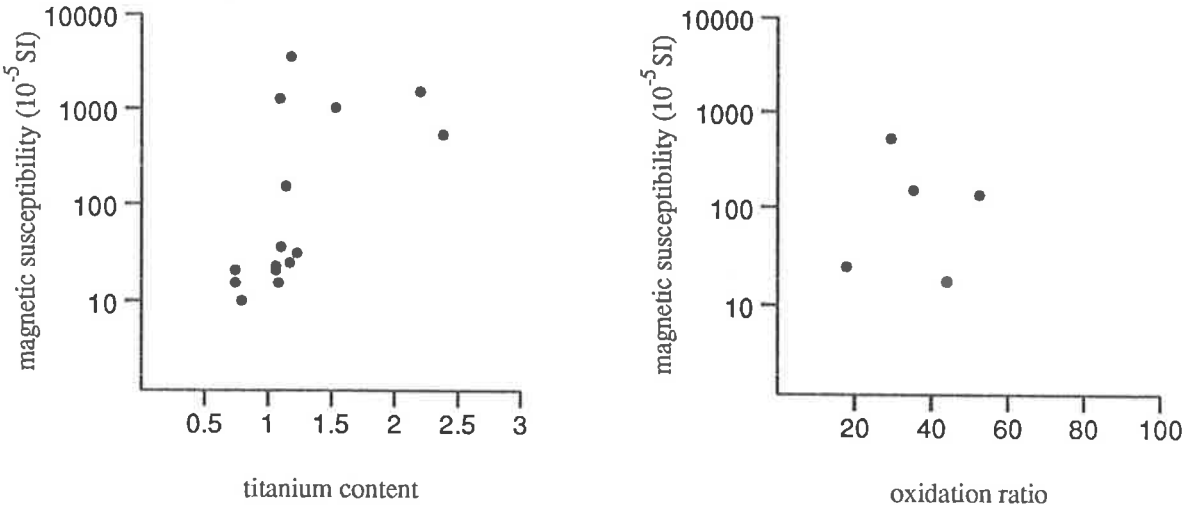

Figure 2.5: Ulupa Siltstone: graphs of susceptibility vs. oxidation ratio and titanium content.

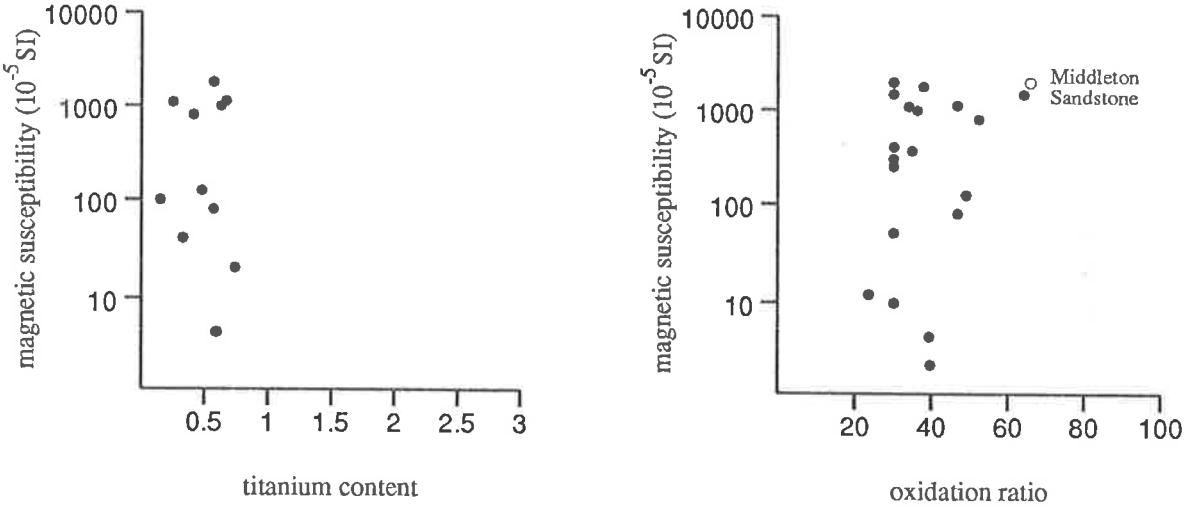

Figure 2.6: Backstairs Passage Formation: graphs of susceptibility vs. oxidation ratio and titanium content. Also shown is one measurement made on the Middleton Sandstone.

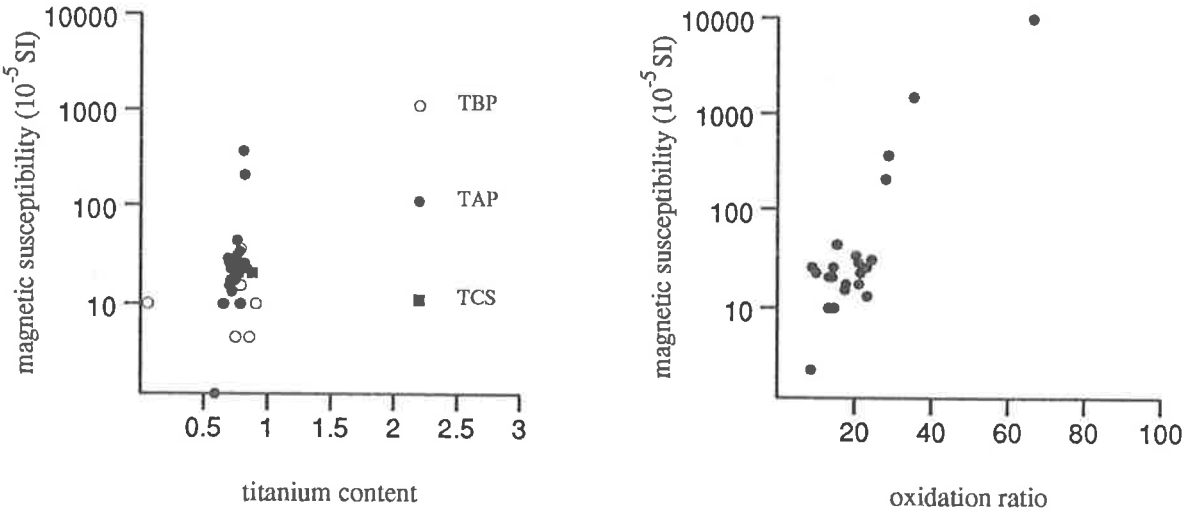

Figure 2.7: Upper Kanmantoo Group: graphs of susceptibility vs. oxidation ratio and titanium content. Code — TCS: Talisker Calc-siltstone, TAP: Tapanappa Formation and TBP: Tunkalilla to Petrel Cove Formation.

which is relatively pure owing to the little titanium in the sediments. Samples of the Backstairs Passage Formation ranged in oxidation ratio from 22 to 70. Magnetite is usually the only iron oxide but is sometimes accompanied by the titanohaematites.

The arenaceous rocks of the Backstairs Passage Formation and the Middleton Sandstone are poor in iron compared to the iron-rich pelitic rocks of the Tapanappa Formation and Ulupa Siltstone. However, given favourable conditions (e.g. in the migmatite zone), and intermediate oxidation ratios, such rocks can be as or more magnetitic than iron-rich rocks and possess high magnetic susceptibilities.

Like the Ulupa Siltstone, the Tapanappa Formation has a high iron content, though much less titanium. Of the Tapanappa Formation samples depicted, all except two are from the Dawesley area. At low oxidation ratios, ilmenite is found in the rocks and with increasing oxidation ratios magnetite appears. Magnetite ore from the Kanmantoo mine has an oxidation ratio of 66.67 and a susceptibility in excess of 1 SI unit. From these graphs, it may be deduced that for oxidation ratios less than 27–30, the opaque composition is dominated by ilmenite. There appears to be a threshold around 30 above which there is a sharp increase in the amount of magnetite.

The three iron oxides have been observed in arenaceous and pelitic rocks varying in oxidation ratio from 30 to 70 indicating that there is considerable overlap between the oxidation ratio field for magnetite alone and for magnetite plus the titanohaematites.

Though there is insufficient data, the available data appear to indicate that the meta-arenites of the Backstairs Passage Formation and Middleton Sandstone have higher oxidation ratios than the pelitic rocks of the Ulupa Siltstone and Tapanappa Formation. It would also appear that the more magnetitic pelitic rocks are more oxidized than the less magnetitic pelitic rocks while the more magnetitic meta-arenites are less oxidized than the less magnetitic meta-arenites. The first relation follows from the usually more oxidizing environment in which arenaceous sediments are deposited compared to argillaceous sediments. The second relation holds because lower oxidation ratios in pelitic rocks favours the production of ilmenite instead of magnetite during metamorphism. In the oxidized arenaceous rocks, too high an oxidation ratio inhibits the production of magnetite with haematite forming instead. Therefore the more magnetitic arenaceous horizons are relatively less oxidized. In general, the pelitic metasediments contain more iron and titanium but are less oxidized.

Magnetite in the metasediments may have formed from the dehydration of chemically precipitated haematite. In migmatites, Whitehead (1975) has noted the formation of magnetite and muscovite from the breakdown of biotite. The absence of chloritoid in Kanmantoo Group metasediments precludes the formation of magnetite by reaction 2.3. Martitization of magnetite is probably due to the weathering of rocks at the surface.

Granites, granitic rocks, norite, dolerite, diorite

The classification of the granitoids into magnetite-series and ilmenite-series given in Section 6.2.1 is based on the opaque mineralogy and magnetic properties. Most exposed granites have high susceptibilities and contain magnetite. Euhedral, MD magnetite grains (as large as 2–4 mm) were observed in samples of the Palmer Granite and the Rathjen Gneiss. Their oxidation ratios are higher than 30 (Table 6.1) and the high oxidation ratios favour the formation of magnetite over ilmenite.

The major opaques in the Black Hill Norite are magnetite and ilmenite. Some pyrite and chalcopyrite has also been reported. The magnetite grains contain fine exsolved non-titaniferous

Formation	Brachina Subgroup		Carrickalinga Head		Backstairs Passage		Talisker		Tapanappa		Tunkalilla		Petrel Cove		Balquhidder		Middleton Sandstone	
SiO_2	61.07	5.95	62.88	6.41	74.75	4.86	55.82	5.97	62.73	6.63	60.31	.93	59.82	2.85	57.37	4.10		
Al_2O_3	16.76	3.29	16.12	2.97	11.83	1.88	15.80	2.53	16.20	3.60	17.65	.62	22.78	7.61	18.60	2.21		
Fe_2O_3	8.01	1.48	8.27	3.70	4.18	1.89	7.22	.84	9.20	3.97	7.51	.34	3.69	1.57	7.63	1.24	2.76	0.00
MnO	.12	.05	.11	.14	.14	.03	.11	.02	.15	.16	.07	0.00	.06	.04	.08	.03		
MgO	3.21	1.03	3.53	1.56	1.29	.76	3.19	.97	3.42	1.03	3.34	.17	4.21	1.65	3.66	1.07		
CaO	1.77	2.48	1.83	3.25	1.06	.91	2.33	2.03	1.22	1.54	.28	.10	1.47	.81	1.49	.72		
Na_2O	1.83	.85	1.99	1.26	3.58	1.34	1.95	.65	1.32	.95	1.42	.11	3.07	2.19	1.87	.90		
K_2O	3.61	1.13	3.03	1.59	2.17	1.31	3.28	.84	3.40	1.10	4.22	.31	1.52	1.13	4.87	1.28		
TiO_2	1.20	.50	.74	.20	.43	.18	.65	.19	.74	.11	.76	.01	.67	.31	.78	.03		
P_2O_5	.19	.08	.16	.06	.15	.08	.13	.03	.17	.07	.12	.04	.16	.07	.15	.03		
FeS_2							10.48	7.15										
$Fe_{.947}S$							9.13	2.18										
The values given above are based on the following number of analyses																		
Fe_2O_3	33		22		22		6		34		2		5		9		1	
sulphides							17											
P_2O_5	26		22		18		23		13		2		5		9		0	
others	26		22		18		23		33		2		5		9		0	

Table 2.7: The upper part of the table gives the average whole rock analyses given as a percentage. The first number in each column represents the mean, the second the standard deviation. These values have been computed from these sources: Brotherton (1967), George (1967), Lindqvist (1969), Fleming (1971), Spry (1976), Allen (1977), Toteff (1977), Mancktelow (1979), Rajagopalan (this thesis). The lower part of the table lists the number of analyses on which each of the averages in the upper part is based.

spinel (possibly hercynite). Some ilmenite grains contain exsolved haematite. A few microprobe measurements (Mortimer, pers. comm.) indicated that the average mole % of haematite in ilmenite was 6.25%, and the average mole % of ulvospinel in magnetite was only .98%. The magnetite is essentially non-titaniferous. The strong NRM component in the Black Hill Norite (Section 6.2.2) is possibly due to the presence of fine-grained magnetite.

2.4 The radiometric method

Gamma ray spectrometry has applications in uranium exploration and geological mapping. This is because only three elements (uranium, thorium and potassium) and their decay products are naturally radioactive. The following summary of the principles of the method has been compiled from these references: IAEA (1979), Killeen (1979), Pitkin (1968) and Faul (1954).

While the specific radioactivity of K^{40} ($3.3\gamma s^{-1}g^{-1}$) is much less than that of U^{238} (12.23 ± 0.027 Bq per mg of total U) and of Th^{232} (4.1 Bq per mg of total Th), its greater abundance in the Earth's crust makes it a significant contributor to radioactive count rates. The effect of varying potassium contents makes the radiometric method an effective mapping tool because potassium minerals (micas, K-feldspars, ...) are major components of rocks and used in their classification.

By means of a Thallium activated NaI detector which converts incoming gamma radiation to charge pulses, an airborne gamma-ray spectrometer measures the count rate in a given interval of time, within several pre-defined energy windows. The incoming radiation is a combination of uncollided and scattered gamma-rays. Scattered gamma-rays contain no information on the nature and position of the source atoms but uncollided 1.46 Me V gamma-rays are diagnostic of K^{40}. Bismuth-214 in the uranium decay chain and Tl^{208} in the thorium decay chain also have gamma-ray emissions in the energy region above 1 Me V in which an uncollided flux component can be distinguished from scattered radiation at all survey altitudes. The count rates can be interpreted in terms of concentration of the emitter. Since radioactive equilibrium must be assumed to compute the concentrations of uranium and thorium, their concentrations are given in terms of "equivalent" units. To interpret the concentrations of the radio-isotopes in the ground, the equipment must be calibrated and the stripping ratios computed.

Traditionally, an airborne sensor is designed to measure count rates in four channels as depicted in figure 2.8. There is always some contribution from all radio-isotopes in all windows. Table 2.8 shows the contributions to the window count rates typically recorded when a 76×76 mm sodium-iodide detector is placed on outcropping granite with 12 ppm eTh, 3 ppm eU and 3% K. About 86% of the signal in the thorium window can be ascribed to thorium and 2% to uranium. In a normal geological environment, thorium produces as many counts as uranium in the uranium window. More than 65% and typically 75% of the count rate in the potassium window can be attributed to potassium in the ground. The total count window produces much more signal than any of the other three windows and consequently makes it possible to detect radioactive anomalies which are not revealed by any of the other windows owing to poor statistics.

An airborne sensor receives terrestrial gamma radiation as well as background radiation due to cosmic rays, airborne radon daughters and radioactive contaminants (nuclear fall-out, detector radioactivity, ...). Terrestrial radiation over a given area is statistical in nature. It also varies with geometry effects, thickness of overburden, soil moisture and matrix effects. Unlike the geomagnetic field, the measured gamma radiation (in a given window and even the total count) is not a continuous function.

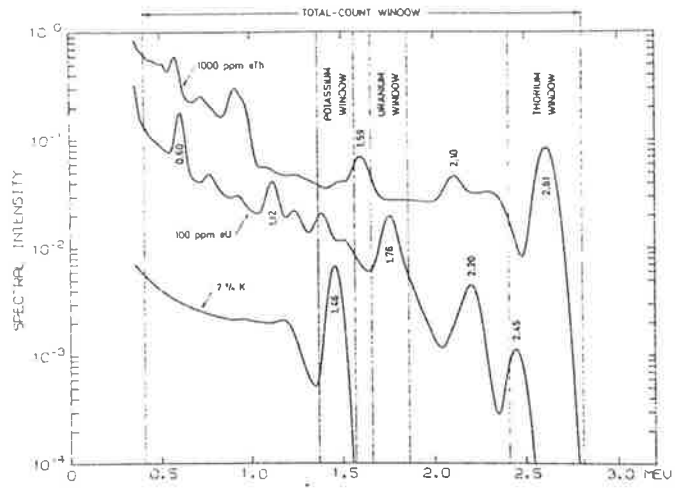

Figure 2.8: Thorium, uranium and potassium gamma-ray spectra obtained at ground level with a 76×76 mm NaI scintillator (after IAEA, 1979).

Radiation source	Counts/100 s within each window			
	Th	U	K	Total count
Thorium	144	75	106	3360
Uranium	4	75	75	1710
Potassium	0	0	900	4200
Background	20	50	100	2000
Total	168	200	1181	11270

Table 2.8: Contributions to the window count rates of a 76×76 mm NaI detector on rock with 12 ppm eTh, 3 ppm eU and 3% K (after IAEA, 1979).

Rock type	K (%)	U (ppm)		Th (ppm) .		Th/U	
	average	average	range	average	range	average	range
Crustal average	2.1	3		12		4	
Mafic igneous	0.5	1	0.2–3	3	0.5–10	3	3–5
Intermediate igneous	1–2.5	2.3	.5–7	9	2–20	4	2–6
Acid igneous	4	4.5	1–12	18	5–20	4	2–10
Arenaceous sediments	1.4	1	0.5–2	3	2–6	3	
Argillaceous sediments	2.7	4	1–13	16	2–47	4	1–12
Limestones	0.3	2	1–10	2		1	
Black shales	2.7	8	3–250	16		2	wide
Laterites	low	10	3–40	50	8–132	5	wide
Metamorphics	depends on parent rock type						

Table 2.9: Radio-element concentrations in crustal rocks (after IAEA, 1979).

The area sampled by an airborne survey system is an oval strip whose length is somewhat greater than the moving distance of the aircraft during a counting period. The width of the strip increases with the survey altitude but is not proportional to the latter because of the greater attenuation of gamma-rays with oblique angles of incidence. Altitude is the most important parameter which affects the area of investigation and topographic features are important if they change the altitude significantly (Duval *et al.*, 1971).

Aerial gamma-ray surveys are invariably surveys of soil radioactivity as the depth of investigation is usually between 8 and 12 inches (Gregory and Horwood, 1961). The main aims in interpreting aeroradiometric data include the correlating of lithology, and hence geology, with anomalous patterns, and the determination of radio-isotope contents in the soil. For successful correlation, the material at ground surface must reflect bedrock composition. Where bedrock is covered by transported soil having a different composition, such as alluvium or loess, correlation is usually impossible (Pitkin, 1968). A study by Schwarzer and Adams (1973) showed that relative concentrations of the radioactive elements in the bedrock is largely preserved in *in situ* soils and that transported soils could be distinguished from *in situ* soils. Their study emphasizes that spectral data converted to concentration units (ppm or %) are superior to qualitative count rates (cps) or total radioactivity for the discrimination and identification of lithologies. The airborne sensor must be properly calibrated if the radio-isotope content of the soil is to be determined.

2.4.1 Radio-element abundances in crustal rocks

The radio-element distribution in common rock types is indicated in Table 2.9. While the K-feldspars and micas are the important potassium bearing minerals, sphene, allanite, apatite, monazite, zircon, thorite, uraninite and pyrochlore contain uranium and/or thorium.

Nearly all felsic igneous rocks are more radioactive than mafic and ultramafic rocks due to the abundance of K-feldspars and more common occurrence of monazite and zircon. Rocks of intermediate composition (granodiorites, monzonites, ...) must be considered individually, though their comparative K-feldspar abundance is a good index to radioactivity. The radioactivity of metamorphic rocks is indicated by the comparative abundances of K-feldspars and micas, by the original composition, and by the addition or depletion of radio-isotopes during metamorphism. Among sedimentary rocks, shales are more radioactive than sandstones and limestones, because of the presence of potassium in clay minerals. Sandstones tend to be more radioactive than limestones if they have heavy mineral bands (containing Th in monazite and U in zircon) and/or interbedded clay-rich shales. Quartzose sandstones and pure limestones are virtually homogenous and devoid of radio-elements. Some carbonaceous shales may be uranium-rich.

Note that radio-isotope content and mappability are independent quantities. No correlation can be established where there is little or no variation in radio-isotope content.

Part II

Processing, presentation and interpretation techniques

Chapter 3

Effective display of aeromagnetic and aeroradiometric data

The information available in aeromagnetic and aeroradiometric data is generally under-utilized, and this is in part due to poor display of the data. The effective display of a data set is crucial to its efficient interpretation (Rajagopalan and Boyd, in press). To maximize the amount of information extracted from the data set and overcome the limitations imposed by using only one kind of display format, several displays should be used to provide different perspectives.

Conventional methods of displaying aeroradiometric data, namely as contour maps or profiles, have tended to downgrade the information content and restrict the integration of this data set into the interpretation model. Digital images have transformed the interpretation of aeroradiometric data and emphasize the importance of matching data sets and displays. This chapter deals mainly with the display of aeromagnetic data as there are fewer ways of displaying aeroradiometric data effectively.

It is assumed here that digital data are available and that all necessary corrections and reductions (diurnal correction, levelling, removal of the International Geomagnetic Reference Field...) have been applied to the data set.

Methods for the display of fine detail in aeromagnetic data and for the production of digital images which have been developed by the author are presented as separate sections.

Examples presented in this chapter are taken from the study area. Except for the image in Figure 3.5 (which covers almost all the study area), every other map shows different presentations of the aeromagnetic data over the lower left part of the study area.

3.1 Systematic approach to displaying geophysical data

Selection of the format and design of the displays (function displayed, whether as contour maps or images or profiles, scale of presentation, use of colour) is dependent on the facilities available and on these geophysical criteria: aims of interpretation, magnetic characteristics and geology of the area, and the survey specifications. This chapter analyzes the qualities of good displays, and the geophysical criteria which govern the choice of displays. A systematic approach leading to the selection of the most effective displays is presented here and demonstrated through examples from the study area.

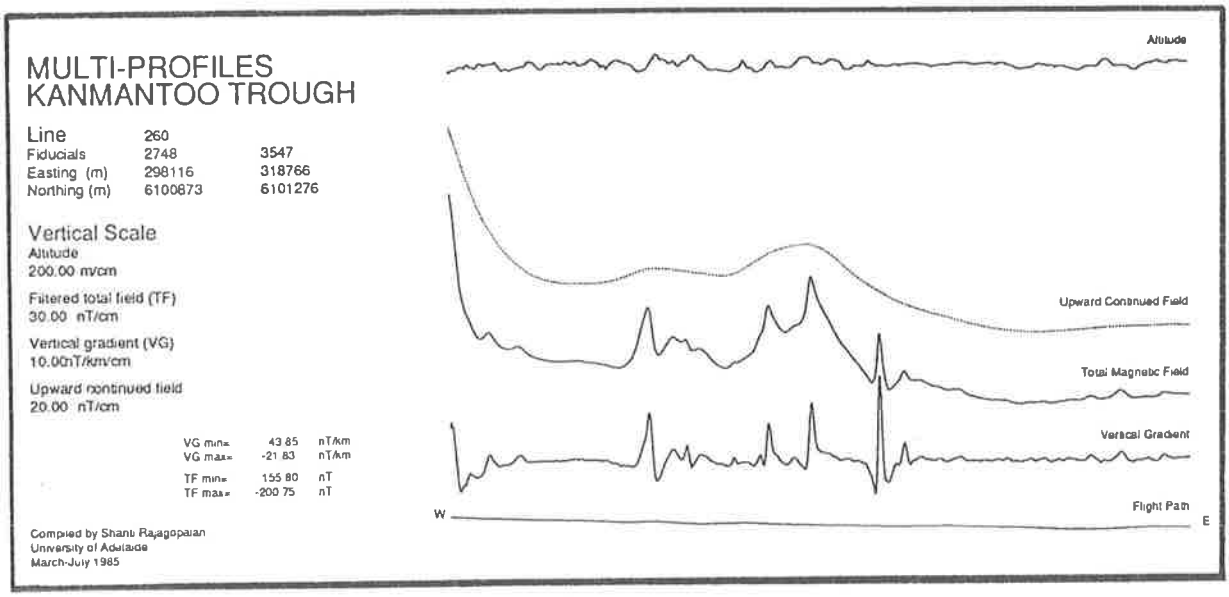

Figure 3.1: Multi-profiles for line 260. These are produced at a large scale for use in quantitative analysis.

3.1.1 Display formats

Airborne geophysical data are generally collected along profiles which are oriented in the same direction. The direction of the flight lines is usually chosen to be perpendicular to the dominant strike of the regional geology. The frequency of data collected along the profiles is the sample spacing and the distance between adjacent lines is the flight line spacing. The nominal flight spacing is 12 times the sample spacing for the CRA data and 6 times the sample spacing for the Pacific Expl. data (see Appendix A). Tie lines used for levelling the survey are also used to display and interpret the survey. The varying density of information in directions parallel and perpendicular to the flight line direction is an important factor when planning displays.

Standard display formats can be classed into two groups: profile displays and gridded data displays. The first group includes single profiles of the measured geophysical field, combinations of different functions of the measured fields, as well as stacked profiles of a single function of the measured data. Contour maps and digital images are examples of gridded data displays. Each display serves different but complementary purposes (these are outlined briefly below and at length in the following sections) and together they highlight different features of the aeromagnetic and, to a lesser extent, the aeroradiometric signal, which would otherwise have remained undetected.

Multi-profiles, for a single flight line, in which several functions of the aeromagnetic field are displayed are invaluable for quantitative interpretation. Figure 3.1 shows, for line 260, the total magnetic field, its upward continued field, its computed one-dimensional vertical gradient (VG), and the flight path and altitude during the flight. Both the total magnetic field and its vertical gradient can be used to interpret anomalies quantitatively (Chapter 4). The one-dimensional vertical gradient was computed from total magnetic field profile data using a quadrature filter (differencing interval: 4, sampling interval: 1) developed by Paine (1986).

On a map of stacked profiles, several flight lines are displayed on the same map sheet with the base line of the displayed function being the flight path. Stacked profiles (see Figure 3.9) provide an alternative map display to contour maps and digital images and can be used to locate anomalies accurately, provide quality control on the survey, and map linear anomalies.

Gridded data displays provide an overview of the data, permit easy correlation with other data sets and aid regional and qualitative interpretation. These displays have several advantages over displayed profiles: they are visually pleasing and provide a good pictorial representation of many recorded data points. However, fine detail in the magnetic field may be obscured, distorted or wrongly represented in such displays (McIntyre, 1981), since gridding packages cannot completely compensate for the varying density of data points in different directions.

Contour maps (Figure 3.2) are familiar to most interpreters. In tightly folded regions, contour maps can help indicate magnetic trends which may otherwise be hard to identify. On the other hand, deviations in flight line paths are hidden,the choice of contour levels is difficult, individual trends may be obscured, significant but low-amplitude anomalies may be overshadowed, and the map may be misleading because of its bias towards certain trends. Small scale contour maps may have poor resolution due to closely spaced contour lines.

Instead of producing contour maps from the gridded data, pixel or digital images may be produced. These may be in colour or in shades of grey (Plates 3 and 4). They can easily be enhanced to delineate directional trends and are particularly effective at very small scales at which other forms of presentation may become too complex to analyze.

3.1.2 Geophysical criteria

The geophysical criteria listed below and the facilities available to the interpreter control the choice of displays. Access to software required to process the data (gridding and contouring packages, derivative operators, image enhancement operators and programs to send it to the output device) and the hardware by which the displays can be produced (computers, pen plotter, colour plotter, laser printer, imaging set up, colour pencils, graphics terminals...) override all other criteria.

The major geophysical criteria when choosing the appropriate set of displays include the following:

1. Aims of the interpretation. If a regional interpretation is to be attempted, then the interpreter will require small scale maps of the total magnetic intensity and may not need to examine individual or stacked profiles. A larger range of maps is necessary to aid geological mapping or search for specific mineral resources.

2. Magnetic characteristics and geology of the study area. The magnetic character of an anomaly are its amplitude, width, anomaly shape, strike length and strike direction. Magnetic characteristics of a study area therefore refers to the dominant magnetic character of the anomalies. While total magnetic intensity maps are standard for any interpretation, the use of upward continued maps (suitable for working out depths to magnetic basement and thickness of sediments), derivative maps (used primarily to study near-surface anomalies and in trend analysis of curvilinear anomalies), enhanced total magnetic intensity maps (e.g. directional filtered maps to delineate large structures and subtle features) will depend on whether the geological terrane and associated magnetic characteristics may be appropriately displayed in these formats.

3. Survey specifications. Surveys are classed as regional or detailed depending on these survey specifications: area covered, nominal flight line and sample spacing and nominal ground clearance. The quality of survey is given by the recovery of fiducials, monitoring of diurnal variations, and variations in ground clearance. Optimum grid spacing and parameters for enhancement operators depend on flight line and sample spacing and on the nominal ground clearance. The scales of the maps produced depend on all survey parameters. Poor quality surveys may be improved by special processing to extract information; on the other hand, additional processing may not be cost-effective.

3.1.3 Design of good displays

Displays vary in their effectiveness to reveal information, partly due to inherent limits and partly due to design flaws. In his book on the display of quantitative information, Tufte (1983) has outlined the major guidelines controlling the design of good displays. These guidelines, adapted for the display of aeromagnetic data, are given below:

1. The display should not be obscured by unnecessary or irrelevant information.

2. Avoid distortion or if deliberately distorting (by using directional filters for example) then make sure that the bias is made known to the interpreter and that other displays exist in which this distortion has not taken place.

Figure 3.2: Contours of total magnetic intensity. The contours are irregularly spaced, and the value increases from blue to black to red contours.

Figure 3.3: Contours of two-dimensional vertical magnetic gradient. As in the above figure, red contours represent the highest values, blue the lowest and black intermediate values.

TOTAL FIELD CONTOURS

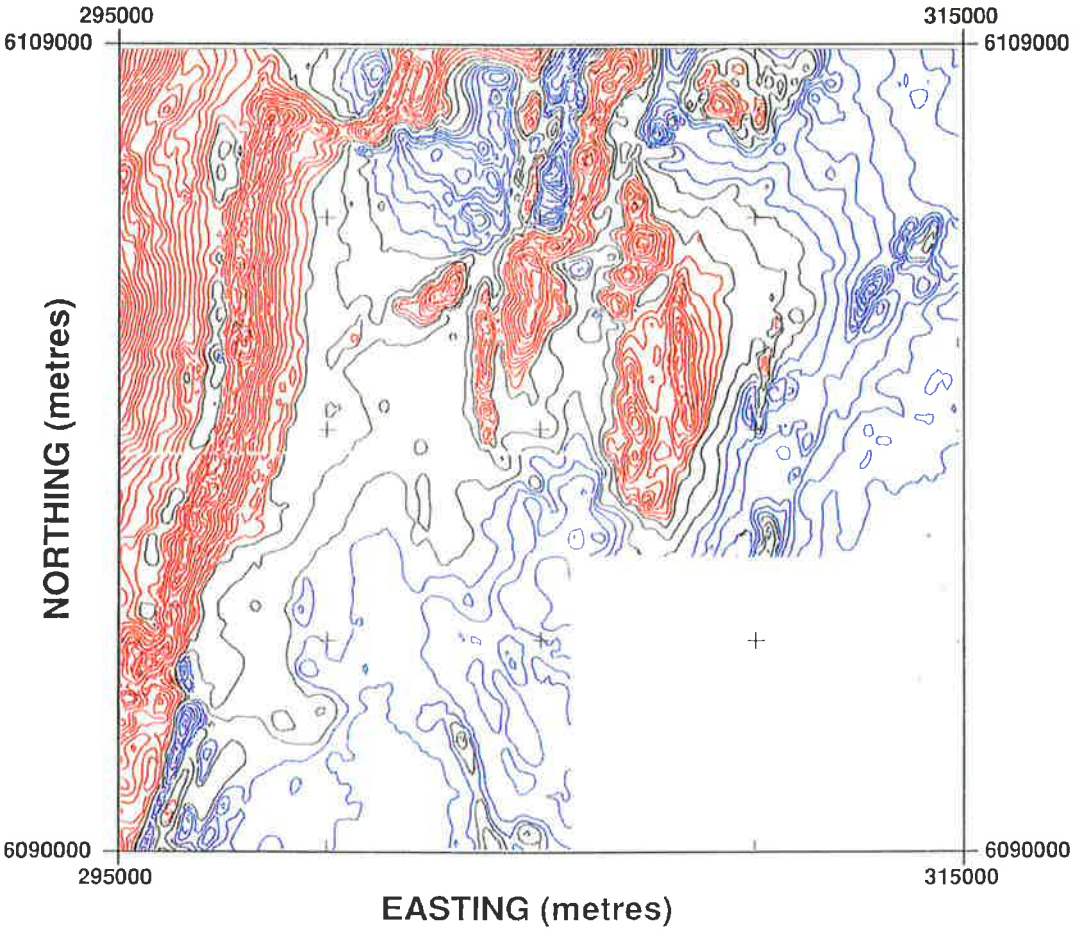

VERTICAL GRADIENT CONTOURS

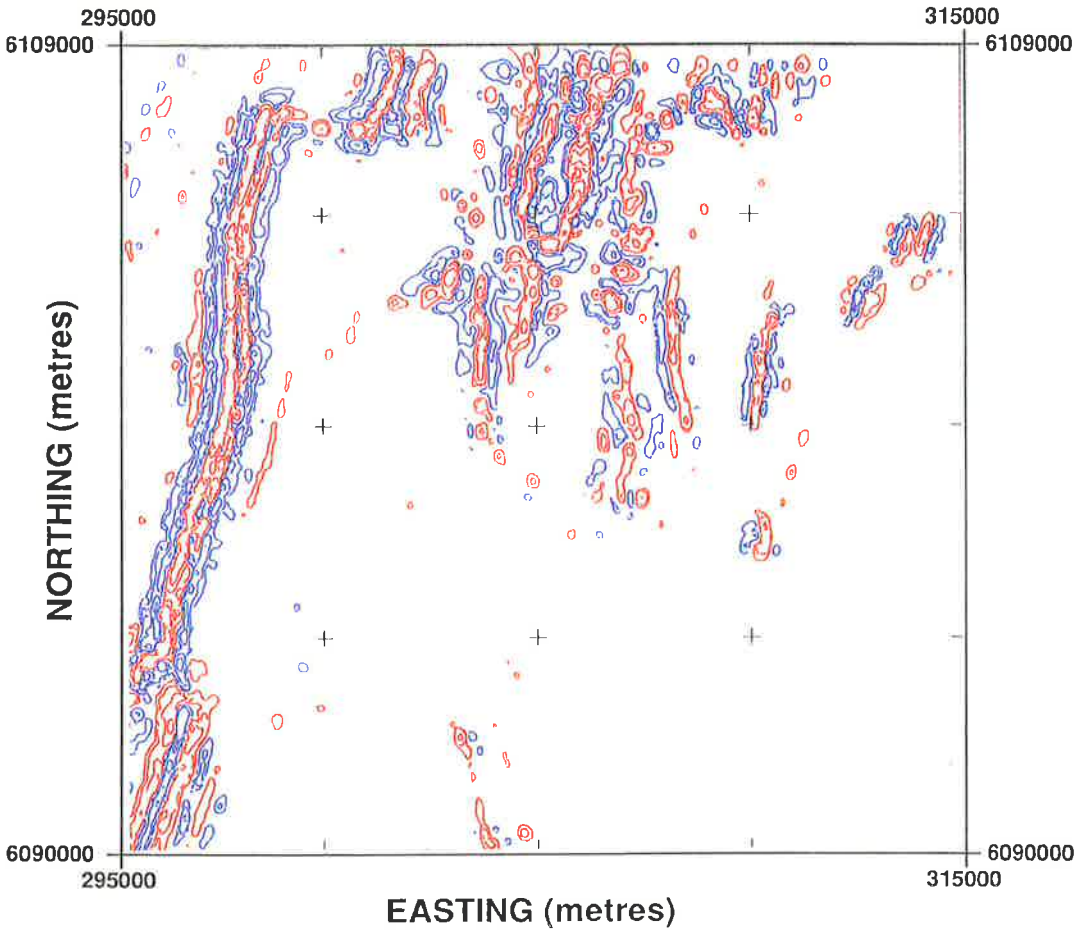

3. Enhance the different characteristics of magnetic data (curvilinear trends, change in gradients, change in anomaly characteristics, breaks in continuity...) so that they are so obvious that the work of the interpreter is more to understand their significance, and less to find them.

4. Display data from a large survey on as few map sheets as possible.

5. Reveal the data at several levels of detail: from a regional overview to detailed, near-surface features.

6. Allow for easy comparison and integration with other data sets (e.g. other geophysical and geochemical data sets, geological maps, aerial photographs, satellite images...).

7. Attract attention to the information being displayed, rather than to the method of display.

The use of colour in displays is debatable. Colour often generates graphical puzzles: shades of grey show varying quantities better than colour as grey levels have a natural visual hierarchy (Tufte, 1983). Contour lines on a map may either be all the same colour (usually black) or divided into several groups, with all levels in a group being coloured the same (e.g. red contours indicating high values, black for intermediate and blue for lows). Images of one function show up better as grey-scale rather than as colour images whereas integrated images, with several variables superimposed, can be more conveniently displayed as colour composites. Similarly graphs showing profiles of several variables may be better displayed in different colours.

The final collection of displays will include maps at different scales: small scale maps to enable the recognition of large structural patterns and working scale maps (at larger scales) to study fine detail. It is essential that geological and other geophysical maps should be available at these scales.

3.1.4 Functions of the total magnetic field

Depths to the top of magnetic sources can vary from near-surface to several kilometres deep. Since high-frequency anomalies tend to be due to shallow sources, and deeper sources give rise to wider anomalies, it is possible to use spectral analysis to separate anomalies on the basis of frequency or wavelength (Bhattacharyya, 1965). The total magnetic field may be continued upwards or filtered using a low-pass filter to remove the effects of shallow sources (e.g. Dods *et al.*, 1985). Alternatively, continuing the field downwards, measuring or computing the derivatives of the field (horizontal or vertical) or filtering using a high-pass filter effectively removes the regional field and emphasizes near-surface features. Apparent-susceptibility maps (Grant, 1973) are similar to derivative maps in that high-frequency anomalies are emphasized. The primary use of the apparent-susceptibility map is in definition of rock type. To remove the effects of the inclination of the earth's magnetic field, it is usual, especially in low magnetic latitudes, to reduce the field to the pole.

Derivative maps reflect near-surface features and are therefore useful in geological mapping. The vertical gradient has a number of advantages over the total magnetic intensity: the regional is almost completely removed, high-frequency anomalies are enhanced, anomaly shape is accentuated and closely spaced anomalies are separated (see Figure 3.1). Several airborne magnetic gradiometer systems are now available and both the horizontal and vertical gradients can be measured (Breiner, 1970; Hood, 1975; Hardwick, 1984). Gradient data, being free of diurnal variations, are generally used to constrain and consequently improve the gridding of the total field. Despite these advantages, gradient data are rarely collected as part of Australian airborne magnetic surveys.

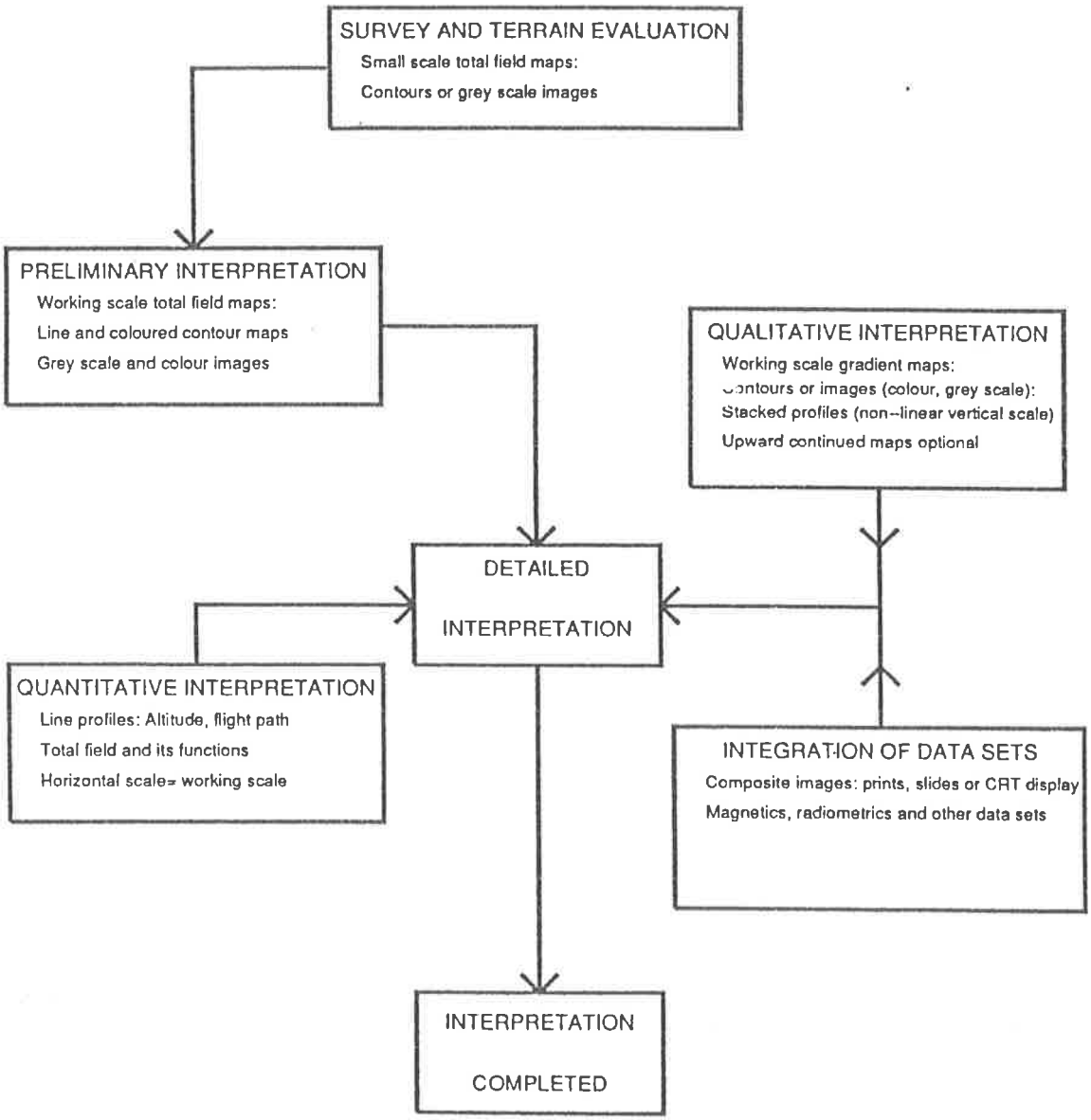

Figure 3.4: The flow chart links map requirements to stages in the interpretation process.

Where vertical gradient data have not been collected, it is possible to approximate both the one-dimensional (Paine, 1986) and the two-dimensional gradient using the profile and gridded total magnetic field data sets respectively. The computed one-dimensional gradient over horizons which are continuous, and whose strike does not parallel the flight path direction, compares favourably with the measured gradient over the same. The two-dimensional vertical gradient was computed from a 15×15 convolution operator supplied by T. H. Whiting.

Unlike the relatively smoothly varying total magnetic field which can be effectively displayed in many different formats, the dominance of high frequencies in the gradient data does not lend itself to clarity in contour map displays. This can be observed by comparing Figures 3.2 and 3.3. The map needs to be in colour to enable easy recognition of highs and lows (this is desirable in maps of the total field but indispensable in those of gradient data). Contouring algorithms designed to handle smoothly varying data cause a large number of closures to be drawn on gradient maps, and the choice of contour levels is restricted by the large order of magnitudes of gradient values. Images of the gradient avoid the problems associated with contouring the function. In any case, the two-dimensional computation introduces spurious anomalies. Stacked profiles of the vertical gradient are a much more satisfactory form of display (compare Figures 3.9 and 3.3) and will be dealt with in Section 3.2.

3.1.5 Interpretation stages

As the interpretation proceeds from the initial evaluation of the survey and terrain, through the various stages, to the final writing of the report, the map requirements of the interpreter varies. The flow chart shown in Figure 3.4 suggests a possible selection of displays at different stages in the interpretation process.

Survey and terrain evaluation

Once located data tapes are made available, the data should be represented as a small scale map of the total field. Gridding the data (either coarsely or on the final grid) and then plotting as a contour map is a good start. From this map, the interpreter will be able to judge whether the survey was flown successfully and the data correctly levelled and reduced. The map will also show what the magnetic terrain is like and the number and characteristics of different zones. This information is used to plan further displays. If the map indicates an unacceptable amount of noise (in the form of stripes, herringbone patterns...), additional processing to smooth and filter the data may be required. Poorly levelled and noisy data sets can be better displayed as pixel images rather than as contour maps.

Preliminary interpretation

The next stage involves the production of maps at a suitable working scale. Black and white contour maps of the total field are standard and relatively inexpensive compared to hard copies of digital images. The grid spacing should be intermediate between the nominal flight line and sample spacing — the closeness to the sample spacing will depend on the quality of the data. The scale of the map should be such that adjacent flight lines are less than 1 cm apart. A scale larger than this makes trend analysis difficult. Colouring the contour maps serves the dual purpose of promoting familiarity with the data and providing a display in which magnetic zones may be more easily identified. A photographically reduced coloured version of the contour

Figure 3.5: Colour composite image of total magnetic intensity (blue) and total gamma radiation count (red). The image was displayed on the AUDIA system (see Section 3.3.1) and photographically reduced and compiled. The colour scale is an increasing scale with light colours representing high values. Data for the lower right part of the study area was not available at the time the image was produced. The single most important advantage of using colour rather than grey-scales is that two or more data sets may be merged.

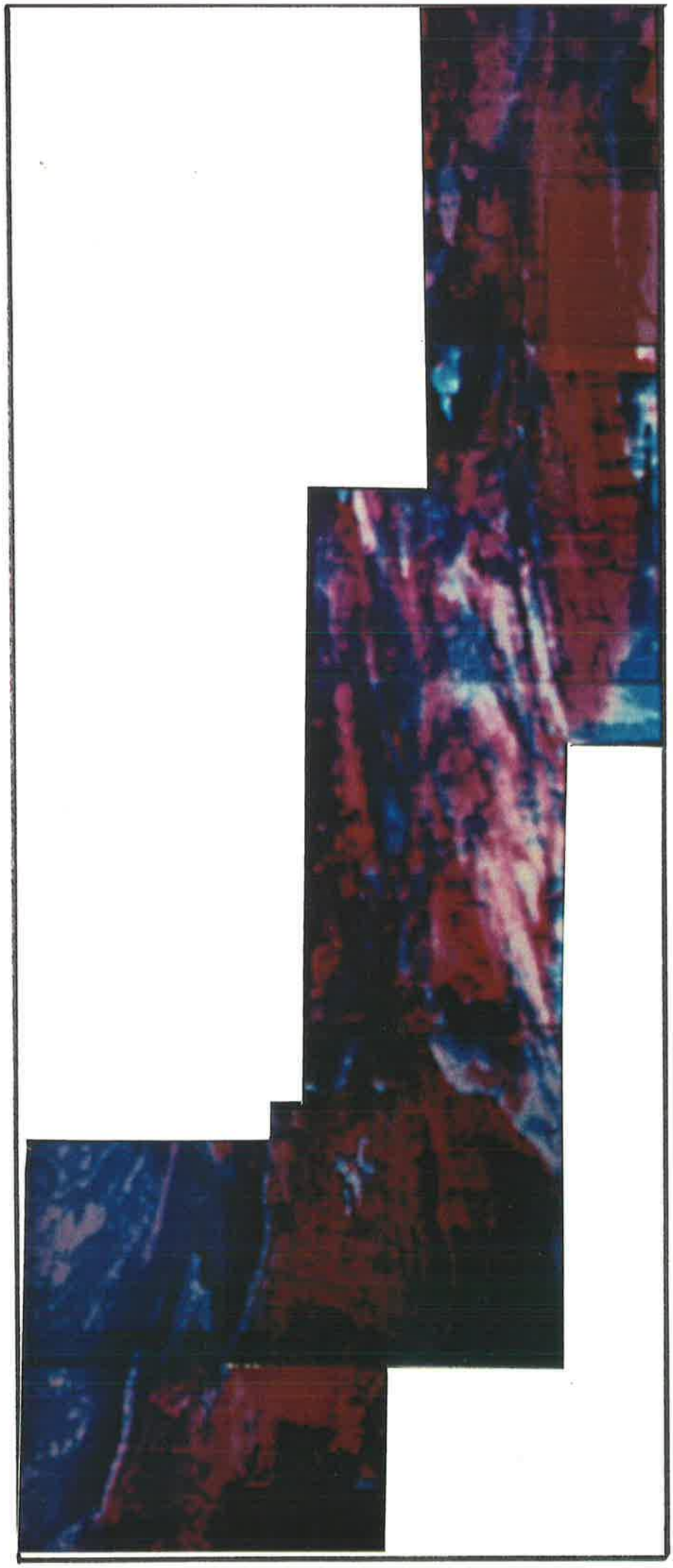

maps of the study area has been reproduced in Figure 5.4. The scale of the original maps was 1 : 50 000.

Detailed interpretation

At this stage, working scale maps of the total magnetic field, and possibly its vertical gradient and upward continued field, and of the geology are desirable. The frequency content of the data set and the aim of the interpretation are used to decide which displays are most suitable. If geological maps are available at scales larger than the working scale, then the interpreter may wish to produce magnetic maps at that same scale for easy comparison. Overlays of black and white geological maps are convenient to use. Stacked profiles of the vertical magnetic gradient (or some other derivative) can be used in trend analysis and mapping of magnetic horizons. Regional structural features may be delineated from enhanced digital images.

Quantitative interpretation

Side by side with maps for qualitative interpretation, the interpreter will need ready access to the recorded total field data, at a vertical scale suitable for quantitative interpretation. Modelling of anomalies is usually carried out on graphs of profiles of the total magnetic field, and these may be displayed on paper or on a graphics terminal connected to a computer. The graph for each line should display some combination of the following functions: the total magnetic field, the ground clearance, flight path, and perhaps functions of the total field such as its upward continued values and derivatives. Stacked profiles of the total field are not usually recommended: they take up too much paper, are cumbersome to handle and are unsuitable for trend analysis.

Integration of information

Overlaying maps on light tables is the conventional method of integrating geological and geophysical information. The difficulties associated with this method (mainly the problems of exact positioning and of comparing data collected at different scales and formats) can be overcome by using imaging techniques. Any data set which is available in digital form, or can be digitized (e.g. geological maps), can be integrated with aeromagnetic data through imaging.

Radiometric total count data integrated with total magnetic field data are presented in Figure 3.5. Such an image permits the visual correlation between the radiometric and magnetic properties of various rocks types. In this figure, a light pink (nearly white) colour characterizes rocks (migmatites and granites) which give rise to magnetic anomalies and radiometric highs. Such rocks are seen in the central portion of the figure. Light blue patterns indicate rocks which have a high magnetic anomaly associated with them but low radiometric count.

3.2 Stacked Profiles

Stacked profiles provide an alternative map display to contour maps and digital images. The most important difference is that no gridding of the data is required and therefore fidelity of the data can be maintained. Stacked profiles can be used to locate anomalies accurately, provide quality control on the survey, and present another perspective.

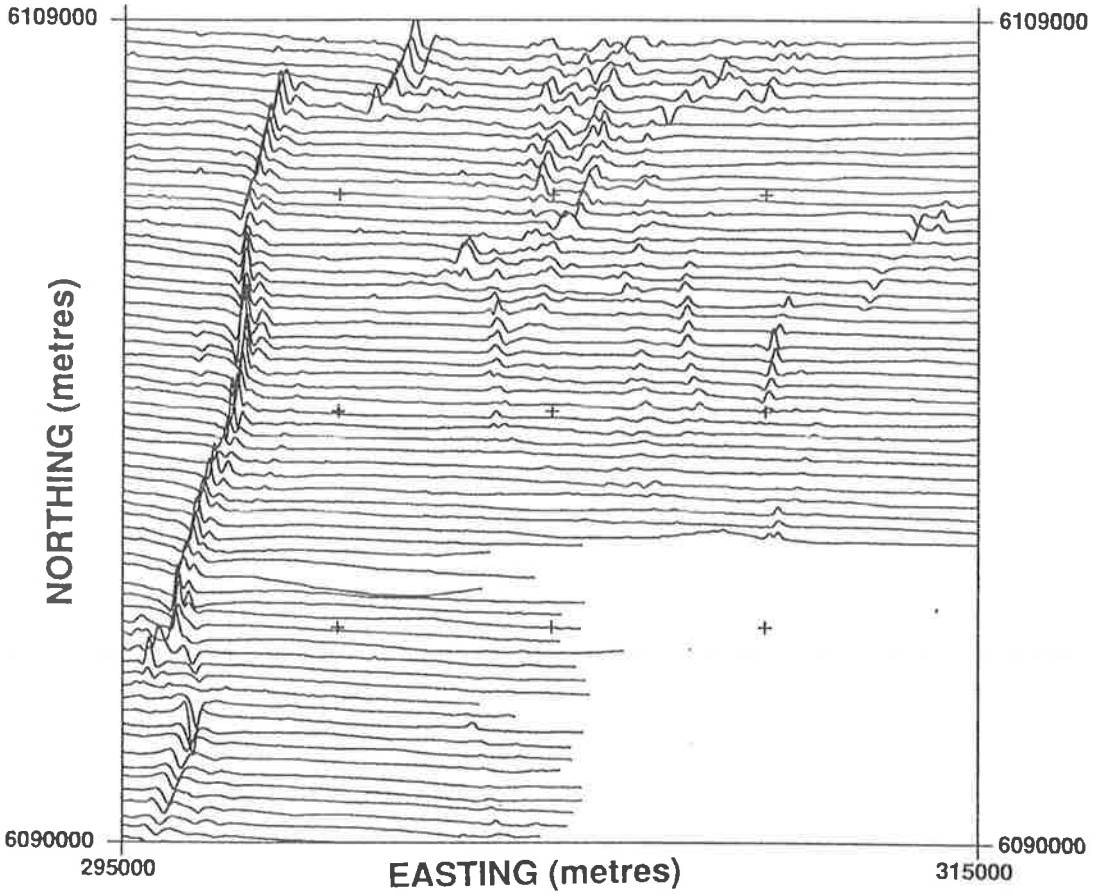

Figure 3.6: Stacked profiles of vertical magnetic gradient using a small vertical scale.

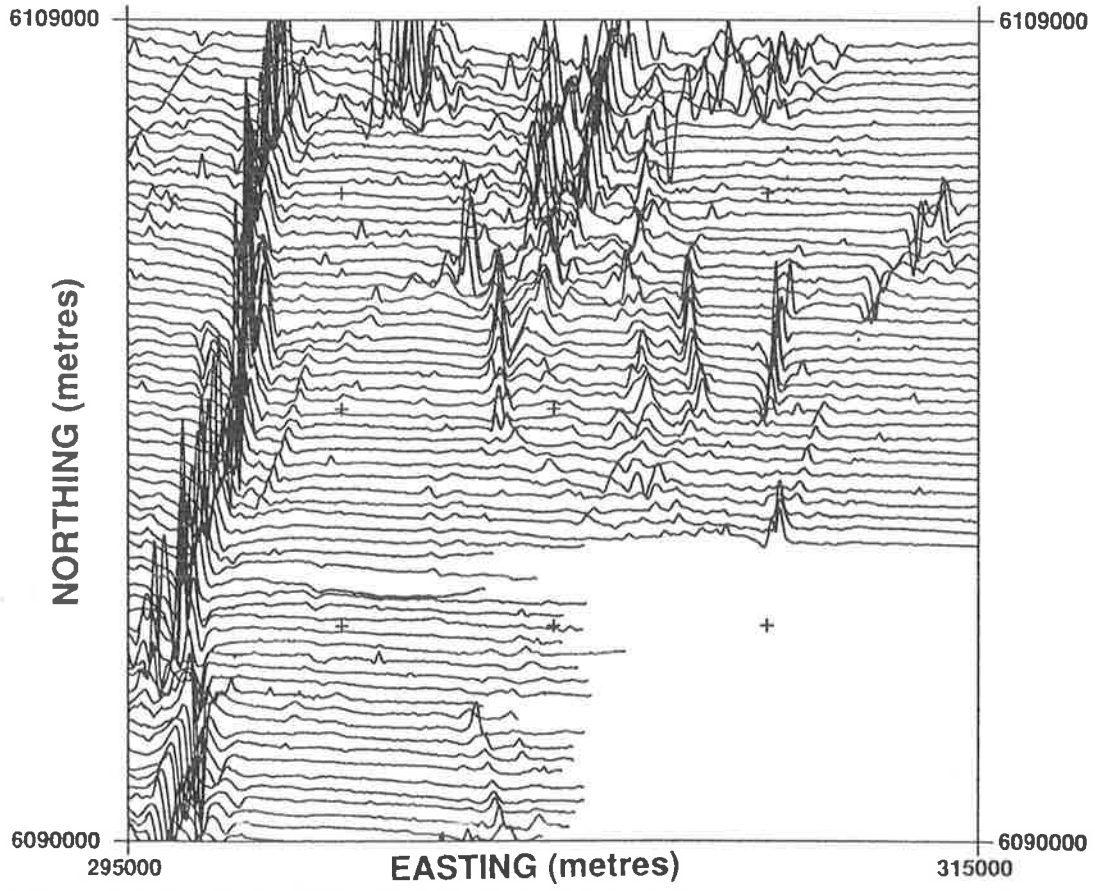

Figure 3.7: Stacked profiles of vertical magnetic gradient using a large vertical scale.

If the profiles are to be represented in a map format, then anomalies must be positioned accurately, anomaly shape preserved, and dynamic range reduced (McIntyre, 1981). The dynamic range of the total magnetic intensity precludes any possibility of identifying small and large order anomalies on the same map. In addition, stacked profiles of the total field often run into several map sheets because the vertical scale chosen causes a large shift from the base line. This shift makes it difficult to locate anomalies accurately on the map and makes such maps of little use in trend analysis.

The smaller dynamic range of derivative data, the greater resolution and isolation of anomalies, and the suppression of the regional combine to make stacked profiles of derivatives of the total magnetic intensity an extremely effective way of accurately displaying fine detail in aeromagnetic data.

Figures 3.6 and 3.7 demonstrate the problem of using linear scales to display the profiles. In both figures, the flight path is taken to be the base line, so that anomalies can be correctly located. In Figure 3.6, the use of a small scale means that while the small, possibly significant, anomalies are amplified, so are the larger amplitude ones, making the map very messy. In Figure 3.7, a larger scale is used — the presentation is clearer, but low-amplitude anomalies are obscured.

While a linear scale preserves the shape of the anomaly, it cannot be used to cope with the large dynamic range of vertical gradient (VG) data. Non-linear vertical scales are preferable to linear scales. One such non-linear operator, the square root operator, is extremely simple to apply. The square root of the absolute VG value, prefixed by the sign, is used instead of the VG. The results are shown in Figure 3.8. Comparison of Figure 3.8 and Figures 3.6 and 3.7 shows the improvement in the clarity and information content obtained through using a non-linear vertical scale. But, anomaly shapes have been distorted, and slopes of the flanks and the number of peaks, information that is crucial to the correlation of anomalies and to trend analysis, are no longer characteristic or distinctive.

An alternative non-linear amplifier, which has been used both in electronics and in the display of seismic data to handle precisely this problem of widely varying input signal amplitude, is the "Automatic Gain Control" or AGC amplifier. In the ideal AGC amplifier the gain of the amplifier varies with the amplitude of the input signal in such a way that the output amplitude is kept constant (Schilling, 1968).

By simulating the electronic amplifier digitally, AGC can be applied to discrete VG data. Within a window sliding along the profile, the root mean square (RMS) value is computed. The inverse of the RMS is taken to be the gain at the midpoint of the window, and thus the amplified value at every point along the profile is computed. This implies that for increasing RMS, gain decreases. To avoid the problem of infinite gain for RMS= 0, add the condition that for RMS = 0, gain = 0.

Along a profile, let

$$\begin{aligned} \text{input amplitude at the jth point} &= V(j) \\ \text{output amplitude at the jth point} &= AMP(j). \end{aligned}$$

Then, if the window length is (2n+1),

$$\text{RMS at the jth point} = \sqrt{\frac{\sum_{i=j-n}^{j+n} V^2(i)}{2n+1}}$$

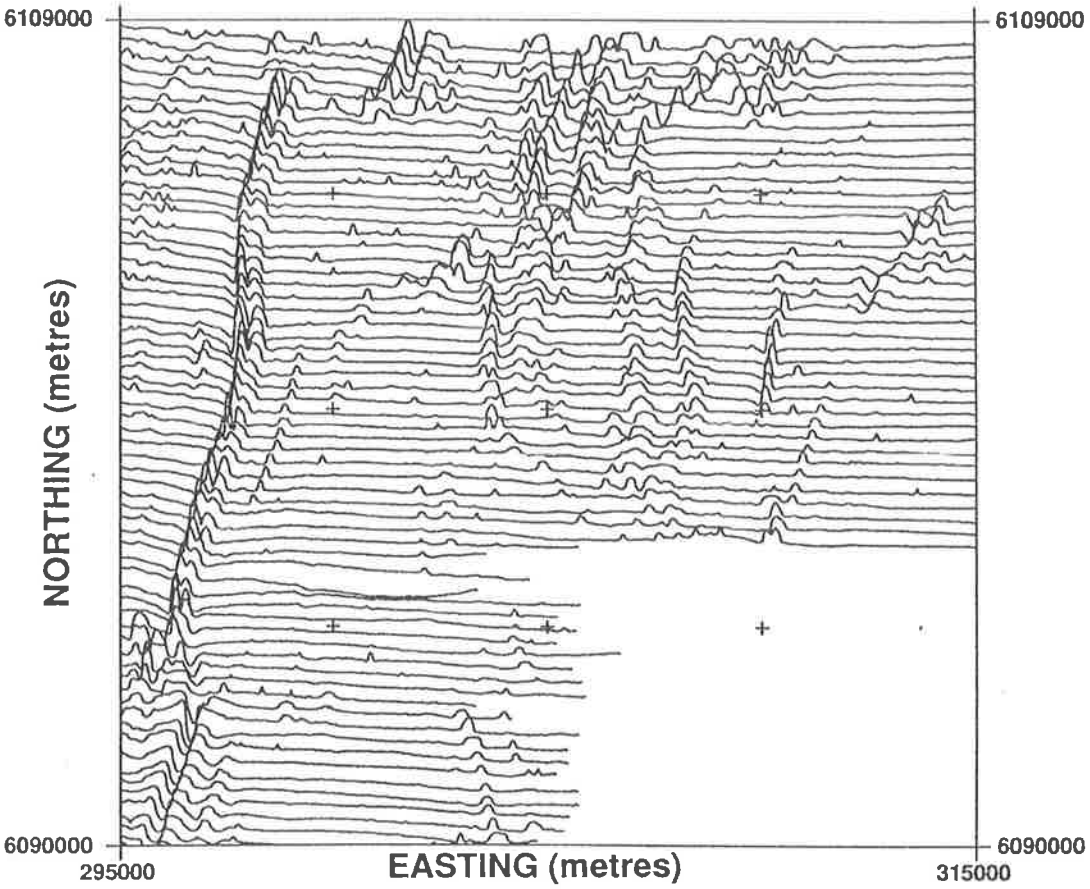

Figure 3.8: Stacked profiles of vertical magnetic gradient using a square root vertical scale.

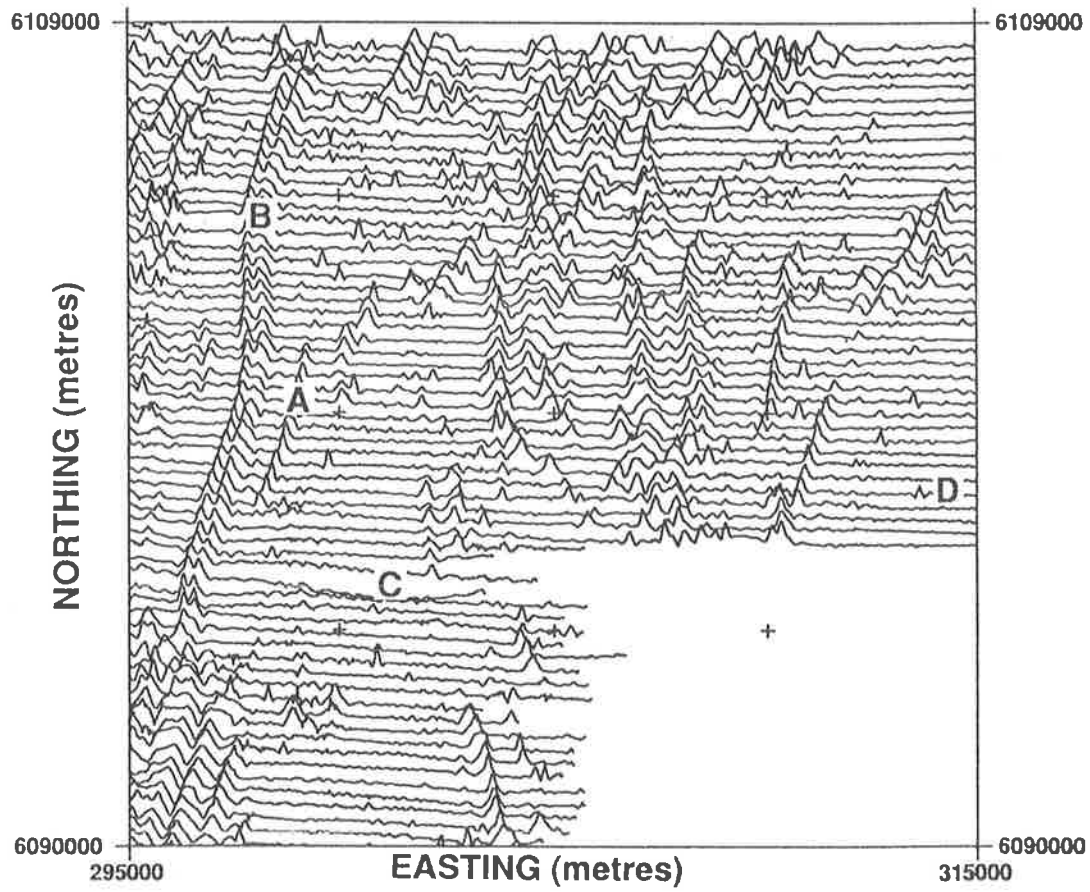

Figure 3.9: Stacked profiles of vertical gradient data amplified using Automatic Gain Control.

$$\begin{aligned} \text{gain} &= 1/\text{RMS} \\ AMP(j) &= V(j) \times \text{gain} \\ &= V(j)/\text{RMS}. \end{aligned}$$

Figure 3.10 shows three amplified profiles (using different window lengths) and the VG profile (sampled every 25 metres). The choice of the length of the window depends on the data set and the sampling interval and can be determined by experimenting with a few different lengths. In general, it must not be so narrow that all non-zero gradient values are amplified to ± 1, nor so wide that there would be loss of detail due to adjacent anomalies overlapping in the output. For an infinitely long profile, the use of an infinitely long window would result in the output being exactly equal to the original VG profile.

From Figure 3.10c it can be seen that for a window length of 15 data points (or 375 m), the dynamic scale has been reduced (thus permitting easy anomaly location), and the characteristic features of the anomaly shape has been reasonably preserved. Unlike a square root operator, the gain of an AGC amplifier varies with anomaly width. To determine the gain function, a model set of profiles was constructed using a discrete sine wave in the centre of each profile to represent a magnetic anomaly. Profiles were 2000 m long and sampled every 25 m. The amplitude of the sine wave in each profile was of unit amplitude, while the wavelength was varied from 100 to 1800 m. Figure 3.11 shows the variation in gain as a function of anomaly width. The AGC amplifier tends to act as a high-pass filter, but as there is little low-frequency information left in the VG data, there is no significant loss of information through amplifying. Noise and narrow anomalies tend to be prominent in the output making them easier to be identified as such. Also, the variation in gain with anomaly width is not significant at the scale at which the amplified profiles will be stacked and plotted as the AGC profiles are scaled linearly to fit between flight lines on the map to avoid profile overlap.

The data used to produce the contour maps in Figures 3.2 and 3.3 have been used to produce the map of stacked profiles shown in Figure 3.9. Using a window length of 15 data points, the vertical gradient profiles were amplified using AGC. The average value of the amplified gradient values along any single profile was used as the baseline for that profile. The original scale of the map was 1:50 000. Low-amplitude anomalies (marked "A") obscured in the total magnetic intensity map showed up clearly and anomalies could be easily correlated along strike. What first appeared to be wide bodies (marked "B"), turned out to made up of narrower magnetic units. The presentation was especially good for picking up linear features. Gaps in the data set ("C") were made obvious and anomalies could be positioned accurately. Single line, narrow anomalies, ("D"), which could be signal or noise, are isolated in the processing and can be quickly picked up by scanning the profiles, and checked against total magnetic intensity profiles. This map can be produced and reproduced easily.

In contrast, there is significantly more processing involved in contouring VG data than in producing stacked profiles. It should be noted here that the resolution observed in the stacked profiles comes through using the VG. If the VG contour map (Figure 3.3) and the stacked profiles (Figure 3.2) are compared, it is easy to see how much more information has been preserved in the stacked profiles and that the display is much better than the VG contour map. The stacked profiles show better resolution than the total magnetic intensity contour map and better display of information than the VG contour map and interpolation between flight lines is in the hands of the interpreter. However, where the strike of the anomaly is almost parallel to the flight path as well as in areas of tight folding, contour maps may be more helpful.

Vertical gradient data can be effectively displayed as stacked profiles by using Automatic Gain Control (Rajagopalan, 1987). The processing involved is simple and requires little computing

[1] See also Appendix K.

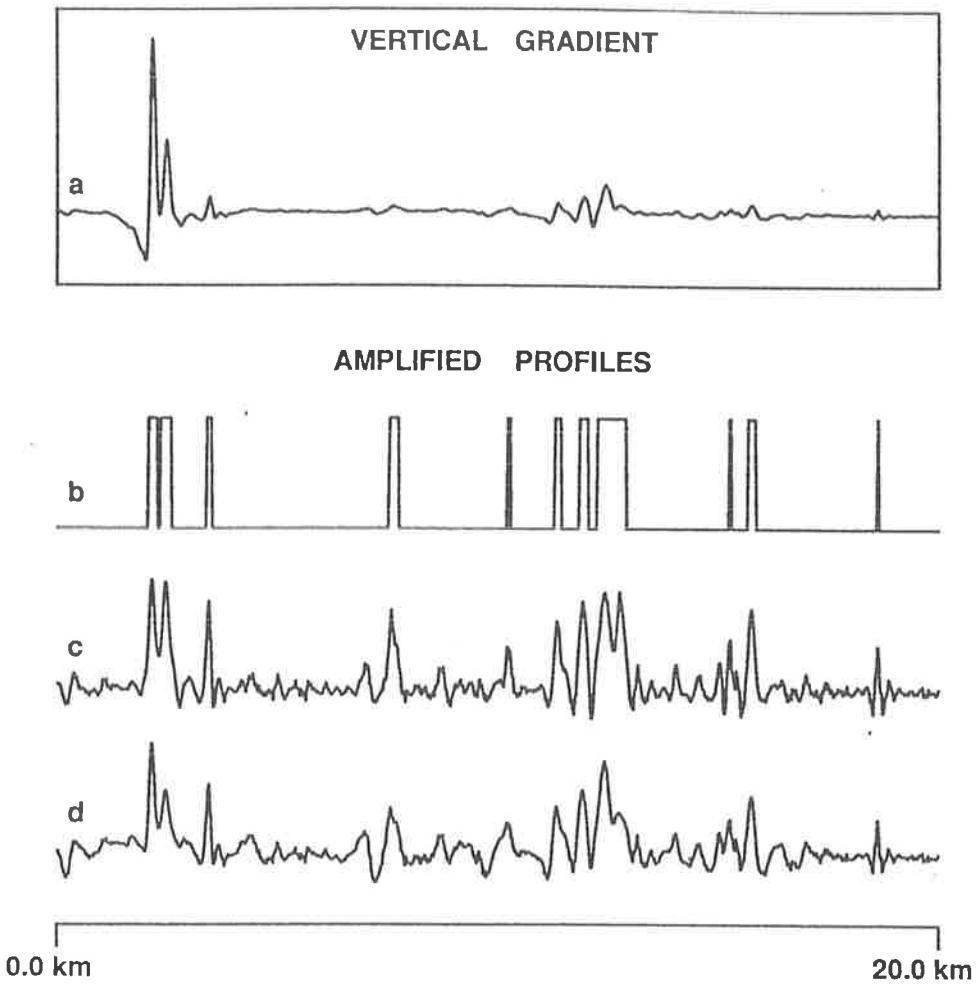

Figure 3.10: Vertical magnetic gradient profiles amplified using Automatic Gain Control. The figure shows the effect of using different window widths.

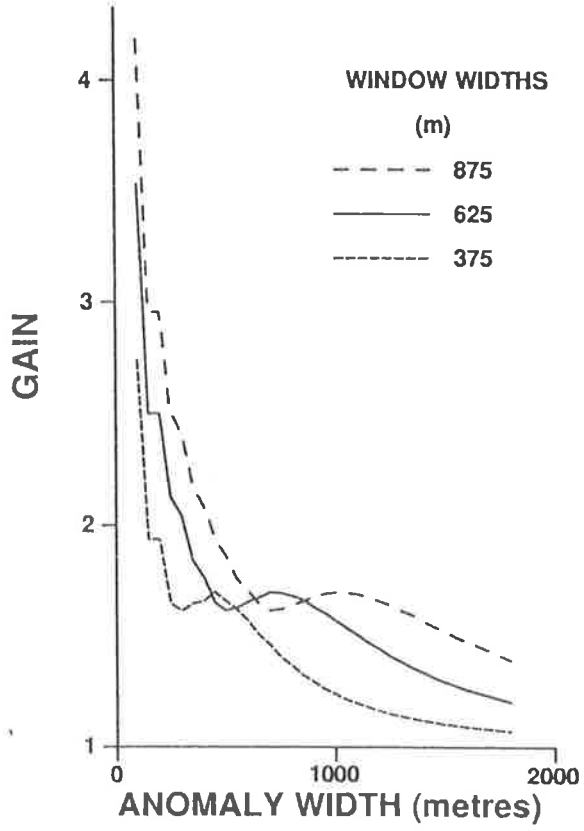

Figure 3.11: The gain of the AGC operator as a function of anomaly width.

time. The display is reasonably faithful to the original data set. The visual display is clear, making it possible for the interpreter to delineate trends, and in the process, to distinguish between signal and noise. The map of the profiles can be overlain on other maps and used, together with profiles and contour maps of the total magnetic intensity, to provide a more complete interpretation of aeromagnetic data.

3.3 Digital images

Imaging techniques have immeasurably improved the display and interpretation of gridded data sets. Techniques for digital image processing applied to LANDSAT data have been and can be extended to all geophysical data sets, including aeromagnetic and aeroradiometric data. Digital images can be produced from gridded data sets using an image processor and display device. Essentially, the gridded data set is defined to consist of pixels which are then mapped to an image where the colour or grey level of the image pixel is a function of the value of the grid pixel.

Digital image processing has a number of advantages: a wide range of data types and formats can be easily incorporated into the same image format for analysis, data collected at different scales or with different resolutions can be processed to a common map projection and scale, and most important of all, two or more data sets can be combined or merged into one display so that correlations can be readily identified (Guinness *et al.*, 1983). The different images may be integrated on a TV screen (or colour printer), by creating a colour composite image, by flickering between the different images registered over each other, or by using a split screen. The colour composite may be a simple "addition" where each of two or three data sets is assigned one of the primary colours, and the composite colour for any pixel is the addition of the primary colour intensities, or a more complex image may be created, where one data set is used to control the intensity and the other data set the hue of the colour for each pixel (see Guinness *et al.*, *op. cit.*).

The major interpretation advantages lie in the visual delineation of large scale features which might not have been recognized in other, more conventional, displays such as contour maps and profiles. Images are the most satisfactory form of displaying aeroradiometric data (see Smith, 1985) as the data set is inherently noisy and the signal to noise ratio is generally low. Digital processing enabled Kowalik and Glenn (1987) to make a direct comparison between LANDSAT and aeromagnetic data and improve structural interpretation. Similarly, Karner *et al.* (1987) have shown that "geotectonic images", formed by integrating British National Gravity and Topographic Data Bank with SEASAT derived gravity anomalies and with gridded bathymetric data, can benefit tectonic studies. Subtle structural associations with gold mineralization have been traced from images of magnetic data of the Yilgarn Province (Isles *et al.*, 1988).

One of the basic activities which constitute digital image processing is image enhancement. This includes increasing or decreasing the contrast, edge sharpening or smoothing, or, more simply, altering the image in some respect which facilitates the interpretation of its information content (Hord, 1982). The image contrast may be enhanced by stretching the histogram either linearly or non-linearly (histogram equalization). Further, the contrast may also be improved by using fewer grey levels than the maximum provided and thus mapping all grid values within a digital range to a specified grey level (density slicing). Linear features are formed by edges. Edges may be enhanced by using non-directional and directional filters. With non-directional filters, linear features in all directions get enhanced, maximum enhancement being obtained for edges parallel to either diagonal of the filter. Directional filters are used to enhance specific linear trends in an image. Usually, the analyst will run filters in different directions (e.g. N-S, NE-SW,

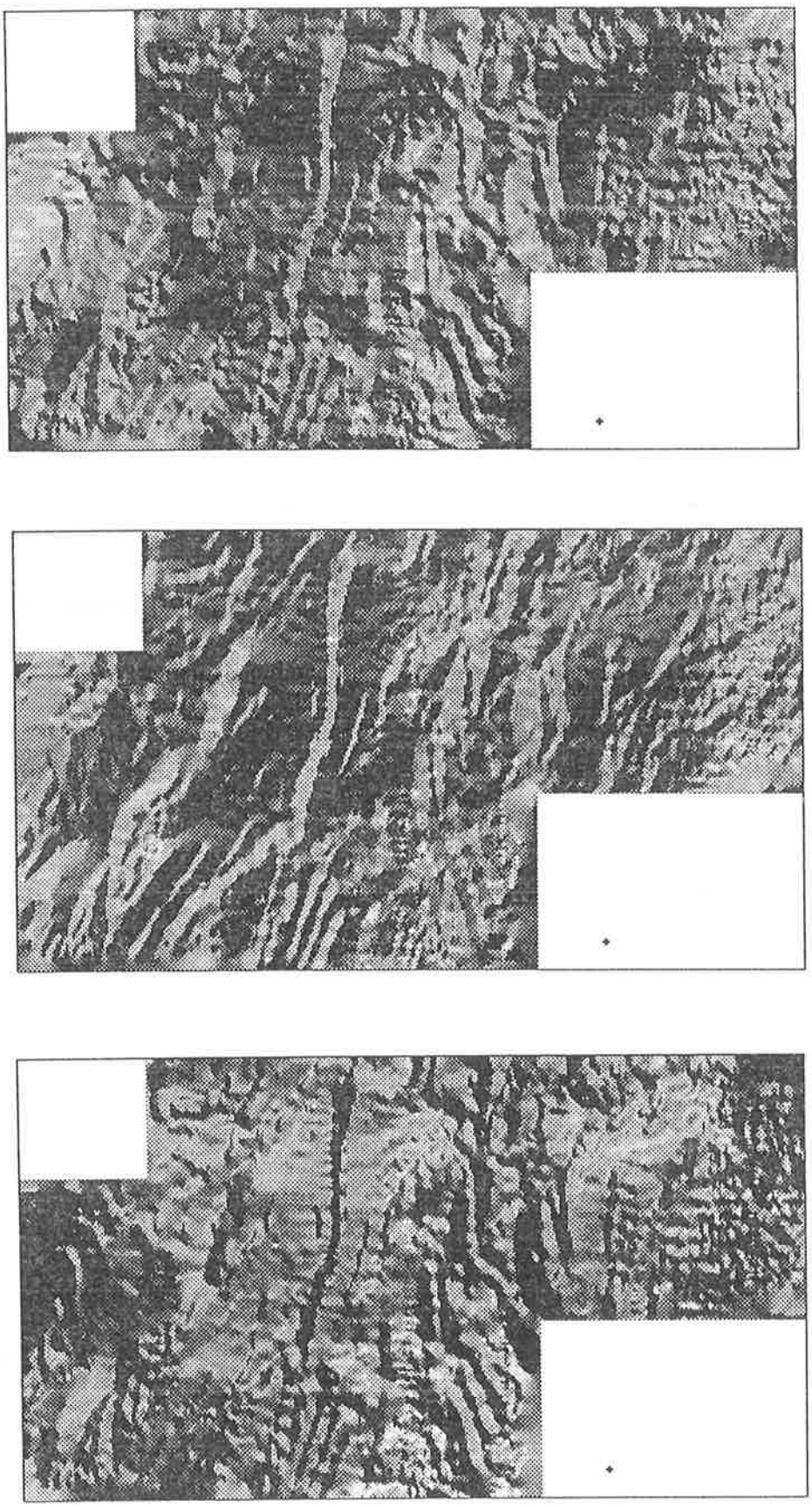

Figure 3.12: Grey-scale shaded-relief images of total magnetic intensity. The elevation and azimuth of the illuminating "source" is given for the three images from top to bottom: 15° and 225°; 30° and 135°; 45° and 45°.

NW-SE and E-W) and produce separate prints of each trend-enhanced image. Examples and use of these filters is described by Sabins (1987).

Especially when viewing extremely large data sets (covering areas of the order of hundreds of thousands of square kilometres), the digital image cannot be matched in its ability to display information in a comprehensible format. The coarseness of contour maps in comparison with the subtle features detected in images can be seen in maps of Canada presented by Dods *et al.* (1985). The maps include shaded-relief images. The impression received is akin to viewing an illuminated topographical surface. This effect is achieved because variation in light and shade is one of the depth cues required by the human eye to identify a three-dimensional shape (Horn, 1981). By this means the magnetic data acquires a "texture" and this texture reflects on the regional geology and is used to subdivide the region into magnetic terranes.

The technique for using light and shade in pictorial representation of three-dimensional shapes has been used by artists for many centuries. Horn (*op. cit.*) developed an algorithm which could simulate the effects of the illumination of a hilly region. The apparent brightness of a surface element depends on its local gradient. Complicating factors such as mutual illumination of surface elements and shading by neighbouring elements, which are in any case irrelevant to magnetic data, were not considered. The brightness of the pixel is taken to be proportional to the cosine of the angle between the direction of the illumination source and the surface normal. The brightness is primarily sensitive to the horizontal gradient in two orthogonal directions and is therefore similar to the horizontal gradient map.

As in directionally filtered maps, shaded relief maps can be varied to highlight trends in different directions. The variables in a shaded relief map are the azimuth and elevation of the illuminating source. The effect of varying the azimuth is similar to directional filtering. If the source is in the NW, then NW trends are suppressed relative to NE trends. If the source is shifted to the SE, the directional enhancement stays the same. But the maximum reflectance is shifted from northwest of the anomalous trend to southeast of it. Lowering the elevation of the source can be used to exaggerate the "terrain elevation" and to highlight subtle and/or weak magnetic features.

Weak but spatially coherent trends, and curvilinear and dendritic patterns can be more clearly delineated from digital images, particularly shaded-relief maps, than from more conventional displays (Chandler, 1985). Figure 3.12 shows a set of digital grey-scale images. The data set is common to most other figures in this chapter. The effect of varying the azimuth and elevation of the source is self evident.

3.3.1 Image display

Images are usually displayed on a TV screen connected to a computer, with hard copies produced only after the interpretation has been finished. The disadvantages are that these copies may be expensive to make. Also, while large scale structures and trends may be delineated easily on images, the positioning of these structures is easier on contour maps than on images. Low-amplitude and regionally restricted anomalies may be obscured on images through the using of only a few grey levels or colours (typically less than 16).

As imaging is often carried out on special purpose interactive processors connected to display systems which may be "ephemeral", e.g. cathode ray tube (CRT) screens, or "hard copy" such as ink-jet printers, the use of this powerful interpretive tool is generally limited to those who have access to dedicated image processing and display equipment.

```
/cm {2.54 div 72 mul}     def              % define cm in terms of points
/T {translate}            def              % set up basic definitions
/M {moveto}               def
/D {lineto}               def
/H {/Helvetica findfont} def
/S {scalefont setfont }   def
/xcentre {stringwidth 0 mul exch 2 div neg exch rmoveto} def

1.00 setlinewidth
20.00 cm  1.00 cm T                        % translate origin
90 rotate                                  % rotate page by 90 degrees

5.88 cm 14.50 cm M      H  10  S
(TOTAL MAGNETIC FIELD)   xcentre
(TOTAL MAGNETIC FIELD)      show           % print legend

gsave

/picstr  236 string def                    % string to hold image data
11.75 cm  13.50 cm scale                   % map image to rectangle
                                           %  (11.75 cm by 13.5 cm)
236 271 8                                  % columns & rows in image
[236 0 0 271 0 0]                          % data format
{currentfile picstr readhexstring pop}     % read image data from source
image                                      % execute image operator

ffffffffffffffffffffffff ...               % image data written out as
48646464809cb8d4d4d4d4f0f0 ...             % 127912 hex digits

grestore

showpage                                   % print page description
```

Figure 3.13: Part of a typical PostScript page description used to print a grey-scale image. The phrases preceded by the % sign are comments explaining the code.

Images used in this thesis have been produced in two different ways. Initially, aeromagnetic and aeroradiometric data were displayed on AUDIA, the University of Adelaide's LANDSAT imaging system developed by J. Willoughby and adapted by him to image geophysical data. Different combinations of the total magnetic intensity and its two-dimensional vertical gradient, and the available radiometric data were integrated as colour composites and these were used to constrain structural and lithologic interpretation. Images of individual fields could be viewed separately. The integration of aeromagnetic and aeroradiometric data was considered particularly useful and a composite image is shown in Figure 3.5.

With the acquisition of a laser printer, it became possible to produce grey-scale images, at different scales and directionally enhanced, on paper (Rajagopalan, in press). Imaging can be carried out on non-dedicated main frame or micro computers connected to a suitable output device which may be a laser printer or bit-mapped screen. The requirements include a gridded data set, image processing software which would describe the image in PostScript and a PostScript output device. PostScript, a registered trademark of Adobe Systems Incorporated (1987), is a simple interpretive programming language with powerful graphics capabilities. The language is device independent and a program in the language can be created or composed using a program in any other language (FORTRAN, MODULA-2...) or with a text editor. A program in PostScript basically describes a display — this is known as a page description. Such a page description can be converted into a display by presenting it to a PostScript interpreter controlling a raster-scan display screen or a laser printer.

Digital images can be easily described in PostScript using the "image" operator (Reid, 1988). The image operator is the mechanism in the PostScript language for printing sampled images of any size. A maximum of 256 grey levels are available. These images may be printed at any size and orientation with a minimum of calculation. The image operator takes data representing an image made up of many small samples and renders it on the current page at a specified location, size, and rotation. The data represents an image which is a certain number of samples wide and high (represented herein by the width and height respectively). Each sample is represented by a one-, two-, four-, or eight-bit value which assigns a shade of grey to that sample. Each sample will eventually be printed as a black, white or grey rectangle on the output page. (Colour PostScript devices will have additional operators to implement full colour images).

I wrote the software[1] to produce colour and grey-scale images. The conversion of a gridded data set to an image is carried out in two stages. At the first stage, the histogram of the input grid is computed. Where survey boundaries are non-rectangular, grid values outside the survey limits are replaced by a dummy value. A number of image-enhancement filters are available: directional filtering, edge enhancement, and artificial illumination (or shaded-relief). (Separate programs were used to compute derivatives of the total field.)

The output from the first program is still a gridded data set. The data could be "coloured" and written to tape in LANDSAT format for display on the AUDIA system. Alternatively, the data can be "grey-scaled" and printed on a laser printer as follows.

The gridded data set is converted at the second stage into a PostScript description (part of a typical page description is shown in Figure 3.13). At this stage, the user must specify the following: the scale at which the image is to be printed, legends to accompany the image (map title, x and y axis titles), and the choice of grey levels.

The grey-scale options can match an increasing "blackness" to increasing field values, or vice versa, or assign arbitrary grey intensities to different ranges of field values. The histogram

[1]These programs and others used to process and present aeromagnetic data are stored in the geophysics computer library at the University of Adelaide.

produced at the first stage is meant for use as a guide to scaling. The number of grey levels which can be used is theoretically 256 though the number which can be comfortably resolved by the human eye is closer to 40. The resolution of the Apple LaserWriter used to produce the images used in this thesis (300 dpi — dots per inch) limited the grey levels to 17 or less (including black and white).

The output at the second stage is a PostScript file which can be sent to a laser printer. Some examples of the different kinds of images which can be produced are shown in Figure 3.12, and in Plates 3 and 4. These demonstrate the considerable improvement obtained by applying image-enhancement techniques.

3.4 Presentation of aeromagnetic interpretation

The final result of aeromagnetic interpretation is usually presented in the form of one or more maps and an accompanying report. The scale of the interpretation map corresponds to the scale of the survey and particularly to the nature of the interpretation. In this thesis, the choice of scale lay between 1:50 000 and 1:100 000. Though the first was the working scale, by using the second scale the individual maps were more manageable and could be spliced to form a single map (Plate 1). Geological maps for the region are only now becoming available at 1:50 000 and since they will also be available at 1:100 000, it should be possible to compare Plate 1 with mapped geology.

The presentation depends on local conditions (geological and magnetic terrane) and on the results obtained. Final results are often presented in the form of a map showing contours of depth to basement, magnetic highs and lows, faults, fold axes, and model positions and parameters (Whiting, 1987). The relation between delineated magnetic axes and local geology is not often straightforward, and while such maps present the information effectively, they are not always comprehensible to geologists. In the study area, the near-complete absence of recognizable deep-seated magnetic sources has made it simple to relate interpreted magnetics directly to near-surface geology.

In this thesis, the interpretation has been presented superimposed on profiles of amplified (AGC) vertical gradient data (Plate 1) at a scale of 1:100 000. By this means, the gradient profiles are accessible to future interpreters of the region. Significant magnetic marker units have been outlined. The outlining of the magnetic markers has been based mainly on trend analysis and anomaly characteristics. In the interests of clarity, not every anomaly could be highlighted. So it is useful that the fine detail which is inherent in the high-resolution aeromagnetic data can still be seen in Plate 1.

The magnetic marker units were coloured according to the accepted stratigraphy (Manck-telow, 1979). While this made the map more comprehensible, it also leaves it open to the risk of being outdated if the stratigraphy were to be revised. However, as mentioned above, in most cases, the interpretation of the markers was based on magnetic considerations and it is only the colouring that is dependent on the stratigraphy. The results of quantitative analyses are included in Appendix I and Appendix J.

Chapter 4

Vertical magnetic gradient analysis of two-dimensional magnetic sources

4.1 Introduction

Quantitative analysis of magnetic anomalies involves the determination of the parameters (depth, thickness, dip, depth extent, strike extent, magnetic susceptibility contrast and magnetization) of the magnetic source. The magnetic signature of the main study area is characterized by numerous anomalies caused by magnetic bands within dipping metasediments. A preliminary interpretation revealed that the majority of magnetic sources were linear to curvilinear, and that depths appeared to be near-surface. Though many techniques for interpreting anomalies caused by two-dimensional sources exist, the parameter usually determined is the depth. Since the majority of magnetic sources appeared to be near-surface, knowledge of the dips of the metasediments would be of great use in structural interpretation.

Graphical methods were used on total magnetic field and vertical gradient anomalies and selected profiles were modelled on computer using GAMMA[1]. The techniques presented in this chapter were used to provide quick depth and dip estimates for two-dimensional sources.

4.1.1 Modelling algorithms

The two most common models which have been successfully applied in magnetic interpretation are the prism and dyke models. Numerous techniques have been devised to solve for the parameters of the total magnetic field anomalies due to these sources (for a review see Åm, 1972). These methods can be grouped into graphical and computer methods. Despite the simplicity of the dyke model, no one technique can be applied to all cases with a reasonable degree of accuracy (Åm, *op. cit.*). Part of the problem is due to imperfect resolution caused by interference from neighbouring magnetic sources and part is due to the errors involved in assigning a simple geometrical model to a complex geological structure.

The parameter estimates obtained from the use of standard techniques on the total magnetic field anomaly can be improved by interpreting the gradient anomaly as well. As has been demonstrated in the previous chapter, the vertical gradient has a number of advantages over

[1]The forward modelling algorithm GAMMA was written by Dr. J. W. Paine of the University of Adelaide.

δ = dip ($0° < \delta < 180°$)

ϕ = strike of the sheet with respect to magnetic north ($0° \leq \phi < 180°$)

T = intensity of the Earth's magnetic field

L = inclination of the Earth's magnetic field ($-90° \leq L \leq 90°$)

$\lambda = \arctan \dfrac{\tan L}{\sin \phi}$

V = vertical gradient of the total field

R = strength of the remanent magnetization (if any)

Q = Koenigsberger ratio $= \dfrac{R}{\kappa T}$

N = inclination of the remanent field ($-90° \leq N \leq 90°$)

C = strike of the remanent magnetic field with respect to magnetic north ($0° \leq C < 180°$)

$\nu = \arctan \dfrac{\tan N}{\sin(\phi - C)}$

M = inclination of the resultant field ($-90° \leq M \leq 90°$)

B = strike of the resultant magnetic field with respect to magnetic north ($0° \leq B < 180°$)

$\mu = \arctan \dfrac{\tan M}{\sin(\phi - B)}$

$\Omega = \sqrt{1 + Q^2 + 2Q(\sin L \sin N + \cos L \cos N \cos C)}$

$\theta = \lambda + \mu - \delta - 90°$

$\Gamma = 2\kappa T \dfrac{\sin L \sin M}{\sin \lambda \sin \mu} \Omega$

Figure 4.1: Nomenclature for symbols used in Chapter 4.

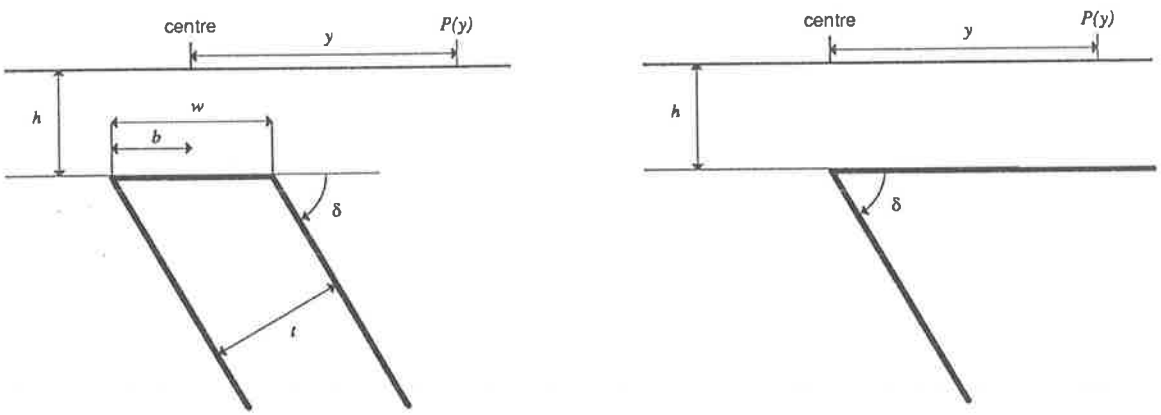

Figure 4.2: Geometry of the thick dyke and edge models.

the total field: resolution is improved, near-surface anomalies are enhanced, and much of the regional field is removed.

In contrast to the abundance of total field interpretation methods, there are few methods directed at the interpretation of gradient data. Those which are available, (Rao and Prakasa Rao, 1970; Nabighian, 1972; Rao *et al.*, 1972; Atchuta Rao *et al.*, 1981), generally require both horizontal and vertical gradient data. Nelson (1988) outlines some techniques which may be applied to total gradient anomalies.

As part of the interpretation procedure used in this thesis, stacked profiles of the one-dimensional vertical gradient were used in visual interpretation (Section 3.2). The aeromagnetic survey data interpreted in this thesis did not include vertical gradient measurements. Therefore the one-dimensional vertical gradient was computed from total magnetic field profile data using a quadrature filter (differencing interval: 4, sampling interval: 1) developed by Paine (1986). For two-dimensional sources, Paine (*op. cit.*) has shown that the approximated gradient (computed by convolution or Fourier analysis) compares favourably with the theoretical gradient. Since profiles of the computed vertical gradient were available and had proved very useful in qualitative interpretation, the next obvious stage was to see whether they could be used for quantitative interpretation as well.

4.1.2 Geometrical models

The geometrical models which have been used in this thesis are the dipping dyke, horizontal edge, prismatic polygon and isolated pole. Vertical cross sections through the dipping dyke and horizontal edge model are shown in Figure 4.2.

The prismatic polygon model is similar to the dipping dyke model in that it has infinite strike extent. However the vertical cross section is polygonal. Such a model allows for a non-horizontal top and non-parallel sides. The prismatic polygon model was only used during forward modelling on the computer.

The isolated pole model is used to model chimney or pipe-like structures. It represents a steeply dipping dipole whose cross section is small compared to its length, so that the lower pole has negligible effect on the measured magnetic field. This model was used in modelling deep basement features.

The models for which techniques are presented here are the dipping dyke (thin and thick) and the edge models. The thin sheet or thin dyke is a special case of a dyke whose width $\ll$ depth. The principal profile is taken to be perpendicular to the strike of the magnetic source. Note that the eastern end of the profile (or the northern end for $\phi = 0°$) is considered positive, and that the dip is to be measured from this end. The parameters of all three models include the depth h, full width w, dyke centre y_0, dip δ, strike ϕ and susceptibility contrast κ. The strike extent and depth extent are assumed to be infinite.

The strike angle, ϕ can be easily determined from contour maps or maps of stacked profiles. The dyke centre y_0 of thin dykes can be located using Werner's (1953) midpoint method. The nomenclature used in this chapter is given in Figure 4.1.

4.1.3 Vertical gradient analysis

The characteristic points which were best resolved on vertical gradient anomalies were the maxima and minima. Inflexion points were poorly defined. The zero-level of the anomaly could be identified in most cases. Simple graphical techniques to interpret thin dykes, thick dykes and the edge model are presented in this chapter. The methods rely on the identification of the maximum, minimum and zero-level of the anomaly and can be quickly and objectively applied. They are similar to Richards (1967) methods for interpreting the total magnetic field anomaly caused by a thin dyke in that the characteristic points used are the maximum and minimum field values and their locations.

The effect of the dip on the shape of the anomaly cannot be separated from the effect of the resultant magnetization. Unless the resultant magnetization is known or can safely be assumed to be induced only, it is not the dip which can be determined independently but the index parameter, θ. The index parameter is a function of the direction of magnetization, and the dip and strike of the sheet (Gay, 1963). For all three models, the vertical gradient field can be separated into the product of an amplitude term and a "shape" term. The amplitude term is a function of the intensity and direction of magnetization, and of all the parameters of the model. The shape term controls the shape of the anomaly. For the thin dyke and edge it is a function of the index parameter and depth, and for the thick dyke it is a function of the index parameter and the width to depth ratio.

Taking h to be positive downwards, the vertical gradient (denoted by V) may be defined as the negative differential of the total field F with respect to depth. Thus $V = -\partial F/\partial h$. By differentiating this equation twice with respect to y, the distance of an observation point along the profile, the locations and values of the maxima and minima can be determined. The maximum and minimum gradient values are defined to be $V_{\max}$ and $V_{\min}$ respectively and they are located at $y_{\max}$ and $y_{\min}$. For the thin dyke and edge models, these values can be described by exact analytical expressions. The thick dyke anomaly can have a maximum of five peaks, and this complicates the solution of the peak positions and values. The equations for the total magnetic field and its vertical gradient over the models are presented in Figure 4.3.

The location of the main minimum with respect to the main maximum on a principal profile can indicate the direction of dip of a dyke model. Provided that the Q factor is small or that the remanent magnetization is in the same direction as the induced component, the direction of the line joining the minimum to the maximum is the direction of dip; i. e. if the dyke strikes NS and the minimum is to the east of the maximum, then the dyke dips towards the west.

The following sections describe the theory and method for the interpretation of the thin dyke, thick dyke and edge models. The accuracy of the approximated vertical gradient constrains the accuracy of the parameter estimates. Error analysis for the interpretation of the thin dyke has been carried out.

4.2 Interpretation of thin dyke anomalies

Equation 4.4 gives the total magnetic field due to a thin sheet at any point $P(y)$ along a principal profile where y is measured from the centre of the dyke. The equation has been adapted from Gay's (1963) and Hood's (1964) equations defining the magnetic anomalies due to dykes. Demagnetization has been ignored.

$$F_{thindyke} = \frac{\Gamma t}{h^2+y^2}[h\cos\theta + y\sin\theta]. \tag{4.4}$$

$$V_{thindyke} = -\frac{\Gamma t}{(h^2+y^2)^2}\left[y^2\cos\theta - 2hy\sin\theta - h^2\cos\theta\right]. \tag{4.5}$$

$$F_{thickdyke} = \Gamma\sin\delta\left[\sin\theta\ln\frac{(y+b)^2+h^2}{(y-b)^2+h^2} + \cos\theta(\arctan\frac{y+b}{h} - \arctan\frac{y-b}{h})\right] \tag{4.6}$$

$$V_{thickdyke} = -\Gamma\sin\delta\left[\frac{2h\sin\theta-(y+b)\cos\theta}{(y+b)^2+h^2} - \frac{2h\sin\theta-(y-b)\cos\theta}{(y-b)^2+h^2}\right] \tag{4.7}$$

$$F_{edge} = \Gamma\sin\delta\left[\frac{\sin\theta}{2}\ln(y^2+h^2) + \cos\theta\arctan\frac{y}{h}\right] \tag{4.8}$$

$$V_{edge} = \frac{\Gamma h\sin\delta}{y^2+h^2}[y\cos\theta - h\sin\theta] \tag{4.9}$$

Figure 4.3: Equations for the total magnetic field and its vertical magnetic gradient over the thin dyke, thick dyke and edge models.

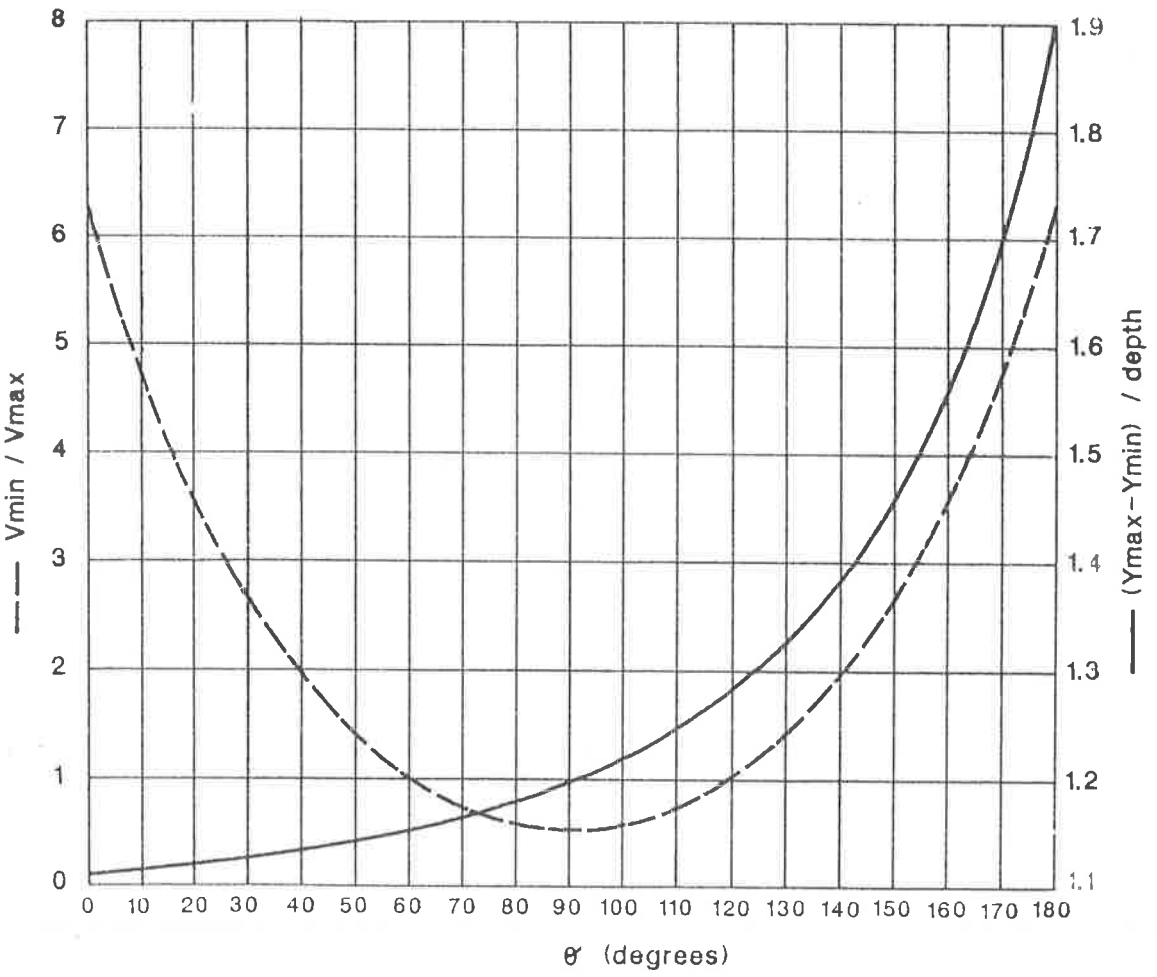

Figure 4.4: Nomogram to determine parameters of a thin dyke model.

The vertical magnetic gradient, given in equation 4.5, is obtained by differentiating Equation 4.4. The main maximum and main minimum of this equation have been determined by differentiation for the two cases outlined below. The mathematics is simple and has therefore not been presented here.

When $\cos\theta = 0$, the gradient anomaly has one minimum and one maximum and is antisymmetrical. The location of the peaks, y_1 and y_2, are given by $y_1 = +h/\sqrt{3}$ and $y_2 = -h/\sqrt{3}$. The gradient values are given by V_1 and V_2 where

$$V_1 = V(y_1) = (3\sqrt{3}/8) \times (\Gamma t \sin\theta/h^2)$$

and

$$V_2 = V(y_2) = -V_1.$$

V_1 is equal but opposite in value to V_2. It represents a maximum or a minimum depending on the value of $\sin\theta$.

For non-zero values of $\cos\theta$, the vertical gradient has three peaks: a minimum on either side of a maximum, or vice versa. Defining $p = \tan(\theta/3)$, these three peaks can be shown to be located at

$$\begin{aligned} y_1 &= hp \\ y_2 &= h(4p + (1+p^2)\sqrt{3})/(1-3p^2) \\ y_3 &= h(4p - (1+p^2)\sqrt{3})/(1-3p^2). \end{aligned}$$

Both $V_{\min}$ and $V_{\max}$ are non-zero and finite for all values of h, θ, and κ. In general, $y_{\min}$ and $y_{\max}$ are functions of θ and depth alone and of the form $h \times \psi(\theta)$ and $V_{\min}$ and $V_{\max}$ are functions of Γ, t, θ and depth and of the form $(-\Gamma t/h^2)\chi(\theta)$. Therefore if $V_{\text{ratio}} = |V_{\min}/V_{\max}|$ and $\Delta_y = (y_{\max} - y_{\min})$, then

$$V_{\text{ratio}} = \chi_1(\theta), \tag{4.1}$$

$$\Delta_y = \psi_1(\theta), \tag{4.2}$$

$$V_{\max} - V_{\min} = -\frac{\Gamma t}{h^2}\chi_2(\theta). \tag{4.3}$$

The nomogram shown in Figure 4.4 was drawn up by computing the ratios V_{ratio} and Δ_y/h for values of θ varying from 0° to 360° in steps of 1°. It was found that both V_{ratio} and $|\Delta_y/h|$ were symmetrical about 180°. The nomogram was then plotted for V_{ratio} and $|\Delta_y/h|$ against θ, for θ varying from 0° to 180°. When Δ_y is negative, take the true value of θ to be $(360° - \theta)$.

From the anomaly, V_{ratio} and Δ_y can be measured. The value of θ most appropriate to the value of V_{ratio} and the sign of Δ_y is estimated from the nomogram and used to estimate the value of $|\Delta_y/h|$. Since Δ_y is known, the depth can be easily determined.

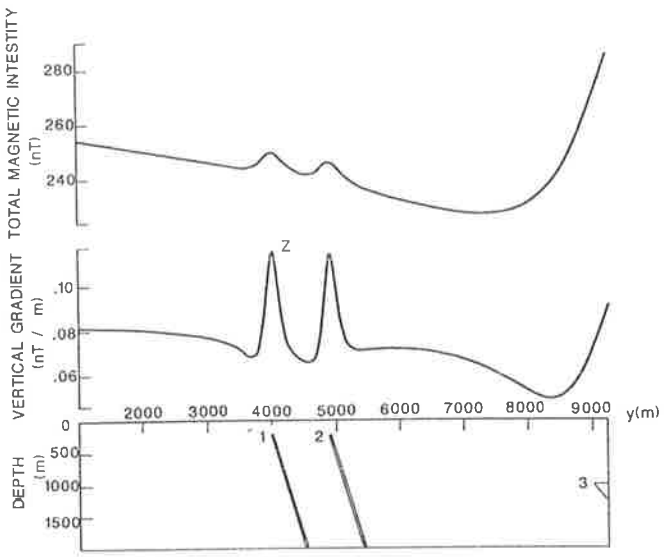

Figure 4.5: Total magnetic field intensity and its vertical gradient over a model consisting of two thin sheets (denoted by 1 and 2) and an edge (only part of which is seen in the figure and is denoted by 3).

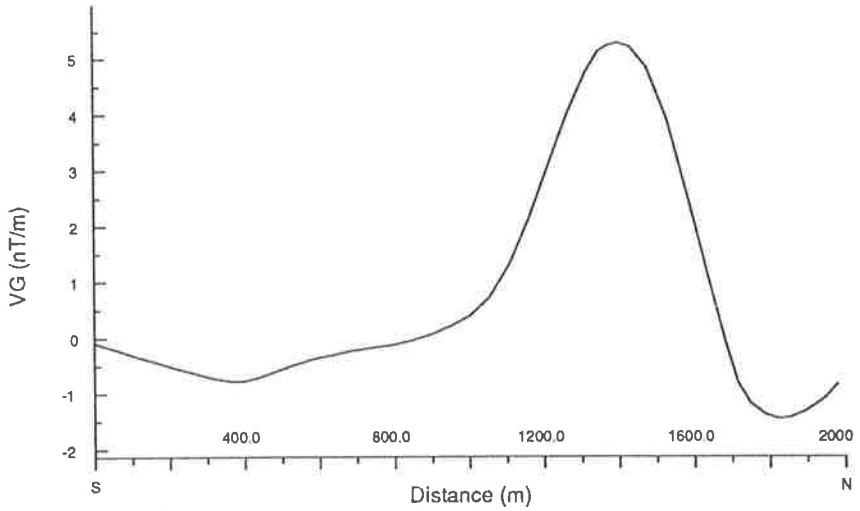

Figure 4.6: Vertical gradient profile from the eastern part of the White Lake region, Canada (after Barongo, 1985).

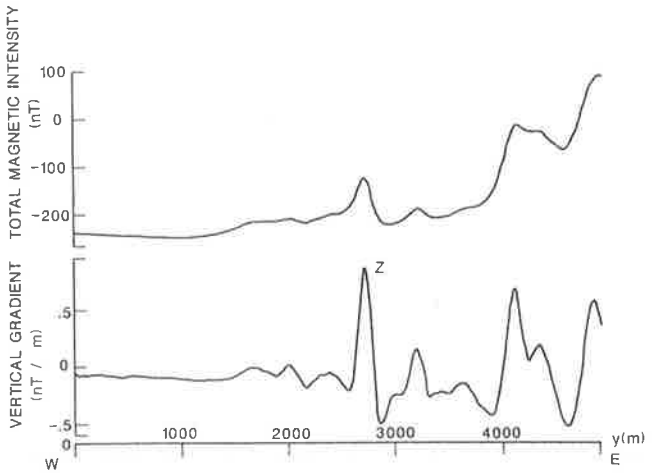

Figure 4.7: Measured total magnetic field intensity and the computed vertical gradient along an E-W profile over the Kanmantoo Trough, South Australia. The interpreted anomaly is denoted by Z.

The method assumes that the profile is perpendicular to the strike of the dyke and that β, the acute angle between the profile and the strike, is 90°. Correcting the depth estimate for $\beta \neq 90°$ can be achieved by multiplying the depth estimate by $\sin\beta$.

In Equation 4.3, the function $\chi_2(\theta)$ lies between 1.125 and 1.299. As a first approximation, the amplitude of the vertical gradient anomaly should give an estimate of $(-\Gamma t/h^2)$. Alternatively, the amplitude may be divided by 1.2. When the magnetization is either known or can safely be assumed to be induced only, Γ/κ can be computed from the equation given for Γ in Figure 4.1. The depth, h, has previously been determined, so the product of susceptibility and thickness, κt can be estimated. Note that the computed vertical gradient may need to be scaled to match the true gradient and this scaling factor can be determined using model data.

Tables of the relation between V_{ratio} and $|\Delta_y/h|$ as functions of θ were also printed (see Appendix G) and it was found that it was quicker to interpret an anomaly using the tables than by checking the nomogram.

4.2.1 Experimental results

The method has been tested on three anomalies. The first represents a theoretical gradient anomaly, the second a measured gradient anomaly and the third was obtained by filtering observed aeromagnetic total field data.

Theoretical example

Figure 4.5 shows the total field and vertical gradient (anomaly Z) due to a thin sheet whose parameters are given by: $h = 215\,\text{m}$, $\phi = 0°$, $\delta = 73°$, $Q = 0$, $\kappa = .001\,\text{SI}$, $t = 22\,\text{m}$. The model is located at $y = 4000\,\text{m}$. An edge model ($h = 1000\,\text{m}$, $\phi = 0°$, $\delta = 45°$, $Q = 0$, $\kappa = .001\,\text{SI}$, $y = 9000\,\text{m}$) has been added to simulate the effect of a regional field, as well as another thin sheet (parameters as for the first sheet, $y = 4900\,\text{m}$) to demonstrate the difficulty in resolving closely-spaced total field anomalies. The intensity of the Earth's magnetic field is taken to be 60 000 nT and its inclination to be −65°. The results of the interpretation are given in Table 4.1. The estimated parameters compare very well with the model parameters and the error in the estimates is minimal.

Measured gradient anomaly

Interpreting observed rather than theoretical anomalies gives similar results. Part of a vertical gradient profile taken from a vertical gradient survey flown by the Geological Survey of Canada over the White Lake region, Canada, (Barongo, 1985), is reproduced in Figure 4.6. Using the maximum and minimum amplitude points, the depth was estimated to be 309 m, θ to be 330°. Barongo (*op. cit.*) computed the depth to be 326 m. If the inclination of the earth's field is assumed to 70° and remanence is ignored, then the dip may be computed from the estimate of θ. This turns out be 80° and though no dip estimate has been made by Barongo (1985), he does mention that the dykes are near-vertical.

Parameter	True value	Estimated Value
Depth	215 m	220 m
Dip	73°	70°
θ	17°	20°
Γ	2168 m	2057 m

Table 4.1: Results of interpreting the models shown in Figure 4.5.

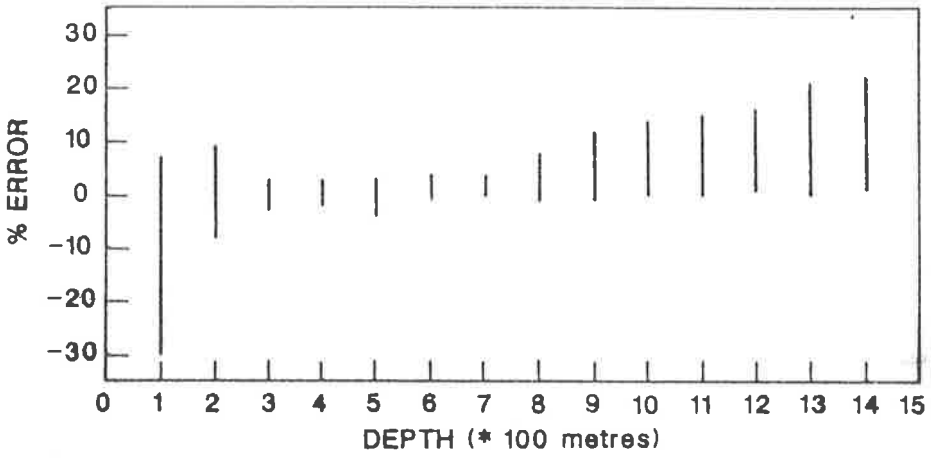

Figure 4.8: Error in the depth estimate (the depth was varied from 60 to 1500 metres).

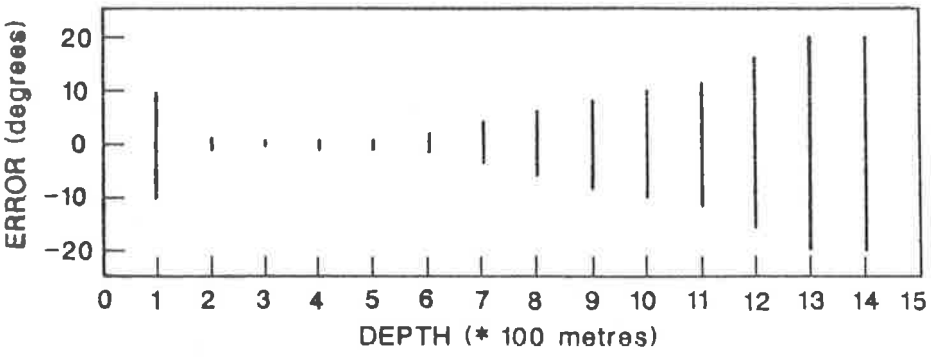

Figure 4.9: Error in the estimate of θ (the depth was varied from 60 to 1500 metres).

Computed gradient anomaly

Part of a total field profile and its computed gradient is reproduced in Figure 4.7. The magnetic anomaly Z can be correlated with a pyrite bearing quartzite (strike $\phi = 5°$) which has been folded into the Monarto Syncline (Mancktelow, 1979). Using stacked profiles of the vertical gradient, this magnetic unit can be followed for over 30 km, and easily traced around the fold of the syncline. A drill hole, located 3.5 km north of Z, intersected bedded layers of sulphides (containing both magnetite and pyrrhotite) within the quartzite, at a depth of 30 metres.

The anomaly Z was interpreted to be due to a thin sheet at a depth of 116 m below the sensor, with an index parameter $\theta = 319°$ and $\Gamma = 15360$. Taking the average sensor height to be 80 m gives the depth below ground surface to be 36 m. Assuming no remanent component, the dip was estimated to be $44°W$ and 0.16 m to be the product of the susceptibility and thickness. The depth estimate is reasonably accurate, considering the undetermined extent of weathering and the shallow depth involved, and while the dip estimate could not be verified, it was consistent with the general dips in the area. Measured susceptibilities vary from 100×10^{-5} SI to 1000×10^{-5} SI. The corresponding thicknesses would then vary from 160 to 16 metres.

4.2.2 Error analysis

Vertical gradient profiles computed from the measured one-dimensional total magnetic field over two-dimensional structures are reasonably accurate when the depth to the top of the source lies between Δ and 10Δ, Δ being the product of the differencing interval and the sample spacing (Paine, 1986). When computed gradient anomalies are interpreted, errors in the gradient values result in inaccurate parameter estimates.

To study the effect of filtering errors on parameter estimates, a FORTRAN program was written to carry out the error analysis for a wide range of parameter (depth and θ) values. The theoretical total field anomaly over a thin sheet was computed for different values of θ and depth, using a sample spacing of 25 metres and with the origin of the model as a sample point. The profiles were taken perpendicular to strike. The vertical gradient was computed from the total field as described in Section 4.1.1.

The errors in the estimates were defined as follows:

$$\begin{aligned} \text{error}_h &= 100 \times (\text{true depth} - \text{estimated depth}) \,/\, \text{true depth} \\ \text{error}_\theta &= \text{true } \theta - \text{estimated } \theta \,. \end{aligned}$$

Depths were varied from 60 m to 1500 m while θ was varied from 0° to 180°. For each depth value the vertical gradient anomaly was interpreted, parameter estimates recorded, and errors computed. The errors varied both with depth as well as θ and for a given depth, varied widely with θ. For each depth value, the minimum and maximum errors in the parameter estimates were used in drawing Figures 4.8 and 4.9.

Where depth to the top of the sheet is $\leq \Delta$, there is a lot of "ringing" in the computed gradient and the accuracy in the estimated depth varies with θ and the error can be as much as 80%. For depth = Δ, the error in depth estimates can go as high as 30%, but is generally within 10% error. For depths between 1.6Δ and 8Δ, depth estimates are well within 10% error and estimates of θ within 6° error. For depths $\geq 9\Delta$, the peaks tend to flatten out and accuracy decreases. Where the origin is not a sampling point, the nearest sampling point can be at

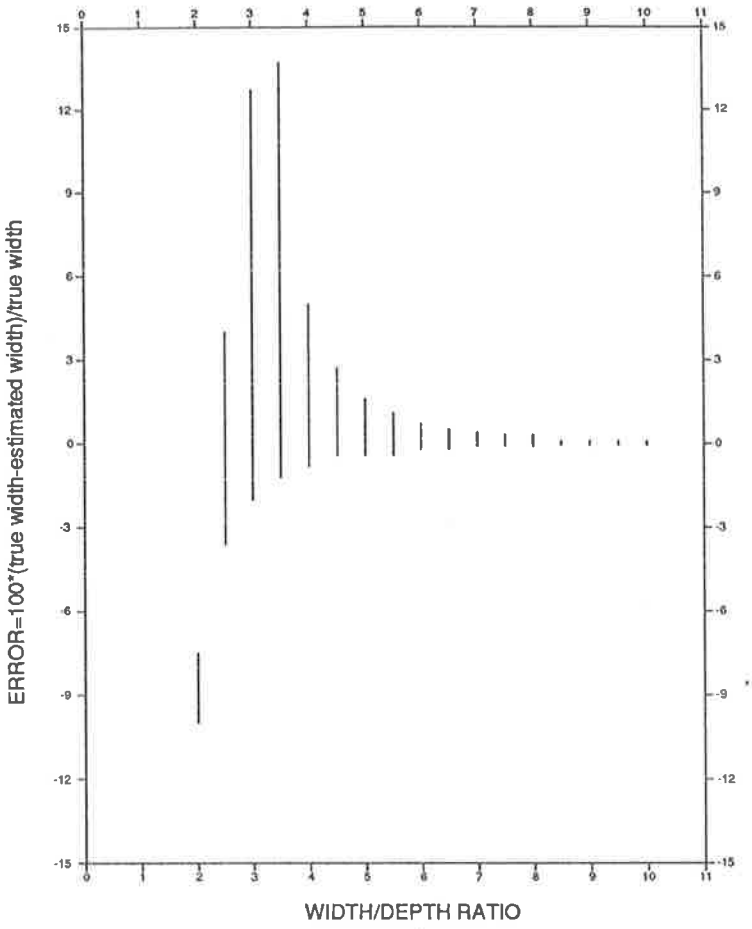

Figure 4.10: Error in using Δ_y as a width estimator of a dyke anomaly.

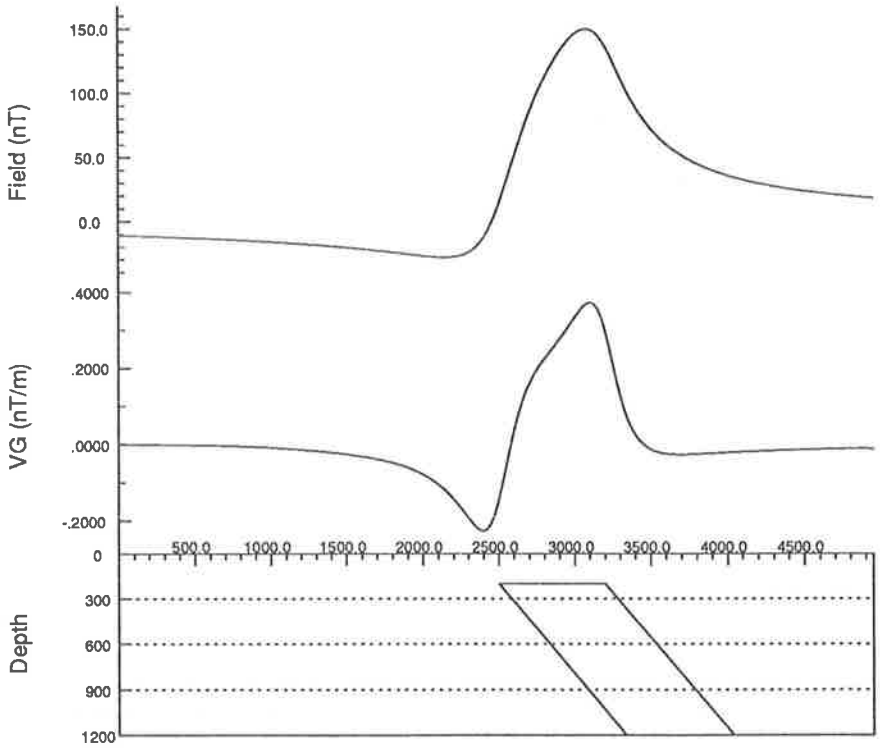

Figure 4.11: Total magnetic field intensity and its vertical gradient over a thick dyke: (Dyke_1).

the most 12.5 metres away. There is no significant change in the parameter estimates and for $1.6\Delta \leq \text{depth} \leq 8\Delta$, accuracy is still within acceptable limits.

The accuracy in parameter estimation in using the nomogram on the computed gradient is dependent on the accuracy of the gradient values. These values are reasonably accurate for two-dimensional structures when the depth to the top lies between Δ and 10Δ, Δ being the product of the differencing interval and the sample spacing. Depth estimates are well within 10% error provided that the true depth lies between 1.6Δ and 8Δ. Estimates of θ are accurate to a few degrees over a wider range of true depth values.

4.3 Interpretation of thick dyke anomalies

The equations for the total magnetic field and its vertical gradient over a thick dyke are given in equations 4.6 and 4.7. As the width to depth ratio of a dyke increases, the number of peaks on its vertical gradient anomaly increases from two to five. The original aim in solving for characteristic points on the gradient anomaly was to find relationships between the peak values and locations which would yield all the parameters of the model. Since peak values could not be described by analytical expressions, they were calculated by forward modelling. The theoretical gradient was computed for model dykes: the width to depth ratio was varied from .5 to 10 in steps of .5, and θ was varied from 0° to 360° in steps of 5°. A computer program was written to search the gradient anomalies for the peak values and positions. As before, the main minimum is V_{min} and the main maximum V_{max}. The distance between the peak positions of V_{min} and V_{max} along the profile is defined to be Δ_y.

The initial ratios which were investigated were vertical ratios (ratios of different combinations of the peak values) and horizontal ratios (ratios of the profile distance between different peaks to Δ_y. No satisfactory width to depth estimator was found. However, the analysis showed that for the dykes investigated:

1. Δ_y is a good width estimator for all values of θ provided that the width to depth ratio is greater than or equal to 2. The error bars in Figure 4.10 indicate the maximum possible errors.

2. Δ_y/h and $V_{\text{ratio}} = |V_{\text{min}}/V_{\text{max}}|$ are complicated functions of the dyke parameters. If the width to depth ratio can be determined by some other method, then V_{ratio} is unique for a given value of θ. Once θ is known, the depth to the top can be determined using the appropriate value of Δ_y/h. The two main sources of error in estimating depth and θ arise from the inaccuracies in the approximation of the vertical gradient and in the estimation of the width to depth ratio. Note that if the anomaly is symmetric, then V_{min} is taken to be the most westerly (or southerly) minimum and V_{max} is the most easterly (or northerly) maximum.

This method was tested on two dykes. Figures 4.11 and 4.12 show the total field and vertical gradient anomaly caused by two different dykes. The intensity of the Earth's magnetic field is taken to be 60 000 nT and its inclination to be $-65°$.

The width to depth ratios for each dyke were determined using Barongo's (1985) "straight slope" method. Tables for the V_{ratio} and Δ_y as functions of the width to depth ratio (these are included in Appendix G) were used to compute the width, depth and θ and the results are given in Table 4.2. The correct determination of the width to depth ratio is critical to the success of

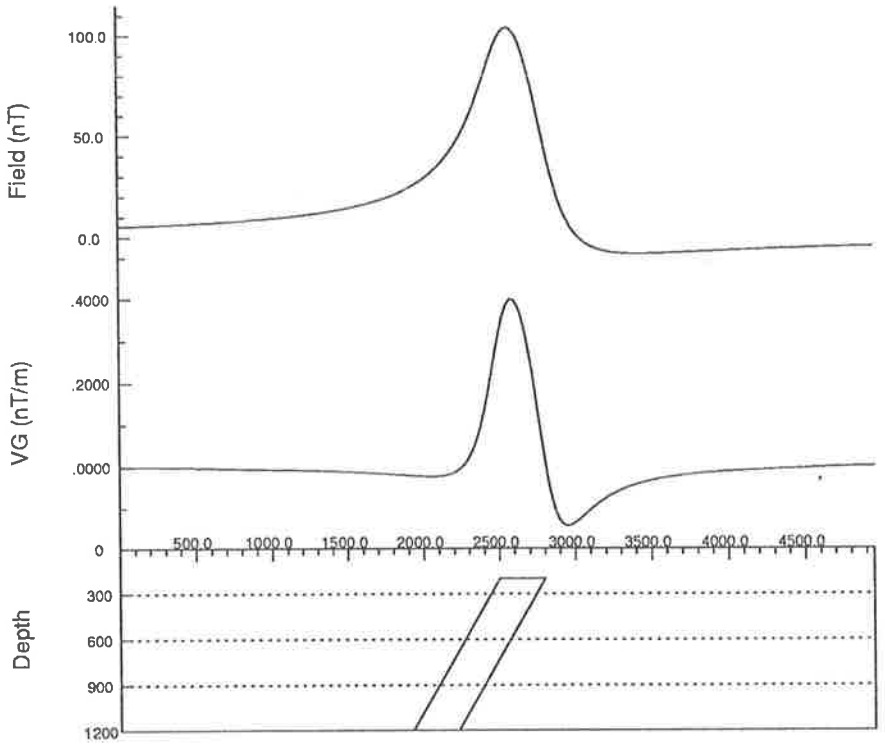

Figure 4.12: Total magnetic field intensity and its vertical gradient over a thick dyke: ($Dyke_2$).

Parameter	Dyke1		Dyke2	
	True value	Estimated Value	True value	Estimated Value
Strike	0°		0°	
Depth	200 m	225 m	200 m	178 m
Width	700 m	675 m	300 m	266 m
θ	40°	45°	30°	30°
Dip	50° E	45° E	60° W	60° W

Table 4.2: Results of interpreting the models shown in Figures 4.11 and 4.12.

the method, particularly to the depth estimate. The estimate of θ is less sensitive to errors, and for wide dykes the distance between the major minimum and maximum is an excellent width estimator.

4.4 Interpretation of edge anomalies

The vertical gradient anomaly over an edge or contact can be quite simply interpreted in terms of the depth and θ. The vertical gradient anomaly has two peaks for all values of θ except 90° and 270°. When $\cos\theta = 0$, the vertical gradient anomaly consists of a single maximum or minimum. The minimum and maximum values and their locations can be represented by simple, analytical solutions.

$$y_{\min} = \frac{h}{\cos\theta}[\sin\theta + 1]$$

$$y_{\max} = \frac{h}{\cos\theta}[\sin\theta - 1]$$

$$V_{\min} = -\frac{\Gamma \sin\delta\cos^2\theta}{2h(1-\sin\theta)}$$

$$V_{\max} = \frac{\Gamma \sin\delta\cos^2\theta}{2h(1+\sin\theta)}.$$

The ratios V_{ratio} and Δ_y/h are functions of the depth, h, and θ only and are given by:

$$V_{\text{ratio}} = \left|\frac{1+\sin\theta}{1-\sin\theta}\right|$$

$$\frac{\Delta_y}{h} = \left|\frac{2.00}{\cos\theta}\right|.$$

The values of the above ratios have been computed for θ varying from 0° to 360° in steps of 5°. The graphs of the two ratios as functions of θ are displayed in Figure 4.13. For angles between 180° and 360°:

$$V_{\text{ratio}}(180° + \theta) = 1/V_{\text{ratio}}(\theta)$$

$$\frac{\Delta_y}{h}(180° + \theta) = \frac{\Delta_y}{h}(\theta).$$

As $\cos\theta \longrightarrow 0$, the vertical gradient anomaly displays only one peak, either a minimum or a maximum, and the method breaks down. The zero-level of the vertical gradient anomaly cannot always be correctly obtained and usually only one peak is distinctly defined. Figure 4.14 shows a model edge which has been interpreted and the results presented in Table 4.3.

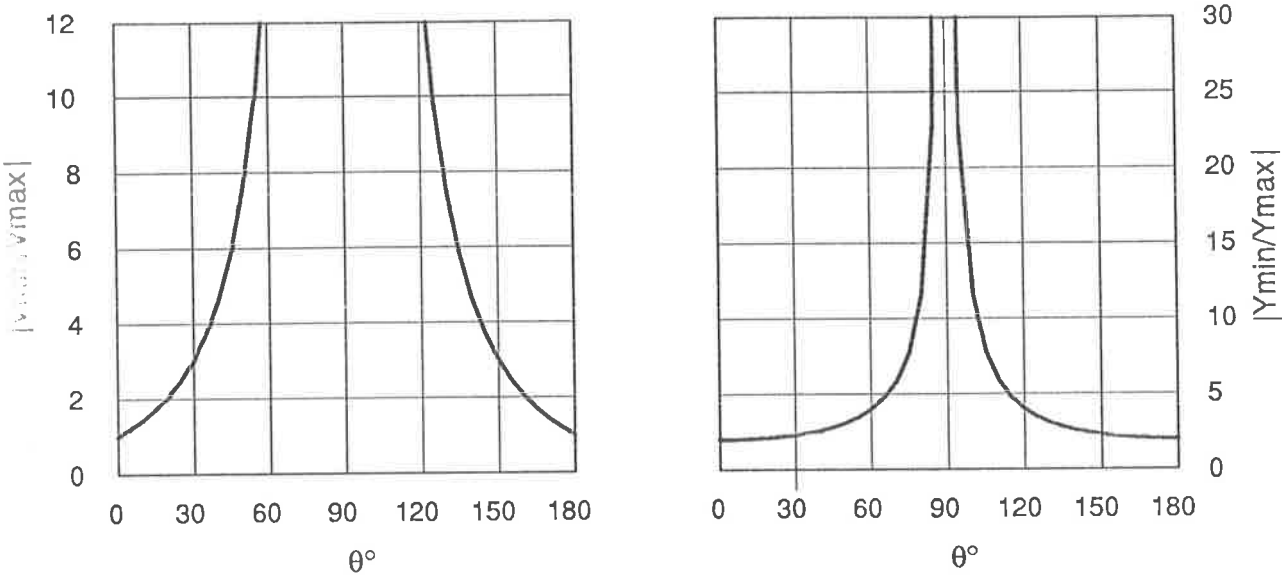

Figure 4.13: Nomogram to determine parameters of an edge model.

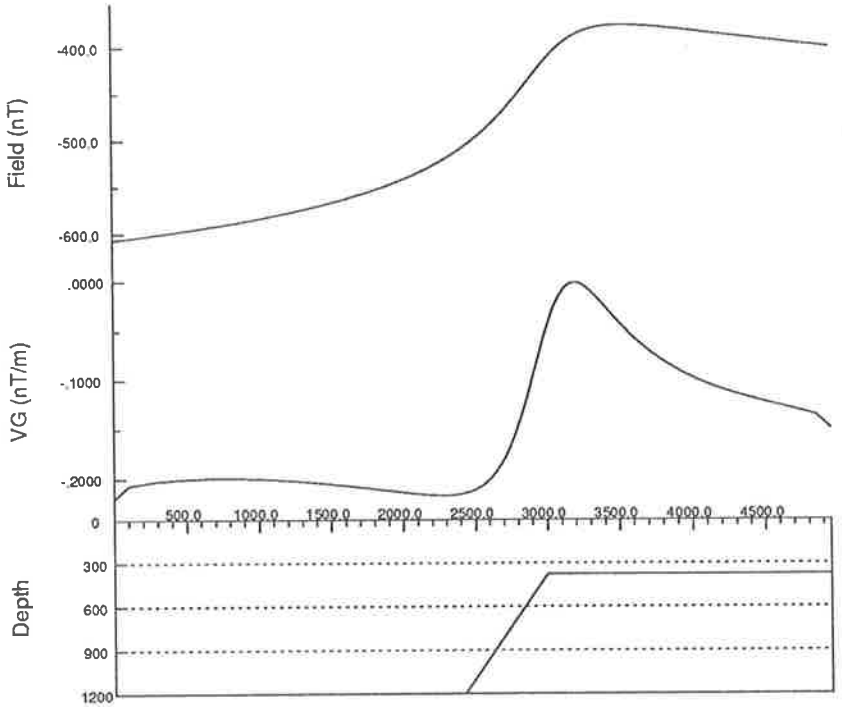

Figure 4.14: Total magnetic field intensity and its vertical gradient over an edge.

Parameter	Edge	
	True value	Estimated Value
Strike	0°	
Depth	375 m	356 m
θ	325°	322°
Dip	55° W	52° W

Table 4.3: Results of interpreting the model shown in Figure 4.14.

4.5 Conclusion

The vertical gradient anomaly over two-dimensional sources generally has well defined peaks. The location and magnitude of the larger minimum and maximum may be quickly applied to the interpretation of the geometry of the source with a reasonable degree of accuracy. The nomograms used are presented in this chapter, and the data on which they are based have been included in Appendices G and H.

Part III

Interpretation

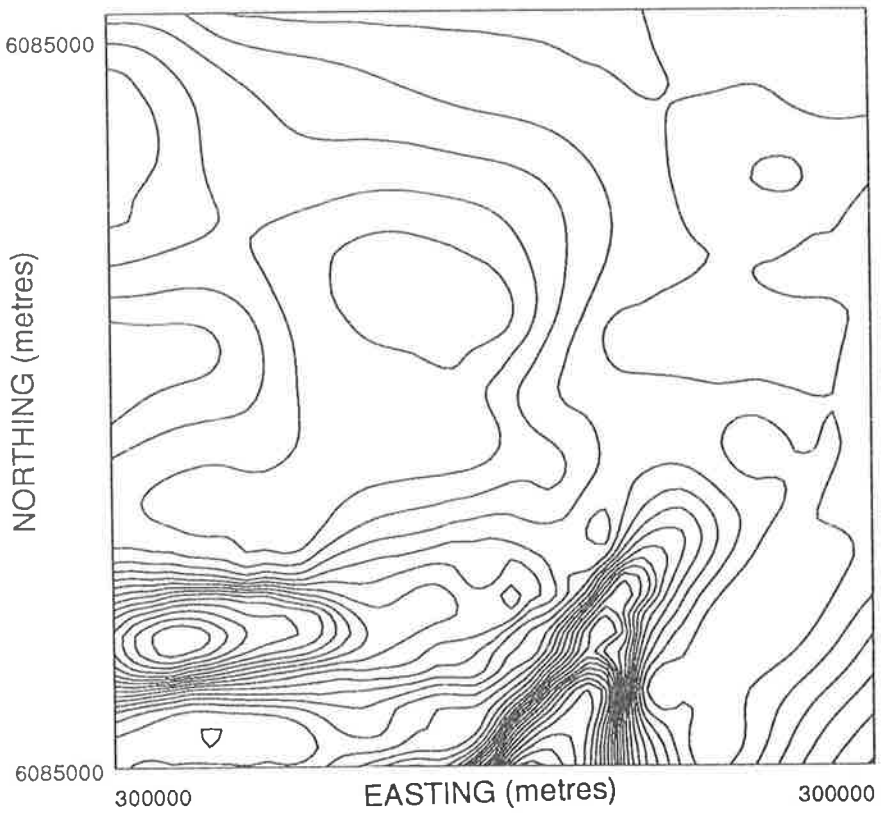

Figure 5.1: Total magnetic field contour map from the *Milang* area (after SADME, 1983). Survey parameters — line spacing: $\frac{1}{4}$ mi, sampling interval: continuous and flying height: 500 ft.

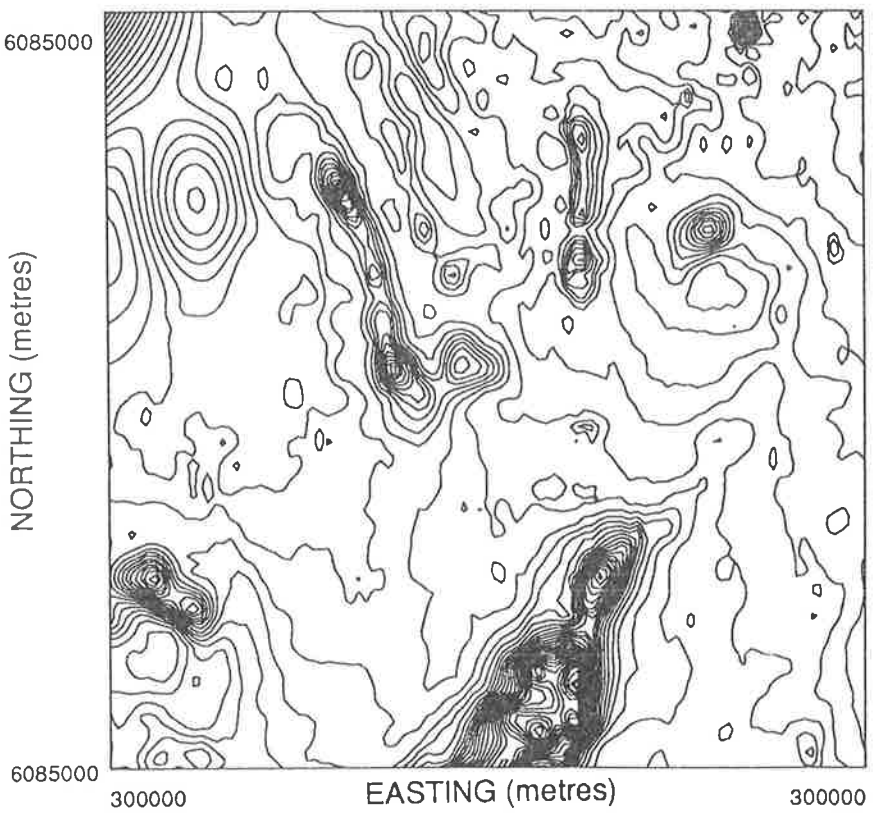

Figure 5.2: Total magnetic field contour map from the *Milang* area (after CRA data). Survey parameters — line spacing: 300 m, sampling interval: 25 m and flying height: 80 m.

Chapter 5

Regional geophysical overview

5.1 Introduction

Magnetometer surveys map the distribution of magnetic minerals in the Earth's crust (Grant, 1985a). While magnetic minerals may not generally be used to identify rock type (for an exception see Ishihara, 1977) and magnetic trends may transgress lithological boundaries (McIntyre, 1980), magnetic data can help solve many geological problems by providing a different perspective to mapped geology.

Rocks which show little variation in lithology may show small but significant variation in the amount and form of magnetic minerals. The resultant magnetic anomalies can be detected by high-quality aeromagnetic surveys. The upgrading of available aeromagnetic data over the Kanmantoo Group rocks proves the point. Older regional survey maps (part of one is shown in Figure 5.1) apparently indicate that the magnetic properties of these metasediments, like their monotonous lithology, shows little variation. Recent data over the same area (Figure 5.2) demonstrates the wealth of geological information inherent in the magnetic data.

The principle underlying the interpretation presented in this and the following chapters, has been to extend the interpretation beyond the delineation and description of magnetic anomalies and by integrating auxiliary information (primarily geological and aeroradiometric) to obtain the maximum geological information in terms of the lithology, stratigraphy and structure. This has been made possible mainly due to the quality of geophysical coverage, and partly due to the processing, presentation and interpretation techniques applied (Part 2) and through the rock property studies undertaken (Chapter 2).

Kanmantoo Group rocks are exposed in an arc which extends from Kangaroo Island to Fleurieu Peninsula and the Mt. Lofty Ranges. As Table A.1 and Figure I.2 show, the high-resolution data covers the Kanmantoo Group in the Mt. Lofty Ranges (excluding the Australia Plains area). The area of high-resolution geophysical coverage is designated the main study area. This area is not confined to Kanmantoo Group rocks and includes Precambrian rocks in the north and west, intrusive rocks in the east and Caenozoic rocks in the east and far south.

To put the geology into a regional perspective, the region around the main study area has been evaluated using regional aeromagnetic surveys (BMR and SADME data). SADME data could not be reprocessed as only analog data in the form of contour maps (SADME, 1980 and 1983) was available. BMR data have been recontoured and imaged (see Appendix A).

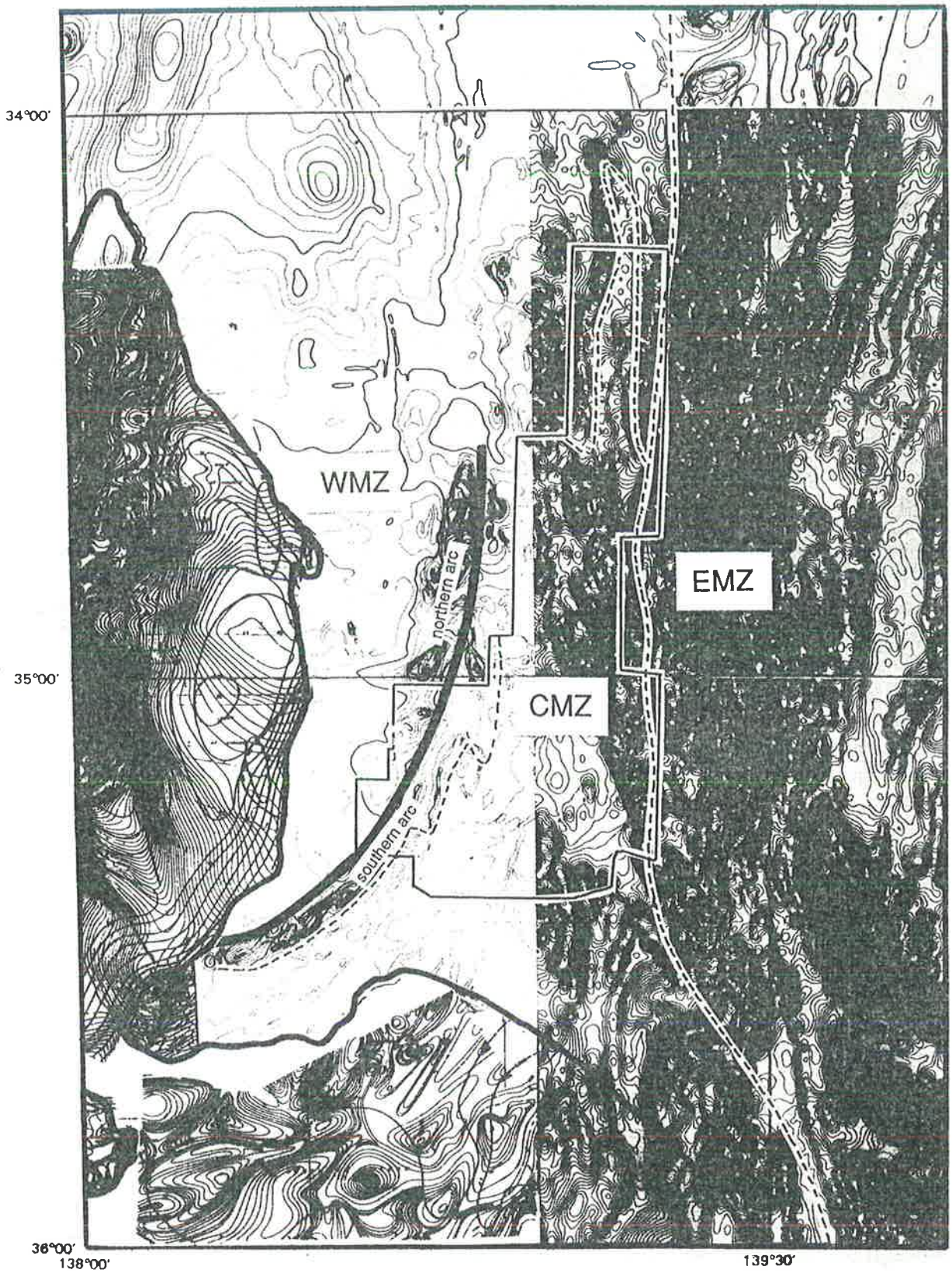

Figure 5.3: Major magnetic zones in the Mt. Lofty Ranges and surrounding area. The study area is shown (continuous line) and the zone limits are outlined (dashed line). A fault (bold line) is inferred to separate the southern and northern arcs of the basement inliers. This map is part of the preliminary regional aeromagnetic map of Adelaide, South Australia, Victoria and New South Wales (BMR, 1980).

5.1.1 Format of Part III

The main interpretation map, Plate 1 (scaled at 1:100 000), is enclosed in the back pocket of this thesis. Profiles of the vertical magnetic gradient (vertically scaled using AGC) form the background of the map. This map is in colour with the different colours used to represent different stratigraphic units (Section 3.4). The same colour key is used in Chapter 7 to illustrate the interpretation of subareas of the study area.

Other maps enclosed are the 1:100 000 total field contour map (Plate 2), grey-scale images at 1:250 000 of the total magnetic field and total radiometric count (Plates 3 and 4) and a regional interpretation map at 1:250 000 (Plate 5). Anomaly names used in Part III are marked on Plate 2. Locality names mentioned in this thesis are marked on Figure I.3. For the location of mineral deposits, readers are referred to Both (in press) and Brown (1908).

The regional geophysical environment of the Kanmantoo Group is discussed in the following section of this chapter. Magnetic data from older surveys by SADME (1980 and 1983) and BMR (1980) have been interpreted on a regional scale. An overview of the interpretation of the detailed aeromagnetic and aeroradiometric surveys is also presented. Relevant gravity and seismic features are also mentioned.

A discussion of the interpretation, intended to supplement Plate 1, is presented in Chapters 6 and 7. The major magnetic anomalies are identified and placed in the appropriate stratigraphic interval in Chapter 6. Macroscopic structures in the study area are discussed in Chapter 7.

The potential of aeromagnetic interpretation to resolve geological issues such as the structural history of a region varies. In Chapter 8, some problems relating to the geology of the Kanmantoo Group are discussed using evidence presented in past and recent studies. Results of aeromagnetic interpretation are included where relevant. Areas have also been identified from aeromagnetic interpretation where detailed geological work is warranted as this might uncover important geological information.

5.2 Regional interpretation

Exposed Kanmantoo Group rocks are flanked to the west, north and northeast by metasediments of the Adelaide Supergroup (Figure 1.1) and in the southwest by the Barossa Complex. Tertiary rocks and Recent sediments of the Murray Basin outcrop to the east and far south and, except for extremely limited outcrop and drill hole cores, obscure the underlying rocks. Since measurements of the magnetic field is not limited by the nature of overburden, magnetic maps provide the most information about basement to the undeformed Murray Basin sediments. Maps of total magnetic intensity over the areas surrounding the study area have been interpreted on a regional scale to identify the major sources of magnetic anomalies and to investigate the possibility of the existence of Kanmantoo Group rocks under Murray Basin cover.

Regional gravity data are available all over South Australia and locally researchers have made closely spaced observations (Sjarif, in prep., Boyd, pers. comm.). Seismic data for crustal analysis are restricted to earthquake and explosion seismic data and in any case are very limited in the Mt. Lofty Ranges.

Figure 5.4: Photographically reduced, hand-coloured contour map of total magnetic intensity (after CRA and Pacific Expl. data). Original maps were at 1:50 000 scale. Part of the EMZ, outside the main study area, is shown in the top right corner of the map. The circular magnetic high, 5 km in diameter, seen in the upper right corner in the EMZ is caused by a magnetic gabbro (Lewis, P., 1985).

Figure 5.5: The transparency shows the boundaries of magnetic subzones in the CMZ relative to the EMZ and WMZ. The study area is outlined.

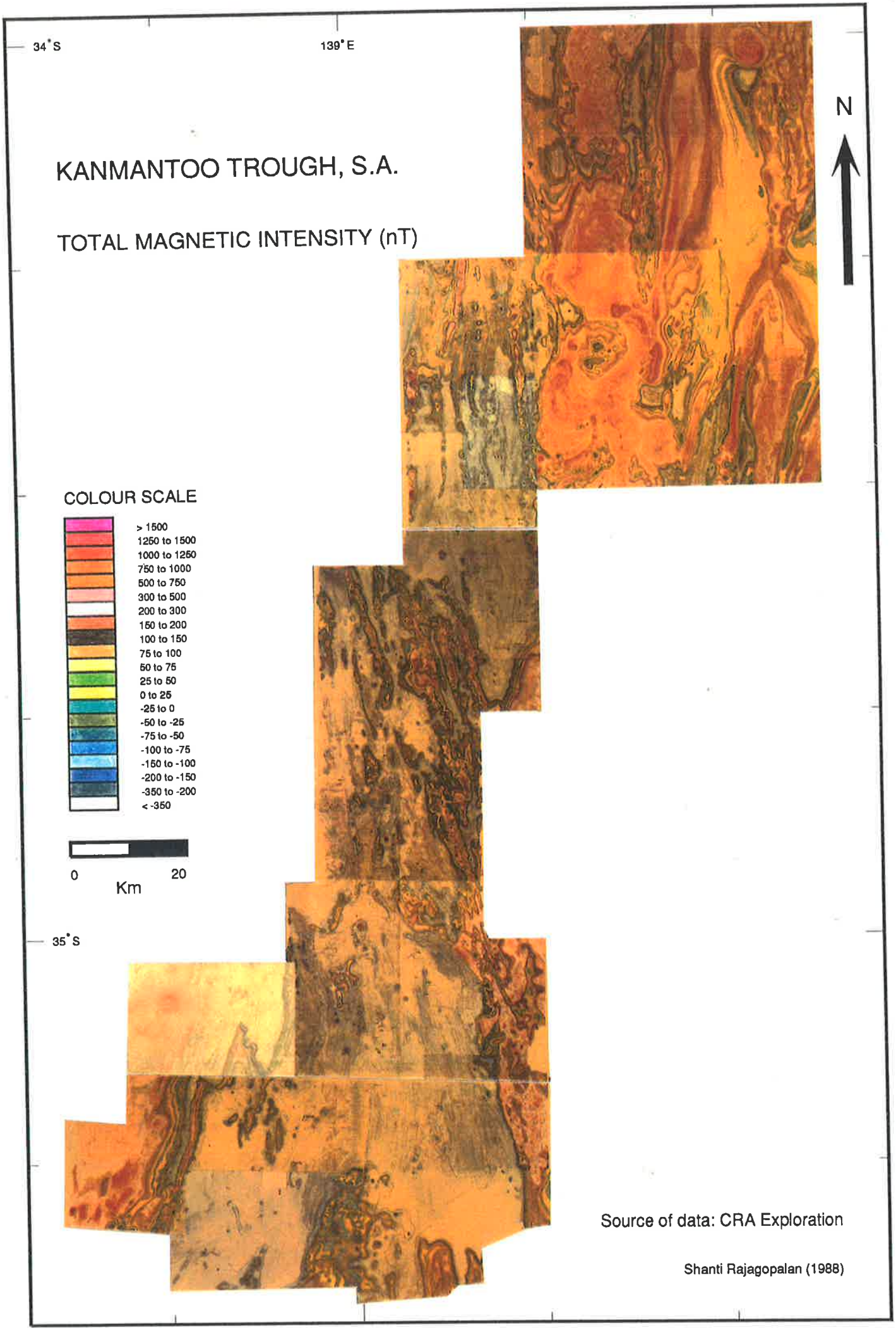
34°S
139°E
N
KANMANTOO TROUGH, S.A.
TOTAL MAGNETIC INTENSITY (nT)
COLOUR SCALE
> 1500
1250 to 1500
1000 to 1250
750 to 1000
500 to 750
300 to 500
200 to 300
150 to 200
100 to 150
75 to 100
50 to 75
25 to 50
0 to 25
-25 to 0
-50 to -25
-75 to -50
-100 to -75
-150 to -100
-200 to -150
-350 to -200
< -350
0
20
Km
35°S
Source of data: CRA Exploration
Shanti Rajagopalan (1988)

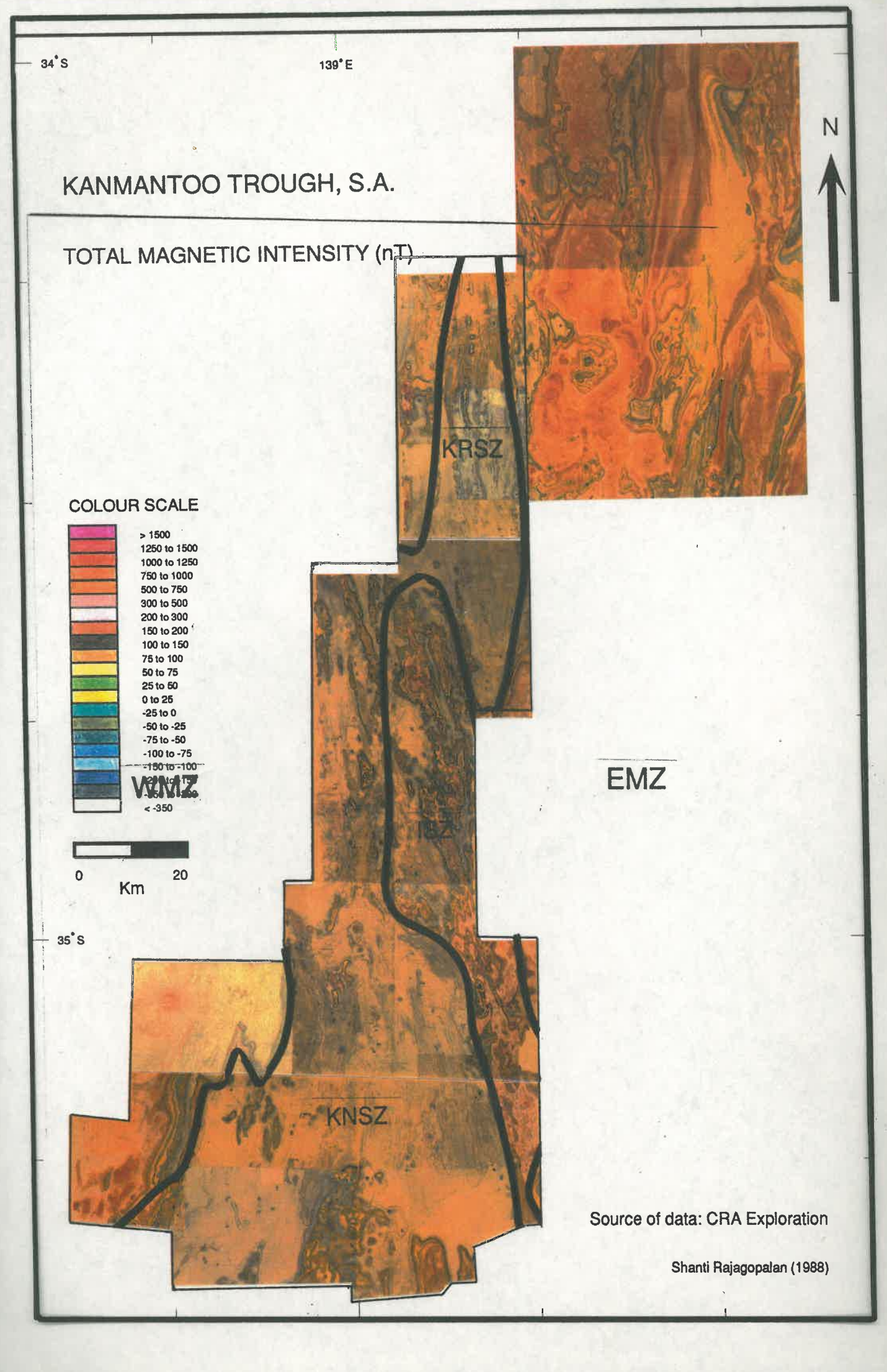
34° S
139° E
N
KANMANTOO TROUGH, S.A.
TOTAL MAGNETIC INTENSITY (nT)
KRSZ
COLOUR SCALE
> 1500
1250 to 1500
1000 to 1250
750 to 1000
500 to 750
300 to 500
200 to 300
150 to 200
100 to 150
75 to 100
50 to 75
25 to 50
0 to 25
-25 to 0
-50 to -25
-75 to -50
-100 to -75
-150 to -100
< -350
WMZ
EMZ
0
20
Km
35° S
KNSZ
Source of data: CRA Exploration
Shanti Rajagopalan (1988)

5.2.1 Magnetic data

The regional aeromagnetic map over the study area and adjacent regions is reproduced in Figure 5.3. This map was compiled from aeromagnetic survey data of differing quality and survey parameters. The study area has been outlined.

The character of magnetic anomalies changes from west to east of the Mt. Lofty Ranges. Anomalies due to outcropping and deeper magnetic basement are found in the western part of the region. In the central part, weakly to moderately magnetic, metamorphosed Kanmantoo Group sediments give rise to linear and curvilinear anomalies. In the Murray Basin, east of the Palmer-Milendella Fault Zone, strong anomalies caused mainly by igneous rocks combine to produce a 40 km wide, meridional magnetic belt, the Murray Magnetic High (MMH).

On the basis of the different magnetic responses, three zones have been demarcated. All three zones trend NS and their boundaries are shown in Figure 5.3. The Central Magnetic Zone (CMZ) covers the exposed and likely Kanmantoo Group rocks. The Western Magnetic Zone (WMZ) lies to the west of the CMZ and is associated with Adelaide Supergroup metasediments and exposed and deep magnetic basement. Immediately east of the CMZ, the undeformed non-magnetic sediments of the Murray Basin and the strongly magnetic, near-surface, igneous and other magnetic sources form the Eastern Magnetic Zone (EMZ).

The CMZ is covered mainly by CRA data (the main study area), and by SADME data in the Australia Plains area, on the south coast and on Kangaroo Island (SADME, 1980 and 1983). Coverage of the WMZ is limited to SADME data except for part of the *Echunga* and *Willunga* sheets for which detailed data is available and the *Eudunda* and *Truro* sheets which are covered by BMR data. BMR data is available for all of the EMZ under consideration in this thesis (see Appendix A).

In the next section a short summary of the typical magnetic and radiometric response in the CMZ is presented and this is followed by a regional magnetic interpretation of the WMZ and EMZ.

Central Magnetic Zone: Magnetic subdivisions

The style of magnetic anomalies in the Central Magnetic Zone (CMZ) varies and is closely linked to changes in metamorphic grade and structural complexity (Figure 5.4). On the basis of similar magnetic character, the study area has been divided into three subzones, which are shown in Figure 5.5. The three subzones are the Kanmantoo Synclinal Subzone (KNSZ) which covers the southern and western parts of the study area, the Karinya Synclinal Subzone (KRSZ) which covers the northern part of the area and the Intermediate Subzone (ISZ) which separates the other two.

In the southern and western part of the CMZ, Kanmantoo Group rocks have been folded into the Kanmantoo Synclinorium which consists of an *en échelon* series of south-plunging synclines. Continuous, linear to curvilinear, well-resolved anomalies outline in detail the open, upright folds against a quiet magnetic background. This subzone is defined as the Kanmantoo Synclinal Subzone or KNSZ.

In the northeast, the major structure is a doubly plunging synclinorium (the Karinya Synclinorium). This forms the Karinya Synclinal Subzone or KRSZ. Anomalies in this subzone are of similar style to those in the KNSZ, though less continuous.

Between the KNSZ and the KRSZ lies a region characterized by closely-spaced, strong, linear anomalies which have a dominant NNW trend. This is the area defined as the Intermediate Subzone or ISZ. The open, upright folds which are common in the KNSZ and KRSZ are rare in this subzone. The ISZ covers most of the *Angaston-Tepko* area. Migmatites are found in the ISZ and the metamorphic grade decreases away from this zone towards the KNSZ and KRSZ.

Magnetic patterns in the Central Magnetic Zone The metasediments of the Kanmantoo Group are generally weakly to moderately magnetic and may be strongly magnetic (typically susceptibilities vary from 0 to 1000×10^{-5} SI). The magnetic metasediments give rise to linear to curvilinear anomalies of varying amplitudes (few nanoTeslas to several hundred) which can be traced for several tens of kilometres. The anomalies tend to be stratiform and delineate major structures. The magnetic minerals which have been identified in the different rock types are magnetite, hemo-ilmenite, ilmeno-haematite and pyrrhotite. There is an increase in the intensity and complexity of the magnetic anomalies with increasing metamorphic grade, with migmatites causing intense and complex anomalies.

Granites and granitic gneisses are characterized by elongate or circular highs or lows which are discordant to surrounding trends and marked by steep gradients along the contact. They have been classified as members of the magnetite-series or ilmenite-series (Section 6.2.1). Some anomalies tend to be a more complex combination of highs and lows, and are not well-defined, and reflect on the origin and formation of the granite. Amphibolites and dolerites range in width from a few centimetres to 20–30 metres, and in length from less than a metre to 1–2 kilometres (Liu and Fleming, 1989). They often occur as small dykes lying between flight lines or on only one flight line making their detection on aeromagnetic maps difficult.

Faults and shears have been detected through the associated displacement of magnetic trends, as contacts between rocks of varying magnetic properties, and as lows which may have formed through the oxidation of magnetite by preferential deep weathering (Henkel and Guzmán, 1977) or by the destruction of magnetite by hot reducing fluids circulating in permeable shears and fractures (McIntyre, 1980).

Mineralization in the Kanmantoo Group is often associated with magnetite and pyrrhotite, and depending on whether the mineralization is stratiform or discordant, the resultant anomalies are stratiform or discordant.

Beneath the Kanmantoo Synclinorium, the magnetic effect of deep-seated rocks has not been detected. Most anomalies have been attributed to metasediments and granitic rocks which are near-surface or outcrop. Therefore, if magnetic basement underlies the Kanmantoo Group it is at depths exceeding many kilometres and there is a corresponding great thickness of sediments in the synclinorium. Alternatively, basement to the Kanmantoo Group is non-magnetic and may be within a few hundred metres of the surface.

Radiometric patterns in the Central Magnetic Zone The image of the total radiometric count displayed in Plate 4 correlates extremely well with gross geology even though the data have not been compensated for altitude and other variations. The major sources of radiometric anomalies are transported soils, lithoradiometric units, zones of pronounced enrichment or depletion in radioactive minerals, and anomalous zones which could not be related to known geology.

Stream channel and drainage patterns show up as radioactive highs (e.g. the Angas River) or lows (e.g. the valley of the Bremer River) depending on the sediment which has been brought

down and on the radioactive response of the adjacent rocks. Caenozoic deposits include limited outcrops of non-radioactive sands and moderately radioactive alluvial. In the far south of the main study area, narrow linear radioactive highs identified in Plate 4 may represent beach strand deposits.

Metasediments are sometimes associated with characteristic curvilinear, radiometric anomalies which can be highs (e.g. Ulupa Siltstone in the region of Macclesfield) or lows (e.g. Milendella Limestone Member, quartzite at Macclesfield). More often, they are associated with large areas of uniform radiometric response owing to their uniform lithology. In general, the more pelitic metasediments are more radioactive than the predominantly arenaceous.

Granites and granitic gneisses are generally enriched in potassium and uranium compared to metasediments. The Palmer Granite is typical of granites in the study area for its high radiometric response.

Metasomatism has resulted in areas which are depleted or enriched in radioactive elements, usually potassium. Such zones are associated with the non-radiometric Mt. Kitchener Granite and the Palmer Fault zone which have been extensively albitized. On the other hand, migmatites west of Palmer give rise to radiometric highs of the same order as the granites.

Western Magnetic Zone

Magnetic anomalies in this zone are caused by weakly to strongly magnetic metasediments of the Adelaide Supergroup, strongly magnetic metamorphic rocks of the Barossa Complex, and unknown, deep-seated magnetic sources which are correlated with Barossa Complex rocks at depth.

Rocks of the Barossa Complex are made up of strongly deformed rocks which are now magnetite-rich micaceous schists in part. They outcrop in inliers along the fold axis of the major anticlinorium and produce intense, complicated anomalies. These anomalies form two arcs (compare Figure 5.3 and Figure 1.3). The Mt. Compass Inlier forms the southern one. The Houghton Diorite and Aldgate Inlier are found in the northern arc. The northern arc is not continuous with the southern arc but offset to the west. Depths to the top of magnetic basement increases from north to south in the northern arc. The deeper magnetic sources have been interpreted to be caused by magnetic basement at depths ranging from 1.5 to 3 km. The two arcs are separated by a fault: downthrown side is to the west, and the throw decreases towards the north. The existence of this fault is supported by a gravity gradient (Sjarif, in prep.). A similar fault may mark the western boundary of the Houghton Diorite.

Metasediments of the Adelaide Supergroup give rise to curvilinear anomalies, e.g. Aldgate Sandstone, Tindelpina Shale Member of the Tapley Hill Shale, Woolshed Flat Shale and Ulupa Siltstone. Of all of them, the Ulupa Siltstone is the most consistent and distinctive in its magnetic properties and makes an excellent magnetic marker. The northern closure of the Karinya Syncline is marked by the continuation of these anomalies around the closure and under Murray Basin sediment cover to the east. North of Australia Plains, linear anomalies either due to dykes or to Adelaide Supergroup rocks strike into oblate magnetic highs typical of the intrusives in the EMZ. The contact with the Kanmantoo Group is folded around the Macclesfield Syncline-Strathalbyn Anticline and the Karinya Syncline.

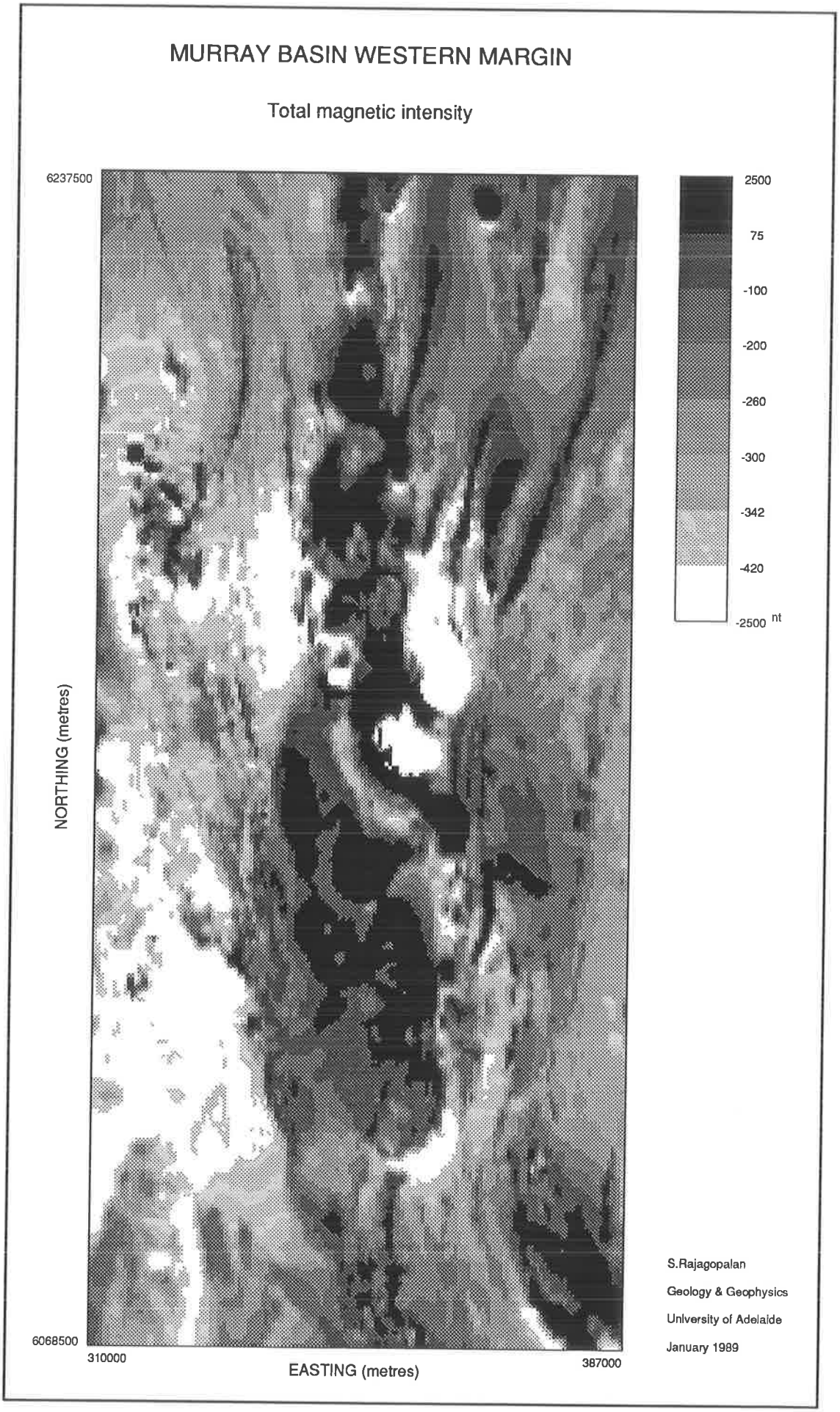

Figure 5.6: Grey-scale image of regional magnetic data (BMR data) over the Eastern Magnetic Zone.

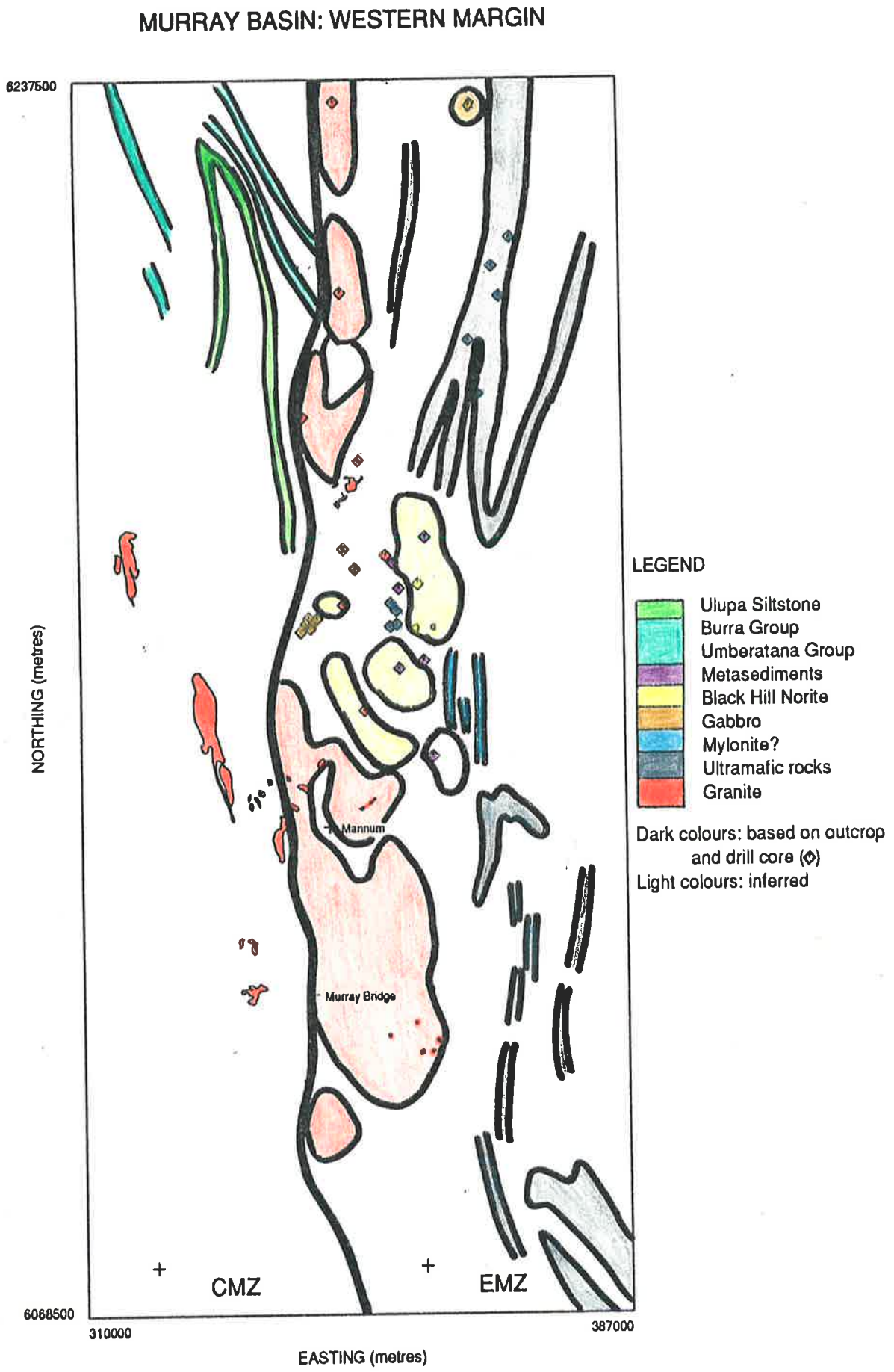

Figure 5.7: Regional interpretation of the Eastern Magnetic Zone: magnetic units outlined (see legend), boundary between EMZ and CMZ indicated by bold line. Drill hole locations after Wegmann (1980) and Lewis, P. (1985).

Eastern Magnetic Zone

The western margin of the Murray Basin forms the present eastern limit of the Kanmantoo Group outcrop. A grey-scale image of the BMR data over the EMZ is shown in Figure 5.6. Intensity and character of magnetic anomalies change sharply across the Palmer-Milendella Fault. Gradients of well over hundreds of nanoTeslas mark the contact between the CMZ and the EMZ establishing the EMZ as a significantly different magnetic "terrane". The contact is essentially linear and trends NS.

Linear, moderately strong magnetic anomalies against a low-relief magnetic background typify the response due to the weak to moderately magnetic Kanmantoo Group in the CMZ. The Murray Magnetic High (MMH) in the EMZ is characterized by multiple, intense anomalies.

The MMH may be separated into an eastern and western band. The western band of the MMH is dominated by a sequence of circular to oblate magnetic anomalies of the order of several thousands of nanoTeslas. The source of these magnetic anomalies are Cambro-Ordovician granitoids and gabbros (e.g. Black Hill Norite) which Foden *et al.* (in press) associate with an extensional post-Delamerian phase. The granitic and gabbroic rocks vary widely in composition (Wegmann, 1980; Foden *et al.*, in press; Turner *et al.*, 1989). The eastern band of the MMH is formed by wide, linear anomalies. Basalt and tholeiite have been discovered in drill holes into these anomalies (Wegmann, 1980; Lewis, P., 1985).

A simplified interpretation based on drill hole data, outcrops and magnetic response is presented in Figure 5.7. The varying magnetic properties and petrology of these intrusions (and extrusions?) are discussed in Section 6.2. Anomalies which could be caused by sediments are only rarely seen as the high magnetic relief caused by the near-surface, igneous sources obscures low-amplitude signals also coming from the same depth. Between the two bands, linear anomalies are occasionally found which could be caused by the metasediments of the Adelaide Supergroup or Kanmantoo Group. Drill holes in a number of these areas have intersected low-grade schists and greywackes which have been tentatively correlated with Kanmantoo Group (Preiss, pers. comm.).

The Murray Magnetic High was identified as "strip 7" by Wellman and Greenhalgh (1988). The abundance of granitoids, gabbros and basalt dykes in the MMH lends credence to the post-Delamerian extensional phase proposed by Foden *et al.* (in press). Further east, a quiet magnetic pattern marks the eastern edge of the MMH. The MMH is sigmoidal in shape. It follows an arc, trending SE near Coonalpyn, NS parallel to the Palmer-Milendella Fault, and swings to a NE trend following the trend of the Nackara Arc. It is a major magnetic feature and delineates the edge of exposed Precambrian rocks in Australia.

Within this magnetic zone, Wegmann (1980) discovered mylonite in the Marne River, just east of longitude 139°30′. Susceptibility measurements on the outcrop returned high values $\sim 1500 \times 10^{-5}$ SI) and the mylonite zone has been correlated with a 15 km long, NS trending narrow magnetic high. It is possible that the Morgan Fault (Firman, 1974) is related to the mylonite zone. There are several similar anomalies in the MMH (Figure 5.7). Mylonite zones are indicative of high strain.

5.2.2 Gravity data

Regional gravity surveys, conducted by SADME and BMR, cover all of South Australia at a spacing of $\approx$ 7 km (Coppin *et al.*, 1973). A detailed coverage of the *Noarlunga, Willunga, Onkaparinga* and *Echunga* sheets has recently been completed by N. Sjarif and Prof. Boyd (spacing

$\approx$ 1.2km). The *Mannum* and *Cambrai* sheets are being covered by Prof. Boyd and S. Turner. Gravity data over small areas have been collected by Honours students at the University of Adelaide: profile across the Mannum to Adelaide pipeline (Middleton, 1973), along the western margin of the Murray Basin (McInerney, 1974; Hansen, 1975) and in the region of the Monarto Granite (Lewis, A. M., 1985).

The main gravity features in the region include:

1. Generally low values over much of the Mt. Lofty Ranges and the Flinders Ranges probably reflect the sequence of thick metasediments in the Adelaide Geosyncline but are otherwise inconclusive.

2. A gravity high runs parallel to and partly coincides with the Murray Magnetic High. It extends further eastwards than the MMH. Mancktelow (1979) identifies the gravity high in the region as the Murray Ridge and suggests that it may represent a cratonic high.

   Several local gravity highs in the broad gravity high have been investigated in more detail (McInerney, 1974; Hansen, 1975; Boyd, pers. comm.). Comparison of magnetic interpretation of the MMH and local gravity observations indicates that the local gravity highs are due to extensive basic intrusion. The Black Hill Norite is more dense than the surrounding granite and this together with its characteristic magnetic properties (Section 6.2.2) permits the identification of similar bodies (Figures 5.7 and Figure 6.1). This interpretation has been confirmed by drilling (drill hole locations given in Wegmann, 1980).

3. Middleton (1973) completed a gravity profile along the pipeline from Mannum to Adelaide. There is no significant density difference between the metasediments of the Adelaide Supergroup and the Kanmantoo Group so that no gravity anomaly would be expected across the contact. There is a high over the migmatites west of the Palmer Granite, and an apparent fault east of the granite.

   Granites may be associated with gravity lows (Hansen, 1975) or highs (e.g. the Monarto Granite in Lewis, A. M., 1985).

   The basement inliers (Barossa Complex) are associated with local gravity highs. The deep-seated magnetic sources in the WMZ which are interpreted to be Barossa Complex rocks at depth (see above) are not obviously related to a gravity anomaly. The fault which was inferred between the southern and northern arcs of the Barossa Complex anomalies (Figure 5.3) is marked by a gravity gradient (Sjarif, in prep.).

4. A steep gradient trends NS and parallel to the Nairne Fault in the *Echunga* region (Boyd, pers. comm.). It follows the contact between the Kanmantoo Group and the Adelaide Supergroup but is caused by a contact at a depth of several kilometres. The source of the gradient may be a fault within deep Barossa Complex rocks in the core of the Strathalbyn Anticline (Plate 5).

   The basement inlier near Normanville is in fault contact with the metasediments of Adelaide Supergroup. Preliminary interpretation suggests that the contact dips east (Sjarif, in prep.). Anderson (1975) in his cross section across the inlier shows that the western limb is overturned and that an easterly dipping late reverse fault displaces the folded beds.

   Both the Morgan Fault (EMZ) and the Encounter Fault (CMZ — this fault trends NE and transects the main study area in the south) were proposed on the basis of gravity gradients (Firman, 1974) . The Morgan Fault has also been related to the right angle change in the course of the Murray River. Several NE trending faults have been mapped using magnetic data (Plate 5) and these are subparallel to the Encounter Fault.

5.2.3 Seismic data

No deep crustal seismic reflection experiments have been carried out in South Australia. However, simple models of the structure of the crust may be deduced from earthquake and explosion seismic data. Greenhalgh *et al.* (1989; in press) have compiled and reinterpreted all available earthquake and explosion seismic (quarry blasts) data. Using a simple average model, they inferred that the thickness of the crust is 38 km with a P wave velocity equal to 6.32 km/s. Results of interpreting quarry blasts within the Adelaide Geosyncline indicate that the crust is layered with an upper layer ranging in thickness from 10 to 18 km, and an average P wave velocity (P_1) of 5.94 kms^{-1} overlying a second layer with velocity 6.42 kms^{-1}. Both crustal discontinuities shallow towards the Murray Basin. The underlying mantle velocity has been calculated to be 8.05 kms^{-1}.

The average P wave velocity in the upper 20 km of the crust varies laterally and ranges between 5.94 and 6.42 kms^{-1}. Greenhalgh *et al.* (1989) found a high velocity ridge which trends NE through the Flinders Ranges. This is coincident with positive Bouguer gravity values. The axis of an elongate conductor mapped using geomagnetic deep sounding arrays (Chamalaun, 1986) runs through the centre of the high velocity ridge. The depth and cause of this conductor are not clear. Parallel to the Torrens Hinge Zone, the P_1 velocity high coincides with a Bouguer gravity low.

From the limited seismic and gravity data available, the Flinders and Mt. Lofty Ranges do not appear to have a significant crustal root. During the Delamerian Orogeny when the Kanmantoo Group formed an orogenic upland, the mountain ranges may have had a corresponding crustal root. However, following subsequent erosion, isostatic compensation would have resulted in the disappearance of the mountain root.

Note that the epicentres of earthquakes are concentrated in the Flinders Ranges, Mt. Lofty Ranges and in the Broken Hill area. Wellman and Greenhalgh (1988) computed the average focal depths and found that seismicity in South Australia is shallow in origin. They determined the predominant principal stress to be NE-SW compression and suggest that this caused the faulting and uplift of the Mt. Lofty Ranges.

Chapter 6

Geophysical responses of known rock types

Magnetic, radiometric and geological data have been compared to determine the geophysical response of different stratigraphic and lithological units. The majority of magnetic anomalies are due to susceptibility differences within metasediments and between igneous rocks and the country rocks. Faults, shear zones and lineaments have distinctive radiometric and magnetic signatures. Basement rocks, i.e. basement to the Adelaide Supergroup, and some mineralized zones have also been correlated with characteristic signatures.

Some magnetic anomalies have been named to make it easier to refer to them. In some cases, an individual magnetic unit has been named (e.g. the curvilinear magnetic anomaly associated with the Talisker Calc-siltstone which is folded by the Macclesfield Syncline has been named TC-MS). In others a group of anomalies has been classified (e.g. magnetic anomalies caused by Tapanappa Formation magnetic horizons in the Dawesley region are referred to as TP-DM). These names have been indicated on Plate 2 and are used in the description of structures in the next chapter.

Only a small part of the main study area is occupied by the WMZ and EMZ, and therefore in detailed discussions (Chapters 6 and 7) the CMZ and main study area are deemed to be equivalent. On this basis, the KNSZ and KRSZ include adjacent WMZ area, and part of the EMZ is included in the ISZ (compare Figures 5.3 and 5.5).

This chapter begins with a discussion of magnetic anomalies in the Kanmantoo Group. This is followed by sections on the other metasedimentary units in the study area: the Normanville Group and the Adelaide Supergroup. The response of the Barossa Complex rocks, granites and granitic gneisses, gabbros, amphibolites and dolerites follows. The radiometric response of the rocks is also discussed. Structures referred to are found on Figure 1.2 and on Plate 5. Measured magnetic susceptibilities are tabulated in Tables 2.4 and 2.5 and listed fully in Appendices B and C. Parameters determined from modelling magnetic anomalies are listed in Appendix I, and the modelled cross-sections are presented in Appendix J. The depths to the tops of magnetic sources are given with reference to the ground surface.

6.1 Metasediments

6.1.1 Kanmantoo Group

Middleton Sandstone

The Middleton Sandstone represents the youngest exposed Kanmantoo Group unit, as its upper boundary is unknown. It must have been overlain by a considerable thickness of sediments, as it is intruded by the coarse-grained Encounter Bay Granites (Daily and Milnes, 1973). On Fleurieu Peninsula the formation has been mapped only near Middleton, its type locality. Better exposures have been identified on the coast of Kangaroo Island. The formation is composed mainly of well laminated arkosic sandstones (see Boord, 1985 for facies descriptions). The lithologies are in sharp contrast to the greywacke facies of the underlying Petrel Cove, Balquhidder and Tunkalilla Formation but are similar to the sandstone facies of the Backstairs Passage Formation. The Middleton Sandstone probably accumulated in a shallow marine environment (Boord, 1985).

Bands rich in the heavy minerals, zircon, ilmenite, magnetite, rutile, sphene, epidote and actinolite have been found in Kanmantoo Group metasediments on Kangaroo Island (Flint, 1976). They occur as lenticular bodies, varying in length from 5–50 metres and in thickness up to 0.75 metres. Of the five localities mentioned by Flint (*op. cit.*), a map of the island produced by Mancktelow (1979) shows that four are located within Middleton Sandstone outcrop. (The heavy minerals at the fifth locality are associated with Recent beach and dune sand deposits). Daily and Milnes (1973) record conspicuous segregations of epidote developed consistently within the Middleton Sandstone at Middleton beach.

Magnetic susceptibility measurements near Middleton (Table 2.4) were of the order of 1000×10^{-5} SI. From the aeromagnetic contour map of Fleurieu Peninsula and part of Kangaroo Island (SADME, 1983), Middleton Sandstone outcrop was found to be associated with strong anomalies. Detrital magnetite is probably the cause for most anomalies as heavy mineral bands are common within the sandstone. One sample measured for ferrous and total iron showed very small total iron content (2.76%) but high oxidation ratio (65.7%). This result is similar to those obtained for the Backstairs Passage Formation (Section 2.3).

Anomalies MS1 to MS4 (Plate 2) are part of a large complex of magnetic anomalies which extends to Middleton beach and into Encounter Bay. Magnetic sources are within a few hundred metres of the surface but are concealed by Tertiary rocks and Recent sediments of the Murray Basin. The anomalies MS1–MS4 are similar in style and very likely share a common source. MS1 appears to be continuous with a magnetic anomaly over exposed Middleton Sandstone near Middleton. The most likely cause of the anomalies MS1–MS4 is the strongly magnetic Middleton Sandstone which forms the core of the south-plunging synclines of the Kanmantoo Synclinorium (see Section 7.2). Without drill hole data, this inference is speculative. Alternatively, the Encounter Bay suite of granites (Mancktelow, 1979) might extend into the region of the MS1–MS4 anomalies, though their low measured susceptibilities makes it unlikely that they could be the cause of the magnetic anomalies.

MS3 is a group of anomalies, "closed" to the north and widening southwards and defined by a steep gradient in the west. The diffuse nature of the eastern boundary indicates probable faulting by the Bremer Fault (Plate 5).

Petrel Cove, Balquhidder and Tunkalilla Formation

Along the south coast of Fleurieu Peninsula, where exposures are good, the rocks between the Tapanappa Formation and the Middleton Sandstone have been divided into the Tunkalilla, Balquhidder and Petrel Cove Formation (Daily and Milnes, 1973). Elsewhere it is difficult to distinguish between these units and the underlying Tapanappa Formation (Mancktelow, 1979) owing to the similarity of their lithologies.

Whole rock analyses (Mancktelow, 1979) gave average values of total iron in these sediments as follows: 2.16% in Petrel Cove, 5.34% in Balquhidder and 5.02% in Tunkalilla Formation. Magnetic susceptibility measurements on samples (Figure 2.5) were uniformly low. Higher quality aeromagnetic data over the south coast of Fleurieu Peninsula would be invaluable in demarcating formations, as the example used in Section 5.1 (Figures 5.1 and 5.2) indicates.

Two curvilinear anomalies YKG-M have been marked on Plate 2. The one in the southwest corner of Plate 2 is a negative anomaly and is terminated against the Encounter Fault. The second YKG-M anomaly is easily identified as a weak, linear anomaly which is caused by younger Kanmantoo Group sediments folded into the Strathalbyn Anticline. Neither anomaly can be delineated in the older survey (SADME, 1983). The cause of magnetic anomalies is likely to be pyrrhotite and magnetite bearing pyrite schists, as bands rich in iron sulphides are common within these formations (Mancktelow, 1979). Several anomalies which have been placed in the Tapanappa Formation (e.g. TP-SM, TP-HH — see below) could instead be in younger Kanmantoo Group formations. However, lack of continuity has prevented correlation.

Tapanappa Formation

The Tapanappa Formation has been mapped as outcropping extensively within the study area. Mancktelow (1979) identified two facies variants: greywacke and sandstone. The proportion of siltstone to sandstone in this facies is variable, but over most of the outcrop area medium-grained greywacke is the dominant lithology. With increasing metamorphic grades, the rocks have been metamorphosed into micaceous quartzites, meta-arkoses, quartz-feldspar-mica schists and andalusite-staurolite schists.

Along the south coast of Fleurieu Peninsula, the dark coloured greywacke facies is more common. In the more northern areas, east and northeast of Truro, grey massive or laminated siltstones crop out. The siltstone units occasionally contain bands which are rich in iron sulphides. On the south coast of Fleurieu Peninsula these bands are rich in pyrrhotite. When strongly metamorphosed the bands are rich in muscovite and pyrite. Even when the more distinctive greywacke facies dominates, the first few metres above the Talisker Calc-siltstone are often sandstones.

Away from the south coast of Fleurieu Peninsula, the lithologies of the Tapanappa Formation are more akin to the sandstone facies of the Backstairs Passage Formation. The rocks are well laminated, light coloured (less biotite) arkosic and quartz-rich sandstones. Mancktelow (1979) has observed thin, heavy mineral beds and laminae containing 80–90 % magnetite $\pm$ haematite in arkosic facies of the Tapanappa Formation. The thickness of these layers ranges up to 30 centimetres.

Continuous linear anomalies, consistent in anomaly characteristics over long distances, is typical of magnetic units within this formation. Anomalies TP-SA and TP-MNS have been correlated with pyrrhotite bearing pyrite schists, which were originally siltstones rich in iron

sulphides and TP-EB (Figure 7.5) is likely to be caused by a similar rock type. Magnetite and pyrrhotite bearing phyllites folded into the Monarto Syncline (Lawrence, 1980) give rise to continuous, narrow, linear anomalies, collectively called TP-MNS. Kleeman and Skinner (1959) suggest that the pyrite, like that of the Nairne pyrite facies of the Talisker Calc-siltstone, is syngenetic in origin. TP-EB outlines what is possibly a large fold in the formation (Figure 7.5). Permian glacials obscure outcrop but the fold is significant in helping to explain the apparent great thickness of the Tapanappa Formation.

Sulphide mineralization within the Tapanappa Formation is often associated with magnetic anomalies. The opaque oxide assemblages of the mineralized zones usually include pyrrhotite ± magnetite (Both, in press). Invariably, pyrite schists in the Tapanappa Formation contain pyrrhotite ± magnetite. Near Wheal Ellen and the Strathalbyn Mine, pyrite schists produce magnetic anomalies, TP-WE and TP-SM respectively. The anomaly TP-WE is negative and may have been caused by the presence of monoclinic pyrrhotite. Monoclinic pyrrhotite has occasionally been found (Askins, 1968; Spry, 1976) and self-reversal in the pyrrhotite may be responsible for the intense negative anomalies. At Kanmantoo Mine (Lindqvist, 1969) and in the Dawesley region (Benlow and Taylor, 1963), sulphide mineralization is associated with andalusite schists. Magnetite is an important component of the opaque oxide assemblages of these schists and this results in strong anomalies (TP-KM and TP-DM respectively).

Magnetite ore from the Kanmantoo Mine had the highest susceptibilities recorded for Kanmantoo Group rocks: over 1 SI unit. The result of mining activity in the region makes it difficult to isolate the magnetic effect of the mineralization. TP-KM consists of a number of bull's-eye anomalies, at least some of which are caused by cultural features.

The maximum amplitude of anomalies in the Dawesley region (Figure 7.10) is $\sim$ 1200 nT. The anomalies are caused by magnetite and pyrrhotite within pelitic schists of the Tapanappa Formation and are collectively defined to be the Dawesley Magnetic Anomaly (DMA). The Dawesley Magnetic Anomaly has been investigated by Mirams (1962), Benlow and Taylor (1963) and Staltari (1974).

Drill hole DDH1 (Benlow and Taylor, *op. cit.*) intersected magnetite bearing sulphide bands. I detected magnetite in staurolite schists (Appendix D). The rocks in the Dawesley area may represent relatively more oxidised rocks compared to the rocks along strike further south. This would then favour production of metamorphic magnetite. The anomaly is right-laterally faulted by the Dawesley Lineament to the north (Plate 5). The axis of the Kanmantoo Syncline passes through this anomaly. At least two generations of folding have combined to produce a complex magnetic anomaly.

There is a major problem in resolving the stratigraphy in the *Tepko* and *Angaston* sheet areas mainly in the area covered by the Intermediate Subzone (ISZ). The lithologies in this area are mainly meta-arenites and migmatites. Mancktelow (1979) has attributed much of the outcrop in this area to the Backstairs Passage Formation but it should be noted here that similar lithologies (meta-arenites) are common in the Tapanappa Formation (see Section 7.4).

In the Karinya Syncline, lower metamorphic grades and pre-metamorphic variations have combined to produce magnetic units which, though linear, are discontinuous, vary rapidly in anomaly characteristics along strike and extend for only few kilometres. TP-KRS is typical of such anomalies.

Talisker Calc-siltstone

The type section of the Talisker Calc-siltstone (calc-siltstone facies) is along the south coast of Fleurieu Peninsula. Talisker Calc-siltstone equivalents have been identified in the KNSZ (Nairne pyrite facies and aluminous siltstone facies) and in the KRSZ (Karinya shale facies). The last three facies variants cause distinctive magnetic anomalies.

The calc-siltstone facies is composed dominantly of light and dark grey banded siltstones (Mancktelow, 1979). The darker siltstones often contain common accessory iron sulphides which Daily and Milnes (1971a) have identified as dominantly pyrrhotite. At Talisker Mine, the intense magnetic anomaly due to the Ulupa Siltstone masks any possible response from the Talisker Calc-siltstone. Linear anomaly TC-EB (Figure 7.5) is possibly due to pyrrhotite bearing rocks.

Between Tinpot and Harrogate, and in the vicinity of Macclesfield, the formation is characterized by a sulphide-rich pyrite facies containing pyrrhotite and accessory galena and sphalerite. This is the Nairne pyrite facies. At Brukunga this facies has been mined for its pyrite content. George (1967) investigated the Nairne pyrite at Brukunga and concluded that the pyrite was syngenetic in origin. The waste bodies around the ores were enriched in pyrrhotite while the ores contained pyrite and significantly less pyrrhotite.

In the vicinity of Macclesfield the anomaly TC-MS traces the Macclesfield Syncline and Strathalbyn Anticline. It is thickest around the anticlinal fold closure and thins out on the western limb of the syncline. Between Strathalbyn and Gemmell, and also near Rockleigh, aluminous siltstones have been equated with the Talisker Calc-siltstone. This facies is dominated by well laminated to banded meta-siltstone, which in medium to high metamorphic grade areas have recrystallized to form schists containing combinations of biotite, andalusite, staurolite, garnet and muscovite. The aluminous siltstone facies near Rockleigh has been correlated with TC-MNS, a curvilinear anomaly folded into the Monarto Syncline. Lawrence (1980) found numerous bands rich in iron sulphides in the siltstones near Rockleigh, and sedimentary and metamorphic pyrrhotite is assumed to be the cause of the anomalies.

The anomaly TC-WKS is a wide, multi-peak, intense, curvilinear anomaly caused by the Nairne pyrite facies of the formation. Variations in amplitude characteristics along strike is related to the variation in pyrrhotite content of the pyrite lenses. The pyrite-rich bands are more strongly weathered than the pyrite-poor bands and the radiometric image shows this up as a curvilinear low following the mapped pyrite bands. At Brukunga, the magnetic anomaly intensity is highest. The unit is sheared by the Mt. Beevor Shear Zone but can be followed further north. The anomaly traces the closure of the Kanmantoo Syncline and there is a corresponding anomaly on the eastern limb of the fold (TC-EKS). The trace of the Bremer Fault partly coincides with the trace of the anomaly TC-EKS.

TC-WKS can be followed for over 40 km along strike and for most of its length can be separated into two major bands: an eastern and a western band, which are associated with two major pyrite bands. Thomson (1969b) suggested that the eastern band was in the Tapanappa Formation while the western band was in the Talisker Calc-siltstone. However, in this thesis, both bands have been interpreted to be in the Talisker Calc-siltstone (Section 7.2.1).

The last facies variant is the Karinya Shale which is found in the doubly-plunging Karinya Syncline and is therefore not continuous with the other facies. The shale is black, very carbonaceous and laminated. Its magnetic response is patchy though linear. The strongest anomaly is developed around the closure of a syncline. Elsewhere, the patchy distribution may be due to variations in the amount of graphite. If the black shale originally contained pyrite, then increased metamorphic grade could result in the production of pyrrhotite. The amount of graphite present

would then control the amount of pyrrhotite which could form from the pyrite (Miyashiro, 1964; Thompson, 1972) and the variation in graphite content along strike might be the cause of the patchy variation in the amplitude and continuity of TC-KRS.

South of the western limb of the Macclesfield Syncline, a blue pyritic shale has been equated by Mancktelow (1979) with the Talisker Calc-siltstone. The interpreted extension of this shale under cover is associated with a strong, negative, linear anomaly, TC-CA.

Backstairs Passage Formation

The characteristic lithology of this formation is light coloured, well laminated, arkose. Arkose beds are separated by thin, well laminated, grey siltstones and phyllites producing a flaggy outcrop pattern (Mancktelow, 1979). Channeling is observed at the base of some arkose units, and on a macroscale, large scale channel structures have been mapped by Mancktelow (1979) between Strathalbyn and Brukunga and possibly west of Tungkillo. Medium-grained greywackes are occasionally found and become more common towards the top of the formation. The thickness of this formation is highly variable and Mancktelow suggests that this is largely a sedimentary feature rather than due to tectonic thinning. Mills (1964) has described heavy mineral scour structures in arkose units within the Karinya Syncline. These are probably part of the Backstairs Passage Formation. In the high metamorphic grade zones, the rocks have been migmatized in part. Magnetic anomalies attributed to this formation increase in amplitude with the increase in metamorphic grade.

The Backstairs Passage Formation has been mapped in the KNSZ (Kanmantoo Synclinal Subzone), the Intermediate Subzone (ISZ) and the KRSZ (Karinya Synclinal Subzone). Anomalies BP-CA, BP-SA, BP-WKS and BP-NKS are to be found in the KNSZ.

In the main study area, the southernmost exposure of the Backstairs Passage Formation is found near Mt. Magnificent. Here a triangular outcrop pattern of greywackes (Wymond, 1950) has been identified by Mancktelow (1979) to be a channel at the base of the Backstairs Passage Formation. This outcrop pattern is associated with a triangular shaped anomalous pattern: the "Channel Anomaly". The Channel Anomaly consists of BP-CA, in the Backstairs Passage Formation, and TC-CA, a negative linear anomaly possibly in the Talisker Calc-siltstone (Figure 7.6). If the Channel Anomaly does represent a channel (see Section 7.2.1), then detrital magnetite concentrated in the channel might be the cause of BP-CA.

North of Ashbourne, BP-CA is cut off and the formation decreases sharply in thickness, possibly disappearing altogether. It reappears around the closure of the Macclesfield Syncline and then widens around the Strathalbyn Anticline where the anomaly BP-SA is found. In this region, several channels have been mapped by Mancktelow (*op. cit.*). As the width of the channels changes so does the width of the anomaly BP-SA.

The anomaly BP-WKS may represent the northern continuation of BP-SA. Near Tinpot, the region separating these two anomalies is characterized by a small zone of NNW trending anomalies. The strike of the Backstairs Passage Formation in this region ranges from N to NE, so that the NNW trending anomalies might represent subsurface amphibolite dykes similar to the Woodside dyke swarm (Pain, 1968). Magnetic susceptibility measurements on Toteff's (1977) samples indicate that the basal member of the Backstairs Passage Formation is the most magnetic. Anomaly BP-WKS is caused by this member.

BP-NKS is attributed to migmatized Backstairs Passage Formation which extends from Pewsey Vale to Harrogate (Offler, 1966). A wide radioactive high is seen over BP-NKS in

keeping with the generally high radioactive anomalies associated with the migmatites. Anomaly BP-NKS is folded into a series of folds and is the first marker described in this region where outcrop is generally poor.

Anomaly BP-KRS is found in the KRSZ. BP-KRS is a discontinuous anomaly. Amplitudes are higher on the western limb of the Karinya Syncline than on the eastern limb.

Magnetic anomalies in the Intermediate Subzone (BP-A1, BP-A2, BP-A3, BP-A4) are distinctly different from those in the KRSZ and KNSZ, though BP-B1 and BP-B2 are similar. A dramatic change in the magnetic character of the formation is evident. The rocks in the Intermediate Subzone are within the sillimanite and migmatite zones and this is reflected in the intense pattern observed. Most anomalies are still linear and continuous and they generally trend NNW.

In the region of Rockleigh, a strong curvilinear anomaly, BP-A1, appears to follow the trend directions mapped by Mancktelow (1979). Where trend lines stop, magnetic maps indicate a folding of the anomaly back onto itself raising many questions about the number of macroscopic deformations in the area (see Section 7.4.1).

BP-A2 includes a number of intense, linear anomalies which may be equivalent to BP-A1. BP-A2 falls into the "zone of veins" (the migmatite zone as described by White, 1956) and exhibits high radioactivity. Similar linear anomalies are found to the north and east of the Rathjen Gneiss and have been collectively named BP-A4. Most of these anomalies are probably due to the dominant middle member of the formation.

Carrickalinga Head Formation

Good exposures of the Carrickalinga Head Formation are found at the type section (Carrickalinga Head), along the south coast of Fleurieu Peninsula, and in the Karinya Syncline. In the KNSZ, outcrop is limited to scattered occurrences above the Nairne Fault. In the Karinya Syncline, a recent road cutting along the Sedan Hill road has uncovered an excellent section through the formation (this section is henceforth referred to as the Sedan Hill section). Elsewhere in the Karinya Syncline, outcrop is poor. Since available aeromagnetic data on the south coast of Fleurieu Peninsula and at Carrickalinga Head is regional, it has not been possible to determine the magnetic effect of the formation in these areas. The best place to study the magnetic response of the formation is in the Karinya Syncline.

Anomalies caused by the Carrickalinga Head Formation have been found on both limbs of the Karinya Syncline. These anomalies are linear. CH1 and CH2 lie on the western limb and CH3 on the eastern limb. CH3 may be the equivalent of CH1 or CH2, but neither continues around the fold closure. CH1 has a strike length of around 20 km, CH2 of 40 km. CH2 is above CH1. CH1 is within the Blowhole Creek Siltstone. The Sedan Hill section was extensively sampled for susceptibility and the results were generally low. This was expected as this section cuts across the Carrickalinga Head Formation on the eastern limb, north of where CH3 terminates, and therefore did not transect any detectable magnetic anomaly.

6.1.2 Normanville Group

The Normanville Group is restricted in the study area. A narrow band of this formation crops out on the western limb of the Macclesfield Syncline in the KNSZ. No more Normanville Group

is seen till the *Angaston-Truro* region (Thomson, 1969b) where the Angaston Marble crops out. Between these two regions, the Kanmantoo Group is in contact with the Adelaide Supergroup. There is limited exposure of the Normanville Group on the east limb of the Karinya Syncline. It crops out more extensively west of the Karinya Syncline.

In the region of Precambrian and Normanville Group outcrop in the KRSZ, the stratigraphy has not been resolved and there are major differences in the interpretation by Coats and Thomson (1959) and Thomson (1969b). What has been mapped by Coats and Thomson (*op. cit.*) as belonging to the Normanville Group has been reinterpreted by Thomson (*op. cit.*) as being part of the Adelaide Supergroup.

The only volcanics which have been found on the Fleurieu Peninsula are the **Truro Volcanics**, which have been found near Truro (Forbes *et al.*, 1972), and at Red Creek and Milendella quarry (Cobb and Farrand, 1984) all on the *Truro* sheet (Coats and Thomson, 1959). The volcanics occur within a Lower Cambrian sedimentary sequence about 490 m in thickness lying with angular unconformity on siltstones and sandstones probably belonging to the Tarcowie Siltstone, Umberatana Group. The volcanics are interbedded with the meta-siltstones which may be equated with the base of the Heatherdale Shale of the Normanville Group (Forbes *et al.*, 1972). In the type section, the volcanics include green-grey amygdaloidal meta-basalt, altered porphyritic andesite, oligoclase andesite and sodic trachytes (Forbes *et al.*, 1972; Farrand, 1985). Susceptibility measurements on outcrops at the type section, Red Creek and Milendella quarry were low. Polished thin sections of the Heatherdale Shale (obtained from C.G.Gatehouse) show abundant, very fine-grained opaques, which are possibly magnetite.

Four linear to curvilinear anomalies have been identified in the Normanville Group: NG1, NG2, NG3 and NG4. NG1 is a weak linear anomaly above US-MS2 on the western limb of the Macclesfield Syncline. NG2 is a curvilinear anomaly seen on the eastern limb of the Karinya Syncline. NG3 is a continuous linear anomaly along the eastern limb of the anticline to the west of the Karinya Syncline. Because of the uncertainty in stratigraphy (see above), this anomaly may be in the Precambrian. Similarly the stratigraphic position of NG4 is uncertain.

6.1.3 Wilpena Group: Ulupa Siltstone

The Wilpena Group represents the last major transgression onto land in the Fleurieu Peninsula before the deposition of Cambrian sediments. Only units of the Brachina Subgroup (Plummer, 1978) outcrop on Fleurieu Peninsula. Preiss *et al.* (1987) equate these units with the Ulupa Siltstone rather than the Brachina Formation since the facies are different — siltstones rather than sandstones. Note that equivalent rocks outcropping near Sellick Hill are called Brachina Formation by Preiss *et al.* (1987) as distinct from Ulupa Siltstone.

In the WMZ, the Ulupa Siltstone equivalents (henceforth referred to as Ulupa Siltstone), cause distinctive magnetic anomalies wherever they outcrop. The intense, characteristic and consistent nature of the anomalies makes this formation an excellent magnetic marker. Magnetic anomalies caused by the Ulupa Siltstone occur over the Mt. Lofty Ranges from Cape Jervis to Eudunda (US-MS1, US-MS2, US-KRS, US-TR and US-PH). The Ulupa Siltstone is therefore the only stratigraphic unit which occurs widely and retains its characteristic magnetic properties. Since the Ulupa Siltstone is the highest distinctive magnetic marker in the Precambrian sequence, information about its occurrence is significant and can be easily noted even where good quality magnetic data are not available.

Brotherton (1967) recognized magnetite, ilmenite and titaniferous haematite in Ulupa Siltstone rocks from Delamere. He concluded that the red siltstones at Sellick Hill contained finely

divided haematite and that at higher metamorphic grades the haematite had been reduced to magnetite because of the presence of graphite. Opaque mineral assemblages in the Mt. Barker Creek area (*Echunga* sheet area) include magnetite, hemo-ilmenite and ilmeno-haematite with the ilmenites and haematites being the dominant opaques. Magnetic susceptibility measurements made on samples and outcrops from Cape Jervis to Eudunda are generally high (800–1300×10^{-5} SI) with lower values reflecting the dominance of haematite-ilmenite assemblages over magnetite (Section 2.3).

The anomaly at Delamere continues under Cambrian outcrop. Near Talisker, the Ulupa Siltstone is shown to have been faulted out by the Talisker Fault against the Backstairs Passage Formation. Stolz (1985) measured the NRM of the Ulupa Siltstone near Delamere and his results showed that the magnetic unit had a weak remanence ($Q \sim .5$) close to the direction of the present field.

North of Ashbourne, the most consistent of all curvilinear magnetic anomalies in the stratigraphic sequence, US-MS1 and US-MS2, trace the Macclesfield Syncline-Strathalbyn Anticline. In the north and south, the anomalies terminate against faults. The anomalies are remarkably consistent with respect to anomaly shape, width and amplitude. Being more ductile than the underlying and overlying rocks, parasitic folds have developed on the shared limb of the Macclesfield Syncline-Strathalbyn Anticline pair. These anomalies have been correlated with unit 2 in Toteff's (1977) subdivision of the "Marino Group". This unit varies between 260 and 290 m in thickness and consists predominantly of distinctive andalusite schists. Intermediate oxidation ratios and a high titanium content favour the presence of all three iron-oxide phases.

Part of anomaly US-MS1 is a distinct negative, suggesting a strong negative polarization probably due to NRM carried by the ilmeno-haematites and hemo-ilmenites. NRM measurements confirmed a direction inconsistent with that of the present field and a Q value of 2.3 (Section 2.3.1). Anomaly US-MS2 is positive throughout. This difference in anomaly sign reflects a difference in remanent components. Polished thin sections and oxidation ratio analyses showed that oxidation states varied rapidly over a single outcrop. It is therefore possible that the lower band (US-MS1) is more oxidized and dominated by titaniferous haematite assemblages while the upper band (US-MS2) is less oxidised and contains magnetite but less haematite and ilmenite. If the remanence is carried in the haematites and ilmenites, US-MS2 would therefore have a smaller remanent component than US-MS1.

The remanent magnetism of the Ulupa Siltstone is obviously related to its degree of metamorphism. During deposition, titanium and iron are no longer as closely combined as they are in igneous and metamorphic rocks. With metamorphism, titaniferous iron oxides and ferrian ilmenites form. With the exsolution of ilmenite from haematites and vice versa, chemical remanent magnetization is acquired.

US-MS1 and US-MS2 extend into the *Onkaparinga* sheet area where they are truncated by the Nairne Fault (Gatley, 1973). No Ulupa Siltstone style anomalies are detected until further north (Figure 1.2), where intense anomalies are observed associated with Ulupa Siltstone outcrop. In these areas the Cambrian is again shown to be in contact with the Ulupa Siltstone. In the Australia Plains area Drummond (1972) has mapped the Ulupa Siltstone on both limbs of the Karinya Syncline. From BMR data (Figure 7.13), anomaly US-KRS can be attributed to the Ulupa Siltstone. In contradiction with Drummond's (*op. cit.*) map, magnetic data clearly shows that the Ulupa Siltstone is continuous around the closure of the syncline.

On the eastern side, the anomaly US-KRS can be traced along the eastern limb under Caenozoic cover where it can be seen to be cross-faulted. The southerly extent of the eastern limb of US-KRS is uncertain as the anomaly is lost in the gradient which marks the contact between the EMZ and the CMZ. Along the western limb of the syncline, the anomaly can be

easily traced well beyond the southern limit of its outcrop as marked on the Truro geological map (Coats and Thomson, 1959). Here Cambrian rocks including the Truro Volcanics are shown as outcropping where the anomaly US-KRS has been traced.

Phosphate deposits at Moculta, St. Kitts and Koonunga (Brown, 1908) are found in Cambrian limestones which occur in synclines and are underlain by Ulupa Siltstone. This is deduced from the location of magnetic anomalies US-PH which are very similar to US-KRS. A number of synclinal closures are seen in the *Barossa-Angaston* region. These synclines have Kanmantoo Group rocks in the core underlain by Ulupa Siltstone. In the Barossa Valley, where Precambrian and Cambrian rocks are completely obscured, magnetic anomalies indicate that Ulupa Siltstone rocks are near the surface.

The maximum intensities of the Ulupa Siltstone magnetic anomalies are observed in the lower metamorphic grade areas (e.g. Delamere and Truro). In the Macclesfield area, the negative magnetic anomaly associated with US-MS1 indicates the presence of a strong remanent component in a direction different to that of the present magnetic field. However, Stolz (1985) measured the NRM of the Ulupa Siltstone near Delamere and his results showed that the direction of the remanent component was similar to that of the present field. It is suggested here that the NRM contained in the Ulupa Siltstone formed during metamorphism and is chemical in origin. In the higher metamorphic grade areas (e.g. Macclesfield) the exsolution of ilmenite from titanhaematite and vice versa has resulted in a strong remanent component.

6.1.4 Adelaide Supergroup: Burra and Umberatana Group

Sediments of the Burra and Umberatana Group cause weak but detectable anomalies particularly where the regional gradient is low. The Aldgate Sandstone contains heavy minerals concentrated from the basement in bands and laminae (Mancktelow, 1979). Other formations associated with magnetic anomalies are the Tindelpina Shale Member of the Tapley Hill Formation (McKirdy *et al.*, 1975), Woolshed Flat Shale, Sturt Tillite and the Rhynie sandstone. These anomalies help outline the Macclesfield Syncline and Strathalbyn Anticline, and the unnamed folds in the *Kapunda-Eudunda* area (Dickinson and Coats, 1957; Robinson, 1966). The northern closure of the Karinya Syncline is defined by a number of these anomalies. These anomalies are of the order of a few tens of nanoTeslas and linear. In the *Eudunda* area, where there is no outcrop, linear anomalies, similar to those described above, apparently follow the strike of sediments folded into the Karinya Syncline and are truncated by post-tectonic granite.

6.1.5 Barossa Complex

The basement to the Adelaide Supergroup crops out in inliers: Houghton Diorite, and Mt. Compass, Warren, Aldgate and Oakbank Inlier (Figure 1.3). The original lithology of much of the older basement has been obscured by strong retrogression or, in the case of the Warren Inlier, by moderate to high grade Palaeozoic metamorphism. The dominant lithology of the Houghton, Aldgate and Mt. Compass inliers is sericite schist (Wicks, 1972; Mancktelow, 1979). Ilmenite, titaniferous haematite and magnetite have been detected in these rocks, accounting for the intense, convoluted magnetic anomalies associated with the inliers. The anomalies are typically of the order of 2000 nT and only anomalies in the EMZ exceed these in amplitude and complexity. A few of the susceptibility measurements made by Horsfall (1973) on outcrops of the Houghton Diorite were of the order of the order of 4000×10^{-5} SI, though typical values were much lower. He suggested that strong retrogression and extensive weathering were responsi-

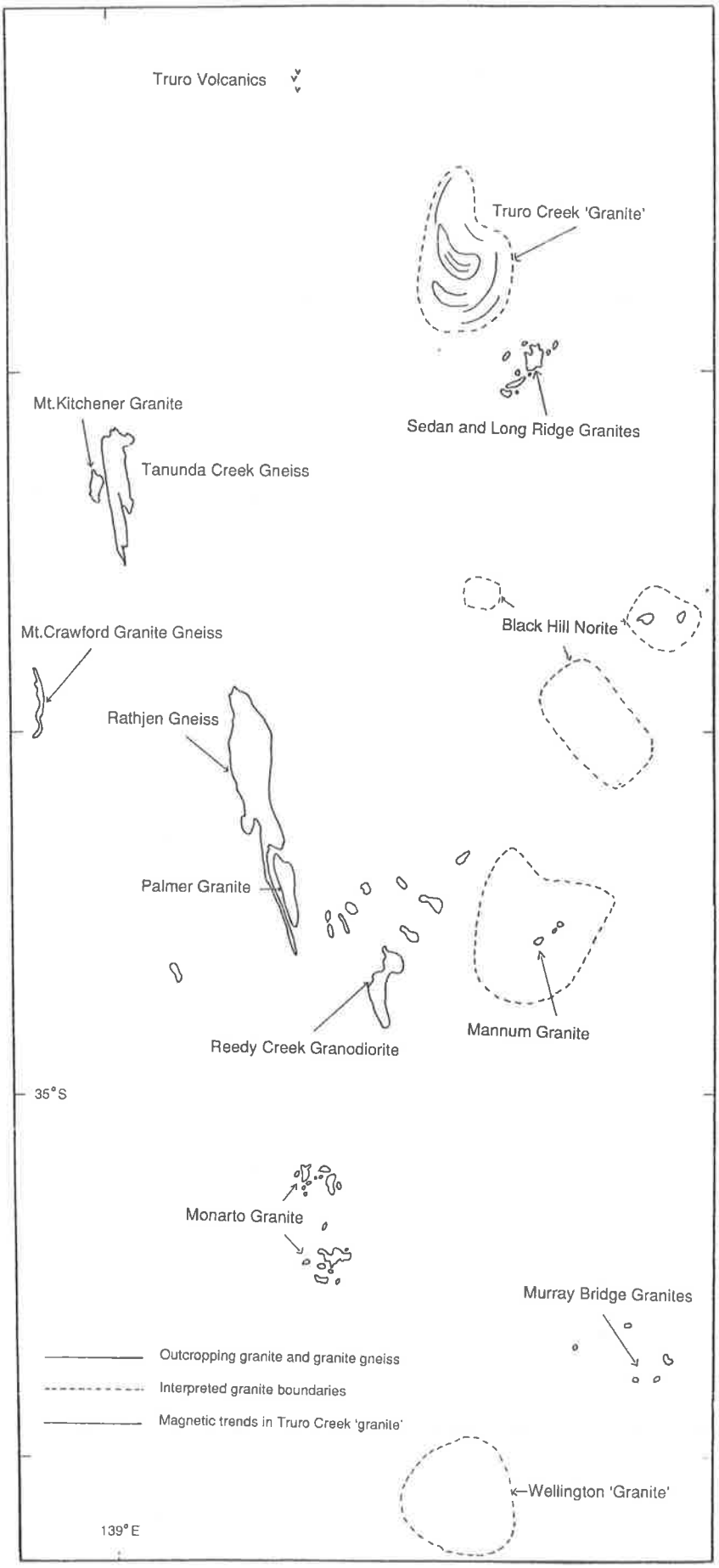

Figure 6.1: Location diagram for granites, granitic gneisses and Black Hill Norite (outcropping and interpreted).

ble for the lower susceptibilities in samples which apparently contained macroscopic magnetite grains. The magnetite was probably martitized to haematite.

Basement anomalies in the Mt. Lofty Ranges form two arcs: the southern one is formed by the Mt. Compass Inlier and anomalies BS1–BS3. The Houghton Inlier, Warren Inlier and anomalies BS4–BS6 form the northern arc. While BS1–BS4 are shallow, BS5 and BS6 range in depth from 1.5 to 3 km. The northern arc is offset to the west of the southern arc and they are separated by a fault (Section 5.2.1).

The northern portion of the Mt. Compass Inlier is covered by CRA magnetic data. On the total magnetic field contour maps, the inliers can be easily related to magnetic highs. The inlier is elongate in shape and bisected by a right-lateral fault. The vertical magnetic gradient contour map highlights the variation in magnetic properties within the inlier. Magnetic lows have been correlated with epidote-diorite assemblages and with the two occurrences of gold mineralization. Susceptibility measurements on outcrops of the Warren Inlier identified coarse-grained micaceous schists as strongly magnetic. In the case of the northern part of the Mt. Compass Inlier, the mica-schists are magnetic while the epidote-diorite is not.

6.2 Igneous rocks

Foden *et al.* (in press) have grouped the different granites and other igneous rocks found within the area into pre-, syn-, and post-tectonic rocks. Some of these are shown in Figures 6.1 and 6.2. The pre-tectonic group include the Truro Volcanics and amphibolites and dolerites in the Cooke Hill and Tungkillo areas (*Tepko* sheet — Gatehouse, 1988a). Syn-tectonic granitoids are common and widespread and include the granites at Palmer, Mt. Crawford, Reedy Creek and Encounter Bay and the Rathjen and Tanunda Creek Gneiss. The post-tectonic phase of Ordovician felsic magmatism was associated with mafic dyke emplacement. Post-tectonic intrusives include the following: Murray Bridge Granites, Mannum Granite, Sedan and Long Ridge Granites, the Black Hill Norite. The swarms of sub-alkaline, dolerite dykes, mostly oriented NW-SE found cross-cutting the Reedy Creek Granodiorite and diorite, and the Mannum Granite are also considered by Foden *et al.*(in press) to be post-tectonic.

6.2.1 Granites and granitic gneisses

Most of the above-mentioned igneous rocks have characteristic magnetic and radiometric signatures and have been classified as belonging to the magnetite-series or ilmenite series based on their opaque mineralogy and magnetic properties (Table 6.1).

A similar classification was made by Webster and Scheibner (1984) of the New England Granitoids on the basis of aeromagnetic interpretation. Magnetite-series granitoids (e.g. Walcha Road Adamellite) were related to well-defined magnetic highs while the magnetic effect of ilmenite-series granitoids (e.g. Mole Granite) resulted in a depression of total magnetic field contours.

The **syn-tectonic granites** vary in their geophysical properties. The Palmer Granite, Reedy Creek Granodiorite, Rathjen and Tanunda Creek Gneiss are magnetic, contain magnetite, and their average magnetic susceptibilities are well in excess of 500×10^{-6} cgs qualifying them as magnetite-series granitoids. Compared to the surrounding metasediments, they appear radioactive though their radioactivity must be due to increased uranium and/or thorium. The amount of potassium present in the granites (Mancktelow, 1979) was compared with that in metasediments (Table 2.7) and was found to be not significantly different.

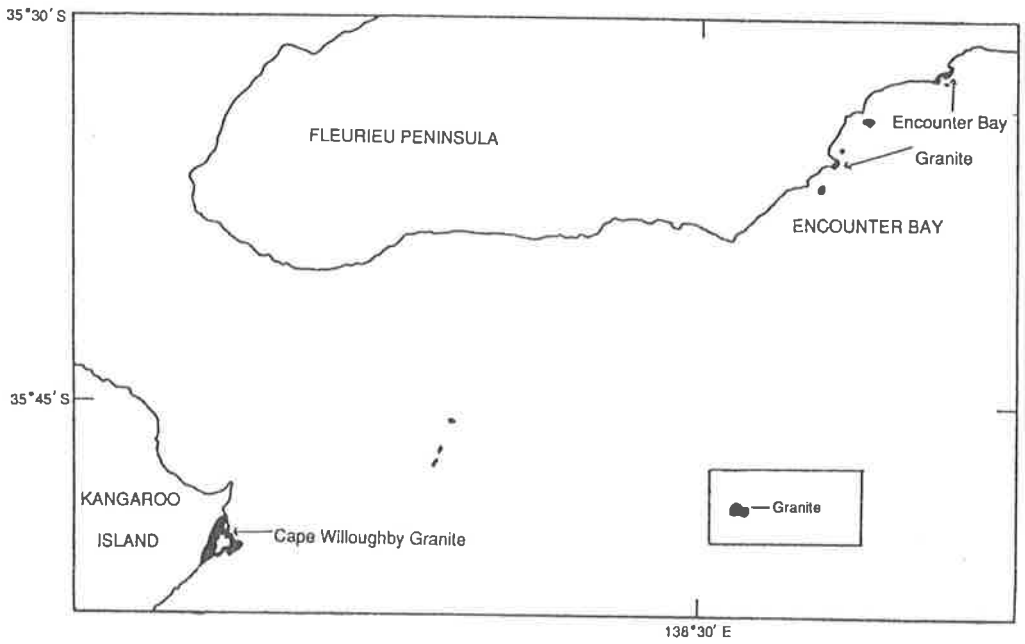

Figure 6.2: Location diagram for Encounter Bay Granite and Cape Willoughby Granite.

The **Palmer Granite** (magnetic anomaly PG) has been described by White *et al.* (1967) as being either fine-grained or coarse-grained, both variants being of granitic composition with accessory magnetite. Pyrite and rare molybdenite have been detected in the fine-grained type. The mapped contact of the granite with the metasediments can be easily traced from both aeromagnetics and radiometrics. The present outcrop pattern shows it to be an oval-shaped body with strike length 5 km and trending NNW. The northern part of the granite is dominated by the coarse-grained type and is more magnetic and radiometric than the southern part, which is dominated by the fine-grained type. Shear zones trending roughly NE are related to albitization of the granite and the albitized zones can be clearly identified as lows on the radiometric image. Magnetic modelling suggests a westerly dipping body. From its geochemistry, Mancktelow (1979) concludes that the Palmer Granite is I-type. Oxidation ratios are well above 50 (Appendix F and Table 6.1) and this too would suggest that it is a magnetite-series granite and therefore I-type.

The **Rathjen Gneiss** (magnetic anomaly RG) is a highly foliated, sheet-like body of strongly deformed granite with a prominent north-trending lineation (White, 1966b). Outcrops gave consistently high susceptibility readings and euhedral magnetite was observed in polished blocks. An oxidation ratio of 37 was computed from an analysis presented in Rattigan and Wegener (1951). NRM measurements on one sample gave a very low Q factor ($\sim .1$). The Rathjen Gneiss can be separated into an eastern and a western block which are separated by a sharp variation in lithology and grain size. This contact trends NNW and is part of the Springton Fault. Madigan (1988) interpreted an igneous origin for the Rathjen Gneiss based on the presence of xenoliths and the igneous nature of the contact with the adjacent biotite schists.

The eastern part is magnetic and radiometric. The northern closure has been modelled as a south-plunging syncline, with a depth extent of 800 metres. The syncline axis can be extended right through the gneiss though several NE trending faults offset the axis. These faults have been identified by breaks in magnetic and radiometric trends and are parallel to and sometimes coincide with a joint system described by White (1956). In contrast the western part appears less magnetic and radiometric. Outcrops are few and no longer exhibit the characteristic lineation and appear to contain less biotite. Since most research has concentrated on the eastern part, it is possible that either the western part is not true Rathjen Gneiss or else it is a variant of the material found on the eastern side. Magnetic susceptibilities are much lower, of the order of 300×10^{-6} cgs. The "tail" of the gneiss is a thin near-vertical sheet outcropping between the migmatites and the Palmer Granite. Its narrow width, less than 25 m, together with the intense magnetic signatures of the surrounding rocks prevented any study of its geophysical properties.

The Springton Fault separates magnetic Rathjen Gneiss from less magnetic Rathjen Gneiss. Just northwest of the Rathjen Gneiss the Springton Fault has vertically displaced a magnetic source. This magnetic source has an arcuate outline and may represent a subsurface extension of the Rathjen Gneiss (Plate 5).

Granitic gneisses east of Mt. Kitchener are collectively known as the **Tanunda Creek Gneiss**. Chinner (1955) recognized three types of gneiss: the predominant type, a quartz-biotite-feldspar gneiss which forms around 90% of the gneiss outcrop, is a buff coloured, medium-grained rock with pronounced foliation and lineation. Occasional "potash-deficient" gneisses occur as narrow bands within the first type. The third type contains hornblende, biotite, feldspar and quartz and crops out as a narrow band which can be followed for several miles. Chinner (*op. cit.*) suggested that these gneisses were the product of the metamorphism of sedimentary material. The Tanunda Creek Gneiss is similar to the Rathjen Gneiss (White, 1956; Offler, 1966) for which Madigan (1988) and Foden *et al.* (in press) favour an igneous origin.

The granite gneisses of the Tanunda Creek Gneiss cause both magnetic (anomaly TCG) and

radiometric anomalies. Together, the gneisses form an elongate body, roughly 4 km long and trending NS, the average width being 800 m. The predominant type, a potassium-rich rock, shows signs of potassium metasomatism. Abundant potassium minerals, mainly microcline, and allanite, together with the excellent quality of the outcrop of these rocks, are probably the main causes for the high radiometric signature. Accessory magnetite has been detected in these rocks (Chinner, *op. cit.*), and since the rocks appear to dip steeply towards the east, their geometry is similar to that of a wide dyke. Magnetic modelling of the edges confirms the easterly dips. If it is igneous in origin, then its magnetic properties together with its high oxidation ratio qualify the Tanunda Creek Gneiss to be a magnetite-series granite.

The **Mt. Crawford Granite Gneiss** is the only granite in the Mt. Lofty Ranges which is seen in contact with Adelaide Supergroup rocks (Mills, 1973). All other granites are in contact with Kanmantoo Group rocks. Quality of aeromagnetic coverage over the granite gneiss was too regional in nature to study its magnetic response.

The **Reedy Creek Granodiorite** is a distinctive, white, coarse-grained, almost porphyritic rock. Major minerals include oligoclase, plagioclase, with lesser quartz, hornblende, biotite and variable microcline. Accessories of sphene, zircon, epidote and magnetite are common (Whitehead, 1975). Fine-grained diorite occurs as elongate bodies and bands within the granodiorite and as a massive dyke cross-cutting the migmatites west of the granodiorite. The diorite intrudes the granodiorite though they exhibit good compositional continuity (Moeller, 1980) suggesting they developed from related magmas (Foden *et al.*, in press). Aeromagnetic data, magnetic susceptibility measurements, oxidation ratio (37.69) and the presence of magnetite indicate that the Reedy Creek Granodiorite belongs to the magnetite-series. Regional aeromagnetic interpretation indicates a much larger body which is now under Caenozoic cover.

The **Encounter Bay Granites** crop out at Cape Willoughby, on the southern coast of Kangaroo Island, and on the south coast of Fleurieu Peninsula in Encounter Bay. They fall within the group of syn-tectonic granites because they are believed to have intruded the younger Kanmantoo Group sediments prior to the culmination of the first folding event (Milnes *et al.*, 1977). The major granite type is a medium to coarse-grained biotite granite which contains opalescent blue quartz. The Encounter Bay Granites have probably become contaminated by digestion of Kanmantoo Group metasedimentary rocks. Magnetic anomalies have not been associated with these granites. Albitized granite at Rosetta Head returned very low susceptibility values but the magnetic properties of the group as a whole have not been investigated.

The syn-tectonic granites described above are mineralogically and geochemically I-type (Foden *et al.*, in press). The Monarto Granite, though also considered to be syn-tectonic, fits into the S-type classification (Hoesni, 1985). It is a medium-grained light grey granite and though Mancktelow (1979) reported magnetite within it, all magnetic susceptibility measurements on samples and outcrops gave uniformly low values. The granite also contains primary muscovite which sets it apart from the Palmer and Murray Bridge granites and is consistent with its classification as an S-type granite, although field relationships indicate that the Palmer and Monarto Granite are of similar age (Mancktelow, 1979). The magnetic response over the Monarto Granite is dissimilar to that over the magnetite-series granitoids. The north Monarto Granite does not affect the magnetic response much though the south Monarto Granite depresses the field and disrupts the pattern. Between the north and south Monarto Granite, a magnetic high is observed which also disturbs the normal gradient in the area. Gravity measurements (Lewis, A. M., 1985) indicated a high over the north and south granites with a slight low between them. Lewis, A. M. (1985) interpreted two granite bodies separated by a thin veneer of granite overlying magnetic metasedimentary rocks of the Kanmantoo Group.

Granite stocks near Rockleigh, in the Springton area and in the south Karinya Syncline are

sometimes magnetic. The generally intense magnetic pattern observed in the ISZ obscures the anomalies due to the small stocks. Granodiorites, diorites, granites and aplites all had high magnetic susceptibilities and contribute to the intense magnetic response in these areas. It is not known which of these are pre-, syn- or post-tectonic.

Foden *et al.* (in press) identified three post-tectonic granites: the Sedan, Murray Bridge and Mannum Granites. The granites all have recognizable magnetic anomalies of the order of $\sim$ 1000 nanoTeslas and the spatial dimensions of the granites exceed the mapped dimensions by several times. The Sedan Granites include the Long Ridge Granites.

The Murray Bridge suite (Milnes *et al.*, 1977) includes the Murray Bridge Granite, Reedy Creek Granodiorite (Sando, 1957; Whitehead, 1975; Moeller, 1980), the Mannum Granite (Goode, 1927), the Swanport Granite (Kleeman, 1934), the Sedan Granites (Wegmann, 1980) and the upper southeast granites (Henstridge, 1970). According to Foden *et al.* (in press), these granites are all very siliceous, true granites and are characterized by smokey quartz. Magnetite has been reported from all of them. Magnetic susceptibility measurements on hand samples and outcrop measurements gave uniformly high values, well over 1000×10^{-6} cgs.

These granites (excluding the Reedy Creek Granodiorite) lie on a north-south trending belt which runs to the east of the Palmer Fault and Milendella Fault and is part of the MMH. Their dimensions as determined from magnetic maps are of the order of several tens of kilometers spatially. This is in sharp contrast to the much smaller dimensions of syn-tectonic granites within the CMZ. The Sedan Granites are very similar in magnetic response and properties to the post-tectonic granites.

The Reedy Creek Granodiorite is the only one of the granites listed by Milnes *et al.* (1977) as part of the Murray Bridge suite which is not within the EMZ but within the CMZ. From the regional interpretation presented in Section 5.2.1 (Figure 5.7), the Reedy Creek Granodiorite does not form part of the Murray Bridge suite. This is consistent with the interpretation by Foden *et al.* (in press) that the Reedy Creek Granodiorite is syn-tectonic while the Sedan, Murray Bridge and Mannum Granites are post-tectonic.

Two other granites have been interpreted (and named) from magnetic maps: the Truro Creek "Granite" and the Wellington "Granite". Both are located within the EMZ, and from aeromagnetic maps appear to have cross sections of many kilometres. Drill hole data confirmed the presence of quartz-diorite in the Truro Creek "granite" (Wegmann, 1980; Figure 5.7). This granite is unusual in that its magnetic pattern is characterized by alternate magnetic and less magnetic arcs. The magnetic anomaly is shown in the top right corner of Figure 5.4 and interpreted magnetic trends are shown in (Figure 6.1). This magnetic layering indicates a lithologic layering in the granite. The Klokken intrusion is a similarly vertically layered granite. Parsons and Brown (1988) describe the inner part of this intrusion as consisting of a spectacular series of layered and laminated syenites. The layered series consists of granular and laminated syenite which are interleaved, the succession forming a pile of inward dipping basins. A similar model is suggested for the Truro Creek "granite" with the alternate layers representing rock of different magnetic properties.

The Wellington "Granite" shows up as a depressed circular low on the magnetic contour maps (lower left corner of Plates 1, 2 and 3 and also shown completely in Figures 5.6 and 5.7). The granite is marked by a steep gradient and magnetic anomalies are truncated at the contact.

All the magnetite-series granites identified as such from their magnetic responses, magnetic susceptibilities and opaque assemblages are I-type granites (Foden *et al.*, in press; Mancktelow, 1979) which is consistent with Ishihara's (1971) observation that all magnetite-series granites are I-type granites, a necessary though not sufficient condition. The Mannum Granite has been

Granite	Magnetic anomaly nT	Radiometric anomaly	Oxidation ratio (average)	susceptibility $\times 10^{-5}$ SI (average)	Opaque oxides	Genetic type	Magnetic classification
SYN-TECTONIC GRANITES							
PG	350	High	54.1	1000	mt	I	mt-series
RG	120	High	37.6	1200	mt		mt-series
TCG	400	High	43.9		mt		mt-series
MKG	400	Low			mt		mt-series
RCG	≈500		37.7	1000	mt	I	mt-series
MNG			31.5	5	ilm	?	ilm-series
POST-TECTONIC GRANITES							
MMG	≈1500		54.8	3000	mt	A	mt-series
MBG	≈500		34.3	600	mt	I	mt-series
SG	≈500			600	mt	I	mt-series
WG	Low						ilm-series

Table 6.1: Magnetic classification of granites. Abbreviations — PG: Palmer Granite, RG: Rathjen Gneiss, TCG: Tanunda Creek Gneiss, MKG: Mt. Kitchener Granite, RCG: Reedy Creek Granodiorite, MNG: Monarto Granite, MMG: Mannum Granite, MBG: Murray Bridge Granites, SG: Sedan and Long Ridge Granites, WG: Wellington "Granite". Magnetite is abbreviated to mt and ilmenite to ilm. Oxidation ratios and susceptibility measurements are listed in Appendices F, B and C.

classified by Foden *et al.* (*op. cit.*) as an A-type granite (high-level, siliceous, "dry" granite) but Ishihara's (*op. cit.*) study deals only with the original classification by Chappell and White (1974) of granites as I or S type. The Mannum Granite had the highest measured susceptibilities of all the granites. The magnetic properties of the Monarto Granite are consistent with it being a member of the ilmenite series.

Ishihara (1981) points out that recognition of the two series of granitoids is an important first step in mineral exploration. The magnetite-series are related to major sulphide mineralization and the ilmenite-series to cassiterite and wolframite mineralization. Since the classification depends on the magnetic properties of granites, it can be accomplished by interpretation of aeromagnetic data and by outcrop susceptibility measurements. Even in weathered outcrops, complete martitization of magnetite to haematite rarely reaches 50%, unless the granite has been hydrothermally altered.

On the basis of magnetic properties, dimension, and location, four groups of granites have been recognized:

1. magnetite-series, generally small (spatial dimensions of the order of a few km) granites in the CMZ which have been deformed during the Delamerian Orogeny. These include the Palmer Granite, Rathjen Gneiss, Tanunda Creek Gneiss and Mt. Kitchener Granite and the much larger Reedy Creek Granodiorite.
2. ilmenite-series Monarto Granite which has intruded Kanmantoo Group metasediments in the CMZ.
3. magnetite-series, large granites (spatial dimensions of the order of many kilometres) which intrude the EMZ and form a belt of intense magnetic anomalies. These include the granites at Murray Bridge, Mannum, Sedan, Swanport and the Truro Creek "Granite".
4. probably ilmenite-series granite (though identification based only on magnetic interpretation) intrusive in the EMZ — the Wellington "Granite".

According to the magmatic history outlined by Foden *et al.* (in press), the first two groups of granitoids were intruded during the Delamerian Orogeny and the granites in the last two groups were post-tectonic. During the Early Ordovician, syn-tectonic, I-type granitic magmas intruded Cambrian metasediments. Most post-tectonic granites discussed above are several times more magnetic than syn-tectonic granites probably due to the extra magnetite. The intrusion of the post-tectonic granites is related to an extensional phase following the close of the Delamerian Orogeny. These granites (and the gabbros, basalt, etc. discussed below) form the Murray Magnetic High (MMH). As mentioned in Chapter 5, the MMH is a major magnetic feature which demarcates the eastern limit of Precambrian outcrop. The extensional phase which resulted in the intrusion of the granites is a significant event in the history of the region.

6.2.2 Gabbros, amphibolites and dolerites

Small scattered outcrops of amphibolites and dolerites (Liu and Fleming, 1989) have variable magnetic properties. However they are generally too small to be picked up on more than one or two flight lines and their magnetic response is not known. The Woodside dyke swarm (Pain, 1968) trends NNW. Ilmenite has been identified (Alderman, 1931) but not magnetite. NNW anomalies in the vicinity of Tinpot may be caused by magnetic dolerite dykes. The magnetic trend is opposite to the trend of the arkoses of the Backstairs Passage Formation as mapped from aerial photographs by Mancktelow (1979).

Gabbro intrusions give rise to distinctive magnetic anomalies. A circular magnetic anomaly, 5 km in diameter, and around 1000 nT in amplitude (top right corner of Figure 5.4) is found in the MMH. Lewis, P. (1985) records that a drill hole into the anomaly intersected gabbro at 244 m.

The Black Hill Norite gives rise to a negative anomaly. The negative intensity implies a strong negative remanent polarization. There are several such anomalies in the vicinity of the original Black Hill Norite which have been interpreted as being caused by similar gabbros. Some of these "Black Hill" style magnetic anomalies have been drilled and confirmed to be Black Hill Norite equivalents (Wegmann, 1980). Wake-Dyster (1974) suggests a field reversal during the Ordovician to account for the negative polarization. According to Foden *et al.* (in press), these mafic intrusions are post-tectonic. The variable magnetic properties of the post-tectonic granites and gabbros may reflect several phases of post-tectonic intrusion.

6.3 Radiometric response

For reasons outlined in the Introduction, it has not been possible to estimate the radio isotope content of the soil and hence, the concentration of potassium and equivalent uranium and thorium in the rocks. Nevertheless, the use of images of the total count channel have been used to confirm and in some cases suggest models for the interpretation of the magnetic data. Colour integration of aeromagnetic and radiometric data helped in the mapping of faults, contacts, and in the correlation of anomalies with similar radiometric and magnetic properties.

Establishing "ground truth" or the correlation between known geology with geophysical response is a first step before extrapolating beyond the areas of geological control. The grey-scale image of total radiometric count and the colour composite image (Figure 3.5) were compared with geological maps.

The main sources of radiometric anomalies include transported and *in situ* soils, and exposed metasediments, migmatites and granites. Other rock units in the area, e.g. pegmatites, dolerites and amphibolites, are generally too small in spatial extent to be readily identified on a total count image, assuming they had a characteristic, anomalous radioactivity. In the higher metamorphic grade areas, zones of pronounced enrichment and depletion in the radioactive elements (usually potassium) are associated with metasomatism, faulting and migmatization. There were also many anomalous areas which could not be readily associated with mapped geology.

In situ soils and bedrock can be generally grouped into zones of pronounced enrichment or depletion in radioactive elements and zones reflecting stratiform anomalies. The main lithoradiometric units are the metasediments and granitic rocks. Possible sources of radioactivity are the K-minerals (particularly orthoclase, microcline and micas), and Th and U bearing minerals (zircon, sphene, monazite, allanite). After the K-minerals, zircons are probably the most important carrier of radioactive minerals. They have been identified in biotites by means of the pleochroic haloes generated. The relation between anomalies and geology is listed below.

1. Transported soils identified in the area include limited outcrops of non-radioactive sands and moderately radioactive alluvial of Tertiary or Quaternary age. Stream channel and drainage patterns show up as radioactive highs or lows depending on the sediment they carry.

2. Stratiform anomalies due to the metasediments show up as curvilinear highs (black and pyritic shales and siltstones), as curvilinear lows (limestones, almost pure marble and

quartzite) and as large areas of uniform radioactivity due to uniform lithology. Curvilinear trends are the result of macroscopic folding. In general, the more pelitic metasediments are more radioactive than the more arenaceous. Migmatites can be easily identified because of their relatively high radioactivity.

The Milendella Limestone Member of the Carrickalinga Head Formation served as an example of a non-radiometric, non-magnetic marker. Its outcrops are easily identified on aerial photographs. On radiometric images it is traced as a low. Several bands and folds within the Milendella Limestone Member have been picked up and verified on Mills' (1964) map of the southern Karinya Syncline. The detail shown in the delineation of this unit from radiometrics is remarkable and probably due to its excellent outcrop and to the sharp change in the radio-isotope content going from the limestone to the more granitic and potassium-rich metasediments on either side of it.

The radiometric response of the metasediments is a complex function of lithology and outcrop pattern: meta-greywackes and semi-pelitic schists bear more potassium and probably less heavy minerals than meta-arkoses, however the latter weather less readily. As a result, large parts of the image indicate quality and abundance of outcrop and cannot be simply related to underlying lithology. This relationship between outcrop and radiometric highs is well illustrated by the Nairne pyrite facies of the Talisker Calc-siltstone. Even against the background of a quiet radiometric response, the pyrite bands can be easily followed as radiometric lows. However at Brukunga, where the outcrop is excellent in an open-cut mine, a well-defined high is observed.

Another major control on resolution of radiometric anomalies is the change in radio-isotope content across the area rather than absolute values. The Milendella Limestone Member is well resolved because the surrounding rocks give high background values; similarly the higher radioactivity of the Ulupa Siltstone in the Macclesfield area is contrasted against the non-radiometric response over the adjacent quartzite and this results in better definition of the Ulupa Siltstone horizon.

Metasomatism, whereby potassium has been introduced into the area, and migmatization of rocks produce well-defined, radiometric anomalies. East of Springton, in the Pewsey Vale area and west of Palmer, meta-arkoses and migmatites cause radiometric anomalies of the same order as the granitic rocks. Significantly, the more magnetic units in the higher metamorphic grade zones are also the more radioactive.

On the *Tepko* and *Angaston* sheets, areas of sodium metasomatism have been mapped. Potash-deficient schists are found around the granitic gneisses in the Pewsey Vale area (Chinner, 1955), north of Rockleigh (White, 1956) and east of Springton (Mills, 1964) and these areas were associated with radiometric lows.

3. The outline of granites and granitic gneisses can be quite easily traced because of their generally high radioactivity e.g. the Palmer Granite and the Rathjen Gneiss. The extensively albitized Mt. Kitchener Granite is characterized by a low in the total radioactive count.

   The Palmer Granite was chosen as an example of a geological unit known to give rise to a magnetic anomaly and expected to be more radioactive than the surrounding metasediments. From the radiometric image, it was verified that the granite causes a radiometric high, and that the southern part is less radioactive than the northern part. Several crush zones which are known to have been albitized show up as lows.

   The Tanunda Creek Gneiss and the Rathjen Gneiss have high radiometric responses. The Rathjen Gneiss has a patchy, variable response possibly due to variation in amount of outcrop. If the western contact between the Rathjen Gneiss and the metasediments has been correctly mapped, then a compositional difference between the eastern and western parts may be the cause of the radioactive and magnetic low to the east (see section above). The

Mt. Kitchener Granite shows up as a high on the magnetic maps but has no anomaly associated with it on the radiometric images. Extensive metasomatism in the area (Chinner, 1955) has enriched the granite in sodium at the expense of potassium.

4. Faults, shear zones, lineaments and contacts have been identified by the sharp change in radioactivity across them. While the causes of these anomalies have not been identified, they may be the result of fluids circulating within fault and shear zones either enriching or depleting the host rocks in radioactive elements, and possibly the result of variable weathering patterns on either side of these structural features. Several fault zones were albitized and therefore associated with radioactive lows.

   Faults, particularly those which have been activated or reactivated during the Tertiary, can be identified from the radiometric images owing to the differing weathering response on either side of the fault zone and perhaps sericitization of the breccia within the crush zone. The scarp associated with the Palmer and Milendella Faults is primarily late Mesozoic-early Tertiary in age (Twidale and Bourne, 1975). These faults are associated with a steep gradient in the radiometric count rates owing to the difference in the radioactive element concentrations between the Kanmantoo Group to the west of the faults and the Caenozoic sediments of the Murray Basin to the east. Most deposits of younger sands and gravels show up as radioactive lows.

Chapter 7

Macroscopic structures within the Central Magnetic Zone

The increased information content of high-quality airborne geophysical data sets, together with the enhanced resolution made possible by modern processing and presentation techniques, has resulted in the successful application of geophysics to the delineation of both major and minor structures. Geophysical interpretation provides an independent source of geological facts and a perspective which can often be quite different from that of the accepted geological model.

Ideally, the interpretation process should consist of two separate stages: the first interpretation should be carried out without reference to geological maps. By this means, new structures may be identified and errors in the geological maps (caused by lack of outcrop, incorrect identification, ...) prevented from unduly influencing the geophysical model. The next stage should involve the integration of geological and geophysical information, with geological mapping used to modify and improve the geophysical "mapping".

Previous geological work has concentrated on small parts of the Mt. Lofty Ranges. The major syntheses of the structural geology of the Kanmantoo Group include the work of Thomson and Horwitz (1962), Offler and Fleming (1968), Thomson (1969b), and Mancktelow (1979). The quality of structural mapping varies and much remains unclear. High-resolution aeromagnetic data are now available over large areas of Kanmantoo Group outcrop. The data has been studied to resolve previously mapped structures, to establish continuity of structural features, to discover new structures and to achieve a uniform approach to the study of the deformation pattern. In this chapter, structures discussed include reexamination of previously recognized features, albeit from a "magnetic" viewpoint. In the main study area, particularly in the intensely metamorphosed region, important new structures are demonstrated which could provide a key to the structural history of the region.

The relative importance and the number and order of the different deformation events is a controversial issue. The two major reviews (Offler and Fleming, 1968; Mancktelow, 1979) differ considerably. The major deformation which produced most of the macroscopic folds in the area has variously been interpreted as being D_1 (Poole, 1969; Daily and Milnes, 1973; Drummond, 1972; Mancktelow, 1979), and as being D_2 (Marlow, 1975; Abbas, 1975). Offler and Fleming (1968) suggest that though the effects of the first deformation D_1 left the most widespread effects, D_3 folds dominated the structural pattern in the eastern Mt. Lofty Ranges. This was later revised by Fleming and White (1984) who state that D_2 folds form the majority of post-D_1 structures, and D_3 macroscopic structures are comparatively less common. Offler and Fleming (1968), Allen (1977), Fleming and White (1984), Hoesni (1985), Madigan (1988) and Foden

et al. (in press) have reported a deformation event prior to what Mancktelow (1979) considers to be D_1. This deformation apparently produced isoclinal and recumbent folds on a mesoscopic scale.

Since the structural history of the Mt. Lofty Ranges is controversial, it has been decided to use a framework of three phases of folding for the whole area. Each phase may include more than one event. The major folding which produced the Kanmantoo Synclinorium is taken to be F_{main}. An early deformation was recognized in some places and these F_{early} folds have been folded by F_{main}. The second phase of folding was pervasive throughout the CMZ. In the ISZ, strong overprinting by a later generation of folds, F_{later}, may have obscured the F_{main} phase of folding. By this means a structural framework applicable to the entire study area, consistent with past structural mapping, and yet independent of the controversies engendered by previous researchers, has been devised. The corresponding deformation events are D_{early}, D_{main} and D_{later}. When the terms F_1, F_2, ..., are used, they are specific to the reference cited.

In the first section, the applicability of aeromagnetic interpretation to structural interpretation is discussed. In the next three sections, the magnetic interpretation of major structures in each of the subzones, KNSZ, KRSZ and ISZ, is presented. The discussion is intended to supplement the interpretation maps, Plates 1 and 5. Some of the figures in this chapter are in colour: the colour key is shown on Plate 1.

The major structures which control the outcrop pattern in the CMZ are the Macclesfield Syncline, Strathalbyn Anticline, Kanmantoo Syncline and Monarto Syncline in the KNSZ, the Karinya Syncline and associated anticlinal folds in the KRSZ, and multiple, unnamed folds in the ISZ. The ISZ has been subdivided into a number of subareas which have similar magnetic characteristics. The main study area includes part of the WMZ in the west and north, and part of the EMZ in the east.

Some magnetic cross sections are illustrated in this chapter but the full results of modelling anomalies are given in Appendices I and J. In the figure captions, the approximate locations of some anomalies are mentioned.

7.1 Scope of aeromagnetic interpretation in structural analysis

On a macroscopic scale, structural geologists use outcrop observations and aerial photographs to map structures. They are limited by lack of access to outcrops and by the amount of soil cover. Even a cursory examination of aeromagnetic maps (Plates 1 to 3, Figure 5.4) reveals the abundance of folds and faults which can be resolved. Continuity of information and depth of penetration make the aeromagnetic method particularly sensitive to changes in structure. In this section, the potential and limitations of applying aeromagnetic interpretation to structural analysis are examined briefly.

All structures discussed in this chapter are macroscopic structures. Magnetic interpretation on its own cannot be used to separate the effects of the sedimentary, metamorphic and igneous history of a region from the structural history. Note too that where there is no detectable magnetic property contrast, there can be no magnetic anomaly.

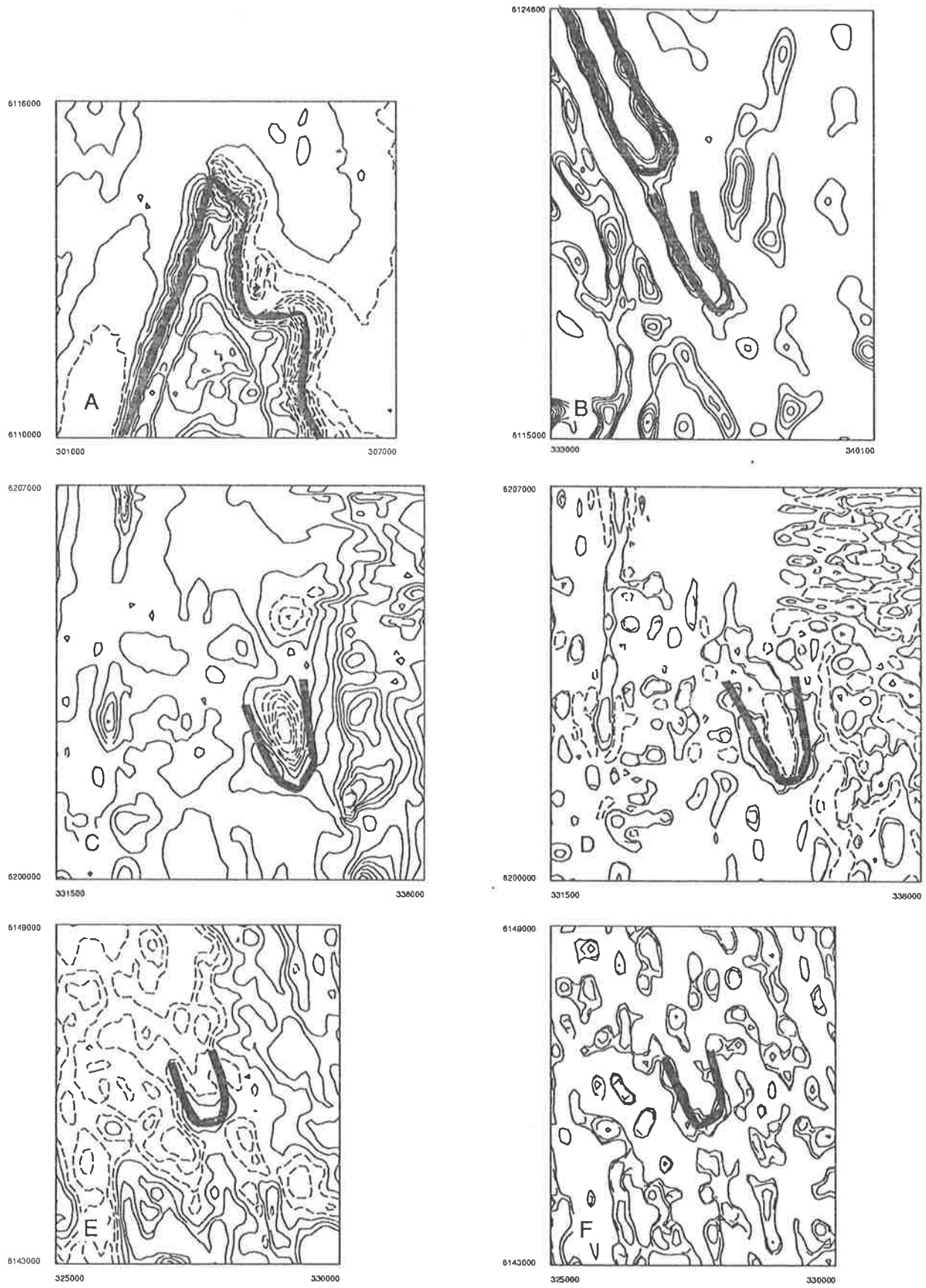

Figure 7.1: Examples of fold anomalies on magnetic maps. The contours are irregularly spaced. Dashed-line contours are lower in value than continuous-line contours. A, B, C and E show the total magnetic field, and D and F show the vertical magnetic gradient.

7.1.1 Magnetic modelling

The different geometric models used to model magnetic anomalies include two-dimensional models (dipping dyke, horizontal edge and prismatic polygon) and the single pole model. For an explanation of these terms refer to Section 4.1.2. The single pole model and the dipping dyke model were used to model deep-seated basement features. Dipping metasedimentary horizons, which had strike extents of several kilometres or more, were modelled using the dipping dyke model and, where this was not suitable, the prismatic polygon model. The polygon model allows for the sides of the body to dip at different angles and for the top of the magnetic source to be non-horizontal. The term "dyke model" or "dipping-dyke model" refers to the geometrical model and not to the intrusive dyke.

Except for the very few anomalies due to deep-seated magnetic basement, depths to the top of magnetic sources were within 100 m and commonly within 30 m. The shallowness of the sources meant that the most significant parameter to be estimated was the dip of the magnetic horizon. Additionally the interpreted magnetic map (Plate 1) is similar to a geological map in that interpreted magnetic units either outcrop or are near-surface.

When modelling magnetic anomalies, a distinction must be made between "magnetic dips" (i.e. dips computed from magnetic modelling) and structural dips. This distinction is due to two important reasons:

1. The assumption that the direction of magnetization is the same as that of the present field of the earth is not always valid. Since it is not possible to separate the effects of geometry (usually structural dip) and NRM from the magnetic anomaly, the use of an incorrect value for the direction of magnetization will result in incorrect dip estimates.

2. The effect of nearby magnetic sources complicates interpretation and increases the ambiguity inherent in magnetic interpretation. By computing the vertical magnetic gradient, an improvement in resolution can be achieved and the definition of the anomalies improved. But in areas of structural complexity, anomalies may still be too close together to be interpreted in isolation.

Additionally, when interpreting folded sequences, the dipping-dyke model is a simplification of a dipping horizon which changes in dip in the vertical plane. Depending on the curvature of the magnetic source, the accuracy in estimating the dip varies.

7.1.2 Folds

Successful interpretation depends on the scale of the folds, the trend of the axial plane and the number of intersections made on the flight paths. Folds can be mapped by tracing a magnetic unit around a fold closure, by changes in the trend of the bedding or the strike of the units, or by comparing the dips on the limbs of the suspected fold. Commonly, there is thickening around the fold hinges and an associated increased magnetic response (Whiting, 1987). If the limbs of the fold have been thinned, a triangular shaped anomaly may be all that is there to identify a fold closure. If the fold closure lies entirely between two flight lines, or is transected by only one flight line, the closure will probably go unnoticed. In the absence of other information, isoclinal and tight folds cannot be distinguished from dipping magnetic units unless the fold closure can be mapped.

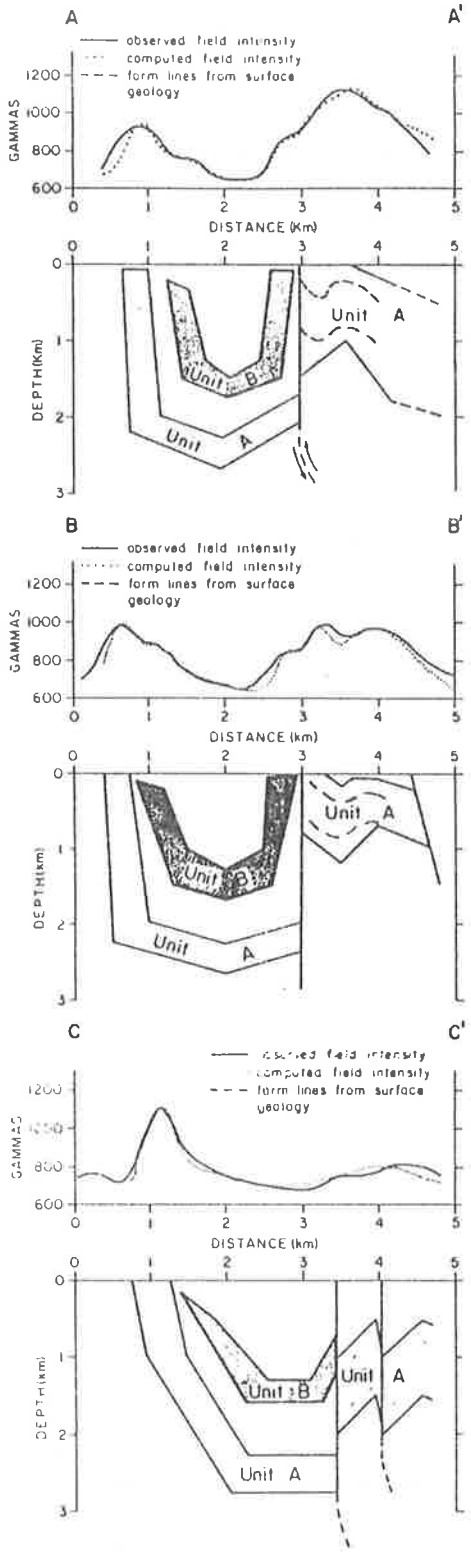

Figure 7.2: Magnetic modelling of synclinal structure (after Robinson *et al.*, 1985).

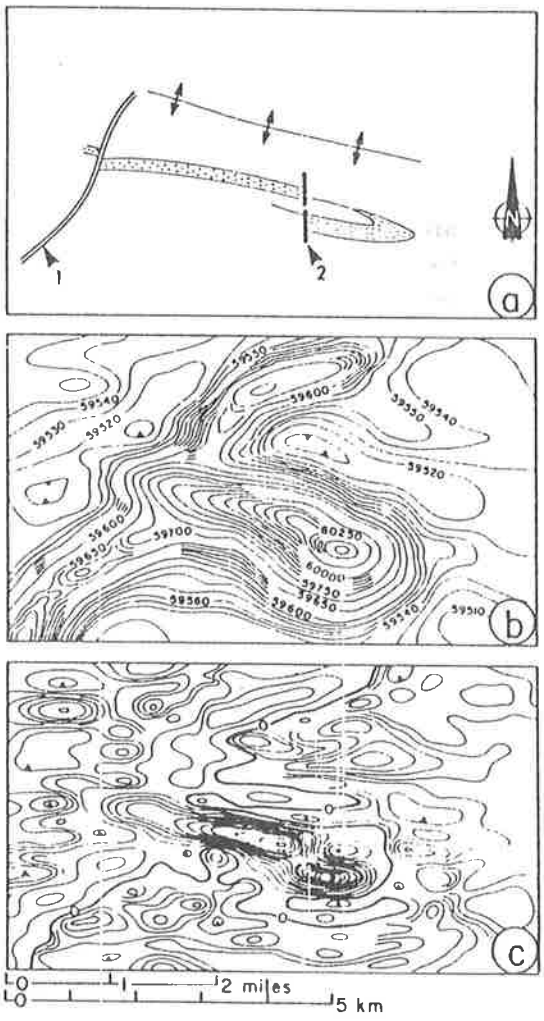

Figure 7.3: Anomaly on a fault: a) Geology (1-dyke, 2-fault). b) Total field. c) Apparent susceptibility, (after Yunsheng *et al.*, 1985).

Intense anomalies which appear to be round or oval on contour maps may be due to small scale, tight folds. Anomalies which start off as wide and then taper off may indicate folded units. Anomalies caused by folded rock units change around the fold. Part of the reason is because of the different dips and sometimes the effect of remanence (NRM) compounded with the change in dip. It is not only the limbs of folds which can be mapped: it is also possible for the dipping axial surface to give rise to a detectable magnetic anomaly. Disruptions in the continuity of magnetic anomalies as a result of faulting can lead to the illusion of a tight fold closure and it may be impossible to resolve this further.

Some examples of interpreted fold anomalies are illustrated in Figure 7.1. In diagram A of this figure, contours of the vertical magnetic gradient delineate the Macclesfield Syncline. Outcrop in the region is very poor and the parasitic folds seen on the eastern limb were not previously known to exist. The second example, B, is taken from the ISZ. The fold closures outlined may represent early isoclinal folds. The limbs are parallel and now form the eastern limb of a regional syncline.

A north-plunging syncline is mapped in diagrams C and D of Figure 7.1, and a south-plunging antiform in diagrams E and F. The contours in diagrams C and E are of the total magnetic field, and in diagrams D and F of the respective vertical magnetic gradient. Resolution is improved in the gradient maps. Similarly, in Figure 7.3, the high-frequency content of apparent susceptibility maps helps in the structural mapping.

The quantitative interpretation of folds is usually restricted to the determination of dips on either limb as shown in Figure 7.2 and in the other models presented in this chapter. The mapping of the axial surface trace can only be schematic. In cases where the axial surface gives rise to a magnetic anomaly, the direction of plunge can be inferred but not always the amount. For example, the nose of a synform might give rise to a triangular magnetic high surrounded by a low. The magnetic anomaly over the closure of an antiform might be similar except that it could be marked by a magnetic high in the form of a "tail" leading along the direction of plunge. This is illustrated in diagrams C and E of Figure 7.1. The presence of such a "tail" would also indicate that the plunge of the antiform is shallow.

7.1.3 Faults, shear zones and lineaments

The magnetic signature of a fault zone may either be "direct" or "indirect". A "direct" anomaly is a high or low caused by the production or destruction of magnetic minerals in the rocks within the fault zone, so that the fault zone is the source of the magnetic anomaly. Retrograde shear zones within which magnetite has been destroyed by circulating fluids are examples of "direct" anomalies (Henkel and Guzmán, 1977). The magnetic low associated with the Palmer Fault (Plate 5) is an example of brecciation and albitization of the fault zone (White, 1956) during which magnetite has been destroyed.

"Indirect" anomalies are much more common. The offset or truncation of one or more magnetic markers is typical of cross faults. The non-appearance of a magnetic unit on the other side of a fold and breaks in continuity of magnetic markers should both be examined for evidence of faulting. Possible faults are indicated where there are breaks in the magnetic pattern (terminations of highs or lows, change in gradient, linear contour patterns) and from alignment of highs and lows. Faults should be suspected where blocks of differing magnetic character have been brought into contact. Different expressions of fault anomalies are demonstrated in Figure 7.3, Figure 7.6, and Figure 7.9.

Changes in the character of a magnetic anomaly from profile to profile can be easily identified

from maps of stacked profiles. Small scale maps such as digital images are invaluable for detecting lineaments — linear features which run for great distances and which may be caused by steeply dipping faults (Gay, 1972).

Accurate mapping of faults is dependent on the trend and sense of movement along the fault plane. Where the trend is at a small angle to the flight path, such that it crosses less than two flight lines, the fault will appear to be subparallel to the flight path. The distinction between faults and contacts may not be obvious or resolvable.

Quantitative interpretation of a fault involves the determination of the direction, sense and amount of movement along the fault plane. Where there has been mainly horizontal movement, the offset of anomalies and of lineaments is used to estimate the sense and amount of movement. Vertical movement can be simply calculated only when the blocks on opposite sides are of the same material. The direction of the downthrown block can be determined qualitatively because where there is substantial throw, the magnetic character of the downthrown side is more "subdued".

But often there has been both horizontal and vertical movement at different times and blocks of different rock types are juxtaposed. In my study area, it is difficult to determine whether there has been vertical movement along the faults as the basement to the Kanmantoo Group is either non-magnetic (if shallow), or if magnetic is very deep. As a result, while cross faults are often obvious, only one fault with definite vertical movement (the Springton Fault) has been mapped. In any case, aeromagnetic maps respond better to net horizontal movement than to the magnetic effect of magnetic blocks overlain vertically (Gay, 1972). Consequently, low-angle thrusts are hard to deduce, let alone analyze quantitatively.

Information about faults may also be obtained from aeroradiometric data which are usually collected as part of modern aeromagnetic surveys. Radiometric images indicate the presence of faults in different ways.

1. Fluids circulating in shear zones might have resulted in metasomatism and the removal of potassium (thus producing a radiometric low) or sericitization (radiometric high).
2. The differential weathering profiles of rocks on either side of the fault can result in a radiometrically anomalous soil profile.
3. Rivers and streams favour fault zones and the sediment which is brought into the river channel may possess radioactive elements in concentrations different to that of the rocks on either side of the fault.

7.2 Structural patterns in the Kanmantoo Synclinal Subzone

The KNSZ covers the southern and western parts of the study area and extends to the south coast of Fleurieu Peninsula. This subzone covers just under two-thirds of the main study area. From the type section along the south coast of Fleurieu Peninsula, Kanmantoo Group rocks outcrop in synclines which form an *en échelon* system migrating northwards (Mancktelow, 1979). Metasediments of the Tapanappa Formation and younger Kanmantoo Group form the bulk of the outcrop as they are found in the core of most of the synclines.

The base of the Kanmantoo Group marks the western margin of the KNSZ. As discussed previously (Section 1.3), the nature of this boundary is controversial and the boundary has

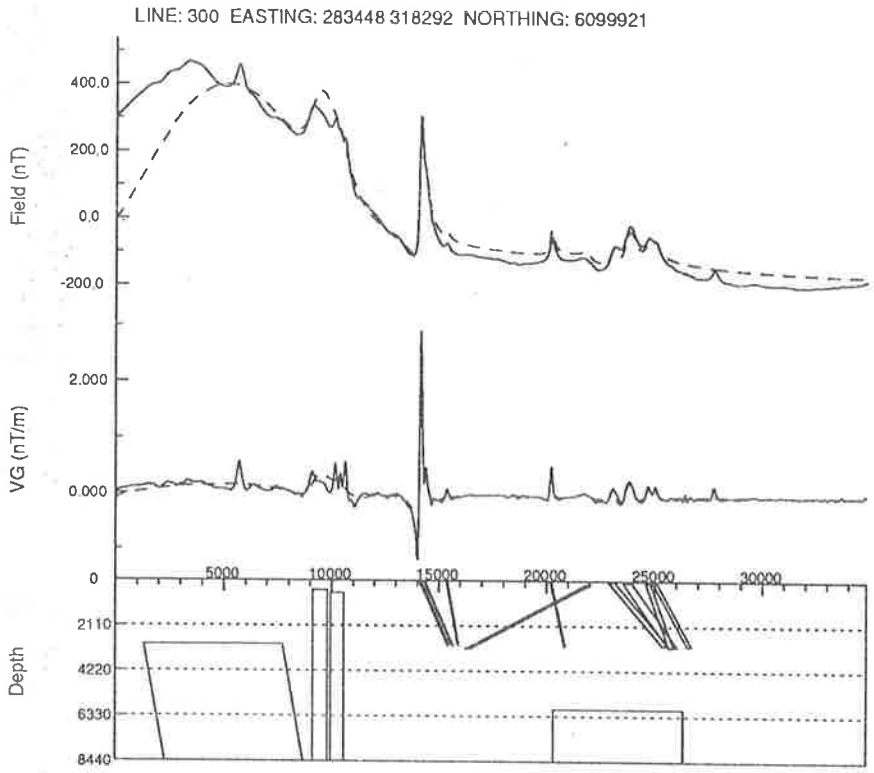

Figure 7.4: Magnetic model of the Macclesfield Syncline-Strathalbyn Anticline. Anomalies: US-MS1 and US-MS2 at 14000, NG1 at 15400, TC-MS at 22000 and 25000.

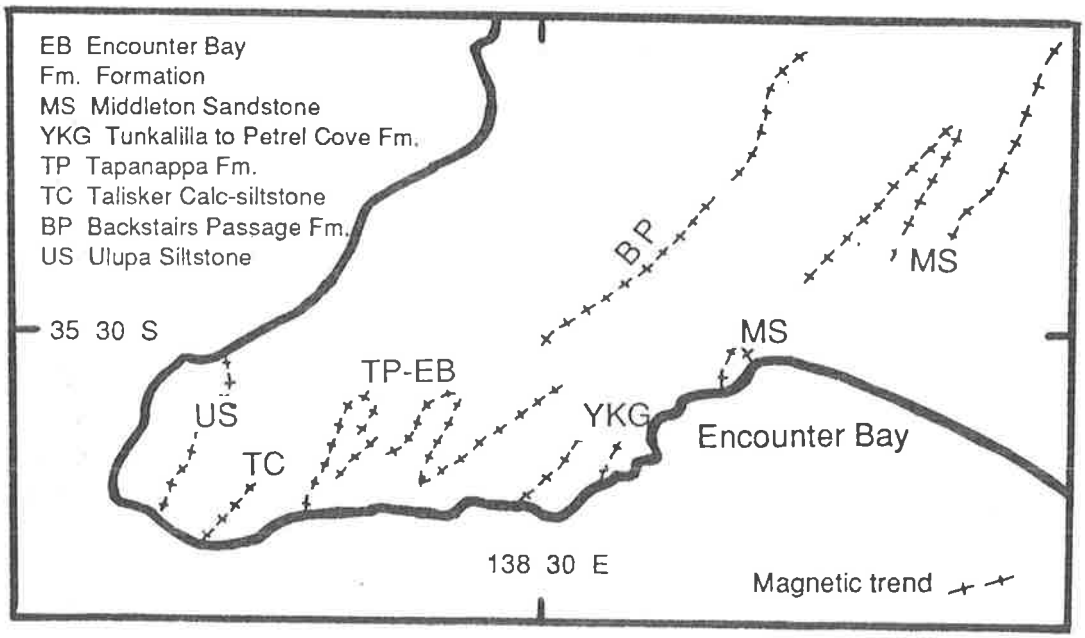

Figure 7.5: Fleurieu Peninsula: folds in the Kanmantoo Group.

been folded during the Delamerian Orogeny. The eastern margin of the KNSZ is the boundary between the KNSZ and the ISZ and the reasons behind its location are given in Section 7.4. In the northwest, south-plunging synclines limit the extent of Kanmantoo Group rocks. In the south and southwest, the synclines open southwards and the southern limit of the KNSZ has not been detected. Kanmantoo Group rocks and their equivalents have been mapped on the south coast of Fleurieu Peninsula (Daily and Milnes, 1971a) and on Kangaroo Island (Daily, 1977).

Barossa Complex rocks are exposed along the axis of the regional anticlinorium which forms the Mt. Lofty Ranges. The magnetite-rich micaceous schists within these rocks are responsible for complex magnetic anomalies (Section 6.1.5). Circular to oblate magnetic anomalies have been interpreted to indicate that the depths to the top of magnetic basement varies from the surface to 4 km. Above the deeper basement, Adelaide Supergroup formations dip at low angles. This has resulted in weak, high-frequency anomalies which are consequently suppressed by the large, low-frequency basement effect. To the east of the anticlinorium axis, the Kanmantoo Synclinorium takes over and the regional magnetic field is characterized by the predominance of high-frequency anomalies and the absence of deep-seated magnetic sources.

Magnetic signatures of the dipping metasediments tend to be linear to curvilinear. Anomaly amplitudes range from negative anomalies (e.g. TP-WE: −50 nT and US-MS1: −300 nT), to small, positive anomalies (e.g. TP-CLS), to high-amplitude anomalies associated with the Ulupa Siltstone (400 nT) and with the Dawesley Magnetic Anomaly (TP-DM: 1200 nT).

Mapped and interpreted granites, granite gneisses and other intrusives include the Mt. Kitchener Granite and Tanunda Creek Gneiss in the north, and the Monarto Granite which crops out on the east limb of the Monarto Syncline (see Section 7.4.1). The Encounter Bay Granites (Milnes, 1973) are within the KNSZ but not within the main study area.

South of the Encounter Fault (Firman, 1974) and north of MS3 and MS4, weak linear anomalies (< 20 nT in amplitude) trend subparallel to the flight paths. These have been interpreted as strandlines and the anomalies are probably caused by magnetite-rich beach deposits.

On Fleurieu Peninsula, the Kanmantoo Group has been folded into folds of large wavelengths (Figure 7.5). Accurate delineation has not been possible owing to the regional nature of the aeromagnetic survey. Lack of digital data also meant that reprocessing was not possible. These folds are apparently on the order of tens of kilometres. Folding on this scale would account for the apparent vast thicknesses of the Kanmantoo Group.

7.2.1 Macclesfield Syncline-Strathalbyn Anticline

In the vicinity of Macclesfield and Strathalbyn, a large syncline-anticline fold couplet has folded the Precambrian and Cambrian metasediments and the boundary between them (Marlow, 1975). The quality of outcrop in the region varies and is often quite poor. However, magnetic and radiometric markers in the Precambrian and Cambrian metasediments clearly delineate the folds. In this section, the terms "western limb" refer to the western limb of the Macclesfield Syncline, "eastern limb" to the eastern limb of the Strathalbyn Anticline, and "shared limb" to the common limb of the Macclesfield Syncline and Strathalbyn Anticline.

The units of the Adelaide Supergroup below the Ulupa Siltstone vary widely in their lithology. Part of the radiometric image shown in Plate 4 was created from detailed data (Pacific Expl. data: 150 m line spacing — see Appendix A). This data covers the Adelaide Supergroup outcrop in the *Echunga* area and illustrates the resolution in lithology which can be achieved by studying radiometric data over areas where lithology and therefore radioactive mineral content varies

with stratigraphy. The radiometrically but not always magnetically distinct lithologies clearly delineate the Macclesfield Syncline. The different rock types include sandstone, shale, siltstone, limestone, dolomite, marble and quartzite (Belperio, 1985). This area is a good example of the complementary nature of magnetic and radiometric information and the advantages obtained through their joint acquisition and integration.

Magnetic anomalies, US-MS1 and US-MS2, are caused by magnetic minerals in andalusite schists near the base of the Ulupa Siltstone. They can be followed for 50 km around the major folds. US-MS2 is the upper unit and US-MS1 the lower unit and the difference in their magnetic properties is evidenced by changes around the folds. The relative ductility of the Ulupa Siltstone with respect to the quartzite above it has resulted in the development of parasitic folds on the shared limb (diagram A in Figure 7.1). These folds are several hundreds of metres across. The fault which offsets US-MS1 and US-MS2 on the western limb might represent the effect of shearing along one such fold. Along the western and eastern limbs, the amplitude of US-MS1 is of the order of 200–400 nT. On the shared limb, anomaly US-MS1 is negative (−300 nT) though anomaly US-MS2 is positive. Around the closure of the Strathalbyn Anticline, the continuity of US-MS1 and US-MS2 is disrupted by a series of faults. On the eastern limb, US-MS1 is continuous but US-MS2 less so.

A quartzite unit crops out sporadically along the eastern limb (quartzite at Mt. Barker) and more continuously along the western limb (quartzite at Macclesfield). BP-SA, in the Backstairs Passage Formation, is found along the eastern and shared limbs. The disappearance of BP-SA and the quartzite around the closure of the Strathalbyn Anticline are probably related. Offler (1963) interpreted the outcrop in this area to indicate that the quartzite at Macclesfield had changed facies into a meta-arkose and was continuous around the fold closures, i.e. that the quartzite and BP-SA were continuous. However, Mancktelow (1979) interpreted the meta-arkose as being in the Backstairs Passage Formation. The anomaly BP-SA is interpreted to be in the basal member of the Backstairs Passage Formation. The termination of the quartzite unit and the anomaly, BP-SA, is considered to be indicative of a fault (see below).

TC-MS has been mapped around the fold closures of the major syncline and anticline, though Offler (1963) in his mapping shows that the pyrite bands are seen only within the syncline and appear to continue as an andalusite schist around the closure of the anticline. On the western limb, TC-MS thins out reappearing as a negative anomaly as part of the Channel Anomaly (see below). On the eastern limb there is a major break between TC-MS and TC-WKS in the Tinpot area. Kleeman and Skinner (1959) have mapped the eastern and western pyrite bands and found that in the vicinity of Tinpot the pyrite bands are not continuous and thin out.

A modelled magnetic profile is shown in Figure 7.4. The effect of magnetic basement is seen in the west but disappears to the east. Modelled susceptibilities (order of 400×10^{-5} SI) of the magnetic Kanmantoo Group rocks are in agreement with measurements made on outcrops. Modelled susceptibilities ($\sim 4000 \times 10^{-5}$ SI) for the Ulupa Siltstone are an order more than measured magnetic susceptibilities and this can be explained by the NRM component (Section 2.3.1). The magnetic dips of the units are generally to the east, indicating that the axial limbs are slightly overturned.

Macclesfield Fault

Marlow (1975) has inferred the presence of two faults in the vicinity of the Macclesfield Syncline area: the Macclesfield Fault which forms the contact between the quartzite at Macclesfield (taken to be Precambrian) and the Cambrian rocks, and the fault between the Normanville Group and the Kanmantoo Group. Both faults have been validated through magnetic interpretation though

the interpretation is slightly different from that of Marlow's (1975). Both faults were probably thrusts considering the large apparent movement and the orientation which is subparallel to bedding.

A fault has been proposed between the Normanville Group and the Kanmantoo Group in the region of the Macclesfield Syncline. The sequence of Adelaide Supergroup rocks and Normanville Group rocks on the western limb is appreciably different from that on the shared and eastern limbs (Marlow, 1975). On the western limb, Normanville Group units disappear or thin out as they approach the Macclesfield Syncline while Kanmantoo Group units thin out away from the fold closure. This may indicate a fault contact between the Normanville Group and the Kanmantoo Group. Steinhardt (in prep.) suggests that the marble at Paris Creek acted as a detachment surface. However this theory is discounted by the discovery by Sprigg (in prep.) of intact *Archaeocyathids* in the marble (Preiss, pers. comm.).

The quartzite at Macclesfield is seen to strike into the magnetic anomaly BP-SA and this formed the basis of Offler's (1963) argument that there had been a facies change from quartzite into meta-arkose. Marlow (1975) reported an increase in the thickness of the quartzite corresponding to the change in facies and a divergence of bedding-cleavage relationships in the quartzite at Macclesfield from the western limb to the hinge of the Strathalbyn Anticline. However, if BP-SA has been correctly interpreted to be in the Backstairs Passage Formation (this follows the mapping of Mancktelow (1979), and the interpretation of BP-SA being the continuation of BP-WKS — see Section 7.2.2) then there must be a fault contact between the quartzite and the Backstairs Passage Formation as it is not possible to account for overlying beds striking into underlying beds by an unconformity. The Macclesfield Fault is likely to represent the extension of the Nairne Fault which has been mapped by Toteff (1977) on the western limb of the Kanmantoo Syncline.

Thrust above Talisker Calc-siltstone?

Along the eastern limb of the Strathalbyn Anticline, magnetic horizons within the Talisker Calc-siltstone give rise to characteristic magnetic anomalies, TC-MS and TC-WKS (Section 6.1.1). TC-WKS is essentially the northern continuation of TC-MS except for a major disruption in magnetic trends in the vicinity of Tinpot.

In this region, magnetic anomalies trend NNW contrary to the mapped NS to NE trends within the Backstairs Passage Formation (trends traced from aerial photographs by Mancktelow, 1979). The anomaly TC-WKS is made up of a number of magnetic horizons of which there are two main ones. These can be related to the two main pyrite bands. The western band had been assigned to the Talisker Calc-siltstone and the eastern to the Tapanappa Formation by Thomson (1969b), though Kleeman and Skinner (1959) interpreted both pyrite bands as being part of the Nairne Pyrite Formation (the old name for what Mancktelow (1979) identifies as the Nairne pyrite facies of the Talisker Calc-siltstone).

The similarity in magnetic response between the two and the suggestion from the contour map that in the vicinity of Tinpot, TC-WKS narrows and the western unit appears to fold into the eastern unit, has been interpreted to indicate that the simple model indicated on geological maps may be incorrect. Instead, one feasible interpretation is that the western and eastern units are equivalent, and the repetition caused by an early thrust during which the pyrite schists acted as a detachment surface. The NNW trending anomalies between the northern end of TC-MS and the southern end of TC-WKS could be due to dykes parallel and similar to the dyke swarm along the Mt. Beevor Shear Zone (Pain, 1968).

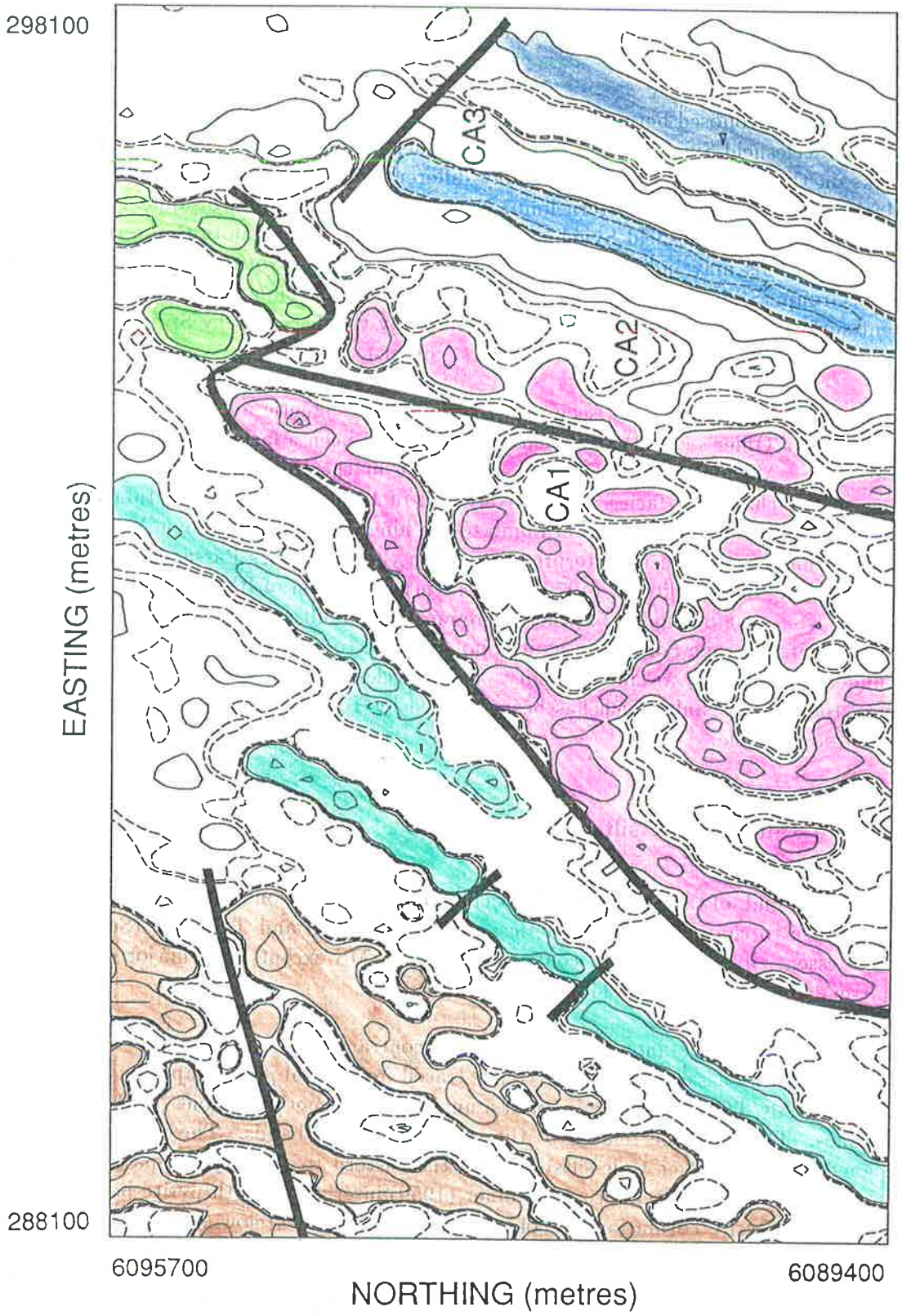

Figure 7.6: Magnetic interpretation of the Channel Anomaly shown superimposed on contours of the vertical magnetic gradient.

Channel Anomaly

The western limb passes into the shared limb near Macclesfield, but in the vicinity of Mt. Magnificent terminates against a triangular shaped magnetic high, the Channel Anomaly (Figure 7.6). Outcrop in the region is poor and covered by Permian glacial sediments in places. Wymond (1950) mapped greywackes in the region which were in fault contact with the underlying Adelaide Supergroup rocks. Horwitz and Thomson (1960) remapped the area and identified impure arkoses which showed cross-bedding and slump structures and, east of the arkoses, mapped phyllites interbedded with greywackes and occasional pyritic schists. Mancktelow (1979) assigned the impure arkoses to the Backstairs Passage Formation, the phyllites to the Tapanappa and younger Kanmantoo Group formations, and indicated that a blue pyritic shale to the northeast of the Channel Anomaly might be the equivalent of the Talisker Calc-siltstone.

There is a sharp increase in the thickness of the Backstairs Passage Formation between the western limb where it is either very thin or disappears altogether and the Channel Anomaly region where it is very thick. The name "Channel Anomaly" for the triangular magnetic high was chosen in accordance with Mancktelow's (1979) interpretation that the triangular wedge of metamorphosed greywackes is in the Backstairs Passage Formation and represents a channel carved into the underlying Precambrian sediments during the deposition of the older Kanmantoo Group rocks.

Based on magnetic character, the anomalous region can be divided into three parts:

CA1 This is the western and southwestern part of the anomaly and from Figure 7.6 curved internal structures can be seen. To the west of CA1, Adelaide Supergroup magnetic units strike at 30° E. The western margin of CA1 is curvilinear and the average trend is 40° E. From the interpretation of the Milang 1 : 100 000 scale total magnetic map (Gerdes, 1986), CA1 is seen to continue southwards. Fold closures similar to those in the northern CA1 may extend southwards.

CA3 The far east part of the anomalous region is characterized by linear magnetic anomalies trending 20° E. There are three distinct units, one of which is a negative anomaly (TC-CA) and may be the extension of the Talisker Calc-siltstone. The strike extent of these units in the main study area is around 6 km. These linear anomalies do not continue to the north and the presence of a fault may be indicated. The southern extent of these units cannot be determined from the regional SADME maps (Gerdes, 1986). The main negative anomaly is similar to TP-WE.

CA2 Between the internal folds in CA1 and the linear anomalies in CA3, CA2 has a single, discontinuous magnetic anomaly which trends 17° E and appears to strike into the anomalies of the Ulupa Siltstone, US-MS1 and US-MS2.

Wymond (1950) described the structure as being simple with beds in the area having a "fairly regular dip, averaging between 60° and 80° to the east". This interpretation appears to be simplistic. The fault at the base of the Channel Anomaly has cut out entire formations of the Adelaide Supergroup. This fault is likely to be the extension of the Macclesfield Fault and therefore the extension of the Nairne Fault. The fault between the Normanville Group and the Kanmantoo Group may continue as the fault inferred between CA1 and CA2.

In the vicinity of the Channel Anomaly, the internal folds indicated in the Backstairs Passage Formation (CA1) are not seen either below or above this formation. The "folds" are of the order of few kilometres, and it is possible that they could be the effect of very large slump structures.

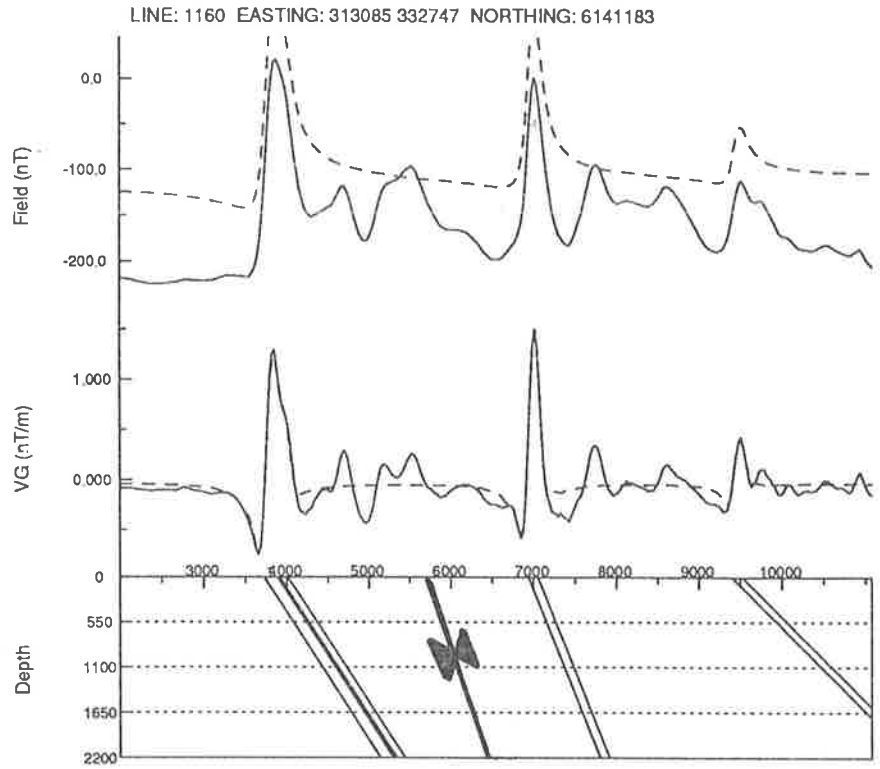

Figure 7.7: Magnetic model of the Kanmantoo Syncline. Anomalies: TC-WKS at 4000 and TC-EKS at 7000.

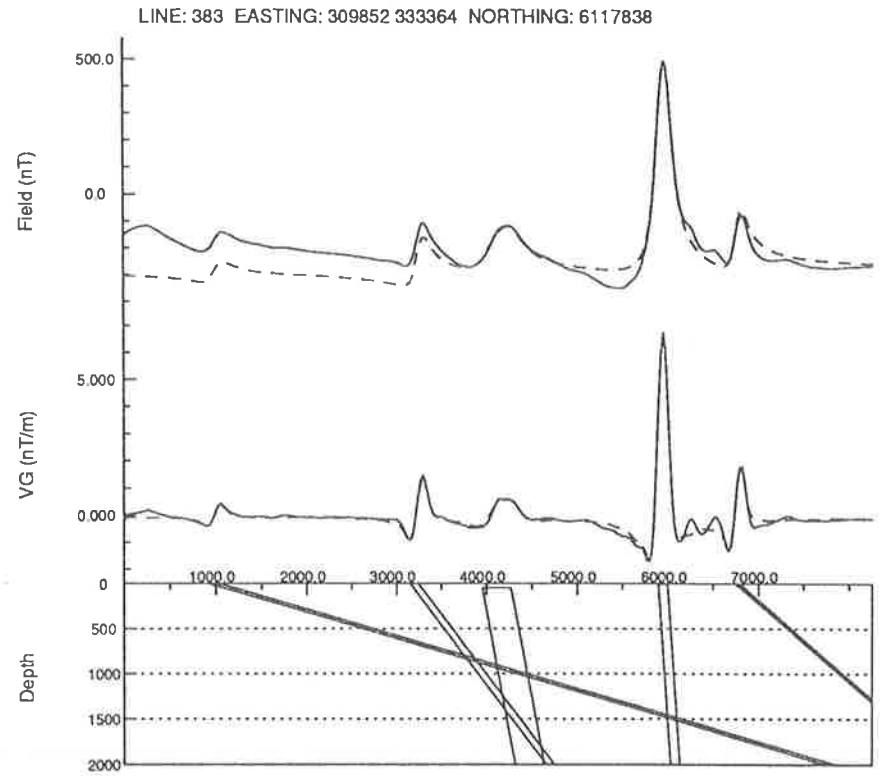

Figure 7.8: West limb of the Kanmantoo Syncline. Anomalies: BP-WKS at 1000, TC-WKS between 3000 and 4500, TP-DM from 5800 onwards.

Alternatively, the increased thickening and the folds within the Backstairs Passage Formation may reflect the effects of a deformation event prior to F_{main}. Evidence presented here and elsewhere in this chapter (Section 7.4.1) is consistent with increased thickening and isoclinal folding of the Backstairs Passage Formation during the F_{early} deformation.

Fold style

Axial planes of these folds trend approximately NS and are subvertical, and the fold axes plunge shallowly to the south. Both folds are several kilometres across and not quite symmetrical. The hinge of both folds is sharp in the north and broadens southwards. The shared limb is shorter than either the western or eastern limbs and from this Marlow (1975) interpreted that the Macclesfield Syncline-Strathalbyn Anticline pair developed principally by rotating the shared limb, after the major anticlinorium was formed. The axis of the Strathalbyn Anticline passes through the town of Strathalbyn. The southernmost anticlinal fold closures are truncated by the Encounter Fault.

Marlow (1975) suggested that the Kanmantoo Group metasediments had undergone two phases of deformation, the first of which produced a penetrative slaty cleavage, the second the Macclesfield Syncline-Strathalbyn Anticline pair. He considered the Macclesfield Syncline and Strathalbyn Anticline to be a single episode of macroscopic folding. He suggested that the two periods of deformation were continuous phases rather than two separate events.

However, Mancktelow (1979) considered the Macclesfield Syncline-Strathalbyn Anticline pair to be F_1 and part of the single, major folding event which resulted in the *en échelon* folding pattern. Offler (1960) suggested that there had been three phases of folding in the area and the Strathalbyn Anticline was an F_2 event. Later, in 1963, he revised the Strathalbyn Anticline to be F_1. And again in 1968, Offler and Fleming stated that the Strathalbyn Anticline was really F_3.

In this thesis, the major folds are interpreted to be part of the F_{main}, the main phase of macroscopic folding.

7.2.2 Kanmantoo Syncline

The Kanmantoo Syncline is the next major fold north of the Strathalbyn Anticline. The eastern limb of the Strathalbyn Anticline forms the western limb of the Kanmantoo Syncline. This major fold extends from north of the Barossa Valley to south of Callington. In general, the axial plane trends approximately NS. The syncline plunges shallowly south. The eastern limb of the syncline is steep to overturned as evidenced by the dips of TC-WKS near Harrogate. Mancktelow's (1979) interpretation of the trace of the axis is shown in Figure 1.2. It passes through the Dawesley Magnetic Anomaly. The general synclinal structure continues southwards with the Middleton Sandstone lying in the core of the syncline. The Middleton Sandstone is covered by the Caenozoic rocks of the Murray Basin. Important centres of mineralization in the KNSZ are at Kanmantoo (TP-KM), Wheal Ellen, Aclare, Brukunga, and South Hill among others.

Magnetic markers include the magnetic horizons which define the eastern limb of the Strathalbyn Anticline, as well as TP-DM (the Dawesley Magnetic Anomaly), and BP-WKS. BP-WKS is interpreted to be an extension of BP-SA (there are minor gaps in the continuity). North of the Mt. Beevor Shear Zone, the magnetic marker TC-WKS is cross-faulted.

Figure 7.9: The Backstairs Passage Formation magnetic marker BP-NKS delineating the closure of the Kanmantoo Syncline shown superimposed on contours of the total magnetic field.

The Mt. Beevor Shear Zone strikes NNW and displaces TC-WKS. Ivezich (1969) interpreted this zone of shears to be a normal "fault", with left-lateral strike slip. The apparent displacement on TC-WKS is ~ 1 km. The shear zone appears to be localized within the hinge of a southeast plunging syncline which has folded the axial plane schistosity associated with the Kanmantoo Syncline (Fleming, 1971). Staltari (1974) suggested that the Mt. Beevor Shear Zone was a regional feature which extended southwards beyond the Dawesley Magnetic Anomaly.

The magnetic anomalies caused by pyrrhotite and magnetite bearing pyrite schists of the Talisker Calc-siltstone, TC-WKS, were used to map the closure of the Kanmantoo Syncline north of Harrogate. TC-WKS was traced on the eastern limb as TC-EKS. Magnetic anomalies on the west limb of the Kanmantoo Syncline dip consistently east. Anomalies on the western limb of the syncline, such as TC-EKS, dip steeply towards the east, indicating that the east limb of the syncline is overturned (Figure 7.7). The syncline plunges shallowly south. Discontinuous anomalies to the south were interpreted as equivalent to TC-EKS. The Kanmantoo Syncline may pass into the Monarto Syncline which is to the east. The Bremer Fault zone coincides partly with the trace of TC-EKS. The effect of the fault on TC-EKS is minor.

North of Harrogate, a group of linear magnetic anomalies in the Backstairs Passage Formation, BP-NKS, trend approximately NNW. These outline a series of northwards migrating, *en échelon* folds. If, as is possible, BP-NKS represents a single horizon within the Backstairs Passage Formation, then an important marker has been determined (Figure 7.9). In keeping with BP-WKS, BP-NKS may also correlate with the basal member of this formation. As has previously been stated, few markers have been identified in the Kanmantoo Group, making stratigraphic correlations difficult, particularly in regions of extensive greywacke and arkose outcrop. BP-NKS is in part related to radiometric highs as well as magnetic highs. The usual lithologies observed are meta-arenites which are in part migmatitic (Offler, 1966). The axis of the Kanmantoo Syncline passes through the Tanunda Creek Gneiss.

Magnetic modelling on a series of profiles confirms the general fold structures illustrated in Figure 7.9: dips tend to be steep and towards the east indicating that the east limbs of the synclines are overturned. Chinner (1955) found that the dip of the foliation of the Tanunda Creek Gneiss was 80° E. To the west the major structure is an F_1 anticline whose axis passes through the Mt. Kitchener Granite. There was shearing along the hinge of the anticline immediately east of the Kanmantoo Syncline (Chinner, *op. cit.*; Offler, *op. cit.*). Later structures were mapped by Offler (*op. cit.*) as overprinting the F_1 structures, however the effect of this later folding has not affected the continuity of the magnetic marker units.

Mancktelow's (1979) maps show the closure of the Kanmantoo Syncline as outlined by the Backstairs Passage Formation, Carrickalinga Head Formation, Normanville Group and Ulupa Siltstone north of the Barossa Valley. From the available magnetic data (SADME, 1980 and 1983) these closures are delineated by the ubiquitous Ulupa Siltstone magnetic markers (Figure 7.13). Several other synclinal closures of Ulupa Siltstone are also clearly defined in magnetic maps, including the Karinya Syncline (Section 7.3.1). These synclines mark the northern limit of the Kanmantoo Group in the KNSZ.

At Callington, synclinal folds are have been interpreted using magnetic anomalies within the Tapanappa and younger Kanmantoo Group Formations. This is in contrast to the complete absence of usable lithological marker beds noted by Grasso and McManus (1954) when they mapped the Callington Syncline. The folds are west of the Bremer Fault and the folded magnetic units are probably extensions of TP-MNS. This would indicate that movement on the Bremer Fault was small. The apparent widths of the limbs are different, with the western limb being thicker than the eastern limb.

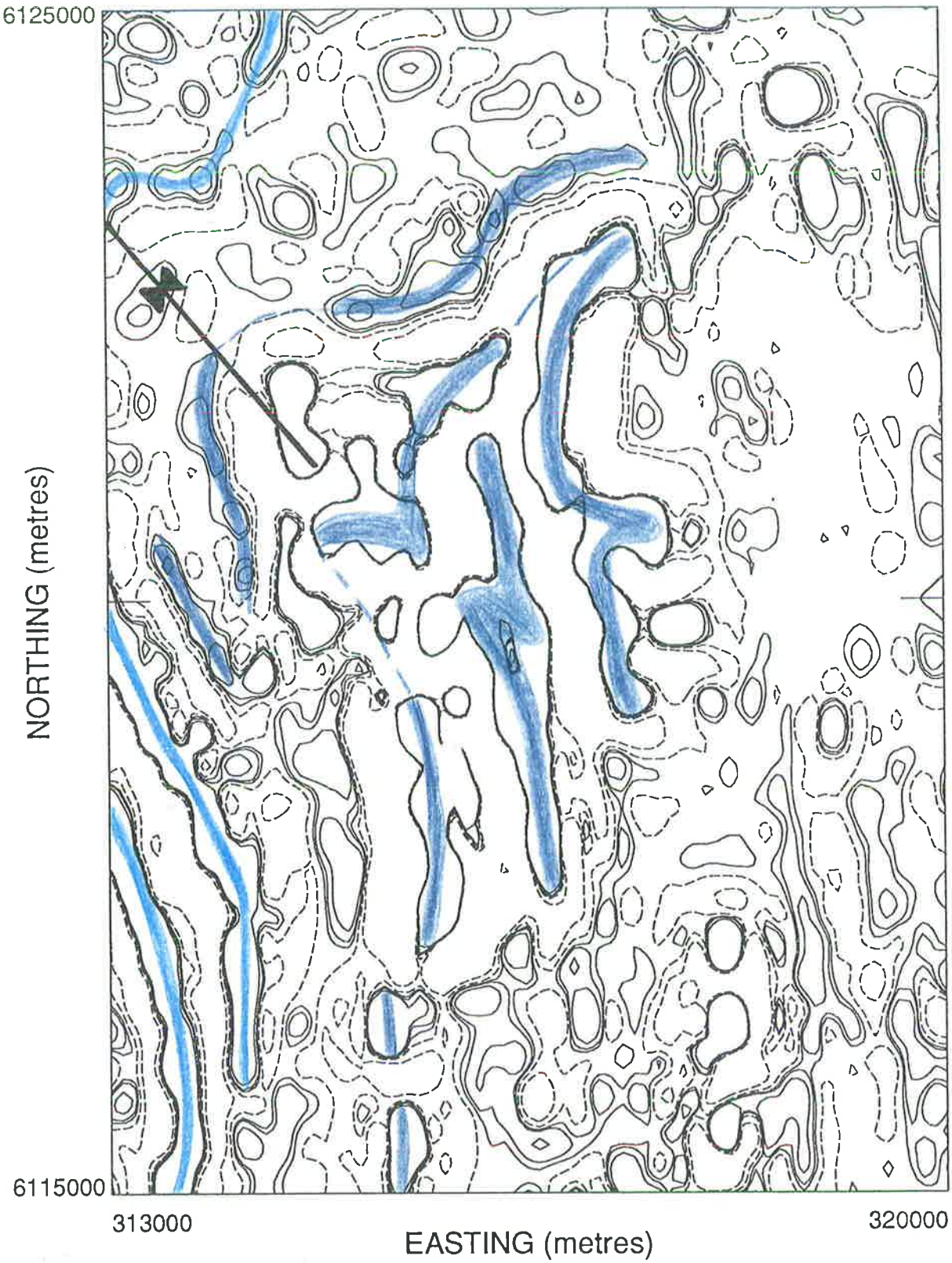

Figure 7.10: Interpretation of the Dawesley Magnetic Anomaly shown superimposed on vertical magnetic gradient contours.

Dawesley Magnetic Anomaly: DMA

The rocks of the Tapanappa Formation generally give rise to only moderate magnetic anomalies except in the vicinity of Dawesley where a group of complexly folded rocks produces the Dawesley Magnetic Anomaly (of the order of 1200 nT). The amplitudes of these anomalies are the largest found in the KNSZ. The lithology includes quartzo-feldspathic schist, micaceous schist with varying amounts of andalusite, staurolite, and garnet, and calc-silicate with occasional pyritic bands (Fleming, 1971).

Diamond drill core (Benlow and Taylor, 1963) has been logged as containing magnetite and sulphides (including pyrite, pyrrhotite, sphalerite and galena). The source of the anomalies appear to be due to magnetite within andalusite-staurolite schists, and due to pyrrhotite ± magnetite within pyrite schists. Interpreted and measured magnetic susceptibilities (of the order of 1000×10^{-5} SI) are higher for Tapanappa Formation rocks in this region than anywhere else (except for magnetite ore from the Kanmantoo mine).

At least two generations of folding have affected the region. The earlier event produced the Kanmantoo Syncline, the axis of which passes through the DMA. The later event overprinted the Kanmantoo Syncline and the form of this fold is a large southeast-plunging synform whose axial plane trace trends 140° E (Fleming, 1971). The later deformation appears to have resulted in the thickening of some rock units. This can be seen in the intensity of magnetic anomalies connected with the fold closures. As Figure 7.10 shows, magnetic units in the Tapanappa Formation have been subjected to at least two phases of macroscopic folding. During the later event, the thickening associated with the fold closures produced relatively intense anomalies. General dips in the area are towards the east (Figure 7.8).

The synformal structure disappears to the southeast but can be traced northwest until it is truncated by the Meadows-Mt. Kitchener Fault (Fleming, 1971). The later event was accompanied by faulting. The Dawesley Lineament, which trends northeast, is a regional feature which limits the DMA in the north.

The rocks of the Tapanappa Formation have unusually high susceptibilities in the Dawesley region. Elsewhere in the CMZ, high magnetic susceptibilities are usually associated with granite intrusion and migmatization. Fleming and White (1984) suggested that pre-tectonic crystallization may have taken place in the Dawesley region. South of Dawesley, base metal mineralization found within the Tapanappa Formation (Kanmantoo, Bremer, Aclare, ...) is considered by Seccombe *et al.* (1985) to be essentially syn-sedimentary. These deposits are interpreted as having formed around hydrothermal discharge points during the deposition of the Tapanappa Formation. Seccombe *et al.* (1985) suggest two alternative mechanisms for convective fluid circulation: major growth faults which focused upwelling fluids and magmatic heating from, as yet undetected, igneous activity.

Other evidence of early thermal activity in the Kanmantoo Group includes igneous intrusion (Encounter Bay Granites: Milnes *et al.*, 1977; pre-tectonic amphibolites: Liu and Fleming, 1989) and partial melting in the migmatite zone (Fleming and White, 1984). The Dawesley Magnetic Anomaly may therefore indicate the presence of subsurface granite. A gravity survey might be effective in testing this hypothesis.

7.2.3 Monarto Syncline

East of the Bremer Fault, Kanmantoo Group metasediments have been folded into the Harriet Hill Folds (see Section 7.2.4) and the Monarto Syncline. The Monarto Syncline developed as a

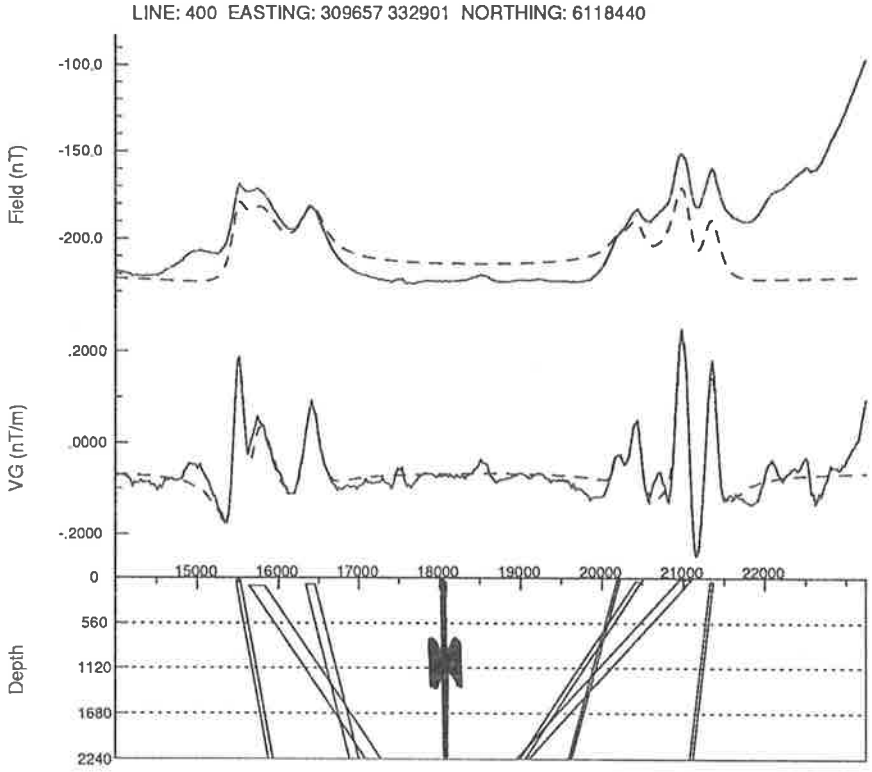

Figure 7.11: Magnetic model of the Monarto Syncline. Anomalies: TP-MNS.

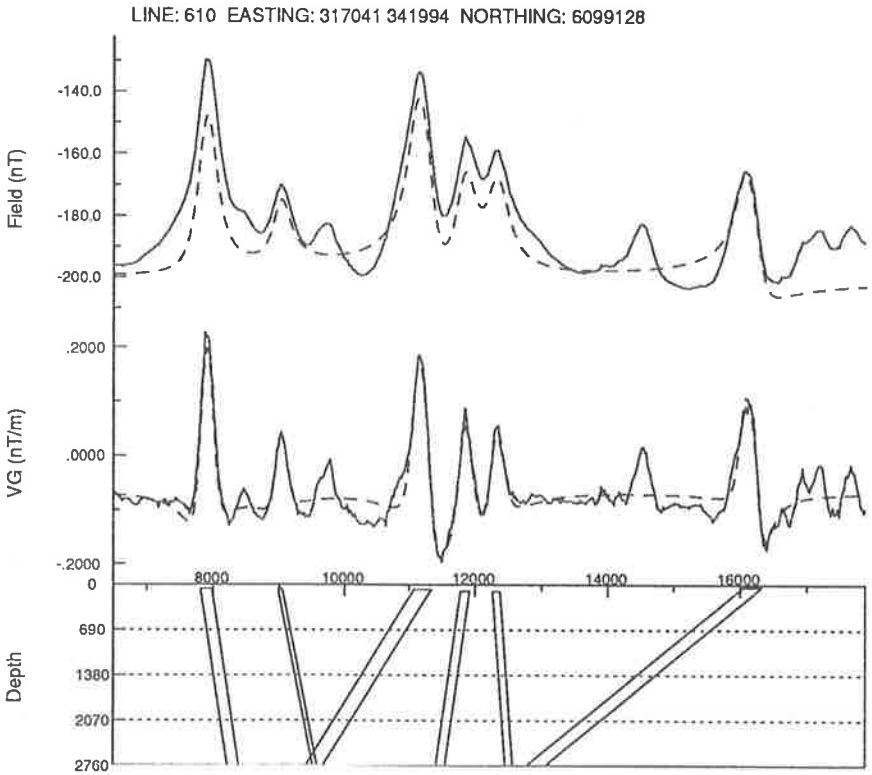

Figure 7.12: Magnetic model of the Harriet Hill Folds. Anomalies: TP-HH between 7800 and 12500, TP-MNS at 16000.

parasitic fold on the limb of the Kanmantoo Syncline (Mancktelow, 1979). The axis trends NS. Lawrence (1980) mapped pyrite and pyrrhotite bearing phyllites in the Tapanappa Formation in the area. These give rise to magnetic anomalies, TP-MNS, which delineate the fold. The general shape of the fold is also seen in radiometric images. The magnetic anomalies can be followed under Tertiary cover. The axis may continue through anomaly MS4. In the southwest, the Monarto Syncline may pass into the Harriet Hill Folds and the Callington Syncline. The Bremer Fault offsets the Callington Syncline to the southwest of the Monarto Syncline. This suggests that along the Bremer Fault, the east block moved north.

The fold as delineated by the magnetic phyllites appears to be a simple upright fold (Figure 7.11). In the Rockleigh region, the Backstairs Passage Formation rocks have been folded by the Monarto Syncline, but the fold closures suggest that there was an earlier macroscopic fold event. In the east, complex structures within the ISZ (Section 7.4.1) cut out the syncline. The total magnetic contours are distorted by the non-magnetic Monarto Granite.

7.2.4 Harriet Hill Folds

The Harriet Hill Folds are a series of south-plunging anticlines and synclines (Plate 5). Their fold axes trend NS and the fold hinges are sharp (Figure 7.12). The magnetic markers (TP-HH) are probably in the younger Kanmantoo Group Formations (between the Tapanappa and Petrel Cove Formation) and similar to the phyllites (rich in pyrrhotite and magnetite) which have been folded into the Monarto Syncline. The simplest explanation is to see the fold as an extension of the Monarto Syncline. It is also possible that the magnetic markers should really be considered as a single unit which has been folded into an isoclinal fold and then refolded into the Harriet Hill Folds. The hypothesis that the Harriet Hill Folds represent macroscopic refolding is difficult to test as the Kanmantoo Group rocks in this region are covered by Murray Basin deposits.

7.2.5 KNSZ: Conclusions

Macroscopic folds initiated during F_{main} control the outcrop of the Kanmantoo Group in the KNSZ. West of the Bremer Fault, the folds form a series of *en échelon* synclines which migrate northwards. The axial planes trend NS, the folds open southwards and plunge towards the south. The Macclesfield Syncline-Strathalbyn Anticline fold couplet shows the effect of F_{main} deformation on the Precambrian and Cambrian rocks. Fold hinges are sharp in the Precambrian units and broader in the Cambrian units. A new marker BP-NKS has been recognized which could be of great benefit to geological mapping.

East of the Bremer Fault, younger Kanmantoo Group rocks have been folded into the Harriet Hill Folds and the Monarto Syncline. Again, the fold axes trend NS and plunge southwards. The Bremer Fault seems to have had little effect on the outcrop pattern. On the radiometric image (Plate 4), the valley of the Bremer River has been associated with a distinct radiometric low, the eastern margin of which coincides with the trace of the Bremer Fault.

Interpretation of regional magnetic data (SADME, 1983) from Middleton on the south coast of Fleurieu Peninsula to the *Milang* and *Alexandrina* sheet areas shows that the anomaly MS2 extends from Middleton to south of the Encounter Fault. Anomaly MS2 is probably caused by the Middleton Sandstone (see Section 6.1.1). The eastern edge of MS2 is delimited by the Bremer Fault.

The structural relationship between the Precambrian and Cambrian is controversial. Geophysical evidence indicates that the bounding surface must be at a low angle to the bedding as

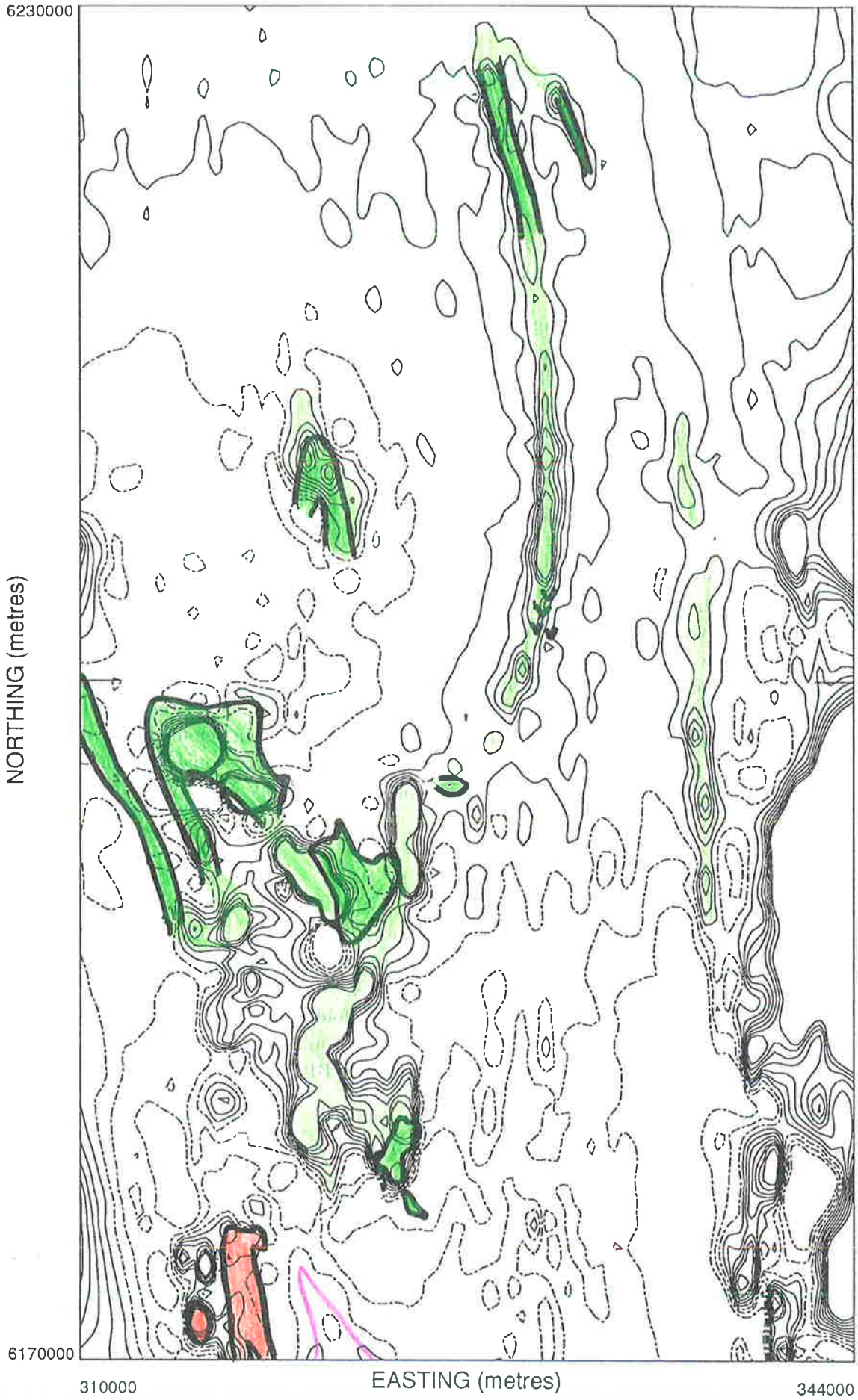

Figure 7.13: Relation between mapped Ulupa Siltstone (shaded dark green) and interpreted Ulupa Siltstone magnetic anomalies (shaded lighter) in the Karinya Syncline area. Truro Volcanics are indicated by "v". The total magnetic field map was produced from digital BMR data.

there is a striking parallelism between the attitude of the magnetic horizons above and below the contact. This would run counter to the theory that the deposition of the Kanmantoo Group was fault controlled. Several examples of structures apparently inconsistent with the F_{main} deformation being the first major deformation have been indicated (Tinpot and the Channel Anomaly — Section 7.2.1) and other examples are provided in the following sections (Section 7.4.1). It is significant that most of these early structures are associated with the basal Kanmantoo Group rocks (Section 7.5).

7.3 Structural patterns in the Karinya Synclinal Subzone

The Karinya Synclinal Subzone lies north and east of the Intermediate Subzone (ISZ) and extends north of the main study area into the *Eudunda* sheet area. The outcrop of Kanmantoo Group metasediments in the northern closure of the Karinya Syncline is the northernmost occurrence of the Group. The eastern margin of the KRSZ is defined to be the western margin of the EMZ. In the south and southwest, the KRSZ passes into the ISZ. The major structures in the KNSZ and KRSZ are synclines which have folded the Kanmantoo Group rocks. West of the Karinya Synclinorium, Proterozoic rocks are found within the cores of anticlinal structures.

About a sixth of the main study area is covered by the KRSZ. CRA aeromagnetic and aeroradiometric data are available over most of the area and BMR aeromagnetic data have been used for the remainder. As mentioned in Section 5.1, the rocks in the main study area are not confined to the Kanmantoo Group. The discussion of structures in the KRSZ has been extended to include structures in the contiguous WMZ.

The magnetic characteristics of this Subzone are very similar to that of the KNSZ. There is no evidence of deep-seated magnetic sources. Magnetic property variations in the metasediments of the Adelaide Supergroup, Normanville Group and Kanmantoo Groups result in linear to curvilinear magnetic trends which dominate the magnetic maps. Amplitudes of anomalies are typically low and less than a few hundreds of nanoTeslas, the exception being the strong anomalies (several hundreds of nanoTeslas) caused by the Ulupa Siltstone magnetic marker US-T. Granitic rocks (aplites, ...) are found in the southern closure of the Karinya Syncline. The stratigraphy in much of the area is uncertain and has not been updated to accommodate the revised classification of Daily and Milnes (1972a).

There is a marked contrast between the intense and complex magnetic character of the Intermediate Subzone and the subdued magnetic response of the KRSZ. Migmatites are common in the ISZ while absent in the KRSZ. Fold axes in the KRSZ trend approximately NS, while the magnetic trends in the ISZ are dominantly NNW. Abrupt termination of magnetic units have been used to infer a fault contact between the northern part of the ISZ and the KRSZ. The western margin of the KRSZ may also be fault bounded.

The regional structure in the KRSZ consists of a doubly-plunging syncline (the Karinya Synclinorium) in the east. To the west of the synclinorium, the Truro Anticlinal structure (new name) consists of a south plunging anticline in the north and a doubly plunging anticline in the south. The fold axes of both these folds trend approximately NS. Both folds are part of the F_{main} macroscopic folding event. The relation between the Truro Anticlinal structure and the Karinya Syncline is uncertain; at least in part the common limb is faulted. The Kanmantoo Group magnetic anomalies, CH2, BP-KRS, and TC-KRS are essentially linear except for occasional bull's-eye anomalies. These deviations may be due to refolding of early folds.

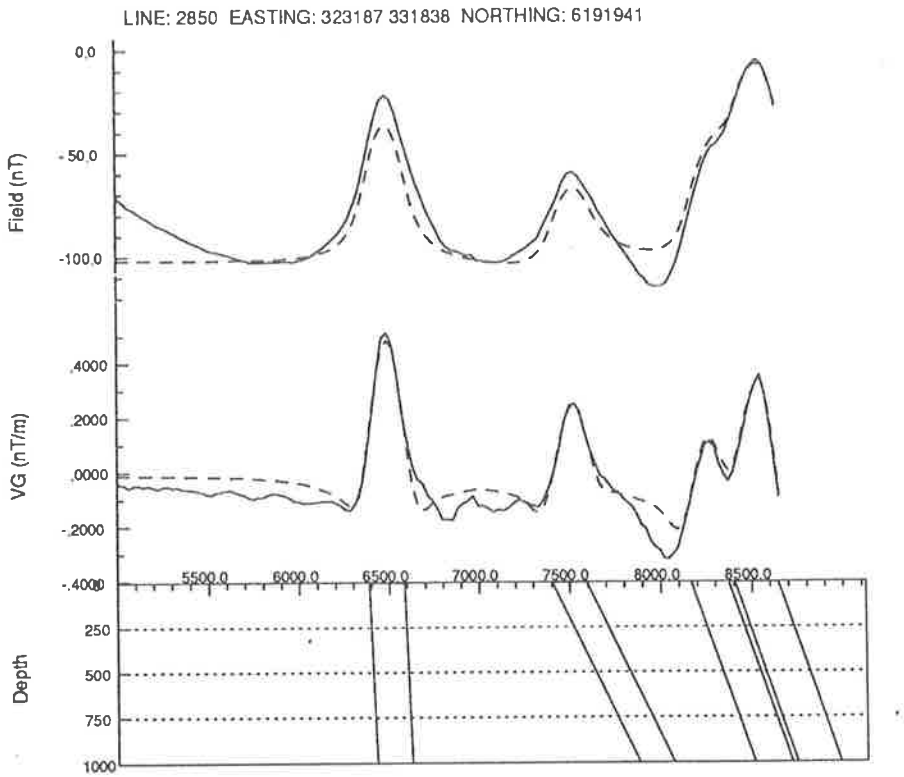

Figure 7.14: West limb of the Karinya Syncline. Anomalies: CH2 at 6500, BP-KRS at 7500 and TC-KRS between 8100 and 8700.

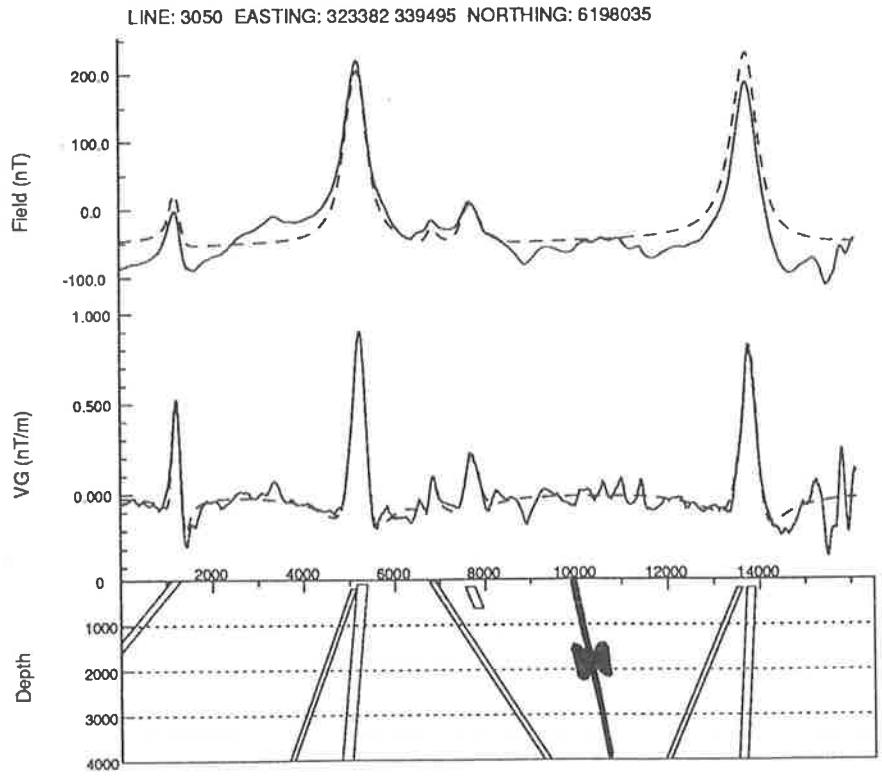

Figure 7.15: Magnetic model of the Karinya Syncline. Anomalies: US-KRS at 5000 and 13700, CH2 at 6800.

7.3.1 The Karinya Synclinorium

The major structure is an oval structure elongated in the NS direction and clearly identifiable from magnetic maps. Drummond (1972) called it the Karinya Synclinorium while Mancktelow (1979) referred to it as the Karinya Syncline. Only lower Kanmantoo Group metasediments outcrop in the core of the syncline. All three subunits of the Carrickalinga Head Formation have been recognized by Gatehouse *et al.* (in press). Normanville Group rocks are found along the eastern limb and also in the northwest. Rocks belonging to the Adelaide Supergroup outcrop around the northern closure and the eastern limb. Several magnetic markers (US-T, CH1, CH2, BP-KRS, TC-KRS and NG2) have been used to delineate the structure. Stratigraphic boundaries are uncertain and since geological information is available mainly on a regional scale, magnetic interpretation can provide the necessary control for future mapping.

The northern closure of the major syncline is best defined by the magnetic marker US-T in the Ulupa Siltstone. US-T can be clearly followed from near Dutton on the west limb of the syncline, around the closure and then under Murray Basin cover east of the Milendella Fault till south of Red Creek. Figure 7.13 shows the relation between mapped outcrop of the Ulupa Siltstone and inferred Ulupa Siltstone magnetic anomaly.

North of Australia Plains, linear magnetic anomalies, possibly in the Adelaide Supergroup, have been followed on the eastern limb of the Syncline. These anomalies are truncated by the post-tectonic intrusives of the EMZ. Kanmantoo Group rocks have also been mapped as forming a fold closure in the north (Coats and Thomson, 1959; Drummond, 1972). But magnetic anomalies within this Group, if present in the north, could not be resolved from BMR data.

Several magnetic markers, CH1, CH2, BP-KRS, and TC-KRS were used to map the southern closure. The hinge of the Karinya Syncline is sharp and this is demonstrated by fold closures in the Talisker Calc-siltstone and Backstairs Passage Formation. Subsequent cross-faulting of the limbs has added to the discontinuous nature of the magnetic markers, which are unlike the more continuous anomalies typical of the KRSZ. Illuminated total magnetic field images (and the detailed geology map produced by Mills, 1964) have been particularly beneficial to the mapping of these folds. This is because on the images anomalies appear to be continuous and the effect of minor faulting is suppressed.

Magnetic anomalies in the Carrickalinga Head Formation and Backstairs Passage Formation are better developed on the western limb than on the eastern limb. The western limb of the Karinya Syncline is shown in Figure 7.14. BP-KRS is folded into a syncline-anticline-syncline combination. The anticline is a tight fold and shearing may have taken place along the hinge or eastern limb. CH2 is similarly folded. CH1 appears on the southwest of the Karinya Syncline but is faulted out and does not appear further north. The anomaly TC-KRS generally follows the mapped Karinya Shale (considered by Coats and Thomson, 1959, as equivalent to the Talisker Calc-siltstone) but there are gaps of several kilometres in places. Bull's-eye anomalies on CH2, BP-KRS and TC-KRS may be the result of tight folding or the effect of several deformations.

In the southern part of the Karinya Synclinorium, the Milendella Limestone Member (which is within the Blowhole Creek Siltstone Member of the Carrickalinga Head Formation — Cooper, 1988) acts as an excellent lithologic marker and forms ridges on the western and eastern limbs. The limestone has a distinct low radiometric signature and because of the contrast between it and the surrounding arkoses, siltstones and granitic rocks, it can be easily mapped from digital images of radiometric data (Plate 4). The incompetent limestones become strongly deformed in the anticlinal fold closures and this is clearly seen in Plate 4. The mapping of the Milendella Limestone Member from aeroradiometric data is another example of the complementary nature of aeromagnetic and aeroradiometric interpretation.

The marker TC-KRS appears on the eastern limb and is folded into a parasitic anticline-syncline fold. The northerly plunge of this syncline and thickening around the fold hinge have contributed to the easy resolution of TC-KRS from aeromagnetic data (diagrams C and D in Figure 7.1). Other markers on the eastern limb include BP-KRS and CH3. CH3 is separated from CH2 and CH1 by a major reverse fault (see below). Outcrop on the eastern limb is terminated by the Milendella Fault. The Heatherdale Shale of the Normanville Group crops out sporadically along the eastern limb and volcanics have been found in several localities (Gatehouse, pers. comm.).

The major fault in the area is a reverse fault on the eastern side of the Karinya Syncline (Mills, 1964). It offsets stratigraphic and magnetic markers, and metamorphic isograds. The fault is seen to dip approximately 45° E and the eastern block has been overthrust to the west. The apparent horizontal displacement is at least a mile, and the eastern side has also moved approximately 2.5 miles northwards (Mills, 1964). The fault is an oblique slip fault. Magnetic anomalies terminate against this fault. West of this major fault, the faults which break up the magnetic markers are either NNW to NW trending sinistral faults or W to SW trending dextral faults (Mills, 1964).

There is clear evidence of reverse faulting on the eastern escarpment of the Mt. Lofty Ranges (Mills, 1964). The Milendella Fault is a reverse fault with brecciated schists of the Kanmantoo Group thrust over Pleistocene fanglomerates, and Miocene limestone has been dragged up along the fault zone to an elevation of 160 m above sea level (Bourman and Lindsay, in press). Unlike the Palmer Fault, the Milendella Fault zone does not appear to have been albitized (Mills, *op. cit.*) and its radiometric expression is due to the effects of the scarp, and the change in outcrop from metasediments west of the fault to sands east of it. The Milendella Fault forms the boundary between the Adelaide Supergroup and the Kanmantoo Group in the region of Australia Plains (Drummond, 1972). The fault has been interpreted as a hinge fault (Drummond, *op. cit.*). However, while a sharp decrease in radiometric total count is observed across the Milendella Fault corresponding to the change in rock type, interpretation of magnetic maps indicate that magnetic markers are relatively unaffected, if at all. The Milendella Fault is important in the uplift of the Mt. Lofty Ranges but may not have not have been a major fault during the Delamerian Orogeny.

Magnetic intrusives of the EMZ limit the KRSZ in the east. The western limit changes in nature from north to south. In the northwest, the fold apparently passes into the north Truro Anticlinal structure (see below). The central part of the western boundary is fault restricted. And in the southwest, the fold passes into an anticline as evidenced by the deformed Milendella Limestone Member of the Carrickalinga Head Formation (Mills, *op. cit.*).

The Karinya Syncline consists of a syncline-anticline-syncline combination. The major structure is a doubly plunging syncline which trends NS (Figure 7.15). The Ulupa Siltstone magnetic anomaly, US-T, is seen on both limbs of the syncline. Magnetic dips obtained for the Ulupa Siltstone may be incorrect owing to the effect of its remanent magnetization. The plunge of the main syncline is shallow in the south (Mills, 1964) and steep in the north (Drummond, 1972). The central portion forms a broad syncline. The syncline is slightly overturned to the east. Drummond (*op. cit.*) considers the fold to be a synclinorium as there is at least one pair of *en échelon* folds in the north. Drummond (*op. cit.*) points out that in the north, the synclines are tight while the anticlines are open. In the south, the anticlines are apparently tight, because often both limbs cannot be resolved.

The formation of the Karinya Syncline was an F_{main} event. Allen (1977) found evidence of deformation prior to the formation of the major syncline. In the south Carrickalinga Head Formation rocks have been mapped on both limbs of the syncline. Mancktelow (1979) has

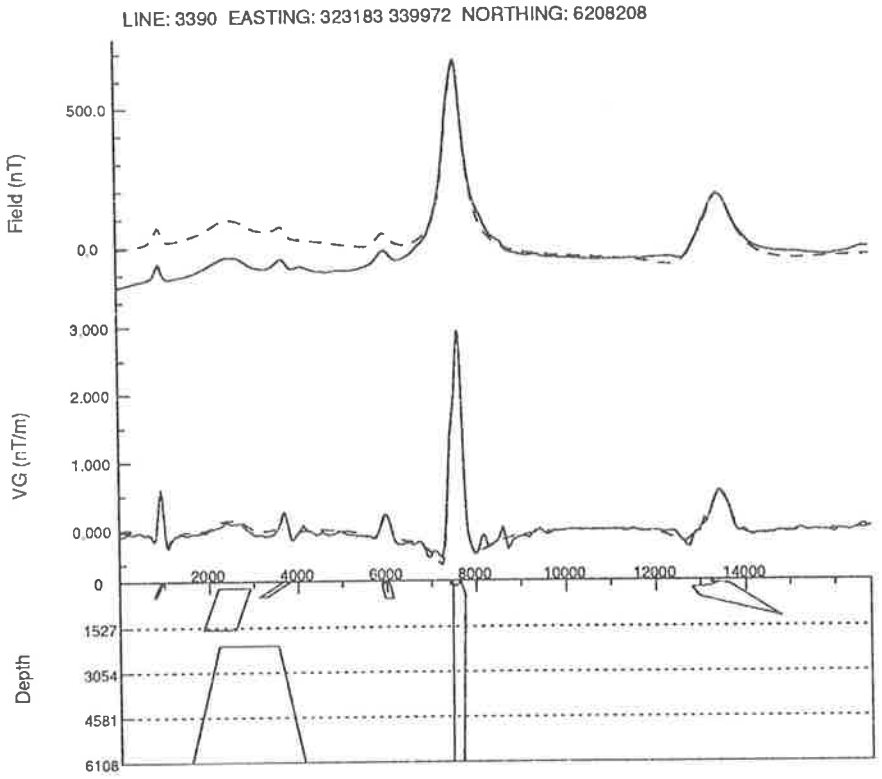

Figure 7.16: Magnetic model of the North Truro Anticline. Anomalies: US-KRS at 7800.

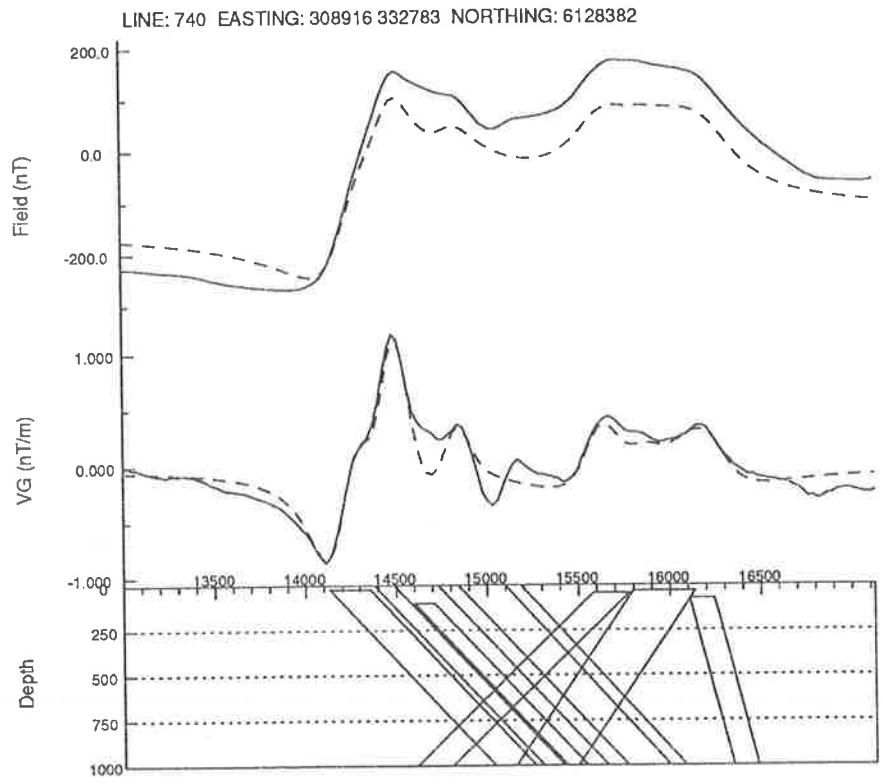

Figure 7.17: Magnetic model of the Rockleigh fold. Anomalies: BP-A1 between 14000 and 16300.

inferred that the meta-arkoses above the Carrickalinga Head Formation belong to the Backstairs Passage Formation. However he has also mapped Backstairs Passage Formation further west of the western limb of the syncline (Figure 1.2). The structural relationship between the south Karinya Syncline and the ISZ in this region is consistent with a deformation event prior to the formation of the major structure.

7.3.2 Truro Anticlinal structure

The anticlinal structures in the Truro-Dutton region have not been formerly defined and are therefore referred to here as the Truro Anticlinal structure. The Truro Anticlinal structure has been mapped by Coats and Thomson (1959) and in part by Kleeman (1965) and Fleming (1965). In Figure 1.2, the major anticlinal structure immediately to the west of the Karinya Syncline is the Truro Anticlinal structure. The Truro Anticlinal structure is made up of two major folds. The northern fold is a southerly plunging anticline which is defined as the north Truro Anticlinal structure (NTA). South of this there lies a doubly plunging anticline and this is the south Truro Anticlinal structure (STA). The axis of the NTA and of the STA both trend approximately NS.

Mancktelow (1979) interpreted the Karinya Syncline and the NTA to be F_1, but the STA to be F_2. Since Adelaide Supergroup rocks on the west limb of the Karinya Syncline form the east limb of the NTA, the NTA and the Karinya Syncline are likely to be of the same generation. However the south plunging STA and the south plunging Karinya Syncline cannot be simply connected (see above). The NTA and the STA are both F_{main} folds.

NTA: north Truro Anticlinal structure

The regional structure consists of a north-plunging anticline with Adelaide Supergroup metasediments in the core of the anticline (Figure 7.16). Minor faulting prior to F_{main} resulted in the disconnected strata on the limbs of the fold. Magnetic anomalies in the Tindelpina Shale member of the Tapley Hill Formation and in the Tarcowie Siltstone delineate the fold. The magnetic anomaly US-T has been identified as the Ulupa Siltstone magnetic marker (Section 6.1.3). The east limb of the NTA continues as the west limb of the Karinya Syncline which is consistent with both folds belonging to the same generation. The fold plane is tilted to the west and plunges 55° in a direction 195° (Kleeman, 1965).

An angular unconformity between the Heatherdale Shale (Normanville Group) and the underlying Adelaide Supergroup was inferred by Kleeman (1965) but the uppermost unit of the Adelaide Supergroup mapped by him is below the Ulupa Siltstone. The Heatherdale Shale is significant because volcanics are intercalated with it. Following US-T from the Australia Plains area, where its identification is reliable, to the eastern limb of the NTA, it was surprising to note that the Ulupa Siltstone has not been mapped in the region.

In the region of the type locality of the Truro Volcanics, work done by Forbes *et al.* (1972) and Kleeman (1965) shows Adelaide Supergroup rocks (below the Ulupa Siltstone) as cutting out against the Normanville Group. The volcanics have been identified as Cambrian and described as intercalated with the Heatherdale Shale. As Figure 7.13 shows, the source of the magnetic anomaly, US-T, is right below the mapped occurrence of the volcanics. The main alternatives to consider are:

1. Anomaly US-T has been mistakenly identified as being caused by the Ulupa Siltstone when it is in fact caused by Heatherdale Shale. The Heatherdale Shale in the region has

abundant, fine-grained opaques which could be magnetite. In the WMZ and CMZ, after the anomalies caused by the Barossa Complex rocks, the most distinctive magnetic anomaly is caused by the Ulupa Siltstone. Wherever the Ulupa Siltstone rocks have been mapped, there is a magnetic anomaly associated with it (Figure 7.13). The magnetic anomalies are of the order of several hundreds of nanoTeslas, and even show up on the SADME (1980) maps. Samples of the Ulupa Siltstone have been taken from areas where the identification is reliable (Delamere: Brotherton (1967), Mancktelow (1979); Mt. Barker Creek: Toteff (1977); Australia Plains: Drummond (1972), Mancktelow (1979)) and the high magnetic susceptibilities, strong Q factor, and percentage and constituents of the magnetic mineral assemblages, are all in favour of the Ulupa Siltstone being the main magnetic marker in the CMZ and WMZ. Anomaly US-T was followed from the Australia Plains area where it coincides with outcrop of the Ulupa Siltstone.

2. The geologic mapping in the area is incorrect and the rocks ascribed to the Heatherdale Shale really belong to the Ulupa Siltstone. The sedimentology of the rocks in the area is very similar to that of the Heatherdale Shale (Gatehouse, pers. comm.) and unlike the green-grey siltstones which are characteristic of the Ulupa Siltstone. So it is unlikely that the Truro Volcanics are in the Precambrian and not in the Cambrian. The identification could be tested by measuring the titanium content of the so-called Heatherdale Shale. The high titanium content of the Ulupa Siltstone (see Table 2.7) could perhaps be used to distinguish it from siltstones of the Heatherdale Shale.

3. The contact between the Cambrian and the Precambrian in this region, which has never clearly been explained before, is not simply an unconformity folded by the F_{main} deformation event. And therefore as the cross section shown in Figure 7.16 implies, the Ulupa Siltstone is near-surface as shown, though it is overlain by the Heatherdale Shale. All the dips are steep.

As explained above, I prefer the third alternative, i.e. US-T is caused by the Ulupa Siltstone; the Truro Volcanics are intercalated with the Heatherdale Shale; and though the dips are steep, the Heatherdale Shale is underlain by the Ulupa Siltstone. It is not enough that there be an unconformity between the Precambrian and the Cambrian, the contact must be fault related, and perhaps part of the F_{early} event.

STA: south Truro Anticlinal structure

The STA is a doubly-plunging anticline south of the NTA. As in the NTA, Adelaide Supergroup rocks are found in the core of the anticline. Fleming (1965) interpreted the major anticline to be a first deformation event. He found that the axial plane dips moderately east and the fold plunge is towards the south and varies from steep to moderately steep.

The stratigraphy in the area is uncertain and different interpretations have been presented in the geological maps of Truro (Coats and Thomson, 1959) and of Adelaide (Thomson, 1969b). Extensive areas of outcrop of the Angaston Marble (Normanville Group) are shown on both maps. The region is also known for its phosphate deposits in the Koonunga Phosphorite Member of the Normanville Group (Brown, 1908). The main lithologies are marbles (Normanville Group) and scapolite schists and the outcrop is poor.

The magnetic marker, NG3, is, for most of its length a single magnetic unit. Similar linear magnetic anomalies elsewhere in the study area have all been stratiform and there is no reason to believe otherwise of NG3. It is possible though that NG3 may really be in the Adelaide Supergroup as there is confusion about the stratigraphy as mentioned above. However, it is

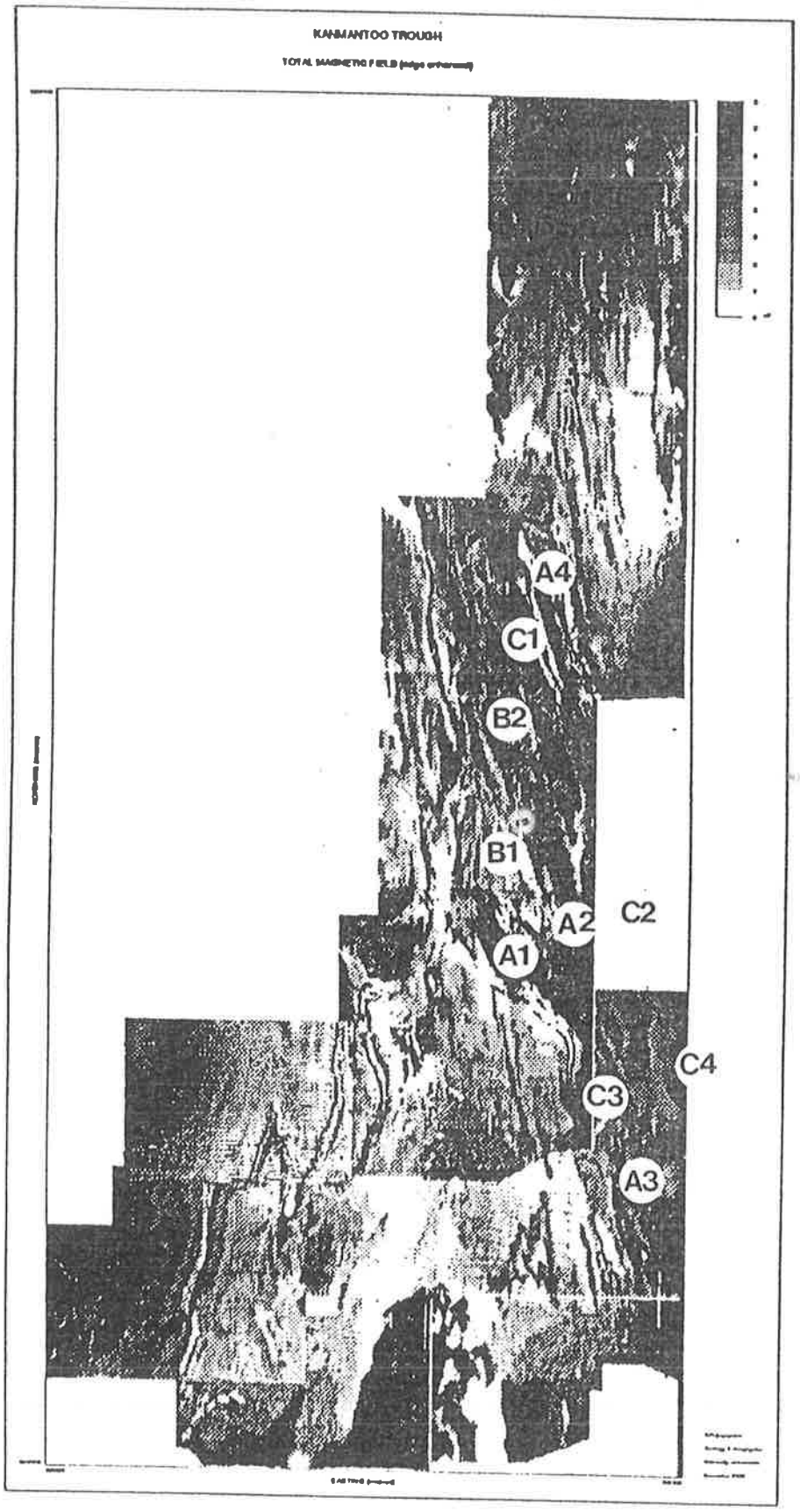

Figure 7.18: Subdivision of the ISZ into subareas. The grey-scale image of total magnetic field was reduced from Plate 3.

unlikely, considering the lower amplitude of the anomaly, that NG3 could be in the Ulupa Siltstone; and though Normanville Group outcrop is limited, there are magnetic anomalies within the Group (e.g. NG1 and NG2) and the Heatherdale Shale contains fine-grained magnetite.

Mancktelow (1979) decided that the STA, unlike the NTA, was an F_2 fold. The structural relationship between the STA and the Karinya Syncline cannot be simple. The western limb of the Karinya Syncline does not form the eastern limb of the STA and the relationship must in part be a fault contact. Fleming (1965) mapped part of the STA and concluded that the contact between the Precambrian and Cambrian could not be stratigraphic but must be structural. He inferred a fault contact but lack of outcrop over the boundary zone prevented any further confirmation. From the available magnetic and geological maps, the following can be inferred:

1. The stratigraphy on the western and eastern limbs are different. The marker NG3 is seen on the eastern limb of STA but has not been found on the western limb.
2. The phosphate deposits in the Koonunga Phosphorite Member are underlain by magnetic Ulupa Siltstone. This is based on the presence of strong magnetic anomalies over the phosphate deposits.
3. Though the regional structure closes in the south, individual units do not. In the southwest, Ulupa Siltstone has been mapped.
4. The western limb of the Karinya Syncline does not form the eastern limb of the STA.

There are several feasible solutions but lack of structural mapping limits the geophysical interpretation. One solution is that the effects of an earlier deformation have been overprinted by the F_{main} STA and Karinya Syncline folds. Alternatively, the STA may be separated from the Karinya Syncline by a fault. Tight "rootless" folds have been observed in the area between the STA and the Karinya Syncline. It is also possible that the Karinya Syncline and STA represent different generations of folding. The folding in this area is much more complex than previously mapped and further structural investigation is required to resolve the deformation style.

7.4 Structural patterns in the Intermediate Subzone

The Intermediate Subzone (ISZ) is a NNW trending elongate region between the KNSZ and the KRSZ and covers about a fifth of the main study area. The pattern of magnetic trends in the ISZ is in sharp contrast to the curvilinear magnetic anomalies which delineate the upright folds of the KNSZ and the KRSZ. Despite this difference in magnetic character, the boundaries of the ISZ are not clear cut. Definition of the western margin is particularly difficult and there is some overlap between the KNSZ and ISZ. The western boundary is taken to be east of the trace of the magnetic markers TC-EKS and TC-MNS and coincides in part with the steep magnetic gradient east of the Monarto Syncline. The northwestern limits follow the Bremer Fault. The western limb of the Karinya Syncline forms part of the eastern margin; the steep gradient which demarcates the EMZ constituting the rest of it.

Compared to the KNSZ and the KRSZ, the ISZ is characterized by an abundance of magnetic anomalies which can range up to hundreds of nanoTeslas in amplitude. Individual anomalies in the ISZ are not all that much higher than those in the KRSZ and KNSZ, but their multiplicity and closeness have resulted in a complex magnetic pattern which at first looks chaotic. The anomalies can be broadly classed into linear and curvilinear anomalies caused by metasediments and migmatites, and oval shaped discrete anomalies caused by granites and granite gneisses.

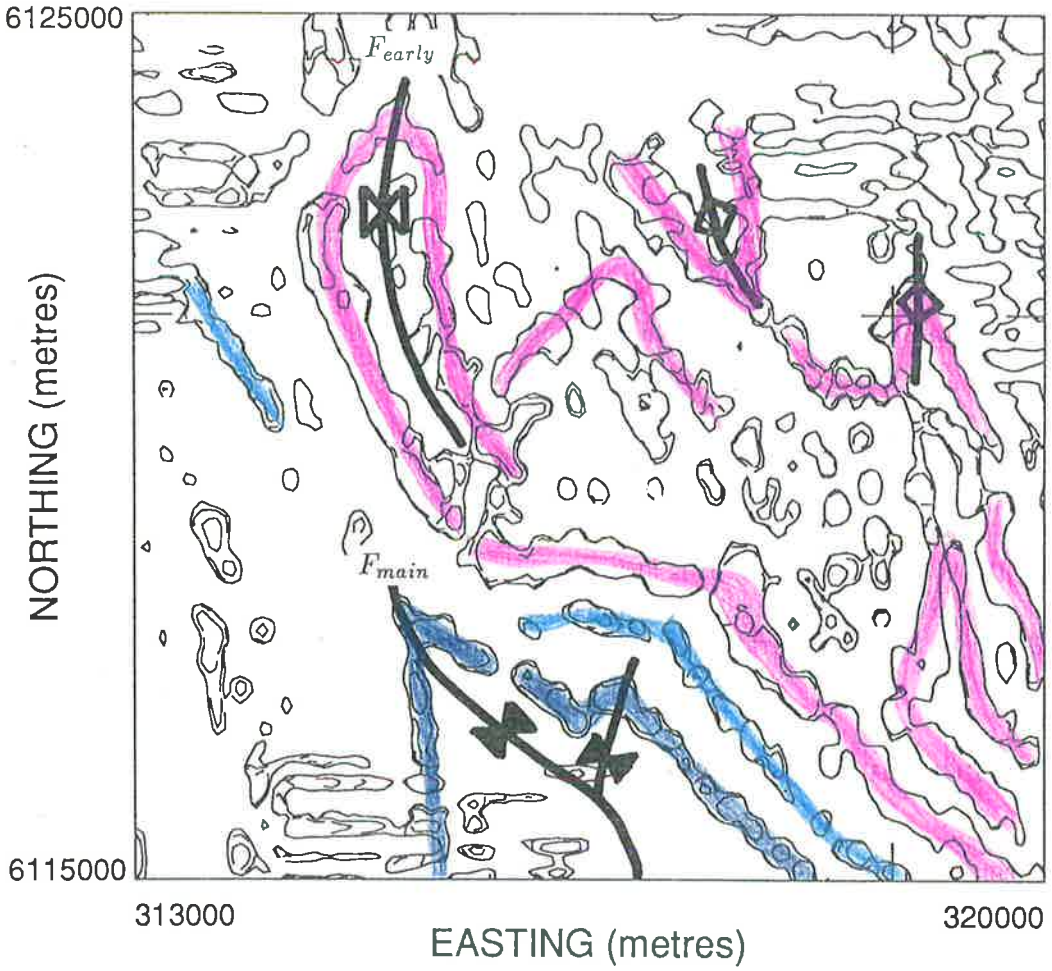

Figure 7.19: F_{early} and F_{main} folds in the Rockleigh area shown superimposed on vertical magnetic gradient contours.

Geologically, the ISZ coincides to a large degree with the migmatite zone (Figure 1.3). The metamorphic grade boundaries trend approximately NNW and this is highly significant. Almost the entire outcrop within the ISZ has been ascribed to the Backstairs Passage Formation. Granites (e.g. Palmer Granite) and granite gneisses (e.g. Rathjen Gneiss) and migmatized rock outcrop together with the meta-arkoses which are typical of the Backstairs Passage Formation. Calc-silicates occasionally occur, as do amphibolite and meta-dolerite dykes.

Unlike the KNSZ and KRSZ, no simple major structure has been mapped by previous workers and the relations of the structures in the ISZ to structures outside the Subzone are difficult to analyze. While a number of folds have been delineated from magnetic interpretation, it has rarely been possible to classify them as being synclines or anticlines. This is because facings are not available and directions of younging are often unknown. Additionally, magnetic dips indicate that most folds are overturned. Fold closures are only rarely seen.

Structures in this area appear to be discordant with structures elsewhere in the KNSZ and the KRSZ. This may be due to the overprinting of F_{main} folds by later folds because temperatures were still high in the ISZ which is within the highest grade metamorphic zone. The open, upright folds common to the KNSZ and the KRSZ are less common in the ISZ. The contact between the ISZ and the KNSZ and KRSZ appears to be discordant. Anomalies of the Truro Anticlinal structures are truncated by the ISZ and the relationship between the ISZ and KRSZ is complex.

7.4.1 Subareas in the ISZ

KNSZ and KRSZ were discussed in terms of the major structures in those subzones. The relatively complex magnetic signatures and the fact that the structure is poorly understood has made it more practical to consider the ISZ in terms of subareas of differing magnetic character.

Based on the magnetic characteristics, the ISZ can be divided into a number of subareas which are shown in Figure 7.18 (compare with Plate 3).

Subarea type A

Multiple, closely spaced, linear anomalies (dominant trend NNW), are caused by migmatites and meta-arenites of the Backstairs Passage Formation. The structural pattern within subareas A1 to A4 is largely unknown. These areas show evidence of previous deformation which could have been isoclinal. The rocks have been mapped as belonging to the Backstairs Passage Formation probably for want of evidence proving otherwise (see Mancktelow, 1979). The structure within these subareas is important, particularly if early macroscopic isoclinal folds interpreted from magnetic data are proved to exist.

The meta-arenites of the Rockleigh region, subarea A1, have been mapped in part by White (1956), Mancktelow (1979) and Lawrence (1980). Structures inferred by Mancktelow (1979) are too simple to explain the magnetic signatures. Magnetic units, TC-MNS and TP-MNS are both folded into the Monarto Syncline. Above TC-MNS, the magnetic units, BP-A1, do not close around the Monarto Syncline. Instead, BP-A1 has been used to delineate a fold closure which must be pre-F_{main} (Figure 7.19). The Monarto Syncline is therefore not an F_1 fold as interpreted by Mancktelow (1979). The magnetic anomaly associated with the pre-F_{main} fold closure suggests the fold was synformal. Part of an aeromagnetic profile over subarea A1 is shown in Figure 7.17.

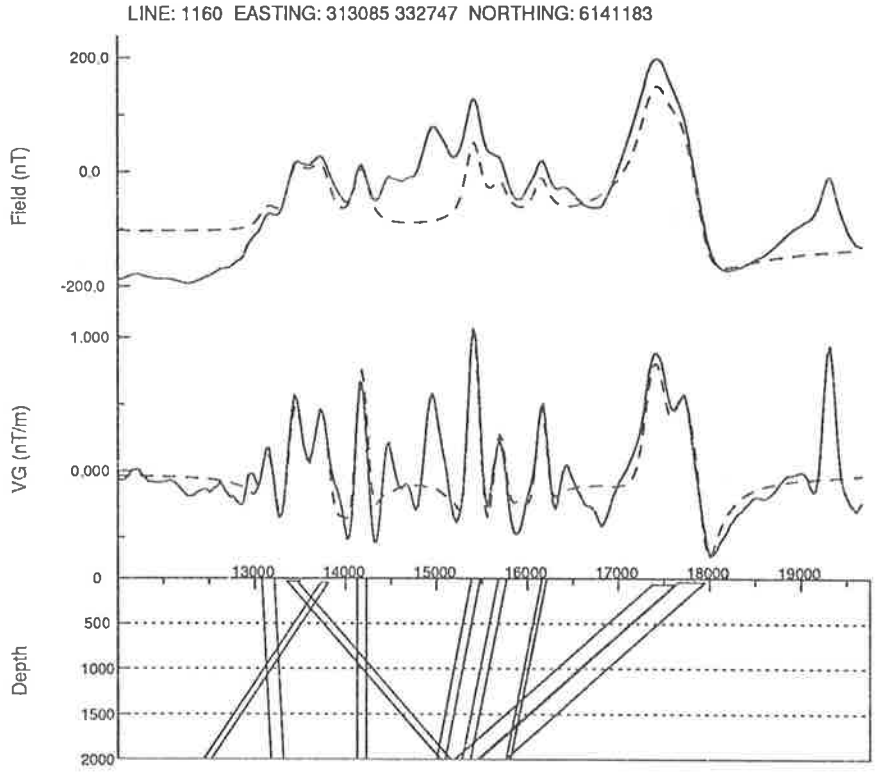

Figure 7.20: Magnetic model of the migmatite belt near Palmer. Anomalies: BP-A2 between 13000 and 17000, Palmer Granite: between 17500 and 18000.

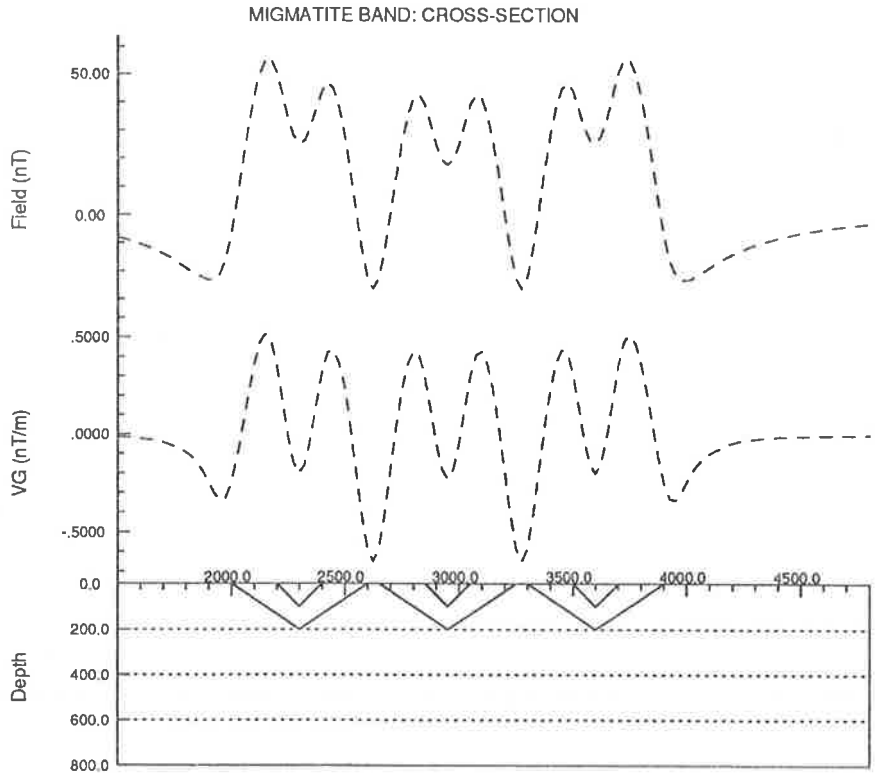

Figure 7.21: Magnetic model of simulated cross section of migmatite belt.

Lawrence (1980) mapped the arkoses as belonging to the middle member of the Backstairs Passage Formation. Trends marked by Mancktelow (1979) follow magnetic trends of BP-A1 and stop just short of the fold closure. North of the fold closure, similar air-photo trends do not continue: this is consistent with the interpretation of an early macroscopic fold refolded by F_{main}.

White (1956) called subarea A2 the "zone of veins". Subarea A2 contains the multiple, linear, NNW trending, magnetic and radiometric rocks west of Palmer. Magnetic anomaly amplitudes and radiometric count increase as rocks pass into the migmatite zone. While linear anomalies predominate on a large scale, individual trends can only be followed for short distances. Despite the ptygmatic folding associated with the migmatite zone, the overall trend of the magnetic units is dominantly NNW. The regional structure is a synform, interpreted by Fleming and White (1984) to be F_3. New, closely spaced gravity data are being collected in the Mt. Lofty Ranges (Boyd, pers. comm.). A gravity high has been located above subarea A2 (Middleton, 1973).

Modelling is difficult and magnetic profiles show a series of peaks in the total magnetic field and its vertical gradient (Figure 7.20). The closeness of the anomalous sources increases the ambiguity of the interpretation. Even on the vertical magnetic gradient profile, the true negative peaks are not seen. An experimental model showing short-wavelength folds is illustrated in Figure 7.21. Such a model also gives rise to a series of linear magnetic anomalies similar to that shown in Figure 7.20. The structure within such a belt is difficult and impossible to resolve from magnetic modelling alone.

The migmatite band east of the Monarto Granite is an extension of subarea A2, with at least two anomalous magnetic units establishing the continuity (there are gaps in detailed aeromagnetic coverage as shown in Figure I.2). Closures from contour maps indicate the presence of isoclinal folds folded by F_{main}. The limbs of the fold are parallel and trend NNW. The closures can be seen in Figure 7.1-B, Plates 1 to 3 and Plate 5, and in Figure 5.4. Attempts to model the isoclinal folds were not successful due to interference from neighbouring magnetic anomalies (Figure 7.22). The isoclinal folds are on the east limb of a regional synform. They may be F_{early} or F_{main} folds.

Subarea A3 is characterized by linear magnetic anomalies trending NS. Subarea A3 lies between the southern extension of the Monarto Syncline and the Wellington "Granite". Fold closures in subarea A3 are probably of the same generation as the isoclinal folds in subarea A2. A strong magnetic gradient separates subarea A3 from the KNSZ and may indicate a structural boundary. Anomalies in the KNSZ adjacent to the contact are of low amplitudes (less than a few hundreds of nanoTeslas) compared to the high amplitude anomalies in subarea A3.

The magnetic character of subareas A2 and A4 are similar, though they are separated by subarea C1. The pronounced NNW trend characteristic of subarea A2 is again seen in subarea A4. Granitic rocks also outcrop in this area, and geological maps (Thomson, 1969b) indicate the presence of granitized sediments (presumably meta-arenites or migmatites). The basic structure of subarea A4 may be anticlinal in keeping with the major syncline, the Karinya Syncline, to the east. Faults to the west and northwest obscure the relation between subarea A4 and the KRSZ. The southwestern contact between the Karinya Syncline and the subarea A4 of the ISZ is a problem area. Carrickalinga Head Formation rocks on the west limb of the Karinya Syncline are flanked on both the east and west by rocks of the younger Backstairs Passage Formation. In the east the younger rocks are folded into a syncline. But for Backstairs Passage Formation rocks to outcrop on the west as well requires further explanation. Abbas (1975) has mapped overturned dips in the ISZ west of the KRSZ. The feasible alternatives include the following: the boundary between subarea A4 and the KRSZ is a fault, the combination of several deformation events has

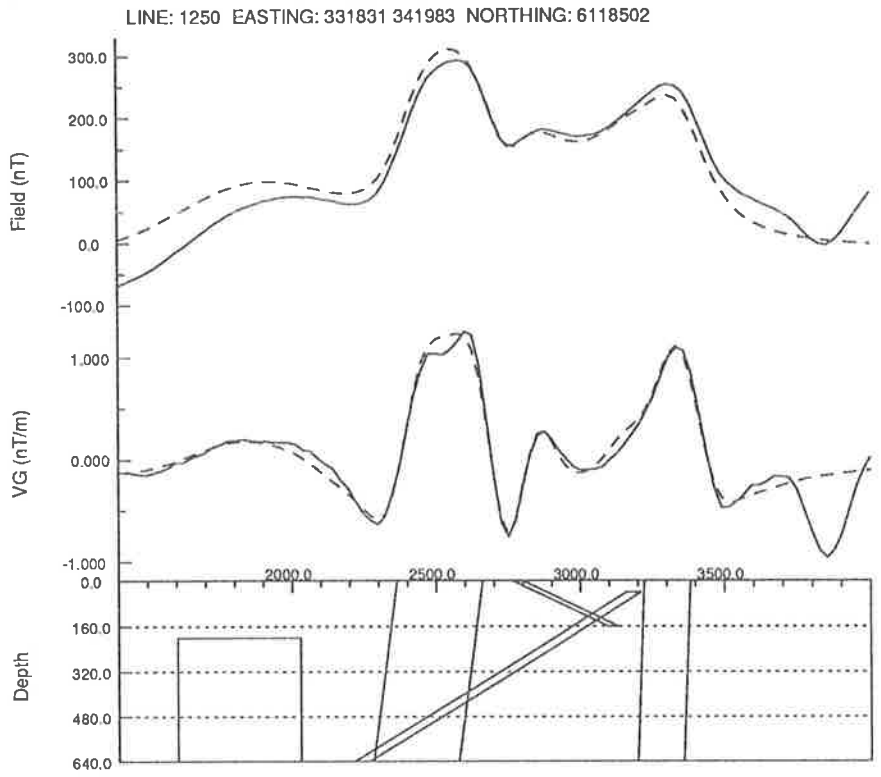

Figure 7.22: Magnetic model of the "isoclinal" folds of subarea A3 of the ISZ. Anomalies: BP-A2 between 2300 and 3500.

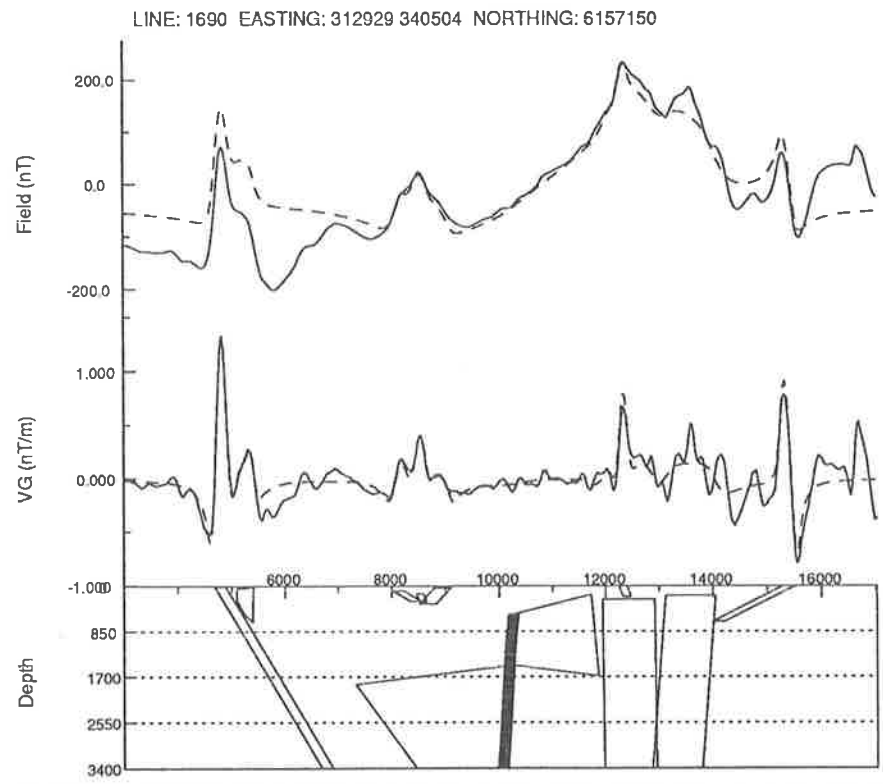

Figure 7.23: Magnetic model of the Springton Fault. The fault is indicated by the bold line. Anomalies: BP-NKS at 4800, possible subsurface granite between 7000 and 12000, BP-A4 between 12000 and 16000.

created this structural anomaly, or even that the meta-arenites which outcrop in subarea A4 have been incorrectly classified as Backstairs Passage Formation.

In the ISZ, the many linear anomalies have been correlated with the Backstairs Passage Formation. Some of the anomalies are obviously repeated by folding but because of the separation between subareas A2 and A4, the "stratigraphy" cannot be resolved. There are also more magnetic markers in this formation in the ISZ than elsewhere because firstly, increased metamorphic grade has increased the magnetite content of subunits within the formation. Secondly, the thickness of the formation may be greater here than elsewhere. The increased thickness may have been caused by thrusts and soft-sediment slumping.

Subarea type B

There are fewer and more widely separated anomalies in these subareas than in subarea A. The anomalies are lower in amplitude and more typical of the KNSZ. Migmatites and granitic rocks are generally limited to subareas A2–A4, and subareas C1–C3. Rocks with lower susceptibilities and simpler magnetic signatures are found in the subareas B1 and B2. The magnetic signature of subarea B1 is typical of the metasediments in the KNSZ and KRSZ. Fold hinges are open, unlike the sharp fold hinges in subareas A1–A4. Different folds do not appear to connect up and folds may be disharmonic. If the fold in subarea A1 does represent an early fold refolded by F_{main} then it is possible that the rocks in subarea B1 do not belong to the Backstairs Passage Formation.

Subarea B2 is separated from subarea C1 by a steeply dipping fault, named here the Springton Fault (Figure 7.23). Subarea B2 is distinctive in that it represents the only part of the CMZ proper where magnetic sources at depths of over two hundred metres have been detected. The fault appears to be a steeply-dipping normal fault and the amount of vertical displacement is 970 m. The downthrown side is towards the west. The fault trends NNW. The "deeper magnetic source" may be part of the Rathjen Gneiss.

On magnetic maps, the arcuate outline of the deeper magnetic source appears to be unaffected by the Bremer Fault though it is faulted by the Springton Fault. A coincident arcuate high is seen on the radiometric image. The source of these anomalies may be a subsurface granite which could be connected to the Rathjen Gneiss. The Springton Fault forms the western magnetic boundary of the Rathjen Gneiss (the radiometric and magnetic anomalies associated with mapped Rathjen Gneiss increase across this boundary). The profile shown in Figure 7.23 lies north of the Rathjen Gneiss.

Subarea type C

Granites and granitic rocks are found mainly in the ISZ. The exceptions are the Mt. Crawford Granite Gneiss in the WMZ, the Tanunda Creek Gneiss and the Mt. Kitchener Granite in the northern end of the KNSZ, small stocks of aplite in the south Karinya Syncline, the Encounter Bay Granites on the south coast and related granites on Kangaroo Island, and the post-tectonic granites of the EMZ.

The Rathjen Gneiss and Palmer Granite fall into a narrow NNW trending area, subarea C1. Both give rise to magnetic and radiometric anomalies (Section 6.2.1). The Rathjen Gneiss has been folded into a syncline. Magnetic modelling suggests that the thickness of the gneiss within the syncline is of the order of 800 m. The joint pattern (NE trending) is reflected in the

magnetic maps as a series of parallel faults and on the radiometric image as parallel lows. The western boundary of the gneiss is faulted and it is possible that more Rathjen Gneiss material is subsurface having been downfaulted by the Springton Fault. The Palmer Granite and Rathjen Gneiss are the only large igneous intrusives known in the region which could have supplied heat to the metasediments of subareas A2 and A4 during metamorphism.

The Reedy Creek Granodiorite and associated intrusives form subarea C2. Only BMR data are available for subarea C2. These granites are not part of the Murray Bridge suite and are syn-tectonic (Section 6.2.1).

The region of the Monarto Granite is defined to be subarea C3. The magnetic signature of the granite is subdued and indicated by the distortion of magnetic contours. The gravity effect suggests a northern and southern body separated by a thin veneer of outcropping granite (Lewis, A. M., 1985). The magnetic contours suggest that, in plan, the granite is oblong shaped (of the order of 5 km by 2.5 km) with the main axis trending NS. In the central area, magnetic anomalies caused by folded metasediments are seen.

Subarea C4 includes the Murray Bridge Granites, Sedan Granites, Truro Creek "Granite" and the Wellington "Granite". These lie in the EMZ and are post-tectonic. Their spatial dimensions are much larger than those of the Palmer Granite and Rathjen Gneiss (Section 6.2.1).

7.4.2 Fold generations

The first example of macroscopic F_{early} folding has been interpreted near Rockleigh where magnetic meta-arkoses of the Backstairs Passage Formation appear to be folded back onto themselves suggesting that an earlier fold axis has been refolded by the F_{main} Monarto Syncline. Other examples of F_{early} folding may include the possibly isoclinal folds in subarea A2.

The NNW trend of D_{later} structures in the ISZ is parallel to the metamorphic grade boundaries. Other significant NNW trends in the CMZ include the Woodside dyke swarm and the trends in the vicinity of Tinpot (Section 7.2.1). The ISZ lies within the G2 gravity corridor which also trends NNW (O'Driscoll, 1983). The NNW trends of magnetic units within the ISZ do not appear to extend outside the subzone. In the southeast, the trends continue across the Palmer Fault. But magnetic anomalies caused by the Reedy Creek Granodiorite and other granite intrusions in subarea C2 create a strong magnetic gradient against which these NNW trends appear to terminate. The intense magnetic anomalies caused by near-surface intrusives within the EMZ suppress the lower amplitude anomalies of the ISZ and it has not been possible to ascertain whether the NNW trend continued into the EMZ. In the northwest, the combination of lower metamorphic grades (and consequently lower magnetic anomalies) and regional magnetic data, prevents the determination of the northern extent of the NNW trends.

The ISZ shows the effect of D_{early} deformation and D_{later} deformation. It would appear that the effects of the D_{main} deformation, which are important in the KNSZ and KRSZ, have been overprinted by D_{later}. The reason behind the comparative influence of D_{later} is probably related to the cooling history of the region. Fleming and White (1984) suggest that as cooling from peak metamorphic temperatures proceeded, the higher grade regions cooled more slowly than the lower grade regions. So temperatures were still high in the ISZ during the D_{later} phase of deformation. The relation of structures in the ISZ to the F_{main} folds of the KNSZ and KRSZ is unclear and this is attributed to the overprinting of F_{main} folds by F_{later}.

It is possible that the deformational history of part of the ISZ is different from that of the KNSZ and the KRSZ (excluding subareas A1, B1 and B2 which show the effect of F_{early} and/or

F_{main}). Madigan (1988) has interpreted NS-stretching lineations observed in the Rathjen Gneiss as evidence of previously unrecorded NS movement in the region. Major NNW trending faults separate subareas A2, C1 and A4. These faults may represent the mechanism by which these subareas were located in their present position. These rocks could be allochthonous. Alternatively, they may have been uplifted in a "pop-up" left-lateral wrench fault system which twisted the Karinya Syncline northwards with respect to the Kanmantoo Syncline. These suggestions are speculative and there is little data to either confirm or deny them.

7.5 Structural history

The Delamerian Orogeny transformed the Proterozoic and Cambrian rocks of the Adelaide Geosyncline into an orogenic upland (Thomson, 1969a). The effects of the orogeny were strongest in the Mt. Lofty Ranges where several deformation events have been recorded (Offler and Fleming, 1968; Mancktelow, 1979).

The earliest known deformation in the region involved the mobilization of the Barossa Complex and subsequent formation of the Adelaide Geosyncline. There was a hiatus between the deposition of Precambrian sediments (the Marinoan) and the Cambrian sediments (Preiss, 1987). The present contact between the Kanmantoo Group and the Precambrian is represented by the Nairne Fault in some places. However it is not known whether this fault represents the original contact. The Nairne Fault, Snelling Fault and Cygnet Fault are believed to have controlled the deposition of the Kanmantoo Group (Preiss, 1987).

The polyphase and complex deformational history of the Kanmantoo Group started with syn-depositional deformation. The effects of syn-depositional events are largely unknown as they have been overprinted by the effects of the Delamerian Orogeny and the accompanying metamorphism. Delamerian Orogeny may have commenced prior to the final stages of deposition.

The main phase of the Delamerian Orogeny, F_{main}, which affected the whole of the Adelaide Geosyncline to varying degrees, produced upright, open macroscopic folds. During F_{main}, the Kanmantoo Synclinorium and Karinya Synclinorium were formed. Faulting was associated with this phase of folding and faults such as the Talisker and Alex Lookout Faults developed on the steep to overturned limbs of F_{main} folds (Mancktelow, 1979).

There is limited evidence to suggest that prior to the F_{main} event, the region had suffered an earlier deformation. Geophysically anomalous areas which may record this event have been identified in previous sections. Detailed geological mapping is warranted in these areas. Several geologists have reported folds prior to F_{main}. How much of what appears to be pre-F_{main} folds is related to syn-depositional events and how much to the Delamerian Orogeny is unknown. It would appear that the onset of the Delamerian Orogeny was marked by the development of thrust faults and isoclinal and recumbent folds as has been documented for most other Palaeozoic foldbelts (e.g. the Caledonides: Elliot and Johnson, 1980). The apparent confinement of F_{early} structures to the ubiquitous Backstairs Passage Formation is probably due to the nature of the event. The effect of the F_{early} phase was strongest near the base of the sedimentary pile where the thickness of sediments was greatest. The upper units of the Kanmantoo Group may have remained relatively undeformed. The Nairne Fault may represent one such thrust. It has been folded by F_{main} (Macclesfield region) and must be older than F_{main}.

Faulting associated with F_{later} is common in the ISZ. The faults run for tens of kilometres and trend NNW. The Springton Fault has vertical movement on it (west block down). The

[2]See also Appendix L.

NNW faults appear to form a set of left-lateral steeply dipping faults. The NE trending faults are common throughout the region though it is not known what the sense of movement along them was. They transect the Delamerian Foldbelt and may have been active post-F_{later}.

The results of magnetic interpretation have drawn attention to a number of areas where structural interpretation is inadequate or needs to be revised. On the basis of available information and constrained by the limitations of geophysical interpretation, it would be imprudent to speculate wildly when what is required are some basic structural facts.

Chapter 8

Discussion and concluding remarks

With the resurgence of interest in the Kanmantoo Group, new theories about the tectonic history of the region have been advanced (e.g. Jenkins, 1986; and in press; Clarke and Powell, 1989; Steinhardt, in prep.). Proofs for the various models are difficult to obtain. In the previous chapters, the magnetic response and structural interpretation was presented. Several subareas requiring further attention were identified. On the basis of the research carried out for this thesis, different models are reviewed using geophysical and geological facts. On many issues, geophysical interpretation may not directly contribute to the geological questions. The following section relates to the central issues listed in Section 1.3 and reviews current theories of the deposition and subsequent history of the Kanmantoo Group in a geophysical perspective.

The following discussion is based on the geophysical interpretation presented in the previous three chapters and on geological work carried out by other researchers. This chapter focuses on those aspects of the deposition, deformation and metamorphism of the sequence which are most controversial.

Of the newer ideas suggested, the most interesting are that the Kanmantoo Group is allochthonous, that part of the Kanmantoo Group has had a different metamorphic history from that of the Adelaide Supergroup, and that the sequence represents a stack of thrust sheets. These ideas have arisen in response to the need to explain the apparent thickness of the sequence and the high grade metamorphism of parts of the Kanmantoo Group (see section 1.3).

The discussion of the important geological issues is followed by the concluding remarks.

8.1 The development of the Kanmantoo Group

The deposition and metamorphism of the Kanmantoo Group are discussed below. The major structures and the structural history were presented in the previous chapter.

8.1.1 Deposition

Age of sediments

Kanmantoo Group metasediments are essentially non-fossiliferous (Section 1.2.1) and early researchers (e.g. Mawson and Sprigg, 1950) and recently Steinhardt (in prep.) have suggested

that the sequence may be partly or wholly coeval with the Proterozoic Adelaide Supergroup. However work by Sprigg and Campana (1953), Daily (1956), Campana and Horwitz (1956) and Gatehouse *et al.* (in press) among others discount this theory. Though there is limited control on the age of the Kanmantoo Group, a Cambrian, rather than partly Precambrian, age is more consistent with all the known geological data.

The Carrickalinga Head Formation is considered by Daily and Milnes (1972a) to be the basal formation of the Kanmantoo Group. Few distinctive fossils have been found within this formation but compared to the other Kanmantoo Group formations, it is the most fossiliferous. Daily (1963) found the brachiopod *Lingulella* in the basal 10 m of the Carrickalinga Head Formation at Carrickalinga Head, and Daily (1977) found the Lower Cambrian trilobite *Redlichia* in what Daily and Milnes (1973) believe to be lower Kanmantoo Group rocks on Kangaroo Island. Gatehouse *et al.* (in press) reported *Hyolithidae* at Carrickalinga Head. This places the age of deposition of the Carrickalinga Head Formation in the Early Palaeozoic. Worm tracks and casts are the only other fossils to have been found in the lower five formations.

Daily and Milnes (1971b) state that "where Lower Cambrian rocks are overlain by Kanmantoo Group rocks without structural discordance, conformity between them can be expected". This is supported by investigations in the following regions: Delamere (Daily, 1963; Leslie, 1962), Red Creek and Sedan Hill sections (Gatehouse *et al.*, in press) and at Carrickalinga Head (Mancktelow, 1979). Note that on the Truro 1 : 63 360 scale map (Coats and Thomson, 1959), the relation has been interpreted to be unconformable though Daily and Milnes (1971b) suggest that a fault contact is more consistent with the evidence. This is supported by magnetic interpretation (Section 7.3). Fault contacts between the two Cambrian Groups have been inferred near Myponga, east of Australia Plains and in the Mount Barker-Mt. Torrens area by Mancktelow (1979). The transitional/conformable relationship between the Carrickalinga Head Formation and the underlying Cambrian Normanville Group reinforces a Cambrian age for the formation. (There is limited palaeontological evidence for a middle Early Cambrian age for the Heatherdale Shale, Normanville Group, (Jago *et al.*, 1984; 1986) which is conformably overlain by the Carrickalinga Head Formation).

The timing of Ordovician granite intrusions into Kanmantoo Group rocks places a lower limit on the age. Dasch *et al.* (1971) dated the granites and metasediments around the Encounter Bay area and determined an age of 487 ± 60 Ma for Kanmantoo Group metasediments.

In the type section, successive Kanmantoo Group units have been shown by Daily and Milnes (1972a and 1973) to be in apparently conformable contact which places the sequence as a whole in the Early Palaeozoic and younger. Questions regarding the acceptance of the stratigraphy proposed by Daily and Milnes (1972a) have been raised by Jenkins (in press) and Steinhardt (in prep.) and will be discussed in a subsequent section. Obviously, while the Carrickalinga Head Formation is Cambrian, if the formations above are not conformable, they could be older than the Carrickalinga Head Formation.

In the Williamstown region, Offler (1966) has recorded three deformations in the Adelaide Supergroup, of which the later two affected the Kanmantoo Group rocks. This is again consistent with a younger age for the Kanmantoo Group compared to the Adelaide Supergroup.

Stratigraphy

The classification developed by Daily and Milnes (1972a) and applied by Mancktelow (1979) has been used throughout in the correlation of magnetic anomalies with stratigraphic units. The classification is based entirely on lithology. The most common lithologies are arkoses,

greywackes, and pelitic units and these may be found in any unit and are not distinctive of any individual formation.

Based on similar lithologies, the sequence can be simplified from the original eight formations into four subunits: KG1 — Carrickalinga Head Formation, KG2 — Backstairs Passage Formation, KG3 — Talisker Calc-siltstone, Tapanappa, Tunkalilla, Balquhidder and Petrel Cove Formation and KG4 — Middleton Sandstone. This subdivision is convenient for analyzing possible repetitions in the sequence. It should not taken to suggest that the classification proposed by Daily and Milnes (1972a) should be revised. Subunit KG1 is characterized by siltstones and occasional argillaceous and pure limestones; KG2 and KG4 are dominated by arkosic sandstones; and KG3 as a whole consists of a sequence of siltstones and greywackes intercalated with siltstones rich in iron sulphides.

The subdivision defined in the coastal section has not been applied far inland. Going inland from the south coast, the thick sequence of greywackes and pelitic rocks can no longer be subdivided into the Tunkalilla, Balquhidder and Petrel Cove Formation and has instead been mapped as Tapanappa Formation (Mancktelow, 1979). This could be due to non-exposure of the younger units or may indicate that the stratigraphy defined was too complex and that subdivision into these formations is not warranted. So KG3 would consist of two formations (Talisker Calc-siltstone and Tapanappa Formation) rather than five. Note that failure to map individual younger units on the *Monarto* sheet may be due to the fact that few detailed mapping studies have been undertaken subsequent to the Daily and Milnes' (1972a) classification.

There is no difference between the arkoses found in the Backstairs Passage Formation and the Tapanappa Formation. These formations cannot be distinguished in regions of arkose outcrop unless the intermediate Talisker Calc-siltstone can be mapped (Mancktelow, 1979). Stratigraphy of large areas of the *Tepko* and *Angaston* sheets is therefore uncertain. The sandstones of the Middleton Sandstone and the Backstairs Passage Formation are also similar but the epidote rich segregations characteristic of the former have not been reported for the latter.

The Kanmantoo Group has been described by Daily and Milnes (1972a) to be a conformable sequence of units as described in the type section along the south coast of Fleurieu Peninsula. The two main problems with accepting this are the enormous inferred thickness of the sequence and the repetition of lithologies both within and across unit boundaries. Current theories (Jenkins, in press; Steinhardt, in prep.) suggest that the thickness has been greatly augmented by thrusting. Jenkins (*op. cit.*) has drawn attention to the appearance of carbonaceous phyllites at the base of the Tunkalilla, Balquhidder and Petrel Cove Formation which he suggests could represent thrust surfaces. Similarly, Steinhardt (in prep.) gives examples of a number of units which could have acted as detachment surfaces during thrusting: the marble at Macclesfield which lies below the Kanmantoo Group, the Talisker Calc-siltstone below the Tapanappa Formation and the various sulphide-rich units in KG3. However, no field data have been produced to support this model.

Steinhardt (*op. cit.*) goes on to suggest that the Tapanappa Formation may represent repeated Carrickalinga Head Formation. There are several differences between these two formations. Though their geochemistry is similar (Table 2.7), fossils found in the Carrickalinga Head Formation have not been found elsewhere, iron sulphides which appear regularly in the Tapanappa Formation first appear in the Kanmantoo Group sequence in the Talisker Calc-siltstone and the argillaceous and pure limestone found in the Carrickalinga Head Formation have not been reported for the Tapanappa Formation. The subdivision of the Carrickalinga Head Formation into three members on the south coast has been repeated by Gatehouse *et al.* (in press) at Sedan Hill. These differences support Daily and Milnes' (1972a) classification of the two as separate formations.

Thickness

Based on thickness estimates along the type section and estimated cover during the intrusion of the Encounter Bay Granites, the thickness has been estimated to be between 15–20 km (Thomson, 1969a). Even accounting for attenuated Adelaide Supergroup below the Kanmantoo Group, the total thickness of the sediments must have been considerable. Note that Daily and Milnes (1972a) gave no estimates of the thickness in their description of the type section. This was probably because parts of the section are inaccessible and thickness estimates would be distorted as significant structures might not have been recognized. The enormous apparent thickness inferred for the Kanmantoo Group might be the result of non-recognition of thrusts and folds which have caused repetition of the sequence in the type section.

A more likely mechanism of augmenting the thickness of the sequence, and one for which some evidence is available, is through folding rather than thrusting. In many places on Fleurieu Peninsula, Permian cover obscures Kanmantoo Group rocks. Interpretation of aeromagnetic maps (SADME, 1983) has revealed previously unrecognized macroscopic folds (Figure 7.5) which appear to have affected Kanmantoo Group rocks, particularly the Tapanappa Formation. Since the Tapanappa Formation appears to be the thickest of the Kanmantoo units, any reduction in its thickness will result in a more plausible thickness of the sequence as a whole. Detailed magnetic traverses will be required to map the folds accurately as available contour maps are liable to be misleading.

Evidence for pre-F_{main} macroscopic folding (some of which may have been isoclinal) has been presented in Sections 7.2.1 and 7.4.1. The eastern and western bands of the magnetic anomaly, TC-WKS, may represent the same magnetic horizon. The absence of a distinct magnetic anomaly in the region between the northern end of TC-MS and the southern end of TC-WKS may represent the magnetic expression of a thrust above the Talisker Calc-siltstone.

Mode of basin formation

The term "Kanmantoo Trough" is a standard reference term. Thomson (1969a) states that the "lack of sorting, sudden thickening across fault hinge zones and abundant sedimentary slump structures point to rapid sedimentary transport and violent downward movements of the sea floor during sedimentation". Thomson (*op. cit.*) in a diagrammatic sketch shows the Kanmantoo Group thickening eastwards across a series of stepped faults. The existence of submarine fault lines is yet to be proved though the present base of the Kanmantoo Group is often marked by a fault.

There is little evidence to suggest that the original basin was a trough. The boundaries of the basin are unknown. The basin may have been a stretch basin (Jenkins, in press). Steinhardt (in prep.) suggests that the Kanmantoo Group may in part be coeval with the Adelaide Supergroup and that the two represent a continental slope-shelf combination deposited off a passive continental margin. Subsequently, the Kanmantoo Group was thrust over the Adelaide Supergroup.

The sequence includes both shallow and deep water sediments and represents a cyclic upward shallowing sequence (Section 1.2.1). Sedimentological work on the sequence is limited to work on the coast (e.g. Daily and Milnes, 1972a; Mancktelow, 1979; Boord, 1985, Gatehouse and Jago, 1988), within the Karinya Syncline (Mills, 1964; Gatehouse *et al.*, in press) and on Kangaroo Island (e.g. Moore, 1983; Mancktelow, 1979; Flint and Grady, 1979).

Mancktelow (1979) and Boord (1985) believe that the Backstairs Passage Formation and Middleton Sandstone were deposited in shallow marine conditions while the other units were deposited in generally deep water conditions. Gatehouse *et al.* (in press) suggest that the Carrickalinga Head Formation was deposited in deep water at Carrickalinga Head, but in shallow water conditions on Kangaroo Island and in the Sedan Hill section. They suggest that the Campana Creek Member of the Carrickalinga Head Formation represents a shallowing upwards sequence which is a precursor to the shallow water, high energy deposits of the Backstairs Passage Formation which prograded across the present area of outcrop.

The Normanville Group and Kanmantoo Group could represent a shelf-slope combination off a passive continental margin (von der Borch, 1980). The term "Adelaide Rift" was proposed by von der Borch (*op. cit.*) but again there is little evidence for rifting. Boord (1985) considers that the basin was a passive continental margin but actively subsiding.

The aeromagnetic map shows two major geophysical boundaries to the west and east of the Mt. Lofty Ranges. To the west, off the coastline of Yorke Peninsula, a wide magnetic anomaly has been interpreted by Gunn (1984) as representing the ancient continental edge with the Adelaide Geosyncline developing as a rift on the "shoulder" to the east. The anomaly has been interpreted to be left-laterally faulted and it continues right into the centre of South Australia. Alternatively, the anomaly could represent moderately deep magnetic basement. The second major boundary is the Murray Magnetic High (MMH) and this is discussed in Section 5.2.1.

Limits of the Kanmantoo Group

Schists intersected in drill holes in the MMH are often very low grade (Wegmann, 1980; Lewis, P., 1985) and cannot be definitely correlated with Kanmantoo Group. Tertiary rocks and Recent sediments obscure basement on the *Milang* and *Alexandrina* sheets and in the Murray Basin. Aeromagnetic interpretation over the *Milang* and *Alexandrina* sheets shows that the synclinal structures continue to open southwards and that the southern limit of the KNSZ, and therefore of the Kanmantoo Group, is not known on Fleurieu Peninsula.

The migmatites and meta-arkoses found in the ISZ are likely to belong to the Backstairs Passage Formation. Further east, the complex magnetic signatures of the igneous intrusives characteristic of the EMZ overshadow the magnetic effect of possible Kanmantoo Group rocks. In a few areas to the east of the *Truro* sheet, linear, relatively smaller magnetic anomalies, which are different to the anomalies caused by the igneous intrusives, may be caused by metasediments. There is no control on the age of these possible metasediments. The Glenelg River beds in Victoria are considered by Wells (1956) and Cooper and Grindlay (1982) to be correlatives of the Kanmantoo Group. However this does not imply that the basin in which the Kanmantoo Group sediments was deposited extended into Victoria.

Basement to the Kanmantoo Group

The Kanmantoo Group may have been deposited on attenuated Normanville Group or Adelaide Supergroup rocks. Alternatively, as Steinhardt (in prep.) and Clarke and Powell (1989) suggest, the sequence may be allochthonous and was later thrust into its present position.

Much of the argument in favour of an allochthon depends on an older age and a separate metamorphic history. As has been shown above, the basal unit of the sequence is likely to be Cambrian. The second point will be discussed in Section 8.1.2.

As the northern closure of the Karinya Syncline shows (refer to Section 7.3.1), Adelaide Supergroup and Kanmantoo Group metasediments are folded together around the syncline. The important Ulupa Siltstone magnetic marker can be followed under cover almost down to Red Creek east of the Palmer-Milendella Fault. In this region, Adelaide Supergroup rocks must lie under the Kanmantoo Group rocks. In the EMZ, the strong magnetic anomalies caused by near-surface intrusive rocks make it difficult to locate narrow, linear anomalies which may be caused by metasediments.

South of this, strong anomalies caused by intrusive rocks of the Murray Magnetic High obscure any analysis of the continuation of metasediment type anomaly in the region to the east of the Palmer Fault and Milendella Fault.

Again in the Red Creek area, Carrickalinga Head Formation overlies Normanville Group, the contact is gradational and the Truro Volcanics may extend into the Carrickalinga Head Formation (Gatehouse, pers. comm.). All this is consistent with the Kanmantoo Group overlying Normanville Group/Adelaide Supergroup in this region and of having done so at the time of deposition.

Sediments of the Carrickalinga Head Formation occur on both sides of the anticlinorium core. There is a difference in facies: deeper water at Carrickalinga Head (which lies west of Mt. Compass Inlier) and shallow water on Kangaroo Island (Moore, 1983). Gatehouse *et al.* (in press) interpreted the formation in the Sedan Hill section as shallow water facies — they were able to apply the same three-fold subdivision of the formation at Sedan Hill corresponding to that exposed on the south coast.

In the Mt. Barker Creek area, the contact between the Adelaide Supergroup and the Kanmantoo Group must be low-angle and the two appear to have been folded and metamorphosed together.

Liu and Fleming (1989) have been studying amphibolites in the Palmer-Tungkillo and surrounding regions. They have noted three generations of amphibolites: pre-D_1, syn- to post-D1, and a third generation of undeformed amphibolite dykes intruded after the close of the Delamerian Orogeny. They deduced from the geochemistry that the dykes have oceanic basalt affinities and that the basic magmas which produced these dykes may have been derived from elevated mantle under the Kanmantoo basin.

The evidence from gravity and seismic data is inconclusive. Magnetic maps provide no direct clues regarding the present basement to the Kanmantoo Group. Indirectly, if magnetic basement exists, it must be more than several kilometres deep. The thickness of low to moderately magnetic metasediments in the Kanmantoo Synclinorium is probably several kilometres.

8.1.2 Metamorphism

Previous researchers (e.g. Tate, 1879; Jenkins, 1986; Clarke and Powell, 1989) have found it incongruous that the "structurally highest sequence", i.e. the Kanmantoo Group, should have been metamorphosed to higher grades than the Adelaide Supergroup. Offler and Fleming (1968) have shown that the metamorphism was of the Buchan style — high T, low P. Undoubtedly, as Figure 1.3 in Chapter 1 shows, the migmatite zone is confined to the metasediments of the Kanmantoo Group.

The Kanmantoo Group is likely (see earlier discussion on stratigraphy) to be stratigraphically higher than the Adelaide Supergroup — the term "structural highest sequence" is ambiguous.

If the metamorphism were due to depth of crustal burial alone, then the difference in maximum metamorphic grade between the Adelaide Supergroup and the Kanmantoo Group might be used to suggest that the Kanmantoo Group was emplaced as a hot allochthon (Clarke and Powell, 1989). However the P-T conditions reflect a severely perturbed thermal regime well in excess of that expected for the conductive heating of tectonically thickened crust (Sandiford *et al.*, in press). Clarke and Powell (1989) also agree that the perturbed geotherm is inconsistent with a tectonically thickened crust alone. Thus it is not necessary to explain the higher metamorphism of the Kanmantoo Group rocks by a separate metamorphic history (the "allochthonous" theory) or by ascribing an older age to the rocks.

Within the CMZ, the Palmer, Monarto and Mt. Kitchener Granite, the Rathjen and Tanunda Creek Gneiss, and the Reedy Creek Granodiorite form one group; and the Encounter Bay Granites and the granites on Kangaroo Island form another. There is a well-defined relationship between the spatial distribution of the first group of granites and the boundaries of the migmatite zone but the metasediments into which they have intruded have not developed discernable contact aureoles (Mancktelow, 1979). Magnetic trends and radiometric highs also bear a strong preferred orientation to the NNW trend of the migmatite zone which lies within the G2 gravity corridor (O'Driscoll, 1983). Of the second group of granites, there is a strong spatial association between the andalusite-staurolite zone boundary and the contact between the Encounter Bay Granites and the country rock. The metamorphism around Victor Harbor appears to be directly related to the intrusion of the Encounter Bay Granites (Mancktelow, 1979).

Mancktelow (*op. cit.*) suggested two explanations for the relation between the first group of granites and the migmatite zone: either the increased heat flow in the region produced the granites, or, alternatively, the granites supplied the energy which caused the metamorphism of the sediments. The first is consistent with the lack of distinct contact aureoles but is incomplete in that the primary heat source is unknown. The second explanation is consistent with the interpretation by Sandiford *et al.* (in press) that additional heat sources are required to explain the conditions of metamorphism. The direct correlation between the location of granites and granite gneisses and the location of the high-grade belt indicates that the simplest solution might be that the positioning of the granite intrusions is the cause of the high grade rocks being apparently confined to the Kanmantoo Group.

The Palmer and Monarto Granite have been interpreted by Mancktelow (*op. cit.*) to have intruded post-D_1 (i.e. after the development of the Kanmantoo and Monarto Syncline). But evidence of early thermal activity in the Central Magnetic Zone has been documented (Encounter Bay Granites: Milnes *et al.*, 1977; partial melting in the migmatite zone, Fleming and White, 1984; base metal mineralization in the Kanmantoo Mine area: Seccombe *et al.*, 1985; pre-tectonic amphibolites: Liu and Fleming, 1989). Apart from the possible subsurface extension of the Rathjen Gneiss and a subsurface granite in the Dawesley area, deep magnetic sources are not apparent in the magnetic data, therefore precluding the existence of subsurface magnetic granites. Other igneous activity includes the Woodside dyke swarm (Pain, 1968) and the only known volcanics in the Mt. Lofty Ranges, the Truro Volcanics which are intercalated with the Heatherdale Shale. Whether these igneous bodies would provide a sufficient quantity of heat to sustain the metamorphism is not known.

Madigan (1988) advocates that metamorphism commenced with the intrusion of granites into the sediments and that metamorphism continued while deformation produced an early stretching lineation. Mancktelow (1979) suggests that peak metamorphic temperatures coincided with D_1 deformation. Prior to the intrusion of the post-Delamerian intrusives in the EMZ, the rocks were cooling.

8.2 Concluding remarks

The geological problem of studying the Kanmantoo Group is typical of some terrains: the area occupied is large, lithological marker horizons are rare and outcrop is often weathered and in some areas non-existent. Though much work has been done, there are gaps in the continuity and also considerable variation in the quality of available information.

The acquisition of high-resolution aeromagnetic data has made it possible to study the entire area independent of the nature of the overburden. It was thus possible to present a unified interpretation of the rocks based on the difference in their magnetic properties. The stratigraphy and structure of the area have been reexamined from a magnetic perspective. Rock property studies, aeroradiometric interpretation and the results of previous geological investigations have been used to constrain and improve the aeromagnetic interpretation.

The advantages of reprocessing geophysical data and of using different presentation formats cannot be over-emphasized. The applications of aeromagnetic data have been extended beyond that of being a reconnaissance tool and an aid to geological mapping. There is a wealth of information inherent in the data set which makes aeromagnetic interpretation relevant to the study of subtle and varied geological problems. The extraction of this information is critically dependent on the processing techniques used. The transformation of the interpretation into a geologically intelligible model requires the study of the relation between the magnetic properties of rocks and their geological evolution.

The interpretation of a geological terrain is an on-going process. As new data are collected and new ideas emerge, previous models will be updated, tested and improved. Basic rock property data, the results of magnetic modelling and the information on the maps included in this thesis should provide more lasting factual information. Anomalous areas have been targeted where detailed geological investigations might reveal evidence crucial to an understanding of the early history of the Kanmantoo Group. It is hoped that the maps and interpretation presented here will provide a basis for future research.

	Detailed data			Regional data	
Flown for	CRA	Pacific Expl.	CRA	SADME	BMR
Year	1979	1979	1980		1978
Digital magnetic data	Yes	Yes	Yes	No	Yes
Digital radiometric data	Yes	Yes	Yes	No	
nominal ground clearance (metres)	80	80	80	152	150
nominal flight line spacing (metres)	300	150	300	1609	1500
nominal sample spacing (metres)	25	25	25	continuous recording	55
flight line direction	EW	EW	EW	EW	EW
Area	Mt. Lofty Ranges	*Echunga*	Murray Bridge	Mt. Lofty Ranges, Kangaroo Island	Adelaide-Renmark

Table A.1: Aeromagnetic survey details.

Appendix A: Geophysical surveys in the study area

Aeromagnetic coverage of Fleurieu Peninsula and the Mt. Lofty Ranges varies in quality and detail. This appendix lists the aeromagnetic and aeroradiometric data used in this thesis. The source and survey specifications are given in Table A.1.

The study area includes part or all of the following 1:50 000 topographic sheet areas: *Alexandrina, Milang, Echunga, Monarto, Tepko, Angaston* and *Truro.* A very small part of the *Willunga, Noarlunga* and *Onkaparinga* 1:50 000 sheet areas is also covered by detailed surveys. The corresponding 1:100 000 sheet names are MILANG (*Milang, Echunga, Noarlunga, Willunga*), MOBILONG (*Mobilong, Monarto, Alexandrina, Wellington*), MANNUM (*Mannum, Cambrai, Angaston, Tepko*) and EUDUNDA (*Eudunda, Truro, Sandleton, Mt. Mary*). Figure A.1 shows the study area and the topographic sheet names.

Figure I.2 shows some of the available aeromagnetic data for the area. The data was acquired from the following sources:

1. CRA data — Except for a small part (see below), all the digital high-resolution aeromagnetic and aeroradiometric data was supplied by CRA Exploration. This data set covers most of the Kanmantoo Group outcrop in the Mt. Lofty Ranges. The digital data was in the form of located data files on magnetic tape. The aeromagnetic data had been corrected for the effects of the International Geomagnetic Reference Field (IGRF) and locations were provided as AMG coordinates. The data are now in the public domain and enquiries should be directed to the South Australian Department of Mines and Energy (SADME). The aeroradiometric data was incomplete and only the uncorrected total radiometric count has been used in this thesis. CRA also generously provided copies of contour maps of the total magnetic field at various scales.

2. Pacific Expl. data — A high-resolution survey (line spacing half that of the CRA survey) was flown for Pacific Exploration. This data set was acquired from SADME as located data files on magnetic tape. The IGRF had to be removed.

3. SADME data — Aeromagnetic data were available in the form of contour maps (Gerdes, 1986; SADME, 1980 and 1983). The data had not been acquired digitally, so no reprocessing was possible.

4. BMR data — All references to BMR data in this thesis relate to the joint acquisition of aeromagnetic data over the Murray Basin in South Australia by the Bureau of Mineral Resources and SADME. Digital aeromagnetic data was generously provided by SADME.

Interpretation of the geophysical data sets was carried out at different scales. Detailed interpretation was carried out at scales of 1 : 50 000 and larger according to the availability of

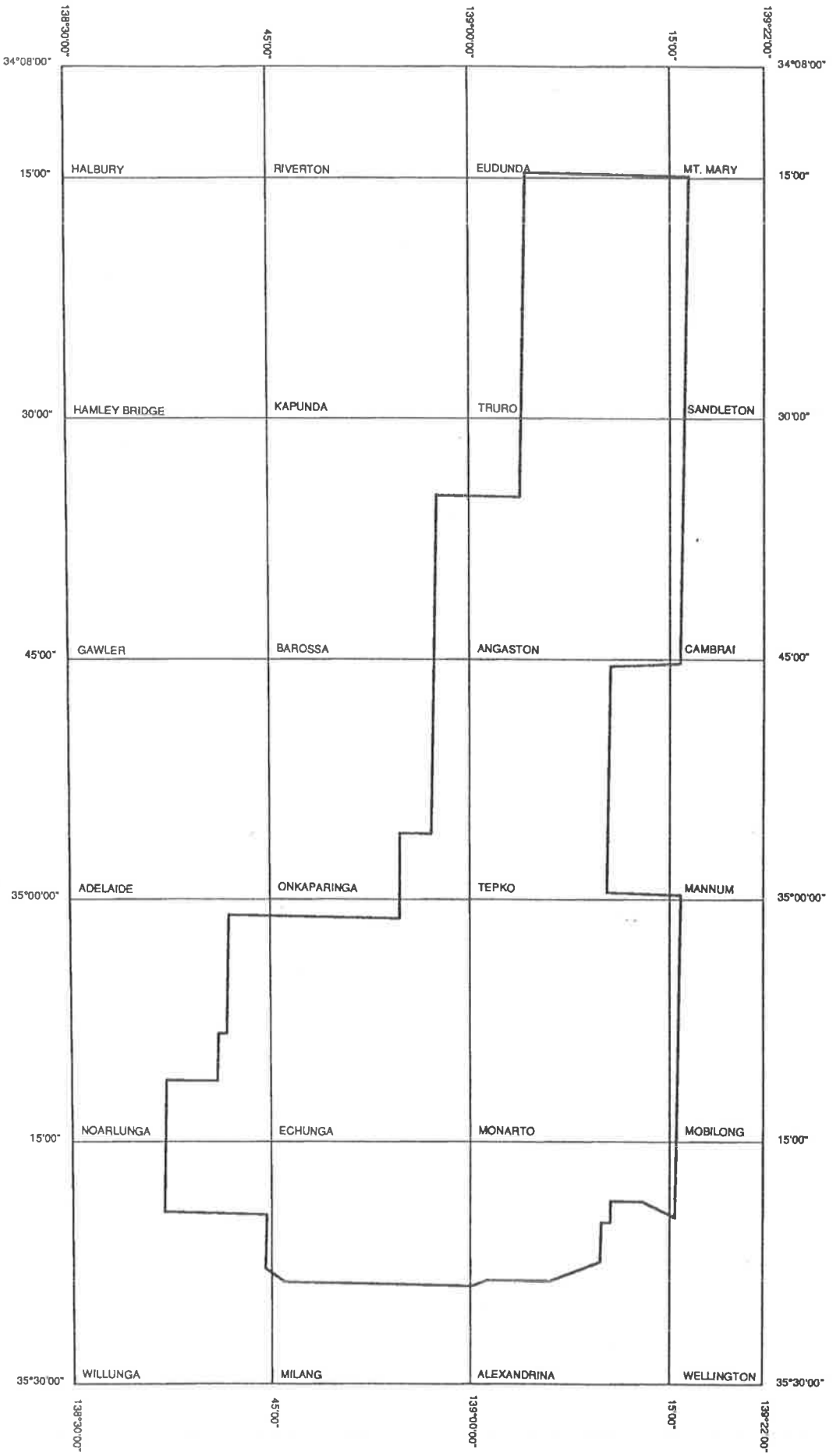

Figure A.1: Study area showing 1:50 000 topographic map sheet areas.

detailed geological maps at the same scale. Access to digital data and computing facilities made it possible to reprocess and enhance different characteristics of the data (Chapter 3). Contour maps of the total magnetic field and its vertical gradient were plotted in colour, using different contour intervals, and at odd scales (to match available geological maps). Profiles (multi-profiles and stacked profiles) were printed for use in quantitative analyses and qualitative interpretation. The different data sets were digitized, integrated into a colour image, and also printed separately as grey-scale images.

The interpretation of the Western Magnetic Zone was carried out at a scale of 1:250 000 using contour maps (SADME, 1980 and 1983). The digital data set (BMR) was gridded and contoured in colour (1:250 000) and also presented as small scale grey-scale images. The complex magnetic pattern characteristic of the EMZ could be more easily interpreted using coloured rather than black and white contour maps.

Appendix B: Outcrop magnetic susceptibility measurements

S.Rajagopalan (1989)

Accession number: 873

University of Adelaide collection

Kanmantoo Group---Adelaide and Barker 1:250000 sheet areas

Column 1: sample number.

Column 2: locality (given in AMG coordinates/ descriptive)

Column 3: average magnetic susceptibility of hand specimen, to be multiplied by E-5 SI units.

Column 4: number of sub-outcrops (if so divided---see note below).

Note: The magnetic susceptibility given for each outcrop visited is based on between 50 to 100 measurements made on each outcrop. Usually, most measurements would fall within a narrow range, so that the average value recorded is representative of the susceptibility of the outcrop. Where the range was wide, it has been so recorded; where the values fell into two or more narrow ranges, the outcrop has been sub-divided and recorded as separate outcrops. Often outcrops were small and isolated; some formations outcropped extensively (e.g. the Rathjen Gneiss) and for the purposes of consistency, the outcrop was sub-divided into smaller outcrops.

Ulupa Siltstone				
X1	309150	6115900	1500	
X2	309150	6115900	1700	
X3	309150	6115900	700	
E2	298225	6105106	50	
E3	298054	6101723		
E8	308051	6111640	900	
E9	308842	6113667	100	
E10	309419	6115879		
Wilpena Group---Quartzite at Macclesfield				
E4	298510	6099184	0	
E5	298963	6099471	0	
Truro Volcanics				
	Truro Volcanics, Dutton		30	3
	Truro Volcanics, Dutton		70	2

Kanmanto Group

Carrickalinga Head Formation

AN5b	336763	6167773	0	
AN6	337689	6159138	0	
S10	326285	6175697	250	
S11	324386	6173479	50	
S14	322175	6177279	200	
S15	323420	6178352	25	
TR1	329010	6191040	20	
TR3a	337013	6191544	20	
TR10	331184	6202297	30	

Backstairs Passage Formation

AN1a	329170	6158733	50	
AN1b	329222	6158533	50	
AN2	332037	6160044	50	
AN3	331702	6162129	50	
AN4a	330902	6165779	400	
AN4b	331133	6165833	0	
AN5a	337387	6168083	400	
ANG	328327	6155706	1500	
N2a	Reedy Creek migmatites		50	10
N2b	Reedy Creek migmatites		900	30
N6	324793	6156880	10	
N7	325861	6155978	20	
S1	326500	6132750	1000	
S4	326887	6156093	50	
S5	327039	6156081	50	
S6	328207	6155890	600	
S7	330209	6156008	350	
S8	325508	6161699	10	
S9	326025	6166971	20	
S12	322327	6168037	100	
S13	319363	6169107	25	
S16	334804	6174097	25	
S17	335573	6173736	25	
S18	336613	6173879	400	
S19	331906	6157612		
S20	331521	6157908	800	
S21	326335	6156862	700	
E6	305153	6099262	0	
E7	307294	6104292	0	
R1	321862	6150872	100	
R2	323782	6150104	100	
R3	325908	6150019	100	
R7	329983	6150910	100	
C5	322350	6144051	50	
C6	322345	6144595	50	
C7	322234	6144986	50	
C8	321814	6145625	50	
C9	320941	6145404	50	
C11	319794	6144684	50	
C12a	324370	6145040	1000	1
C12b	324370	6145040	400	1
C13a	326323	6144953	1000	1
C13b	326323	6144953	400	1
T1	321419	6138054	50	
T2	322277	6137243	0	
T3	323367	6132591	1500	
T4	324102	6132479	300	
T5	324460	6132207	1000	
T6	319360	6148462	600	
T7	318598	6150854	0	
T8a	319812	6150726	50	
T8b	319946	6150474	50	
T9	318864	6146367	600	
T10	322113	6145699	100	
T11	323294	6144150	1500	
T12	324670	6144612	800	
T13	326233	6144481	100	
T15	331031	6135505	1000	
T16	328458	6136409	100	
A1	320700	6145600	0	
A2	Reedy Creek cutting		0	
A3	324300	6145500	700	
A4	324100	6145600	150	15
A5	329562	6156890		

TR4	334329	6191837	220	21
TR5	333960	6191726	210	18
TR7	331553	6191622	30	

Talisker Calc-siltstone

E11	312017	6120279	200	
E14	311600	6124000	450	
E15	311600	6124000	700	
E16	311600	6124000	800	
E17	311600	6124000	50	
E18	314644	6121173	1500	
C3	320371	6141229	50	
C4	320635	6141365	20	
TR6	333402	6191748	0	
TR8	332005	6198288	10	
TR9	332588	6202580	50	

Tapanappa Formation

E12	312672	6120467	0	
E13	312949	6120517	0	
E19	316926	6122217	1500	
J3	316692	6117923	200	wide range
J4	316423	6118750	50	few highs
J5	316596	6120173	50	
C1	317432	6139853	50	
C2	318055	6140259	0	

Middleton Sandstone

Middleton Beach		1200	5
Flinders Chase Nat. Pk. KI		1000	2

Granites, granitic gneisses, norites and mylonite

Rathjen Gneiss

BH10	328700	6143900	1125	4
R5	326884	6150556	500	
R6	328179	6150111	800	
P1	327650	6145550	0	
P2	327650	6145550	200	
P3	Rathjen Gneiss		800	
P4	Rathjen Gneiss		1000	
P5	Rathjen Gneiss		500	
P6	Rathjen Gneiss		500	
P7	Rathjen Gneiss		1500	
P8	Rathjen Gneiss		500	
P9	Rathjen Gneiss		400	
P10	Rathjen Gneiss		1500	
P11	Rathjen Gneiss		400	
P12	Rathjen Gneiss		1000	
P13	Rathjen Gneiss		0	
P16	Rathjen Gneiss		50	
P17	Rathjen Gneiss		1000	
P18	Rathjen Gneiss		800	
S2	328700	6143350	1500	
S3	326391	6155952	1200	

Monarto Granite

	Monarto Granite		10	10
	Monarto Granite		60	5.

Palmer Granite

BH9	330625	6142550	1100	16
T14	329596	6145069	600	
N3	330750	6141900	800	

Mannum Granite

BH3	Mannum Granite		3500	13
BH4	Mannum Granite		6450	9
BH5, 6,7	Mannum Granite		2270	22
BH8	Mannum Granite		3250	6

Encounter Bay Granite

	Encounter Bay Granite		0	5

Reedy Creek Granodiorite

	Reedy Creek		650	2
	Reedy Creek		680	3
	Reedy Creek		1100	3
	Reedy Creek		1200	2
	Reedy Creek		1000	1
	Reedy Creek		1500	4
	Reedy Creek		2500	2

Black Hill Norite

BH1	Black Hill Norite		4000	18
BH2	Black Hill Norite		4000	13

Mylonite

M1	Marne River (Renmark)		1500	5

---

undifferentiated (mainly Kanmantoo Group)

M2			50	
R8	331608	6151493	20	
R9	335285	6151862	20	
R10				
R11			1500	
R12			20	
R13			200	
R14				
R15			100	
C10	320416	6144899	0	
C14			0	
C15			0	
E1	298212	6106033	50	
Z1	Mount Barker Creek			possibly Backstairs Passage Fm.
EBC1	Mount Barker Creek			possibly Ulupa Siltstone
EBC2	Mount Barker Creek			possibly Ulupa Siltstone
BC1				
BC40				
TR2			15	10
TR3b	337848	6191484		

Appendix C: Sample magnetic susceptibility measurements

University of Adelaide collection

Column 1: average magnetic susceptibility of hand specimen,
to be multiplied by E-5 SI units.
Column 2: number of specimens
Column 3: locality
Column 4: lithology

Igneous Rocks			
315.0	7	Murray Bridge	Granite
875.0	8	Mannum	Tonalite
44.0	5	Tungkillo	Amphibolite
4000.0	2	Mannum	Granite
60.0	2	Pallamana	Amphibolite
1750.0	2	Mannum	Granite
Backstairs Passage Formation			
17.0	15	Tungkillo	Diopside-Scapolite
Normanville Group			
0.0	17	Angaston	Marble
Tapanappa Formation			
25.0	28	Dawesley	Andalusite schists

P.D.Fleming (1971)

Accession number: A281
University of Adelaide collection
Monarto 1:50000 sheet---Dawesley area
Column 1: sample number.
Column 2: average magnetic susceptibility of hand specimen,
to be multiplied by E-5 SI units.
Column 3: number of specimens measured

Tapanappa Formation
semi-pelitic and pelitic schists, garnet, staurolite and andalusite schists,
calc-silicate units and pyritic schist units and quartzo-feldspathic schists

11	15.0	1
731	17.5	2
377	23.0	3
631	32.0	2
254	50.0	2
652	25.0	2
246	975.0	2
216	15.0	2
567	60.0	3
420	15.0	2
834	5.0	3
602	30.0	3
762	45.0	2
730	15.0	4
233	208.0	3
734	15.0	3
05	30.0	1
717	40.0	1
337	25.0	1
718	42.5	2
F18	35.0	2
749	17.5	2
673	17.5	4
646	12.5	2

812	0.0	3
636	20.0	4
419	0.0	2
400	10.0	2
146b	2.0	3
279a	10.0	2
102	5.0	1
153	15.0	1
936	10.0	1
946	20.0	2
719	30.0	1
A32	50.0	3
31	37.5	2
438a	18.0	3
247	15.0	2
620b	20.0	2
353a	20.0	1
293	20.0	2
240	30.0	1
236	10.0	3
438b	26.5	3
592	22.5	2
940a	10.0	2
242a	20.0	1
352a	35.0	1
241	20.0	1
228	43.0	3
230	25.0	3
98	0.0	1
Y65	0.0	1
120b	10.0	1
3	23.0	3
109	15.0	1
708	25.0	2
689a	25.0	2
235	22.5	2
234	25.0	2
709	35.0	2
689c	20.0	2
688a	32.5	2
232	366.5	3
45	20.0	3
217	20.0	2
222	17.5	2
215	33.5	3
221	15.0	3
226	13.5	3
223	20.0	1
184	5.0	2
X12	45.0	2
214	10.0	2
220	28.5	3
225	22.5	2
210	25.0	2
219	2.5	2
218	30.0	1
715	25.0	2
716	17.5	2

S.Fermio

South Australian Institute of Technology collection
Granitic rocks: Murray Basin
Column 1: average magnetic susceptibility of hand specimen,
to be multiplied by E-5 SI units.
Column 2: number of different specimens.
Column 3: lithology.
Column 4: sample location.

Igneous Rocks			
520.0	5	Granite	Swanport
1200.0	3	Granite	Reedy Creek
600.0	4	Granite	Sedan, Long Ridge, and Black Hill
2500.0	4	Granite	Mannum
2300.0	3	Granite	Reedy Creek
360.0	3	Adamellite	
Mylonite			
1500.0	7	Mylonite	Marne River
Backstairs Passage Formation			
300.0	8	Migmatite	

R.Gerdes

South Australian Department of Mines and Energy
Brukunga Mine
Column 1: rock type
Column 2: range of magnetic susceptibility of core,
to be multiplied by E-5 SI units.
Column 3: mean susceptibility
Column 4: number of samples.
Note: These measurements were carried out on drill-hole core by staff at SADME. Refer to Mason (1966) for drill-hole data.

Talisker Calc-siltstone---Nairne pyrite facies			
Grenofels amphibolite	862 to 3192	2003	8
Amphibolite	0 to 372	137	15
Schist	78 to 1596	743	27
Gneiss/Meta-siltstone	0 to 1324	456	33
Gneiss	0 to 2101	382	56

M.J.Hoesni (1985)

Accession number: 848
University of Adelaide collection
Monarto 1:50000 sheet area
Column 1: sample number.
Column 2: average magnetic susceptibility of hand specimen,
to be multiplied by E-5 SI units.
Column 3: locality---
GQ: Guerin's quarry
SC: Salt Creek
RG: Rocky Gully
PR: Pallamanna Railway cutting
SF: Schubert's farm
KQ: Kinchina Quarry

Backstairs Passage Formation

Migmatite			
79	100.0	GQ	2
22/8	50.0		11
1/11	200.0	GQ	21
1/11	100.0	RG	26
83	100.0	GQ	38
45	0.0	GQ	39
14/2	0.0	SC	54
45B	0.0	GQ	55
60	400.0	SF	70
R.C.	300.0		75
45	0.0	GQ	76
46	0.0	SF	77
69	0.0	GQ	78
16/10	0.0	RG	82
71	0.0	RG	83
6	500.0	RG	84
30/20	1000.0	RG	85
31/1	0.0	RG	86
	1000.0	GQ	1
	100.0	RG	3
	50.0		12
	0.0	RG	18
	0.0	RG	19
	0.0	GQ	36
	0.0	RG	37
	1000.0	GQ	41
	0.0	RG	42
	500.0	GQ	44
	50.0	GQ	46
	0.0	RG	48
	100.0	GQ	50
	400.0	GQ	51
	300.0	GQ	52
	700.0	GQ	59
	500.0	GQ	60
	0.0	RG	80
	0.0	RG	81
	400.0	GQ	87
Quartzite sillimanite schist			
24/5	0.0	RG	47
65	0.0	SC	57
474-17	300.0		74
9J	0.0	SC	79
4/3	0.0	SC	88
27/21	0.0	SC	30
Meta-arenite			
	1500.0	SC	62
	1700.0	SC	63
Cummingtonite schists			
27/1	200.0	RG	4
81	350.0	RG	6
?2	0.0	RG	23
81	350.0	RG	25
	250.0	RG	14
81	200.0	RG	15
81	200.0	RG	32
82	200.0		33
Anthophyllite schists			
43	1250.0	SC	9
27/12	50.0	RG	29
	1500.0	GQ	61
43	1500.0	SC	73

```
Chlorite pseudomorph
     41   150.0  GQ       7
     41   100.0  GQ      72
     41   100.0  GQ      53
Tremolite
   25/3   200.0  RG      13
          1000.0          31
     77   850.0           56

Igneous rocks
Murray Bridge Granite
     34   700.0  MB       5
          1000.0 MB      43
          600.0  MB      49
Monarto Granite
          0.0    PR      35
    PC3   0.0    PR      45
     30   0.0    KQ      58
          0.0            65
    PC3   0.0    PR      66
     32   0.0    PR      71
Granite
     42   0.0    GQ      10
     59   0.0    GQ      16
          0.0    GQ      20
     66   0.0    GQ      22
     21   50.0   SC      24
     LS   0.0    GQ      34
          0.0    GQ      40
          0.0    GQ      68
          0.0    GQ      69

Amphibolite
     84   0.0    RG       8
          0.0    RG      17
          300.0  GQ      64
```

A.G.Kremor (1980)

South Australian Institute of Technology collection
Eden Valley
Column 1: sample number.
Column 2: average magnetic susceptibility of hand specimen,
to be multiplied by E-5 SI units.
Column 3: number of different specimens.
Column 4: sample location (AMG coordinates).

```
 Carrickalinga Head Formation
 sandy biotite schist
  4214        7.5  2

 Backstairs Passage Formation
 sandy and micaceous schist
  4218       15.0  2
  4219       17.5  2
  4220       25.0  2
  4221       55.0  3
  4221a      57.0  3
  4222       13.0  3
  4228        0.0  2
 banded plag-gar-qua-scap-diop "fels"
  4224       22.5  2
  4225       20.0  4
```

hornblende quartz "fels"
4223 1350.0 3 330490 6167955
4223 0.0 2
feldspathic meta sandstone
4215 0.0 1
4216 0.0 1
4217 470.0 3 328960 6168200
actinolite quartzite
4226 2.0 3
staurolite schist
4238 16.0 3
4227 18.0 4

Igneous Rocks
microgranodiorite
4229 850.0 3 327880 6167160
4230 370.0 3 328285 6167505
4231 0.0 3
4232 0.0 2
4237 5.0 2
hornblende tonalite
4234 0.0 3
pegmatite
4236 10.0 2

Triassic Laterite
4227 18.0 4

Amphibolite
amphibolite/ metadolerite
4235 60.0 3
4239 25.0 2

M.D.Lucas (1980)

South Australian Institute of Technology collection
Springton
Column 1: sample number.
Column 2: average magnetic susceptibility of hand specimen,
to be multiplied by E-5 SI units.
Column 3: number of different specimens.

Backstairs Passage Formation
meta-arkoses, quartzites, micaceous and sandy schists
4130 0.0 3
4131 800.0 3
4132 5.0 2
4135 0.0 1
4136 10.0 2
4138 25.0 4
4140 400.0 2
4141 90.0 2
4142 17.0 2
4143 15.0 2
4144 10.0 3
4146 5.0 2
4148 225.0 2
4151 15.0 2
4152 25.0 3
4153 10.0 2
4155 0.0 2
4156 15.0 2
4157 5.0 2
4158 225.0 2

4159	40.0	3
4162	10.0	2
4164	5.0	2
4165	15.0	3
4166	10.0	2
Amphibolite		
4133	17.0	2
4154	25.0	3
4160	65.0	6
4161	75.0	3
Igneous Rocks		
Pegmatite		
4134	10.0	2
Granodiorite		
4139	200.0	3
4147	7.0	3
4149	150.0	2
4150	7.0	2
4163	0.0	2

R.W.Lawrence (1980)

Accession number: 766 (unless stated otherwise, e.g. 171-71).
University of Adelaide collection
Monarto 1:50000 sheet---Rockleigh and South-Eastern Freeway.
Column 1: sample number.
Column 2: average magnetic susceptibility of hand specimen,
to be multiplied by E-5 SI units.
Column 3: number of specimens measured
Column 4: locality
Note : LO number following gives the location (see Lawrence, 1980)
TS thin section available with this number
HS hand sample available
Column 5: a "?" in this column means that stratigraphic
identification is uncertain.

Backstairs Passage Formation				
LO/384b	10.0	1		
TS/54	0.0	1		
LO/387	20.0	1		
TS/57	0.0	1		
LO/350	30.0	1		
LO/239	30.0	1		
TS/33	0.0	1		
Talisker Formation				
pyritic metasiltstone			Nairne Pyrite	
HS/B	0.0	1	Freeway Cutting	
TS/2	0.0	1	Freeway Cutting	
HS/C	0.0	1	Freeway Cutting	
TS/9	0.0	1	Freeway Cutting	
HS/PS2	0.0	1	Brukunga Mine	
HS/D	0.0	1	Freeway	
HS/F	0.0	1	Monarto	?
TS/18	0.0	1	Monarto	?
Pyritic calc-silicate			Nairne pyrite	
E	1000.0	1	Brukunga Mine	
LO/524	20.0	1		?
TS/55	0.0	1		?
Garnet Pyrite laminated arkose				
HS/4	15.0	1		

Crenulated biotite schist
 TS/43 0.0 1
 HS/3 30.0 1
Layered Mica Quartz Rocks
 TS/40 0.0 1
 HS/5 20.0 1
 TS/36 0.0 1
 HS/6 30.0 1
 TS/38 0.0 1
 HS/7 50.0 1
 TS/37 0.0 1

Tapanappa Formation
Meta-sandstone and meta-arkose
 LO/5 25.0 1 ?
 TS/24 0.0 1 ?
 TS/25 0.0 1 ?
 LO/21 25.0 1 ?
 TS/56 0.0 1 ?
Meta-sandstone with climbing ripples
 LO/96 40.0 1
 TS/30 0.0 1
Phyllite chip conglomerate
 LO/99 30.0 1
 TS/27 0.0 1
 TS/28 0.0 1
Calc-silicate
 LO/479 10.0 1
 TS/51 0.0 1
Porphyroblastic Andalusite Schists
 LO/91b 40.0 1
 TS/35 0.0 1
 LO/91c 40.0 1
Biotite schists
 LO/296 35.0 1
 TS/32 0.0 1
 TS/31 0.0 1
 LO/91a 20.0 1

undifferentiated Backstairs Passage, Talisker Calc-Siltstone or Tapanappa Formation
Pyritic Meta-arkose
 HS/A 0.0 1 Freeway Cutting
 HS/G 0.0 1 Monarto 237239
 TS/16 0.0 1 Monarto 237239
Porphyroblastic Andalusite Schists
 HS/H 20.0 1 Tepko 266263
 TS/6 0.0 1 Tepko 266263
 TS/7 0.0 1 Tepko 266263
Biotite Schists
 HS/J 25.0 1 Monarto 308223
 TS/11 0.0 1 Monarto 308223
 LO/232e 20.0 1 Monarto 308223
Amphibolites
 LO/404a 30.0 1

K.J.Mills (1964)

Accession number: A 185
University of Adelaide collection
East of Springton---south Karinya Syncline
Column 1: sample number.
Column 2: average magnetic susceptibility of hand specimen,
to be multiplied by E-5 SI units.
Column 3: number of specimens measured.
Column 4: remarks on lithology or mineralogy
Column 5: locality---refer to Mills (1964) for grid reference

Backstairs Passage Formation				
quartzo-feldspathic schists				
618	0.0	3	qfs laminated arkose	196.218
630	10.0	2		
366	45.0	4	heavy mineral banding in arkose	188.156
pelitic schists				
626	20.0	3		
617	10.0	2		
625	10.0	3		
calc-silicate rocks				
336a	10.0	1		
649a	10.0	1		
quartz-potash feldspar rocks				
703	10.0	1		
358	10.0	1		
701	1000.0	1	mic. hem. sch	147.181
702	70.0	1		146.183
702a	15000.0	1		146.183
363	200.0	1		155.150
other metasomatic rocks				
311	10.0	1		
269b	10.0	1		
257b	30.0	1		
325	25.0	1		
segregation veins				
603	10.0	1		
arkoses				
790	0.0	1		
790(1)	0.0	1		
790(3)	0.0	1		
608	10.0	1		
607	10.0	1		
621	10.0	1		
610	0.0	1		
Carrickalinga Head Formation				
pelitic schists				
816a	10.0	2		
588	10.0	3		
581	20.0	2		
581	10.0	1		
586	20.0	3		
579b	10.0	2		
720a	47.5	2	spess. sch.	157.213
446	40.0	3	almandine	216.118
448	16.5	3		
474	25.0	2		
453	10.0	2		
428b	12.0	3		
490	32.5	2		
362	10.0	1		

aluminous pelitic schists				
718b	20.0	2		
718a	10.0	2		
503	10.0	2		
738	35.0	3		
cordierite-anthophyllite schists				
cordierite bearing				
829	45.0	3		221.141
calc-silicate rocks				
600a	10.0	1		
24a	10.0	1		
24d	10.0	1		
388c	27.5	2		
15	15.0	3		
336b	10.0	1		
251	30.0	2		
540	10.0	1		
99b	10.0	1		
833	10.0	1		
marbles				
555	0.0	2		
811	10.0	1		
61a	10.0	1		
258a	0.0	2		
731	10.0	1		
406a	10.0	1		
487	10.0	1		
30	20.0	2		
30a	10.0	1		
30c	10.0	1		
metasomatic rocks				
quartz-albite rocks				
265	10.0	1		
411	40.0	1	albz. qtz-felds sch.	210.118
411b	10.0	1		
411c	10.0	1		
516a	10.0	1		
516b	10.0	1		
516c	10.0	1		
825a	10.0	1		
other metasomatic rocks				
437	40.0	1	Kanappa mine skarn	217.118
440	45.0	2	Kanappa mine skarn	216.117
442	40.0	1	Kanappa mine skarn	216.117
298a	10.0	1	powdery hem. rock	178.098
segregation veins				
22a	10.0	1		
307	10.0	1		
673	10.0	1		
509	10.0	1		
limestones				
669	10.0	1		
794	0.0	1		
803	0.0	1		
802	0.0	1		
800	0.0	1		
796	0.0	1		
796(1)	0.0	1		
796(2)	0.0	1		
809	0.0	1		
799	0.0	1		
813	0.0	1		
812	15.0	1		
793	5.0	1		

arkoses

798	20.0	1		
727	30.0	1		

cordierite schists

302	20.0	1		
302a	15.0	1		
302b	20.0	1		
302c	20.0	1		
302d	30.0	1		

Backstairs Passage Formation or Carrickalinga Head Formation

quartzo-feldspathic schists

756	0.0	2		
715	0.0	1		
629	90.0	4	bio-rich	212.201
23	10.0	1		
595	22.0	2		

pelitic schists

594	12.5	2		
824	0.0	2		
276a	52.5	2	almandine	165.131

aluminous pelitic schists

750	10.0	2		
532	28.0	3		

Intrusive rocks

amphibolites (meta-dolerites)

152	25.0	1		
133	10.0	1		
571b	32.5	2		
27a	25.0	1		
27b	10.0	1		
27c	30.0	1		
28	27.5	2		
823	10.0	1		
25	10.0	1		
139	25.0	1		
820	10.0	1		
571c	10.0	1		
571c	10.0	1		
146	75.0	2		182.085
103	25.0	1		
111	10.0	1		
150b	23.0	3		
131	10.0	1		
131b	10.0	1		
131c	10.0	1		
131d	25.0	2		
131f	32.5	2		
316	65.0	1		166.110
501	25.0	1		

granodiorites

423a	10.0	1		
412	650.0	3	fine-grained gran.	220.123
463	185.0	3	bio-rich	214.109
200	10.0	1		
187	500.0	3	med. grained	148.113
170	515.0	3	fine-grained	160.089
439	10.0	1		

aplites

417	10.0	1			
379	10.0	1			

diorites

378a	1500.0	3			236.172
378b	250.0	1			236.172
821	10.0	1			
822	10.0	1			
327	35.0	3			
332c	10.0	1			
91	285.0	3	fine-grained		210.096
405	10.0	1			
268	10.0	1			
694	10.0	1			
655	100.0	2	fine-grained		182.185

unclassified

791	30.0	1			
784	10.0	1	banded plag-hast rock		166.123
656	0.0	1			
283	10.0	1			
108	0.0	1			

M.J.Moore (1980)

South Australian Institute of Technology collection
Keyneton
Column 1: sample number.
Column 2: average magnetic susceptibility of hand specimen,
to be multiplied by E-5 SI units.
Column 3: number of different specimens.
Column 4: percent magnetite (if determined)
Column 5: sample location (AMG coordinates).

Carrickalinga Head Formation
Grey-green meta-siltstone/meta-greywacke with mica schist unit.

4188	950.0	2	1%	330845	6169041
4189	10.0	2			
4191	10.0	2			
4192	10.0	2			
4193	10.0	2			

Backstairs Passage Formation
Meta-arkose and feldspathic meta-sandstone with calc-silicate units.

4197	0.0	3			
4198	135.0	3	trace	330490	6169005
4201	0.0	2			
4203	5.0	1			
4205	15.0	2			
4206	5.0	1			
4209	325.0	4	5%	329179	6170320
4212	40.0	3			

Meta-greywacke and meta-siltstone with calc-silicate and mica schist units.

4194	25.0	3			
4195	5.0	3			
4196	0.0	3			
4199	15.0	3			
4200	0.0	2			
4202	0.0	2			
4204	7.0	2			
4207	10.0	3			
4208	7.0	2			
4213	0.0	2			

Igneous Rocks
Dolerite Dyke

4211	25.0	2	

N.S.Mancktelow (1979)

Accession number: 474 (unless other source quoted, e.g. Whitehead (1975).)
University of Adelaide collection
Mt Lofty Ranges and Kangaroo Island
Column 1: sample number.
Column 2: average magnetic susceptibility of hand specimen,
to be multiplied by E-5 SI units.
Column 3: number of specimens measured
Column 4: locality---six figure grid reference from the South Australian Lands
Department 1:50000 topographic map series (e.g. Monarto 292115).
Column 5: Source quoted by Mancktelow (1979).

Mount Compass inlier

206	10.0	1	
206	5.0	1	

Precambrian below Ulupa Siltstone

186e	0.0	1	
186	10.0	1	
186d	5.0	1	
186b	0.0	1	
186	5.0	1	
347	10.0	1	

Ulupa Siltstone
Aluminous siltstones, quartzites, sandstones,
andalusite-garnet-staurolite schists.

121	15.0	1	
W	1500.0	1	Echunga 065082
234B	3500.0	1	Cape Jervis 441600
245	0.0	1	
309	30.0	1	
340	10.0	1	
342	15.0	1	
352	1250.0	2	Echunga 970978
352	700.0	1	Echunga 970978
359	20.0	1	
425	35.0	1	
426	1000.0	1	Echunga 102146
428	20.0	1	
502	22.5	2	
502	15.0	1	
504	22.5	2	
620	37.5	2	
620	40.0	2	

Meta-dolerite within Brachina Subgroup

505	1500.0	1	Adelaide (1:250 000) 213787
505	800.0	1	Adelaide (1:250 000) 213787

Carrickalinga Head Formation
Siltstones, feldspathic greywackes and phyllites

81	10.0	1	
87N	15.0	1	
87	15.0	1	
259	15.0	1	
293	20.0	1	
293	22.5	2	
537	20.0	1	

Backstairs Passage Formation
Arkoses, sandstones and greywackes

318	20.0	1	
327	70.0	3	
331	40.0	1	
332	25.0	1	
503	15.0	1	
417-B	35.0	2	Whitehead (1975)
417-C	10.0	1	Whitehead (1975)

Talisker Calc-Silicate
Calc-silicates, aluminous siltstones, pyrite units and black shales

K37	20.0	1	
316	20.0	1	
317(B?)	30.0	1	
317B	25.0	1	
321	35.0	1	
321	12.5	2	
321	40.0	1	
321B	10.0	1	
333	15.0	1	
333	20.0	1	
333A	25.0	1	
333B	20.0	1	
335	30.0	1	
562	15.0	1	Talisker?
541	10.0	1	
K38	0.0	1	
315B	32.5	2	
297	10.0	1	

Tapanappa Formation
Greywackes, sandstones

K44	25.0	1	
SC50A	10.0	1	Daily and Milnes (1973)
317	20.0	2	
317D	55.0	1	
389	15.0	1	Tapanappa?
390	0.0	1	
390	15.0	1	
390B	25.0	1	
574A	22.5	2	
574B	25.0	1	

Kanmantoo Group: younger formations
Tunkalilla Formation

289	20.0	1	
354	0.0	1	

Balquihidder Formation

K27	20.0	1	
288	20.0	1	
384	20.0	1	
403	35.0	1	
404	25.0	1	
405	20.0	1	
526	10.0	1	

Petrel Cove Formation

BF2	20.0	1	
BF2	10.0	1	
CN1	20.0	1	
263C	10.0	1	
263C	20.0	1	
380	20.0	1	
380	17.5	2	
399	0.0	1	
407(401?)	10.0	1	

401	10.0	1
401	5.0	2
Middleton Sandstone		
264C	200.0	1
265	22.5	2
unclassified		
416	0.0	1
416B	0.0	1
KM	40.0	1
17	150.0	2
176	10.0	1
48	15.0	1
306	10.0	1
185B	10.0	1
391	20.0	1
419	10.0	1
508	42.5	2
47	15.0	1
67	15.0	1
1	25.0	1
371	5.0	1
531	20.0	1
156	22.5	2
533	10.0	1
402	0.0	1
514	1750.0	2
381	15.0	1
534	0.0	1
531A	15.0	1
332	50.0	1
182	45.0	1
392	30.0	1
90	0.0	1
619	15.0	1
393	22.5	2
621	10.0	1
K34	20.0	1
622	550.0	1
257	20.0	1
95B	20.0	1
105	15.0	1
87	25.0	1
88	20.0	1
282	30.0	1
618	7.5	2
530	5.0	1
622	625.0	2
619	10.0	1
237	20.0	1
530	15.0	1
393	10.0	1
337	30.0	1
617	15.0	1
104	20.0	1
621	15.0	1
125	15.0	1

G.Nader(1976)

South Australian Institute of Technology collection
Macclesfield
Column 1: sample number.
Column 2: average magnetic susceptibility of hand specimen,
to be multiplied by E-5 SI units.
Column 3: number of different specimens.
Column 4: sample location (AMG coordinates).

Precambrian (Tapley Hill)			
meta-sandstones and marble			
4001	5.0	2	
4002a	0.0	2	
4002b	0.0	2	
4002c	2.5	2	
Ulupa Siltstone			
porphyroblastic mica schists			
4000	17.0	3	
4003	10.0	2	
4005	1000.0	2	305100 6106650
4006	2250.0	3	305300 6106750
4007	1000.0	2	304650 6106700
4017	15.0	2	
4018	18.0	3	
Wilpena Group			
Quartzite at Macclesfield			
4008	0.0	2	
4009	0.0	2	
Normanville Group			
Marble at Macclesfield			
4012a	0.0	1	
4012b	0.0	1	
4012c	2.5	2	
4013	0.0	2	
Backstairs Passage Formation			
meta-sandstones and coarse grained schists			
4004	27.0	3	
4010a	200.0	2	303400 6106300
4010b	70.0	2	303400 6106300
4011	10.0	2	
4014	7.0	3	
4015	9.0	3	
4016	5.0	2	
Talisker Formation			
4019	10.0	2	
Triassic: Laterite			
4020	0.0	3	

S.Rajagopalan (1989)

Accession number: 873
University of Adelaide collection
Kanmantoo Group---Adelaide and Barker 1:250000 map sheet areas
Column 1: sample number.
Column 2: average magnetic susceptibility of hand specimen,
to be multiplied by E-5 SI units.
Column 3: number of specimens measured

Tapanappa Formation
magnetite ore, Kanmantoo mine

KCU	>100000.0	1

S.Toteff (1977)

Accession number: A405
University of Adelaide collection
Echunga 1:50000 sheet Nairne-Mount Barker Creek
Onkaparinga 1:50000 sheet Birdwood-Brukunga areas
Column 1: sample number.
Column 2: average magnetic susceptibility of hand specimen,
to be multiplied by E-5 SI units.
Column 3: number of specimens measured.
Column 4: locality (AMG coordinates).

Precambrian
Meta-siltstones, meta-arkoses, andalusite schists, feldspathic meta-sandstones

3(1)	11.0	4		
4	13.0	9		
5	2.0	4		
5(1)	0.0	4		
6	10.0	7		

Marino Group
Unit 1
Feldspathic meta-siltstone, meta-sandstone, calc-silicate,
scapolite-rich meta-siltstone,feldspathic meta-sandstone and meta-arkose

7	11.0	2		
8	11.0	4		
9	150.0	3	308807	6116092
9	0.0	1	308807	6116092
9(1)	2.0	2		
10	85.0	3	308842	6116020

Hallett Arkose Equivalent
Meta-arkose

11	12.5	4		
11(1)	12.5	4	308888	6115949
11a	10.0	3	308888	6115949
11(2)	485.0	3	308888	6115949
12	0.0	1		
12	7.5	4		
13	20.0	3		
14	0.0	1		
15	10.0	4		
15	1.0	4		
16	0.0	1		
17	15.0	6		
17(2)	10.0	2		
17(1)	5.0	2		
18(1)	5.0	2		
23	425.0	6	309092	6115443
23(1)	10.0	4		

Upper Arkose Equivalent				
Meta-arkose				
21	0.0	1		
22	0.0	3		
22(1)	0.0	5		
25	15.0	6		
25	0.0	1		
25(1)	1.0	2		
26	5.0	4		
Ulupa Siltstone				
Unit 2				
Micaschist and andalusite schist				
27	15.0	7		
27(1)	19.0	6		
29	20.0	7		
30	965.0	8	309455	6115435
30	0.0	1		
31	935.0	6	309658	6115517
33	1075.0	4	309681	6115499
33a	525.0	8	309681	6115499
34	250.0	5	309707	6115485
34a	150.0	1	309707	6115485
34b	300.0	2	309707	6115485
34c	290.0	10	309707	6115485
34b?	350.0	3	309707	6115485
34a,b,?	635.0	7	309707	6115485
Unit 3 a				
Meta-siltstone, quartz micaschist, andalusite schist				
36	870.0	5	309808	6115140
36	105.0	7	309808	6115140
36	0.0	1		
37a	25.0	8		
39	0.0	1		
40	0.0	1		
40	10.0	3		
Unit 3 b				
Meta-siltstone, quartz micaschist, andalusite schist				
41	250.0	4	309962	6115212
Unit 3 d				
Meta-siltstone, quartz micaschist, andalusite schist				
44	475.0	7	310218	6115277
Mount Barker Quartzite				
White orthoquartzite				
45	15.0	5		
46	15.0	7		
47	17.5	6		
47(1)	20.0	4		
47(2)	0.0	2		
Backstairs Passage Formation				
Feldspathic meta-sandstone and meta-arkose				
a: more pelitic				
48	1800.0	3	310455	6115294
48(1)	125.0	6	310455	6115294
48	785.0	3	310455	6115294
49	15.0	6		
49(1)	12.5	4		
49(2)	5.0	4		
50	0.0	2		
50(1)	7.5	2		
51	20.0	5		
52	15.0	3		
53	435.0	3	310473	6114357
53(2)	475.0	2	310473	6114357

54	30.0	4
54(1)	20.0	3
55	20.0	3
56	5.0	5
57	1.0	2
58	0.5	4
b:		
59	0.0	3
60	0.0	5
62	5.0	4
65	55.0	2
c: Impure feldspathic meta-sandstone		
66	5.0	2
67	10.0	2
68	12.0	7
69(1)	6.0	4
70	0.0	1
70	0.0	3
70(1)	5.0	5
71	0.0	8
71(1)	10.0	4
73(1)	5.0	2
74	15.0	5
76	7.0	5

Collected by S.Toteff for R.Wiltshire

South Australian Institute of Technology collection
Monarto 1:50000 sheet---along Mount Barker Creek
Column 1: sample number.
Column 2: average magnetic susceptibility of hand specimen,
to be multiplied by E-5 SI units.
Column 3: number of specimens measured.
Column 3: locality given in AMG coordinates

Backstairs Passage Formation				
1	405.0	5	310496	6115205
2	510.0	5	310428	6114328
3	1000.0	2	310533	6114354
4	765.0	3	310560	6114299
5	40.0	4	310596	6114305
6	3250.0	4	310633	6114305
7	10.0	2	310687	6114340
8	10.0	2		
9	5.0	2		
10	20.0	4		
Talisker Formation				
11	25.0	5		
11a	250.0	4	311803	6112959
12	80.0	5	312497	6112570
13	12.0	3		
14	10.0	3		
15	25.0	6		
16	13.0	4		
Tapanappa Formation				
17	5.0	2		
19	15.0	2		
20	10.0	2		
18?	5.0	2		
23	12.0	4		
24	12.0	2		
25	15.0	2		
26	19.0	4		

27	15.0	2
28	12.0	2
29	16.0	3
30	21.0	3
31	23.0	3
32	13.0	3
33	10.0	2
34	12.0	2
35	12.0	2
36	10.0	2
37	15.0	3
38	15.0	3
39	15.0	2
40	7.0	2
41	10.0	2
42	10.0	2
43	7.0	2
44	10.0	2
45	15.0	2
46	11.0	2
47	12.0	5
48	10.0	2
49	10.0	2
51	12.0	4
53	12.0	2
54	12.0	2
55	10.0	2
56	10.0	2
57	8.0	4
58	11.0	2
59	10.0	2
60	12.0	2
61	10.0	4
62	8.0	3
63	8.0	3
64	10.0	2
65	17.0	2
66	10.0	3
67	11.0	3
68	13.0	3
69	12.0	2
70	6.0	2
71	8.0	3
72	16.0	3
73	13.0	3
74	15.0	2
75	11.0	2
76	10.0	2
77	20.0	2
78	11.0	3

Appendix D: Mineralogy of polished thin sections and polished blocks

Abbreviations
qtz: quartz
plg: plagioclase
mic: microcline
bio: biotite
mus: muscovite
grp: graphite
chl: chlorite
str: staurolite
and: andalusite
sil: sillimanite
gnt: garnet
clc: calcite
amp: amphibole
scp: scapolite
epi: epidote
hnb: hornblende
zrc: zircon
sph: sphene
tou: tourmaline
apa: apatite
rut: rutile
mt: magnetite
ilm: ilmenite
hem: haematite

no.	qtz	plg	mic	kfs	mus	grp	chl	str	and	sil	gnt	clc	amp	scp	epi	hnb	zrc	sph	tou	apa	rut	mt	ilm	hem
Ulupa Siltstone																								
X1	*	*		*	*		*	*	*	*												*	*	*
X2	*			*	*		*		*	*									*	*		?	*	*
X3	*			*	*				*														*	*
E8	*	*		*	*		*	*	*										*			*	*	*
E8b	*	*			*				*	*												*	*	*
Carrickalinga Head Formation																								
TR1	*	*		*	*																			
Backstairs Passage Formation																								
AN2	*	?		*	*						*										*	?	?	?
AN4a	*	*		*	*			*										*				*	*	*
ANG	non-opaque minerals not studied																					*		
T1	non-opaque minerals not studied (polished block)																					?		
T3(1)	non-opaque minerals not studied (polished block)																					*	*	*
T3(2)	non-opaque minerals not studied (polished block)																					*	*	*
T3(3)	non-opaque minerals not studied (polished block)																					*	*	*
T3(4)	non-opaque minerals not studied (polished block)																					*	*	*
T4	non-opaque minerals not studied (polished block)																					*	*	*
T6	*	*	*	*	*																	*		
T7b	*	*		*	*										*							*		
T8b	*	*		*	*																?			
T9a	*	*		*	*										*			*			?	*	*	*
T10a														*	*	*		*						
T11	*	*		*	*							*	*					*				*		
T12	*	*		*	*													*				*		
T13	*	*		*	*													*				*		
T15	*	*		*	*																	*		
TR4a	*	*	*	*	*																	*		
TR5	*	*										*			?			*		*		*		
TR4b																						*		
Talisker Calc-siltstone																								
E11	*	*		*	*																			
TR8						*																		
TR9	*	*		*	*													*		*		*		
Tapanappa Formation																								
E13	*	*		*	*										*					*	*			
E19	*			*	*			*		*												*	*	?
Palmer Granite																								
T14	non-opaque minerals not studied																					*		
Rathjen Gneiss																								
RG1	non-opaque minerals not studied (polished block)																					*		
RG2	non-opaque minerals not studied (polished block)																					*		
undifferentiated																								
EBC1	*	*		*	*													*				*		
EBC2	*	*	*	*			*								*		*	*				*	*	*
Z1	*	*		*						*					*			*				*		
E1	*	*		*	*																		?	?

Appendix E: Oxidation ratio and whole rock analyses determined by the author

S.Rajagopalan (1989)
Accession number: 873

ox. ratio : oxidation ratio after Chinner (1960).
susc. : average magnetic susceptibility (multiply by E-5 SI units).

Whole rock analyses: Fe2O3 was determined by by atomic absorption and XRF and FeO by titration. All other oxides determined by XRF only. XRF analyses carried out by Mr John Stanley. Mr P. McDuie assisted with the chemical analyses. Samples prefixed by BC are from Toteff's (1977, accession: A405) collection.

Note: ms-Middleton Sandstone; tap-Tapanappa Formation; us-Ulupa Siltstone; chf-Carrickalinga Head Formation; bpf-Backstairs Passage Formation; ???-undifferentiated.

sample	J1	KCU	E19	E8b	S15	E1	E1
formation	ms	tap	tap	us	chf	???	???
ox. ratio	65.782	66.658	35.192	52.522	46.359	18.386	17.594
susc.	2000	>100000	1500	135	25	50	50
Fe2O3	1.816	44.392	2.945	4.389	3.717	0.686	0.643
FeO	0.850	19.980	4.880	3.570	3.870	2.740	2.710

sample	BC56	BC63	BC48	T12	T13	T9a	T1
formation	bpf	bpf	bpf	bpf	bpf	bpf	bpf
ox. ratio	39.670	39.350	37.671	36.168	34.834	33.962	23.628
susc.	0	5	1800	1000	366	1100	12
SiO2	75.39	72.18	68.78	70.76		80.02	
Al2O3	11.23	11.97	12.65	12.72		9.85	
Fe2O3	1.330	1.644	2.230	2.418	2.002	0.743	1.530
FeO	1.820	2.280	3.320	3.840	3.370	1.300	4.450
MnO	0.04	0.04	0.02	0.04		0.06	
MgO	1.11	1.04	1.59	1.42		0.94	
CaO	1.72	1.38	0.86	0.55		2.92	
Na2O							
K2O	1.41	3.68	4.16	3.45		1.88	
TiO2	0.60	0.59	0.57	0.63		0.25	
P2O5	0.21	0.21	0.08	0.23		0.08	
loss	0.64	0.60	1.57	0.82		0.74	
total	95.50	95.61	95.83	96.88		98.78	

sample	T3(1)	T3(4)	ANG	T6	BC48'	BC62	T11
formation	bpf	bpf	bpf	bpf	bpf	bpf	bpf
ox. ratio	85.314	77.693	64.121	52.326	48.955	46.841	46.740
susc.	1500		1500	800	125	80	1133
SiO2	78.30			73.64	74.55	75.61	75.49
Al2O3	10.19			12.52	11.48	10.73	11.80
Fe2O3	4.261	3.832	1.430	2.159	1.716	1.699	0.829
FeO	0.660	0.990	0.720	1.770	1.610	1.735	0.850
MnO	0.00			0.02	0.06	0.03	0.09
MgO	0.31			1.11	1.09	0.99	0.46
CaO	0.47			0.87	1.25	1.44	3.60
Na2O							
K2O	0.04			3.54	1.59	2.83	3.47
TiO2	0.15			0.41	0.48	0.57	0.67
P2O5	0.06			0.10	0.24	0.24	0.34
loss	0.17			0.57	1.06	0.38	0.59
total	94.61			96.71	95.13	96.23	98.19

Appendix F: Oxidation ratios computed or obtained from previous researchers

OXIDATION RATIO VALUES COMPUTED/OBTAINED FROM PREVIOUS RESEARCHERS

tot. Fe : total iron
Fe2+ : amount of iron present in ferrous state
Fe3+ : amount of iron present in ferric state
ox_ratio : oxidation ratio computed after Chinner (1960)

R.A.Brotherton (1967)
Delamere area
Brachina Sub-Group

SAMPLE	tot. Fe	FeO	Fe2O3	Fe2+	Fe3+	ox_ratio
	all wts in wt %					
67BD23	6.161	4.160	4.210	3.216	2.945	47.661
67BSC6	6.555	4.190	4.740	3.239	3.315	50.444
67BD38	5.926	4.100	3.940	3.170	2.756	46.372
67BMC10	4.754	1.680	4.940	1.299	3.455	72.572
67BMC4	5.642	3.200	4.530	2.474	3.169	56.021
67BMC7	4.491	0.960	5.360	0.742	3.749	83.400

P.D.Fleming (1971)
Accession number: A281
University of Adelaide collection
Monarto 1:50000 sheet---Dawesley area
Tapanappa Formation: meta-shales & meta-greywackes

SAMPLE	tot. Fe	FeO	Fe2O3	Fe2+	Fe3+	ox_ratio
	all wts in wt %					
236	5.603	6.180	1.180	4.778	0.825	14.662
220	8.478	8.650	2.560	6.687	1.791	21.030
228	9.380	10.260	2.070	7.932	1.448	15.365
222	7.627	8.110	1.940	6.270	1.357	17.712
223	6.847	7.590	1.400	5.868	0.979	14.235
715	6.731	7.440	1.400	5.752	0.979	14.480
716	6.798	6.930	2.060	5.358	1.441	21.103
215	10.217	10.510	2.990	8.125	2.091	20.381
232	5.448	5.020	2.240	3.881	1.567	28.648
233	5.301	4.930	2.130	3.811	1.490	27.993
234	6.498	6.460	2.150	4.994	1.504	23.046
235	5.896	5.980	1.820	4.623	1.273	21.498
218	6.964	6.800	2.440	5.257	1.707	24.407
210	4.710	5.540	0.610	4.283	0.427	9.015
214	3.423	3.840	0.650	2.969	0.455	13.218
217	3.934	4.410	0.750	3.409	0.525	13.272
219	3.057	3.610	0.380	2.791	0.266	8.652
221	3.712	3.960	0.930	3.061	0.650	17.445
225	3.840	4.470	0.550	3.456	0.385	9.968
226	4.603	4.570	1.530	3.533	1.070	23.151

S.Toteff (1977)
Accession number: A405
University of Adelaide collection
Echunga 1:50000 sheet Nairne-Mount Barker Creek
Onkaparinga 1:50000 sheet Birdwood-Brukunga areas

All samples from Marino Group Unit 2 except E4E which is from Marino Group Unit 3.

SAMPLE	tot. Fe	FeO	Fe2O3	Fe2+	Fe3+	ox_ratio
	all wts in wt %					
		Meta-shales				
M24	5.834	4.570	3.290	3.533	2.301	39.313
E4E (unit 3)	6.069	4.430	3.780	3.425	2.644	43.432
BC38	5.848	5.130	2.690	3.966	1.882	32.057
BC34a	4.711	3.940	2.380	3.046	1.665	35.214
BC37a	5.646	6.000	1.440	4.639	1.007	17.760
E2a (unit 3)	6.845	6.140	3.000	4.747	2.098	30.539
M21	6.193	4.220	4.190	3.262	2.931	47.185
BC27'	5.770	4.170	3.640	3.224	2.546	43.992
	Meta-siltstones & meta-sandstone					
E4b	5.139	3.960	2.970	3.061	2.077	40.293
BC33a	3.254	2.970	1.370	2.296	0.958	29.332
BC43	4.752	4.030	2.340	3.116	1.637	34.317

Alderman (1929)
Granites

SAMPLE	tot. Fe	FeO	Fe2O3	Fe2+	Fe3+	ox_ratio
	all wts in wt %					
aplite-Mannum	1.415	0.690	1.260	0.533	0.881	62.166
granite-Mannum	2.128	0.970	1.970	0.750	1.378	64.632
granite-Palmer	1.650	1.030	1.220	0.796	0.853	51.593
granite-Monarto	1.104	1.030	0.440	0.796	0.308	27.766
granite-Swanport	1.493	0.900	1.140	0.696	0.797	53.266
tonalite-Mannum	3.680	2.960	1.990	2.288	1.392	37.692

Bowes (1954)
Rosetta Head

SAMPLE	tot. Fe	FeO	Fe2O3	Fe2+	Fe3+	ox_ratio
	all wts in wt %					
q-bio-hornf	5.039	5.070	1.600	3.920	1.119	22.116
q-alb-chl-sch	5.154	5.500	1.290	4.252	0.902	17.427
q-alb-chl-sch	5.025	5.650	0.940	4.368	0.657	13.021
alb-chl-sch	4.519	4.000	2.040	3.092	1.427	31.455
coarse alb-chl	2.314	2.080	1.010	1.608	0.706	30.407

Abbas (1975)
Cooke Hill intrusives

SAMPLE	tot. Fe	FeO	Fe2O3	Fe2+	Fe3+	ox_ratio
	all wts in wt %					
75	1.701	1.730	0.520	1.337	0.364	21.289
140	1.974	2.020	0.590	1.562	0.413	20.812
199	1.637	1.720	0.440	1.330	0.308	18.711
233	1.706	1.890	0.350	1.461	0.245	14.283
295	1.449	1.530	0.380	1.183	0.266	18.266
511	1.870	1.930	0.540	1.492	0.378	20.113
137	1.344	1.340	0.440	1.036	0.308	22.807
232	1.291	1.200	0.520	0.928	0.364	28.053
208	2.317	2.110	0.980	1.631	0.685	29.474

average Palmer Granite (White, 1967)	1.463	0.870	1.130	0.673	0.790	53.890
Swanport Granite (AMDL)	1.460	1.110	0.860	0.858	0.602	41.078

N.S.Mancktelow (1979)
Accession number: 474
University of Adelaide collection
Mt Lofty Ranges and Kangaroo Island

PG : Palmer Granite
TCGG : Tanunda Creek Granite Gneiss
MON_G : Monarto Granite
RCG : Reedy Creek Granodiorite
MAN : Mannum Granite
MB : Murray Bridge Granite
SW : Swanport Granite

SAMPLE	tot. Fe	FeO	Fe2O3	Fe2+	Fe3+	ox_ratio
	all wts in wt %					
PG3	1.650	1.030	1.220	0.796	0.853	51.593
PG4	0.942	0.440	0.860	0.340	0.602	63.751
PG5	1.092	0.480	1.030	0.371	0.720	65.880
PG6	1.477	0.970	1.040	0.750	0.727	49.103
PG7	1.558	1.020	1.100	0.789	0.769	49.249
PG8	1.657	1.130	1.120	0.874	0.783	47.142
PG9	1.861	1.050	1.500	0.812	1.049	56.245
PG10	1.720	1.040	1.310	0.804	0.916	53.127
TCGG11	0.746	0.540	0.470	0.417	0.329	43.920
MON_G3	1.066	0.800	0.640	0.618	0.448	41.855
MON_G4	1.104	1.030	0.440	0.796	0.308	27.766
RCG5	3.680	2.960	1.990	2.288	1.392	37.692
MB13	1.785	1.640	0.740	1.268	0.518	28.877
SW15	1.493	0.900	1.140	0.696	0.797	53.266
SW16	0.423	0.420	0.140	0.325	0.098	23.073

M.J.Hoesni (1985)
Accession number: 848
University of Adelaide collection
Monarto 1:50000 sheet area

Mon. : Monarto
MB : Murray Bridge
Gr. : granite
Peg. : pegmatite
Ton. : tonalite
mig. : migmatites probably from the Backstairs Passage Formation
sch. : schist
anth. : anthophyllite
sill. : sillimanite
qtz. : quartz
nonmig. m.arn. : nonmigmatized meta-arenite
mig. mas. gne. : migmatized massive gneiss

SAMPLE		tot. Fe	FeO	Fe2O3	Fe2+	Fe3+	ox_ratio
		all wts in wt %					
30	Mon. Gr.	0.794	0.720	0.340	0.557	0.238	29.820
32	"	1.184	1.070	0.510	0.827	0.357	30.015
13	Peg. Gr.	0.884	0.800	0.380	0.618	0.266	29.943
14	"	1.626	1.470	0.700	1.136	0.490	29.996
40	"	1.206	1.090	0.520	0.843	0.364	30.034
59	"	0.914	0.830	0.390	0.642	0.273	29.716
66	"	1.117	1.010	0.480	0.781	0.336	29.954
34	MB. Gr. ton.	1.641	1.480	0.710	1.144	0.497	30.151

5	Whole rock mig.	2.930	2.650	1.260	2.049	0.881	29.964
33	"	3.289	2.970	1.420	2.296	0.993	30.080
46	"	2.847	2.570	1.230	1.987	0.860	30.102
60	"	1.873	1.690	0.810	1.307	0.567	30.132
45L	leucosome	0.982	0.890	0.420	0.688	0.294	29.806
45M	mesosome	2.068	1.870	0.890	1.446	0.623	29.984
68L	leucosome	0.839	0.760	0.360	0.588	0.252	29.885
79L	"	2.413	2.180	1.040	1.685	0.727	30.034
79M	mesosome	4.758	4.300	2.050	3.324	1.434	30.020
15	amphibolite	9.307	8.410	4.010	6.502	2.805	30.023
43	anth. sch.	2.698	2.440	1.160	1.886	0.811	29.961
41	gr. anth. sch.	2.608	2.360	1.120	1.825	0.783	29.924
65	qtz-sill. sch.	1.626	1.470	0.700	1.136	0.490	29.996
44	nonmig. m.arn.	2.121	1.920	0.910	1.484	0.636	29.897
67	mig. mas. gne.	1.701	1.540	0.730	1.191	0.511	29.900

Appendix G: Vertical gradient parameters for the dyke model

DYKE MODEL
VERTICAL GRADIENT PARAMETERS

w : full width
h : depth to top
theta : index parameter
vmin : minimum on dyke vertical magnetic gradient anomaly
vmax : maximum on dyke vertical magnetic gradient anomaly
vratio : abs(vmin/vmax)
deltay : (peak separation)/depth

w/h	theta	vratio	deltay	w/h	theta	vratio	deltay
0.1	0.	0.1250	1.7320				
0.1	5.	0.1448	1.6503	0.1	95.	1.1060	1.1560
0.1	10.	0.1667	1.5786	0.1	100.	1.2236	1.1599
0.1	15.	0.1908	1.5156	0.1	105.	1.3543	1.1665
0.1	20.	0.2173	1.4601	0.1	110.	1.5000	1.1758
0.1	25.	0.2463	1.4111	0.1	115.	1.6630	1.1879
0.1	30.	0.2780	1.3680	0.1	120.	1.8458	1.2030
0.1	35.	0.3127	1.3301	0.1	125.	2.0517	1.2212
0.1	40.	0.3507	1.2969	0.1	130.	2.2845	1.2428
0.1	45.	0.3923	1.2679	0.1	135.	2.5490	1.2679
0.1	50.	0.4377	1.2428	0.1	140.	2.8508	1.2969
0.1	55.	0.4873	1.2212	0.1	145.	3.1969	1.3301
0.1	60.	0.5417	1.2030	0.1	150.	3.5962	1.3680
0.1	65.	0.6013	1.1879	0.1	155.	4.0597	1.4111
0.1	70.	0.6666	1.1758	0.1	160.	4.6014	1.4601
0.1	75.	0.7383	1.1665	0.1	165.	5.2351	1.5156
0.1	80.	0.8172	1.1599	0.1	170.	5.9961	1.5786
0.1	85.	0.9041	1.1560	0.1	175.	6.9028	1.6503
0.1	90.	1.0000	1.1547	0.1	180.	8.0000	1.7320

w/h	theta	vratio	deltay	w/h	theta	vratio	deltay
0.5	0.	0.1308	1.7675				
0.5	5.	0.1514	1.6894	0.5	95.	1.1027	1.2275
0.5	10.	0.1739	1.6211	0.5	100.	1.2162	1.2310
0.5	15.	0.1987	1.5614	0.5	105.	1.3421	1.2370
0.5	20.	0.2258	1.5090	0.5	110.	1.4820	1.2455
0.5	25.	0.2553	1.4631	0.5	115.	1.6382	1.2565
0.5	30.	0.2876	1.4227	0.5	120.	1.8130	1.2703
0.5	35.	0.3228	1.3874	0.5	125.	2.0096	1.2870
0.5	40.	0.3610	1.3566	0.5	130.	2.2314	1.3067
0.5	45.	0.4027	1.3298	0.5	135.	2.4831	1.3298
0.5	50.	0.4481	1.3067	0.5	140.	2.7698	1.3566
0.5	55.	0.4976	1.2870	0.5	145.	3.0984	1.3874
0.5	60.	0.5516	1.2703	0.5	150.	3.4771	1.4227
0.5	65.	0.6104	1.2565	0.5	155.	3.9163	1.4631
0.5	70.	0.6747	1.2455	0.5	160.	4.4293	1.5090
0.5	75.	0.7451	1.2370	0.5	165.	5.0330	1.5614
0.5	80.	0.8222	1.2310	0.5	170.	5.7493	1.6211
0.5	85.	0.9069	1.2275	0.5	175.	6.6073	1.6894
0.5	90.	1.0000	1.2263	0.5	180.	7.6453	1.7675

w/h	theta	vratio	deltay	w/h	theta	vratio	deltay
1.0	0.	0.1475	1.8671				
1.0	5.	0.1700	1.7998	1.0	95.	1.0938	1.4344
1.0	10.	0.1945	1.7420	1.0	100.	1.1968	1.4369
1.0	15.	0.2211	1.6923	1.0	105.	1.3101	1.4412
1.0	20.	0.2499	1.6495	1.0	110.	1.4353	1.4472
1.0	25.	0.2810	1.6125	1.0	115.	1.5741	1.4552
1.0	30.	0.3146	1.5807	1.0	120.	1.7288	1.4652
1.0	35.	0.3508	1.5532	1.0	125.	1.9018	1.4774
1.0	40.	0.3898	1.5295	1.0	130.	2.0962	1.4920
1.0	45.	0.4318	1.5093	1.0	135.	2.3159	1.5093
1.0	50.	0.4771	1.4920	1.0	140.	2.5655	1.5295
1.0	55.	0.5258	1.4774	1.0	145.	2.8508	1.5532
1.0	60.	0.5785	1.4652	1.0	150.	3.1788	1.5807
1.0	65.	0.6353	1.4552	1.0	155.	3.5587	1.6125
1.0	70.	0.6967	1.4472	1.0	160.	4.0019	1.6495
1.0	75.	0.7633	1.4412	1.0	165.	4.5231	1.6923
1.0	80.	0.8356	1.4369	1.0	170.	5.1413	1.7420
1.0	85.	0.9142	1.4344	1.0	175.	5.8817	1.7998
1.0	90.	1.0000	1.4335	1.0	180.	6.7777	1.8671

w/h	theta	vratio	deltay	w/h	theta	vratio	deltay
1.5	0.	0.1736	2.0156				
1.5	5.	0.1990	1.9678	1.5	95.	1.0824	1.7531
1.5	10.	0.2262	1.9289	1.5	100.	1.1719	1.7544
1.5	15.	0.2554	1.8970	1.5	105.	1.2695	1.7566
1.5	20.	0.2865	1.8707	1.5	110.	1.3764	1.7597
1.5	25.	0.3196	1.8490	1.5	115.	1.4939	1.7638
1.5	30.	0.3548	1.8308	1.5	120.	1.6239	1.7690
1.5	35.	0.3921	1.8156	1.5	125.	1.7684	1.7753
1.5	40.	0.4317	1.8028	1.5	130.	1.9298	1.7829
1.5	45.	0.4737	1.7920	1.5	135.	2.1112	1.7920
1.5	50.	0.5182	1.7829	1.5	140.	2.3164	1.8028
1.5	55.	0.5655	1.7753	1.5	145.	2.5502	1.8156
1.5	60.	0.6158	1.7690	1.5	150.	2.8183	1.8308
1.5	65.	0.6694	1.7638	1.5	155.	3.1284	1.8490
1.5	70.	0.7266	1.7597	1.5	160.	3.4899	1.8707
1.5	75.	0.7877	1.7566	1.5	165.	3.9151	1.8970
1.5	80.	0.8533	1.7544	1.5	170.	4.4200	1.9289
1.5	85.	0.9239	1.7531	1.5	175.	5.0256	1.9678
1.5	90.	1.0000	1.7527	1.5	180.	5.7600	2.0156

w/h	theta	vratio	deltay	w/h	theta	vratio	deltay
2.0	0.	0.2071	2.1974				
2.0	5.	0.2360	2.1838	2.0	95.	1.0711	2.1493
2.0	10.	0.2665	2.1766	2.0	100.	1.1476	2.1497
2.0	15.	0.2984	2.1726	2.0	105.	1.2301	2.1504
2.0	20.	0.3317	2.1700	2.0	110.	1.3197	2.1514
2.0	25.	0.3665	2.1679	2.0	115.	1.4174	2.1526
2.0	30.	0.4028	2.1659	2.0	120.	1.5245	2.1541
2.0	35.	0.4405	2.1638	2.0	125.	1.6425	2.1557
2.0	40.	0.4799	2.1617	2.0	130.	1.7734	2.1576
2.0	45.	0.5210	2.1596	2.0	135.	1.9195	2.1596
2.0	50.	0.5639	2.1576	2.0	140.	2.0838	2.1617
2.0	55.	0.6088	2.1557	2.0	145.	2.2700	2.1638
2.0	60.	0.6560	2.1541	2.0	150.	2.4829	2.1659
2.0	65.	0.7055	2.1526	2.0	155.	2.7284	2.1679
2.0	70.	0.7577	2.1514	2.0	160.	3.0144	2.1700
2.0	75.	0.8129	2.1504	2.0	165.	3.3514	2.1726
2.0	80.	0.8714	2.1497	2.0	170.	3.7530	2.1766
2.0	85.	0.9336	2.1493	2.0	175.	4.2372	2.1838
2.0	90.	1.0000	2.1491	2.0	180.	4.8284	2.1974

w/h	theta	vratio	deltay	w/h	theta	vratio	deltay
2.5	0.	0.2463	2.4009				
2.5	5.	0.2790	2.4549	2.5	95.	1.0614	2.5914
2.5	10.	0.3123	2.4998	2.5	100.	1.1268	2.5914
2.5	15.	0.3463	2.5312	2.5	105.	1.1968	2.5914
2.5	20.	0.3810	2.5521	2.5	110.	1.2721	2.5913
2.5	25.	0.4164	2.5659	2.5	115.	1.3534	2.5911
2.5	30.	0.4527	2.5750	2.5	120.	1.4419	2.5908
2.5	35.	0.4898	2.5810	2.5	125.	1.5385	2.5902
2.5	40.	0.5280	2.5850	2.5	130.	1.6448	2.5892
2.5	45.	0.5674	2.5875	2.5	135.	1.7625	2.5875
2.5	50.	0.6080	2.5892	2.5	140.	1.8938	2.5850
2.5	55.	0.6500	2.5902	2.5	145.	2.0415	2.5810
2.5	60.	0.6935	2.5908	2.5	150.	2.2092	2.5750
2.5	65.	0.7388	2.5911	2.5	155.	2.4016	2.5659
2.5	70.	0.7861	2.5913	2.5	160.	2.6249	2.5521
2.5	75.	0.8356	2.5914	2.5	165.	2.8876	2.5312
2.5	80.	0.8875	2.5914	2.5	170.	3.2018	2.4998
2.5	85.	0.9422	2.5914	2.5	175.	3.5845	2.4549
2.5	90.	1.0000	2.5914	2.5	180.	4.0598	2.4009

w/h	theta	vratio	deltay	w/h	theta	vratio	deltay
3.0	0.	0.2899	2.6183				
3.0	5.	0.3257	2.8320	3.0	95.	1.0534	3.0586
3.0	10.	0.3605	2.9267	3.0	100.	1.1099	3.0584
3.0	15.	0.3951	2.9753	3.0	105.	1.1699	3.0582
3.0	20.	0.4297	3.0037	3.0	110.	1.2340	3.0577
3.0	25.	0.4647	3.0216	3.0	115.	1.3027	3.0571
3.0	30.	0.5000	3.0333	3.0	120.	1.3768	3.0562
3.0	35.	0.5358	3.0412	3.0	125.	1.4572	3.0549
3.0	40.	0.5722	3.0467	3.0	130.	1.5448	3.0531
3.0	45.	0.6093	3.0504	3.0	135.	1.6411	3.0504
3.0	50.	0.6473	3.0531	3.0	140.	1.7477	3.0467
3.0	55.	0.6863	3.0549	3.0	145.	1.8664	3.0412
3.0	60.	0.7263	3.0562	3.0	150.	2.0001	3.0333
3.0	65.	0.7676	3.0571	3.0	155.	2.1521	3.0216
3.0	70.	0.8104	3.0577	3.0	160.	2.3270	3.0037
3.0	75.	0.8547	3.0582	3.0	165.	2.5311	2.9753
3.0	80.	0.9010	3.0584	3.0	170.	2.7738	2.9267
3.0	85.	0.9493	3.0586	3.0	175.	3.0702	2.8320
3.0	90.	1.0000	3.0586	3.0	180.	3.4496	2.6183

w/h	theta	vratio	deltay	w/h	theta	vratio	deltay
3.5	0.	0.3368	3.0220				
3.5	5.	0.3727	3.3533	3.5	95.	1.0470	3.5392
3.5	10.	0.4071	3.4284	3.5	100.	1.0964	3.5391
3.5	15.	0.4411	3.4673	3.5	105.	1.1486	3.5388
3.5	20.	0.4749	3.4906	3.5	110.	1.2039	3.5383
3.5	25.	0.5086	3.5055	3.5	115.	1.2629	3.5376
3.5	30.	0.5425	3.5156	3.5	120.	1.3261	3.5367
3.5	35.	0.5766	3.5226	3.5	125.	1.3942	3.5354
3.5	40.	0.6110	3.5275	3.5	130.	1.4679	3.5335
3.5	45.	0.6459	3.5310	3.5	135.	1.5483	3.5310
3.5	50.	0.6812	3.5335	3.5	140.	1.6366	3.5275
3.5	55.	0.7173	3.5354	3.5	145.	1.7343	3.5226
3.5	60.	0.7541	3.5367	3.5	150.	1.8433	3.5156
3.5	65.	0.7918	3.5376	3.5	155.	1.9661	3.5055
3.5	70.	0.8306	3.5383	3.5	160.	2.1059	3.4906
3.5	75.	0.8706	3.5388	3.5	165.	2.2671	3.4673
3.5	80.	0.9121	3.5391	3.5	170.	2.4562	3.4284
3.5	85.	0.9551	3.5392	3.5	175.	2.6832	3.3533
3.5	90.	1.0000	3.5393	3.5	180.	2.9694	3.0220

w/h	theta	vratio	deltay	w/h	theta	vratio	deltay
4.0	0.	0.3820	3.8042				
4.0	5.	0.4163	3.9004	4.0	95.	1.0418	4.0274
4.0	10.	0.4497	3.9458	4.0	100.	1.0856	4.0272
4.0	15.	0.4826	3.9721	4.0	105.	1.1315	4.0269
4.0	20.	0.5152	3.9889	4.0	110.	1.1801	4.0265
4.0	25.	0.5475	4.0002	4.0	115.	1.2315	4.0259
4.0	30.	0.5798	4.0079	4.0	120.	1.2863	4.0251
4.0	35.	0.6121	4.0134	4.0	125.	1.3450	4.0239
4.0	40.	0.6445	4.0174	4.0	130.	1.4082	4.0224
4.0	45.	0.6772	4.0203	4.0	135.	1.4768	4.0203
4.0	50.	0.7101	4.0224	4.0	140.	1.5516	4.0174
4.0	55.	0.7435	4.0239	4.0	145.	1.6337	4.0134
4.0	60.	0.7774	4.0251	4.0	150.	1.7247	4.0079
4.0	65.	0.8120	4.0259	4.0	155.	1.8264	4.0002
4.0	70.	0.8474	4.0265	4.0	160.	1.9411	3.9889
4.0	75.	0.8837	4.0269	4.0	165.	2.0721	3.9721
4.0	80.	0.9212	4.0272	4.0	170.	2.2236	3.9458
4.0	85.	0.9599	4.0274	4.0	175.	2.4022	3.9004
4.0	90.	1.0000	4.0274	4.0	180.	2.6180	3.8042

w/h	theta	vratio	deltay	w/h	theta	vratio	deltay
4.5	0.	0.4223	4.3815				
4.5	5.	0.4555	4.4316	4.5	95.	1.0376	4.5198
4.5	10.	0.4878	4.4602	4.5	100.	1.0768	4.5196
4.5	15.	0.5195	4.4782	4.5	105.	1.1178	4.5194
4.5	20.	0.5507	4.4902	4.5	110.	1.1608	4.5190
4.5	25.	0.5816	4.4985	4.5	115.	1.2063	4.5185
4.5	30.	0.6123	4.5043	4.5	120.	1.2545	4.5178
4.5	35.	0.6428	4.5086	4.5	125.	1.3060	4.5169
4.5	40.	0.6734	4.5116	4.5	130.	1.3611	4.5156
4.5	45.	0.7039	4.5139	4.5	135.	1.4206	4.5139
4.5	50.	0.7347	4.5156	4.5	140.	1.4851	4.5116
4.5	55.	0.7657	4.5169	4.5	145.	1.5556	4.5086
4.5	60.	0.7971	4.5178	4.5	150.	1.6332	4.5043
4.5	65.	0.8290	4.5185	4.5	155.	1.7193	4.4985
4.5	70.	0.8615	4.5190	4.5	160.	1.8158	4.4902
4.5	75.	0.8946	4.5194	4.5	165.	1.9251	4.4782
4.5	80.	0.9287	4.5196	4.5	170.	2.0502	4.4602
4.5	85.	0.9638	4.5198	4.5	175.	2.1956	4.4316
4.5	90.	1.0000	4.5198	4.5	180.	2.3678	4.3815

w/h	theta	vratio	deltay	w/h	theta	vratio	deltay
5.0	0.	0.4584	4.9202				
5.0	5.	0.4904	4.9511	5.0	95.	1.0341	5.0147
5.0	10.	0.5216	4.9704	5.0	100.	1.0695	5.0146
5.0	15.	0.5520	4.9832	5.0	105.	1.1064	5.0144
5.0	20.	0.5820	4.9919	5.0	110.	1.1451	5.0141
5.0	25.	0.6114	4.9981	5.0	115.	1.1858	5.0137
5.0	30.	0.6406	5.0025	5.0	120.	1.2288	5.0131
5.0	35.	0.6695	5.0058	5.0	125.	1.2744	5.0123
5.0	40.	0.6982	5.0082	5.0	130.	1.3232	5.0113
5.0	45.	0.7270	5.0100	5.0	135.	1.3756	5.0100
5.0	50.	0.7557	5.0113	5.0	140.	1.4322	5.0082
5.0	55.	0.7847	5.0123	5.0	145.	1.4937	5.0058
5.0	60.	0.8138	5.0131	5.0	150.	1.5611	5.0025
5.0	65.	0.8433	5.0137	5.0	155.	1.6355	4.9981
5.0	70.	0.8733	5.0141	5.0	160.	1.7183	4.9919
5.0	75.	0.9038	5.0144	5.0	165.	1.8115	4.9832
5.0	80.	0.9350	5.0146	5.0	170.	1.9173	4.9704
5.0	85.	0.9670	5.0147	5.0	175.	2.0392	4.9511
5.0	90.	1.0000	5.0147	5.0	180.	2.1816	4.9202

w/h	theta	vratio	deltay	w/h	theta	vratio	deltay
5.5	0.	0.4906	5.4429				
5.5	5.	0.5215	5.4639	5.5	95.	1.0312	5.5112
5.5	10.	0.5516	5.4776	5.5	100.	1.0635	5.5111
5.5	15.	0.5809	5.4869	5.5	105.	1.0970	5.5109
5.5	20.	0.6095	5.4934	5.5	110.	1.1321	5.5107
5.5	25.	0.6376	5.4981	5.5	115.	1.1688	5.5104
5.5	30.	0.6653	5.5015	5.5	120.	1.2076	5.5099
5.5	35.	0.6927	5.5041	5.5	125.	1.2486	5.5093
5.5	40.	0.7199	5.5060	5.5	130.	1.2922	5.5085
5.5	45.	0.7469	5.5074	5.5	135.	1.3389	5.5074
5.5	50.	0.7739	5.5085	5.5	140.	1.3892	5.5060
5.5	55.	0.8009	5.5093	5.5	145.	1.4437	5.5041
5.5	60.	0.8281	5.5099	5.5	150.	1.5031	5.5015
5.5	65.	0.8555	5.5104	5.5	155.	1.5684	5.4981
5.5	70.	0.8833	5.5107	5.5	160.	1.6407	5.4934
5.5	75.	0.9115	5.5109	5.5	165.	1.7216	5.4869
5.5	80.	0.9403	5.5111	5.5	170.	1.8130	5.4776
5.5	85.	0.9698	5.5112	5.5	175.	1.9174	5.4639
5.5	90.	1.0000	5.5112	5.5	180.	2.0383	5.4429

w/h	theta	vratio	deltay	w/h	theta	vratio	deltay
6.0	0.	0.5195	5.9575				
6.0	5.	0.5494	5.9725	6.0	95.	1.0287	6.0087
6.0	10.	0.5783	5.9826	6.0	100.	1.0583	6.0086
6.0	15.	0.6064	5.9896	6.0	105.	1.0891	6.0085
6.0	20.	0.6338	5.9947	6.0	110.	1.1211	6.0083
6.0	25.	0.6607	5.9983	6.0	115.	1.1546	6.0080
6.0	30.	0.6870	6.0010	6.0	120.	1.1898	6.0076
6.0	35.	0.7130	6.0030	6.0	125.	1.2270	6.0072
6.0	40.	0.7387	6.0045	6.0	130.	1.2664	6.0065
6.0	45.	0.7642	6.0056	6.0	135.	1.3085	6.0056
6.0	50.	0.7896	6.0065	6.0	140.	1.3537	6.0045
6.0	55.	0.8150	6.0072	6.0	145.	1.4025	6.0030
6.0	60.	0.8405	6.0076	6.0	150.	1.4555	6.0010
6.0	65.	0.8661	6.0080	6.0	155.	1.5136	5.9983
6.0	70.	0.8920	6.0083	6.0	160.	1.5777	5.9947
6.0	75.	0.9182	6.0085	6.0	165.	1.6490	5.9896
6.0	80.	0.9449	6.0086	6.0	170.	1.7291	5.9826
6.0	85.	0.9721	6.0087	6.0	175.	1.8202	5.9725
6.0	90.	1.0000	6.0087	6.0	180.	1.9250	5.9575

w/h	theta	vratio	deltay	w/h	theta	vratio	deltay
6.5	0.	0.5455	6.4674				
6.5	5.	0.5744	6.4786	6.5	95.	1.0266	6.5069
6.5	10.	0.6022	6.4863	6.5	100.	1.0540	6.5068
6.5	15.	0.6292	6.4917	6.5	105.	1.0823	6.5067
6.5	20.	0.6555	6.4956	6.5	110.	1.1118	6.5066
6.5	25.	0.6811	6.4985	6.5	115.	1.1425	6.5063
6.5	30.	0.7062	6.5006	6.5	120.	1.1748	6.5060
6.5	35.	0.7309	6.5023	6.5	125.	1.2088	6.5056
6.5	40.	0.7553	6.5035	6.5	130.	1.2447	6.5051
6.5	45.	0.7794	6.5044	6.5	135.	1.2830	6.5044
6.5	50.	0.8034	6.5051	6.5	140.	1.3240	6.5035
6.5	55.	0.8273	6.5056	6.5	145.	1.3681	6.5023
6.5	60.	0.8512	6.5060	6.5	150.	1.4159	6.5006
6.5	65.	0.8752	6.5063	6.5	155.	1.4682	6.4985
6.5	70.	0.8995	6.5066	6.5	160.	1.5256	6.4956
6.5	75.	0.9239	6.5067	6.5	165.	1.5892	6.4917
6.5	80.	0.9488	6.5068	6.5	170.	1.6605	6.4863
6.5	85.	0.9741	6.5069	6.5	175.	1.7410	6.4786
6.5	90.	1.0000	6.5069	6.5	180.	1.8332	6.4674

w/h	theta	vratio	deltay	w/h	theta	vratio	deltay
7.0	0.	0.5690	6.9743				
7.0	5.	0.5969	6.9830	7.0	95.	1.0247	7.0056
7.0	10.	0.6237	6.9890	7.0	100.	1.0502	7.0055
7.0	15.	0.6497	6.9933	7.0	105.	1.0765	7.0054
7.0	20.	0.6748	6.9964	7.0	110.	1.1038	7.0053
7.0	25.	0.6993	6.9987	7.0	115.	1.1322	7.0051
7.0	30.	0.7233	7.0005	7.0	120.	1.1619	7.0048
7.0	35.	0.7468	7.0017	7.0	125.	1.1932	7.0045
7.0	40.	0.7700	7.0027	7.0	130.	1.2262	7.0041
7.0	45.	0.7928	7.0035	7.0	135.	1.2613	7.0035
7.0	50.	0.8155	7.0041	7.0	140.	1.2988	7.0027
7.0	55.	0.8381	7.0045	7.0	145.	1.3390	7.0017
7.0	60.	0.8607	7.0048	7.0	150.	1.3825	7.0005
7.0	65.	0.8832	7.0051	7.0	155.	1.4299	6.9987
7.0	70.	0.9060	7.0053	7.0	160.	1.4818	6.9964
7.0	75.	0.9289	7.0054	7.0	165.	1.5393	6.9933
7.0	80.	0.9522	7.0055	7.0	170.	1.6033	6.9890
7.0	85.	0.9759	7.0056	7.0	175.	1.6754	6.9830
7.0	90.	1.0000	7.0056	7.0	180.	1.7576	6.9743

w/h	theta	vratio	deltay	w/h	theta	vratio	deltay
7.5	0.	0.5903	7.4794				
7.5	5.	0.6172	7.4862	7.5	95.	1.0231	7.5046
7.5	10.	0.6431	7.4910	7.5	100.	1.0469	7.5045
7.5	15.	0.6680	7.4945	7.5	105.	1.0714	7.5044
7.5	20.	0.6922	7.4970	7.5	110.	1.0968	7.5043
7.5	25.	0.7157	7.4989	7.5	115.	1.1232	7.5042
7.5	30.	0.7386	7.5003	7.5	120.	1.1508	7.5039
7.5	35.	0.7610	7.5014	7.5	125.	1.1797	7.5037
7.5	40.	0.7830	7.5022	7.5	130.	1.2102	7.5033
7.5	45.	0.8048	7.5028	7.5	135.	1.2426	7.5028
7.5	50.	0.8263	7.5033	7.5	140.	1.2771	7.5022
7.5	55.	0.8477	7.5037	7.5	145.	1.3141	7.5014
7.5	60.	0.8690	7.5039	7.5	150.	1.3540	7.5003
7.5	65.	0.8903	7.5042	7.5	155.	1.3973	7.4989
7.5	70.	0.9118	7.5043	7.5	160.	1.4447	7.4970
7.5	75.	0.9334	7.5044	7.5	165.	1.4969	7.4945
7.5	80.	0.9552	7.5045	7.5	170.	1.5550	7.4910
7.5	85.	0.9774	7.5046	7.5	175.	1.6202	7.4862
7.5	90.	1.0000	7.5046	7.5	180.	1.6942	7.4794

w/h	theta	vratio	deltay	w/h	theta	vratio	deltay
8.0	0.	0.6096	7.9832				
8.0	5.	0.6357	7.9887	8.0	95.	1.0217	8.0038
8.0	10.	0.6606	7.9926	8.0	100.	1.0440	8.0037
8.0	15.	0.6846	7.9954	8.0	105.	1.0669	8.0037
8.0	20.	0.7078	7.9975	8.0	110.	1.0907	8.0036
8.0	25.	0.7304	7.9991	8.0	115.	1.1153	8.0034
8.0	30.	0.7523	8.0002	8.0	120.	1.1410	8.0033
8.0	35.	0.7737	8.0011	8.0	125.	1.1680	8.0030
8.0	40.	0.7947	8.0018	8.0	130.	1.1963	8.0027
8.0	45.	0.8154	8.0023	8.0	135.	1.2264	8.0023
8.0	50.	0.8359	8.0027	8.0	140.	1.2583	8.0018
8.0	55.	0.8562	8.0030	8.0	145.	1.2925	8.0011
8.0	60.	0.8764	8.0033	8.0	150.	1.3293	8.0002
8.0	65.	0.8966	8.0034	8.0	155.	1.3692	7.9991
8.0	70.	0.9169	8.0036	8.0	160.	1.4127	7.9975
8.0	75.	0.9373	8.0037	8.0	165.	1.4606	7.9954
8.0	80.	0.9578	8.0037	8.0	170.	1.5137	7.9926
8.0	85.	0.9787	8.0038	8.0	175.	1.5732	7.9887
8.0	90.	1.0000	8.0038	8.0	180.	1.6404	7.9832

w/h	theta	vratio	deltay	w/h	theta	vratio	deltay
8.5	0.	0.6273	8.4861				
8.5	5.	0.6525	8.4906	8.5	95.	1.0205	8.5032
8.5	10.	0.6766	8.4938	8.5	100.	1.0414	8.5031
8.5	15.	0.6997	8.4962	8.5	105.	1.0630	8.5031
8.5	20.	0.7220	8.4979	8.5	110.	1.0853	8.5030
8.5	25.	0.7436	8.4992	8.5	115.	1.1084	8.5029
8.5	30.	0.7646	8.5002	8.5	120.	1.1325	8.5027
8.5	35.	0.7851	8.5009	8.5	125.	1.1576	8.5025
8.5	40.	0.8052	8.5015	8.5	130.	1.1841	8.5022
8.5	45.	0.8250	8.5019	8.5	135.	1.2121	8.5019
8.5	50.	0.8445	8.5022	8.5	140.	1.2419	8.5015
8.5	55.	0.8638	8.5025	8.5	145.	1.2737	8.5009
8.5	60.	0.8830	8.5027	8.5	150.	1.3078	8.5002
8.5	65.	0.9022	8.5029	8.5	155.	1.3448	8.4992
8.5	70.	0.9214	8.5030	8.5	160.	1.3850	8.4979
8.5	75.	0.9407	8.5031	8.5	165.	1.4292	8.4962
8.5	80.	0.9602	8.5031	8.5	170.	1.4780	8.4938
8.5	85.	0.9799	8.5032	8.5	175.	1.5326	8.4906
8.5	90.	1.0000	8.5032	8.5	180.	1.5942	8.4861

w/h	theta	vratio	deltay	w/h	theta	vratio	deltay
9.0	0.	0.6435	8.9884				
9.0	5.	0.6679	8.9921	9.0	95.	1.0194	9.0027
9.0	10.	0.6911	8.9948	9.0	100.	1.0391	9.0026
9.0	15.	0.7134	8.9968	9.0	105.	1.0595	9.0026
9.0	20.	0.7349	8.9982	9.0	110.	1.0805	9.0025
9.0	25.	0.7557	8.9993	9.0	115.	1.1022	9.0024
9.0	30.	0.7759	9.0001	9.0	120.	1.1249	9.0023
9.0	35.	0.7955	9.0007	9.0	125.	1.1485	9.0021
9.0	40.	0.8148	9.0012	9.0	130.	1.1733	9.0019
9.0	45.	0.8336	9.0016	9.0	135.	1.1996	9.0016
9.0	50.	0.8523	9.0019	9.0	140.	1.2274	9.0012
9.0	55.	0.8707	9.0021	9.0	145.	1.2570	9.0007
9.0	60.	0.8890	9.0023	9.0	150.	1.2889	9.0001
9.0	65.	0.9072	9.0024	9.0	155.	1.3233	8.9993
9.0	70.	0.9255	9.0025	9.0	160.	1.3607	8.9982
9.0	75.	0.9438	9.0026	9.0	165.	1.4017	8.9968
9.0	80.	0.9623	9.0026	9.0	170.	1.4469	8.9948
9.0	85.	0.9810	9.0027	9.0	175.	1.4973	8.9921
9.0	90.	1.0000	9.0027	9.0	180.	1.5540	8.9884

w/h	theta	vratio	deltay	w/h	theta	vratio	deltay
9.5	0.	0.6584	9.4902				
9.5	5.	0.6820	9.4933	9.5	95.	1.0184	9.5023
9.5	10.	0.7045	9.4956	9.5	100.	1.0371	9.5022
9.5	15.	0.7260	9.4972	9.5	105.	1.0563	9.5022
9.5	20.	0.7467	9.4985	9.5	110.	1.0762	9.5021
9.5	25.	0.7667	9.4994	9.5	115.	1.0967	9.5021
9.5	30.	0.7861	9.5001	9.5	120.	1.1181	9.5020
9.5	35.	0.8049	9.5006	9.5	125.	1.1403	9.5018
9.5	40.	0.8234	9.5010	9.5	130.	1.1637	9.5016
9.5	45.	0.8415	9.5014	9.5	135.	1.1884	9.5014
9.5	50.	0.8593	9.5016	9.5	140.	1.2145	9.5010
9.5	55.	0.8769	9.5018	9.5	145.	1.2423	9.5006
9.5	60.	0.8944	9.5020	9.5	150.	1.2721	9.5001
9.5	65.	0.9118	9.5021	9.5	155.	1.3043	9.4994
9.5	70.	0.9292	9.5021	9.5	160.	1.3392	9.4985
9.5	75.	0.9467	9.5022	9.5	165.	1.3774	9.4972
9.5	80.	0.9642	9.5022	9.5	170.	1.4195	9.4956
9.5	85.	0.9820	9.5023	9.5	175.	1.4663	9.4933
9.5	90.	1.0000	9.5023	9.5	180.	1.5189	9.4902

w/h	theta	vratio	deltay	w/h	theta	vratio	deltay
10.0	0.	0.6721	9.9916				
10.0	5.	0.6949	9.9943	10.0	95.	1.0174	10.0020
10.0	10.	0.7167	9.9962	10.0	100.	1.0352	10.0019
10.0	15.	0.7375	9.9976	10.0	105.	1.0535	10.0019
10.0	20.	0.7575	9.9987	10.0	110.	1.0723	10.0018
10.0	25.	0.7768	9.9995	10.0	115.	1.0918	10.0018
10.0	30.	0.7954	10.0001	10.0	120.	1.1120	10.0017
10.0	35.	0.8136	10.0005	10.0	125.	1.1330	10.0015
10.0	40.	0.8313	10.0009	10.0	130.	1.1551	10.0014
10.0	45.	0.8486	10.0012	10.0	135.	1.1784	10.0012
10.0	50.	0.8657	10.0014	10.0	140.	1.2030	10.0009
10.0	55.	0.8826	10.0015	10.0	145.	1.2292	10.0005
10.0	60.	0.8993	10.0017	10.0	150.	1.2572	10.0001
10.0	65.	0.9159	10.0018	10.0	155.	1.2874	9.9995
10.0	70.	0.9326	10.0018	10.0	160.	1.3201	9.9987
10.0	75.	0.9492	10.0019	10.0	165.	1.3559	9.9976
10.0	80.	0.9660	10.0019	10.0	170.	1.3953	9.9962
10.0	85.	0.9829	10.0020	10.0	175.	1.4390	9.9943
10.0	90.	1.0000	10.0020	10.0	180.	1.4879	9.9916

Appendix H: Vertical gradient parameters for the edge model

EDGE MODEL
VERTICAL GRADIENT PARAMETERS

theta: index parameter (function of magnetization and dip --- degrees)
vmin : minimum vertical gradient value of edge anomaly
vmax : maximum vertical gradient value of edge anomaly
dy : profile distance between peak gradient positions
depth: depth to the top of the edge model

For further explanations, refer to Chapter 4.

theta	abs(vmin/vmax)	dy/depth	theta	abs(vmin/vmax)	dy/depth
0.	1.0000000000	2.0000000000			
5.	1.1909542084	2.0076396465	185.	0.8396628499	2.0076396465
10.	1.4202766418	2.0308530331	190.	0.7040881515	2.0308530331
15.	1.6983964443	2.0705523491	195.	0.5887906551	2.0705523491
20.	2.0396068096	2.1283555031	200.	0.4902905822	2.1283555031
25.	2.4639129639	2.2067558765	205.	0.4058585167	2.2067558765
30.	3.0000000000	2.3094010353	210.	0.3333333433	2.3094010353
35.	3.6901724339	2.4415490627	215.	0.2709900439	2.4415490627
40.	4.5989103317	2.6108145714	220.	0.2174428105	2.6108145714
45.	5.8284268379	2.8284270763	225.	0.1715728790	2.8284270763
50.	7.5486321449	3.1114475727	230.	0.1324743330	3.1114475727
55.	10.0590143204	3.4868934155	235.	0.0994133130	3.4868934155
60.	13.9282016754	4.0000000000	240.	0.0717967749	4.0000000000
65.	20.3464851379	4.7324032784	245.	0.0491485372	4.7324032784
70.	32.1634368896	5.8476085663	250.	0.0310912058	5.8476085663
75.	57.6955604553	7.7274065018	255.	0.0173323564	7.7274065018
80.	130.6464080811	11.5175409317	260.	0.0076542478	11.5175409317
85.	524.5855102539	22.9474258423	265.	0.0019062668	22.9474258423
90.	infinity	infinity	270.	0.0000000000	infinity
95.	524.5855102539	22.9474258423	275.	0.0019062668	22.9474258423
100.	130.6464080811	11.5175409317	280.	0.0076542478	11.5175409317
105.	57.6955604553	7.7274065018	285.	0.0173323564	7.7274065018
110.	32.1634368896	5.8476085663	290.	0.0310912058	5.8476085663
115.	20.3464851379	4.7324032784	295.	0.0491485372	4.7324032784
120.	13.9282016754	4.0000000000	300.	0.0717967749	4.0000000000
125.	10.0590143204	3.4868934155	305.	0.0994133130	3.4868934155
130.	7.5486321449	3.1114475727	310.	0.1324743330	3.1114475727
135.	5.8284268379	2.8284270763	315.	0.1715728790	2.8284270763
140.	4.5989103317	2.6108145714	320.	0.2174428105	2.6108145714
145.	3.6901724339	2.4415490627	325.	0.2709900439	2.4415490627
150.	3.0000000000	2.3094010353	330.	0.3333333433	2.3094010353
155.	2.4639129639	2.2067558765	335.	0.4058585167	2.2067558765
160.	2.0396068096	2.1283555031	340.	0.4902905822	2.1283555031
165.	1.6983964443	2.0705523491	345.	0.5887906551	2.0705523491
170.	1.4202766418	2.0308530331	350.	0.7040881515	2.0308530331
175.	1.1909542084	2.0076396465	355.	0.8396628499	2.0076396465
180.	1.0000000000	2.0000000000	360.	1.0000000000	2.0000000000

Appendix I: Results of modelling magnetic anomalies

The CRA and PACIFIC EXPL. aeromagnetic profiles were broken up into four surveys: Bull Creek, Kanmantoo, Murray Bridge and Echunga surveys. Anomalies were interpreted using graphical techniques and using GAMMA, a forward modelling interactive graphics computer program (see Chapter 4). The results of the quantitative analyses are given for each survey.

RESULTS OF INTERPRETATION USING GAMMA

For each line modelled, the average northing of the line is given. The location of the model is given in terms of the easting. Both the northing and the easting are in metres (AMG coordinates). The parameters of the model are given below. For details, refer to Chapter 4. All profiles are east-west profiles, and the minimum easting is west of the maximum easting.

Model: Dyke, sheet (thin dyke), edge, polygon, pole and index dyke. For an explanation of the the dyke, sheet, edge, polygon and pole models refer to Chapter 4. The index dyke (I Dyke) and index sheet (I Sheet) are identical to the dyke and sheet model respectively except that the index parameter 'theta' (+ - dip - 90) has been modelled instead of the dip.
Susc: Magnetic susceptibility (SI).
Phi: Strike of the model.
Dip: Dip measured from the east.
Theta: Index parameter = + - Dip - 90.
Depth: Depth to the top of the source. The altitude of the aircraft (not the sensor height) has been subtracted.
Width: Width of the model measured along the profile.
Depthext: For non-zero values, the Depthext refers to the depth extent of the model. Where Depthext = 0.0, the depth extent is infinite.

For the polygon model, the easting and depth to each corner are given.

All linear parameters are given in metres and all angles in degrees.

Diagrams for the modelled profiles are presented in Appendix J except for the lines marked with an asterisk (*).

The results for the Bull Creek, Kanmantoo and Murray Bridge surveys follows.

BULL CREEK SURVEY
BULL CREEK SURVEY
CRA Data
Lines: 10 to 670

Line: 20 Easting: 289897 318279 Northing: 6108516 *

Model	Easting	Susc	Phi	Dip Theta	Depth	Width	Depthext
I Dyke	301460.0	1138.6	0	38	20.2	274.8	0.0
I Dyke	301959.2	545.8	0	63	29.5	3[illegible].3	0.0

Line: 40 Easting: 290011 318764 Northing: 6107879 *

Model	Easting	Susc	Phi	Dip Theta	Depth	Width	Depthext
I Dyke	301244.4	1508.8	0	33	47.4	217.7	0.0
I Dyke	304996.6	1487.1	0	-85	37.9	89.0	0.0

Line: 101 Easting: 318321 290163 Northing: 6106028 *

Model	Easting	Susc	Phi	Dip Theta	Depth	Width	Depthext
I Dyke	304844.5	926.4	0	-54	4.6	208.6	0.0
I Dyke	304484.0	548.6	0	-78	7.2	97.2	0.0
I Dyke	304166.4	238.7	0	-10	8.4	100.0	0.0

Line: 140 Easting: 289926 319125 Northing: 6104906 *

Model	Easting	Susc	Phi	Dip Theta	Depth	Width	Depthext
I Dyke	313554.8	607.5	20	149	-1.0	121.5	0.0
I Dyke	314149.4	583.7	20	-33	4.9	123.8	0.0

Line: 200 Easting: 289784 318528 Northing: 6103050

Model	Easting	Susc	Phi	Dip Theta	Depth	Width	Depthext
I Dyke	312551.5	499.2	30	156	27.2	147.5	0.0

Line: 260 Easting: 283716 318766 Northing: 6101442

Model	Easting	Susc	Phi	Dip Theta	Depth	Width	Depthext
Dyke	303656.0	477.5	0	125	2.0	178.0	0.0
Dyke	308192.7	477.5	0	87	3.2	146.4	0.0
Dyke	310167.0	1193.7	12	79	0.9	75.0	0.0
Dyke	307015.0	397.9	0	86	8.6	122.1	0.0
Dyke	304766.0	238.7	0	134	1.0	80.0	0.0

Line: 300 Easting: 283448 318292 Northing: 6100205

Model	Easting	Susc	Phi	Dip Theta	Depth	Width	Depthext
Dyke	289798.0	1989.4	0	90	10500.0	9000.0	0.0
Dyke	292598.0	1432.4	0	90	451.0	700.0	10000.0
Dyke	293448.0	1591.5	0	90	583.0	600.0	10000.0
Dyke	284798.0	3581.0	0	80	3000.0	6400.0	7000.0
Dyke	297559.5	3787.9	15	67	10.0	94.0	3000.0
Dyke	297824.5	3071.7	15	67	57.0	36.0	3000.0
Dyke	298825.5	318.3	15	80	11.0	50.0	3000.0
Dyke	303668.7	1597.6	0	78	41.0	49.4	3000.0
Dyke	306323.0	238.6	0	50	20.0	295.0	3000.0
Dyke	307016.0	477.9	0	55	84.0	422.0	3000.0
Dyke	308055.0	397.9	0	70	90.0	225.0	3000.0
Dyke	308383.0	238.7	0	61	45.0	191.9	3000.0
Dyke	305316.1	477.5	0	151	161.0	221.4	3000.0
Dyke	303798.0	596.8	0	90	6000.0	6000.0	5000.0

Line: 401 Easting: 283665 305714 Northing: 6097348 *

Model	Easting	Susc	Phi	Dip Theta	Depth	Width	Depthext
Dyke	283665.0	3581.0	0	80	3000.0	3000.0	0.0
Dyke	289958.4	3313.4	0	90	442.0	778.0	0.0
Dyke	286665.0	1591.5	0	90	10000.0	8000.0	0.0
Dyke	290958.2	4036.3	0	83	577.0	660.0	0.0

Line: 540 Easting: 283236 305728 Northing: 6093130 *

Model	Easting	Susc	Phi	Dip Theta	Depth	Width	Depthext
I Dyke	296550.6	2481.2	0	197	4.7	167.2	0.0
I Dyke	303134.8	791.0	0	-14	47.7	96.6	0.0

Line: 600 Easting: 283343 305507 Northing: 6091251 *

Model	Easting	Susc	Phi	Dip	Theta	Depth	Width	Depthext
Dyke	279343.0	4615.5	0	92		2500.0	5200.0	0.0
Dyke	286293.0	1591.5	0	90		950.0	1200.0	0.0
Dyke	287943.0	1989.4	0	90		850.0	1100.0	0.0
Dyke	291493.0	1034.5	0	90		1200.0	1750.0	0.0

Line: 610 Easting: 283794 305370 Northing: 6090953

Model	Easting	Susc	Phi	Dip	Theta	Depth	Width	Depthext
Dyke	294294.2	319.3	15	90		100.0	1200.0	0.0
I Dyke	296226.8	397.6	15		-63	27.9	539.0	0.0
I Dyke	295711.9	413.8	15		260	0.0	288.7	0.0
Dyke	296859.3	318.1	15	107		69.6	416.9	0.0

Line: 650 Easting: 283796 305486 Northing: 6089767

Model	Easting	Susc	Phi	Dip	Theta	Depth	Width	Depthext
Dyke	292073.4	1582.3	0	130		300.0	735.0	4000.0
Dyke	294649.0	1640.6	0	130		520.0	500.0	4000.0
Dyke	281230.0	7957.7	0	100		920.0	2000.0	0.0
Dyke	284230.0	795.8	0	90		20.0	3000.0	1900.0
Dyke	284230.0	1193.7	0	90		1920.0	3000.0	0.0
Dyke	288682.7	2249.5	30	69		18.9	47.5	1000.0

Line: 670 Easting: 283230 301451 Northing: 6089285

Model	Easting	Susc	Phi	Dip	Theta	Depth	Width	Depthext
Dyke	292073.4	1582.3	0	130		300.0	735.0	4000.0
Dyke	294649.0	1640.6	0	130		520.0	500.0	4000.0
Dyke	281230.0	7957.7	0	100		920.0	2000.0	0.0
Dyke	284230.0	795.8	0	90		20.0	3000.0	1900.0
Dyke	284230.0	1193.7	0	90		1920.0	3000.0	0.0
Dyke	288341.4	875.3	30	76		1.0	121.0	0.0

KANMANTOO SURVEY
KANMANTOO SURVEY
CRA Data
Lines: 10 to 3410

Line: 370 Easting: 309758 332906 Northing: 6117480

Model	Easting	Susc	Phi	Dip	Theta	Depth	Width	Depthext
Dyke	313142.0	2677.9	-20	57		30.8	54.8	0.0
Dyke	315655.5	6141.2	10	80		0.8	98.3	0.0
Dyke	315784.5	5766.3	10	80		12.1	58.3	0.0

Line: 383 Easting: 309852 333364 Northing: 6117838

Model	Easting	Susc	Phi	Dip	Theta	Depth	Width	Depthext
Dyke	310787.1	1842.5	0	16		8.5	119.7	0.0
Dyke	313001.3	1831.4	-20	54		0.9	86.7	0.0
Dyke	313803.9	795.7	-20	79		50.0	300.0	0.0
Dyke	315748.2	6260.3	10	86		4.4	99.8	0.0

Dyke	316603.2	5776.9	0	41		0.9	41.8	0.0

Line: 400 Easting: 309657 332901 Northing: 6118440

Model	Easting	Susc	Phi	Dip	Theta	Depth	Width	Depthext
Dyke	325130.3	717.3	-10	79		29.1	54.3	0.0
Dyke	325291.7	318.1	-10	56		98.3	188.4	0.0
Dyke	325992.9	358.1	0	75		79.9	116.3	0.0
Dyke	329841.4	159.7	0	104		15.9	37.6	0.0
Dyke	330068.8	398.3	0	122		44.1	70.5	0.0
Dyke	330612.2	427.3	0	131		13.4	148.7	0.0
Dyke	330985.9	1069.4	0	96		44.5	39.1	0.0

Line: 400 Easting: 309657 332901 Northing: 6118440

Model	Easting	Susc	Phi	Dip	Theta	Depth	Width	Depthext
Dyke	310623.4	3076.4	0	14		60.4	215.4	0.0
Dyke	312721.7	480.0	-20	81		37.9	316.4	0.0
Dyke	313599.9	1530.9	-20	88		7.4	53.8	0.0
Dyke	315648.2	6046.2	0	83		37.3	90.2	0.0
Dyke	316507.6	7024.4	0	46		35.2	69.7	0.0
Dyke	313707.9	1591.5	-20	46		3.0	75.3	0.0
Dyke	315976.6	2893.7	0	115		3.9	102.1	0.0

Line: 460 Easting: 309363 333031 Northing: 6120139

Model	Easting	Susc	Phi	Dip	Theta	Depth	Width	Depthext
Dyke	316056.8	8236.6	-5	65		49.8	57.8	0.0
Dyke	317011.0	16803.3	-10	13		33.1	93.5	0.0
Dyke	316469.0	8832.8	-5	132		60.1	57.8	0.0
Dyke	315713.3	7755.4	-15	74		104.1	97.4	0.0

Line: 530 Easting: 309605 333309 Northing: 6122208

Model	Easting	Susc	Phi	Dip	Theta	Depth	Width	Depthext
Dyke	316664.3	10488.0	0	41		16.7	58.3	0.0
Dyke	316165.8	1762.6	0	76		115.7	140.1	0.0
Dyke	310505.0	1591.5	0	90		50.0	150.0	0.0

Line: 660 Easting: 309779 333427 Northing: 6126163

Model	Easting	Susc	Phi	Dip	Theta	Depth	Width	Depthext
Dyke	317529.1	2483.7	-10	89		42.5	98.3	0.0
Dyke	318417.8	1881.6	-10	66		33.7	103.7	0.0
Dyke	317694.1	707.8	-10	77		19.3	104.6	0.0

Line: 740 Easting: 308916 332783 Northing: 6128382

Model	Easting	Susc	Phi	Dip	Theta	Depth	Width	Depthext
Dyke	311416.3	135.3	-25	75		0.0	200.0	1000.0
Dyke	315495.5	5628.5	17	143		96.3	115.5	6000.0
Dyke	315563.0	1305.2	17	59		15.5	166.8	6000.0
Dyke	317887.4	477.1	17	118		1.0	47.0	0.0
Dyke	323049.8	1674.7	-25	50		23.0	201.0	0.0

Dyke	323294.7	1671.1	-25	50	0.0	100.0	0.0
Dyke	323645.6	557.0	-25	50	0.0	100.0	0.0
Dyke	324012.3	0.0	-21	50	0.0	82.0	0.0
Dyke	324498.6	1123.7	-23	133	44.3	181.1	0.0
Dyke	325024.5	1578.7	-25	77	73.6	122.8	0.0
Dyke	324715.8	841.0	-20	122	33.2	320.0	0.0
Dyke	323515.7	795.8	-25	50	100.0	100.0	0.0

Polygon	1949.6	-6	

Corner	Easting	Depth
1	309205.8	80.0
2	309305.8	80.0
3	309405.8	30.0
4	309455.8	30.0
5	309475.8	50.0
6	309505.8	45.0
7	309570.8	30.0
8	309711.8	23.0
9	309437.8	580.0
10	309105.8	580.0

Line: 780 Easting: 309183 333001 Northing: 6129742

Model	Easting	Susc	Phi	Dip Theta	Depth	Width	Depthext
Dyke	321136.1	1004.6	-30	128	0.0	150.8	0.0
Dyke	318199.9	477.5	17	88	-3.9	51.8	0.0
Dyke	322494.8	309.0	-25	68	1.0	130.0	0.0
Dyke	322655.3	3602.7	-25	70	62.4	138.4	0.0
Dyke	322884.0	655.6	-25	77	0.8	205.2	0.0
Dyke	323433.7	795.8	-25	80	20.0	275.0	0.0
Dyke	329953.5	1989.4	-15	110	40.0	40.0	0.0
Dyke	330532.1	4579.1	-15	117	82.6	94.4	0.0
Dyke	331651.1	4986.8	-15	151	59.4	86.3	0.0
Dyke	331847.5	791.3	-15	73	25.7	146.5	0.0
Dyke	332183.0	2003.3	-15	88	80.4	225.0	0.0
Dyke	332537.0	1137.5	-15	115	39.1	83.5	0.0

Line: 830 Easting: 309053 333004 Northing: 6131214

Model	Easting	Susc	Phi	Dip Theta	Depth	Width	Depthext
Dyke	317549.9	583.4	7	71	1.1	315.3	0.0
Dyke	319349.4	630.6	3	108	18.0	50.5	0.0
Dyke	319939.9	817.6	0	84	91.2	233.3	0.0
Dyke	320079.4	1906.4	0	34	115.1	96.3	0.0

Line: 980 Easting: 313553 332818 Northing: 6135775

Model	Easting	Susc	Phi	Dip Theta	Depth	Width	Depthext
Dyke	316132.9	238.7	0	99	49.1	295.1	0.0
Dyke	317507.1	1140.0	-10	48	57.9	153.9	0.0
Dyke	318196.2	323.9	-5	66	17.9	56.0	0.0
Dyke	320189.5	866.4	16	70	64.1	128.3	0.0
Dyke	317802.5	238.7	-10	120	20.0	100.0	100.0
Sheet	319764.7	3522.1	0	22	1.2	32.1	200.7

Line: 1040 Easting: 313620 332545 Northing: 6137638

Model	Easting	Susc	Phi	Dip Theta	Depth	Width	Depthext
Dyke	317230.9	1017.2	-12	87	36.1	354.6	1000.0
Dyke	317687.5	763.1	-12	94	13.2	183.5	1000.0
Dyke	326811.4	800.2	-20	32	32.1	399.9	15074.9
Dyke	328433.3	1326.6	-22	153	0.9	126.6	0.0
Dyke	329000.6	795.8	-22	90	0.0	220.0	0.0
Dyke	329520.7	1114.1	-22	50	0.0	65.0	0.0
Dyke	322769.0	1794.8	0	54	33.0	100.0	375.0
Dyke	320202.0	5172.5	0	75	100.0	79.0	0.0
Dyke	321366.0	2928.5	0	103	18.0	50.0	0.0
Dyke	329697.8	522.1	-22	137	-23.3	68.2	0.0

Polygon	238.7	-12	

Corner	Easting	Depth
1	315954.9	25.6
2	316149.8	5.9
3	315167.1	3107.6
4	316133.7	2751.6

Polygon	545.4	1	

Corner	Easting	Depth
1	322014.8	27.4
2	322393.2	229.1
3	322064.8	2527.4
4	322034.8	2527.4

Line: 1160 Easting: 313085 332747 Northing: 6141183

Model	Easting	Susc	Phi	Dip Theta	Depth	Width	Depthext
Dyke	316810.3	1409.8	0	57	2.5	156.8	0.0
Dyke	316995.0	716.2	0	57	0.0	100.0	0.0
Dyke	320024.5	1468.1	5	68	0.9	113.1	0.0
Dyke	322485.0	557.0	0	45	0.9	124.0	0.0
Dyke	328470.7	1173.8	-13	100	0.9	92.9	0.0
Dyke	328765.2	477.5	-13	101	0.0	90.0	0.0
Dyke	329245.3	954.9	-13	101	0.0	50.0	0.0
Dyke	330457.4	1761.0	-10	137	64.4	245.2	0.0
Dyke	330745.3	1538.0	-10	137	40.0	286.4	0.0
Dyke	327215.0	795.8	0	90	0.0	100.0	0.0
Dyke	326164.2	238.7	0	87	0.9	135.4	0.0
Dyke	326439.6	1073.6	0	49	31.3	112.3	0.0
Dyke	326816.8	1434.4	0	123	46.2	82.1	0.0

Line: 1160 Easting: 313085 332747 Northing: 6141183

Model	Easting	Susc	Phi	Dip Theta	Depth	Width	Depthext
Dyke	328470.7	1173.8	-13	100	0.9	92.9	0.0
Dyke	328765.2	477.5	-13	101	0.0	90.0	0.0
Dyke	329245.3	954.9	-13	101	0.0	50.0	0.0
Dyke	330457.4	1761.0	-10	137	64.4	245.2	0.0
Dyke	330745.3	1538.0	-10	137	40.0	286.4	0.0
Dyke	327215.0	795.8	0	90	0.0	100.0	0.0
Dyke	326164.2	238.7	0	87	0.9	135.4	0.0
Dyke	326439.6	1073.6	0	49	31.3	112.3	0.0

Dyke	326816.8	1434.4	0	123	46.2	82.1	0.0

Line: 1410 Easting: 313709 332519 Northing: 6148391

Model	Easting	Susc	Phi	Dip Theta	Depth	Width	Depthext
Dyke	320158.3	580.2	-6	79	22.4	100.6	946.0
Dyke	314289.3	1591.5	5	120	0.0	140.0	5000.0
Dyke	317531.4	629.5	6	68	77.4	147.3	3542.8
Dyke	320716.6	238.7	-5	75	21.5	124.7	0.0

Line: 1460 Easting: 313828 332926 Northing: 6150266

Model	Easting	Susc	Phi	Dip Theta	Depth	Width	Depthext
Dyke	315827.8	762.3	-12	81	88.7	148.9	508.2
Dyke	317641.8	629.5	6	94	70.5	123.1	508.7
Dyke	331965.9	1281.5	-23	124	45.5	160.1	0.0
Dyke	332457.8	318.3	-23	133	9.7	221.0	0.0

Polygon	570.2	-6	

Corner	Easting	Depth
1	319792.2	84.5
2	319909.9	44.5
3	320012.1	128.4
4	320019.8	58.2
5	320115.3	45.7
6	319981.3	827.7
7	319839.8	1469.4
8	319992.2	3084.5
9	319631.8	2586.0

Line: 1550 Easting: 313767 340235 Northing: 6152920

Model	Easting	Susc	Phi	Dip Theta	Depth	Width	Depthext
Dyke	328811.6	712.3	-12	95	1.0	180.0	0.0
Dyke	313900.2	1855.6	-5	112	0.9	74.8	0.0
Dyke	320125.6	17416.4	-8	13	0.9	15.3	0.0
Dyke	314532.6	480.4	-5	120	117.4	450.0	0.0
Dyke	315355.7	812.7	-10	75	53.0	70.6	0.0
Dyke	314928.3	397.9	-10	38	57.0	182.2	0.0
Dyke	318633.9	803.3	-22	99	19.1	318.7	0.0

Line: 1640 Easting: 313422 340657 Northing: 6155605 *

Model	Easting	Susc	Phi	Dip Theta	Depth	Width	Depthext
Dyke	327435.4	1159.9	0	144	10.1	255.0	536.5
Dyke	327674.3	929.3	0	144	9.8	214.6	511.7

Polygon	794.3	0	

Corner	Easting	Depth
1	325926.0	23.0
2	326122.0	1.0
3	326251.5	30.9
4	326331.7	46.4
5	326297.8	124.7

Corner	Easting	Depth
6	326619.0	1.0
7	326832.0	0.0
8	326436.0	223.0
9	326404.0	199.3
10	326220.2	109.1

Line: 1650 Easting: 313094 340367 Northing: 6155925 *

Model	Easting	Susc	Phi	Dip Theta	Depth	Width	Depthext
Dyke	313466.0	159.2	0	49	0.9	124.0	0.0
Dyke	336793.6	1683.0	0	90	0.0	52.0	201.0
Dyke	327512.7	1933.8	0	145	3.4	276.1	0.0
Dyke	327380.8	775.4	0	128	0.0	98.7	0.0
Dyke	329223.0	535.7	0	105	0.0	900.0	0.0
Dyke	332011.8	2434.9	0	52	44.5	193.0	0.0
Dyke	332494.0	507.1	0	54	-11.4	46.9	0.0

Polygon	397.9	0	

Corner	Easting	Depth
1	318003.0	40.0
2	318697.0	0.0
3	318478.0	371.0
4	318176.0	1189.0
5	317843.0	1991.0

Polygon	238.7	0	

Corner	Easting	Depth
1	328094.0	0.0
2	328594.0	0.0
3	328672.3	587.2
4	328694.4	1991.2
5	328294.0	2000.0
6	328143.7	587.2

Line: 1690 Easting: 312929 340504 Northing: 6157150 *

Model	Easting	Susc	Phi	Dip Theta	Depth	Width	Depthext
Dyke	321390.4	2748.9	0	66	143.3	132.9	150.0
Dyke	324871.1	950.2	0	89	256.7	976.6	0.0
Dyke	326053.6	630.7	0	91	283.6	926.6	0.0
Dyke	320951.3	1054.8	0	31	89.8	204.8	200.0
Dyke	317606.3	1216.8	0	59	5.9	206.5	0.0
Dyke	328231.5	1627.4	0	152	1.5	221.2	666.0
Dyke	325179.0	477.5	0	70	0.0	150.0	200.0
Dyke	321728.4	318.3	0	132	35.4	307.8	300.0

Polygon	373.9	0	

Corner	Easting	Depth
1	318022.9	46.0
2	318170.7	42.8
3	318339.3	0.3
4	318327.9	346.0
5	318324.7	671.2
6	318190.3	553.9
7	318023.5	273.0

Polygon 318.3 0

Corner	Easting	Depth
1	323286.0	512.0
2	324658.0	161.0
3	324794.0	1683.0
4	323182.0	1489.0

Polygon 318.3 0

Corner	Easting	Depth
1	323182.0	1489.0
2	320252.0	1841.0
3	322782.0	5312.0

Line: 1762 Easting: 313209 340428 Northing: 6159254

Model	Easting	Susc	Phi	Dip	Theta	Depth	Width	Depthext
Dyke	317445.3	479.6	0	102		0.0	153.3	0.0
Dyke	317679.1	299.2	0	97		0.0	179.8	0.0
Dyke	327054.6	1418.3	-22	151		7.6	111.6	0.0
Dyke	327489.3	1847.2	-22	70		19.0	53.9	0.0
Dyke	326432.3	1440.7	-22	155		24.0	157.4	0.0
Dyke	327735.4	-729.0	-22	88		61.4	153.0	350.0
Dyke	328924.5	1432.4	-22	59		50.0	125.0	0.0
Dyke	328389.6	397.9	-22	75		35.5	416.7	0.0
Dyke	331394.3	5570.4	-8	137		1.5	125.0	0.0
Dyke	331396.9	39788.7	-8	5		26.5	182.1	0.0

Line: 1820 Easting: 313662 340057 Northing: 6161047

Model	Easting	Susc	Phi	Dip	Theta	Depth	Width	Depthext
Dyke	323462.3	159.2	-22	90		0.0	100.0	0.0
Dyke	324262.3	159.2	-22	110		0.0	100.0	0.0
Dyke	326677.1	1716.3	-22	148		7.1	259.4	0.0
Dyke	317393.2	2383.1	0	43		39.7	61.7	0.0
Dyke	321162.5	477.2	-10	61		1.1	180.4	0.0
Dyke	321402.2	557.0	-10	60		10.0	40.0	0.0
Dyke	320349.2	318.3	-16	94		34.0	337.0	0.0
Dyke	322092.7	1427.8	-10	21		1.0	76.4	0.0
Dyke	316069.2	397.9	0	82		45.3	166.8	0.0
Dyke	328522.3	4774.6	-18	80		32.6	23.0	0.0
Dyke	329596.9	776.2	-18	93		0.9	226.8	0.0
Dyke	330902.1	4774.6	-10	110		6.2	110.0	0.0
Dyke	331870.5	3801.0	-10	17		0.9	122.9	0.0

Line: 2150 Easting: 313217 340489 Northing: 6170997

Model	Easting	Susc	Phi	Dip	Theta	Depth	Width	Depthext
Dyke	319592.4	318.3	-10	102		25.2	141.6	0.0
Dyke	320143.8	5177.0	-12	122		0.9	23.2	0.0
Dyke	320676.9	1304.9	-20	111		38.2	76.8	0.0
Dyke	321073.7	655.7	0	41		3.5	103.3	0.0
Dyke	331793.6	523.7	0	80		0.9	98.1	1000.0
Dyke	332508.6	1255.2	0	80		34.9	133.2	0.0
Dyke	332898.2	159.1	0	49		3.8	307.4	0.0

Line: 2200 Easting: 323059 339896 Northing: 6172511 *

Model	Easting	Susc	Phi	Dip	Theta	Depth	Width	Depthext
Dyke	331834.3	546.2	-10	76		95.0	180.0	0.0
Dyke	332377.4	801.0	-10	48		57.3	153.6	0.0
Dyke	332933.4	1033.7	-10	91		104.3	126.3	0.0

Line: 2300 Easting: 323524 339467 Northing: 6175535 *

Model	Easting	Susc	Phi	Dip	Theta	Depth	Width	Depthext
Dyke	329743.0	1032.4	0	52		1.2	149.0	0.0
Dyke	331474.1	520.6	0	94		3.6	350.5	0.0
Dyke	331729.1	489.1	0	129		10.4	267.5	0.0
Dyke	326042.3	1183.7	0	73		0.9	67.2	0.0
Dyke	326497.1	1867.4	0	66		60.9	81.1	0.0
Dyke	327068.9	1045.6	-20	111		95.5	103.7	0.0

Line: 2550 Easting: 323629 332363 Northing: 6182986

Model	Easting	Susc	Phi
Polygon		1039.9	0

Corner	Easting	Depth
1	328111.8	33.8
2	328207.1	12.3
3	328339.8	249.7
4	328344.8	245.1
5	328602.0	1279.9
6	327966.0	1271.0
7	328025.4	228.2
8	328061.1	224.5

Polygon 1416.5 0

Corner	Easting	Depth
1	324158.5	179.4
2	324715.8	195.2
3	324653.1	445.7
4	324425.1	541.5
5	324286.1	3742.0
6	323853.1	10820.9
7	323835.7	289.3
8	324048.5	387.4
9	324159.8	220.5

Line: 2750 Easting: 323545 332088 Northing: 6188937

Model	Easting	Susc	Phi
Polygon		1416.9	0

Corner	Easting	Depth
1	323532.1	62.9
2	323876.6	121.4
3	323944.5	295.4
4	324146.4	279.0

5	323806.0	18155.8
6	323377.6	13003.9
7	323420.5	252.3
8	323359.3	244.2
9	323464.2	55.3

Line: 2850 Easting: 323187 331838 Northing: 6191941

Model	Easting	Susc	Phi	Dip	Theta	Depth	Width	Depthext
Dyke	329575.2	318.3	0	87		0.9	195.6	0.0
Dyke	330590.4	200.8	0	64		2.5	188.6	0.0
Dyke	331352.0	238.7	0	71		0.0	205.0	0.0
Dyke	331591.7	358.1	0	71		1.0	239.1	0.0

Line: 2950 Easting: 322643 339817 Northing: 6194958

Model	Easting	Susc	Phi	Dip	Theta	Depth	Width	Depthext
Dyke	327865.4	964.3	0	128		19.8	121.7	252.9
Dyke	323981.7	3940.4	0	91		0.0	154.1	0.0
Dyke	324158.0	11538.7	0	63		1.0	110.0	0.0
Dyke	324493.0	2785.2	0	65		25.0	125.0	0.0
Dyke	329665.3	397.9	8	100		65.1	199.6	0.0

Line: 3050 Easting: 323382 339495 Northing: 6198035

Model	Easting	Susc	Phi	Dip	Theta	Depth	Width	Depthext
Dyke	330132.2	198.9	10	57		28.6	142.5	38591.6
Dyke	328419.0	2819.0	15	109		190.1	109.0	0.0
Dyke	328047.1	1254.7	15	95		91.2	222.2	0.0
Dyke	324505.6	466.4	-15	128		0.9	193.2	0.0
Dyke	330949.2	848.7	10	69		164.1	201.9	477.4
Dyke	336882.3	1070.8	0	112		200.0	118.0	0.0
Dyke	337101.6	3270.7	0	93		191.1	186.6	0.0

Line: 3250 Easting: 323194 339340 Northing: 6203953

Model	Easting	Susc	Phi	Dip	Theta	Depth	Width	Depthext
Dyke	324008.0	159.2	0	147		1.0	123.0	0.0
Dyke	330148.3	14968.1	0	63		103.5	30.3	0.0
Dyke	330452.4	4750.2	0	115		86.9	176.1	0.0

Line: 3350 Easting: 323405 339382 Northing: 6207071

Model	Easting	Susc	Phi	Dip	Theta	Depth	Width	Depthext
Dyke	324160.0	795.8	0	140		20.4	58.9	0.0
Dyke	330377.0	12598.6	0	86		109.5	65.6	0.0
Dyke	330501.8	2693.2	0	60		14.9	283.2	0.0
Dyke	332556.2	738.0	0	61		1.1	114.6	0.0

Line: 3390 Easting: 323183 339972 Northing: 6208208

Model	Easting	Susc	Phi	Dip	Theta	Depth	Width	Depthext
Dyke	324102.4	1032.6	0	106		0.8	48.9	501.0
Dyke	325388.5	286.1	0	103		219.8	718.2	1374.1

Dyke	330634.8	12179.5	0	135		89.7	82.6	0.0
Dyke	330746.6	20078.2	0	54		93.3	65.5	0.0
Dyke	326843.0	318.3	0	137		10.0	165.0	501.0
Dyke	329060.0	526.4	0	81		84.0	183.0	498.0

Polygon 1110.6 0

Corner	Easting	Depth
1	325972.0	2145.0
2	326722.0	2145.0
3	327472.0	7349.0
4	325972.0	8286.0
5	324526.0	7517.0
6	325399.5	2145.0

Polygon 1254.2 0

Corner	Easting	Depth
1	336408.0	84.0
2	336814.0	140.0
3	337977.0	1215.0
4	336162.3	565.4
5	335985.0	259.0
6	336228.0	233.0
7	336399.7	210.9
8	336548.3	127.8

Line: 3390 Easting: 323183 339972 Northing: 6208208

Model	Easting	Susc	Phi	Dip	Theta	Depth	Width	Depthext
Dyke	324102.4	1032.6	0	106		0.8	48.9	501.0
Dyke	325388.5	286.1	0	103		219.8	718.2	1374.1
Dyke	326843.0	318.3	0	137		10.0	165.0	501.0
Dyke	329060.0	526.4	0	81		84.0	183.0	498.0

Polygon 5219.5 0

Corner	Easting	Depth
1	330596.0	139.3
2	330602.8	47.3
3	330737.2	198.7
4	330777.4	138.8
5	330831.4	21.8
6	330937.2	485.7
7	330542.8	31693.0
8	330465.0	129.6

Polygon 1110.6 0

Corner	Easting	Depth
1	325972.0	2145.0
2	326722.0	2145.0
3	327472.0	7349.0
4	325972.0	8286.0
5	324526.0	7517.0
6	325399.5	2145.0

Polygon 1254.2 0

Corner	Easting	Depth
1	336408.0	84.0
2	336814.0	140.0
3	337977.0	1215.0
4	336152.3	565.4
5	335985.0	259.0
6	336228.0	233.0
7	336399.7	210.9
8	336548.3	127.8

MURRAY BRIDGE SURVEY
MURRAY BRIDGE SURVEY
CRA Data
Lines: 10 to 1720

Line: 30 Easting: 327278 317964 Northing: 6081650

Model	Easting	Susc	Phi	Dip	Theta	Depth	Width	Depthext
Edge	318686.3	636.6	187	104		724.0	0.0	0.0
I Dyke	320843.0	397.8	0		52	337.6	334.3	1879.5
I Dyke	325504.7	498.5	0		69	174.4	324.5	290.5
I Dyke	326464.0	795.8	0		0	310.0	660.0	1000.0
I Dyke	325964.0	1989.4	0		30	1710.0	8000.0	0.0

Polygon 1351.6 0

Corner	Easting	Depth
1	321908.0	230.0
2	322598.0	195.0
3	322922.0	845.0
4	321048.0	321.0

Line: 40 Easting: 328966 317811 Northing: 6082019

Model	Easting	Susc	Phi	Dip	Theta	Depth	Width	Depthext
Edge	319611.0	573.0	180	104		1910.0	0.0	0.0
I Dyke	320811.0	159.2	0		30	110.0	800.0	1000.0
I Dyke	325485.4	477.5	0		69	122.5	274.5	0.0
I Dyke	326611.0	477.5	0		0	310.0	1000.0	1400.0
I Dyke	325965.0	1591.5	0		30	1710.0	8000.0	0.0
I Dyke	319958.8	318.3	0		65	244.0	516.7	2826.0

Polygon 1351.6 0

Corner	Easting	Depth
1	321861.0	230.0
2	322551.0	195.0
3	322875.0	845.0
4	321001.0	321.0

Line: 80 Easting: 317767 331864 Northing: 6083318

Model	Easting	Susc	Phi	Dip	Theta	Depth	Width	Depthext
I Dyke	325098.9	397.9	0		60	77.2	243.1	0.0
Edge	320191.8	398.3	180	71		271.7	0.0	0.0
I Dyke	331085.0	662.9	0		22	195.0	1651.0	0.0
I Dyke	326024.5	669.8	0		5	210.4	1532.4	0.0

I Dyke	327926.8	991.5	0		-2	417.5	1419.8	0.0

Polygon 1351.6 0

Corner	Easting	Depth
1	321608.0	230.0
2	322298.0	195.0
3	322622.0	845.0
4	320748.0	321.0

Line: 91 Easting: 332983 317813 Northing: 6083671

Model	Easting	Susc	Phi	Dip	Theta	Depth	Width	Depthext
I Dyke	325013.0	398.0	0		130	95.0	156.0	0.0
Edge	320191.8	398.3	180	71		271.7	0.0	0.0
I Dyke	331085.0	662.9	0		22	195.0	1651.0	0.0
I Dyke	326046.7	640.5	0		14	244.2	1523.0	0.0
I Dyke	328248.8	896.2	0		-23	408.3	1323.5	0.0

Polygon 1351.6 0

Corner	Easting	Depth
1	321608.0	230.0
2	322298.0	195.0
3	322622.0	845.0
4	320748.0	321.0

Line: 106 Easting: 294468 318225 Northing: 6083473

Model	Easting	Susc	Phi	Dip	Theta	Depth	Width	Depthext
I Dyke	301359.2	159.0	0		-25	91.3	591.1	0.0
I Dyke	301815.4	159.0	0		5	141.6	554.8	0.0
I Dyke	304468.0	795.8	0		0	4910.0	5000.0	0.0
I Dyke	304487.0	557.0	0		60	126.0	207.0	600.0
I Dyke	305515.0	596.8	0		-60	178.0	429.0	500.0
I Dyke	304768.0	-1193.7	0		0	610.0	700.0	100.0
I Dyke	311141.5	1328.3	0		5	216.2	2153.7	763.8

Line: 120 Easting: 332879 294723 Northing: 6084234

Model	Easting	Susc	Phi	Dip	Theta	Depth	Width	Depthext
I Dyke	305507.2	354.0	0		-36	115.0	206.7	0.0
I Dyke	304071.6	483.3	0		-6	167.8	489.8	0.0
I Dyke	304596.7	483.3	0		-6	103.1	252.2	0.0
I Dyke	305792.3	357.9	0		-40	143.1	212.4	0.0
I Dyke	295880.8	397.9	0		152	86.8	177.4	0.0

Polygon 877.5 0

Corner	Easting	Depth
1	311523.2	308.2
2	312371.8	264.5
3	312900.1	195.3
4	313649.8	826.7
5	315811.6	837.5
6	315889.0	1387.4
7	318894.9	841.5

	8	318038.6	5595.2
	9	312200.2	9778.7
Polygon		1193.7	0

Corner	Easting	Depth
1	311723.0	270.0
2	313676.8	740.7
3	316541.4	1186.3
4	318514.7	2220.7
5	319103.5	3287.0
6	311723.0	3270.0

Line: 160 Easting: 332722 294782 Northing: 6085524

Model	Easting	Susc	Phi	Dip Theta	Depth	Width	Depthext
I Dyke	331273.2	526.0	0	25	94.5	943.4	2864.7
I Dyke	306187.0	1625.9	0	-50	158.0	98.0	0.0
Polygon		611.4	0				

Corner	Easting	Depth
1	325096.3	138.4
2	325699.7	138.4
3	326479.5	210.7
4	327151.4	101.2
5	327717.0	87.1
6	328337.8	246.1
7	328651.0	209.1
8	328964.2	172.1
9	330555.3	22718.4
10	325096.3	22718.4
11	325096.3	5138.4

Line: 180 Easting: 332728 294906 Northing: 6086052

Model	Easting	Susc	Phi	Dip Theta	Depth	Width	Depthext
I Dyke	331156.0	795.8	0	35	267.0	650.0	0.0
I Dyke	306187.0	1625.9	0	-50	158.0	98.0	0.0

Line: 290 Easting: 294570 333560 Northing: 6089342

Model	Easting	Susc	Phi	Dip Theta	Depth	Width	Depthext
I Dyke	323717.3	1187.3	0	6	311.9	440.5	254.3

Line: 400 Easting: 302232 341985 Northing: 6092779

Model	Easting	Susc	Phi	Dip Theta	Depth	Width	Depthext
I Dyke	338512.9	2669.4	0	26	677.4	548.4	0.0

Line: 530 Easting: 310123 341983 Northing: 6096653

Model	Easting	Susc	Phi	Dip Theta	Depth	Width	Depthext
I Sheet	333412.2	965.9	0	10	135.9	50.0	0.0
I Dyke	321064.3	1714.0	0	18	173.5	101.4	0.0

I Dyke	321543.0	369.1	0	-49	95.5	146.2	0.0
I Dyke	324586.5	415.8	0	22	104.0	177.8	0.0
I Dyke	335908.7	467.6	0	-12	45.4	54.8	0.0
I Dyke	338633.6	4458.4	0	14	219.3	160.2	0.0

Line: 580 Easting: 341999 316998 Northing: 6098214

Model	Easting	Susc	Phi	Dip Theta	Depth	Width	Depthext
I Dyke	329418.8	347.9	0	28	112.5	134.1	0.0
I Dyke	329022.7	347.9	0	3	168.1	244.1	0.0
I Sheet	331601.7	318.3	0	20	137.4	50.0	0.0
I Sheet	333310.9	679.6	0	-48	50.4	50.0	0.0
I Dyke	319055.1	1087.9	0	24	123.7	108.8	0.0
I Dyke	319449.0	369.1	0	-35	108.7	123.0	0.0

Line: 610 Easting: 341994 317041 Northing: 6099128

Model	Easting	Susc	Phi	Dip Theta	Depth	Width	Depthext
Dyke	324847.3	397.9	0	81	62.1	173.2	0.0
Dyke	326020.0	398.0	0	78	74.5	70.2	0.0
Dyke	328113.8	98.2	-5	121	72.4	262.1	0.0
Dyke	328818.8	397.9	-15	97	97.0	133.0	0.0
Dyke	329301.6	397.9	-8	85	103.4	113.0	0.0
Dyke	333079.8	284.1	-10	139	40.8	277.4	0.0

Line: 660 Easting: 317167 341989 Northing: 6100648

Model	Easting	Susc	Phi	Dip Theta	Depth	Width	Depthext
Dyke	326793.4	397.9	0	39	71.9	149.9	0.0
Dyke	328214.9	863.5	0	41	114.1	97.0	0.0
Dyke	329076.7	397.8	-10	68	84.6	152.3	0.0
Dyke	333002.4	397.9	-10	158	-5.5	129.9	0.0
Dyke	334242.1	479.9	-10	91	10.0	156.2	0.0

Line: 1250 Easting: 331831 341983 Northing: 6118502

Model	Easting	Susc	Phi	Dip Theta	Depth	Width	Depthext
Dyke	334195.6	1191.6	-20	96	0.8	278.3	0.0
Dyke	333434.2	795.8	-20	90	200.0	400.0	0.0
Dyke	339262.2	545.1	0	93	236.2	3320.9	0.0
Dyke	334594.4	4405.2	-20	26	1.0	34.0	160.0
Dyke	334992.1	5340.6	-20	146	41.0	48.0	0.0
Dyke	335054.1	1193.7	-20	92	0.0	150.0	0.0

Line: 1400 Easting: 341985 331843 Northing: 6123019

Model	Easting	Susc	Phi	Dip Theta	Depth	Width	Depthext
Dyke	332420.8	803.3	-20	121	-11.9	137.6	134.8
Dyke	331641.8	795.8	-20	95	0.0	150.0	0.0
Dyke	338055.6	2706.0	0	155	127.1	283.5	0.0
Polygon		1281.2	-20				

Corner	Easting	Depth
1	332800.2	-27.1

2	332863.1	-31.0
3	332986.8	-37.1
4	332924.5	1.2
5	332789.6	5.9

Polygon 1465.4 -20

Corner	Easting	Depth
1	333211.0	-30.1
2	333310.0	-42.1
3	333417.0	-46.1
4	332628.0	259.9
5	332458.0	257.9

Polygon 759.8 -20

Corner	Easting	Depth
1	333583.7	-18.2
2	333823.8	7.6
3	334067.5	16.6
4	334054.5	241.8
5	333628.6	160.9

Polygon 540.1 -20

Corner	Easting	Depth
1	332061.9	-18.9
2	331961.3	-60.4
3	332223.1	-36.3
4	332627.1	349.0
5	332120.5	353.2

Line: 1400 Easting: 341985 331843 Northing: 6123019

Model	Easting	Susc	Phi	Dip	Theta	Depth	Width	Depthext
Dyke	332420.8	803.3	-20	121		-11.9	137.6	134.8
Dyke	331641.8	795.8	-20	95		0.0	150.0	0.0
Dyke	338055.6	2:06.0	0	155		127.1	283.5	0.0

Polygon 1465.4 -20

Corner	Easting	Depth
1	333211.0	-30.1
2	333310.0	-42.1
3	333417.0	-46.1
4	332628.0	259.9
5	332458.0	257.9

Polygon 759.8 -20

Corner	Easting	Depth
1	333583.7	-18.2
2	333823.8	7.6
3	334067.5	16.6
4	334054.5	241.8
5	333628.6	160.9

Polygon 696.0 -20

Corner	Easting	Depth
1	334441.2	76.8
2	334815.9	92.9
3	335089.8	449.8
4	334675.3	557.6
5	334597.7	898.9

ECHUNGA SURVEY

ECHUNGA SURVEY

BASEMENT ANOMALIES: BS5 AND BS6

Depths to deep basement anomalies, BS5 and BS6 were determined using spectral analysis. This gave average depths for deep basement features. Both BS5 and BS6 were caused by magnetic sources at an average depth of 1.5 and 3.5 km.

BULL CREEK SURVEY
CRA Data
Lines: 10 to 670
Results of quantitative analysis using graphical techniques

For each anomaly modelled, the easting and the average northing of the line are given. Both the northing and the easting are in metres (AMG coordinates). The parameters of the model are given below. For details, refer to Chapter 4.

Model: Dyke, sheet (thin dyke), edge, pole (see Chapter 4).
Aml.: Amplitude of the anomaly in nanoTeslas.
Phi: Strike of the model.
Depth: Depth to the top of the source. The altitude of the aircraft (not the sensor height) has been subtracted.
Width: Width of the model measured along the profile.
Theta: Index parameter = + - Dip - 90.
Dip: Dip is measured from the east. The dip was computed from theta assuming that the resultant direction of magnetization is in the direction of the present field of the earth.

All linear parameters are given in metres and all angles in degrees.

Line	Model	Easting (m)	Northing (nT)	Aml (m)	Phi (m)	Depth	Width	Theta	Dip
200	Dyke	312528	6103050	-78	30	42	198	140	
220	Dyke	308017	6102671	135	0	8	245	20	70
250	Dyke	303820	6101714	100	0	49	249	330	120
260	Dyke	303866	6101442	80	0	14	218	315	135
270	Dyke	309901	6101125	80	12	12	220	65	36
280	Dyke	310156	6100836	8	12	0	200	75	26
290	Dyke	307104	6100307	120	0	80	400		
310	Dyke	297481	6099859	480	15	10	80	15	89
320	Sheet	298628	6099585	20	18	29	119	85	21
320	Dyke	297403	6099585	260	15	47	110	30	74
420	Dyke	302190	6096725	12	0	23	192	295	155
540	Dyke	303236	6093130	72	-16	77	184	0	105
600	Dyke	303443	6091251	40	-16	84	244	10	95
630	Sheet	302352	6090395	30	-16	9		304	161
650	Sheet	288896	6089767	125	30	59		38	78
650	Sheet	293046	6089767	10	15	34		283	177
650	Sheet	295546	6089767	-85	18	43			
670	Sheet	288280	6089285	128	28	69		46	69

KANMANTOO SURVEY
CRA Data
Lines: 10 to 3410
Results of quantitative analysis using graphical techniques

For each anomaly modelled, the easting and the average northing of the line are given. Both the northing and the easting are in metres (AMG coordinates). The parameters of the model are given below. Not all parameters were determined for all models. See Chapter 4 for further details.

Model: Dyke, sheet (thin dyke), edge, pole (see Chapter 4).
Amp.: Amplitude of the anomaly in nanoTeslas.
Phi: Strike of the model.

Depth: Depth to the top of the source. The altitude of the aircraft (not the sensor height) has been subtracted.
Width: Width of the model measured along the profile.
Theta: Index parameter = + - Dip - 90.
Dip: Dip measured from the east. Where magnetic dip cannot be = structural dip, only theta is given.

All linear parameters are given in metres and all angles in degrees.

Line	Model	Easting (m)	Northing (m)	Amp (nT)	Phi	Dep (m)	Width (m)	Dip	Theta
200	Dyke	312340	6112324	165	16	57	221	40	65
210	Dyke	320357	6112607	42	25	10	230		117
210	Dyke	323857	6112607	21	0	118	353	7	83
210	Dyke	325707	6112607	45	-13	72	210		114
210	Dyke	328007	6112607	45	-16	86	352	5	100
231	Dyke	323817	6113238	45	0	38	294	27	63
240	Dyke	323775	6113472	54	0	51	211	55	45
240	Dyke	327875	6113472	54	-16	53	215	25	80
360	Dyke	313299	6117173	138	-15	4	141	40	64
360	Dyke	314024	6117173	150	-15	4	141	40	69
370	Dyke	313258	6117480	120	-20	19	218	45	63
370	Dyke	315558	6117480	810	6	35	313	30	66
383	Dyke	310852	6117838	66	0	3	186	75	15
383	Dyke	313102	6117838	165	-20	0	175	60	46
390	Dyke	312913	6118153	165	-20	10	220	30	78
390	Dyke	313663	6118153	255	-20	51	183	62	46
390	Dyke	315613	6118153	420	0	26	290	45	45
400	Dyke	315657	6118440	591	6	75	289	42	54
410	Dyke	330758	6118699	60	0	7	146		130
420	Dyke	310526	6118991	96	0	34	186	35	55
420	Dyke	318976	6118991	60	-15	-10	120	42	62
431	Dyke	324935	6119278	42	-13	7	146	15	87
431	Dyke	325765	6119278	40	0	7	145	5	85
441	Dyke	325770	6119604	45	0	39	129	10	80
441	Dyke	330770	6119604	114	0	18	162		115
450	Dyke	325809	6119870	36	5	4	94	27	68
450	Dyke	330809	6119870	99	-5	-8	123		125
460	Dyke	325813	6120139	45	0	5	95	15	75
460	Dyke	352263	6120139	108	0	20	165		125
460	Dyke	331313	6120139	45	0	-7	83		95
480	Dyke	324733	6120787	45	-5	6	96	35	60
480	Dyke	330633	6120787	120	-10	6	96		134
490	Dyke	324699	6121065	30	-7	1	91	30	67
490	Dyke	325799	6121065	50	0	31	121	2	88
490	Dyke	330499	6121065	120	-10	27	117		126
600	Dyke	311411	6124362	285	0	71	161	7	83
600	Dyke	313661	6124362	15	0	-3	44	60	30
600	Dyke	318811	6124362	225	-5	13	205	2	93
610	Dyke	311483	6124627	255	0	60		61	29
610	Dyke	317733	6124627	45	-5	66		23	72
610	Dyke	325783	6124627	90	-30	35	223		119
610	Dyke	327983	6124627	90	-20	3	140	60	48
621	Dyke	311490	6124922	345	0	31	61	27	63
621	Dyke	314415	6124922	30	0	-44			2
621	Dyke	318090	6124922				-10	75	600
621	Dyke	323765	6124922	60	-10	38	128	36	63
621	Dyke	327615	6124922	50	-42	-13		90	35

621	Dyke	328715	6124922	120	-32	3	336		
621	Dyke	332915	6124922	90	-20	-7	296		
630	Dyke	311541	6125268	90	-10	9	238	5	94
630	Dyke	312491	6125268	100	0	-9	81	55	35
630	Dyke	312941	6125268	15	0	-10	192		
630	Dyke	317891	6125268	240	-15	55	507		
630	Dyke	323691	6125268	60	-10	42	132	50	49
630	Dyke	313691	6125268	15	0	-15	150		
640	Dyke	317650	6125555	195	-10	74	164	20	88
700	Sheet	315379	6127341	300	18	-8		0	106
720	Dyke	329047	6127990	105	-15	28		54	50
740	Dyke	315816	6128575	270	18	44	134		121
751	Dyke	315770	6128876	270	18	-3	174		111
751	Dyke	331020	6128876	216	-20	36	126	50	58
760	Dyke	315916	6129163	300	18	56	73		131
760	Dyke	321616	6129163	105	-30	31	303	10	106
760	Dyke	328766	6129163	90	-30	-7	110	55	61
780	Dyke	321233	6129742	170	-30	72	81		138
800	Dyke	320838	6130319	1[illegible]0	-30	38	64		121
810	Dyke	315855	6130591	130	-5	-7	24[illegible]	10	89
810	Edge	322405	6130591	300	0	-2		3	87
830	Dyke	317703	6131213	105	3	18	323	25	68
840	Dyke	317780	6131548	75	3	60	300	30	43
840	Dyke	319480	6131548	45	0	18	54		
850	Dyke	319517	6131795	120	0	4	47	45	45
850	Dyke	328117	6131795	90	-10	-4	128	0	99
870	Dyke	319410	6132401	300	0	18		28	62
890	Dyke	315603	6133072	120	-28	24			135
900	Dyke	315515	6133358	75	-25	10	650		
900	Dyke	317615	6133358	45	-15	-1	178	20	84
920	Sheet	319722	6133956	60	5	-9		51	44
940	Dyke	316153	6134583	75	-20		450		
940	Dyke	322403	6134583	300	0		300		
960	Dyke	322329	6134842	300	0	60	300		105
980	Dyke	317653	6135775	100	-10	24	227	40	59
980	Dyke	319803	6135775	45	0	17		32	18
980	Dyke	321953	6135775	30	0	4		35	55
990	Dyke	317675	6136109	90	0	0	350	55	35
1000	Dyke	318028	6136407	120	-5	6	108	35	60
1000	Dyke	318178	6136407	20	-5	28	118		110
1000	Dyke	325478	6136407	30				126	227
1010	Dyke	322379	6136703	60	0	50	210		145
1020	Dyke	317625	6137044	120		30	350		
1020	Dyke	320075	6137044	300	0	3	185	40	50
1030	Dyke	320134	6137350	300	0	31	121	20	70
1030	Dyke	322884	6137350	150	0	51	212	62	28
1030	Dyke	317784	6137350	180		10			
1030	Dyke	325884	6137350	60	-5	84			
1040	Dyke	316120	6137638	45	0	32	250		142
1040	Dyke	320120	6137638	300	0	71	407	5	85
1040	Dyke	322820	6137638	210	-5	30	240	30	65
1040	Dyke	327220	6137638	90	-10	91	453	35	64
1040	Dyke	328420	6137638	80	-20	46			166
1040	Dyke	331720	6137638	120	0	14	93	65	25
1070	Dyke	317572	6138540	90	-5	22	180		
1070	Dyke	322122	6138540	180	0	-22	170	35	55
1070	Dyke	322872	6138540	150	0	34	370	0	90
1100	Dyke	320125	6139420	150	-5	50	209	45	50
1100	Dyke	322625	6139420	120	0	4	234	0	90
1111	Dyke	314714	6139721	30	0	14	208		132

1130	Dyke	316889	6140268	75	-10	10	116	48	52
1130	Dyke	320089	6140268	120	0	49	139	75	15
1150	Dyke	316794	6140884	75	-10	77	167	57	42
1150	Dyke	319919	6140884	90	0	48	138	67	23
1150	Dyke	322469	6140884	60	-5	38	128	52	43
1150	Dyke	324219	6140884	60	-10	46	136		166
1160	Dyke	316835	6141183	210	-5	60	150	50	45
1160	Dyke	322485	6141183	75	-5	43	133	50	45
1630	Dyke	314610	6155312	20	-10	4	94		131
1630	Dyke	336685	6155312	20	0	8	98	40	50
1630	Dyke	320856	6155312	60	15	102	192	45	59
1680	Dyke	319613	6156846		0	7	97	37	53
1680	Dyke	324713	6156846		0	46	136	20	70
1680	Dyke	328413	6156846		-23	35	125		171
1770	Dyke	318809	6159576		-5	-4	86	62	33
1780	Dyke	333271	6159843		0	29	119	60	30
1790	Dyke	333221	6160109		0	13	103	65	25
1810	Dyke	313140	6160776		-2	49			94
1810	Dyke	317390	6160776		0	10	100	47	43
1810	Dyke	326990	6160776		-16	43	133		172
1820	Dyke	317362	6161046	90	0	9	99	45	45
1820	Dyke	322112	6161046	45	-5	10	100	50	45
1820	Dyke	326912	6161046	100	-16	89	179		160
1820	Dyke	331912	6161046	150	-15	62	152	85	19
1840	Dyke	317543	6161677	45	0	12	108	55	35
1840	Dyke	318918	6161677	60	-5	11	101	55	40
1840	Dyke	321968	6161677	50	-10	12	102	67	32
1840	Dyke	325643	6161677	70	-16	1	91		135
1840	Dyke	326668	6161677	300	-16	3	93		170
1840	Dyke	330468	6161677	1376	-12	38	128	40	61
1840	Dyke	331918	6161677	450	-10	35	125	32	67
1860	Dyke	314092	6162250	45	0	37	127	47	43
1860	Dyke	315592	6162250	20	0	49	139	72	18
1860	Dyke	317342	6162250	90	0	13	103	62	28
1860	Dyke	321892	6162250	20	-10	13	103		
1860	Dyke	323842	6162250	30	-10	28	118	63	36
1860	Dyke	318992	6162250	45	-10	9	99	50	49
1901	Dyke	317265	6163505	75	0	26	290	37	53
1910	Dyke	336868	6163823	20	0	-10	120		110
1920	Dyke	338887	6164026	20	0	13	103	62	28
1930	Dyke	337917	6164492	20	0	13	103	63	27
2000	Dyke	337722	6166608	45	0	7	97		127
2000	Dyke	320063	6166608	360	-5	59	149	17	78
2080	Dyke	337538	6168864	30	0	1	91		110

Appendix J: Aeromagnetic profiles modelled using GAMMA

This appendix includes diagrams of some of the aeromagnetic profiles which were modelled using GAMMA. On each diagram, the line number, the easting of the start and finish, and the northing are given. Distances along the profile are with respect to the easting of the start of the line.

Bull Creek Survey

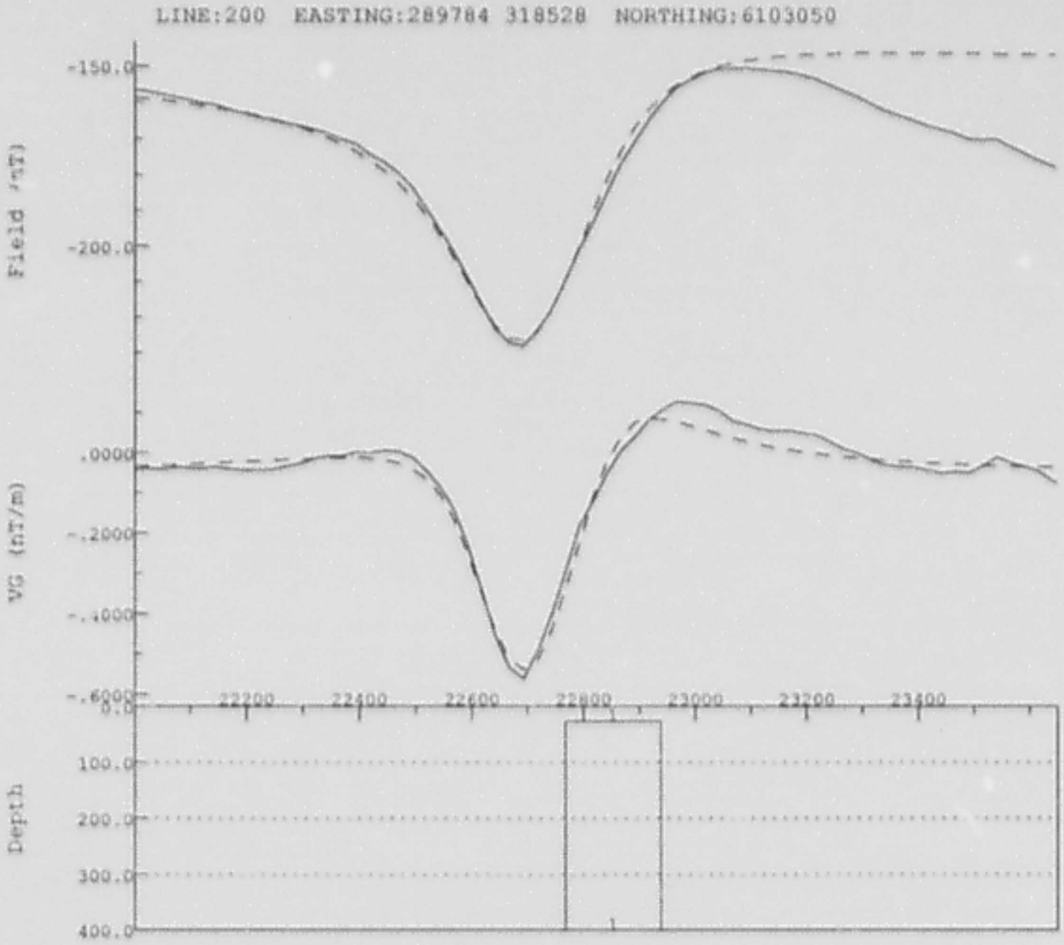
LINE:200 EASTING:289784 318528 NORTHING:6103050
Field (nT)
-150.0
-200.0
VG (nT/m)
.0000
-.2000
-.4000
-.6000
22200
22400
22600
22800
23000
23200
23400
Depth
0.0
100.0
200.0
300.0
400.0

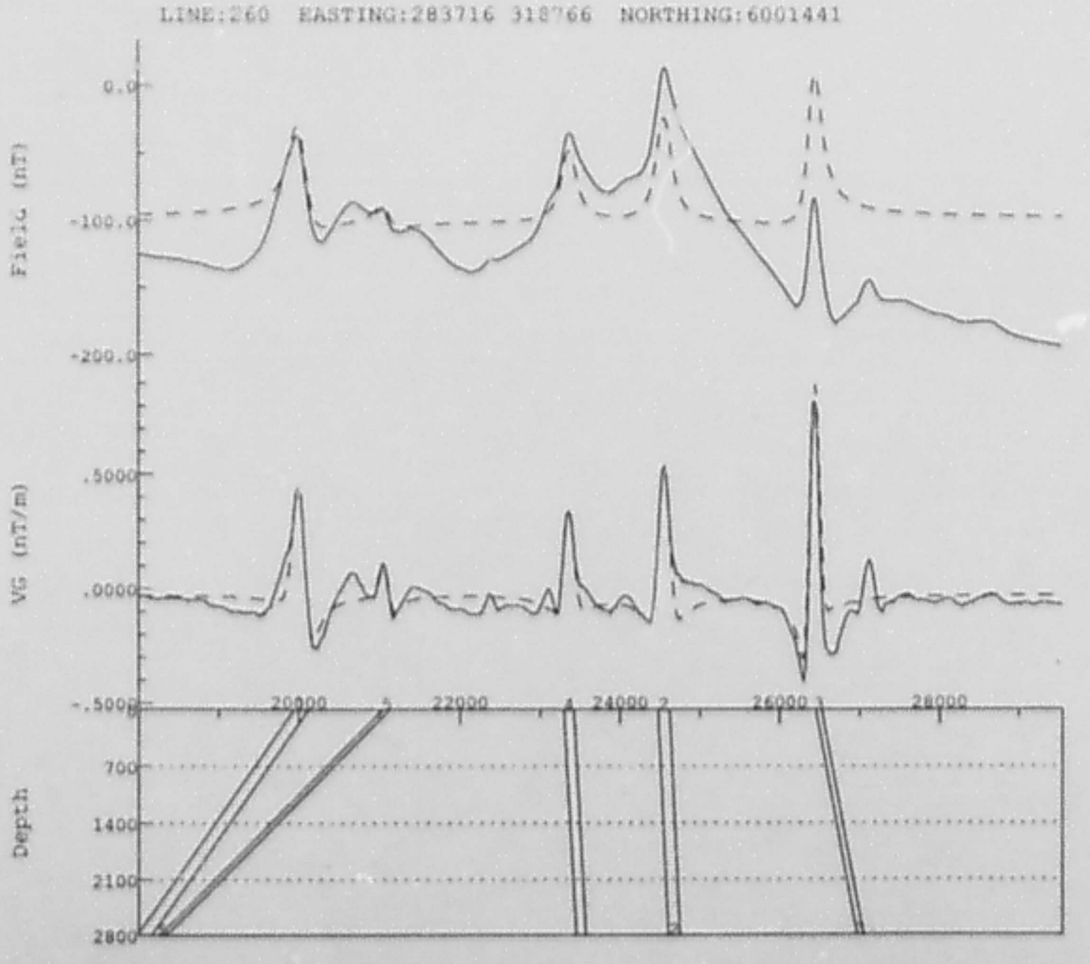
LINE:260 EASTING:283716 318766 NORTHING:6001441
Field (nT)
0.0
-100.0
-200.0
VG (nT/m)
.5000
.0000
-.5000
20000
22000
24000
26000
28000
Depth
700
1400
2100
2800

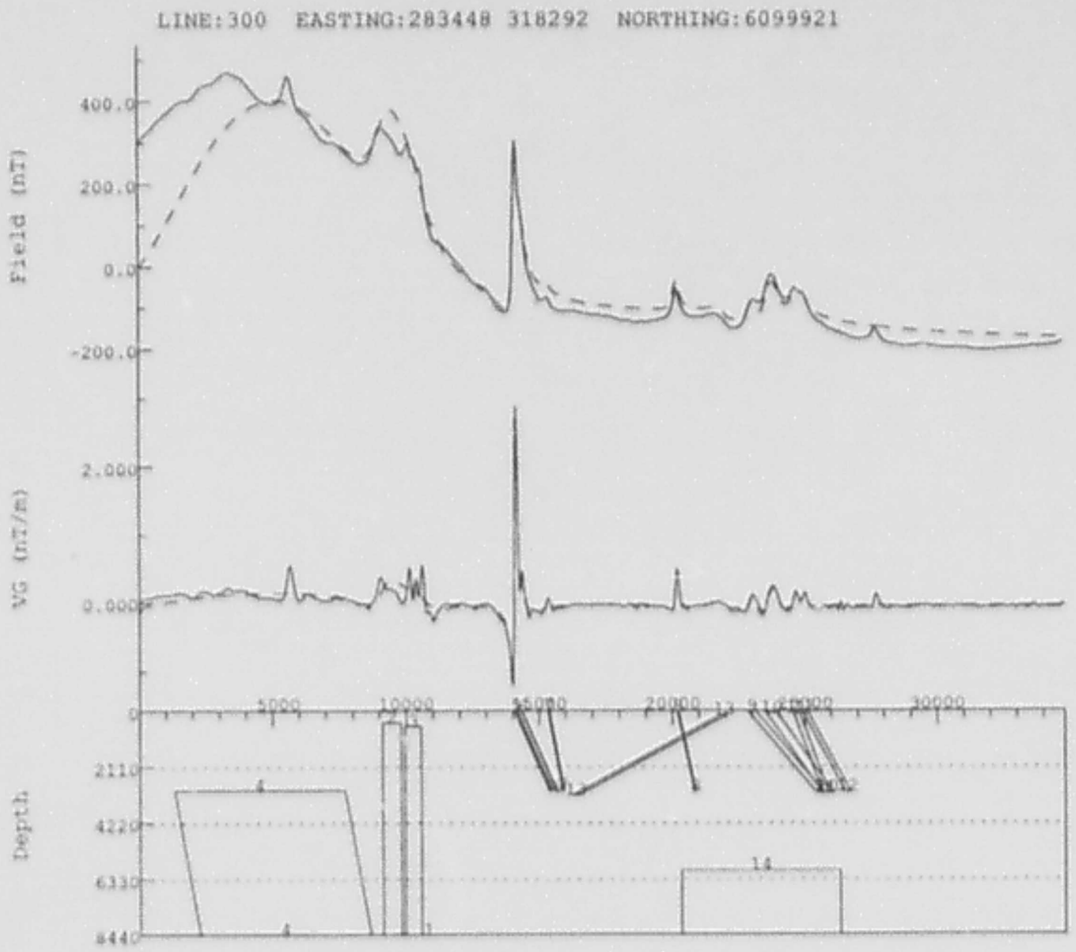
LINE:300 EASTING:283448 318292 NORTHING:6099921
Field (nT)
400.0
200.0
0.0
-200.0
VG (nT/m)
2.000
0.000
5000
10000
15000
20000
25000
30000
Depth
0
211.0
422.0
633.0
844.0

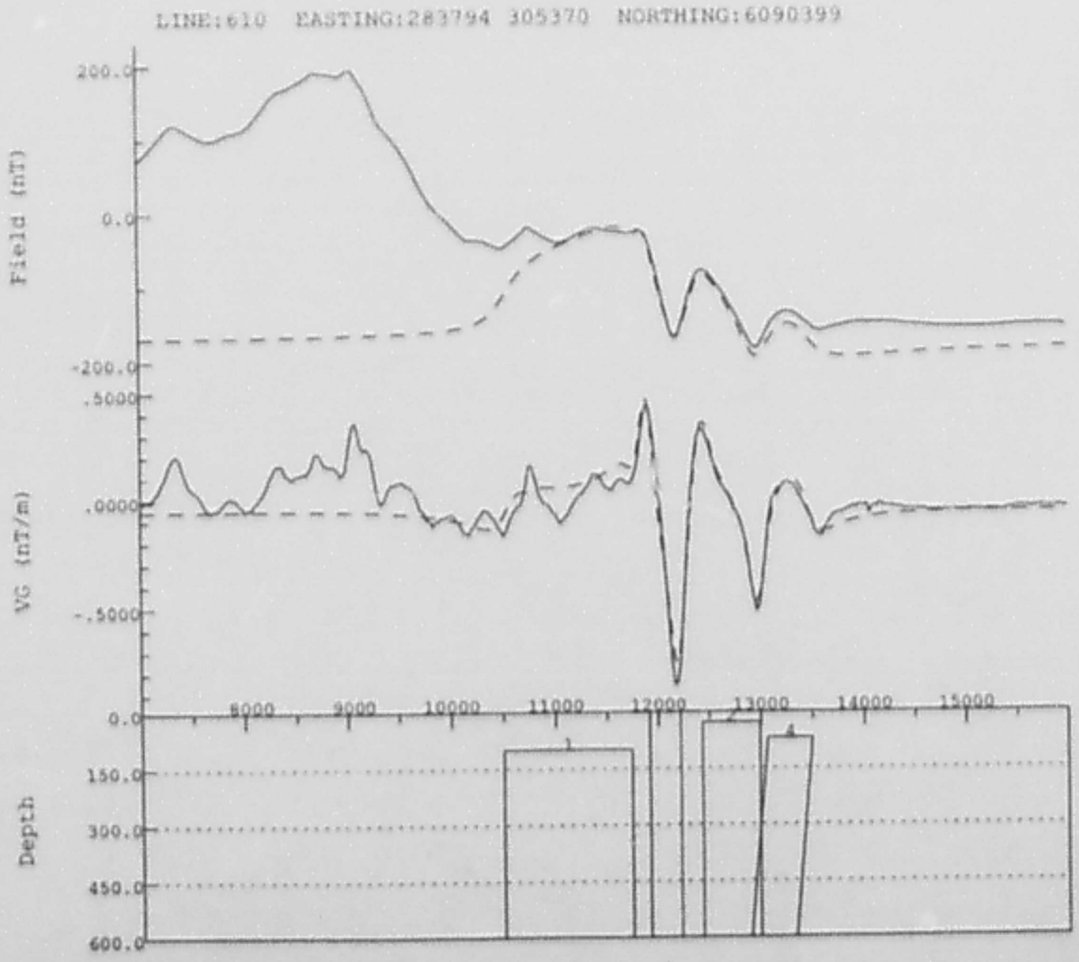
LINE:610 EASTING:283794 305370 NORTHING:6090399
Field (nT)
200.0
0.0
-200.0
VG (nT/m)
.5000
.0000
-.5000
8000
9000
10000
11000
12000
13000
14000
15000
Depth
0.0
150.0
300.0
450.0
600.0

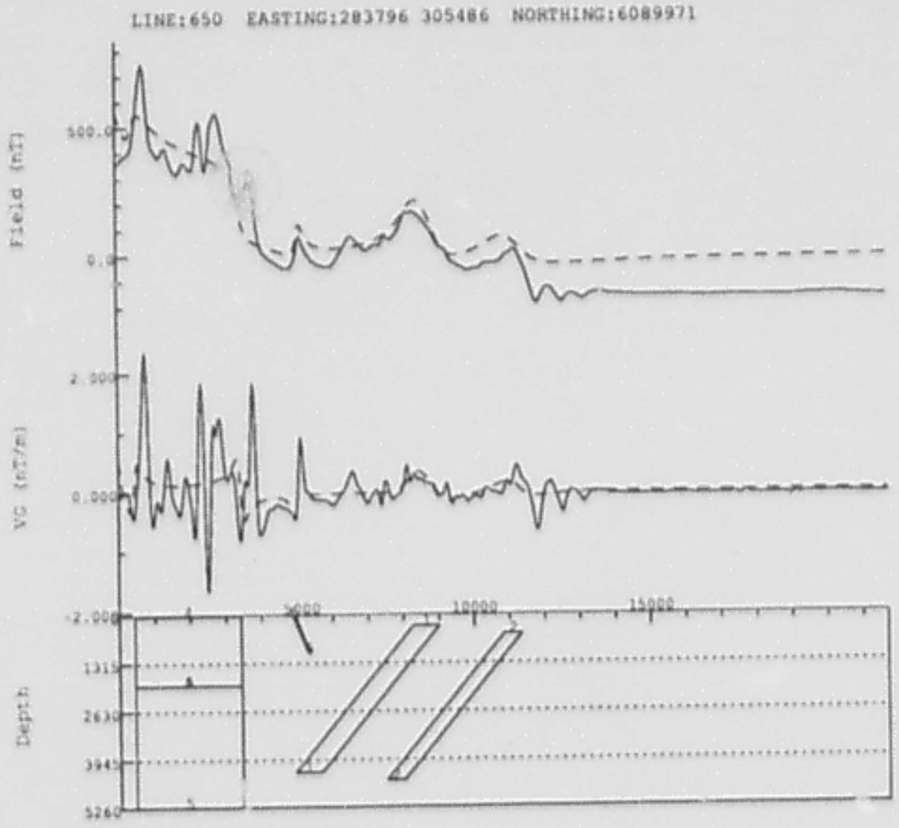
LINE:650 EASTING:283796 305486 NORTHING:6089971
Field (nT)
500.0
0.0
VG (nT/m)
2.000
0.000
-2.000
5000
10000
15000
Depth
1315
2630
3945
5260

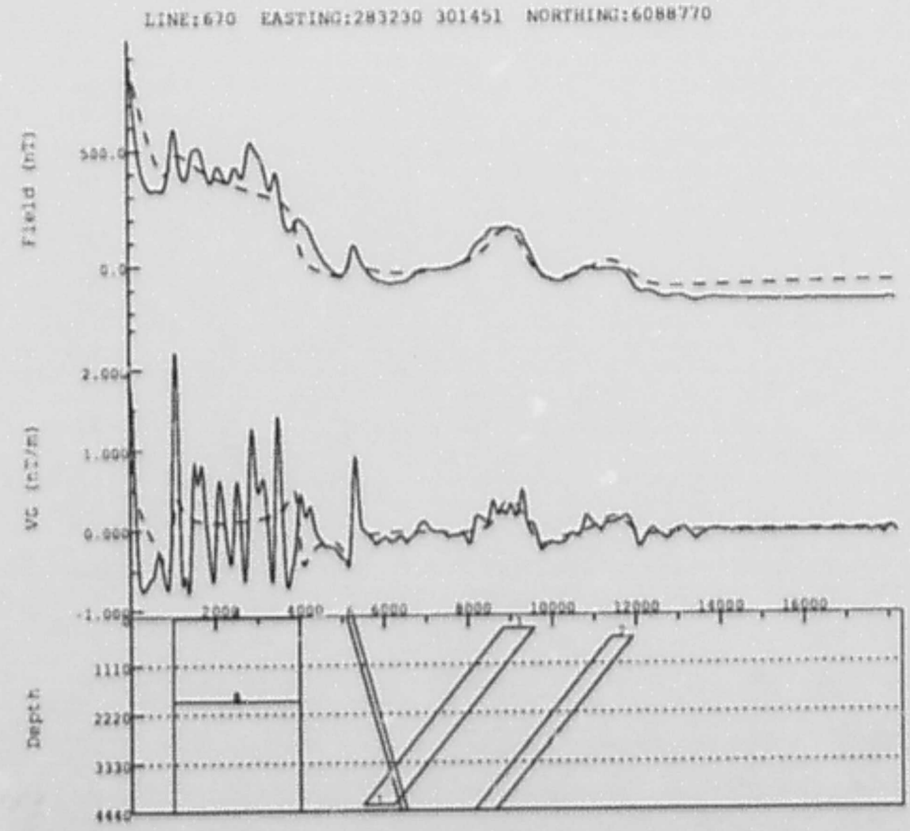
LINE:670 EASTING:283230 301451 NORTHING:6088770
Field (nT)
500.0
0.0
VG (nT/m)
2.000
1.000
0.000
-1.000
2000
4000
6000
8000
10000
12000
14000
16000
Depth
1110
2220
3330
4440

Kanmantoo Survey

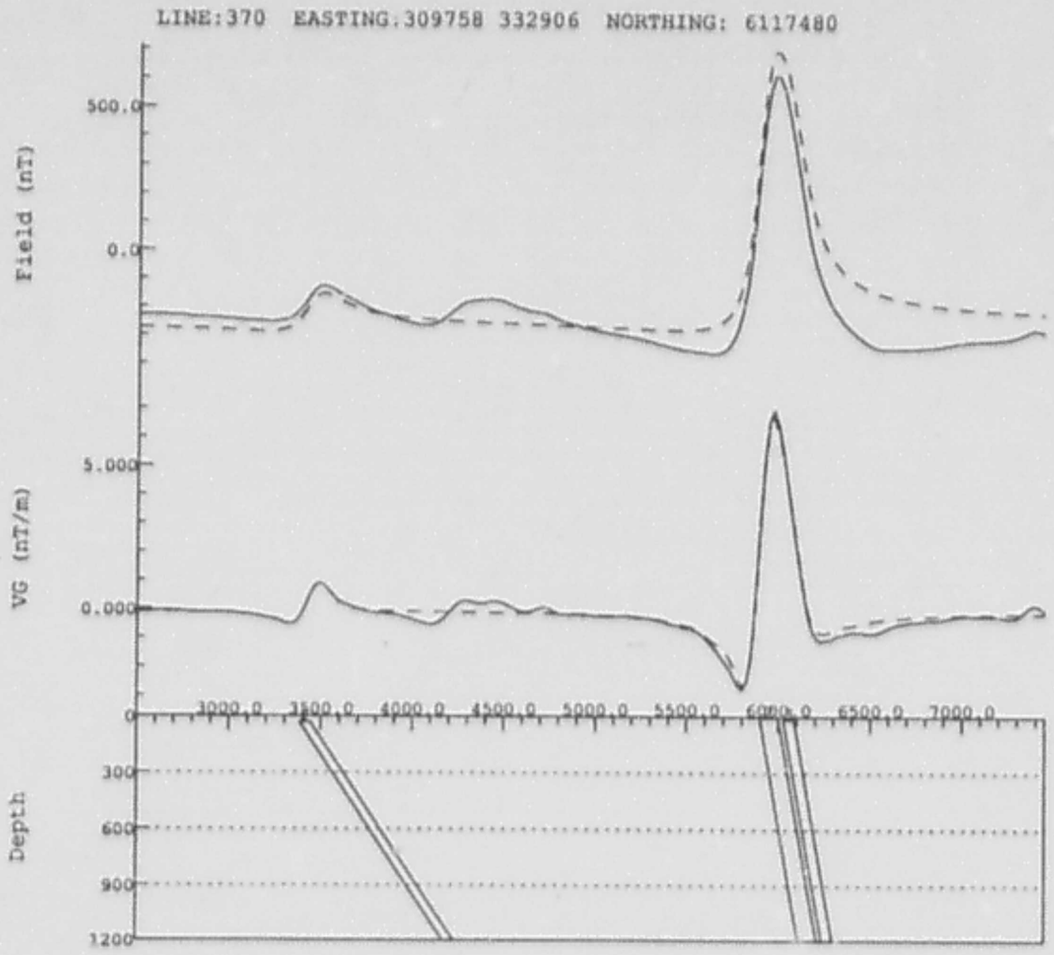
LINE:370 EASTING.309758 332906 NORTHING: 6117480
Field (nT)
500.0
0.0
VG (nT/m)
5.000
0.000
3000.0
3500.0
4000.0
4500.0
5000.0
5500.0
6000.0
6500.0
7000.0
Depth
0
300
600
900
1200

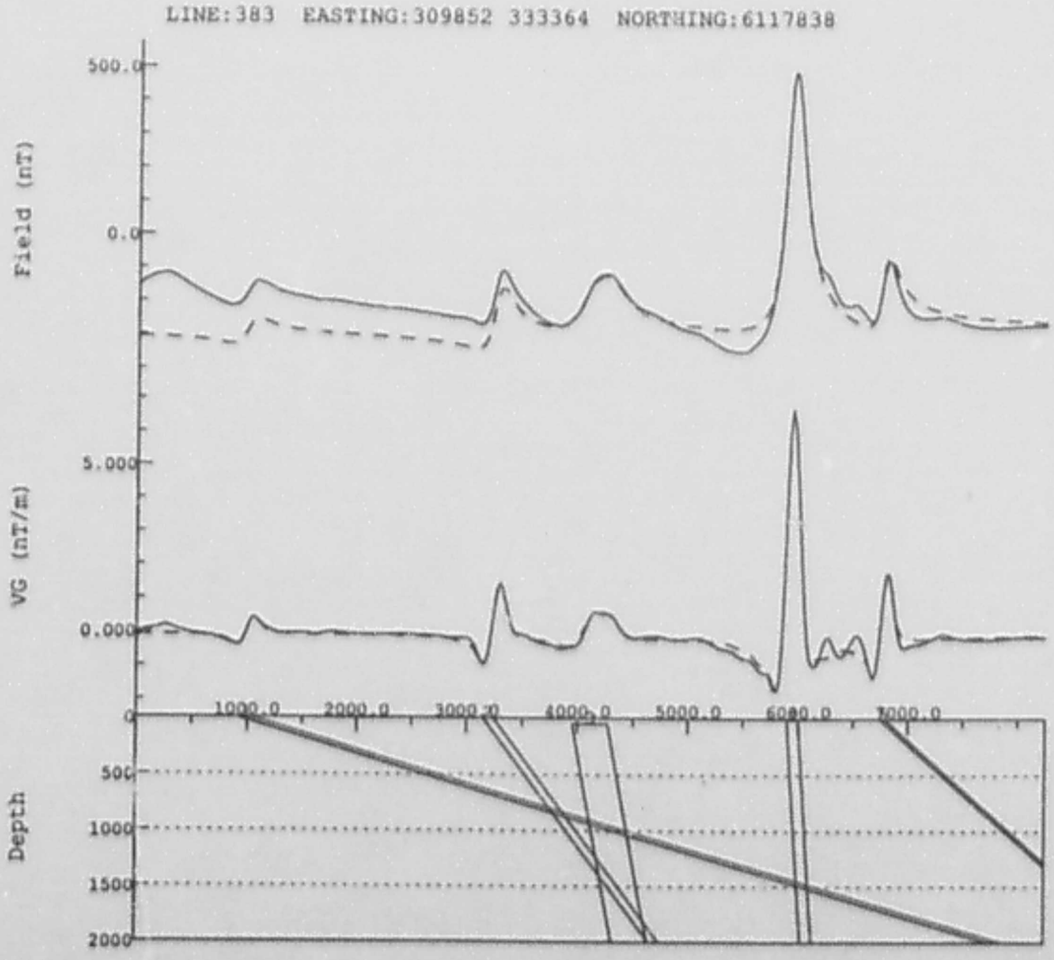
LINE:383 EASTING:309852 333364 NORTHING:6117838
Field (nT)
500.0
0.0
VG (nT/m)
5.000
0.000
1000.0
2000.0
3000.0
4000.0
5000.0
6000.0
7000.0
Depth
0
500
1000
1500
2000

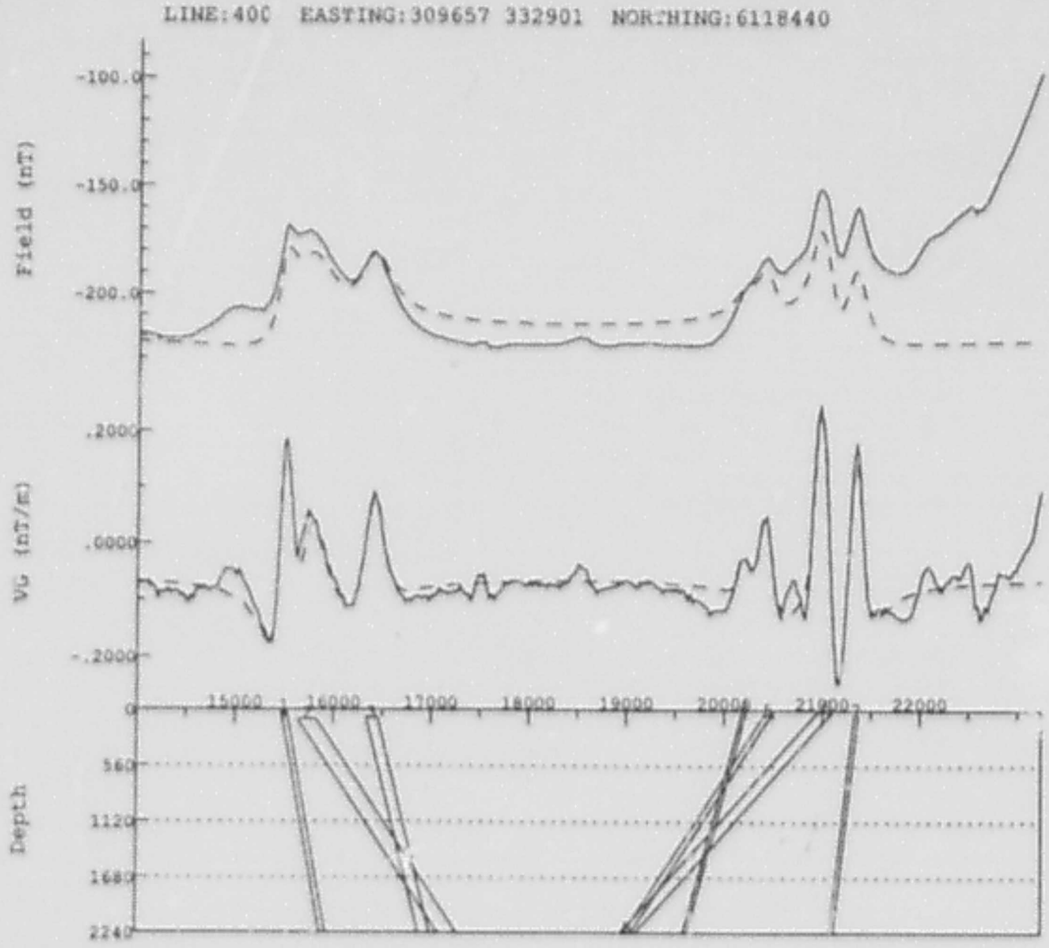
LINE:400 EASTING:309657 332901 NORTHING:6118440
Field (nT)
-100.0
-150.0
-200.0
VG (nT/m)
.2000
.0000
-.2000
15000
16000
17000
18000
19000
20000
21000
22000
Depth
0
560
1120
1680
2240

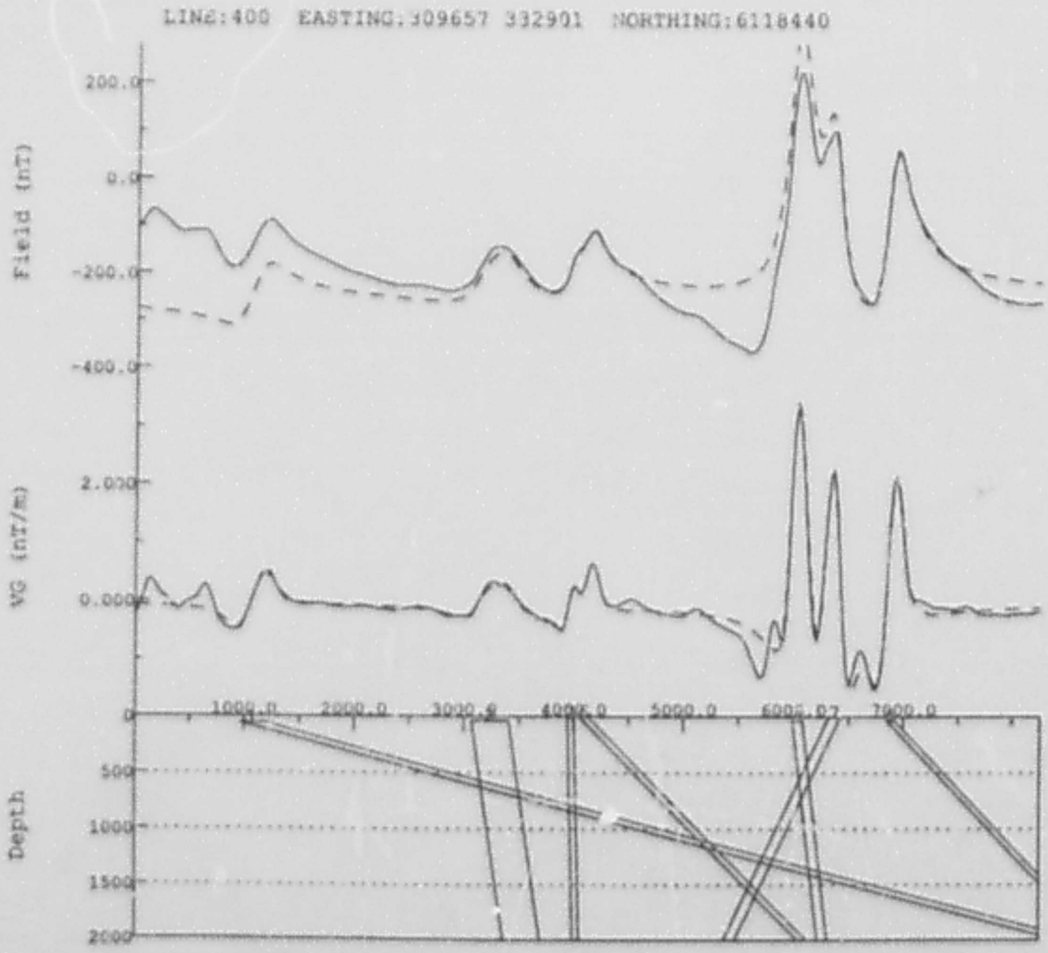
LINE:400 EASTING:309657 332901 NORTHING:6118440
Field (nT)
200.0
0.0
-200.0
-400.0
VG (nT/m)
2.000
0.000
1000.0
2000.0
3000.0
4000.0
5000.0
6000.0
7000.0
Depth
0
500
1000
1500
2000

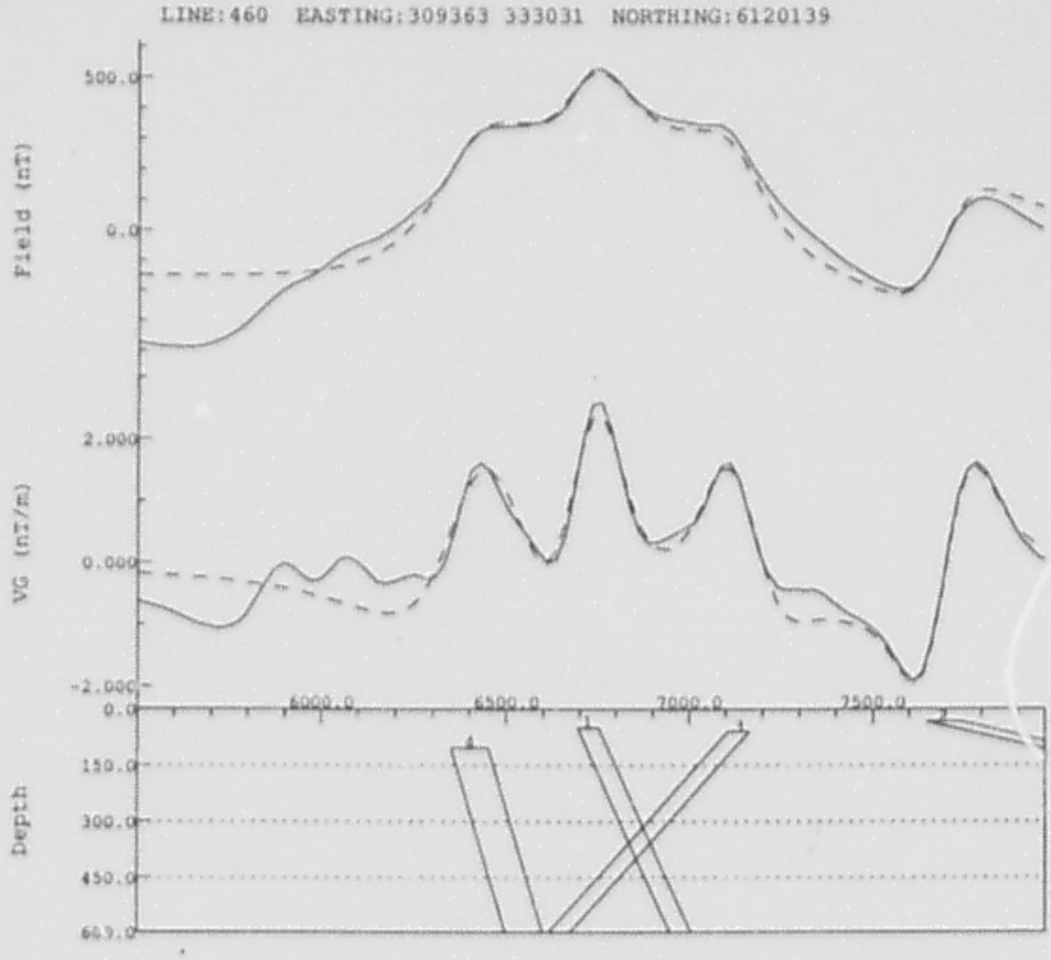
LINE:460 EASTING:309363 333031 NORTHING:6120139
Field (nT)
500.0
0.0
VG (nT/m)
2.000
0.000
-2.000
6000.0
6500.0
7000.0
7500.0
Depth
0.0
150.0
300.0
450.0
669.0

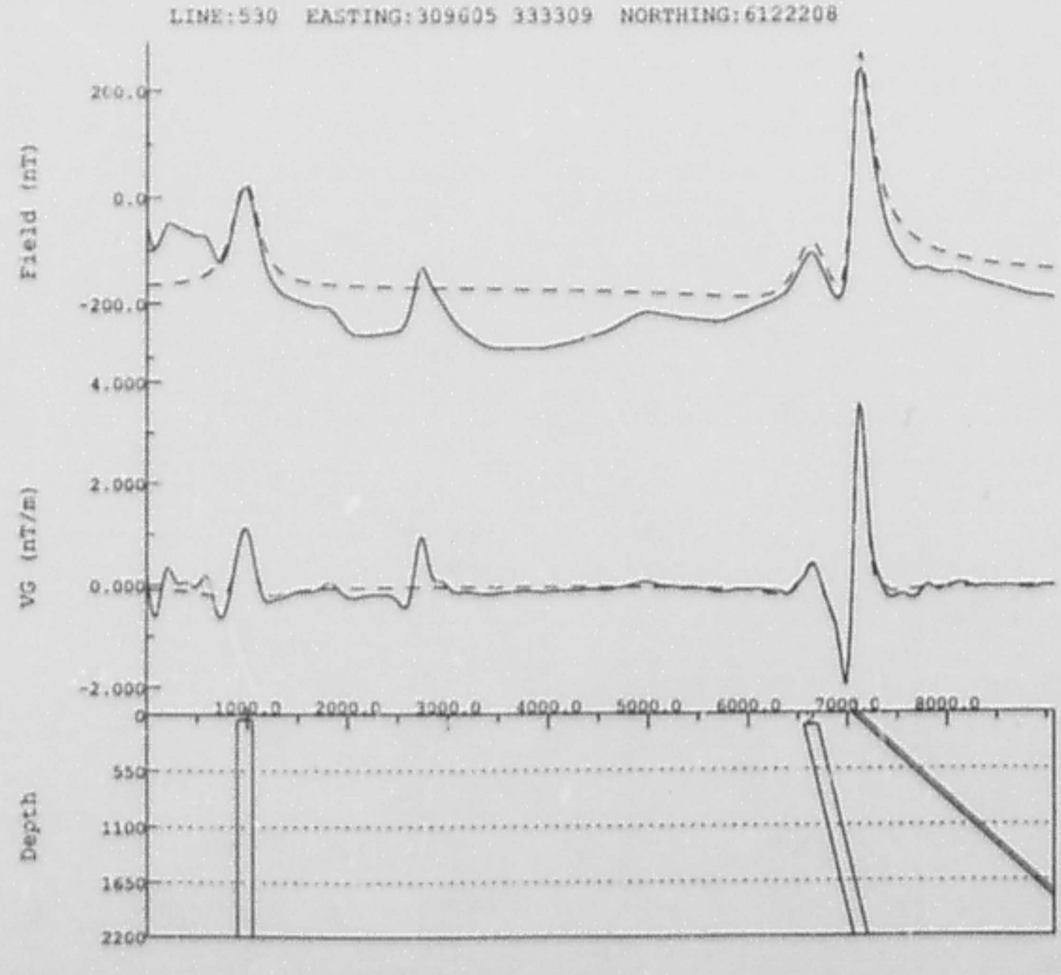
LINE:530 EASTING:309605 333309 NORTHING:6122208
Field (nT)
200.0
0.0
-200.0
VG (nT/m)
4.000
2.000
0.000
-2.000
1000.0
2000.0
3000.0
4000.0
5000.0
6000.0
7000.0
8000.0
Depth
0
550
1100
1650
2200

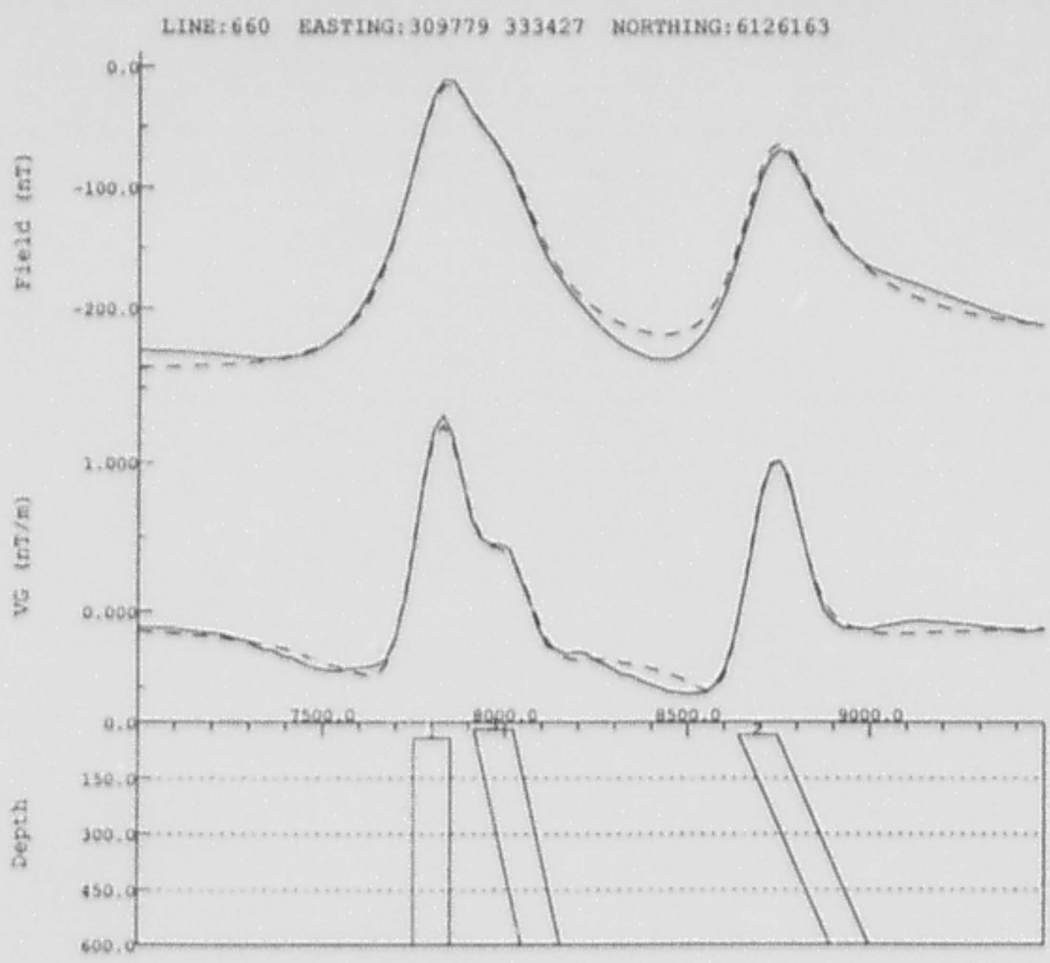
LINE:660 EASTING:309779 333427 NORTHING:6126163
Field (nT)
0.0
-100.0
-200.0
VG (nT/m)
1.000
0.000
Depth
0.0
150.0
300.0
450.0
600.0
7500.0
8000.0
8500.0
9000.0

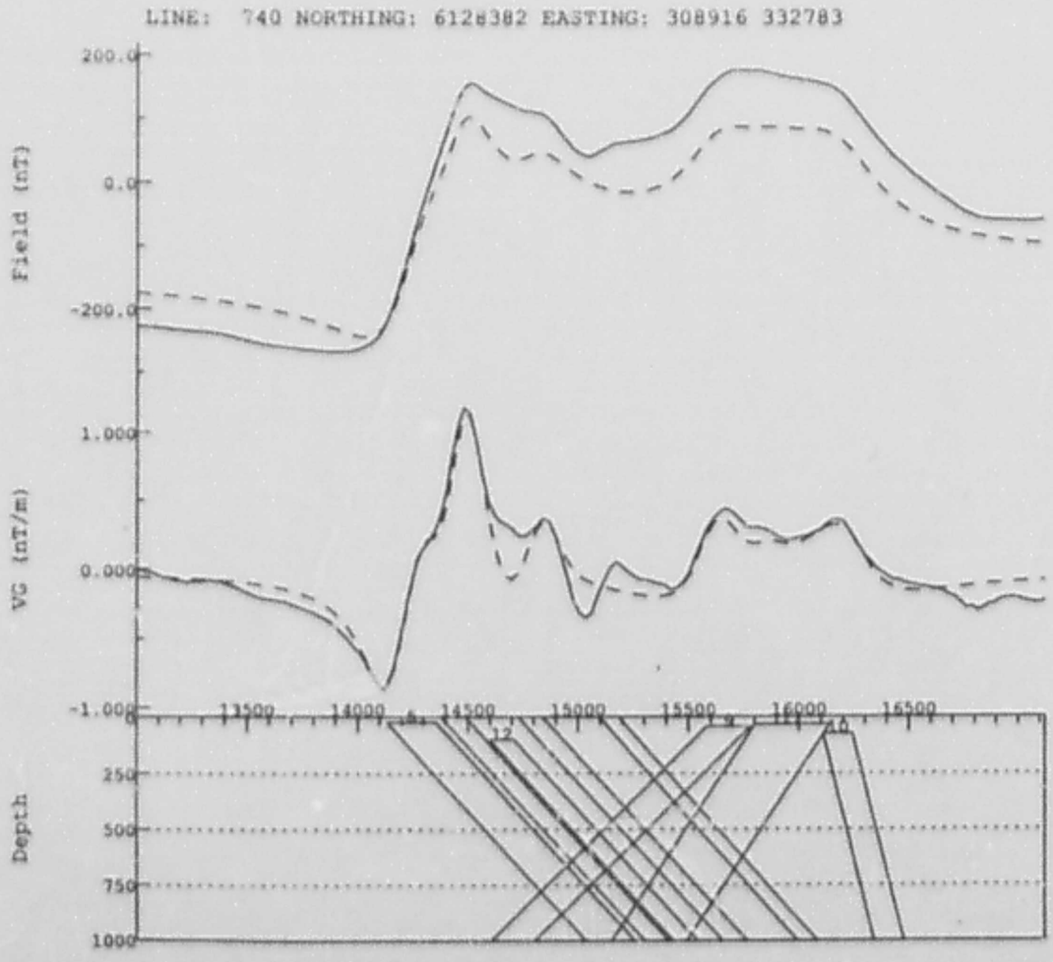
LINE: 740 NORTHING: 6128382 EASTING: 308916 332783
Field (nT)
200.0
0.0
-200.0
VG (nT/m)
1.000
0.000
-1.000
Depth
0.0
250
500
750
1000
13500
14000
14500
15000
15500
16000
16500

LINE: 740 NORTHING: 6128382 EASTING: 308916 332783

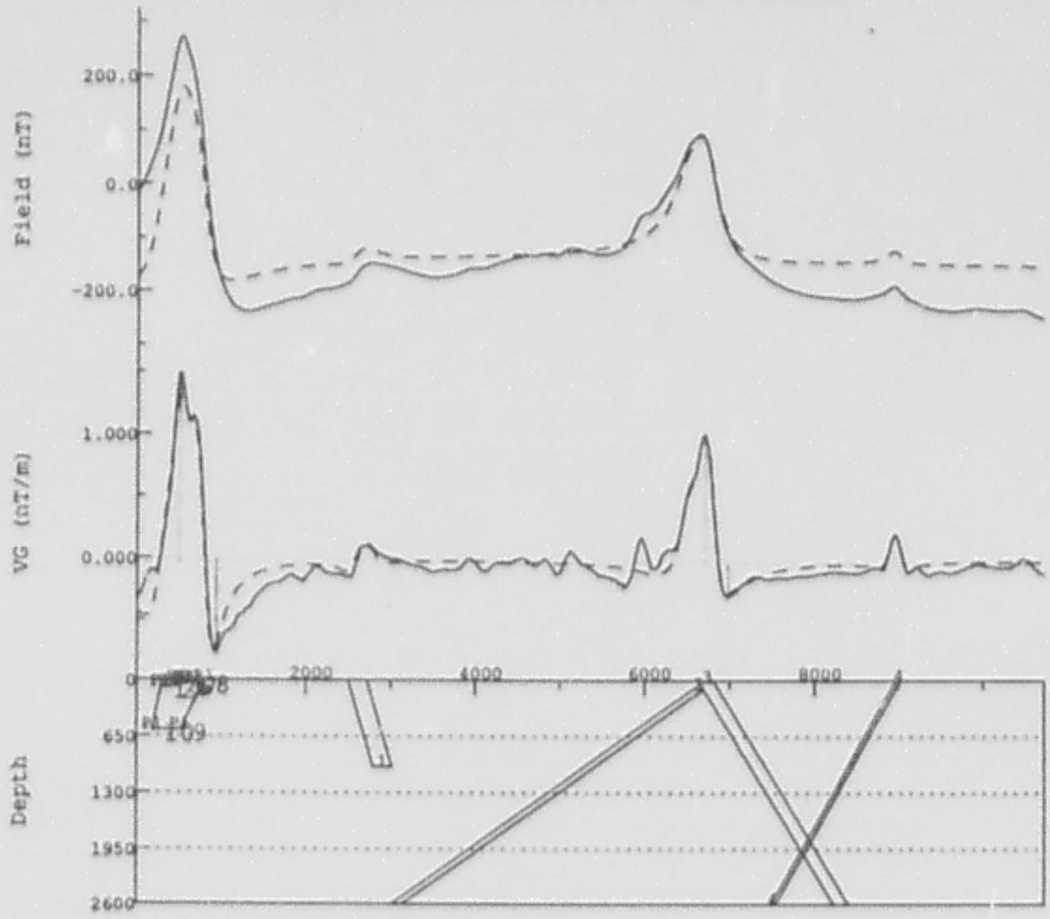

LINE:780 EASTING:309183 333001 NORTHING:6129742

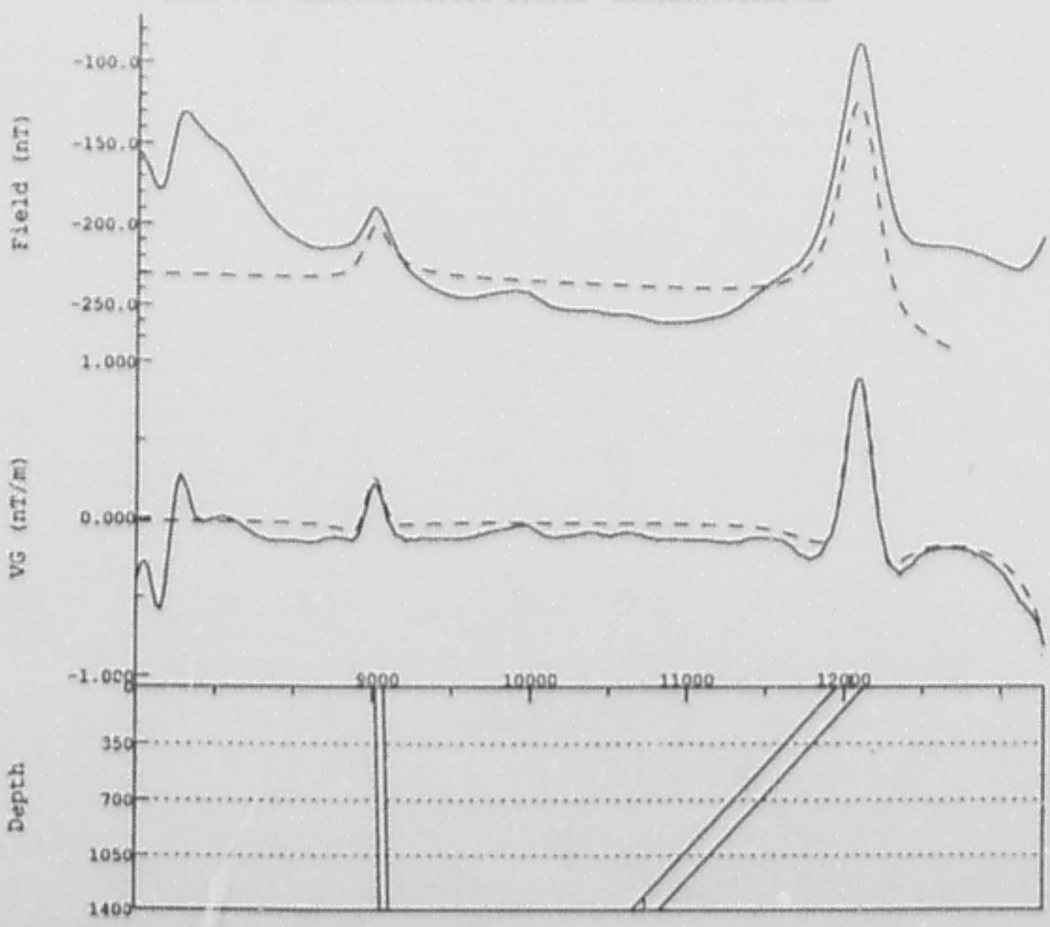

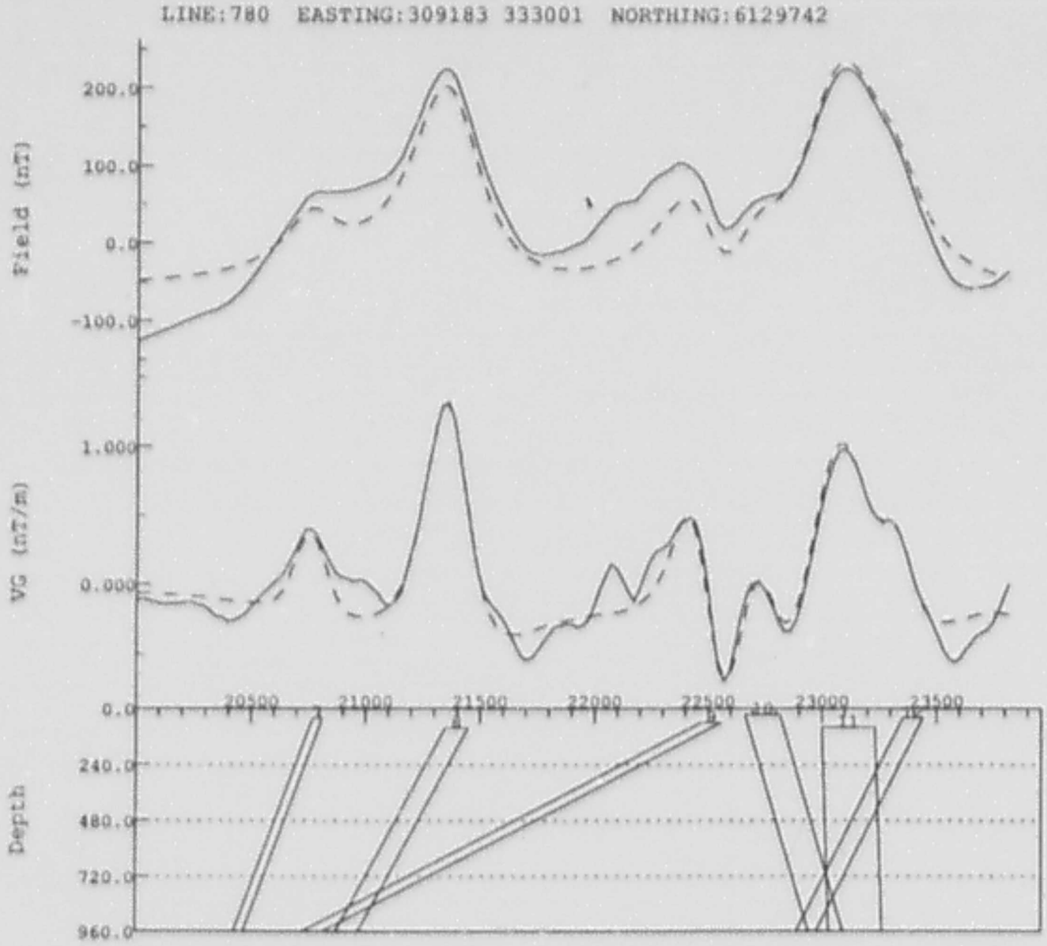
LINE:780 EASTING:309183 333001 NORTHING:6129742
Field (nT)
200.0
100.0
0.0
-100.0
VG (nT/m)
1.000
0.000
0.0
20500
21000
21500
22000
22500
23000
23500
Depth
240.0
480.0
720.0
960.0

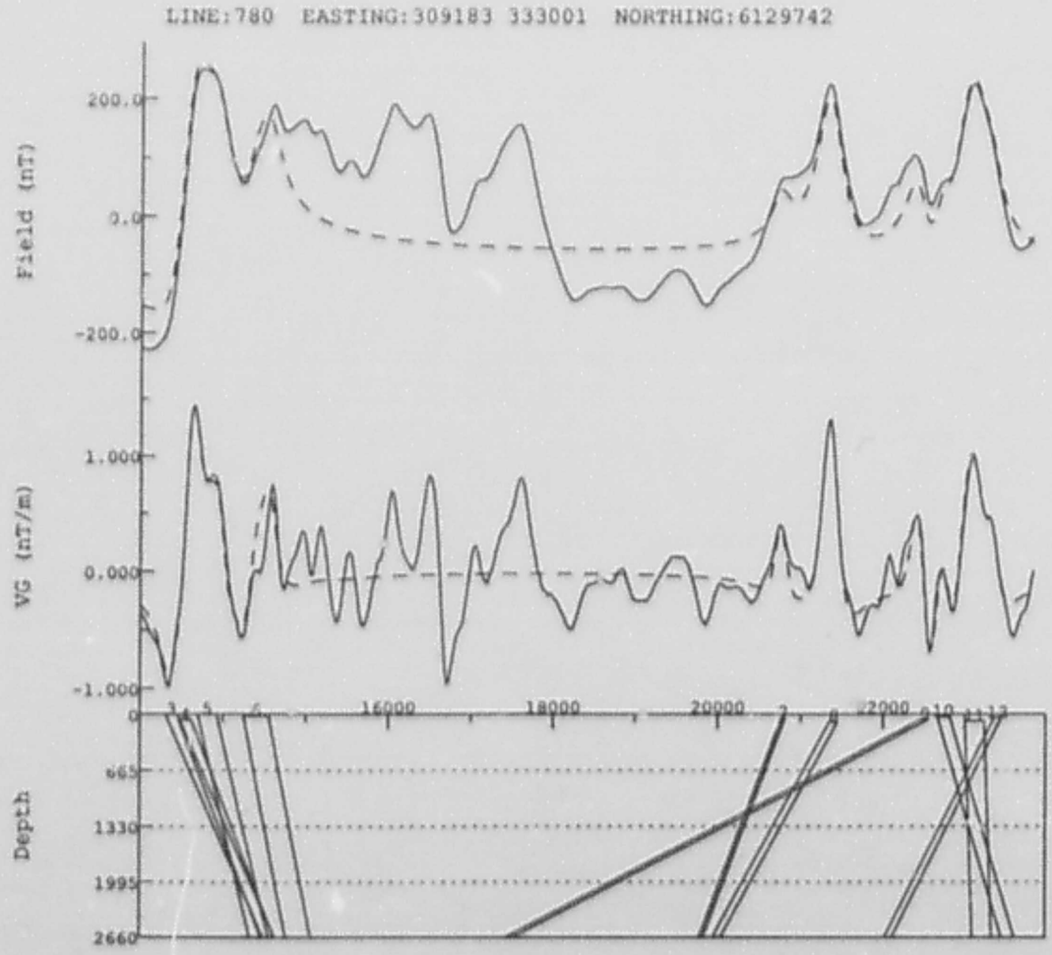
LINE:780 EASTING:309183 333001 NORTHING:6129742
Field (nT)
200.0
0.0
-200.0
VG (nT/m)
1.000
0.000
-1.000
16000
18000
20000
Depth
665
1330
1995
2660

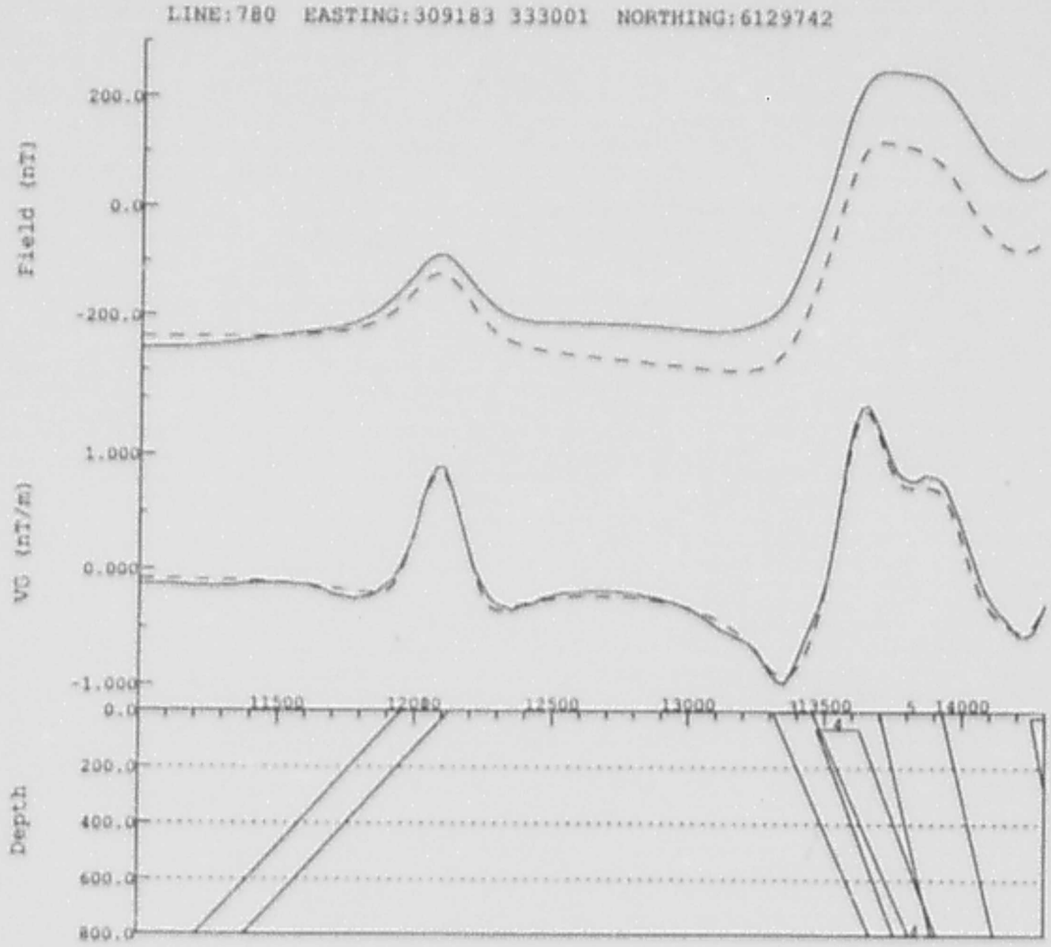
LINE:780 EASTING:309183 333001 NORTHING:6129742
Field (nT)
200.0
0.0
-200.0
VG (nT/m)
1.000
0.000
-1.000
11500
12000
12500
13000
13500
14000
Depth
0.0
200.0
400.0
600.0
800.0

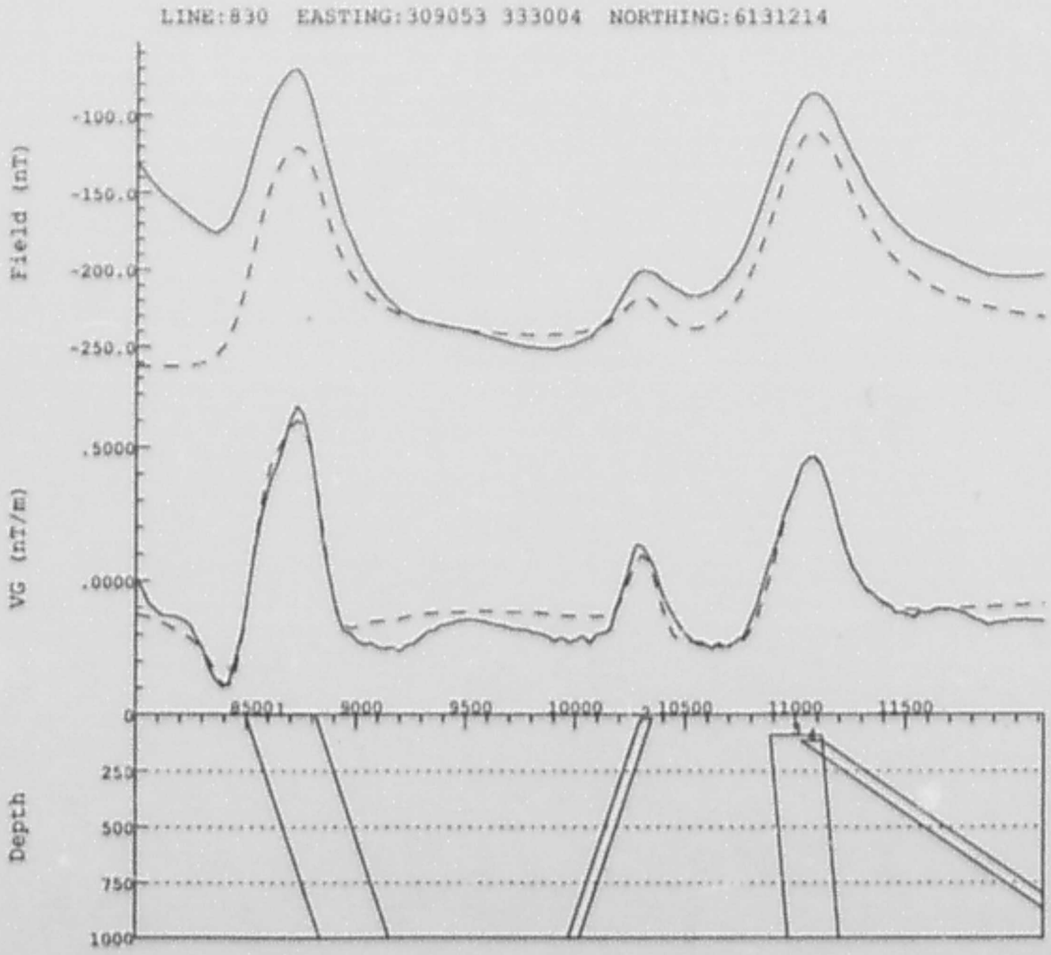
LINE:830 EASTING:309053 333004 NORTHING:6131214
Field (nT)
-100.0
-150.0
-200.0
-250.0
VG (nT/m)
.5000
.0000
8500
9000
9500
10000
10500
11000
11500
Depth
0
250
500
750
1000

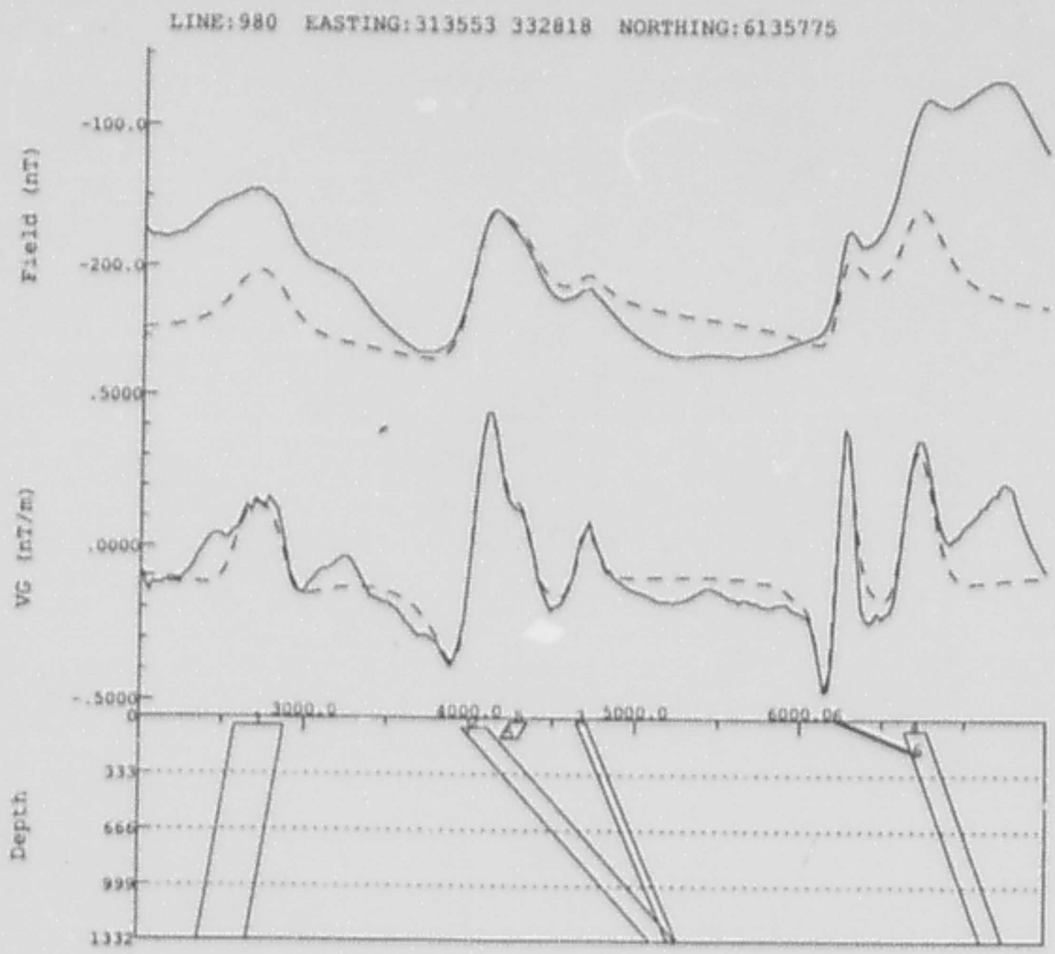
LINE:980 EASTING:313553 332818 NORTHING:6135775
Field (nT)
-100.0
-200.0
VG (nT/m)
.5000
.0000
-.5000
3000.0
4000.0
5000.0
6000.0
Depth
0
333
666
999
1332

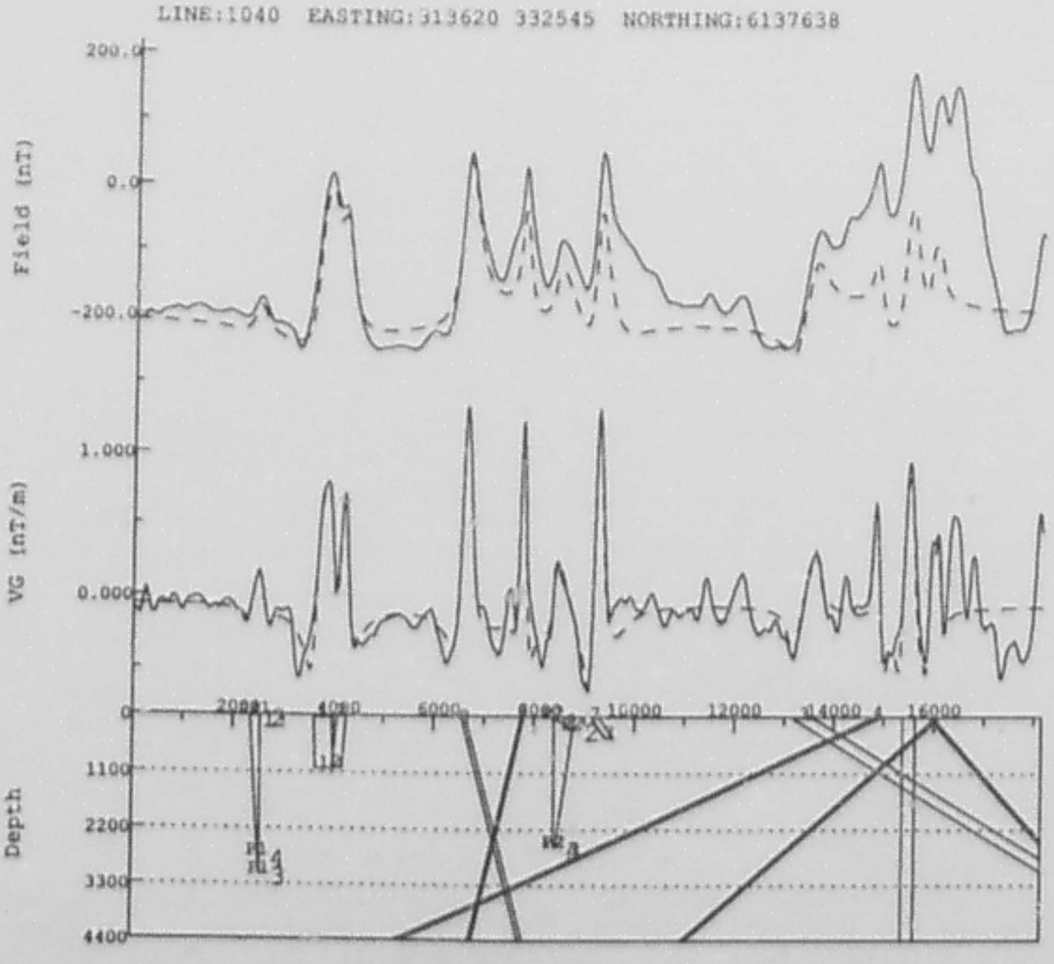
LINE:1040 EASTING:313620 332545 NORTHING:6137638
Field (nT)
200.0
0.0
-200.0
VG (nT/m)
1.000
0.000
Depth
0
1100
2200
3300
4400

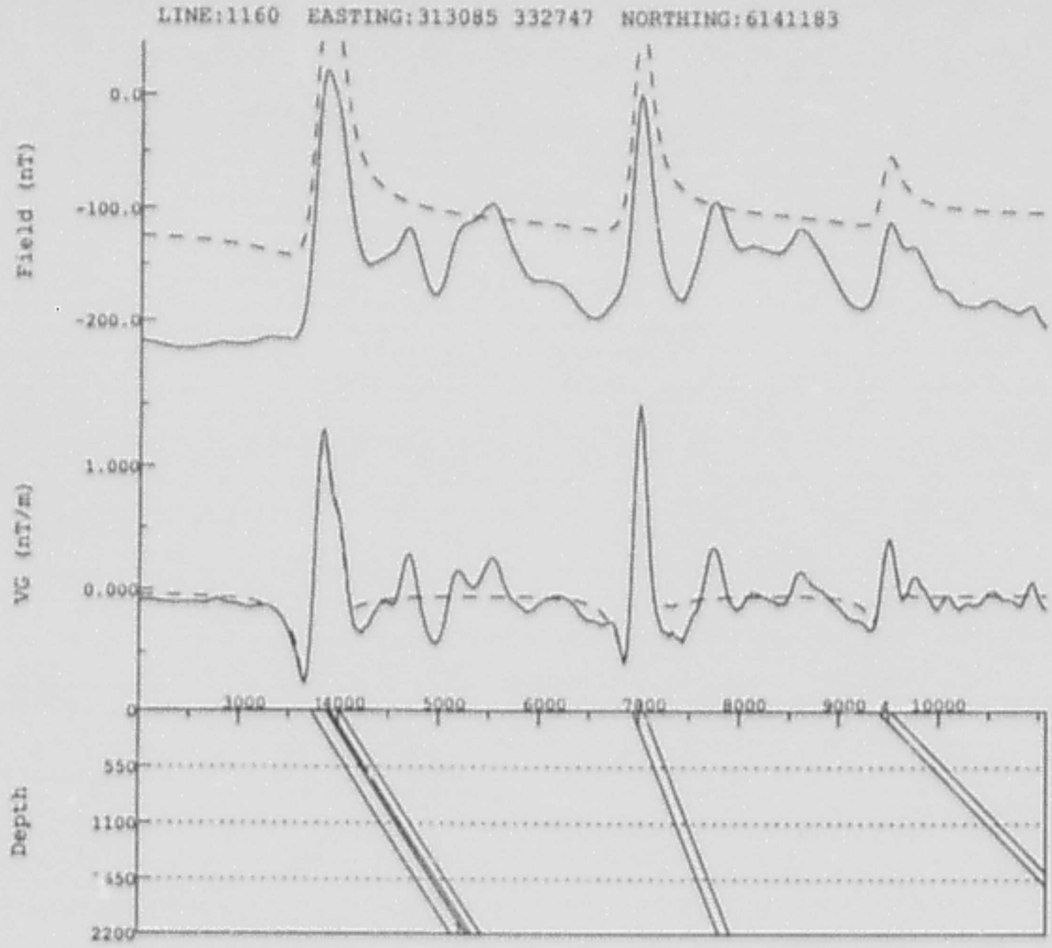
LINE:1160 EASTING:313085 332747 NORTHING:6141183
Field (nT)
0.0
-100.0
-200.0
VG (nT/m)
1.000
0.000
3000
4000
5000
6000
7000
8000
9000
10000
Depth
0
550
1100
1650
2200

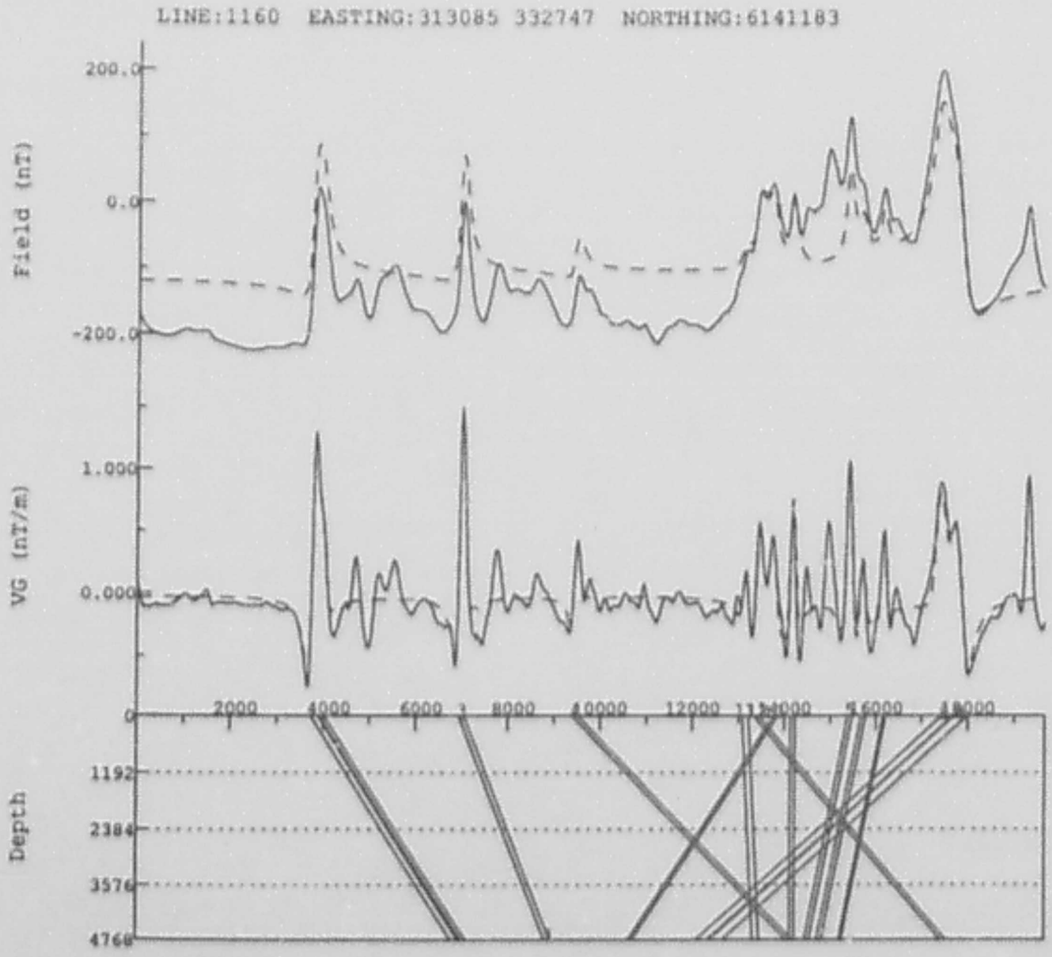
LINE:1160 EASTING:313085 332747 NORTHING:6141183
Field (nT)
200.0
0.0
-200.0
VG (nT/m)
1.000
0.000
2000
4000
6000
8000
10000
12000
14000
16000
18000
Depth
0
1192
2384
3576
4768

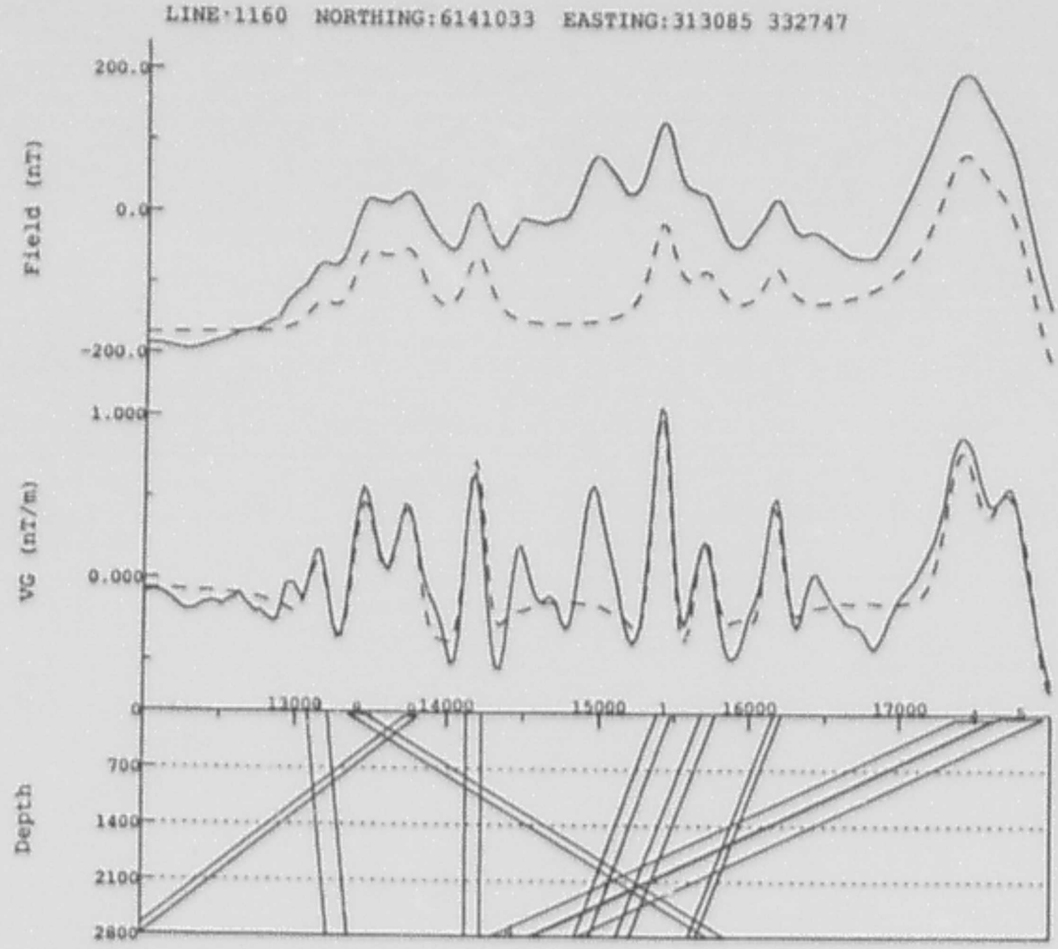
LINE·1160 NORTHING:6141033 EASTING:313085 332747
Field (nT)
200.0
0.0
-200.0
VG (nT/m)
1.000
0.000
Depth
0
700
1400
2100
2800
13000
14000
15000
16000
17000

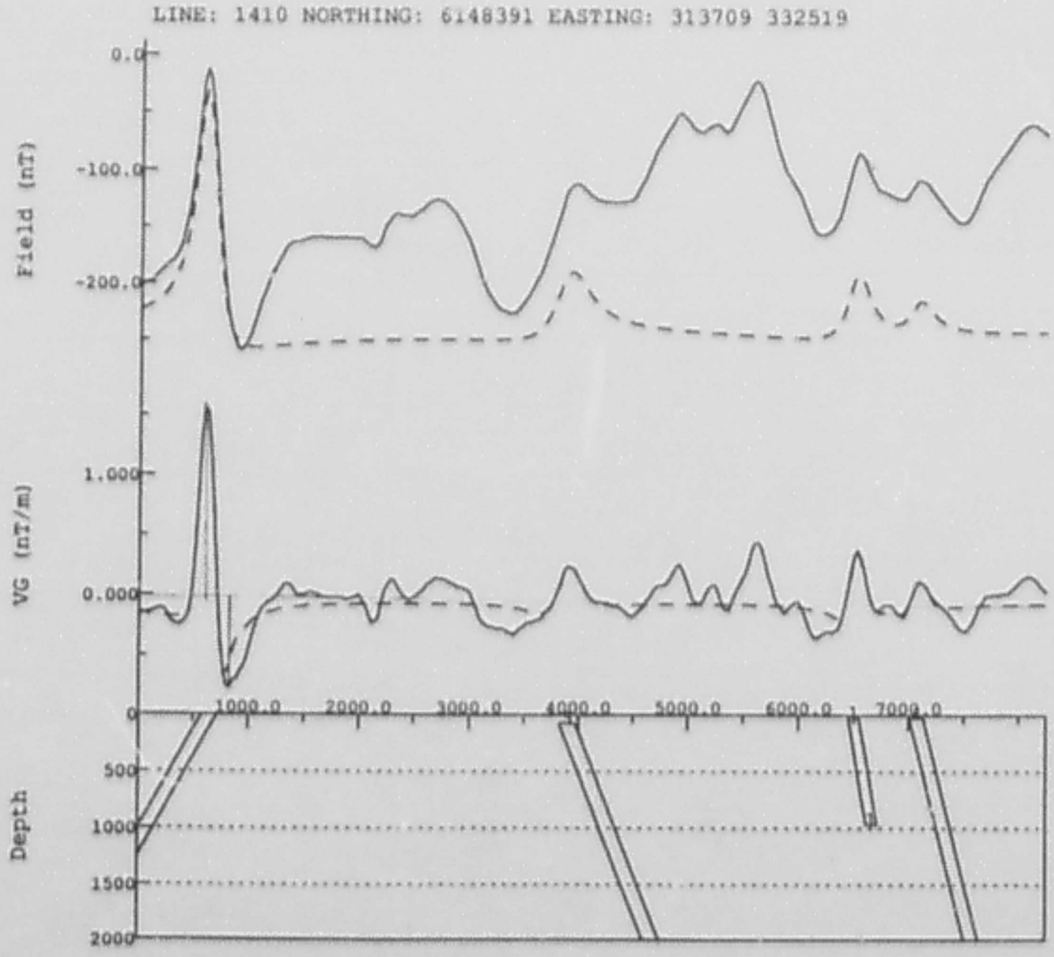
LINE: 1410 NORTHING: 6148391 EASTING: 313709 332519
Field (nT)
0.0
-100.0
-200.0
VG (nT/m)
1.000
0.000
Depth
0
500
1000
1500
2000
1000.0
2000.0
3000.0
4000.0
5000.0
6000.0
7000.0

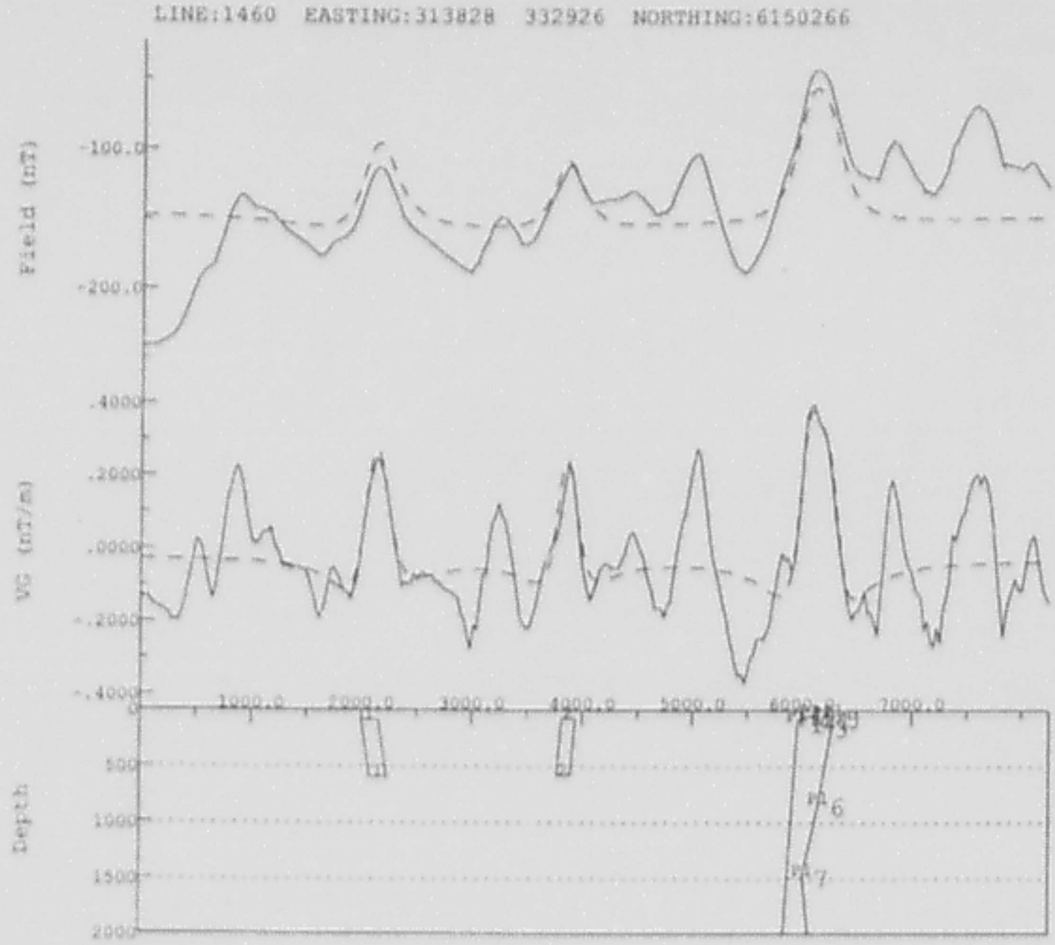
LINE:1460 EASTING:313828 332926 NORTHING:6150266
Field (nT)
-100.0
-200.0
VG (nT/m)
.4000
.2000
.0000
-.2000
-.4000
1000.0
2000.0
3000.0
4000.0
5000.0
6000.0
7000.0
Depth
0
500
1000
1500
2000
6
7

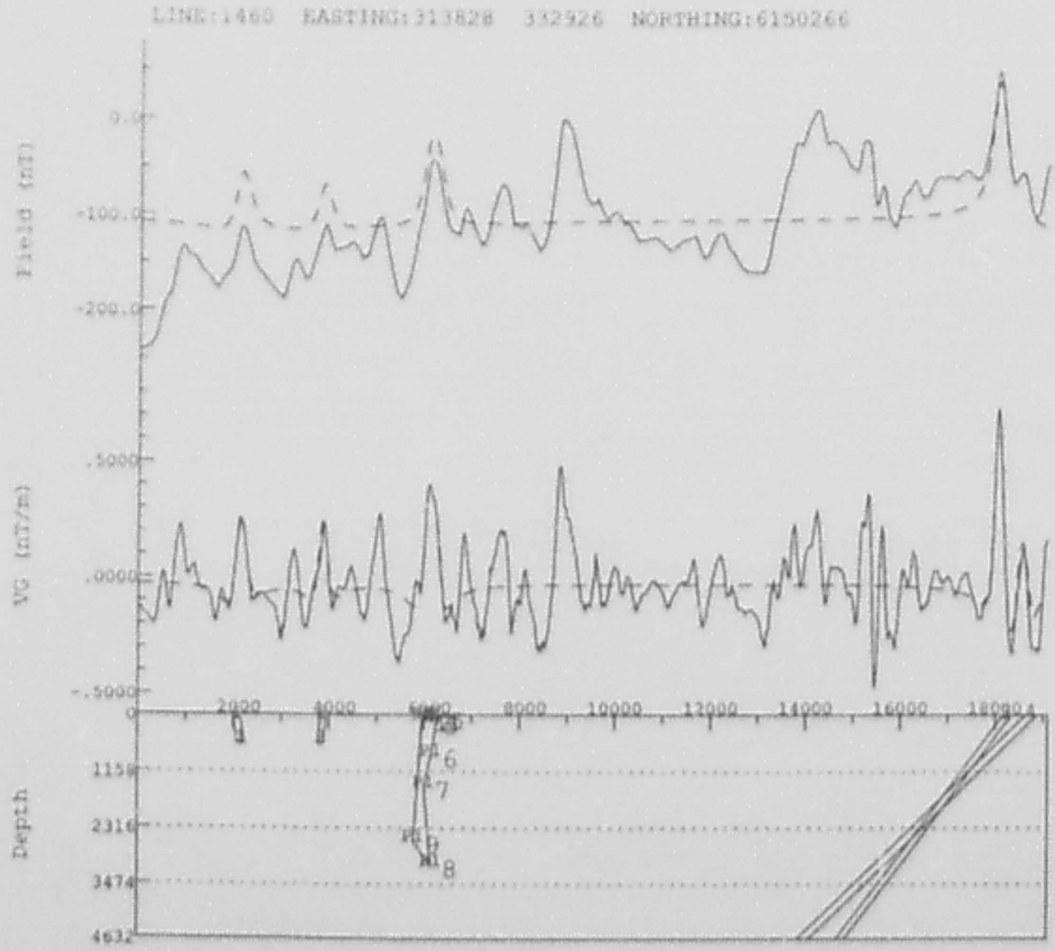
LINE:1460 EASTING:313828 332926 NORTHING:6150266
Field (nT)
0.0
-100.0
-200.0
VG (nT/m)
.5000
.0000
-.5000
2000
4000
6000
8000
10000
12000
14000
16000
18000
Depth
1158
2316
3474
4632
6
7
8

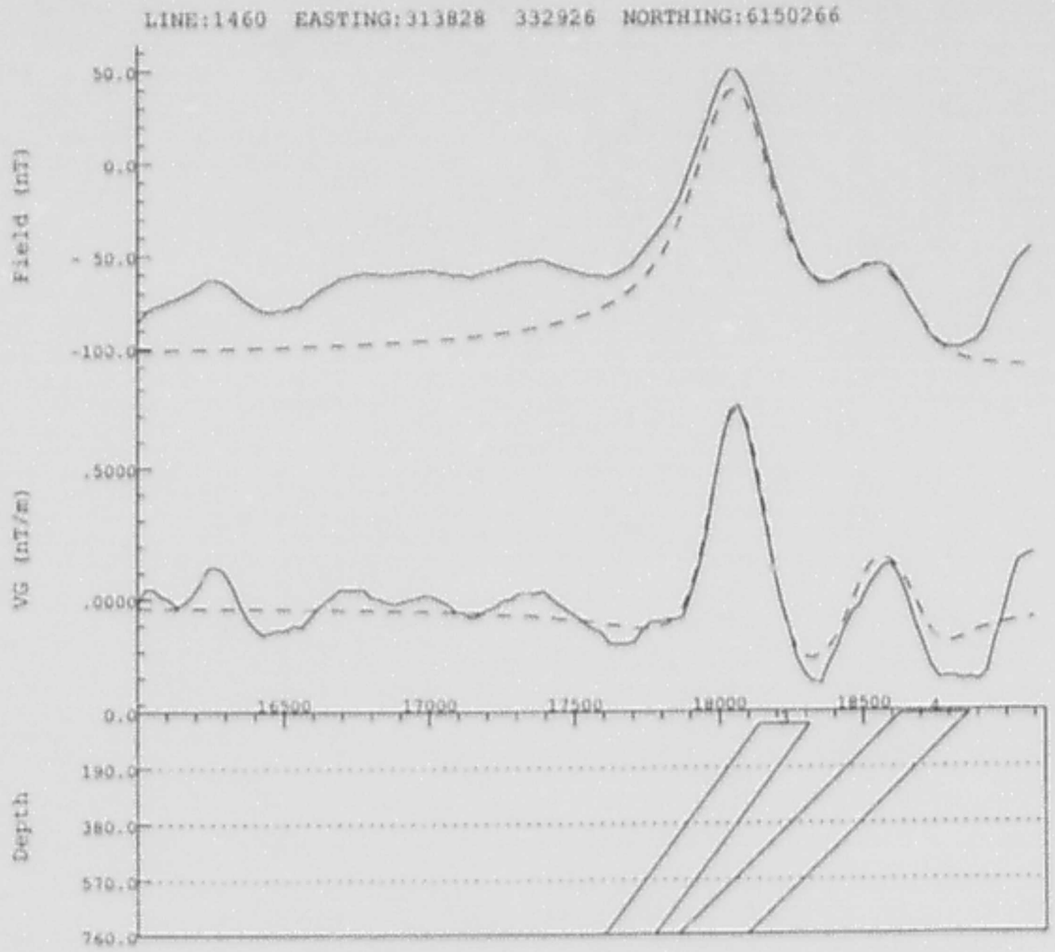
LINE:1460 EASTING:313828 332926 NORTHING:6150266
Field (nT)
50.0
0.0
-50.0
-100.0
VG (nT/m)
.5000
.0000
0.0
16500
17000
17500
18000
18500
Depth
190.0
380.0
570.0
760.0

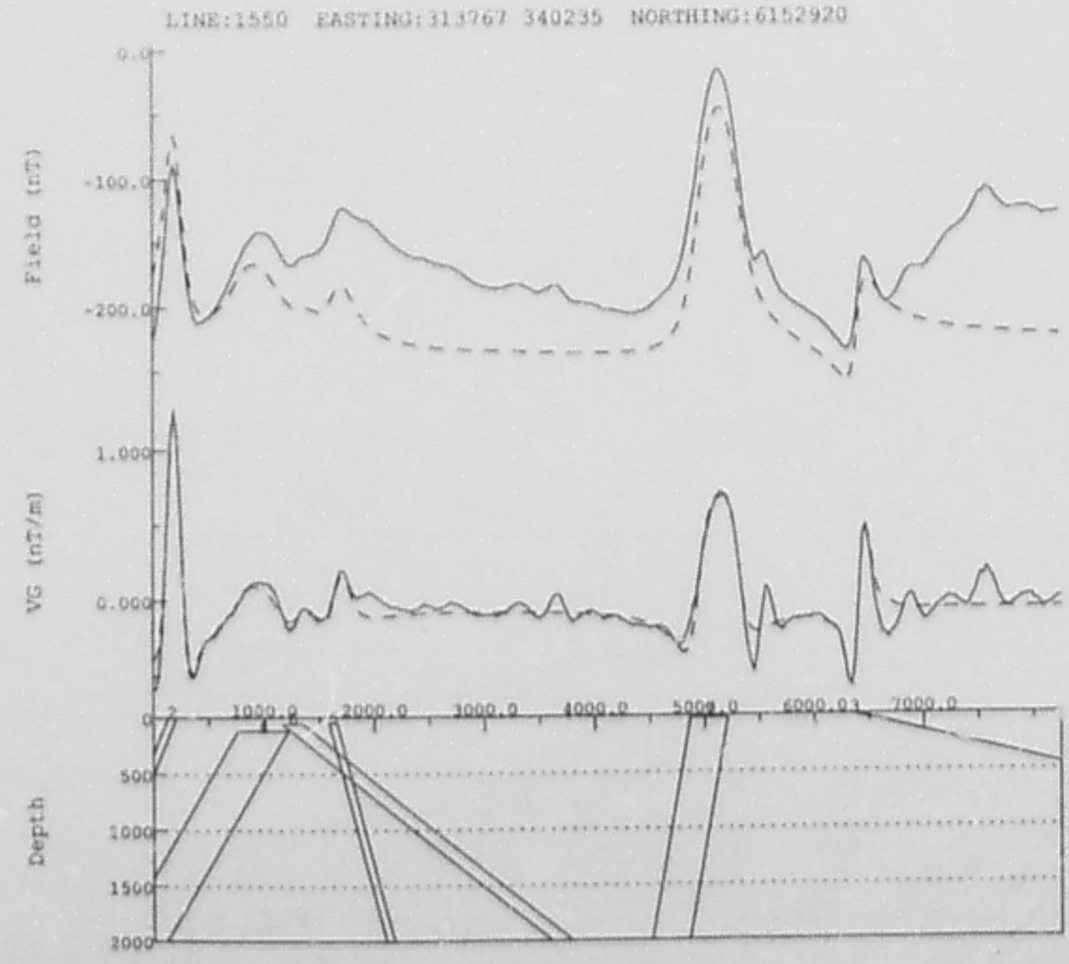
LINE:1550 EASTING:313767 340235 NORTHING:6152920
Field (nT)
0.0
-100.0
-200.0
VG (nT/m)
1.000
0.000
0
1000.0
2000.0
3000.0
4000.0
5000.0
6000.0
7000.0
Depth
500
1000
1500
2000

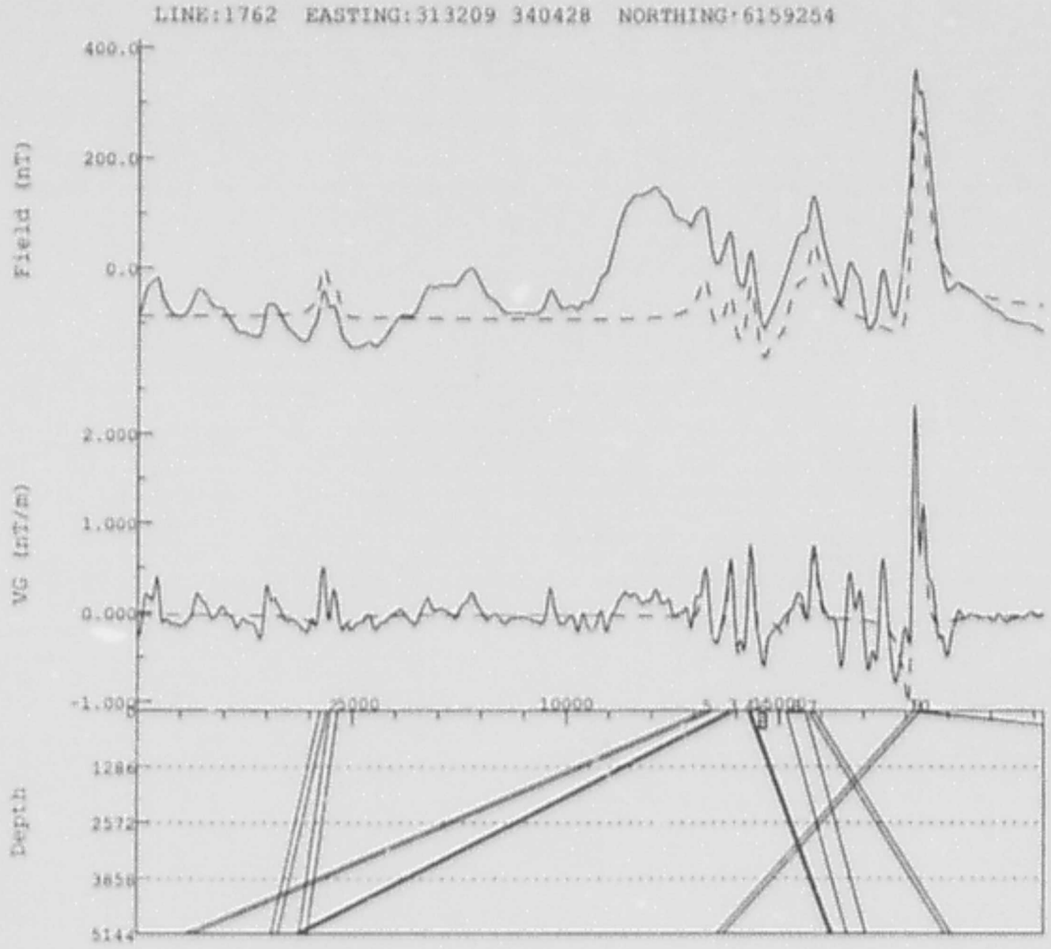
LINE:1762 EASTING:313209 340428 NORTHING:6159254
Field (nT)
400.0
200.0
0.0
VG (nT/m)
2.000
1.000
0.000
-1.000
20000
10000
Depth
1286
2572
3858
5144

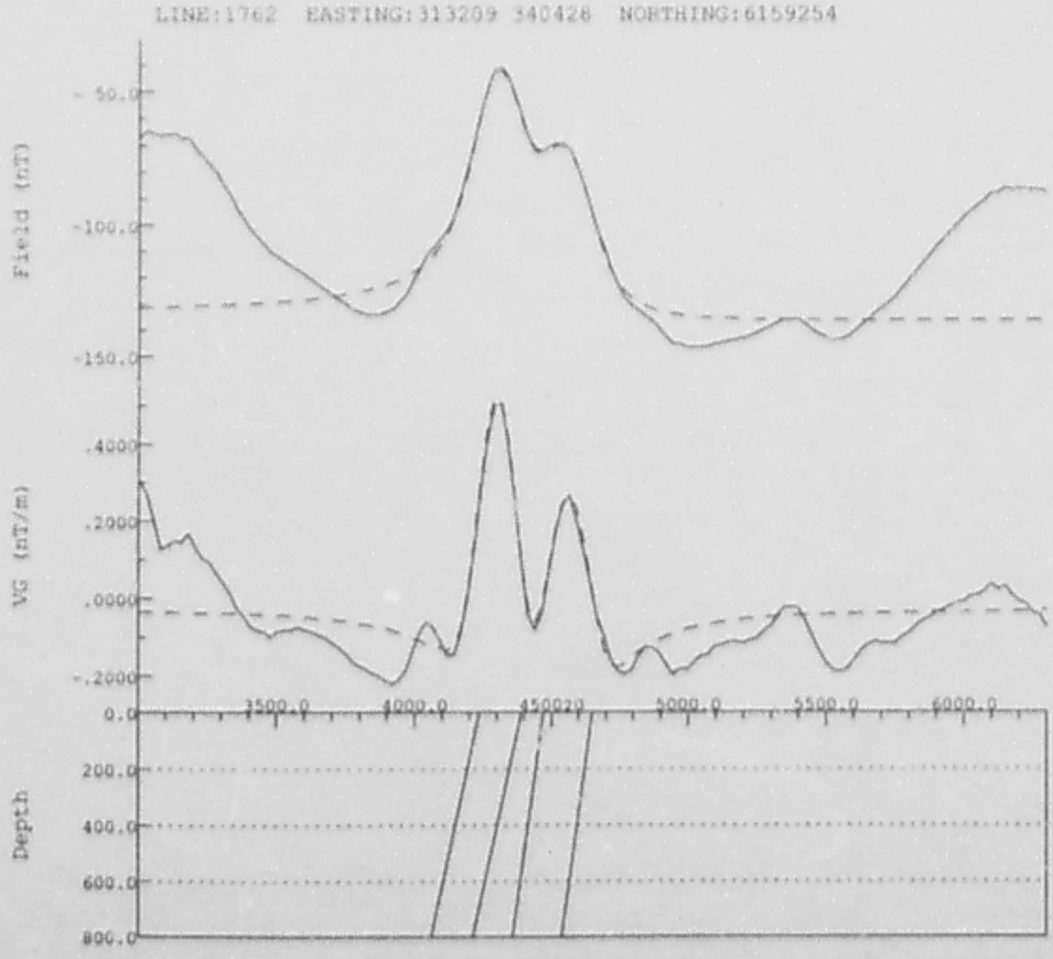
LINE:1762 EASTING:313209 340428 NORTHING:6159254
Field (nT)
-50.0
-100.0
-150.0
VG (nT/m)
.4000
.2000
.0000
-.2000
3500.0
4000.0
4500.0
5000.0
5500.0
6000.0
Depth
0.0
200.0
400.0
600.0
800.0

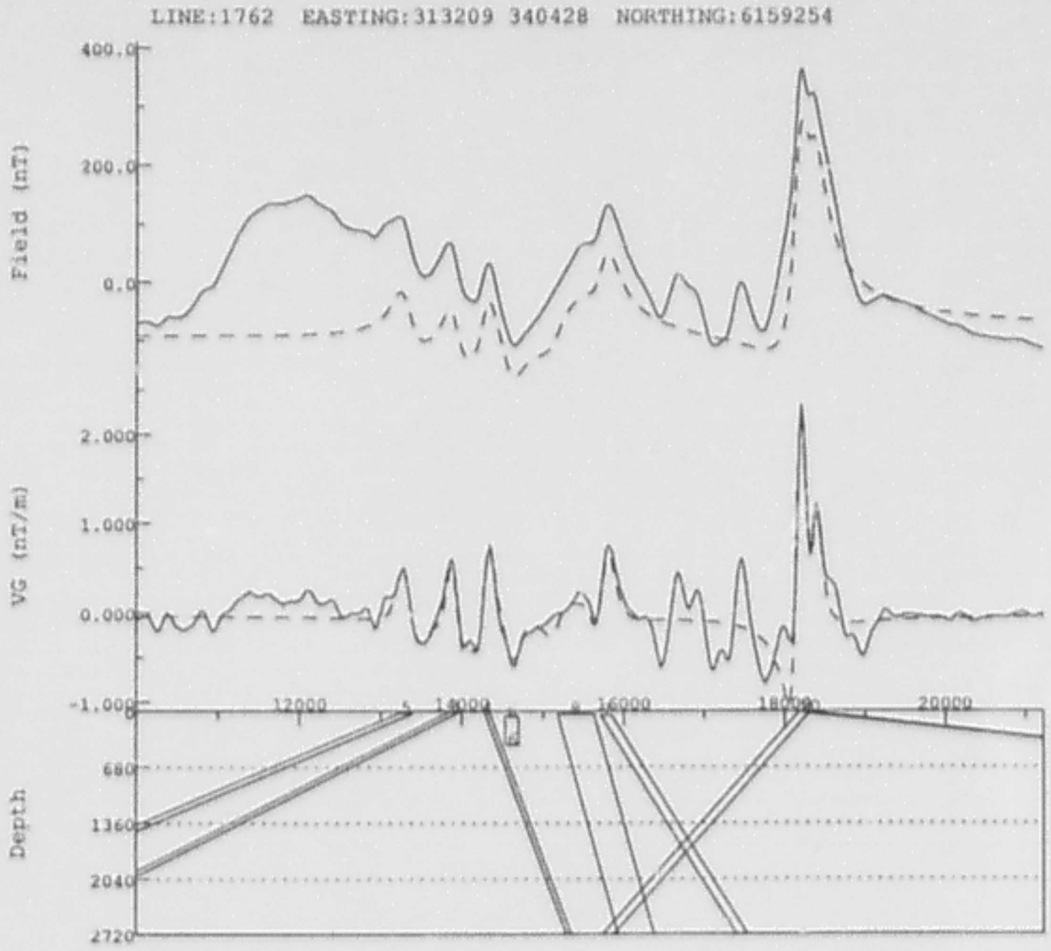
LINE:1762 EASTING:313209 340428 NORTHING:6159254
Field (nT)
400.0
200.0
0.0
VG (nT/m)
2.000
1.000
0.000
-1.000
12000
16000
20000
Depth
680
1360
2040
2720

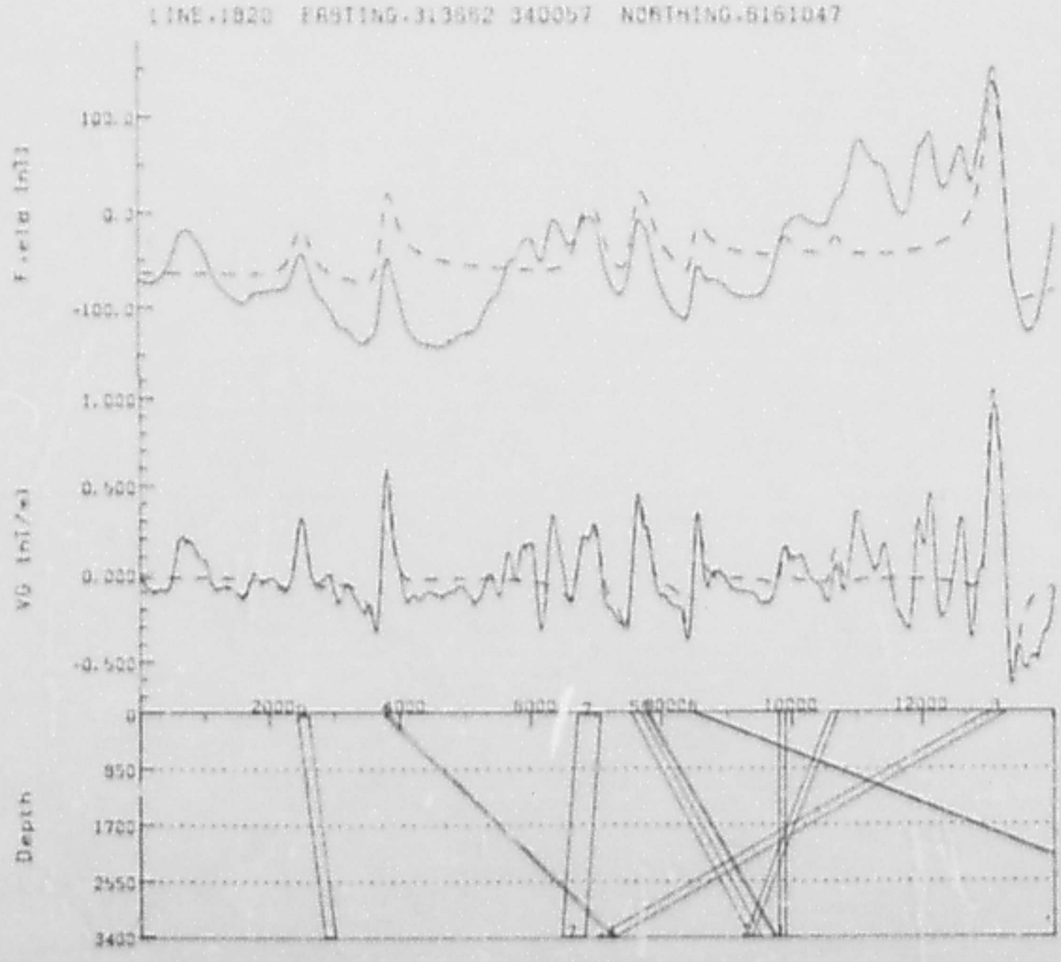
LINE:1820 EASTING:313882 340057 NORTHING:6161047
Field (nT)
100.0
0.0
-100.0
VG (nT/m)
1.000
0.500
0.000
-0.500
Depth
950
1700
2450
3400

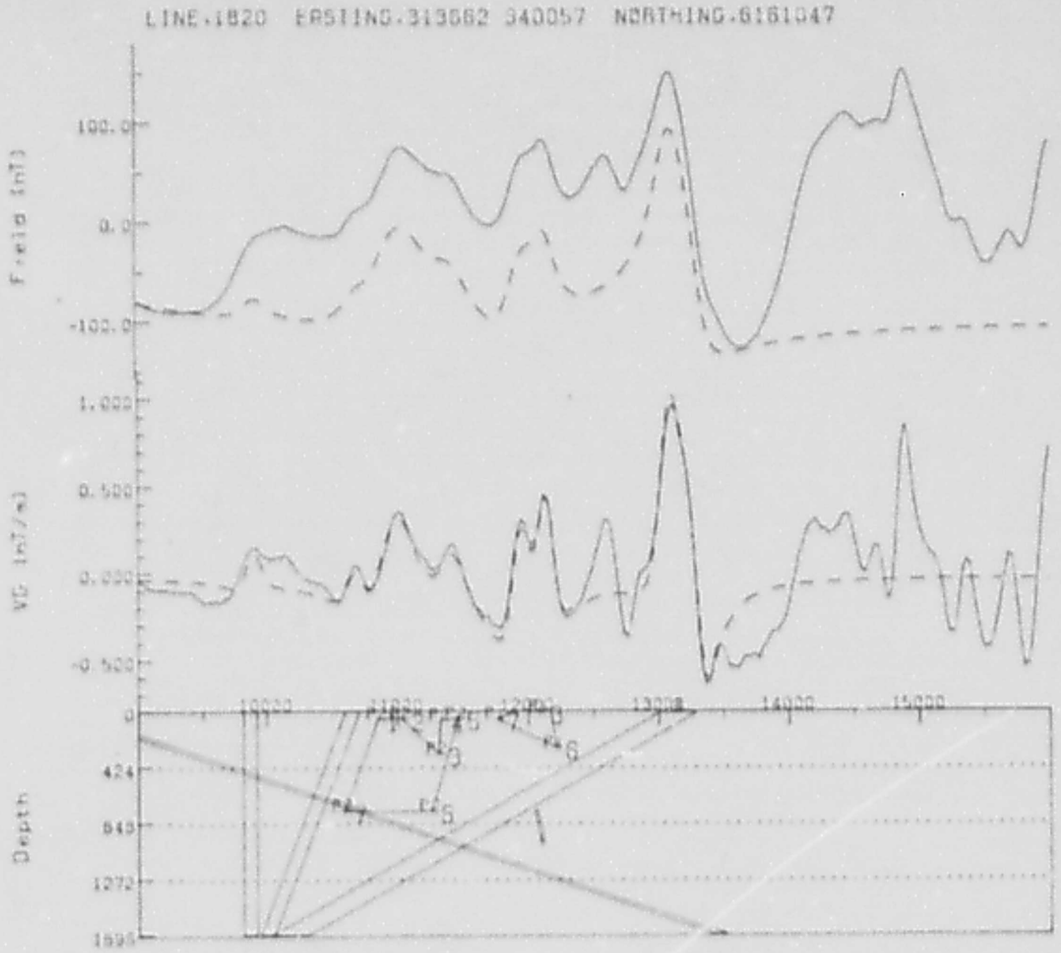
LINE.1820 EASTING.313662 340057 NORTHING.6161047
Field (nT)
100.0
0.0
-100.0
VG (nT/m)
1.000
0.500
0.000
-0.500
Depth
0
424
848
1272
1696

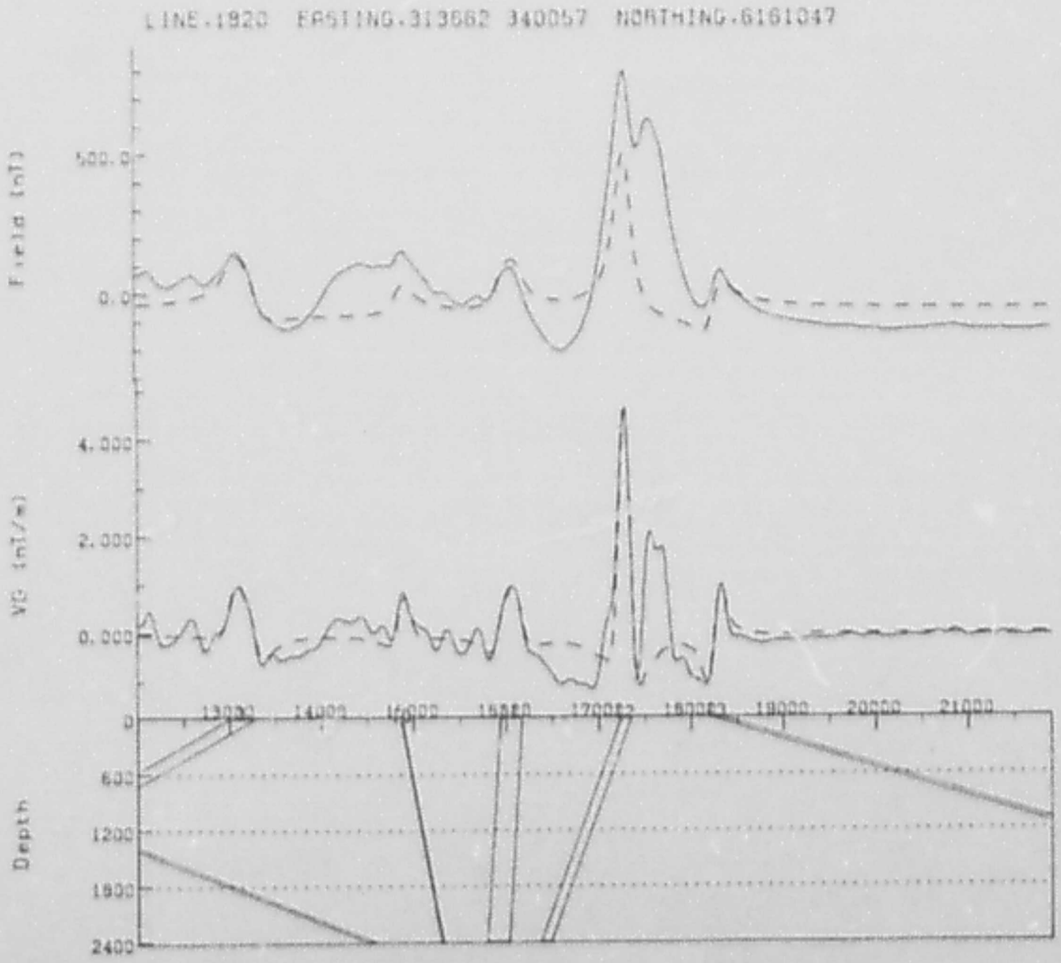
LINE.1820 EASTING.313662 340057 NORTHING.6161047
Field (nT)
500.0
0.0
VG (nT/m)
4.000
2.000
0.000
Depth
0
600
1200
1800
2400

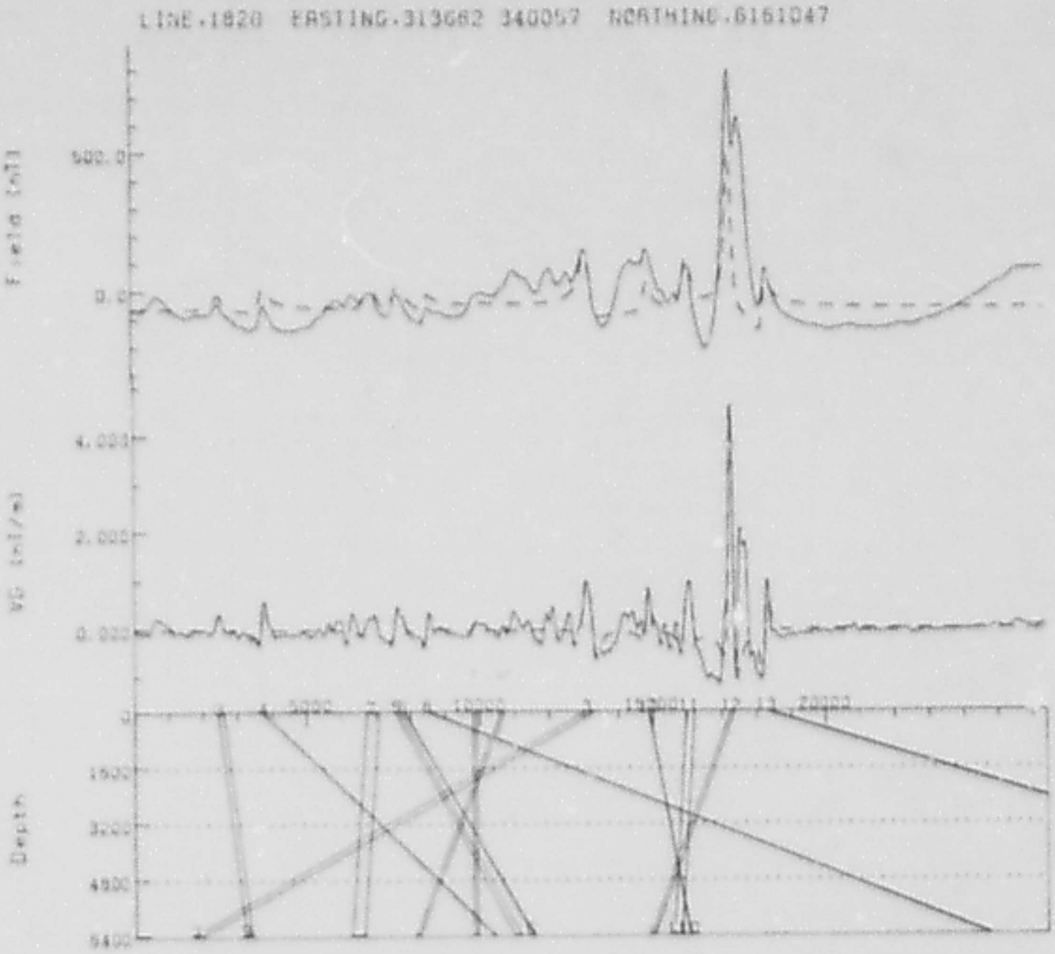
LINE-1820 EASTING-313682 340057 NORTHING-6161047
Field (nT)
500.0
0.0
VG (nT/m)
4.000
2.000
0.000
Depth
0
1600
3200
4800
6400

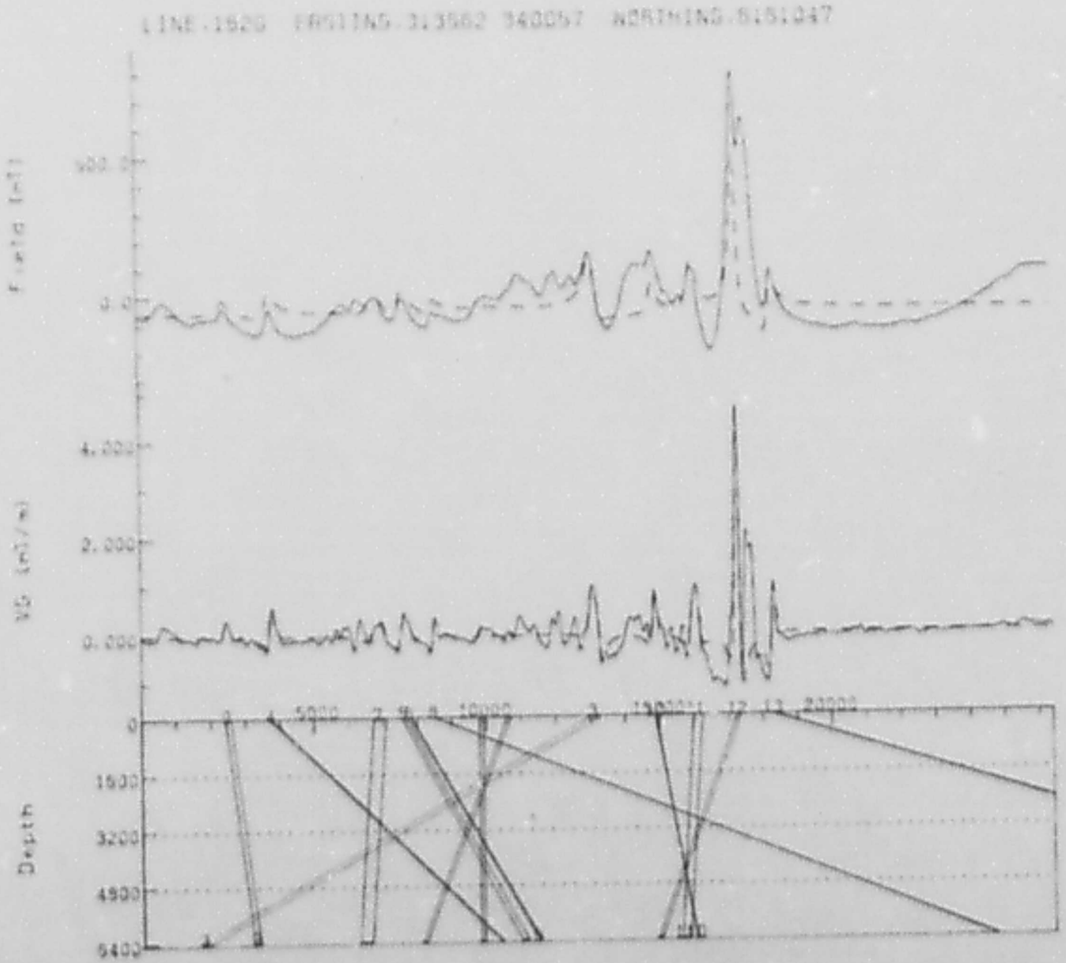
LINE-1820 EASTING-313682 340057 NORTHING-6161047
Field (nT)
500.0
0.0
VG (nT/m)
4.000
2.000
0.000
Depth
0
1600
3200
4800
6400

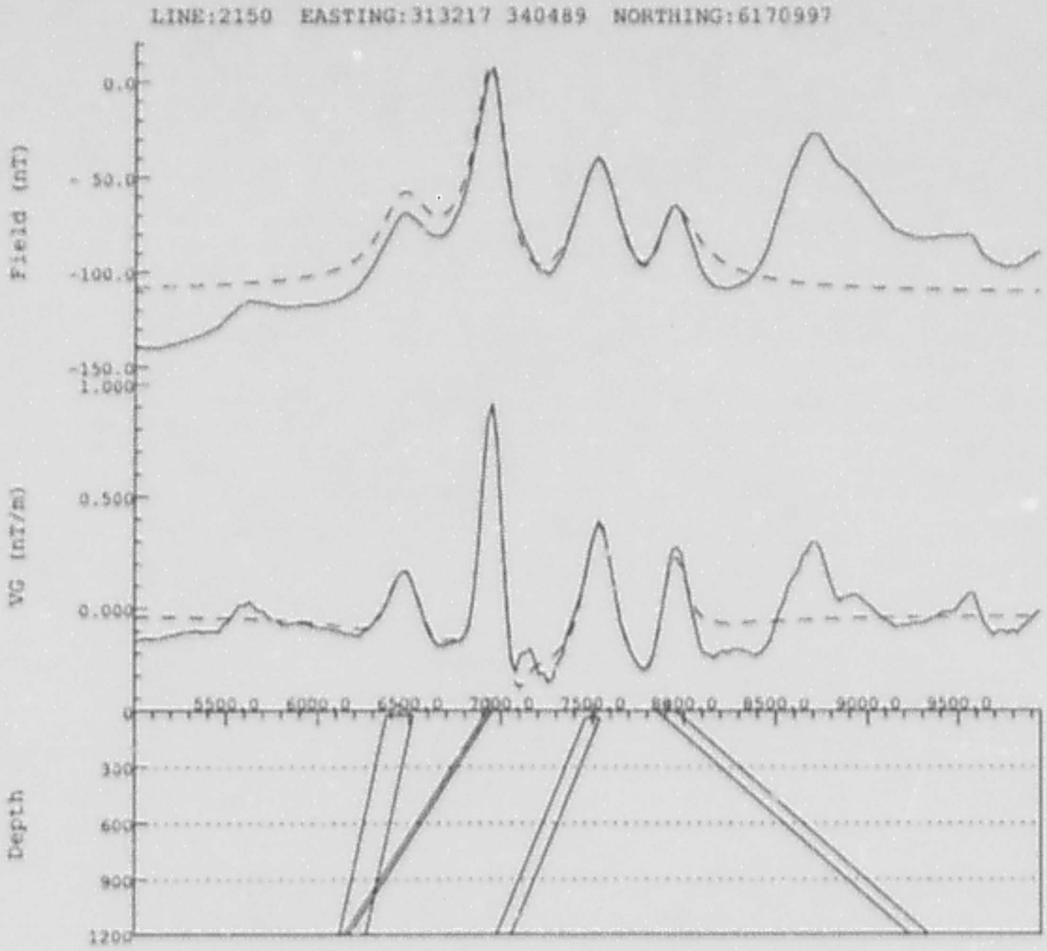
LINE:2150 EASTING:313217 340489 NORTHING:6170997
Field (nT)
0.0
- 50.0
-100.0
-150.0
VG (nT/m)
1.000
0.500
0.000
5500.0
6000.0
6500.0
7000.0
7500.0
8000.0
8500.0
9000.0
9500.0
Depth
0
300
600
900
1200

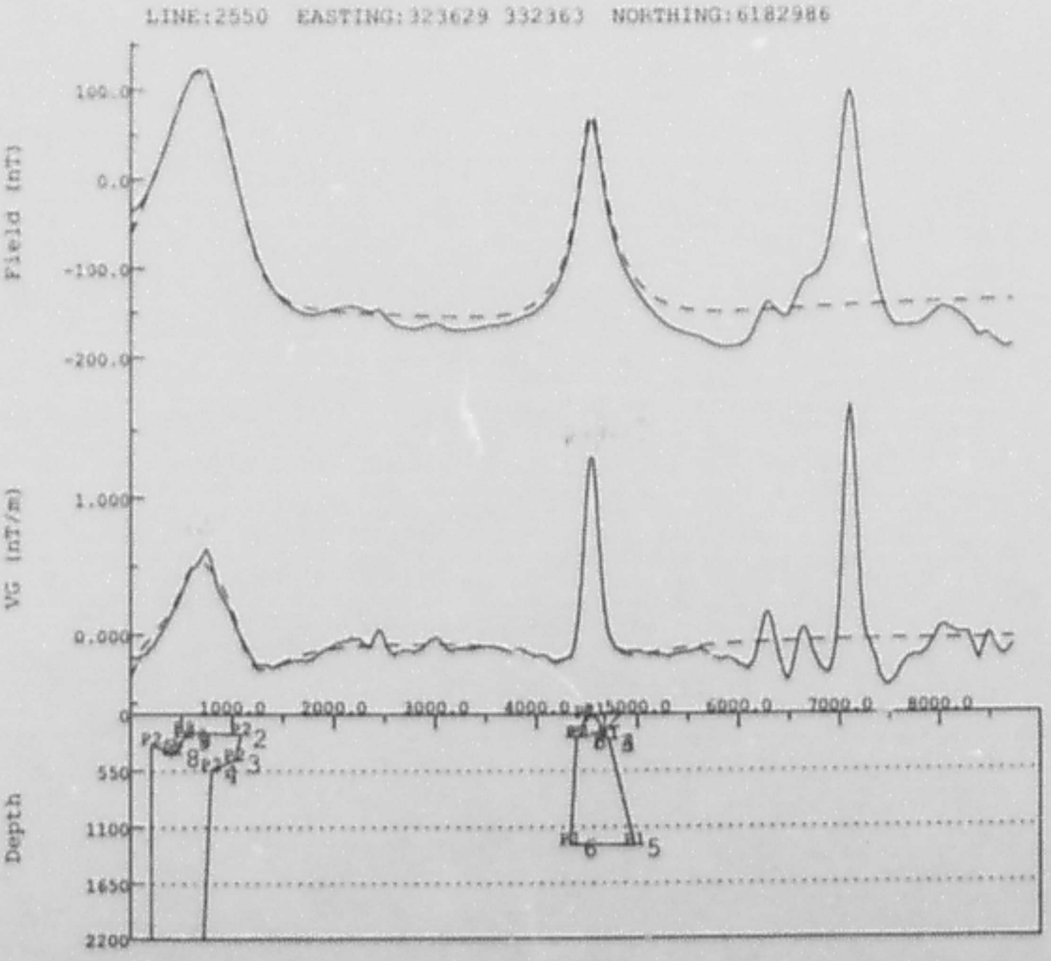
LINE:2550 EASTING:323629 332363 NORTHING:6182986
Field (nT)
100.0
0.0
-100.0
-200.0
VG (nT/m)
1.000
0.000
1000.0
2000.0
3000.0
4000.0
5000.0
6000.0
7000.0
8000.0
Depth
0
550
1100
1650
2200

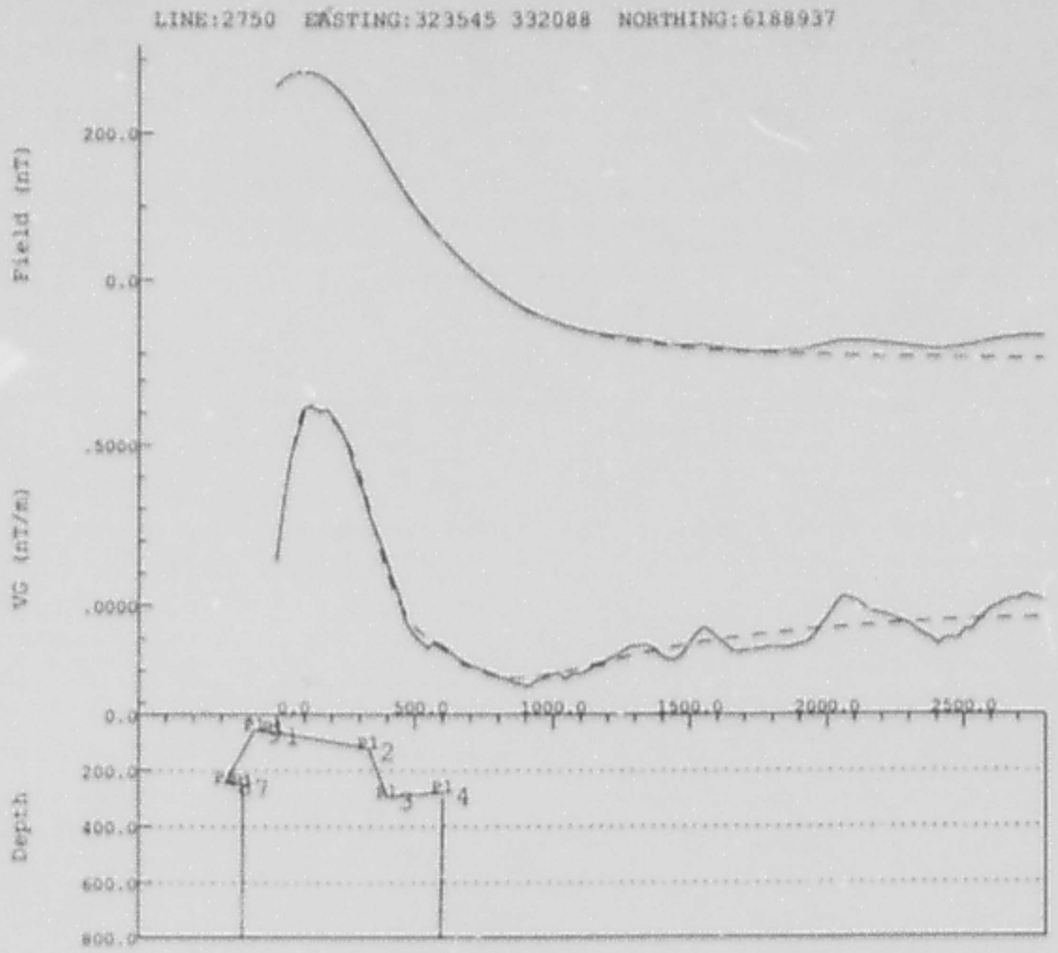
LINE:2750 EASTING:323545 332088 NORTHING:6188937
Field (nT)
200.0
0.0
.5000
.0000
VG (nT/m)
0.0
500.0
1000.0
1500.0
2000.0
2500.0
Depth
200.0
400.0
600.0
800.0
1
2
3
4
7

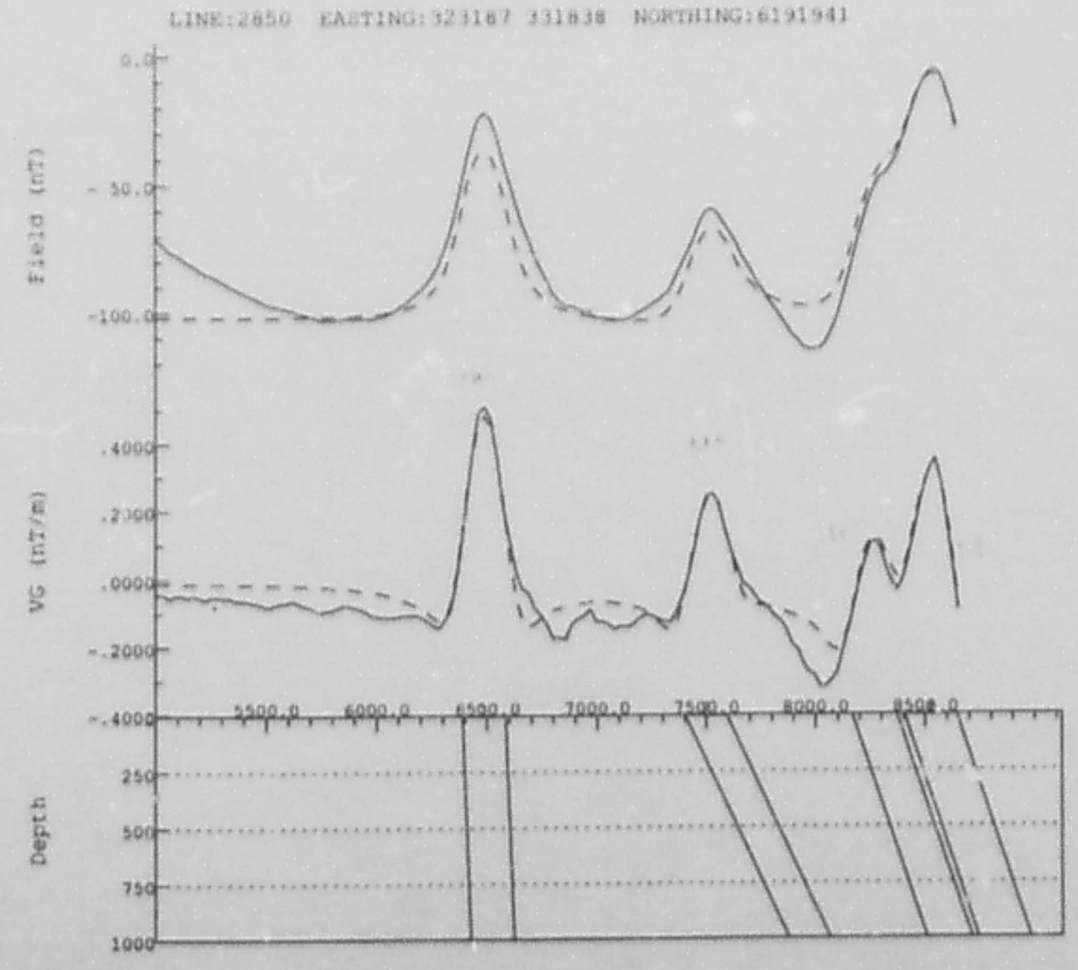
LINE:2850 EASTING:323167 331838 NORTHING:6191941
Field (nT)
0.0
- 50.0
-100.0
.4000
.2000
.0000
-.2000
-.4000
VG (nT/m)
5500.0
6000.0
6500.0
7000.0
7500.0
8000.0
8500.0
Depth
250
500
750
1000

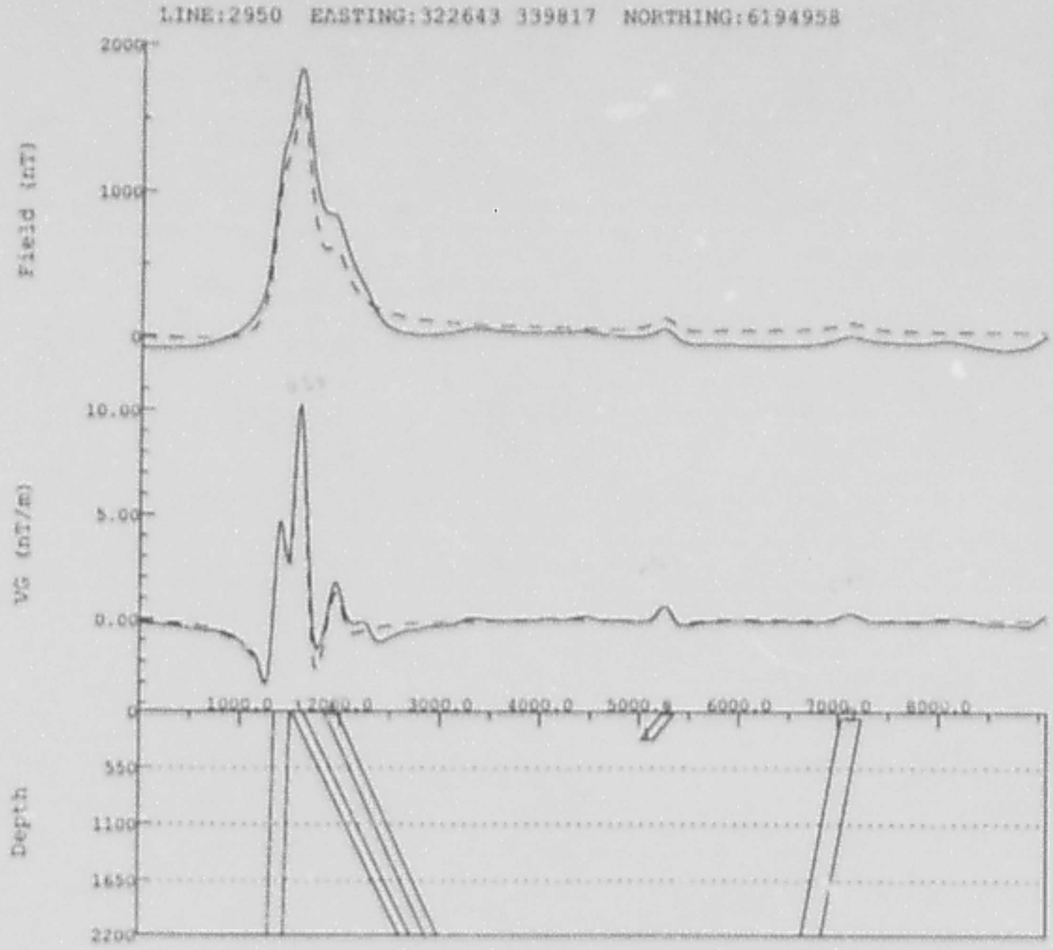
LINE:2950 EASTING:322643 339817 NORTHING:6194958
Field (nT)
2000
1000
0
VG (nT/m)
10.00
5.00
0.00
1000.0
2000.0
3000.0
4000.0
5000.0
6000.0
7000.0
8000.0
Depth
550
1100
1650
2200

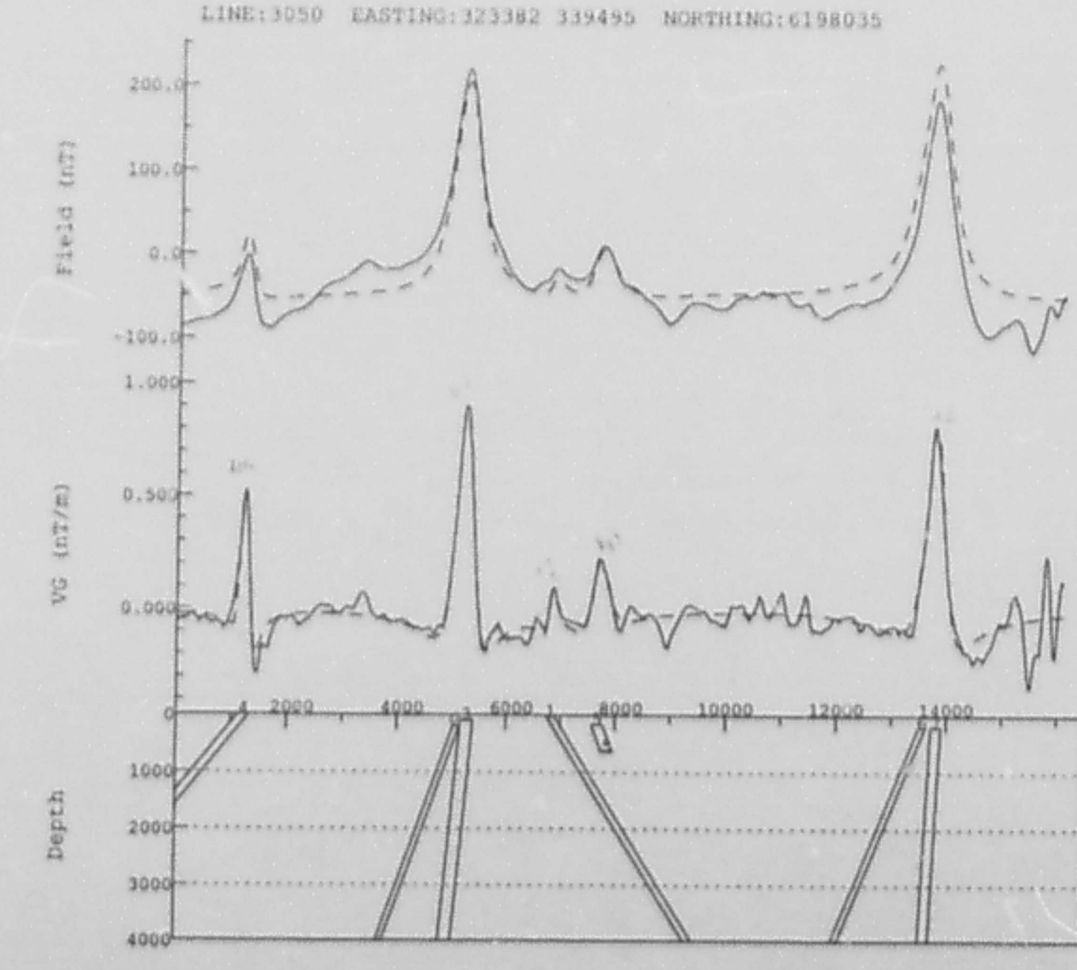
LINE:3050 EASTING:323382 339495 NORTHING:6198035
Field (nT)
200.0
100.0
0.0
-100.0
VG (nT/m)
1.000
0.500
0.000
2000
4000
6000
8000
10000
12000
14000
Depth
1000
2000
3000
4000

LINE:3250 EASTING:323194 339340 NORTHING:6203953

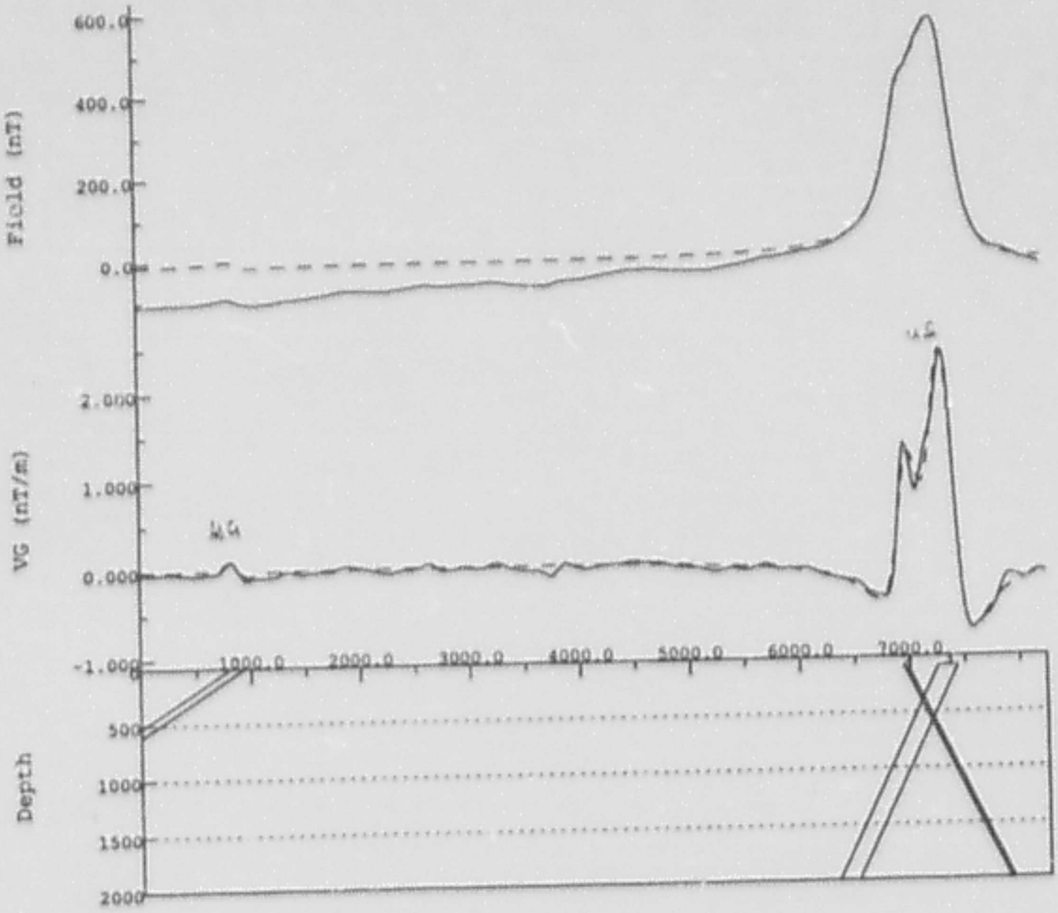

LINE:3350 EASTING:323405 339382 NORTHING:6207126

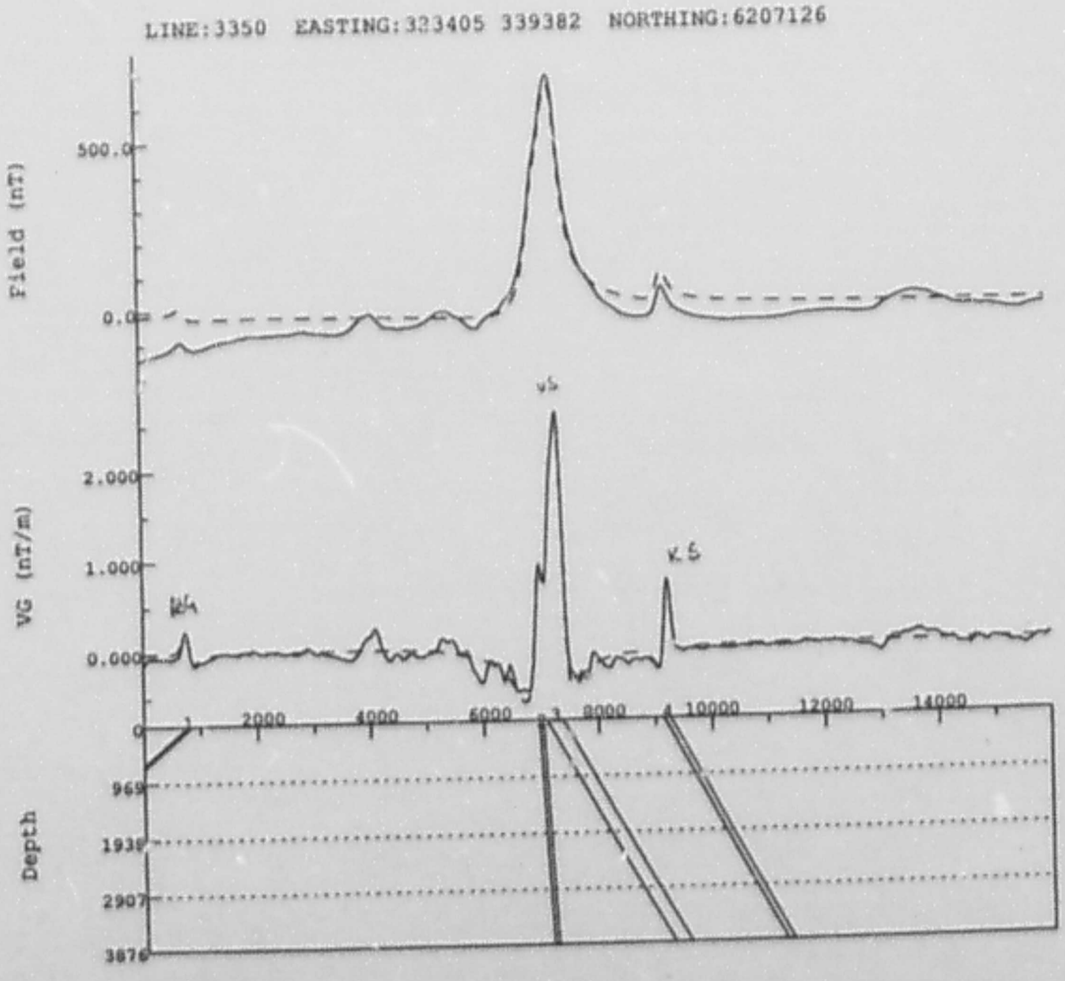

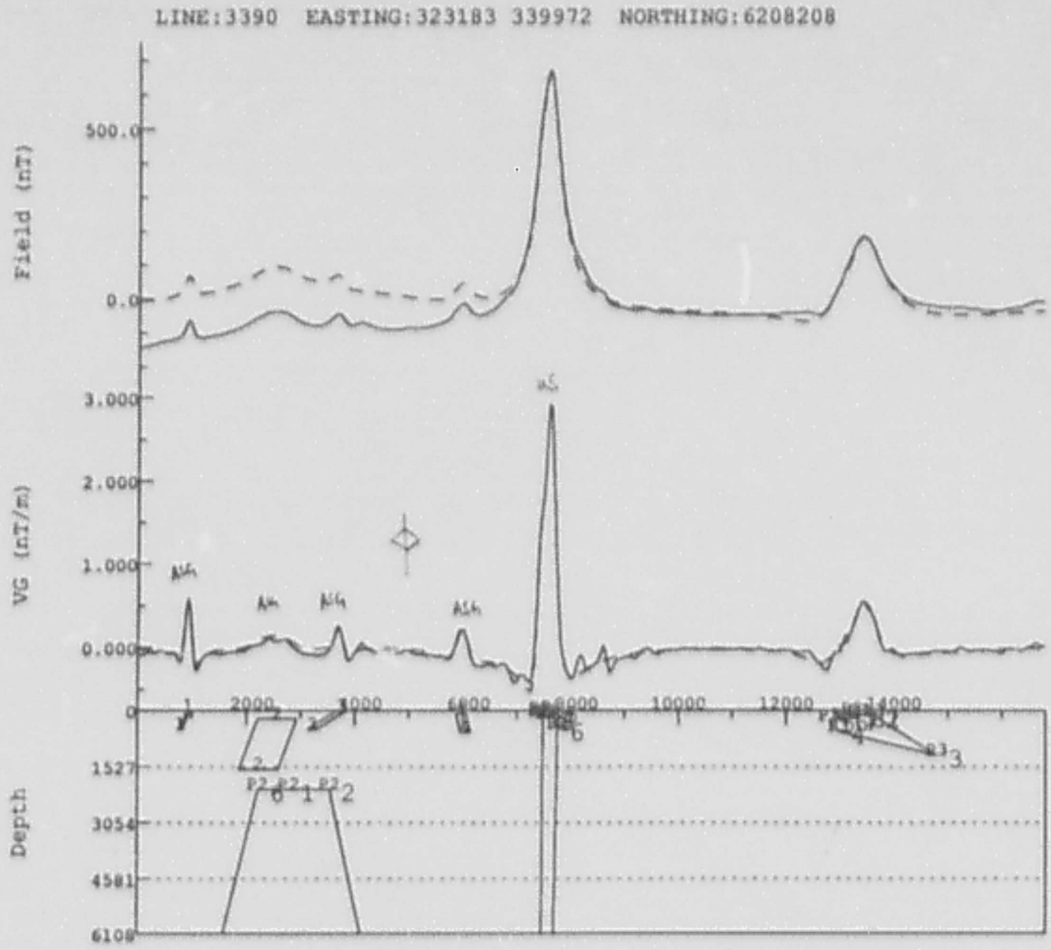
LINE:3390 EASTING:323183 339972 NORTHING:6208208
Field (nT)
500.0
0.0
VG (nT/m)
3.000
2.000
1.000
0.000
Depth
1527
3054
4581
6108

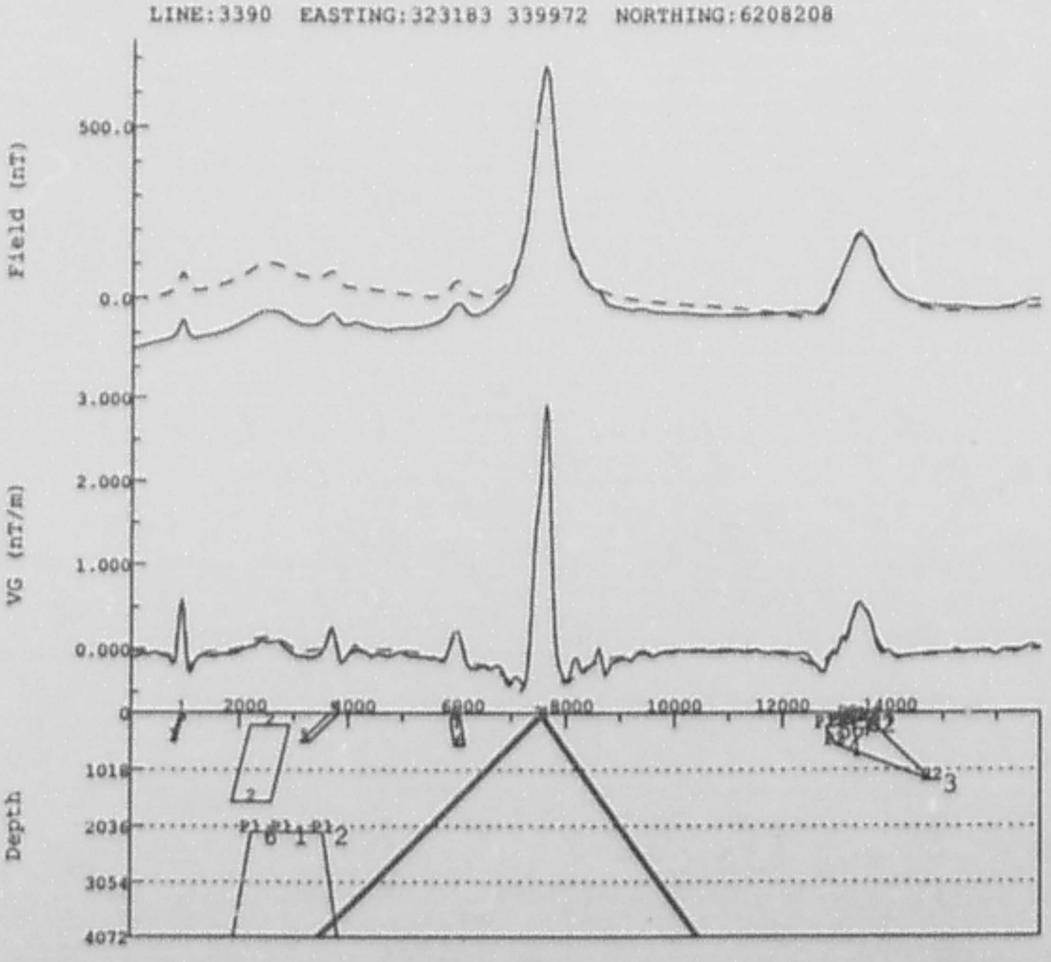
LINE:3390 EASTING:323183 339972 NORTHING:6208208
Field (nT)
500.0
0.0
VG (nT/m)
3.000
2.000
1.000
0.000
Depth
1018
2036
3054
4072

Murray Bridge Survey

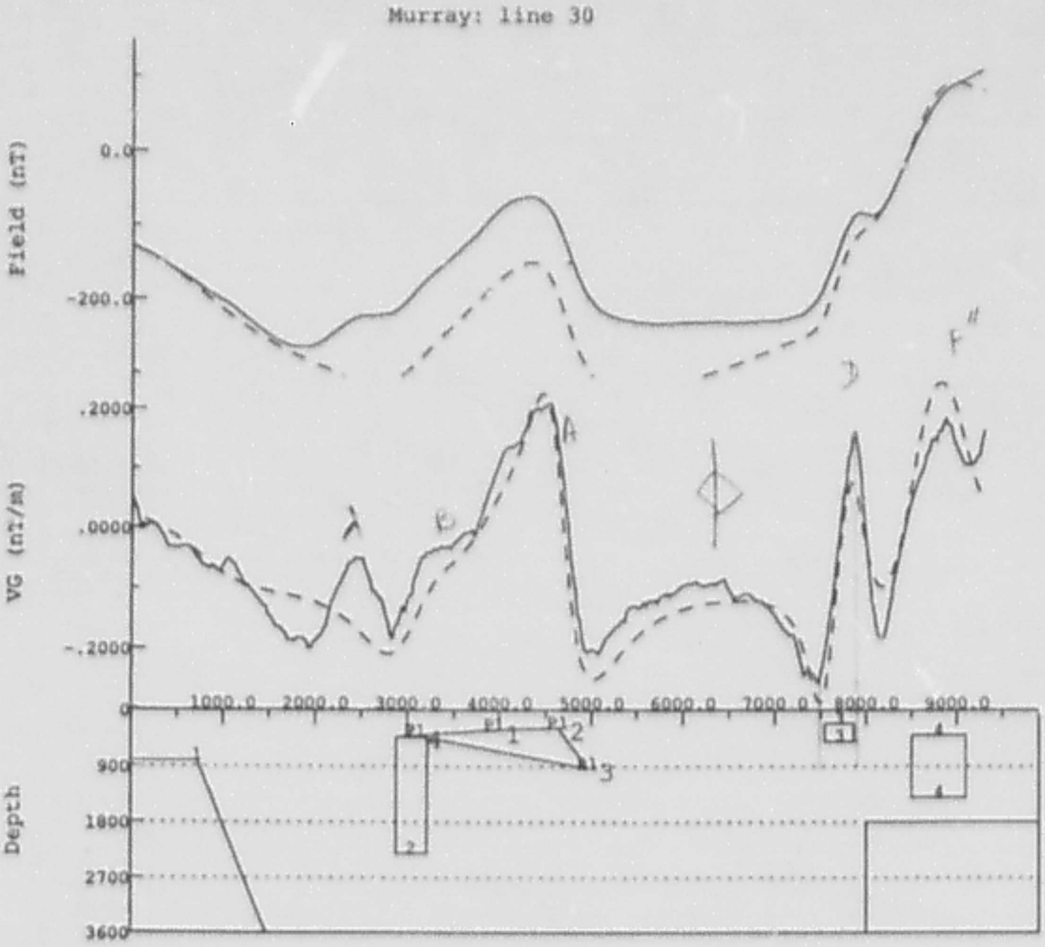
Murray: line 30
Field (nT)
0.0
-200.0
VG (nT/m)
.2000
.0000
-.2000
A
B
D
F"
1000.0
2000.0
3000.0
4000.0
5000.0
6000.0
7000.0
8000.0
9000.0
Depth
900
1800
2700
3600

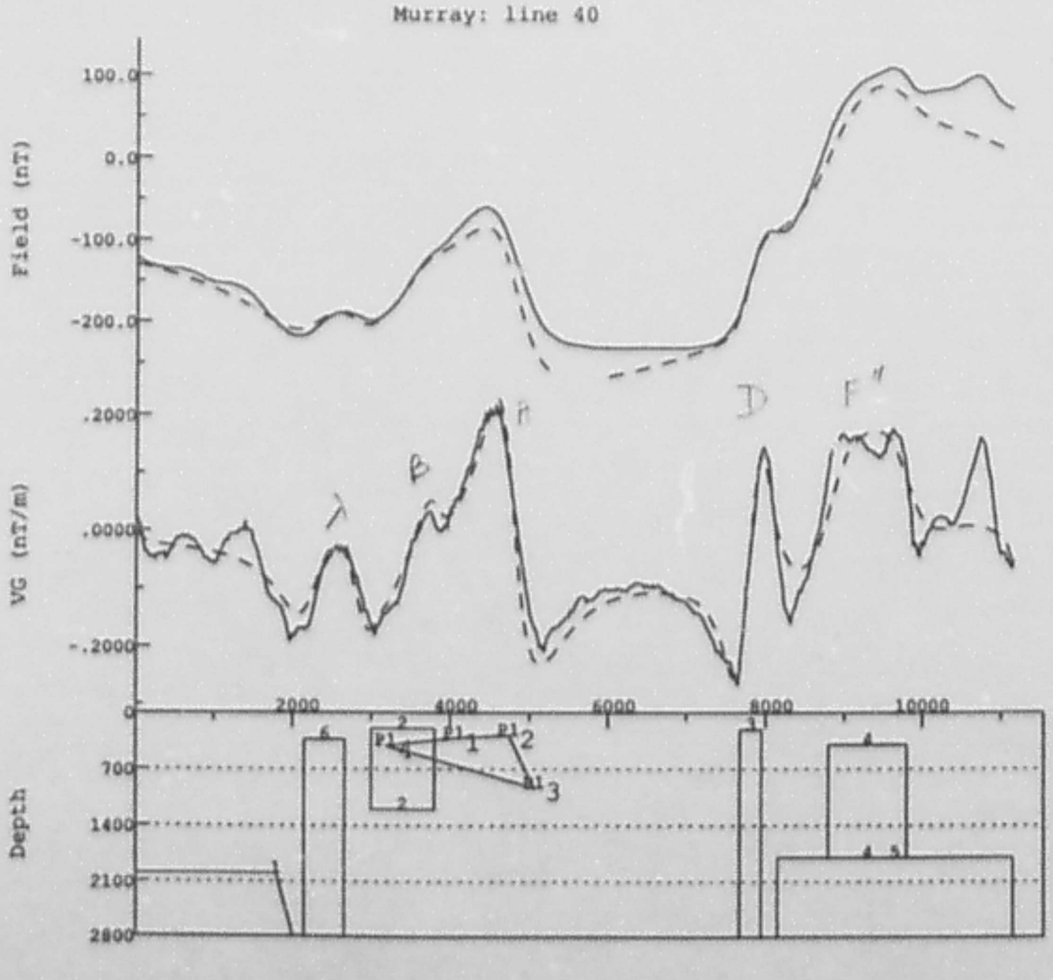
Murray: line 40
Field (nT)
100.0
0.0
-100.0
-200.0
VG (nT/m)
.2000
.0000
-.2000
A
B
D
F"
2000
4000
6000
8000
10000
Depth
700
1400
2100
2800

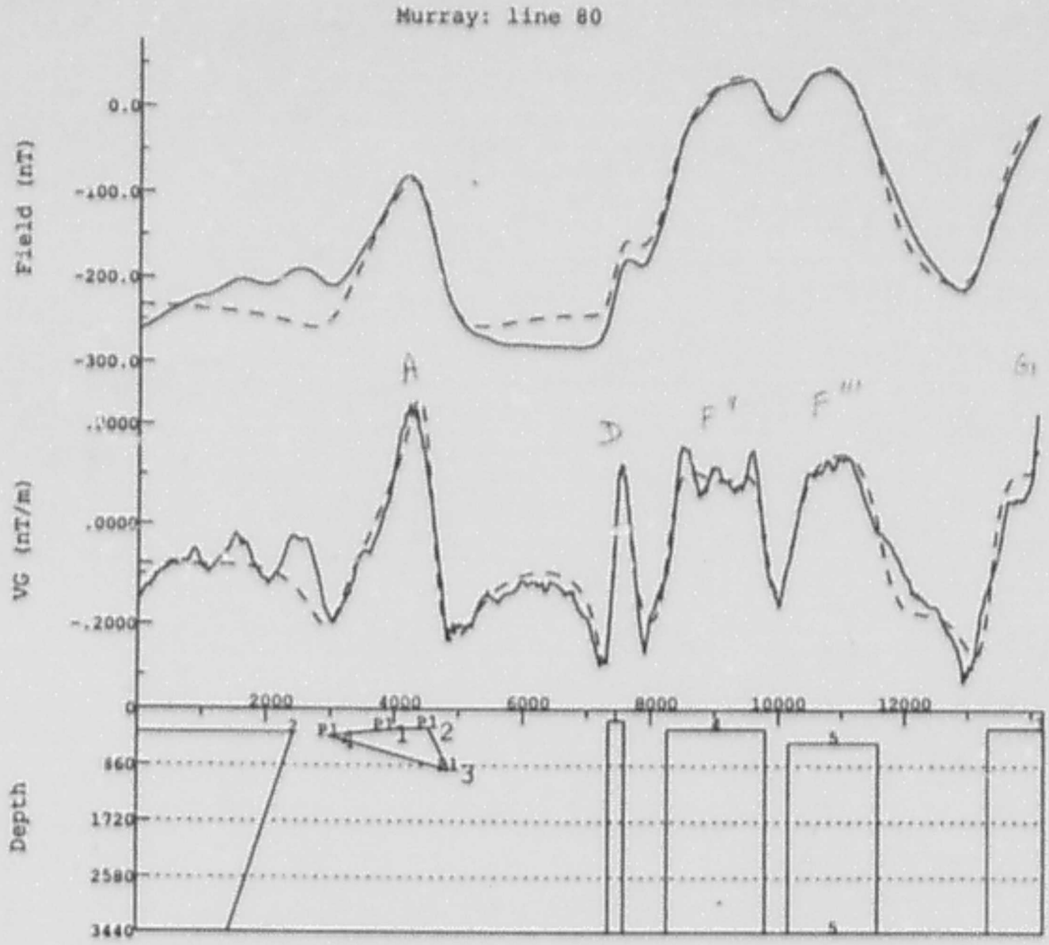
Murray: line 80
Field (nT)
VG (nT/m)
Depth
A
D
F'
F''
G1
2000
4000
6000
8000
10000
12000
660
1720
2580
3440

Hex

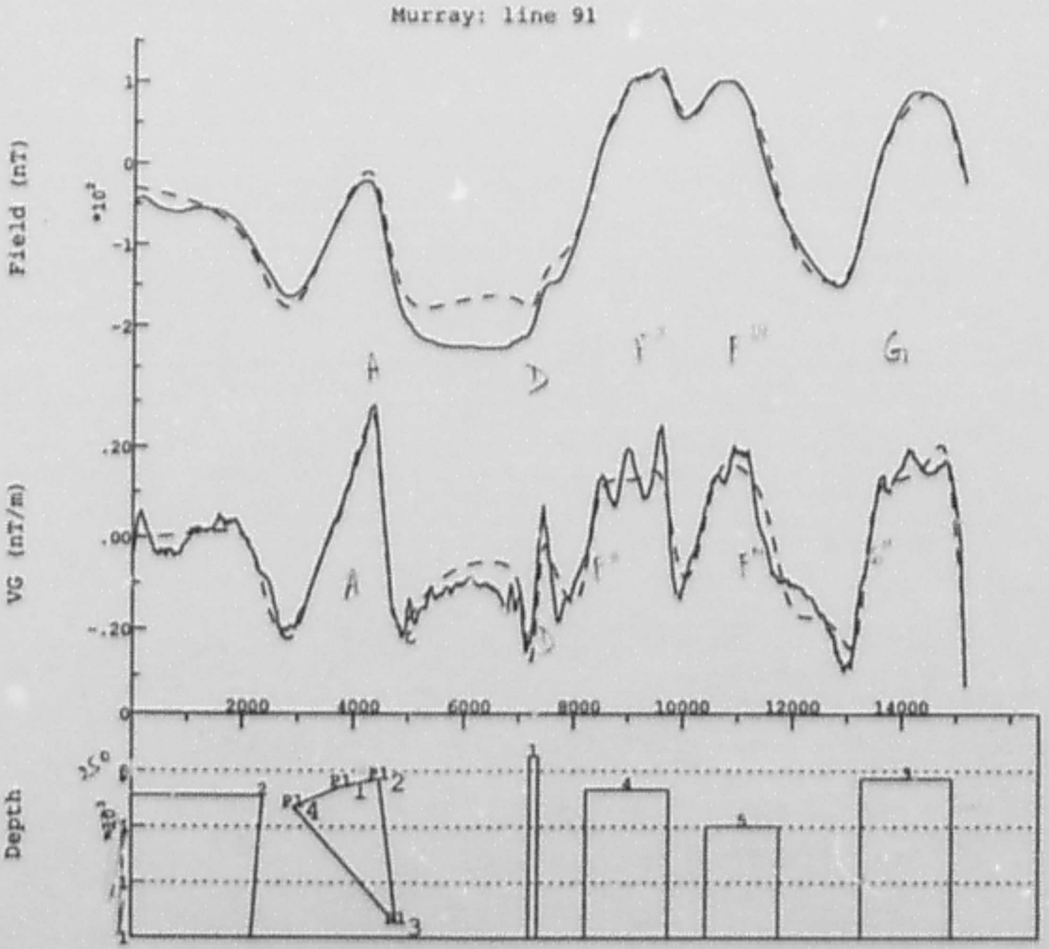
Murray: line 91
Field (nT)
VG (nT/m)
Depth
A
D
F'
F''
G1
2000
4000
6000
8000
10000
12000
14000

Hex

Murray: line 530

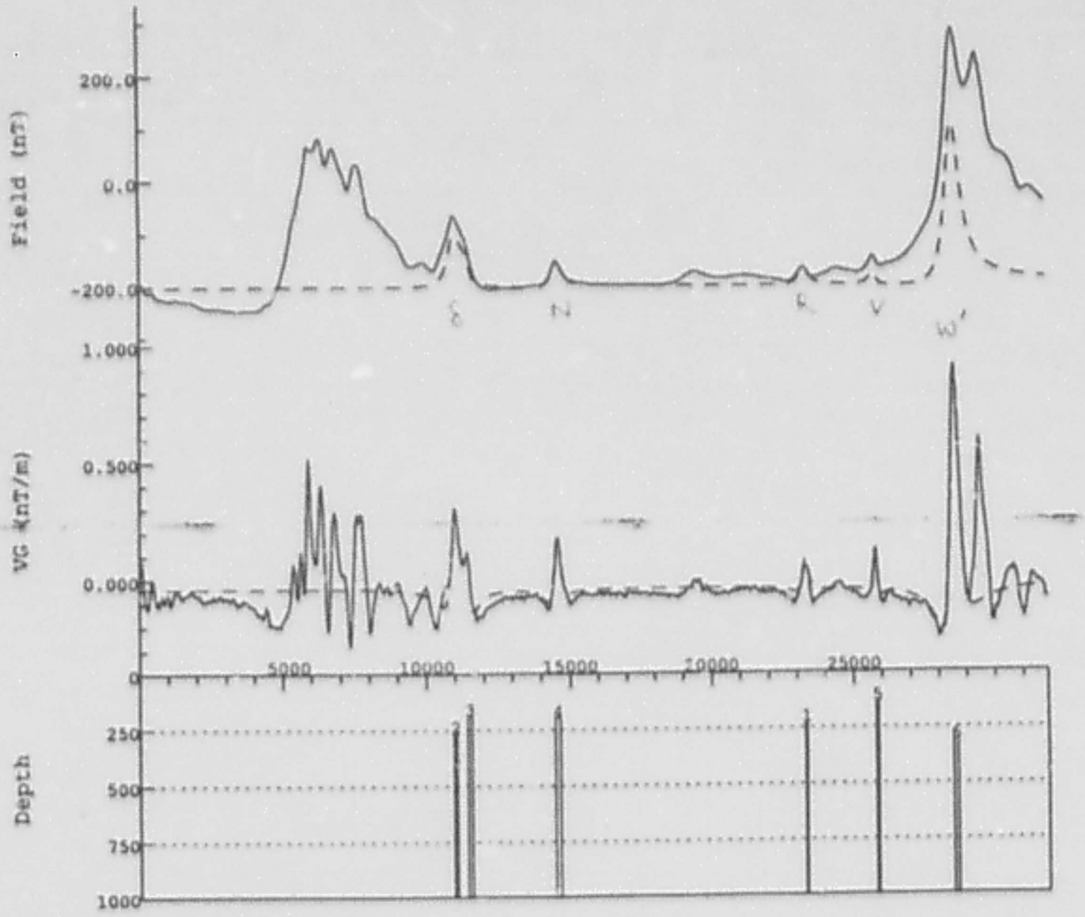

1 R
2 } S
3 }
4 N
5 V
6 W'

Murray: line580

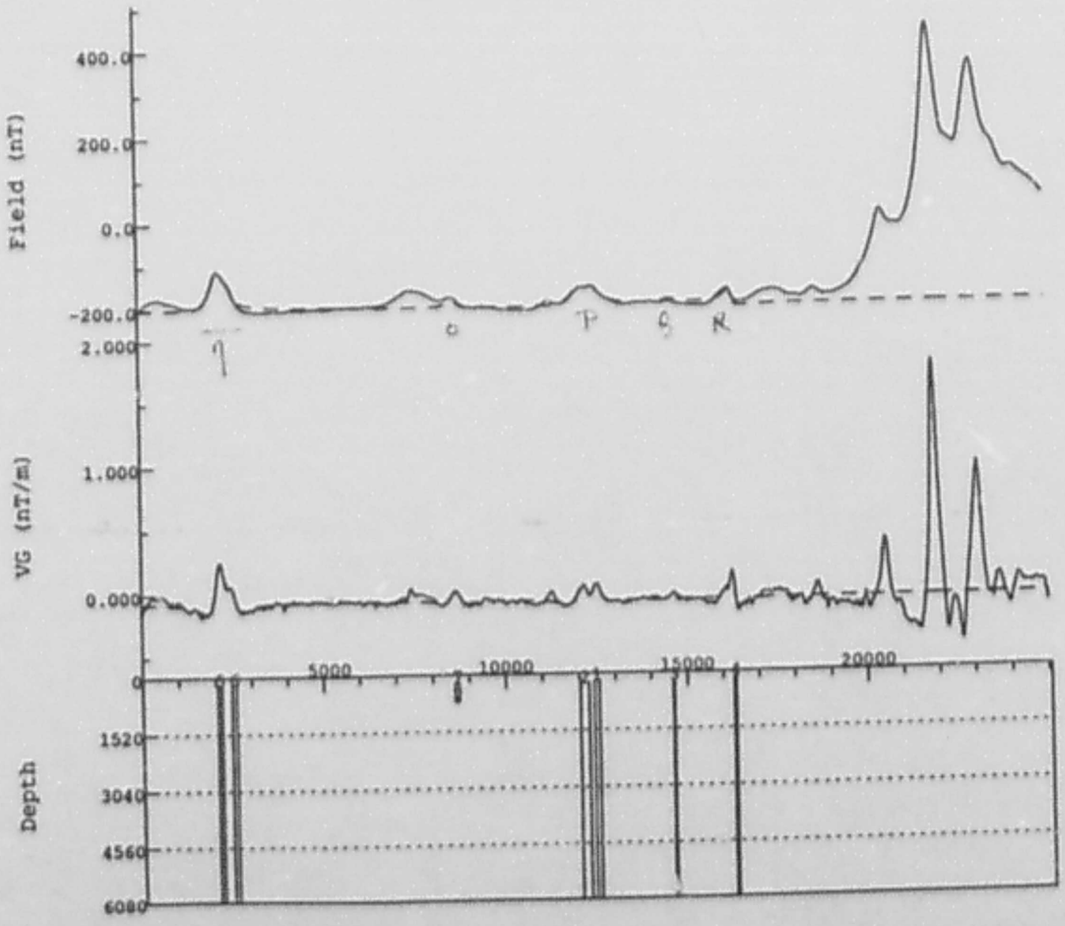

1 } P
2 }
3 Q
4 R
5 }
6 } T
7 U

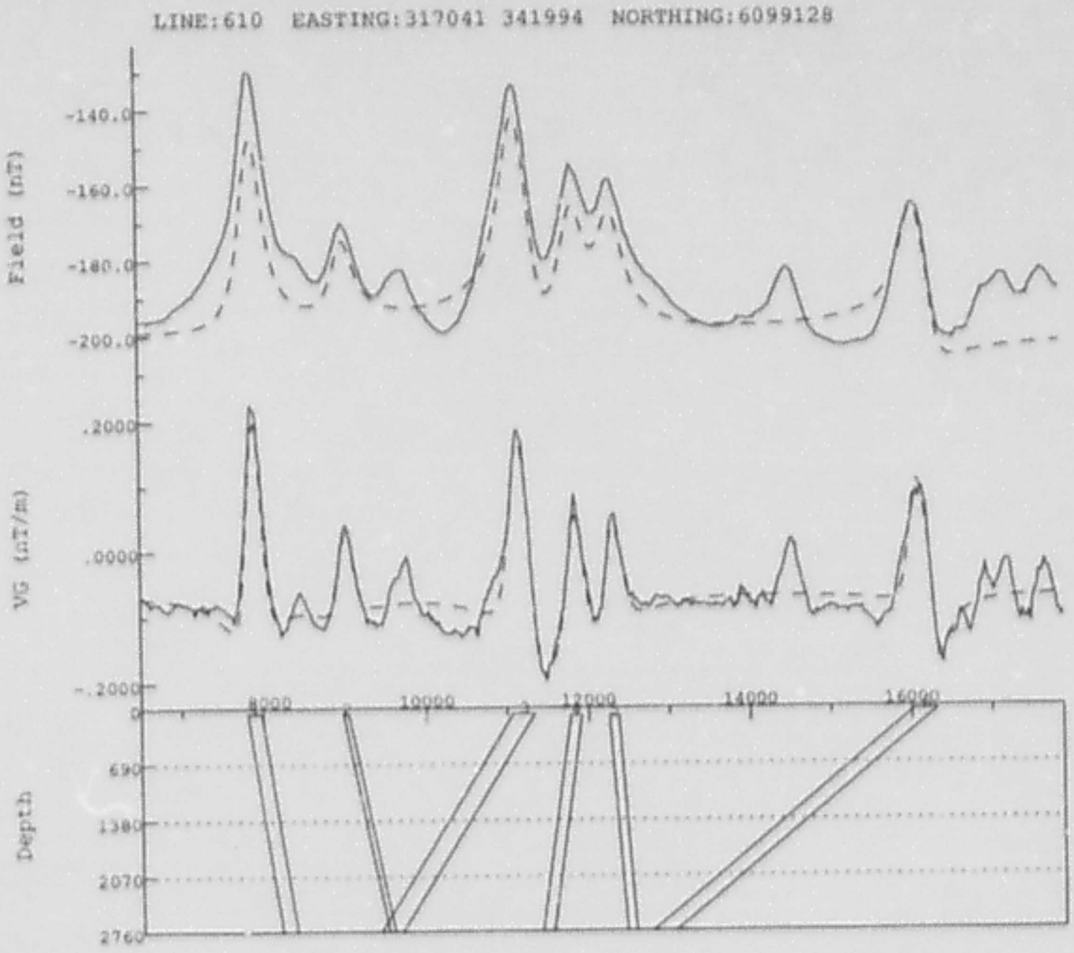
LINE:610 EASTING:317041 341994 NORTHING:6099128
Field (nT)
-140.0
-160.0
-180.0
-200.0
VG (nT/m)
.2000
.0000
-.2000
8000
10000
12000
14000
16000
Depth
0
690
1380
2070
2760

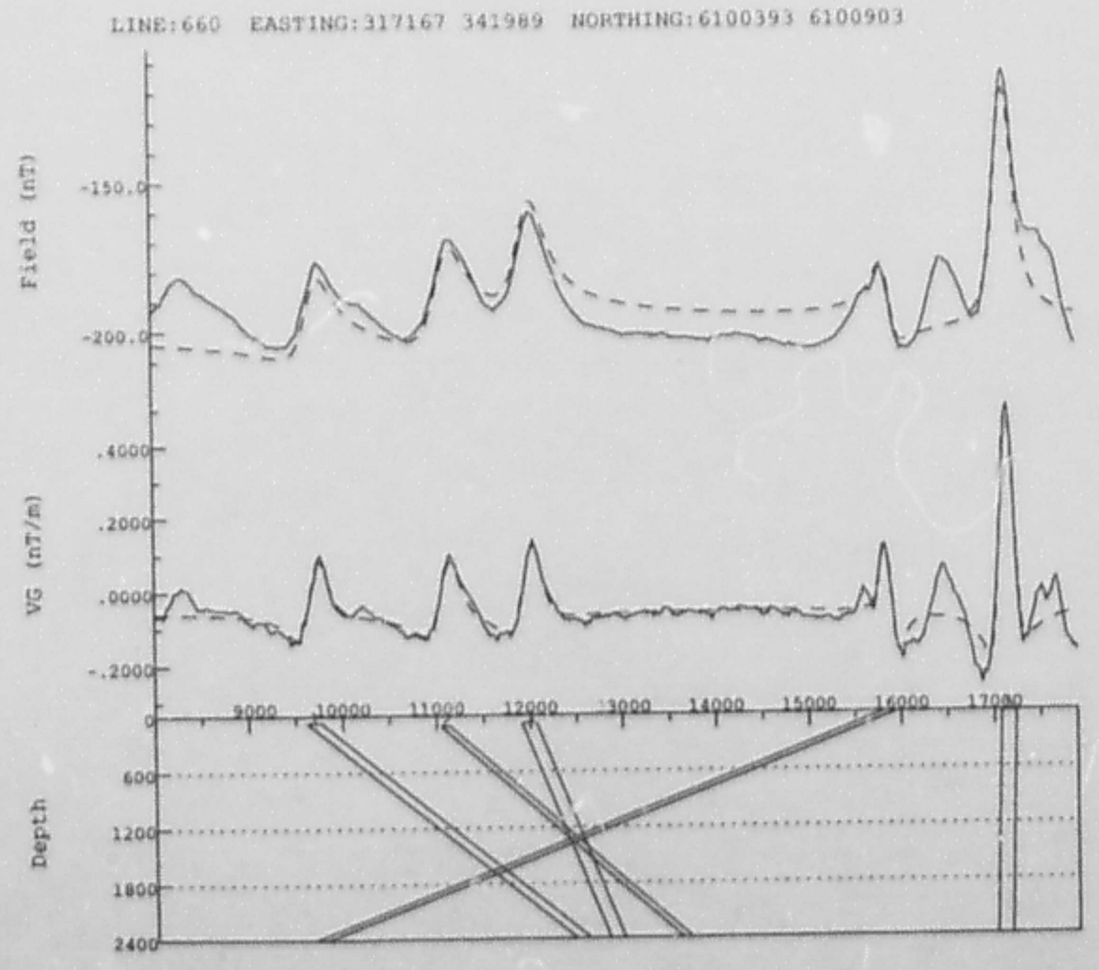
LINE:660 EASTING:317167 341989 NORTHING:6100393 6100903
Field (nT)
-150.0
-200.0
VG (nT/m)
.4000
.2000
.0000
-.2000
9000
10000
11000
12000
13000
14000
15000
16000
17000
Depth
0
600
1200
1800
2400

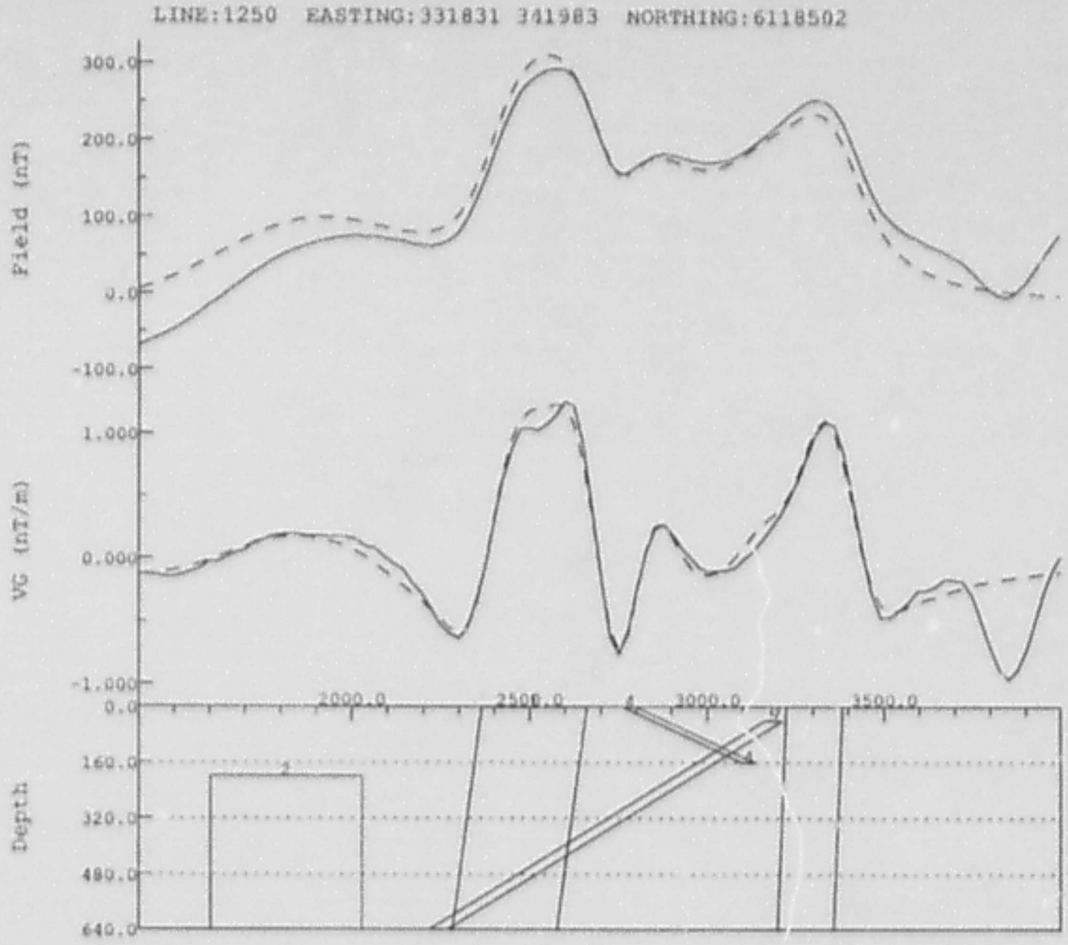
LINE:1250 EASTING:331831 341983 NORTHING:6118502
Field (nT)
300.0
200.0
100.0
0.0
-100.0
VG (nT/m)
1.000
0.000
-1.000
2000.0
2500.0
3000.0
3500.0
Depth
0.0
160.0
320.0
480.0
640.0

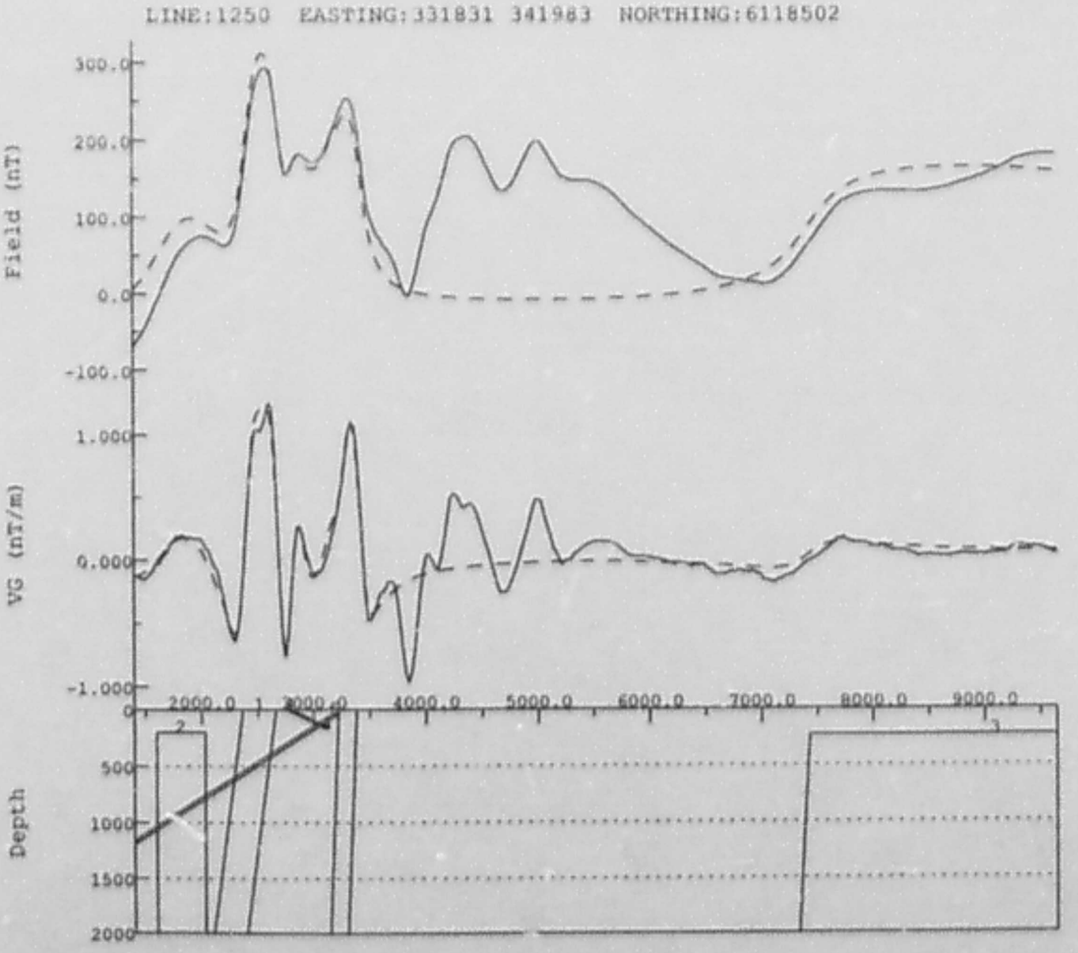
LINE:1250 EASTING:331831 341983 NORTHING:6118502
Field (nT)
300.0
200.0
100.0
0.0
-100.0
VG (nT/m)
1.000
0.000
-1.000
2000.0
3000.0
4000.0
5000.0
6000.0
7000.0
8000.0
9000.0
Depth
0
500
1000
1500
2000

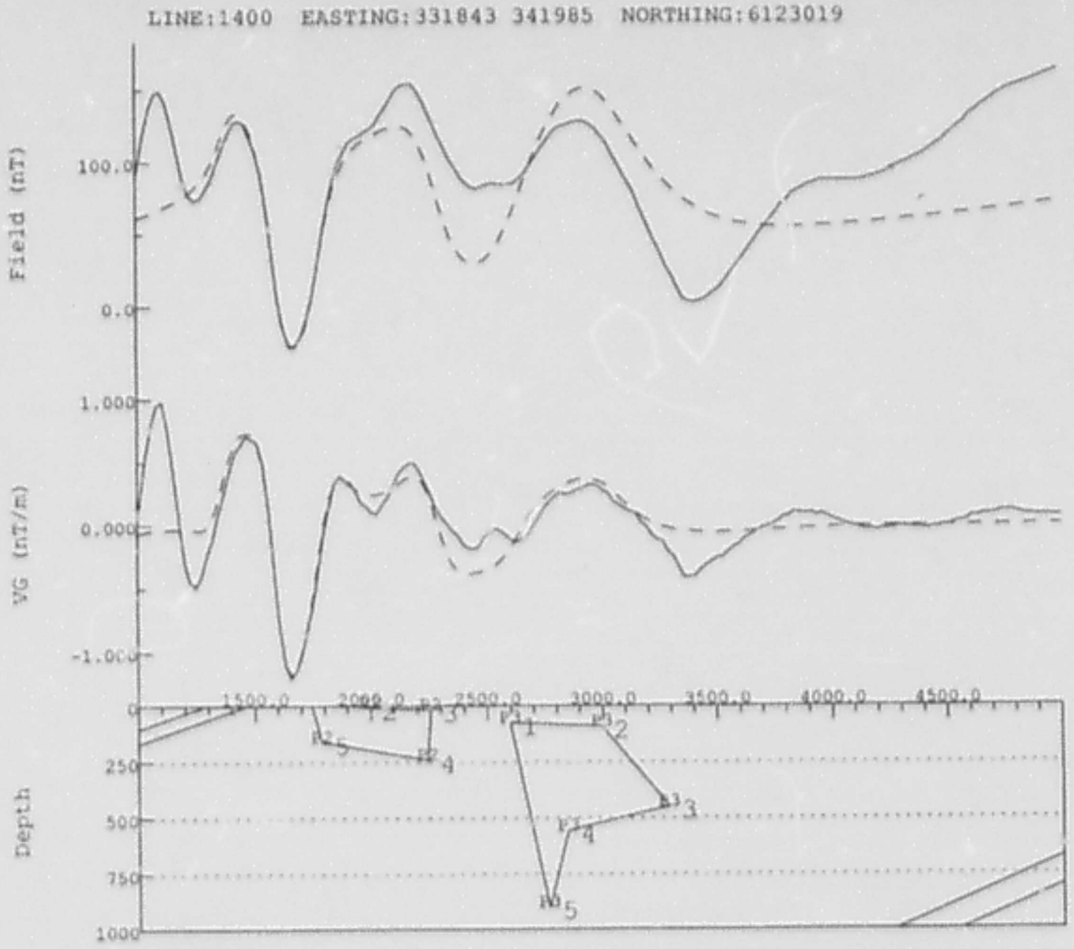
LINE:1400 EASTING:331843 341985 NORTHING:6123019
Field (nT)
100.0
0.0
VG (nT/m)
1.000
0.000
-1.000
1500.0
2000.0
2500.0
3000.0
3500.0
4000.0
4500.0
Depth
0
250
500
750
1000

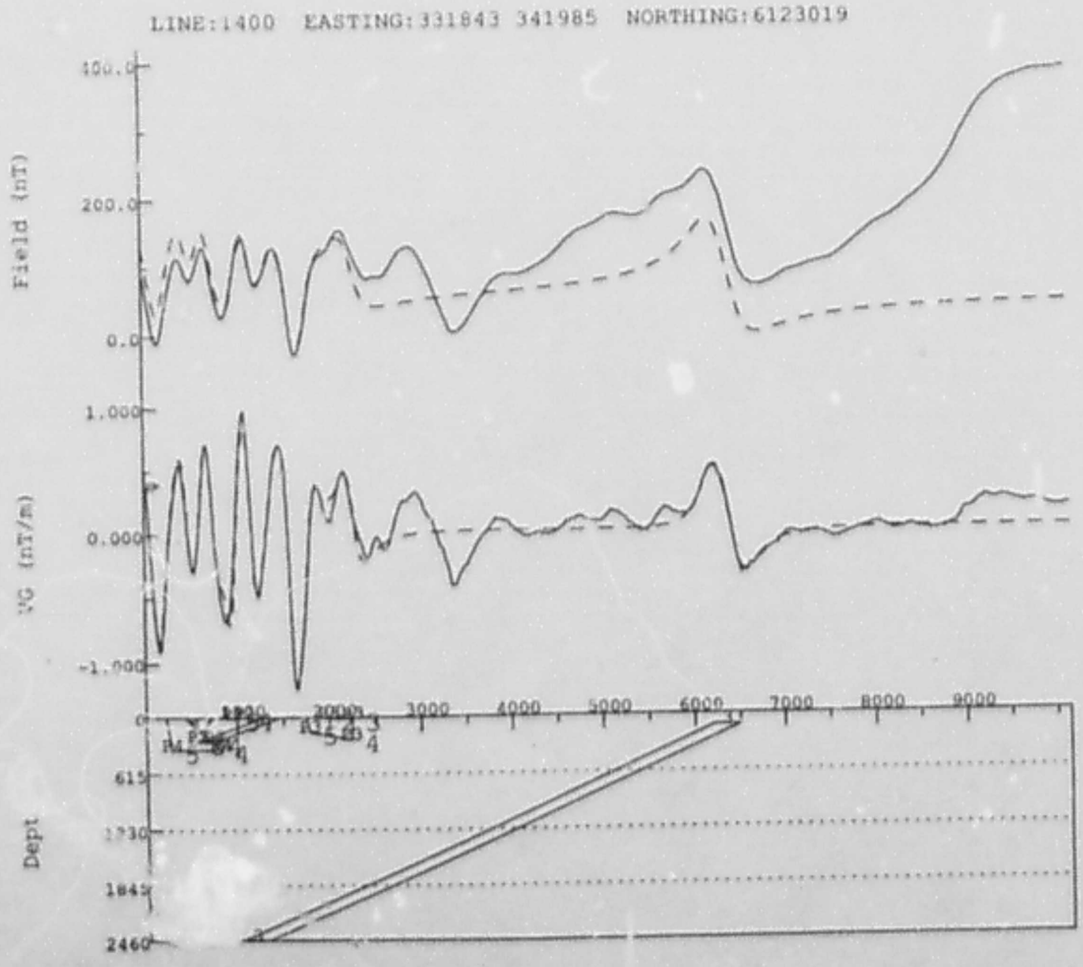
LINE:1400 EASTING:331843 341985 NORTHING:6123019
Field (nT)
100.0
200.0
0.0
VG (nT/m)
1.000
0.000
-1.000
1000
2000
3000
4000
5000
6000
7000
8000
9000
Dept
615
1230
1845
2460

KANMANTOO TROUGH

TOTAL MAGNETIC FIELD (edge enhanced)

Shanti Rajagopalan
Geology & Geophysics
University of Adelaide
October 1988

KANMANTOO TROUGH

TOTAL RADIOMETRIC COUNT

Shanti Rajagopalan
Geology & Geophysics
University of Adelaide
October 1988

Appendix K: Automatic Gain Control

The aim in applying any enhancement technique is to improve the display by highlighting weak trends which might otherwise have been overlooked. The amplitude, width (or frequency) and the relative peak positions and values represent the recognizable characteristics of a vertical gradient anomaly. Trend analysis involves tracing a signal across profiles. Even if the signal has been distorted in the output, provided it is still distinguishable from nearby, unconnected anomalies, successful trend analysis is possible. In any signal enhancement technique there is a trade-off between amplification of weak anomalies and distortion of signal character. The optimal display is one which maximizes the first while minimizing the second.

Downward continuation and first and second derivatives are conventionally computed from total magnetic field data in order to bring out and resolve anomalies from shallow sources. Such techniques are distinct from display operators such as the square-root and "Automatic Gain Control" (or AGC) which are used to enhance the display of derivative data. Automatic Gain Control is a very effective way of enhancing low-amplitude anomalies while preserving high-amplitude anomalies. Much amplitude information is lost but the resolution of anomalies is high. The results of applying AGC to vertical gradient data depend very much on the amplitude and frequency content of the original data and on the choice of the window width. The square-root (or similar power) operator is much simpler to apply though not as effective.

This appendix is intended to supplement the discussion in Chapter 3. The efficiency of the AGC and square-root operators are discussed in terms of anomaly enhancement and distortion. The effect on the output of different window widths is also demonstrated.

For any profile, let the input and output amplitudes at the j^{th} point be given as follows:

$$\begin{aligned} \text{input amplitude} &= V(j) \\ \text{output amplitude using AGC} &= AG(j) \\ \text{output amplitude using a square-root operator} &= SQRT(j). \end{aligned}$$

Then, if the window length is (2n+1),

$$\begin{aligned} RMS(j) &= \sqrt{\frac{\sum_{i=j-n}^{j+n} V^2(i)}{2n+1}} \\ AG(j) &= \frac{V(j)}{RMS(j)} \end{aligned}$$

PR1: anomaly 1						
x	V	$SQRT$	AG			
			window widths			
			9	13	19	25
$j-3$	0.85	0.92	0.90	0.85	0.83	0.86
$j-2$	0.93	0.97	0.95	0.93	0.92	0.94
$j-1$	0.98	0.99	0.98	0.98	0.98	0.98
j	1.00	1.00	1.00	1.00	1.00	1.00
$j+1$	0.98	0.99	1.00	0.98	0.97	0.98
$j+2$	0.93	0.97	0.98	0.93	0.90	0.93
$j+3$	0.85	0.92	0.94	0.85	0.81	0.85
PR2: anomaly 2						
x	V	$SQRT$	AG			
			window widths			
			9	13	19	25
$j-3$	0.70	0.84	0.76	0.70	0.69	0.69
$j-2$	0.87	0.93	0.90	0.86	0.85	0.86
$j-1$	0.97	0.99	0.98	0.97	0.96	0.96
j	1.00	1.00	1.00	1.00	1.00	1.00
$j+1$	0.95	0.98	0.97	0.95	0.96	0.96
$j+2$	0.84	0.92	0.90	0.85	0.87	0.86
$j+3$	0.71	0.85	0.82	0.73	0.74	0.74

Table K.1: Rounding of anomaly peaks in the output $SQRT$ and AG profiles. Anomaly 1 is taken from PR1 (Figure K.4) and anomaly 2 from PR2 (Figure K.5).

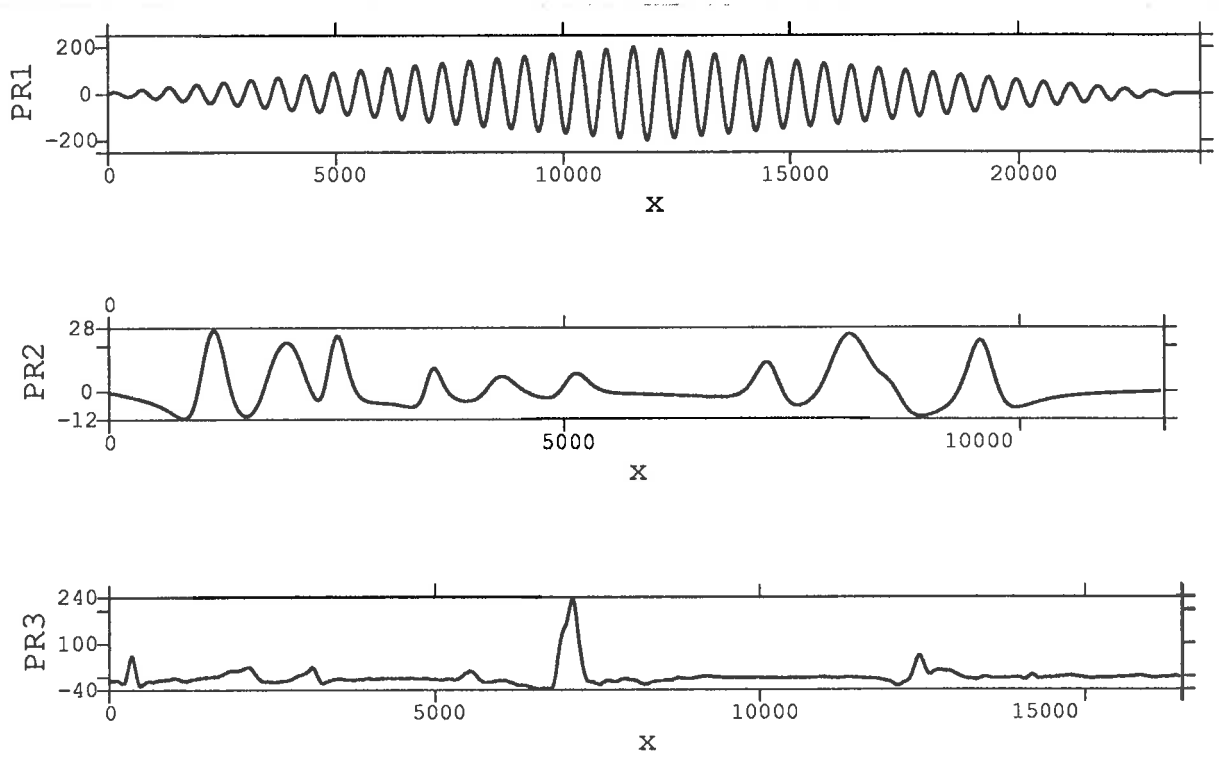

Figure K.1: Three test input profiles — PR1: a periodic sine wave of varying amplitude, PR2: a vertical magnetic gradient profile over a model comprising dipping dykes and PR3: a vertical gradient profile computed from total magnetic field data from the north of the main study area.

And

$$SQRT(j) = \begin{cases} \sqrt{V(j)}, & \text{if } V(j) \geq 0; \\ -\sqrt{-V(j)}, & \text{otherwise.} \end{cases}$$

Three test input profiles were used (see Figure K.1) — PR1: a periodic sine wave of varying amplitude, PR2: a vertical magnetic gradient profile over a model comprising dipping dykes and PR3: a vertical gradient profile computed from total magnetic field data from the north of the main study area. Each profile was sampled every 25 metres. The width of the window is specified in number of data points unless stated otherwise.

Distortion

1. Effect of scaling input data

   If the input vertical gradient profile is multiplied by a constant, say k^2, then all values in the output $SQRT$ profile are multiplied by k. However, scaling the input profile leaves the output AG profile unchanged.

2. Effect of non-zero DC level

   The profile PR3 was used as input to test the effect of shifting the DC level. To all the values of this profile, a constant value corresponding to 10^{-2}, 10^{-1}, 1, 10 and 10^2 times the total range was added. These DC-shifted profiles were used as input to the square-root operator and the results are shown in Figure K.2. Using a window width of 31 data points, the corresponding AG profiles were also computed and these are shown in Figure K.3.

   For both the square-root and AGC operators, if a small DC level is added to the original data, the shape and relative amplitudes of the output are not much affected. When the amount added is less than a tenth of the range, the output values are very little changed. However,when the DC level exceeds this, the output is distorted and unacceptable. The distortion in the output was most evident when the non-zero DC level is of the same order as or greater than the range.

   The DC level of a vertical gradient profile would be expected to be near zero and the average value of the profile (taken to be the DC level) may be subtracted from all data points if this is not the case.

3. Location of characteristic points

   By definition, the location of the zeroes, maxima and minima in the original vertical gradient profile are exactly reproduced in the $SQRT$ profile. Similarly, the location of the zeroes of the input profile are unchanged in the AG profile.

   For very small window widths, the maxima and minima may be shifted in the output. For the three test profiles and for window widths below 13, the peaks were very occasionally offset by one data point. Below 9, the offsets were much more common and could be 2 and sometimes even 3 data points. Such small window widths (related to anomaly widths) are not recommended (see below) and as the window width increases, this problem disappears.

4. Flattening of peaks

   Peaks appear more flattened in the $SQRT$ profile than in the AG profile (compare the outputs in Figures K.4, K.5 and K.6). Consider two points $V(1)$ and $V(2)$ on the left and right flanks of a gradient anomaly with peak value $V(peak)$. Then $V(1) = \frac{V(peak)}{k^2}$ and $V(2) = \frac{V(peak)}{l^2}$ where k and l are greater than 1.

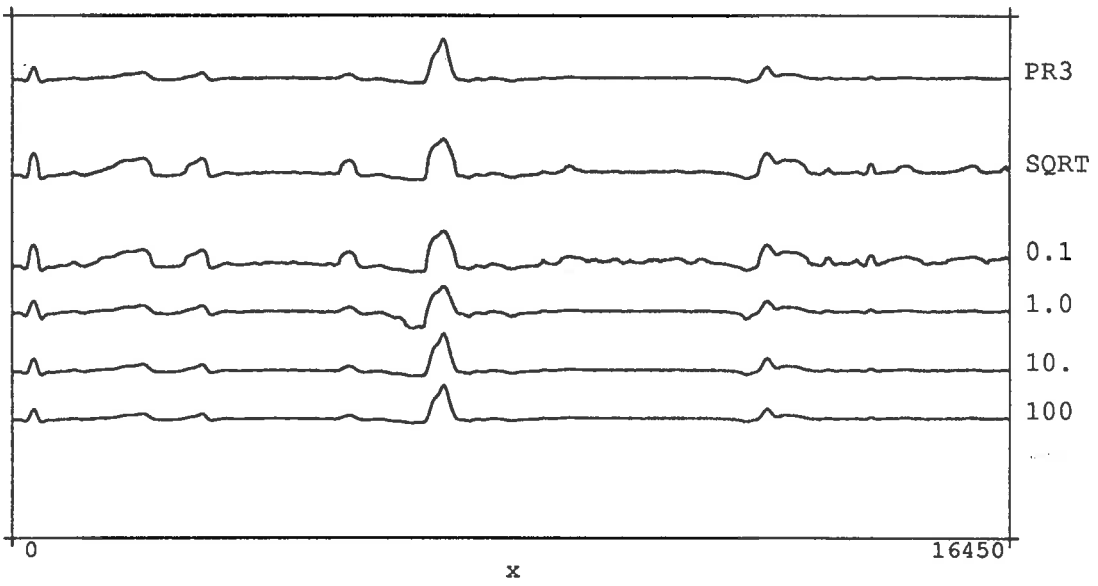

Figure K.2: The input profile is PR3. The output profiles are *SQRT* profiles corresponding to DC shifts in the input (DC shift is marked against each profile and is with respect to the total range of input values.)

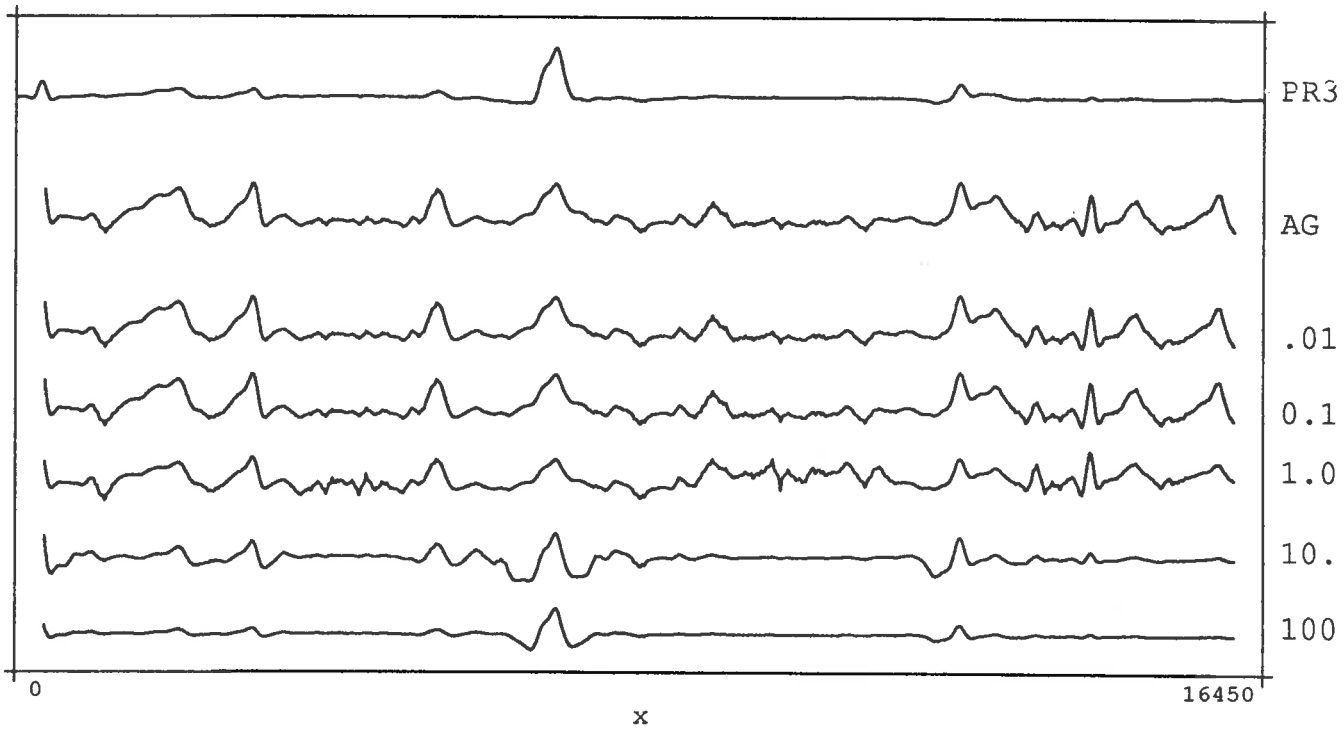

Figure K.3: The input profile is PR3. The output profiles are *AG* profiles corresponding to DC shifts in the input (DC shift is marked against each profile and is with respect to the total range of input values.)

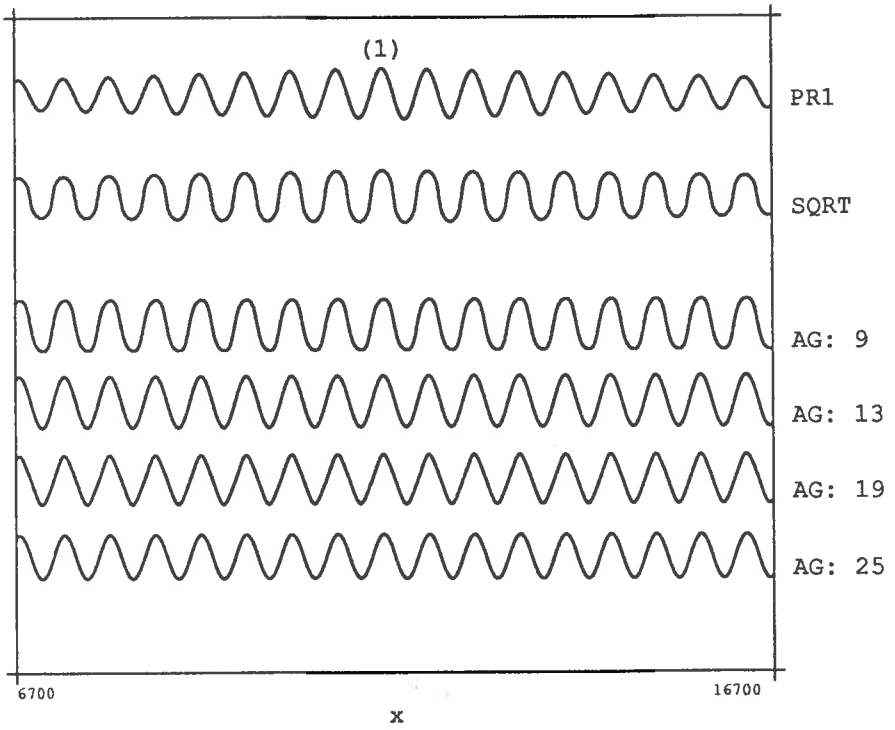

Figure K.4: The input profile is PR1. The output profiles are $SQRT$ and AG profiles (window width shown against AG profiles). Note anomaly 1.

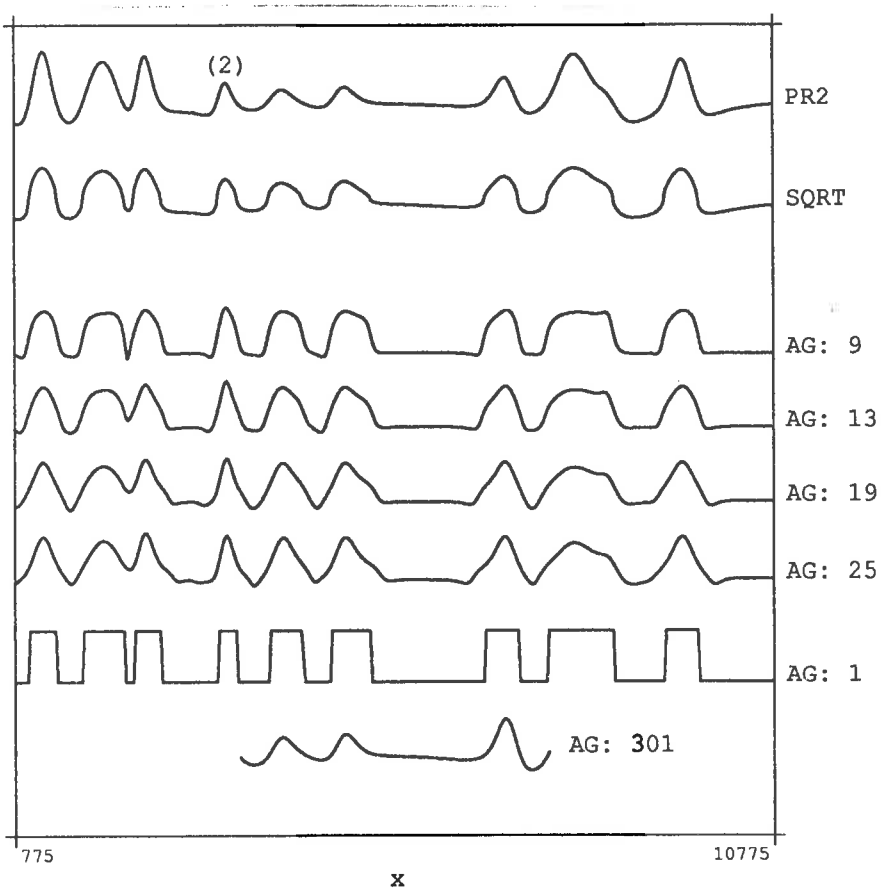

Figure K.5: The input profile is PR2. The output profiles are $SQRT$ and AG profiles (window width shown against AG profiles). Note anomaly 2.

Then

$$SQRT(1) = \frac{SQRT(peak)}{k}$$
$$SQRT(2) = \frac{SQRT(peak)}{l}.$$

However if the points are very close to one another, then RMS(1), RMS(2) and RMS(peak) will be nearly equal, and

$$AG(1) = \frac{AG(peak)}{k^2}$$
$$AG(2) = \frac{AG(peak)}{l^2}.$$

Therefore, the points $V(1)$ and $V(2)$ are closer in amplitude to $V(peak)$ in the $SQRT$ output than in the AG output and so the peak appears rounded in the $SQRT$ profile but is better defined in the AG profile. To demonstrate this, two anomalies were chosen (marked 1 and 2 in Figures K.4 and K.5). Selecting that part of the profile which covered the anomaly, the values in the vertical gradient, $SQRT$ and AG profiles were scaled to fit between 0 and 1. The values adjacent to the maxima in each case are presented in Table K.1. For both anomalies, the AG values show a steeper dropping off resulting in a sharper definition of the peaks.

5. Effect of noise

   Very low-amplitude noise may not be always identifiable on a $SQRT$ profile. Noise is characterized by high frequency, i.e. narrow width. The chosen window width is bound to be much larger than the width of the noise anomaly and therefore noise is readily identifiable on the AG profile. Though its amplitude is enhanced, the character of the anomaly is maintained. This is an asset as the distinction between noise and a high-frequency signal should be left to the interpreter.

Enhancement

The square-root operator acts as an amplitude filter rather than a frequency filter: i.e. it attenuates large anomalies and amplifies small anomalies regardless of their frequency content (McIntyre, 1981). The AGC operator is far more successful at amplifying weak signals than the square-root operator. This can be seen in Table K.2 in which the range of peak values in the input profiles and the corresponding range in the output $SQRT$ and AG profiles are tabulated. All profiles were first scaled to lie between 0 and 1.

The output of the AGC operator is dependent on the input frequency and therefore on the choice of window width chosen. It is designed to be independent of input amplitude and both weak and strong signals appear relatively equally strong in the output. The square-root operator amplifies weak signals but not as efficiently. The background level in the $SQRT$ profiles is quiet compared with the AG profiles (Figures K.4 to K.6) showing that very weak signals which can be detected on the AG profiles are not highlighted in the $SQRT$ profiles.

Profile: PR1						
	V	$SQRT$	AG			
			window widths			
			9	13	19	25
Smallest maxima	0.55	0.61	1.00	1.00	0.99	0.92
Biggest maxima	1.00	1.00	1.00	1.00	1.00	1.00
Smallest minima	0.00	0.00	0.00	0.00	0.00	0.00
Biggest minima	0.45	0.39	0.00	0.00	0.04	0.19

Table K.2: Comparison of anomaly enhancement in the output $SQRT$ and AG profiles.

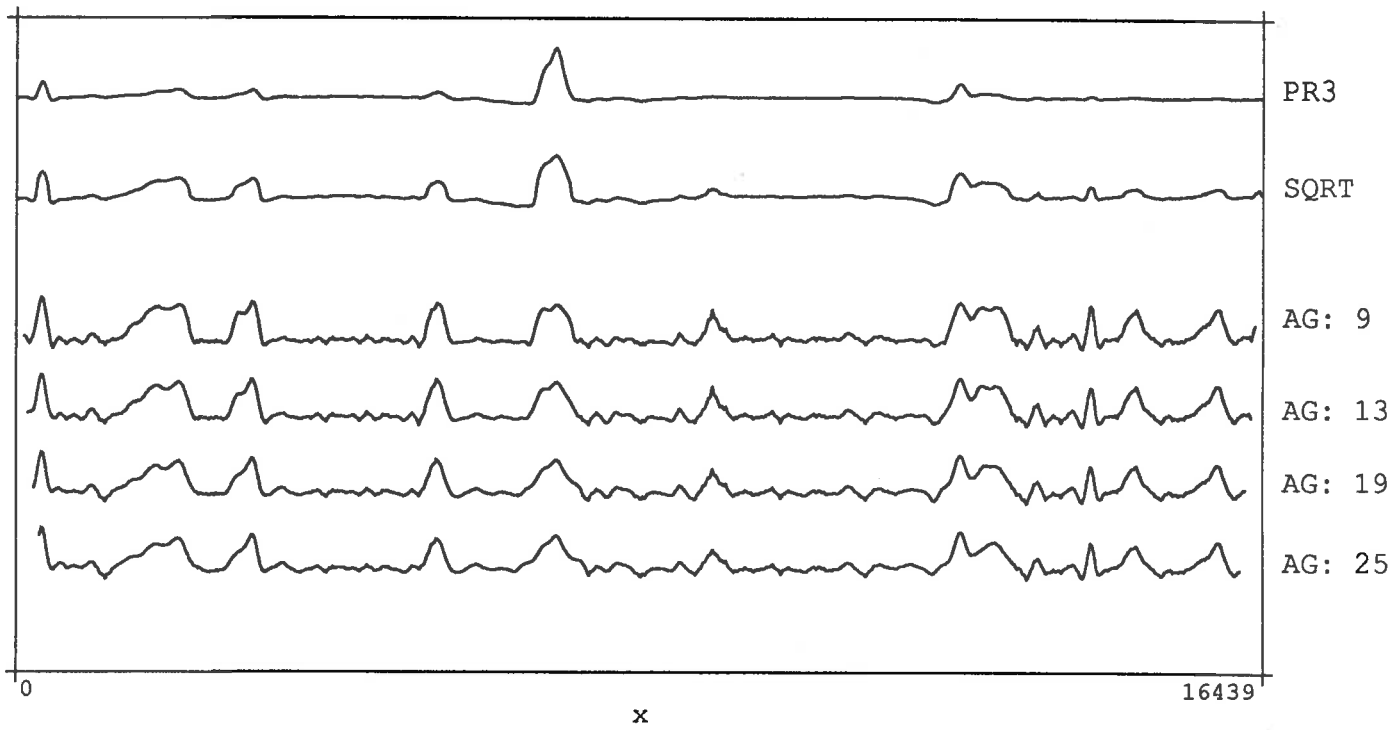

Figure K.6: The input profile is PR3. The output profiles are $SQRT$ and AG profiles (window width in data points shown against AG profiles).

The AGC operator: choice of window width

Very small window widths can cause a significant loss of signal character — strong and weak anomaly amplitudes become very similar in the output, peaks are flattened and slopes of anomaly flanks become near-vertical. In Figure K.5, when the window width = 1, all non-zero values are amplified to ± 1 depending on whether they are positive or negative while zeroes remain unchanged. This profile is useless as anomalies from different sources are indistinguishable in the output.

If an extremely large window width is chosen, then for any data point, the RMS value within this extremely large window will not be very different from that for any other point along the profile. Consequently, the output will be very similar to the input except that it will appear scaled down (see Figure K.5). Also for larger windows more data are lost on the ends of the profile during calculation.

To find the optimal range for the window width, the profile PR1 was used as the input. The ideal enhanced output with input as PR1 is a periodic sine wave of the same frequency but constant peak amplitude.

Comparing the *SQRT* and *AG* profiles (window widths of 9, 13, 19 and 25 data points), we can see that the *SQRT* and *AG* (width=9) profiles both show rounding of the anomaly peaks. In Figure K.6, the profiles with widths of 13, 19 and 25 are similar with better resolution brought out with the bigger window.

The root mean square error between the *AG* (width=13 data points) output and the ideal output (both scaled to fit between 0 and 1) was 0.00. This window corresponds to half the period or the distance between an adjacent high and low. In this example, all peaks are amplified to the same value and the shape of the input sine wave is preserved.

Vertical gradient profiles show a variety of different anomaly widths. In general, a vertical gradient anomaly consists of a low-high-low combination or vice-versa. The peak-to-peak distance is the distance between adjacent low and high. To bring the peaks out clearly, the chosen window width must be greater than or equal to the peak-to-peak distance. For anomalies investigated in the study area, this distance was commonly less than 1000 metres and often around 300 to 500 metres. The optimal window width is the smallest window which will produce the best visual output and provide the necessary enhancement with the minimum distortion.

As a guide, the window width should lie between 375 and 600 metres, possibly going up to 800 metres and this should achieve the desired result. As the window gets wider, more information is lost on the edges and there is less amplification of the weak signals.

Appendix L: The structural history of the Kanmantoo Group — a summary

The geology of the Kanmantoo Group, particularly its structural history, is complex and controversial. Many previous researchers have concentrated on small areas and as a result the interpreted importance and number and order of the different deformation events varies from area to area. The two major reviews (Offler and Fleming, 1968; Mancktelow, 1979) differ considerably. Through the interpretation of the available high-quality aeromagnetic data and integrating these results with known geology, the Kanmantoo Group was deduced to have undergone three phases of macroscopic folding: F_{early}, F_{main} and F_{later}. Each phase may have included more than one event.

The three subzones, the Kanmantoo Synclinal Subzone (KNSZ), the Karinya Synclinal Subzone (KRSZ) and the Intermediate Subzone (ISZ) comprise the Central Magnetic Zone (CMZ). The major folding which produced the Kanmantoo Synclinorium is taken to be F_{main}. An early deformation was recognized in some places and these F_{early} folds have been folded by F_{main}. The second phase of folding was pervasive throughout the CMZ. In the ISZ, strong overprinting by a later generation of folds, F_{later}, may have obscured the F_{main} phase of folding.

The Delamerian Orogeny transformed the Proterozoic and Cambrian rocks of the Adelaide Geosyncline into an orogenic upland (Thomson, 1969a). The effects of the orogeny were strongest in the Mt. Lofty Ranges where several deformation events have been recorded (Offler and Fleming, 1968; Mancktelow, 1979).

The earliest known deformation in the region involved the mobilization of the Barossa Complex and subsequent formation of the Adelaide Geosyncline. There was a hiatus between the deposition of Precambrian sediments (the Marinoan) and the Cambrian sediments (Preiss, 1987). The present contact between the Kanmantoo Group and the Precambrian is represented by the Nairne Fault in some places. The Nairne Fault, or its equivalent, has been extended into the vicinity of the Channel Anomaly where the basal Kanmantoo Group rocks are in faulted contact with the Adelaide Supergroup and Normanville Group rocks. The Nairne Fault, Snelling Fault and Cygnet Fault are believed to have controlled the deposition of the Kanmantoo Group (Preiss, 1987).

The polyphase and complex deformational history of the Kanmantoo Group started with syn-depositional deformation. The effects of syn-depositional events are largely unknown as they have been overprinted by the effects of the Delamerian Orogeny and the accompanying metamorphism. Delamerian Orogeny may have commenced prior to the final stages of deposition.

The main phase of the Delamerian Orogeny, F_{main}, which affected the whole of the Adelaide Geosyncline to varying degrees, produced upright, open macroscopic folds. During F_{main}, the Kanmantoo Synclinorium and Karinya Synclinorium were formed. The fold pattern and metamorphic history are similar in the KNSZ and KRSZ and this has resulted in similar magnetic patterns. Faulting was associated with this phase of folding and faults such as the Talisker and Alex Lookout Faults developed on the steep to overturned limbs of F_{main} folds (Mancktelow, 1979).

Prior to the F_{main} event, the region suffered an earlier deformation. Geophysically anomalous areas which may record this event have been identified in the areas of the Channel Anomaly, Tinpot Anomaly and Rockleigh Anomaly. Several geologists have reported folds prior to F_{main} and also early thermal activity. How much of what appears to be pre-F_{main} folds is related to syn-depositional events and how much to the Delamerian Orogeny is unknown. It is likely that the onset of the Delamerian Orogeny was marked by the development of thrust faults and isoclinal and recumbent folds as has been documented for most other Palaeozoic foldbelts (e.g. the Caledonides: Elliot and Johnson, 1980). The apparent confinement of F_{early} structures to the ubiquitous Backstairs Passage Formation is probably due to the nature of the event. The effect of the F_{early} phase was strongest near the base of the sedimentary pile where the thickness of sediments was greatest. The upper units of the Kanmantoo Group may have remained relatively undeformed. The Nairne Fault may represent one such thrust. It has been folded by F_{main} (Macclesfield region) and must be older than F_{main}. The two main pyrite bands of the Talisker Calc-silicate may also be examples of repetition as a result of early thrust movements.

Faulting associated with F_{later} is common in the ISZ. The faults run for tens of kilometres and trend NNW. The Springton Fault has vertical movement on it (west block down). The NNW faults appear to form a set of left-lateral steeply dipping faults. The NE trending faults are common throughout the region though it is not known what the sense of movement along them was. They transect the Delamerian Foldbelt and may have been active post-F_{later}.

There is a marked contrast between the intense and complex magnetic character of the Intermediate Subzone and the relatively subdued magnetic response of the KNSZ and KRSZ. The region is characterized by multiple linear anomalies which trend NNW and are parallel to the metamorphic grade boundaries. Structures in this area appear to be discordant with structures elsewhere in the KNSZ and the KRSZ. The open, upright folds common to the KNSZ and the KRSZ are less common in the ISZ. This may be due to the overprinting of F_{main} folds by later folds because temperatures were still high in the ISZ which is within the highest grade metamorphic zone. The increased number of magnetic anomalies may be due to repetition, increased magnetite content in the higher-grade rocks, and increased thickness caused by thrusts and soft-sediment slumping.

It is possible that the deformational history of part of the ISZ is different from that of the KNSZ and the KRSZ. Madigan (1988) has interpreted NS-stretching lineations observed in the Rathjen Gneiss as evidence of previously unrecorded NS movement in the region. Major NNW trending faults separate subareas A2, C1 and A4 of the ISZ. These faults may represent the mechanism by which these subareas were located in their present position. These rocks could be allochthonous. Alternatively, they may have been uplifted in a "pop-up" left-lateral wrench fault system which twisted the Karinya Syncline northwards with respect to the Kanmantoo Syncline. These suggestions are speculative and there is little data to either confirm or deny them.

Errata

1. Chapter 3, page 38, paragraph 3
   For "In Figure 3.6, the use of a small scale" read "In Figure 3.7, the use of a large scale".
   For "In Figure 3.7, a larger scale is used" read "In Figure 3.6, a smaller scale is used".

2. Chapter 5, page 54
   In Figures 5.1 and 5.2, change the limits of the axes as follows: the easting varies from "300000 to 305000" and the northing from "6085000 to 6090000".

3. Chapter 7, page 99
   In Figure 7.19, change "313000" to "320000", "320000" to "332000", "6115000" to "6122500" and "6125000" to "6134000".

4. Appendix I, page 1
   In two places, replace "(+ - dip - 90)" with "$(\lambda + \mu - \delta - 90°)$".

References

Abbas, S. A. F., 1975, *Granitic and migmatitic rocks of the Cooke Hill area, South Australia, and their structural setting*, Ph. D. thesis, Univ. Adelaide (unpubl.).

Abele, C. and McGowran, B., 1959, *The geology of the Cambrian south of Adelaide (Sellick Hill to Yankalilla)*, Trans. R. Soc. S. Aust., 82: 301–320.

Alderman, A. R., 1929, *Magmatic Differentiation at Mannum*, Trans. R. Soc. S. Aust., 53: 249–257.

Alderman, A. R., 1931, *Petrographic notes on some basic rocks from the Mount Barker and Woodside districts*, Trans. R. Soc. S. Aust., 55: 163–167.

Allen, R., 1977, *Metamorphic phase relationships in the Kanmantoo*, B. Sc. (Hons.) thesis, Univ. Adelaide (unpubl.).

Åm, K., 1972, *The arbitrarily magnetized dyke: interpretation by characteristics*, Geoexploration, 10: 63–90.

Anderson, J. A., 1975, *Structural and strain analysis of the nose of the Myponga-Little Gorge Inlier, Fleurieu Peninsula, S.A.*, B. Sc. (Hons.) thesis, Univ. Adelaide.

Annersten, H., 1968, *A mineral chemical study of a metamorphosed iron formation in northern Sweden*, Lithos, 1: 374–397.

Askins, P. W., 1968, *Geochemical exploration around the Aclare mine and mineral deposits of the surrounding region*, B. Sc. (Hons.) thesis, Univ. Adelaide (unpubl.).

Atchuta Rao, D., Ram Babu, H. V. and Sanker Narayan, P. V., 1981, *Interpretation of magnetic anomalies due to dykes: The complex gradient method*, Geophysics, 46: 1572–1578.

Banno, S. and Kanehira, K., 1961, *Sulphide and oxide minerals in schists of the Sanbagawa and central Abukama metamorphic terranes*, Jpn. J. Geol. Geogr., 23: 331–348.

Barongo, J. O., 1985, *Method for depth estimation and aeromagnetic vertical gradient anomalies*, Geophysics, 50: 963–968.

Belperio, A.P. (compiler), 1985, *Echunga map sheet, 1:50 000 geological series*, S.A. Department of Mines and Energy.

Benlow, J. C. and Taylor, B. J., 1963, *Geophysical investigation of the Dawesley aeromagnetic anomaly*, S.A. Department of Mines and Energy, Mining Review, 119: 43–49.

Bhattacharyya, B. K., 1965, *Two-dimensional harmonic analysis as a tool for magnetic interpretation*, Geophysics, 30: 829–857.

BMR, 1980, *Regional aeromagnetic contour map of Adelaide, South Australia, New South Wales and Victoria*, Preliminary edition, Bureau of Mineral Resources.

Boord, R., 1985, *Sedimentology of the Cambrian upper Kanmantoo Group, southern Fleurieu Peninsula, South Australia*, B. Sc. (Hons.) thesis, Univ. Adelaide (unpubl.).

Both, R. A., in press, *Geology and mineral deposits of the Kanmantoo Trough*, In: Hughes, F. (ed.) Geology of the mineral deposits of Australia and Papua New Guinea, Australas. Inst. Min. Met.

Bourman, R. P. and Lindsay, J. M., in press, *The timing, extent and character of faulting on the eastern margin of the Mount Lofty Ranges, South Australia*, Trans. Roy. Soc. S. Aust.

Bowes, D. R., 1954, *The metamorphic and igneous history of Rosetta Head, South Australia*, Trans. R. Soc. S. Aust., 77: 182–214.

Boyd, D. M., 1967, *The contribution of airborne magnetic surveys to geological mapping*, In: Morley, L. W. (ed.), Mining and Groundwater Geophysics, Geological Survey of Canada, Economic Geology Report, 26: 213–227.

Breiner, S., 1970, *Transverse and longitudinal magnetic gradiometers for exploration*, Presented at the 40th Ann. Internat. Mtg. Soc. Expl. Geophys.

Brotherton, R. A., 1967, *A metamorphic study of the Marino Group phyllites, Delamere and Sellick Hill sections with special reference to the iron oxides.*, B. Sc. (Hons.) thesis, Univ. Adelaide (unpubl.).

Brown, H. Y. L., 1883, *Geological sketch map of South Australia exclusive of the Northern Territory, 1inch/40 miles (1:2,534,400)*, Adel. Surv. Gen. Off.

Brown, H. Y. L., 1908, *Record of the mines of South Australia*, Government printer, Adelaide.

Buddington, A. F., Fahey, J. and Vlisidis, A., 1963, *Degree of oxidation of Adirondack iron oxide and iron-titanium oxide minerals in relation to petrogeny*, J. Petrol., 4: 138–169.

Campana, B. and Horwitz, R.C., 1956, *The Kanmantoo Group of South Australia considered as a transgressive sequence*, Aust. J. Sci., 18: 128–129.

Carroll, D., 1958, *The role of clay minerals in the transportation of iron*, Geochim. Cosmochim. Acta, 14: 1.

Chamalaun, F. H., 1986, *Extension of the Flinders Ranges anomaly*, Expl. Geophy., 17: 31.

Chandler, V. W., 1985, *Interpretation of Precambrian geology in Minnesota using low-altitude, high-resolution aeromagnetic data*, In: Hinze, W. J. (ed.), The utility of regional gravity and magnetic anomaly maps, Society of Exploration Geophysicists, 375–391.

Chappell, B. W. and White, A. J. R., 1974, *Two contrasting granite types*, Pacific Geology, 8: 173–174.

Chinner, G. A., 1955, *The granite gneisses of the Barossa ranges*, M. Sc. thesis, Univ. Adelaide (unpubl.).

Chinner, G. A., 1960, *Pelitic gneisses with varying ferrous/ferric ratios from Glen Clova, Angus, Scotland*, J. Petrol., 1: 178–217.

Clark, D. A., 1983, *Comments on magnetic petrophysics*, Bull. Aust. Soc. Explor. Geophys., 14: 49–62.

Clarke, G. L. and Powell, R., 1989, *Basement-cover interaction in the Adelaide Foldbelt, South Australia: the development of an arcuate foldbelt*, Tectonophysics, 158: 209–226.

Coats, R. P. and Thomson, B. P., 1959, *Truro map sheet, 1:63 360 geological series*, S.A. Department of Mines and Energy.

Cobb, M.A. and Farrand, M.G., 1984, *A new occurrence of the Truro Volcanics*, Geol. Surv. S. Aust., Quart. Geol. Notes, 89: 8–10.

Compston, W., Crawford, A. R. and Bofinger, V. M., 1966, *A radiometric estimate of the duration of sedimentation in the Adelaidean Geosyncline*, J. Geol. Soc. Aust., 13: 229.

Cooper, B. J., 1988, *The Milendella Limestone Member (Early Cambrian, Kanmantoo Group), a stratigraphic marker horizon in the Karinya Syncline*, S.A. Department of Mines and Energy, Report Book, 88/47: 13 pages.

Cooper, R. A. and Grindlay, G. W. (eds.), 1982, *Late Proterozoic to Devonian sequences in southeastern Australia, Antarctica and New Zealand and their correlation*, Geol. Soc. Aust. Special Publication, 9: 103 pages.

Coppin, R. J., Hall, J. McG. and Milton, B. E., 1973, *Bouguer gravity anomaly map of South Australia, 1:1 000 000 scale*, S.A. Department of Mines and Energy.

Curtis, C. D. and Spears, D. A., 1968, *The formation of sedimentary iron minerals*, Econ. Geol., 63: 257–270.

Daily, B., 1956, *The Cambrian in South Australia*, Ph. D. thesis, Univ. Adelaide (unpubl.).

Daily, B., 1963, *The fossiliferous Cambrian succession on Fleurieu Peninsula, South Australia*, Rec. S. Aust. Mus., 14: 579–601.

Daily, B., 1977, *Notes on the geology of Kangaroo Island*, Kangaroo Island field conference, October 1977, Geol. Soc. Aust., S. Aust. division (unpubl.).

Daily, B., Firman, B. J., Forbes, B. G. and Lindsay, J. M., 1976, *Geology*, In:Twidale, C. R. and others (eds.), Natural history of the Adelaide region, Roy. Soc. S. Aust., 5–42.

Daily, B. and Milnes, A. R., 1971a, *Stratigraphic notes on Lower Cambrian fossiliferous metasediments between Campbell Creek and Tunkalilla Beach in the type section of the Kanmantoo Group, Fleurieu Peninsula, South Australia*, Trans. R. Soc. S. Aust., 95: 199–214.

Daily, B. and Milnes, A. R., 1971b, *Discovery of Late Precambrian Tillites (Sturt Group) and younger metasediments (Marino Group) on Dudley Peninsula, Kangaroo Island, South Australia*, Search, 2: 431–433.

Daily, B. and Milnes, A. R., 1972a, *Revision of the stratigraphic nomenclature of the Cambrian Kanmantoo Group, South Australia.*, J. Geol. Soc. Aust., 19: 197–202.

Daily, B. and Milnes, A. R., 1972b, *Significance of basal Cambrian metasediments of andalusite grade, Dudley Peninsula, Kangaroo Island, South Australia*, Search, 3: 89–90.

Daily, B. and Milnes, A. R., 1973, *Stratigraphy, structure and metamorphism of the Kanmantoo Group (Cambrian) in its type section east of Tunkalilla Beach, South Australia*, Trans. R. Soc. S. Aust., 97: 213–242.

Dalgarno, C. R., 1964, *Lower Cambrian stratigraphy of the Flinders Ranges*, Trans. R. Soc. S. Aust., 88: 129–144.

Dasch, E. J., Milnes, A. R. and Nesbitt, R. W., 1971, *Rubidium-strontium geochronology of the Encounter Bay Granite and adjacent metasedimentary rocks, South Australia*, J. Geol. Soc. Aust., 18: 259–266.

Dickinson, S. B. and Coats, R. P., 1957, *Kapunda map sheet, 1:63 360 geological series*, S.A. Department of Mines and Energy.

Dods, S. D., Teskey, D. J. and Hood, P. J., 1985, *The new series of 1:1 000 000-scale magnetic-anomaly maps of the Geological Survey of Canada: Compilation techniques and interpretation*, In: Hinze, W. J. (ed.), The utility of regional gravity and magnetic anomaly, maps, Society of Exploration Geophysicists, 69–87.

Drummond, A. J., 1972, *The geology of the Australia Plains area, northern Mt. Lofty Ranges, South Australia*, B. Sc. (Hons.) thesis, Univ. Adelaide (unpubl.).

Duval, J. S., Jr., Cook, B. and Adams, J. A. S., 1971, *Circle of investigation of an air-borne gamma-ray spectrometer*, J. Geophys. Res., 76: 8466–8470.

Elliot, D. and Johnson, M. R. W., 1980, *The structural evolution of the northern part of the Moine thrust belt*, Trans. R. Soc. Edin., 71: 69–96.

Fander, H. W., 1960, *Accessory minerals of South Australian granites*, M. Sc. thesis, Univ. Adelaide (unpubl.).

Farrand, M., 1985, *Rocks from the Kanmantoo Trough near Sedan Hill including possible equivalents to the Truro Volcanics*, S.A. Department of Mines and Energy, Report Book, 85/32: 33 pages.

Faul, H. (ed.), 1954, *Nuclear Geology*, John Wiley, New York, 414 pages.

Firman, J. B., 1974, *Structural lineaments in South Australia*, Trans. R. Soc. S. Aust., 98: 153–171.

Fleming, P. D., 1965, *The geology of an area east of Angaston, South Australia*, B. Sc. (Hons.) thesis, Univ. Adelaide (unpubl.).

Fleming, P. D., 1971, *Metamorphism and folding in the Mt. Lofty Ranges, South Australia, with particular reference to the Dawesley-Kanmantoo area.*, Ph. D. thesis, Univ. Adelaide (unpubl.).

Fleming, P. D., 1973, *Mg-Fe distribution between coexisting garnet and biotite, and the status of fibrolite in the andalusite-staurolite zone of the Mt. Lofty Ranges, South Australia*, Geol. Mag., 109: 477–482.

Fleming, P. D. and Offler, R., 1968, *Pre-tectonic metamorphic crystallization in the Mt. Lofty Ranges, South Australia*, Geol. Mag., 105: 356–359.

Fleming, P. D. and White, A. J. R., 1984, *Relationships between deformation and partial melting in the Palmer migmatites, South Australia*, Aust. J. Earth Sci., 31: 351–360.

Flint, D. J., 1976, *Heavy mineral rich sediments within the Kanmantoo Group, Kangaroo Island*, Geol. Surv. S. Aust., Quart. Geol. Notes, 59: 11–12.

Flint, D. J., 1978, *Deep sea fan sedimentation of the Kanmantoo Group, Kangaroo island*, Trans. R. Soc. S. Aust., 102: 203–222.

Flint, D. J. and Grady, A. E., 1979, *Structural geology of Kanmantoo Group sediments between West Bay and Breakneck River, Kangaroo Island, South Australia*, Trans. R. Soc. S. Aust., 103: 45–56.

Foden, J. D., Turner, S. P. and Morrison, R. S., in press, *Tectonic implications of Delamerian magmatism in South Australia and western Victoria.*, In: Brian Daily Memorial Volume, Geol. Soc. Aust. Special Publ.

Forbes, B. G. (compiler), 1979, *Onkaparinga map sheet, 1:50 000 preliminary geological map*, S.A. Department of Mines and Energy.

Forbes, B. G. (compiler), 1983, *Noarlunga map sheet, 1:50 000 geological series*, S.A. Department of Mines and Energy.

Forbes, B. G., Coats, R. P. and Daily, B., 1972, *Truro Volcanics*, Geol. Surv. S. Aust., Quart. Geol. Notes, 44: 1–5.

French, B. M., 1968, *Progressive contact metamorphism of the Biwabik iron-formation, Mesabi Range, Minnesota*, Minn. Geol. Surv. Bull., 45: 103 pages.

Gatehouse, C. G. (compiler), 1988a, *Tepko map sheet, 1:50 000 geological series*, S.A. Department of Mines and Energy.

Gatehouse, C. G. (ed.), 1988b, *Kanmantoo Field Symposium excursion guide*, S.A. Department of Mines and Energy, Report Book, 88/35: 89 pages.

Gatehouse, C. G. and Jago, J. B., 1988, *Carrickalinga Head — Carrickalinga Head Formation*, In: Gatehouse, C. G. (ed.) Kanmantoo Field Symposium excursion guide, S.A. Department of Mines and Energy, Report Book, 88/35: 22–24.

Gatehouse, C. G., Jago, J. B. and Cooper, B. J., in press, *Stratigraphy and sedimentology of the Carrickalinga Head Formation, Kanmantoo Group, South Australia.*, In: Brian Daily Memorial Volume, Geol. Soc. Aust. Special Publ.

Gatley, P. A., 1973, *Geology of the Brukunga area*, III Year Project, S. Aust. Inst. Tech. (unpubl.).

Gay, S. P., Jr., 1963, *Standard curves for interpretation of magnetic anomalies over long tabular bodies*, Geophysics, 28: 161–200.

Gay, S. P., Jr., 1972, *Fundamental characteristics of aeromagnetic lineaments, their geological significance and their significance to geology*, American Stereo Map Company, Salt Lake City, Utah, 94 pages.

George, R. J., 1963, *The geology of the Talisker Mine area.*, B. Sc. (Hons.) thesis, Univ. Adelaide (unpubl.).

George, R. J., 1967, *Metamorphism of the Nairne Pyrite Deposit*, Ph. D. thesis, Univ. Adelaide (unpubl.).

George, R. J., 1969, *Sulphide-silicate reactions during metamorphism of the Nairne Pyrite Deposit*, Proc. Australas. Inst. Min. Metall., 230: 1–7.

Gerdes, R.A. (compiler), 1986, *Milang map sheet, 1:100 000 aeromagnetic map of total intensity, sheet 6627*, S. A. Department of Mines and Energy.

Goode, B. F., 1927, *The Mannum Granite*, Trans. R. Soc. S. Aust., 51: 126–128.

Grant, F. S., 1973, *The magnetic susceptibility mapping method for interpreting aeromagnetic surveys*, Presented at the 43rd Ann. Internat. Mtg. and Expos., Soc. Explor. Geophys., Mexico City.

Grant, F. S., 1985a, *Aeromagnetics, geology and ore environments, I. Magnetite in igneous, sedimentary and metamorphic rocks: An overview*, Geoexploration, 23: 303–333.

Grant, F. S., 1985b, *Aeromagnetics, geology and ore environments, II. Magnetite and ore environments*, Geoexploration, 23: 335–382.

Grasso, R. and McManus, J., 1954, *The geology of the Callington area.*, B. Sc. (Hons.) thesis, Univ. Adelaide (unpubl.).

Greenhalgh, S. A., Tapley, D. and Singh, R., 1989, *Crustal heterogeneity in South Australia, earthquake evidence*, Geophy. Jour. of the RAS, DGG and EGS, 96: 85–99.

Greenhalgh, S. A., Tapley, D. and von der Borch, C. C., in press, *Explosion seismic determination of crustal structure beneath the Adelaide Geosyncline, South Australia*, Physics of the Earth and Planetary Interiors.

Gregory, A. F. and Horwood, J. L., 1961, *A laboratory study of gamma-ray spectra at the surface of rocks*, Dep. Energy, Mines and Resources, Ottawa, Mines branch, Res. Rep., R85: 52 pages.

Guinness, E. A., Arvidson, R. E., Leff, C. E., Edwards, M. H. and Bindschadler, D. L., 1983, *Digital image processing applied to analysis of geophysical and geochemical data for southern Missouri*, Economic Geology, 78: 654–663.

Gunn, P. J., 1984, *Recognition of ancient rift systems: examples from the Proterozoic of South Australia*, Bull. Aust. Soc. Explor. Geophys., 15: 85–98.

Hansen, A. K., 1975, *Gravity and magnetic interpretation in the Sedan-Cambrai region of the Murray Basin*, B. Sc. (Hons.) thesis, Univ. Adelaide (unpubl.).

Hardwick, C. D., 1984, *Nonoriented cesium sensors for airborne magnetometry and gradiometry*, Geophysics, 49: 2024–2031.

Harms, J., 1951, *The geology of part of the Cambrai Military sheet*, B. Sc. (Hons.) thesis, Univ. Adelaide (unpubl.).

Henkel, H. and Guzmán, M., 1977, *Magnetic features of fracture zones*, Geoexploration, 15: 173–181.

Henstridge, D. A., 1970, *The petrology and geochemistry of the upper south-east granites, South Australia*, B. Sc. (Hons.) thesis, Univ. Adelaide (unpubl.).

Hildenbrand, T. G., 1985, *Magnetic terranes in the central United States determined from the interpretation of digital data*, In: Hinze, W. J. (ed.), The utility of regional gravity and magnetic anomaly maps, Society of Exploration Geophysicists, 248–266.

Hoesni, M. J., 1985, *The granitoids and migmatites of the Monarto area, South Australia.*, B. Sc. (Hons.) thesis, Univ. Adelaide (unpubl.).

Hood, P. J., 1964, *The Koenigsberger ratio and the dipping-dyke equation*, Geophysical Prospecting, 12: 440–456.

Hood, P. J., 1975, *The GSC aeromagnetic gradiometer, a new mapping tool for mineral exploration*, The Northern Miner, 61: A20–21.

Hood, P. J., Holroyd, M. T. and McGrath, P. H., 1979, *Magnetic methods applied to base metal exploration*, In: Hood, P. J. (ed.) Geophysics and geochemistry in the search for metallic ores, Geological Survey of Canada, Economic Geology Report, 31: 77–104.

Hord, M. R., 1982, *Digital image processing of remotely sensed data*, Academic Press, New York, 256 pages.

Horn, B. K. P., 1981, *Hill shading and the reflectance map*, Proc. IEEE, 69: 14–47.

Horsfall, C. L., 1973, *Interpretation of aeromagnetic and ground magnetic data over the Houghton Inlier, S. A., as an aid to geological mapping*, B. Sc. (Hons.) thesis, Univ. Adelaide (unpubl.).

Horwitz, R. C., Thomson, B. P. and Webb, B. P., 1959, *The Cambrian-Precambrian boundary in the eastern Mt. Lofty Ranges: South Australia*, Trans. R. Soc. S. Aust., 82: 205–218.

Horwitz, R. C. and Thomson, B. P., 1960, *Milang map sheet, 1:63360 geological series*, S.A. Department of Mines and Energy.

IAEA, 1979, *Gamma-ray surveys in uranium exploration*, International Atomic Energy Agency, Vienna, Technical Reports series number 186, 89 pages.

Ishihara, S., 1977, *The magnetite-series and ilmenite-series granitic rocks*, Mining Geol., 27: 293–305.

Ishihara, S., 1981, *The granitoid series and mineralization*, In: Skinner, B. J. (ed.) Econ. Geol. 75th Anniv. Vol., 458–484.

Isles, D. J., Harman P. G. and Cunneen, J. P., 1988, *Aeromagnetics and the Yilgarn gold rush*, In: Goode, A. D. T. and Bosma, L. I. (eds.) Bicentennial Gold 88, Extended Abstracts, Geol. Soc. Aust., Abstracts No. 22: 259–264.

Ivezich, M. M., 1969, *A geophysical investigation of the Mt. Beevor shear zone and the Nairne pyrite member*, B. Sc. (Hons.) thesis, Univ. Adelaide (unpubl.).

Jago, J. B., Daily, B., von der Borch, C. C., Cernovskis, A. and Saunders, N., 1984, *First reported trilobites from the Lower Cambrian Normanville Group, Fleurieu Peninsula*, Trans. R. Soc. S. Aust., 108: 207–211.

Jago, J. B., Gehling, J. G. and Daily, B., 1986, *Cambrian sediments of the Sellick Hill-Carrickalinga Head area, Fleurieu Peninsula, South Australia*, In: Parker, A. J. (compiler), One day geological excursions of the Adelaide region, Geol. Soc. Aust., S. Aust. division, 67–81.

Jenkins, R. J. F., 1986, *Ralph Tate's enigma — and the regional significance of thrust faulting in the Mt. Lofty Ranges*, Eighth Australian Geological Convention, Geol. Soc. Aust., Abstracts, 15: 101.

Jenkins, R. J. F., in press, *The Adelaide Fold Belt: tectonic reappraisal*, In: Brian Daily Memorial Volume, Geol. Soc. Aust. Special Publ.

Karner, G. D., Weissel, J. K., Dewey, J. F. and Munday, T. J., 1987, *Geotectonic imaging of the north-western European continent and shelf*, Marine and Petroleum Geology, 4: 94–102.

Killeen, P. G., 1979, *Gamma ray spectrometric methods in uranium exploration — application and interpretation*, In: Hood, P. J. (ed.) Geophysics and geochemistry in the search for metallic ores, Geological Survey of Canada, Economic Geology Report, 31: 163–229.

Kleeman, A. W., 1934, *The Murray Bridge Granite*, Trans. R. Soc. S. Aust., 58: 237–241.

Kleeman, A. W. and Skinner, B. J., 1959, *The Kanmantoo Group in the Strathalbyn-Harrogate region, South Australia*, Trans. R. Soc. S. Aust., 82: 61–71.

Kleeman, J. D., 1965, *Notes on the geologic map "Geology north of Truro"*, B. Sc. (Hons.) thesis, Univ. Adelaide (unpubl.).

Kowalik, W. S. and Glenn, W. E., 1987, *Image processing of aeromagnetic data and integration with Landsat images for improved structural interpretation*, Geophysics, 52: 875–884.

Kremor, A. G., 1980, *The geology of an area east of Eden Valley*, III Year Project, S. Aust. Inst. Tech. (unpubl.).

LaGanza, R. F., 1959a, *The Nairne Sulfide Deposit, Nairne, South Australia*, M. Sc. thesis, Univ. Adelaide (unpubl.).

LaGanza, R. F., 1959b, *Pyrite investigations at Nairne, South Australia*, Econ. Geol., 54: 895–902.

Large, R. L., 1977, *Chemical evolution and zonation of massive sulphide deposits in volcanic terrains*, Econ. Geol., 72: 549–572.

Lawrence, R. W., 1980, *Stratigraphy and structure in and adjacent to the Talisker Formation (Nairne Pyrite equivalent) in the eastern Mount Lofty Ranges*, B. Sc. (Hons.) thesis, Univ. Adelaide (unpubl.)

Leslie, W. C., 1962, *Geology of the Delamere area, South Australia*, B. Sc. (Hons.) thesis, Univ. Adelaide (unpubl.).

Lewis, A. M., 1985, *A gravity and magnetic investigation of the Monarto granite, S.A.*, B. Sc. (Hons.) thesis, Univ. Adelaide (unpubl.).

Lewis, P., 1985, *CRA Exploration 13 E. L.'s reports*, S.A. Department of Mines and Energy, Open File Report, 3957, XIV: page 402.

Lindqvist, W. F., 1969, *Geology and metamorphic history of the Kanmantoo copper Deposit, South Australia*, Ph. D. thesis, Univ. London (unpubl.).

Liu, S. F. and Fleming, P. D., 1989, *Amphibolites/metadolerites and their tectonic implications from the Mt. Lofty Ranges metamorphic belt, S. A.*, Australasian tectonics, Specialist group in tectonics and structural geology, Geol. Soc. Aust., Abstracts, 24: 89–90.

Lucas, M. D., 1980, *Geology of the area between Springton and Eden Valley*, III Year Project, S. Aust. Inst. Tech. (unpubl.).

Madigan, T. L. A., 1988, *The Rathjen Gneiss: Constraints on the tectonic history of the Kanmantoo Group around Springton, South Australia*, B. Sc. (Hons.) thesis, Univ. Adelaide (unpubl.).

Mancktelow, N. S., 1979, *The structure and metamorphism of the southern Adelaide Fold Belt*, Ph. D. thesis, Univ. Adelaide (unpubl.).

Marlow, P. C., 1975, *Structural investigations near Macclesfield, South Australia*, M. Sc. thesis, Univ. Adelaide (unpubl.).

Mawson, D. and Sprigg, R. C., 1950, *Subdivision of the Adelaide System*, Aust. J. Sci., 13: 69–70.

McInerney, P. M., 1974, *Interpretation of a major Bouguer gravity anomaly in the western Murray Basin*, B. Sc. (Hons.) thesis, Univ. Adelaide (unpubl.).

McIntyre, J. I., 1980, *Geological significance of magnetic patterns related to magnetite in sediments and metasediments — a review*, Bull. Aust. Soc. Explor. Geophys., 11: 19–33.

McIntyre, J. I., 1981, *Accurate display of fine detail in aeromagnetic data*, Bull. Aust. Soc. Explor. Geophys., 12: 82–88.

McKirdy, D. M., Sumartojo, J., Tucker, D. H. and Gostin, V., 1975, *Organic, mineralogic and magnetic indications of metamorphism in the Tapley Hill Formation, Adelaide Geosyncline*, Precambrian Research, 2: 345–374.

Middleton, M. A., 1973, *A gravity survey across the Mt. Lofty Ranges, S.A.*, B. Sc. (Hons.) thesis, Univ. Adelaide (unpubl.).

Mills, K. J., 1964, *The structural petrology of an area east of Springton, South Australia*, Ph. D. thesis, Univ. Adelaide (unpubl.).

Mills, K. J., 1973, *The structural geology of the Warren National Park and the western portion of the Mount Crawford State Forest, South Australia*, Trans. R. Soc. S. Aust., 97: 281–315.

Milnes, A. R., 1973, *The Encounter Bay Granites, South Australia, and their environment*, Ph. D. thesis, Univ. Adelaide (unpubl.).

Milnes, A. R., Compston, W. and Daily, B., 1977, *Pre- to syn-tectonic emplacement of Early Palaeozoic granites in south-eastern South Australia*, J. Geol. Soc. Aust., 24: 87–106.

Mirams, R. C., 1962, *Investigation of the Dawesley aeromagnetic anomaly*, S.A. Department of Mines and Energy, Mining Review, 116: 10–13.

Miyashiro, A., 1964, *Oxidation and reduction in the Earth's crust with special reference to the role of graphite*, Geochimica et Cosmochimica, 28: 717–729.

Miyashiro, A., 1973, *Metamorphism and metamorphic belts*, G. Allen and Unwin, London, 492 pages.

Moeller, T., 1980, *The petrology and geochemistry of the Reedy Creek granitoids and migmatites.*, B. Sc. (Hons.) thesis, Univ. Adelaide (unpubl.).

Moore, M. J., 1980, *The geology of an area south of Keyneton*, III Year Project, S. Aust. Inst. Tech. (unpubl.).

Moore, P. S., 1983, *Geological field guide to the northeast coast of Kangaroo Island*, Australasian Sedimentologists Group, Adelaide, 54 pages.

Morris, B. J., 1974, *Basic rocks of the Kanmantoo Group at Tailem Bend*, Geol. Surv. S. Aust., Quart. Geol. Notes, 51: 9–12.

Morris, B. J., 1988, *Distribution of mineralization*, In: Gatehouse, C. G. (ed.) Kanmantoo Field Symposium excursion guide, S.A. Department of Mines and Energy, Report Book, 88/35: 15–16.

Nabighian, M. N., 1972, *The analytic signal of two-dimensional magnetic bodies using Hilbert transforms*, Geophysics, 47: 376–387.

Nader, G. L., 1977, *A geological study and structural interpretation of the Macclesfield Syncline, Macclesfield, within the eastern Mt. Lofty Ranges*, III Year Project, S. Aust. Inst. Tech. (unpubl.).

Nelson, J. B., 1988, *Comparison of gradient analysis techniques for linear two-dimensional magnetic sources*, Geophysics, 53: 1088–1095.

Nenke, J. A., 1972, *Geochemistry and mineragraphy of the Nairne Pyrite Deposit, Brukunga, S.A.*, B. Sc. (Hons.) thesis, Univ. Adelaide (unpubl.).

O'Driscoll, E. S. T., 1983, *Deep tectonic foundations of the Eromanga Basin*, APEA Journal, 23: 5–17.

Offler, R., 1960, *The structure, petrology and stratigraphy of the Strathalbyn Anticline.*, B. Sc. (Hons.) thesis, Univ. Adelaide (unpubl.).

Offler, R., 1963, *Structural geology of the Strathalbyn anticline*, Trans. R. Soc. S. Aust., 87: 199–208.

Offler, R., 1966, *The structure and metamorphism of the Pewsey Vale area northeast of Williamstown, South Australia*, Ph. D. thesis, Univ. Adelaide (unpubl.).

Offler, R. and Fleming, P. D., 1968, *A synthesis of folding and metamorphism in the Mt. Lofty Ranges, South Australia*, J. Geol. Soc. Aust., 15: 245–266.

O'Reilly, W., 1984, *Rock and mineral magnetism*, Blackie & Son Limited, Glasgow, 220 pages.

Pain, A. M., 1968, *A study of the metadolerite dyke swarm in the Woodside district, South Australia*, B. Sc. (Hons.) thesis, Univ. Adelaide (unpubl.).

Paine, J. W., 1986, *A comparison of methods for approximating the vertical gradient of one-dimensional magnetic field data*, Geophysics, 51: 1725–1735.

Parker, A. J., 1986, *Tectonic development and metallogeny of the Kanmantoo Trough in South Australia*, Ore Geology Reviews, 1: 203–212.

Parker, A. J., Rickwood, P. C., Baillie, P. W., Boyd, D. M., Freeman, M. J., McClenaghan, M. P., Murray, C. G., Myers, J. S. and Pietsch, B. A., 1987, *Mafic dyke swarms of Australia*, In: Halls, H. C. and Fahrig, W. F. (eds.), Mafic dyke swarms, Geological Association of Canada, Special Paper, 34: 401–417.

Parsons, I. and Brown, W. L., 1988, *Sidewall crystallization in the Klokken intrusion: zoned ternary feldspars and coexisting minerals*, Contrib. Mineral. Petrol., 98: 431–443.

Paterson, N. R. and Reeves, C. V., 1985, *Applications of gravity and magnetic surveys — the state of the art in 1985*, Geophysics, 50: 2558–2594.

Pitkin, J. A., 1968, *Airborne measurements of terrestrial radioactivity as an aid to geologic mapping*, USGS Professional paper, 516-F, 29 pages.

Plummer, P. S., 1978, *The Brachina Subgroup — a late Precambrian intertidal sequence, Flinders Ranges, South Australia*, Ph. D. thesis, Univ. Adelaide (unpubl.).

Poole, L. E., 1969, *The structural geology of an area south of Kanmantoo, South Australia*, B. Sc. (Hons.) thesis, Univ. Adelaide (unpubl.).

Preiss, W. V., 1979, *Adelaidean Sedimentation: the Adelaide Geosyncline and Stuart Shelf*, S.A. Department of Mines and Energy, Report Book, 79/34: 37 pages.

Preiss, W. V. (compiler), 1987, *The Adelaide Geosyncline — late Proterozoic stratigraphy, sedimentation, palaeontology and tectonics*, Bull. Geol. Surv. S. Aust., 53: 438 pages.

Rajagopalan, S., 1987, *The use of "Automatic Gain Control" to display vertical magnetic gradient data*, Bull. Aust. Soc. Explor. Geophys., 18: 166–169.

Rajagopalan, S., in press, *Digital images from a laser printer*, Computers & Geosciences.

Rajagopalan, S. and Boyd, D. M., in press, *A systematic approach to the display of aeromagnetic data*, Bull. Ass. Explor. Geophys.

Ramdohr, P., 1969, *The ore minerals and their intergrowths*, Oxford, New York: Pergamon Press, 1174 pages.

Rao, B. S. R. and Prakasa Rao, T. K. S., 1970, *Easy method of interpreting dyke anomalies*, Pure Appl. Geophys., 78: 32–36.

Rao, B. S. R., Prakasa Rao, T. K. S., Gopala Rao, D. and Kesavamani, M., 1972, *Derivatives and dyke anomaly interpretation*, Pure Appl. Geophys., 99: 120–129.

Rattigan, J. H. and Wegener, C. F., 1951, *Granites of the Palmer area and associated granitized sediments*, Trans. R. Soc. S. Aust., 74: 149–164.

Reid, G. C., 1988, *PostScript Language Program Design*, Addison-Wesley, Reading, Ma., 226 pages.

Richards, D. J., 1967, *Three rapid direct methods for estimating depth to thin two-dimensional magnetic slabs*, Ann. Geol. Surv. S. Afr., 10: 101–106.

Robinson, E. S., Poland, P. V., Glover, L., III and Speer, J. A., 1985, *Some effects of regional metamorphism and geologic structure on magnetic anomalies over the Carolina Slate belt near Roxboro, North Carolina*, In: Hinze, W. J. (ed.), The utility of regional gravity and magnetic anomaly maps, Society of Exploration Geophysicists, 320–324.

Robinson, W. B., 1966, *Eudunda map sheet, 1:63 360 geological series*, S.A. Department of Mines and Energy.

Rochette, P., 1987, *Metamorphic control of the magnetic mineralogy of black shales in the Swiss Alps; toward the use of "magnetic isograde"*., Earth and Planetary Science Letters, 84: 446–456.

Rumble, D., III, 1973, *Fe-Ti oxide minerals from regionally metamorphosed quartzites*, Contrib. Mineral. Petrol., 42: 181–195.

Rumble, D., III, 1976, *Oxide minerals in metamorphic rocks*, In: Rumble, D., III (ed.) Oxide minerals, Mineral. Soc. Am., Short course notes (Washington), 502 pages.

Sabins, F. F., 1987, *Remote Sensing principles and interpretation*, W. H. Freeman and Co., New York, 447 pages.

SADME, 1980, *Adelaide map sheet, 1:250 000 aeromagnetic map of total intensity, SI 54-9*, S. A. Department of Mines and Energy.

SADME, 1983, *Barker map sheet, 1:250 000 aeromagnetic map of total intensity, sheet SI 54-13*, S. A. Department of Mines and Energy.

Sandiford, M., Oliver, R. L., Mills, K. J. and Allen, R. V., in press, *A cordierite-staurolite-muscovite association, east of Springton, Mt. Lofty Ranges: implications for the metamorphic evolution of the Kanmantoo Group*, In: Brian Daily Memorial Volume, Geol. Soc. Aust. Special Publ.

Sando, M., 1957, *The granite and metamorphic rocks of the Reedy Creek area, Mannum, South Australia*, M. Sc. thesis, Univ. Adelaide (unpubl.).

Schilling, D. L., 1968, *Electronic circuits: Discrete and Integrated*, McGraw-Hill, 671 pages.

Schwarzer, T. F. and Adams, J. A. S., 1973, *Rock and soil discrimination by low altitude airborne gamma-ray spectrometry in Payne County, Oklahoma*, Econ. Geol., 68: 1297–1312.

Seccombe, P. K., Spry, P. G., Both, R. A., Jones, M. T. and Schiller, J. C., 1985, *Base Metal Mineralisation in the Kanmantoo Group, South Australia: A Regional Isotope Study*, Econ. Geol., 80: 1824–1841.

Selwyn, A. R. C., 1859, *Preliminary report by R.C.Selwyn of a geological survey of portions of South Australia.*, Parl. Pap. S. Aust., 119: 1.

Sjarif, N., in prep., *A gravity survey of the southern Mount Lofty Ranges*, M. Sc. thesis, Univ. Adelaide.

Skinner, B. J., 1958, *The geology and metamorphism of the Nairne Pyritic Formation, a sedimentary sulphide deposit in South Australia*, Econ. Geol., 53: 546–562.

Smith, R. J., 1985, *Geophysics in Australian mineral exploration*, Geophysics, 50: 2637–2665.

Sprigg, R. C. and Campana, B., 1953, *The age and facies of the Kanmantoo Group*, Aust. J. Sci., 16: 12–14.

Spry, P. G., 1976, *Base metal mineralization in the Kanmantoo Group, S. A.: The South Hill, Bremer and Wheal Ellen areas*, B. Sc. (Hons.) thesis, Univ. Adelaide (unpubl.).

Spry, P. G., Schiller, J. C. and Both, R. A., 1988, *Structure and metamorphic setting of base metal mineralization in the Kanmantoo Group, South Australia*, Proc. Australas. Inst. Min. Metall., 293: 57–65.

Staltari, G., 1974, *Aeromagnetic interpretation of the Kanmantoo area, South Australia.*, B. Sc. (Hons.) thesis, Univ. Adelaide (unpubl.).

Steinhardt, C., in prep., *Thrusting and the tectonic development of the Adelaide Geosyncline*, Tectonics.

Stolz, E. M., 1985, *A magnetic study of the Brachina Formation on southern Fleurieu Peninsula, South Australia*, B. Sc. (Hons.) thesis, Univ. Adelaide (unpubl.).

Stuart, W. J., Jr. and von Sanden, A. T., 1972, *Palaeozoic history of the St. Vincent Gulf region, South Australia.*, A.P.E.A. Journal, 12: 9–16.

Sun Yunsheng, Strangway, D. W., and Urquhart, W. E. S., 1985, *Geologic interpretation of a high-resolution aeromagnetic survey in the Amos-Barraute area of Quebec*, In: Hinze, W. J. (ed.), The utility of regional gravity and magnetic anomaly maps, Society of Exploration Geophysicists, 413–425.

Takahashi, M., Aramaki, S. and Ishihara, S., 1980, *Magnetite-series/Ilmenite series vs. I-type/S-type granitoids*, Mining Geology Special Issue, Granitic magmatism and related mineralization, 8: 13–28.

Tate, R., 1879, *The anniversary address of the President*, Trans. Phil. Soc. S. Aust., 2: 39–75.

Thiele, W. K., 1961, *The magnetics of the Nairne Pyrite Formation*, B. Sc. (Hons.) thesis, Univ. Adelaide (unpubl.).

Thompson, J. B., Jr., 1972, *Oxides and sulphides in regional metamorphism of pelitic schists*, Int. Geol. Congr., 24th, Montreal, 10: 27–35.

Thompson, R. L., 1970, *A study of the mineralization at the Kitticoola Copper Mine, Palmer, S.A.*, B. Sc. (Hons.) thesis, Univ. Adelaide (unpubl.).

Thomson, B. P., 1969a, *The Kanmantoo Group and Early Palaeozoic Tectonics.*, In: Parkin, L. W. (ed.) Handbook of South Australian Geology, Geol. Surv. S. Aust., Govt. Printer, Adelaide, 97–108.

Thomson, B. P., 1969b, *Adelaide map sheet, 1:250 000 geological series, sheet SI 54-9*, S.A. Department of Mines and Energy.

Thomson, B. P., 1970, *A review of the Precambrian and lower Palaeozoic tectonics of South Australia*, Trans. R. Soc. S. Aust., 94: 192–221.

Thomson, B. P., 1975, *Kanmantoo Trough — regional geology and comments on mineralization*, In: Knight, C. L. (ed.), Economic geology of Australia and Papua New Guinea, Aust. Inst. Min. Met., 1: 555–565.

Thomson, B. P., Daily, B., Coats, R. P. and Forbes, B. G., 1976, *Late Precambrian and Cambrian geology of the Adelaide "Geosyncline" and Stuart Shelf, South Australia*, Excursion Guide 33A, 25th. Int. Geol. Congr., Sydney, Australia.

Thomson, B. P. and Horwitz, R. C., 1961, *Cambrian-Precambrian unconformity in Sellick Hill-Normanville area of South Australia*, Aust. J. Sci., 24: 40–41.

Thomson, B. P. and Horwitz, R. C., 1962, *Barker map sheet, 1:250 000 geological series, sheet SI 54-13*, S.A. Department of Mines and Energy.

Toteff, S., 1977, *The geology of the Adelaidean-Kanmantoo sequences in the eastern Mount Lofty Ranges*, Ph. D. thesis, Univ. Adelaide (unpubl.).

Toteff, S., in press, *The Adelaide Supergroup-Kanmantoo Group contact, eastern Mount Lofty Ranges, South Australia*, In: Brian Daily Memorial Volume, Geol. Soc. Aust. Special Publ.

Tufte, E. R., 1983, *The visual display of quantitative information*,, Graphics Press, Connecticut, 197 pages.

Turner, S., Foden, J. D. and Cooper, J., 1989, *Post-Delamerian magmatism: tectonic controls on magma chemistry and evidence for post-Delamerian extension*, Australasian tectonics, Specialist group in tectonics and structural geology, Geol. Soc. Aust., Abstracts, 24: 155–156.

Twidale, C. R. and Bourne, J. A., 1975, *Geomorphological evolution of part of the eastern Mount Lofty Ranges, South Australia*, Trans. R. Soc. S. Aust., 99: 197–210.

Vokes, F. M., 1969, *A review of metamorphism of sulphide deposits*, Earth-Sci. Rev., 5: 99–143.

von der Borch, C. C., 1980, *Evolution of the late Proterozoic to early Palaeozoic Adelaide Foldbelt, Australia: comparisons with post-Permian rifts and passive margins.*, Tectonophysics, 70: 115–134.

Wake-Dyster, K., 1974, *An investigation of the magnetic characteristics of the Black Hill Norite, western Murray Basin*, B. Sc. (Hons.) thesis, Univ. Adelaide (unpubl.).

Webb, A. W., 1976, *Geochronology of the granitic rocks of south-eastern South Australia*, Aust. Mineral Dev. Labs., Report No. 1138, Adelaide, Aust. (unpubl.).

Webster, S. S. and Scheibner, E., 1984, *Introduction to the magnetic properties of New England granitoids*, Bull. Aust. Soc. Explor. Geophys., 15: 67–73.

Wegmann, D., 1980, *Pre-Tertiary geology of the Black Hill region in the western Murray Basin of S.A.; with special emphasis on the petrology and geochemistry of the gabbroic rocks*, B. Sc. (Hons.) thesis, Univ. Adelaide (unpubl.).

Wellman, P. and Greenhalgh, S. A., 1988, *Flinders/Mount Lofty Ranges, South Australia: Their uplift, erosion and relationship to crustal structure*, Trans. R. Soc. S. Aust., 112: 11–19.

Wells, B. E., 1956, *Geology of the Casterton district*, Proc. Roy. Soc. Vic., 68: 85–110.

Werner, S., 1953, *Interpretation of magnetic anomalies at sheet-like bodies*, Stockholm, Sveriges Geologiska Undersokning.

White, A. J. R., 1956, *The granites and associated metamorphic rocks of Palmer, South Australia*, Ph. D. thesis, Univ. London (unpubl.).

White, A. J. R., 1966a, *Genesis of migmatites from the Palmer region of South Australia.*, Chem. Geol., 1: 165–200.

White, A. J. R., 1966b, *Petrology and structure of the Rathjen Granitic Gneiss of the Palmer region, South Australia*, J. Geol. Soc. Aust., 13: 471–489.

White, A. J. R., Compston, W. and Kleeman, A. W., 1967, *The Palmer Granite — a study of a granite within a regional metamorphic environment*, J. Petrol., 8: 29–50.

Whitehead, B. R., 1975, *The structure and the petrology and geochemistry of the migmatites and igneous rocks of the Reedy Creek area near Palmer, S. A.*, B. Sc. (Hons.) thesis, Univ. Adelaide (unpubl.).

Whiting, T. H., 1987, *A study of the lithology and structure of the eastern Arunta Inlier based on aeromagnetic interpretation*, Ph. D. thesis, Univ. Adelaide (unpubl.).

Wicks, S. P., 1972, *Geology of part of the basement inlier northeast of Mt. Compass*, B. Sc. (Hons.) thesis, Univ. Adelaide (unpubl.).

Willan, R. C. R. and Hall, A. J., 1980, *Sphalerite geobarometry and trace-element studies on stratiform sulphide from McPhun's Cairn, Loch Fyne, Argyll, Scotland*, Inst. Min. Metal. Trans., 89: B31–B40.

Wymond, A. P., 1950, *The geology of the Bulls Creek-Mount Magnificent area*, M. Sc. thesis, Univ. Adelaide (unpubl.).